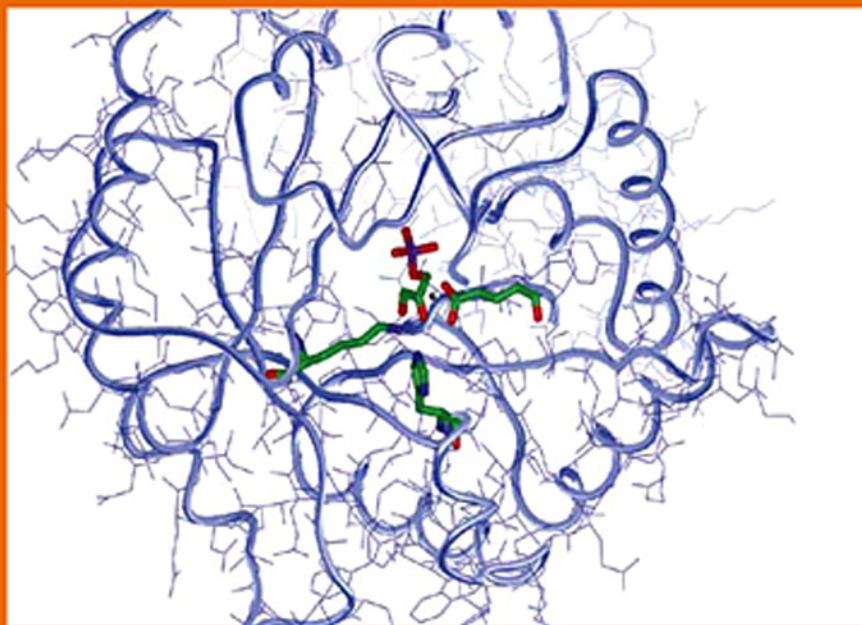


# **Chemical Kinetics**

## **From Molecular Structure to Chemical Reactivity**

Luis Arnaut, Sebastiao Formosinho  
and Hugh Burrows



# **Chemical Kinetics**

## **From Molecular Structure to Chemical Reactivity**

This page intentionally left blank

# **Chemical Kinetics**

## **From Molecular Structure to Chemical Reactivity**

Luis Arnaut  
Sebastiao Formosinho  
Hugh Burrows

*Chemistry Department  
University of Coimbra  
Coimbra, Portugal*



ELSEVIER

Amsterdam • Boston • Heidelberg • London • New York • Oxford  
Paris • San Diego • San Francisco • Singapore • Sydney • Tokyo

Elsevier  
Radarweg 29, PO Box 211, 1000 AE Amsterdam, The Netherlands  
The Boulevard, Langford Lane, Kidlington, Oxford OX5 1GB, UK

First edition 2007

Copyright © 2007 Elsevier B.V. All rights reserved

No part of this publication may be reproduced, stored in a retrieval system or transmitted in any form or by any means electronic, mechanical, photocopying, recording or otherwise without the prior written permission of the publisher

Permissions may be sought directly from Elsevier's Science & Technology Rights Department in Oxford, UK: phone (+44) (0) 1865 843830; fax (+44) (0) 1865 853333; email: permissions@elsevier.com. Alternatively you can submit your request online by visiting the Elsevier web site at <http://elsevier.com/locate/permissions>, and selecting *Obtaining permission to use Elsevier material*

#### Notice

No responsibility is assumed by the publisher for any injury and/or damage to persons or property as a matter of products liability, negligence or otherwise, or from any use or operation of any methods, products, instructions or ideas contained in the material herein. Because of rapid advances in the medical sciences, in particular, independent verification of diagnoses and drug dosages should be made

#### Library of Congress Cataloging-in-Publication Data

A catalog record for this book is available from the Library of Congress

#### British Library Cataloguing in Publication Data

A catalogue record for this book is available from the British Library

ISBN-13: 978-0-444-52186-6

ISBN-10: 0-444-52186-0

For information on all Elsevier publications  
visit our website at [books.elsevier.com](http://books.elsevier.com)

Printed and bound in The Netherlands

07 08 09 10 11 10 9 8 7 6 5 4 3 2 1

Working together to grow  
libraries in developing countries

[www.elsevier.com](http://www.elsevier.com) | [www.bookaid.org](http://www.bookaid.org) | [www.sabre.org](http://www.sabre.org)

ELSEVIER BOOK AID International Sabre Foundation

# Contents

<i>Preface</i> .....	<i>xi</i>
<b>1 Introduction</b> .....	<b>1</b>
1.1 Initial Difficulties in the Development of Chemical Kinetics in the Twentieth Century .....	2
1.2 Chemical Kinetics: The Current View .....	4
References .....	14
<b>2 Reaction Rate Laws</b> .....	<b>15</b>
2.1 Reaction Rates .....	15
2.2 Factors that Influence the Velocities of Reactions .....	17
2.2.1 Nature of the reagents .....	17
2.2.2 Reactant concentration .....	19
2.2.3 Temperature .....	25
2.2.4 Light .....	26
2.2.5 Catalysts .....	29
2.2.6 Reaction medium .....	30
References .....	32
<b>3 Experimental Methods</b> .....	<b>33</b>
3.1 Application of Conventional Techniques to Study Reactions .....	34
3.1.1 First-order reactions .....	34
3.1.2 Second-order reactions .....	36
3.1.3 Complex reactions .....	39
3.1.4 Activation energy .....	41
3.1.5 Dependence of light intensity .....	43
3.1.6 Enzyme catalysis .....	46
3.1.7 Dependence on ionic strength .....	47
3.2 Application of Special Techniques for Fast Reactions .....	50
3.2.1 Flow methods .....	51
3.2.2 Relaxation methods .....	52
3.2.3 Competition methods .....	56
3.2.4 Methods with enhanced time resolution .....	61
References .....	75
<b>4 Reaction Order and Rate Constants</b> .....	<b>77</b>
4.1 Rates of Elementary Reactions .....	77
4.1.1 First-order reactions .....	77

4.1.2	Second-order reactions . . . . .	80
4.1.3	Zero-order reactions . . . . .	82
4.1.4	Third-order reactions . . . . .	83
4.2	Rates of Complex Reactions . . . . .	84
4.2.1	Parallel first-order reactions . . . . .	85
4.2.2	Consecutive first-order reactions . . . . .	86
4.2.3	Reversible first-order reactions . . . . .	88
4.3	Methods for Solving Kinetic Equations . . . . .	89
4.3.1	Laplace transforms . . . . .	89
4.3.2	Matrix method . . . . .	94
4.3.3	Runge–Kutta method . . . . .	97
4.3.4	Markov chains . . . . .	99
4.3.5	Monte Carlo method . . . . .	103
4.4	Simplification of Kinetic Schemes . . . . .	106
4.4.1	Isolation method . . . . .	106
4.4.2	Pre-equilibrium approximation . . . . .	107
4.4.3	Steady-state approximation . . . . .	108
4.4.4	Rate-determining step of a reaction . . . . .	111
	References . . . . .	113
<b>5</b>	<b>Collisions and Molecular Dynamics . . . . .</b>	<b>115</b>
5.1	Simple Collision Theory . . . . .	117
5.2	Collision Cross Section . . . . .	122
5.3	Calculation of Classical Trajectories . . . . .	128
5.4	PES Crossings . . . . .	135
5.5	Molecular Dynamics . . . . .	137
	References . . . . .	142
<b>6</b>	<b>Reactivity in Thermalised Systems . . . . .</b>	<b>143</b>
6.1	Transition-State Theory . . . . .	143
6.1.1	Classical formulation . . . . .	144
6.1.2	Partition functions . . . . .	147
6.1.3	Absolute rate calculations . . . . .	149
6.1.4	Statistical factors . . . . .	151
6.1.5	Beyond the classical formulation . . . . .	154
6.2	Semi-Classical Treatments . . . . .	156
6.2.1	Kinetic isotope effects . . . . .	156
6.2.2	Tunnel effect . . . . .	160
6.3	Intersecting-State Model . . . . .	167
6.3.1	Activation energies . . . . .	170
6.3.2	Classical rate constants . . . . .	176
6.3.3	Absolute semi-classical rates . . . . .	180
6.3.4	Relative rates . . . . .	183
	References . . . . .	187
<b>7</b>	<b>Relationships between Structure and Reactivity . . . . .</b>	<b>189</b>
7.1	Quadratic Free-Energy Relationships (QFER) . . . . .	189

7.2	Linear Free-Energy Relationships (LFER) . . . . .	193
7.2.1	Brönsted equation . . . . .	194
7.2.2	Bell–Evans–Polanyi equation . . . . .	196
7.2.3	Hammett and Taft relationships . . . . .	196
7.3	Other Kinds of Relationships between Structure and Reactivity . . . . .	202
7.3.1	The Hammond postulate . . . . .	202
7.3.2	The reactivity–selectivity principle (RSP) . . . . .	203
7.3.3	Relationships of the electronic effect: equation of Ritchie . . . . .	205
7.3.4	An empirical extension of the Bell–Evans–Polanyi relationship . . . . .	205
	References . . . . .	207
<b>8</b>	<b>Unimolecular Reactions . . . . .</b>	<b>209</b>
8.1	Lindemann–Christiansen Mechanism . . . . .	209
8.2	Hinshelwood’s Treatment . . . . .	212
8.3	Rice–Rampsberger–Kassel–Marcus (RRKM) Treatment . . . . .	215
8.4	Local Random Matrix Theory (LRMT) . . . . .	218
8.5	Energy Barriers in the Isomerisation of Cyclopropane . . . . .	220
	References . . . . .	222
<b>9</b>	<b>Elementary Reactions in Solution . . . . .</b>	<b>223</b>
9.1	Solvent Effects on Reaction Rates . . . . .	223
9.2	Effect of Diffusion . . . . .	225
9.3	Diffusion Constants . . . . .	229
9.4	Reaction Control . . . . .	235
9.4.1	Internal pressure . . . . .	237
9.4.2	Reactions between ions . . . . .	240
9.4.3	Effect of ionic strength . . . . .	244
9.4.4	Effect of hydrostatic pressure . . . . .	246
	References . . . . .	249
<b>10</b>	<b>Reactions on Surfaces . . . . .</b>	<b>251</b>
10.1	Adsorption . . . . .	251
10.2	Adsorption Isotherms . . . . .	256
10.2.1	Langmuir isotherm . . . . .	256
10.2.2	Adsorption with dissociation . . . . .	257
10.2.3	Competitive adsorption . . . . .	258
10.3	Kinetics on Surfaces . . . . .	259
10.3.1	Unimolecular surface reactions . . . . .	259
10.3.2	Activation energies of unimolecular surface reactions . . . . .	260
10.3.3	Reaction between two adsorbed molecules . . . . .	261
10.3.4	Reaction between a molecule in the gas phase and an adsorbed molecule . . . . .	263
10.4	Transition-State Theory for Reactions on Surfaces . . . . .	263
10.4.1	Unimolecular reactions . . . . .	263
10.4.2	Bimolecular reactions . . . . .	265

10.5 Model Systems . . . . .	268
10.5.1 Langmuir–Hinshelwood mechanism . . . . .	268
10.5.2 Eley–Rideal mechanism . . . . .	270
References . . . . .	271
<b>11 Substitution Reactions . . . . .</b>	<b>273</b>
11.1 Mechanisms of Substitution Reactions . . . . .	273
11.2 S <sub>N</sub> 2 and S <sub>N</sub> 1 Reactions . . . . .	274
11.3 Langford–Gray Classification . . . . .	276
11.4 Symmetrical Methyl Group Transfers in the Gas-Phase . . . . .	280
11.5 State Correlation Diagrams of Pross and Shaik . . . . .	282
11.6 Intersecting-State Model . . . . .	285
11.7 Cross-Reactions in Methyl Group Transfers in the Gas Phase . . . . .	288
11.8 Solvent Effects in Methyl Group Transfers . . . . .	289
References . . . . .	294
<b>12 Chain Reactions . . . . .</b>	<b>295</b>
12.1 Hydrogen–Bromine Reaction . . . . .	295
12.2 Reaction between Molecular Hydrogen and Chlorine . . . . .	298
12.3 Reaction between Molecular Hydrogen and Iodine . . . . .	300
12.4 Calculation of Energy Barriers for Elementary Steps in Hydrogen–Halogens Reactions . . . . .	301
12.5 Comparison of the Mechanisms of the Hydrogen–Halogen Reactions . . . . .	303
12.6 Pyrolysis of Hydrocarbons . . . . .	305
12.6.1 Pyrolysis of ethane . . . . .	306
12.6.2 Pyrolysis of acetic aldehyde . . . . .	308
12.6.3 Goldfinger–Letort–Niclause rules . . . . .	309
12.7 Explosive Reactions . . . . .	310
12.7.1 Combustion between hydrogen and oxygen . . . . .	310
12.7.2 Thermal explosions . . . . .	314
12.7.3 Combustion of hydrocarbons . . . . .	316
12.8 Polymerisation Reactions . . . . .	317
References . . . . .	320
<b>13 Acid–Base Catalysis and Proton-Transfer Reactions . . . . .</b>	<b>321</b>
13.1 General Catalytic Mechanisms . . . . .	321
13.1.1 Fast pre-equilibrium: Arrhenius intermediates . . . . .	322
13.1.2 Steady-state conditions: van't Hoff intermediates . . . . .	324
13.2 General and Specific Acid–Base Catalysis . . . . .	326
13.3 Mechanistic Interpretation of the pH Dependence of the Rates . . . . .	329
13.4 Catalytic Activity and Acid–Base Strength . . . . .	338
13.5 Salt Effects . . . . .	342
13.6 Acidity Functions . . . . .	343
13.7 Hydrated Proton Mobility in Water . . . . .	345
13.8 Proton-Transfer Rates in Solution . . . . .	350

13.8.1 Classical PT rates . . . . .	351
13.8.2 Semiclassical absolute rates . . . . .	356
References . . . . .	358
<b>14 Enzymatic Catalysis . . . . .</b>	<b>361</b>
14.1 Terminology . . . . .	361
14.2 Michaelis–Menten Equation . . . . .	363
14.3 Mechanisms with Two Enzyme–Substrate Complexes . . . . .	368
14.4 Inhibition of Enzymes . . . . .	370
14.5 Effects of pH . . . . .	373
14.6 Temperature Effects . . . . .	375
14.7 Molecular Models for Enzyme Catalysis . . . . .	376
14.8 Isomerisation of Dihydroxyacetone Phosphate to Glyceraldehyde 3-Phosphate Catalysed by Triose-Phosphate . . . . .	379
14.9 Hydroperoxidation of Linoleic Acid Catalysed by Soybean Lipoxygenase-1 . . . . .	381
References . . . . .	383
<b>15 Transitions between Electronic States . . . . .</b>	<b>385</b>
15.1 Mechanisms of Energy Transfer . . . . .	385
15.2 The “Golden Rule” of Quantum Mechanics . . . . .	391
15.3 Radiative and Radiationless Rates . . . . .	395
15.4 Franck–Condon Factors . . . . .	400
15.5 Radiationless Transitions within a Molecule . . . . .	407
15.6 Triplet-Energy (or Electron) Transfer between Molecules . . . . .	410
15.7 Electronic Coupling . . . . .	421
15.8 Triplet-Energy (and Electron) Transfer Rates . . . . .	430
References . . . . .	434
<b>16 Electron Transfer Reactions . . . . .</b>	<b>437</b>
16.1 Rate Laws for Outer-Sphere Electron Exchanges . . . . .	437
16.2 Theories of Electron-Transfer Reactions . . . . .	440
16.2.1 The classical theory of Marcus . . . . .	440
16.2.2 Solute-driven and solvent-driven processes . . . . .	443
16.2.3 Critique of the theory of Marcus . . . . .	445
16.2.4 ISM as a criterion for solute-driven electron transfers . . . . .	449
16.3 ISM and Electron-Transfer Reactions . . . . .	452
16.3.1 Representing ET reactions by the crossing of two potential-energy curves . . . . .	452
16.3.2 Adiabatic self-exchanges of transition-metal complexes . . . . .	454
16.3.3 Outer-sphere electron transfers with characteristics of an inner-sphere mechanism . . . . .	456
16.4 Non-Adiabatic Self-Exchanges of Transition-Metal Complexes . . . . .	458
16.4.1 A source of non-adiabaticity: orbital symmetry . . . . .	458
16.4.2 Electron tunnelling at a distance . . . . .	458
16.4.3 Non-adiabaticity due to spin forbidden processes . . . . .	459

16.5	Electron Self-Exchanges of Organic Molecules . . . . .	460
16.6	Inverted Regions . . . . .	462
16.7	Electron Transfer at Electrodes . . . . .	469
16.7.1	The Tafel equation . . . . .	469
16.7.2	Calculations of rate constants . . . . .	475
16.7.3	Asymmetry in Tafel plots . . . . .	478
16.7.4	Electron transfer at surfaces through a blocking layer . . . . .	479
References . . . . .		482
<b>Appendix I: General Data . . . . .</b>		<b>485</b>
<b>Appendix II: Statistical Thermodynamics . . . . .</b>		<b>487</b>
<b>Appendix III: Parameters Employed in ISM Calculations . . . . .</b>		<b>495</b>
<b>Appendix IV: Semi-classical Interacting State Model . . . . .</b>		<b>499</b>
IV.1	Vibrationally Adiabatic Path . . . . .	499
IV.2	Tunnelling Corrections . . . . .	502
IV.3	Semi-classical Rate Constants . . . . .	503
References . . . . .		504
<b>Appendix V: The Lippincott-Schroeder Potential . . . . .</b>		<b>505</b>
V.1	Lippincott—Schroeder (LS) Potential . . . . .	505
V.2	The LS-ISM Reaction Path . . . . .	508
V.3	Rate Constants for Proton Transfer along an H-bond . . . . .	508
References . . . . .		509
<b>Appendix VI: Problems . . . . .</b>		<b>511</b>
<i>Subject Index . . . . .</i>		543

## Preface

Chemical kinetics is the area of science devoted to the study of the rates as well as the mechanisms of reactions. Its applications range from the understanding of the interplay between metabolic processes, where the intricate control of the rates of enzymatic processes is fundamental for the overall wellbeing of biological systems, through industrial synthesis of both fine and heavy chemicals to the long-term geological and atmospheric changes occurring on our planet since the evolution of the Universe and those expected to occur in future. At the economic level, the overwhelming majority of industrial chemical syntheses involves heterogeneous or homogeneous catalysis, and an understanding of the inherent processes and interactions is fundamental for the optimisation of reaction conditions. Moreover, a kinetic and mechanistic understanding of the complex series of interrelated reactions occurring between molecules such as oxygen, carbon dioxide, hydrogen, nitrogen and its oxides in the stratosphere and the study of processes induced by the absorption of light or high-energy radiation is fundamental to our appreciation of effects such as global warming or the depletion of the ozone layer. The timescales involved in these dynamic processes vary by many orders of magnitude, from less than the time of vibration of a chemical bond up to the age of the Universe.

All textbooks in physical chemistry have sections dedicated to kinetics. However, generally, owing to space constraints, they cannot treat the topic in the depth that is necessary for its full appreciation, and frequently, they treat its mechanics rather than its practical applications or its relations to the other areas of physical sciences such as thermodynamics and structural studies. Further, although a number of excellent student texts (at the undergraduate as well as postgraduate levels) are devoted to this topic, some of the most important ones were published several decades ago and cannot be expected to reflect the numerous significant research advances that have been acknowledged by the award of many Nobel prizes and other important distinctions in this area.

This book aims to provide a coherent, extensive view of the current situation in the field of chemical kinetics. Starting from the basic theoretical and experimental background, it gradually moves into specific areas such as fast reactions, heterogeneous and homogeneous catalysis, enzyme-catalysed reactions and photochemistry. It also focusses on important current problems such as electron-transfer reactions, which have implications at the chemical as well as biological levels. The cohesion between all these chemical processes is facilitated by a simple, user-friendly model that is able to correlate the kinetic data with the structural and the energetic parameters.

While the book is primarily meant for chemists, we feel that it can also be useful to students and research workers in related disciplines in the physical sciences, the biological and biomedical areas and in the earth and atmospheric sciences. It is hoped that this text will be beneficial to students at the undergraduate as well as postgraduate levels. In addition, the programs available free of cost at a dedicated website (<http://www.ism.qui.uc.pt:8180/ism/>) will be valuable to many research workers whose investigations necessitate the use of the tools of chemical kinetics.

The task of compiling this book would have been impossible without the excellent collaboration of many of our colleagues and co-workers, whose studies have been cited throughout the text. The feedback on the earlier versions of this text from our students at the University of Coimbra have contributed greatly to the improvement of the same. Very special thanks are due to Dr. Carlos Serpa and Dr. Monica Barroso for their contribution to the design of experiments and models that have helped us to understand the relationship between chemical structure and reactivity.

Luis Arnaut  
Sebastiao Formosinho  
Hugh Burrows

# - 1 -

## Introduction

---

It is easy with the hindsight of the twenty-first century to think that chemical kinetics has developed in a logical and coherent fashion. But this was far from the case. However, an understanding of the way we achieved our present ideas on chemical kinetics is a very good basis for truly understanding the subject. In the first chapter we start by looking at some of the milestones and pitfalls in the development of chemical kinetics. We then consider the relationship between kinetics and thermodynamics and finally, we consider the relationship between the macroscopic world we live in and the microscopic world of molecules.

The great success of Newtonian mechanics in the areas of mechanics and astronomy, which involved the idea of explaining phenomena by simple forces acting between particles, led scientists in the nineteenth century to try to introduce such a mechanical explanation to all areas involving natural phenomena. In chemistry, for example, these concepts were applied to interpret “chemical affinity”, leading to the so-called “chemical mechanics”. We will see that this is not far removed from many of our modern ideas in this area, and we will develop our understanding of chemical kinetics within this context.

In this chapter, we will see that the concepts of chemical kinetics evolved relatively late in terms of the overall studies of reactions and reactivity. The study of chemical kinetics can be traced back to Ludwig Wilhelmy [1], who carried out in 1850 the first study of the inversion of cane sugar (sucrose) in the presence of acids that he formulated in terms of a first-order mathematical expression to interpret the progress of the reaction. Unfortunately, this work went unrecognised until Ostwald [2] drew attention to it some 34 years later. It may seem strange today that such an idea of studying the variation of “chemical affinity” with time had not occurred earlier. Farber [3] had tried to explain this and has shown that, in fact, there were some earlier attempts to study the time evolution of reactions, even before Wilhelmy, but that these tended to be isolated observations. Most probably, the practical importance of such studies did not exist at the end of the eighteenth century, and it was only with the advent of the chemical industry at the beginning of the nineteenth century that chemists, rather late, needed to consider this problem. Eventually, this became of great importance for the development of industrial research at the end of that century. An excellent discussion of this problem is given by Christine King [4–6] in her studies on the *History of Chemical Kinetics*, where she analyses the impact of the various theoretical, experimental and conceptual works of Berthelot and Péan de St Giles [7–9], Guldberg and Waage [10] and Harcourt and Essen [11–14]. These researchers can truly be considered to be the founders of this new branch of chemistry, chemical kinetics.

## 1.1 INITIAL DIFFICULTIES IN THE DEVELOPMENT OF CHEMICAL KINETICS IN THE TWENTIETH CENTURY

One of the major difficulties in the development of chemical kinetics stemmed from the lack of mathematical preparation of chemists of that period. For example, Morris Travers [4,5,15] in his biography of William Ramsay noted that his lack of mathematical preparation was the determining factor that made him decide not to become a physicist. Harcourt also notes his own mathematical weakness and his inability to understand many of the mathematical treatments that were made on his experimental data on chemical reactions. These were due to the mathematician Esson, professor of geometry at Oxford. Such developments were sufficiently complex that they were not even understood by many of his contemporary mathematicians, let alone by the chemists of the period. Also, the work of Guldberg and Waage in this area resulted from a collaboration between a professor of applied mathematics and a chemist, while the extremely promising work of Berthelot and Péan de St Gilles on kinetics was finally abandoned by the premature death of the latter scientist at the age of 31.

Berthelot and St Giles, in their kinetic study of esterification reactions, showed that the amount of ester formed at each instant was proportional to the product of the “active masses” of the reactants and inversely proportional to the volume. Rather inexplicably, these authors did not take into account the role of these factors in defining the rate law of the reaction [4,5,15]. A possible explanation for this can be seen in a note on the life and work on Marcelin Berthelot [16]. In this work, indications are given of Berthelot’s understanding of the role of mathematics in chemistry: “the mathematicians make an incoherent block out of physical and chemical phenomena. For better or for worse, they force us to fit our results to their formulae, assuming reversibility and continuity on all sides, which, unfortunately, is contradicted by a large number of chemical phenomena, in particular the law of definite proportions.”

Guldberg and Waage arrived at the concept of chemical equilibrium during 1864–1867 through the laws of classical mechanics: that there are two opposing forces, one owing to the reactants and the other to the products, which act during a chemical reaction to achieve equilibrium. In an analogy with the theory of gravity, such forces will be proportional to the masses of the different substances; actually, they established two separate laws, one relating to the effect of masses and the other to that of volume, and it was only later that they were combined into a single law, involving concentrations or “active masses”.

Guldberg and Waage also initially experienced difficulties in finding the proper exponents involved in the description of the variations in the concentrations of the different substances; this problem was resolved in 1887, in terms of molecular kinetic theory. However, far more importantly, these authors did not manage to distinguish the rate laws (what we would call today the initial conditions) from the derivatives of the equilibrium conditions. This considerably complicated and delayed the future development of chemical kinetics. The dynamic nature of chemical equilibrium was never in doubt. However, the complexity of the systems was far from being considered and the link between equilibrium and kinetics was weak. The works of Harcourt and Esson are models of meticulous experimental and theoretical work, but on reading them, it is also obvious that these authors had to confront many conceptual and technical problems. Their kinetic studies

needed fairly slow reactions that could be started and stopped quickly and easily. The reactions that best satisfied these experimental conditions were, in fact, fairly complex in mechanistic terms. In spite of the fact that Harcourt knew that such reactions did not happen in a single step, he was far from being able to recognise all their complexities. It was this difficulty in seeing simplicity in the macroscopic observations and extending it to the corresponding microscopic interpretation that became one of the main obstacles to the proper development of chemical kinetics.

Another area of chemical kinetics that has been the focus of various historical studies, involved the interpretation of the effect of temperature on the rates of chemical reactions. For rates measured under standard concentration conditions, Arrhenius expressed this effect by the equation

$$k = A e^{-(E_a/RT)} \quad (1.1)$$

where  $k$  is the rate under standard conditions and  $A$  and  $E_a$  constants, which are practically independent of temperature.  $A$  is called the *frequency factor* or *pre-exponential factor* and  $E_a$  the *activation energy*.

The Arrhenius law took a long time to become accepted; many other expressions were also proposed to explain the dependence of rate on temperature [17–19]. However, the Arrhenius expression eventually became dominant, as it was the model that was the easiest to relate to in terms of physical significance. Nevertheless, its acceptance did not come quickly, and was compounded by great difficulties in scientific communication at the time, with lack of interaction between different research groups often carrying out similar, and often parallel studies, instead of drawing on the progress that had already been achieved in this area.

Many of these conceptual and experimental difficulties would disappear with the brilliant work of van't Hoff [20], who introduced the concept of order of reaction and, through it, the possibility of knowing the mechanism of a chemical reaction just on the basis of chemical kinetics [21]. In fact, van't Hoff used the term *molecularity* for what we would call today reaction *order* (the power to which a concentration of a component enters into the rate equation). When referring to the actual concept of *molecularity*, this author used the explicit expression “the number of molecules that participate in the reaction” [6]. The term *order* is due to Ostwald. Van't Hoff received the first Nobel Prize in 1901 for his discovery of the laws of chemical dynamics.

During this period, interest in chemical kinetics remained fairly high until 1890, and then declined “due to the lack of stimulus from kinetic theories which could suggest appropriate experiments, sufficient to stimulate a discussion” [22] and, in essence, it needed something to allow a connection between molecular structure and chemical reactivity. This is true, not just of chemical kinetics: all areas of science suffer in the absence of appropriate theories, which help to guide development of experiments.

A revival of interest in this area began around 1913 with the “radiation hypothesis”, due to M. Trautz, Jean Perrin and William Lewis. The particular challenge they tackled would probably have escaped notice of the scientific community, except for the fact that Perrin and Lewis were two highly respected scientists. Their developments required a strong mathematical preparation. Lewis was the first chemist to develop a theory of chemical

kinetics based on statistical mechanics and quantum theory. It is clear that Lewis was an exception in terms of mathematical background to the majority of British chemists, who even in the 1920s had a mathematical background that was insufficient to address, or even understand such problems.

The “radiation theory”, which was received with enthusiasm, was later seen to be mistaken. However, it was important as it stirred up a lively debate that greatly contributed to the development of the correct theories of chemical kinetics.

In this first phase of development, the theories of chemical kinetics tried to resolve the problem of the calculation of the pre-exponential factor and activation energy in the Arrhenius equation. The difficulties in calculating  $A$  stemmed in large part from the confusion that had existed ever since the first quarter of the nineteenth century over the role of molecular collisions on the rates of reaction. Today, we know that molecular collisions lead to the distribution of energy between molecules, but the rate of chemical reactions is determined both by the frequency of these collisions and the factors associated with the distribution of energy.

Max Trautz in 1916 and William Lewis in 1918 developed mathematical expressions that allowed the formulation of a collision theory for pre-exponential factors. In 1936 Henry Eyring, and almost independently, Michael Polanyi and M.G. Evans came to develop the transition state theory, having as its bases thermodynamics and statistical mechanics.

The concept of potential energy surface (PES) was developed to calculate the activation energy. Based on quantum mechanics, the first PES was constructed, at the start of the 1930s by Eyring and Polanyi for the reaction  $H + H_2$ . But the concept of PES is much more comprehensive because it allows the dynamic study of the rates of elementary reactions. This is based on the study of the forces that cause molecular motions that will lead to chemical reaction.

## 1.2 CHEMICAL KINETICS: THE CURRENT VIEW

Chemistry is concerned with the study of molecular structures, equilibria between these structures and the rates with which some structures are transformed into others. The study of molecular structures corresponds to study of the species that exist at the minima of multi-dimensional PESs, and which are, in principle, accessible through spectroscopic measurements and X-ray diffraction. The equilibria between these structures are related to the difference in energy between their respective minima, and can be studied by thermochemistry, by assuming an appropriate standard state. The rate of chemical reactions is a manifestation of the energy barriers existing between these minima, barriers that are not directly observable. The transformation between molecular structures implies varying times for the study of chemical reactions, and is the sphere of chemical kinetics. The “journey” from one minimum to another on the PES is one of the objectives of the study of molecular dynamics, which is included within the domain of chemical kinetics. It is also possible to classify nuclear decay as a special type of unimolecular transformation, and as such, nuclear chemistry can be included as an area of chemical kinetics. Thus, the scope of chemical kinetics spans the area from nuclear processes up to the behaviour of large molecules.

The range of rates of chemical reactions is enormous. Figure 1.1 gives a general panorama of the variety of reaction rates of processes in the world around us. Nuclear transformations and geological processes can be considered to be some of the slowest reactions that we come across. The corrosion of some metals frequently takes place during the life expectancy of a human (80 years =  $2.5 \times 10^9$  sec). The time of cooking food is readily measurable simply by visual observation, and extends from minutes to hours. We can contrast this with the case of reactions such as the precipitation of a salt or neutralisation of an acid that occur in  $<0.1$  sec, because visually we can no longer distinguish images on this timescale. There are, however, special techniques which allow much shorter time resolution in our observation window, and which allow study of extremely rapid reactions. The limit of time resolution of interest for chemical kinetics is defined by the movement of nuclei in molecules in their vibrational or rotational motion.

The chemical reaction can be considered as a voyage on a multi-dimensional PES (Figure 1.2). The definition of the PES has its origin in the separation of the movement of electrons and nuclei. This separation is justified on the basis of the difference in mass between an electron and a proton (the mass of the former is 1/1800 times the rest mass of the second), which means that the movement of electrons is much more rapid than that of the nuclei. Because of this, the electrons can be considered to re-adjust *instantaneously* to each of the geometries that the nuclei might adopt. The PES results from solving the Schrödinger equation for each of the possible nuclear geometries. The sum of the electronic energy and the nuclear repulsion governs the movement of the nuclei. Ideally, the Schrödinger equation must be solved for a great number of nuclear geometries using only the laws of quantum mechanics and the universal constants, which are given in Appendix 1. From this, a set of points will be obtained, and the energy determined for each of the possible geometries. This type of calculation, known as *ab initio*, is very time consuming

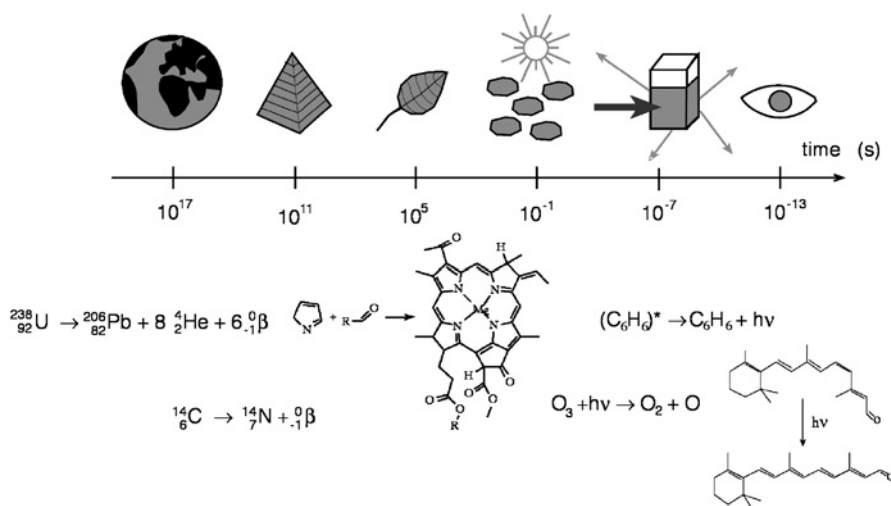


**Figure 1.1** Range of rates of chemical reactions.

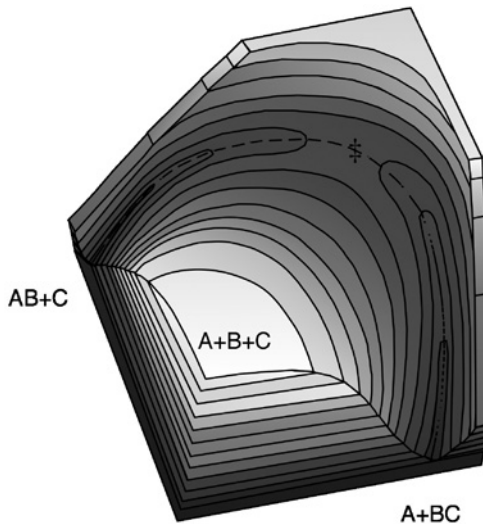


**Figure 1.2** PES for collinear approach of atom A to the diatomic molecule BC in the triatomic system  $A + BC \rightarrow AB + C$ , with the most important topographical regions: reactant valley ( $A + BC$ ), transition state ( $\ddagger$ ), product valley ( $AB + C$ ), dissociation plateau for all bonds ( $A + B + C$ ) and lowest energy pathway from reactants to products (dashed line).

and difficult for polyatomic systems. As a consequence, many PESs include experimental information and are described by more or less complex functions, which are fitted to results of *ab initio* calculations and experimental information on the system.

In a hypersurface of a polyatomic system there can exist a number of more or less stable structures, which correspond to deeper or shallower potential wells. The separation between these wells is made up of hills, that is, potential barriers with variable heights. The height of the potential barriers determines the energy necessary to convert from one structure into another, that is, for a chemical reaction to occur. In the passage from a reactant well, or valley, to that of products, there is normally one that goes by a path, whose point of highest energy is termed the saddle point, given the topographic similarity to the saddle of a horse. A saddle point corresponds to a maximum energy on the route that leads from reactants to products, but a minimum one on the direction orthogonal to this. The reaction pathway, which goes through the lowest energy path, is called the *minimum energy path*. It is natural that a chemical reaction, which occurs on a single PES will follow preferentially the minimum energy pathway or route. The surface orthogonal to the minimum energy pathway between reactants and product and which contains the saddle point, corresponds to a set of nuclear configurations that is designated the *transition state*. Its existence can be considered as virtual or conceptual, because the transition state corresponds to a region on the potential energy hypersurface from which the conversion of reactants to products leads to a decrease in the potential energy of the system. The transition state is, therefore, intrinsically unstable.

The minimum energy pathway for a given reaction can be defined by starting from the transition state as being the path of the largest slope that leads to the reactants valley on

one side and the product valley on the other. This minimum energy pathway is shown in Figure 1.2 for a typical reaction that involves breaking one bond in the reactants and forming a new bond in the products. Normally, the PES for a chemical system cannot be determined accurately since for a molecule containing  $N$  atoms the PES is a function of  $3N$  nuclear coordinates. Some of these coordinates can be separated, in particular the three coordinates which describe translational motion, given the conservation of the movement of the centre of mass, and the coordinates corresponding to rotational motion, given the conservation of angular momentum. After separation of these motions, the PES will be a function of  $3N-5$  internal, interdependent coordinates for linear configurations and  $3N-6$  for non-linear configurations. The complexity of the PES for polyatomic systems justifies the use of simplified models that simulate the variation of the potential energy of the system as a function of a reaction coordinate of the reaction. The reaction coordinate starts to have a particular significance for each model that represents the variation of the energy of the system on the conversion of reactants to products. Given that these models are simplified representations of the PES, the reaction coordinate given by a model may not correspond to the minimum energy pathway.

Figure 1.2 shows the case of a very simple PES. In fact, the topography of the PESs can be very diverse. Figure 1.3 shows an example of a PES, where instead of a maximum (saddle point), there is a minimum (intermediate) in the middle of the minimum energy pathway.

The movement of atoms across the reaction coordinate can, in an elementary approximation, be compared with that of atoms in a bond with a low-frequency vibration. The vibrational frequency  $v$  of a bond between atoms A and B is characteristic of the AB bond

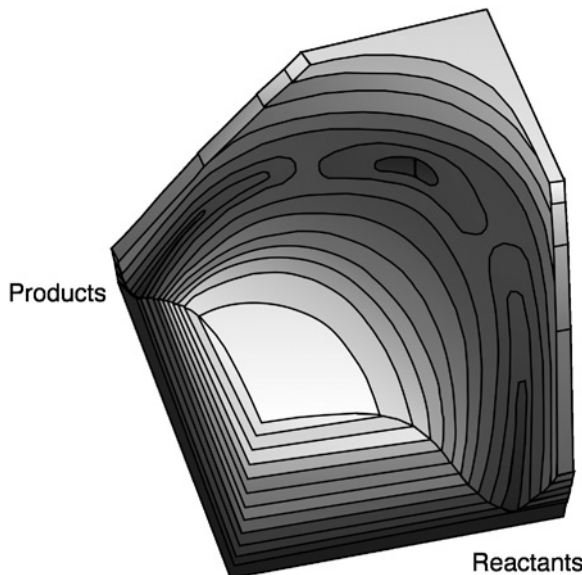


**Figure 1.3** Reaction occurring on a surface with a potential well separating reactants and products, and corresponding to the formation of a reactive intermediate. The reaction is exothermic.

and depends, to a first approximation, on the force constant of the bond  $f$  and the reduced mass of its atoms,  $\mu$

$$\nu = \frac{1}{2\pi} \left( \frac{f}{\mu} \right)^{1/2} \quad (1.2)$$

where the reduced mass is given by

$$\mu = \frac{m_A m_B}{m_A + m_B} \quad (1.3)$$

The energies where vibrations of AB are expected to occur lie between 300 and 3000 cm<sup>-1</sup> (4–40 kJ mol<sup>-1</sup>) such that they can be seen in the infrared. These energies can be related to the corresponding vibrational frequencies by the Planck equation

$$E = \hbar\nu \quad (1.4)$$

where Planck's constant,  $\hbar = 6.626 \times 10^{-34}$  J sec =  $6.626 \times 10^{-34}$  N m sec. Thus, it is possible to calculate that a bond AB typically will undergo  $10^{13}$ – $10^{14}$  oscillations per second, or that there will be one vibration for each 100–10 fsec. As the vibrational energy of a bond is given by

$$E_v = \left( v + \frac{1}{2} \right) \hbar\nu, \quad v = 0, 1, 2, 3, \dots \quad (1.5)$$

where  $v$  is the vibrational quantum number, the minimum distortion that a diatomic molecule suffers relative to its equilibrium bond length,  $r_{eq}$ , can be calculated by considering that the bond is in its lowest vibrational energy,  $v = 0$ , and using a harmonic oscillator as the model of the variation of energy with the distortion (Figure 1.4). The variation of the energy with the distortion is given by the equation of a parabola

$$V(r) = \frac{1}{2} f (r_{eq} - r)^2 \quad (1.6)$$

where  $f$  is the force constant characteristic of the oscillator. By substituting eq. (1.2) into expression (1.5) with  $v = 0$ , and equating to (1.6), we obtain

$$r_{eq} - r = \sqrt{\frac{\hbar}{f}} \sqrt{\frac{f}{\mu}} \quad (1.7)$$

To apply this equation to the real case of the <sup>35</sup>Cl–<sup>35</sup>Cl bond, it is necessary to know its reduced mass and vibrational frequency. The reduced mass of Cl<sub>2</sub> calculated from the atomic mass of chlorine and eq. (1.3) leads to  $\mu = 2.905 \times 10^{-26}$  kg. The Cl–Cl vibration is seen at 559.71 cm<sup>-1</sup> with  $\nu = c\bar{\nu}$ , where  $c = 2.998 \times 10^8$  m sec<sup>-1</sup> is the speed of light in vacuum and the frequency is  $1.68 \times 10^{13}$  sec<sup>-1</sup>. Using eq. (1.2), the force constant for this bond is  $f = 322.7$  N m<sup>-1</sup>, since by definition 1 N = 1 kg m sec<sup>-2</sup>. Force constants are often

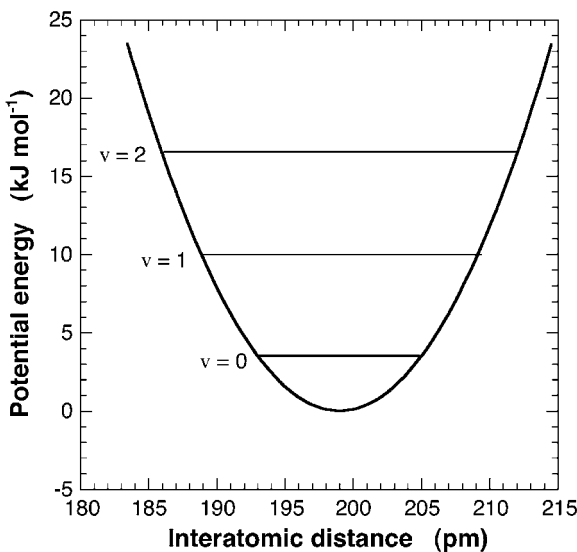


**Figure 1.4** Harmonic oscillator with the characteristic behaviour of  $\text{Cl}_2$  molecule.

expressed in  $\text{mdyn \AA}^{-1}$ ,  $\text{kcal mol}^{-1} \text{\AA}^{-2}$  or  $\text{J mol}^{-1} \text{pm}^{-2}$ , so that it is useful to know the conversion factors for these units:

$$1 \text{ mdyn \AA}^{-1} = 100 \text{ N m}^{-1} = 143.8 \text{ kcal mol}^{-1} \text{\AA}^{-2} = 60.17 \text{ J mol}^{-1} \text{pm}^{-2}.$$

Knowing the values of  $f$  and  $\mu$ , eq. (1.7) gives  $(r_{\text{eq}} - r) = 5.87 \times 10^{-12} \text{ m}$ . As such, a vibration goes through  $1.17 \times 10^{-11} \text{ m}$  in  $5.95 \times 10^{-14} \text{ sec}$ , or, in other words, the speed at which the atoms undergo vibrational movement is about  $200 \text{ m sec}^{-1}$  ( $720 \text{ km h}^{-1}$ ) in the fundamental vibrational level. It should be noted that the Cl–Cl bond, whose equilibrium bond length is  $1.99 \times 10^{-10} \text{ m}$ , is distorted by about 3% of its length.

Today, a technique called transition state spectroscopy that uses lasers with pulse widths around 10 fsec facilitates the detection of transient species with extremely short lifetimes. In this time interval, a bond in its fundamental vibration covers a distance of only  $2 \times 10^{-12} \text{ m}$ . As such, this technique enables one to obtain a sequence of images of vibrational motion of a chemical bond in the act of breaking. However, it is worth remembering that owing to the Heisenberg uncertainty principle:

$$\Delta E \Delta t \geq \frac{1}{2} \hbar \quad (1.8)$$

observations on the time scale  $10^{-14} \text{ sec}$  correspond to an uncertainty in energy of  $3 \text{ kJ mol}^{-1}$ . A better time resolution leads to greater uncertainties in energy, which will not be of much use in chemical kinetics, given that, according to eq (1.1), an uncertainty of  $3 \text{ kJ mol}^{-1}$  in transition state energy leads to a factor of 3 in the rate of a reaction at  $25^\circ\text{C}$ .

Nevertheless, these ultrashort pulse techniques do find applications in areas of spectroscopy where one is dealing with broad bands in terms of frequency distribution, and spectral bandwidth is not the limiting factor.

It is anticipated that the most rapid chemical reactions will be those that occur every time there is a bond vibration, that is, when the energy barrier is equal or less than that of the vibrational energy. This corresponds to a purely repulsive PES that could be obtained, for example, by electronic excitation. Figure 1.5 gives a typical example of a reaction of this type. For molecules with more than two atoms the situation becomes significantly more complicated, because it is necessary to consider energy distribution between the various bonds involved. For a bimolecular reaction, the maximum rate will be achieved for an exothermic reaction that occurs on every collision between reactant molecules. This limit is reached in some reactions of free radicals in the gas phase that occur without any activation barrier. In fact, however, even in some of these reactions potential wells are seen instead of barriers separating reactants and products, as in the surface shown in Figure 1.3. In these cases, the rate of the reaction may be limited by the formation of a complex or intermediate with a finite lifetime. In this case, the reaction is no longer elementary, and follows a two-step mechanism: formation of an intermediate, followed by its decay. In fluid solutions the maximum rate of a bimolecular reaction is limited by the rate at which the reactants can diffuse in the medium to achieve the reaction radius.

Beyond the above limiting situation, in a chemical reaction of the general type



energy barriers are always found. The simplest model for the origin of these energy barriers consists in assuming that to break the B–C bond, we need to supply to the BC molecules an energy equal to the energy of this bond. However, frequently, the observed energy barriers

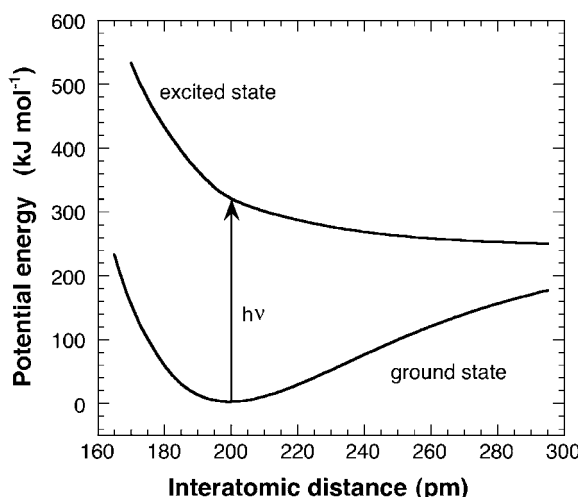


**Figure 1.5** Reaction occurring on a barrier-free surface, obtained by electronic excitation of the reactants.

of these reactions are only *ca* 10% of the energy of the bonds being broken. As such, we can see that, in general, the reaction cannot proceed in one step in which the B–C bond is broken followed by a subsequent and independent step in which there is formation of the A–B bond. In all the steps of the reaction there must be a strong correlation between the bond which is broken and that which is being formed. The transition state appears to have an electronic configuration that maximises the bonding in all of the parts (A–B and B–C) of which it is composed. The energy barrier results from two opposing factors: on one hand, the approach between the species A and BC allows the formation of a new bond, AB, which lowers the energy of the system, while on the other, this approach results in an increase in the energy of the system, given the repulsion between the molecules at short distances. The total energy depends on the correlation between the breaking and formation of the bonds.

The potential energy is a microscopic variable. For any configuration of the reactive system, in principle it is possible to calculate a potential energy. Knowing the potential energy along the minimum energy path, it is possible to define a continuous analytical function that will describe the evolution of the system from reactants to products. The knowledge of the PES allows estimation of the potential energy of activation of a chemical reaction, that is, following classical mechanics, the minimum energy necessary, for the isolated reactants to be transformed to isolated product molecules. To make a comparison between the potential energy of activation calculated from the PES and the experimental activation energy, it is necessary to make the change from the microscopic to the macroscopic domain. The energy of the system, which is observed macroscopically, is a thermodynamic energy. The energy differences between reactants and products in solution are normally measured in terms of their equilibrium constants. As the equilibrium constant of a reaction is related to the free energy

$$\Delta G^0 = -RT \ln K_{\text{eq}} \quad (1.9)$$

the barrier height to be surmounted in the course of a reaction must be expressed in macroscopic terms by a free energy of activation. The variation of potential energy calculated in this way thus corresponds to the variation in free energy when the entropy differences are negligible. The relation between the microscopic models and the experimental macroscopic reality can be made through statistical mechanics. In statistical terms, although a chemical species is a group of particles with a determined range of properties, all the particles of one species have to have the same equilibrium configuration. So, as many species exist as equilibrium configurations that can be statistically defined along the reaction coordinate.

In this context, equilibrium configuration denotes a geometry in mechanical equilibrium, that is, a geometry corresponding to a point for which the derivative of the potential energy function is zero. This derivative is zero for potential maxima and minima. As such, along the reaction coordinate, we can define three configurations that fulfil these requisites: the reactants, the products and the transition state. The first two correspond to minima and are in stable equilibria, while the latter corresponds to a maximum along the reaction coordinate, and is in unstable equilibrium (or pseudo-equilibrium). Then, although the reaction coordinate is continuous, the thermodynamic energy along it is discontinuous, containing only three points. Nevertheless, it is useful to formulate the variation of free energy as a function of the reaction coordinate in terms of a continuous function. It should be noted,

however, that the interpolated points between the equilibrium configurations do not have any thermodynamic significance.

In the transformation from the microscopic world to the macroscopic one, we also need to consider the effect of molecular collision on the distribution of molecular velocity or energy in these systems. The majority of molecules will have a velocity close to the mean value for the molecules, but there are always some molecules with velocity much greater than and others with velocity much lesser than the mean velocity. The distribution of velocities of gas molecules was first described by Maxwell in 1860. The Maxwell distribution of velocities is given by

$$f(s) = 4\pi \left( \frac{M}{2\pi RT} \right)^{3/2} s^2 \exp\left(-\frac{Ms^2}{2RT}\right) \quad (1.10)$$

The mean velocity can be calculated from the integral

$$\bar{s} = \int_0^\infty sf(s) ds = 4\pi \left( \frac{M}{2\pi RT} \right)^{3/2} \int_0^\infty s^3 \exp\left(-\frac{Ms^2}{2RT}\right) ds = \sqrt{\frac{8RT}{\pi M}} \quad (1.11)$$

where  $M$  is the molar mass of the molecules, and  $f(s) ds$  the fraction of molecules which have velocities between  $s$  and  $s+ds$ . Figure 1.6 illustrates the distribution of molecular velocities of a gas at various temperatures.

For the case of  $\text{N}_2$  molecules at 298 K, using the constants from Appendix I, we obtain a mean velocity of  $475 \text{ m sec}^{-1}$ .

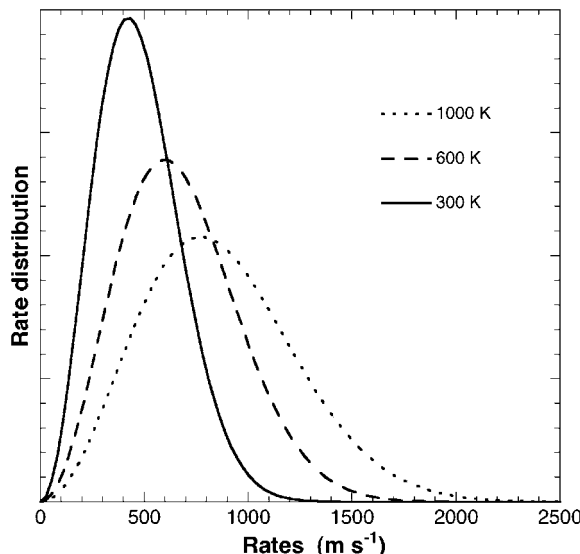
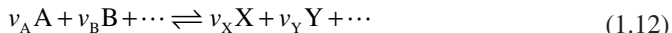


**Figure 1.6** Distribution of molecular velocities for  $\text{N}_2$  at three different temperatures (in Kelvin).

Until now, we have only considered elementary reactions, that is, ones that occur in a single step. These reactions are observed between a certain number (that must be a whole number) of atoms, molecules or ions. The number of species involved in an elementary reaction is designated as the molecularity of an elementary reaction. A chemical reaction is generally described by an equation of the type



where  $v_A, v_B, v_X, v_Y, \dots$  are the stoichiometric coefficients of the species A, B, X, Y, ... These coefficients are also whole numbers, but as the overall reaction can occur with a sequence of elementary steps of molecularity one, two or three, the stoichiometric coefficients will only correspond to the molecularity of the reaction if this is an elementary reaction. The sequence of these microscopic elementary steps is known as the mechanism of the reaction. In any case, the balance of all the microscopic elementary steps has to result in the macroscopic process described by the above general chemical equation, whose equilibrium constant is

$$K_{\text{eq}} = \frac{(a_X)^{v_X} (a_Y)^{v_Y}}{(a_A)^{v_A} (a_B)^{v_B}} \quad (1.13)$$

where  $a_i$  represents the activity of species  $i$ .

The mechanism of a reaction is normally determined experimentally, but although it is possible to disprove a mechanism, it is impossible to confirm that a proposed mechanism is correct simply on the basis of the experimental results available. It is also possible that a reaction can occur by two distinct mechanisms.

In the above explanation, we did not consider the possibility of an elementary process having a molecularity greater than 3. The probability that elementary kinetic processes involve the simultaneous collision of four particles is negligible. When more than three reactant molecules are involved, it is certain that the chemical transformation which occurs does not take place in a single elementary step.

Current practice in chemical kinetics tries to identify the one particular elementary step that has a very large effect on the overall reaction rate. This elementary process is known as the rate-determining step of the reaction. This rate-determining step depends on the relative magnitudes of the energy barriers for each elementary reaction as well as on the concentrations of the reactants and intermediates. When such a step exists, the rate of the overall reaction is either the value for this rate-determining step, or it is this value multiplied by some equilibrium constants of steps preceding it (pre-equilibria).

In Chapters 2 and 3, we will consider, respectively, the factors involved in determining the rates of chemical reaction and the techniques that allow the experimental study of their kinetics. In Chapter 4, we will start from empirical knowledge of the variation of concentration of reactants and products with time to establish the rate laws for the corresponding elementary reactions. Chapters 5–8 will consider some theories that allow us to calculate or rationalise the numerical values in the above rate laws. Chapters 9–14 will discuss in detail some of the most important reactions that have been studied using chemical kinetics. The last two chapters will focus on some less familiar topics in textbooks in this area,

but we believe they will lead to a conceptual awareness of the role of energy and electron transfer in chemical kinetics.

## REFERENCES

- [1] L Wilhelmy, *Pogg. Ann.* **81** (1850) 423.
- [2] W Ostwald, *J. Prakt. Chem.* **29** (1884) 358.
- [3] E Farber, *Chymia* **7** (1961) 135.
- [4] MC King, *Ambix* **29** (1982) 49.
- [5] MC King, *Ambix* **31** (1984) 16.
- [6] MC King, KJ Laidler, *Arch. Hist. Exact. Sci.* **30** (1984) 45.
- [7] M Berthelot, LP St. Gilles, *Ann. Chim.* **65** (1862) 385.
- [8] M Berthelot, LP St. Gilles, *Ann. Chim.* **66** (1862) 5.
- [9] M Berthelot, LP St. Gilles, *Ann. Chim.* **68** (1863) 255.
- [10] J. Lamor, *Manchester Mem.* **32** (1908) 10.
- [11] AV Harcourt, W Esson, *Chem. News* **10** (1864) 171.
- [12] AV Harcourt, W Esson, *Proc. Roy. Soc. (London)* **14** (1865) 470.
- [13] AV Harcourt, W Esson, *Philos. Trans.* **156** (1866) 202.
- [14] AV Harcourt, W Esson, *Chem. News* **18** (1868) 13.
- [15] MC King, *Ambix* **28** (1981) 70.
- [16] E Jungfleische, *Bull Soc. Chem.* (1913) 102.
- [17] EW Lund, *J. Chem. Educ.* **45** (1968) 125.
- [18] SR Logan, *J. Chem. Educ.* **59** (1982) 279.
- [19] KJ Laidler, *J. Chem. Educ.* **61** (1984) 494.
- [20] JH van't Hoff, *Études de Dynamique Chimique*, Muller Amsterdam, 1884.
- [21] A Findlay, T William, *A Hundred Years of Chemistry*, University Paperbacks, Methuen, London, 1965.
- [22] AJ Ihde, *The Development of Modern Chemistry*, Harper & Row, New York, 1964.

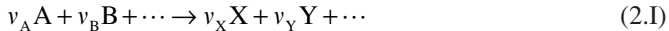
## - 2 -

# Reaction Rate Laws

---

### 2.1 REACTION RATES

The rate of conversion for the general form of a chemical reaction,



where  $v_A$ ,  $v_B$ ,  $v_X$  and  $v_Y$  are the stoichiometric coefficients of the species involved, can be expressed in terms of a single parameter  $\xi$ , which is known as the extent of reaction, and is defined by [1]

$$\xi = \frac{n_i(\xi) - n_i(0)}{v_i} \quad (2.1)$$

Here,  $i$  represents any of the reactants or products,  $n_i$  the number of moles of  $i$  in the chemical reaction (positive for products and negative for reactants),  $n_i(0)$  the amount of  $i$  present when  $v = 0$  (that is before the start of the reaction) and  $n_i(\xi)$  the amount of  $i$  present at extent of reaction  $\xi$ .

The rate of conversion in a chemical reaction is defined as the variation of  $\xi$  with time,  $t$ ,

$$r = \frac{d\xi}{dt} \quad (2.2)$$

Using the definition of  $\xi$  from eq. (2.1), we obtain

$$\frac{d\xi}{dt} = \frac{1}{v_i} \frac{dn_i}{dt} \quad (2.3)$$

where, to simplify the notation, we will write  $n_i$  instead of  $n_i(\xi)$ .

The reaction velocity is defined by

$$v = \frac{r}{V} = \frac{1}{v_i V} \frac{dn_i}{dt} \quad (2.4)$$

The distinction between the rate of conversion  $r$  and the reaction velocity (rate)  $v$  can be made on the basis of the units that are used. Normally, the amount of substance  $i$  is given in moles and the rate of conversion is expressed as mol sec<sup>-1</sup>, while for the case of the volume

being given in  $\text{dm}^3$ , the reaction velocity is given in  $\text{mol dm}^{-3} \text{ sec}^{-1}$ . If the volume stays constant during the reaction, it is more common to give the concentration of  $i$ , that is,  $[i]$  in  $\text{mol L}^{-1}$  ( $1 \text{ L} = 1 \text{ dm}^3$ ) in the determination of the rate of conversion of reactions. Thus, for a total constant volume  $V$ ,

$$\left( \frac{d\xi}{dt} \right)_V = \frac{V}{v_i} \left( \frac{d[i]}{dt} \right)_V \quad (2.5)$$

The experimental determination of the velocity of a reaction in solution is made by measuring the change in the concentration of reactants or products with time, since the volume of the environment in which the reaction occurs does not vary appreciably during the reaction. This is also true of reactions in the gas phase when the reactor is kept at constant volume.

Sometimes for a reaction in the gas phase at constant temperature and volume, it is more convenient to measure the partial pressure  $P_i$  of one component  $i$  rather than its concentration. Assuming ideal mixing behaviour of the gases, we can express the rate of conversion as a function of partial pressure of any one of the components

$$\left( \frac{d\xi}{dt} \right)_{T,V} = \frac{V}{v_i RT} \left( \frac{dP_i}{dt} \right)_{T,V} \quad (2.6)$$

When there is a change in the total number of moles of gas in the system,  $\sum v_i \neq 0$ , the total pressure will vary proportionally with the extent of reaction. From eq. (2.1), for the set of all the components of the reaction we can write

$$\sum v_i \xi = \sum n_i(\xi) - \sum n_i(0) \quad (2.7)$$

or rearranging,

$$\xi = \frac{\sum n_i(\xi) - \sum n_i(0)}{\sum v_i} \quad (2.8)$$

If all the gases follow ideal behaviour

$$n_i(\xi) = \frac{P_i(\xi)}{RT} V \quad (2.9)$$

and we can write

$$\xi = \frac{V}{RT} \frac{\sum P_i(\xi) - \sum P_i(0)}{\sum v_i} \quad (2.10)$$

As  $\sum P_i(x)$  and  $\sum P_i(0)$  are the total pressures of the systems for the extent of reaction  $\xi$  and for the start of the reaction, respectively, the previous equation can be simplified to give

$$\xi = \frac{V}{RT} \left( \frac{P(\xi) - P(0)}{\sum v_i} \right) \quad (2.11)$$

As a consequence, where there is a change in the total number of moles of gas, the rate of conversion for a reaction at constant volume and temperature will be given by

$$\left(\frac{d\xi}{dt}\right)_{V,T} = \frac{V}{RT \sum_i v_i} \left(\frac{dP}{dt}\right)_{V,T} \quad (2.12)$$

where  $P$  represents the total pressure of the reaction system.

From the perfect gas equation, if a gas phase reaction in which  $\sum v_i \neq 0$  occurs at constant temperature and pressure, the volume must change. In this case, if all the components follow ideal behaviour

$$n_i(\xi) = \frac{P_i(\xi)V(\xi)}{RT} \quad (2.13)$$

where  $V(\xi)$  is the total volume of the system for an extent of reaction  $\xi$ . Substituting into eq. (2.8) and considering that the volume remains constant,  $\Sigma P_i(\xi) = \Sigma P_i(0) = P$ ,

$$\xi = \frac{P}{RT \sum_i v_i} [V(\xi) - V(0)] \quad (2.14)$$

and

$$\left(\frac{d\xi}{dt}\right)_{T,P} = \frac{P}{RT \sum_i v_i} \left(\frac{dV}{dt}\right)_{T,P} \quad (2.15)$$

It is important to prove that eq. (2.2) defines the rate of conversion in the reaction, that eq. (2.4) defines the velocity of the reaction and that in the expressions (2.5), (2.6), (2.12) and (2.15), the quantities  $(d[i]/dt)_{V,T}$ ,  $(dP/dt)_{V,T}$ ,  $(dP/dt)_{V,T}$  and  $(dV/dt)_{T,P}$  are proportional to the velocity of the reaction. It must also be emphasised that, generally, the rate can be defined in terms of any of the reactant or product molecules, provided that the stoichiometry of the reaction is included. In other words, eq. (2.16) is valid

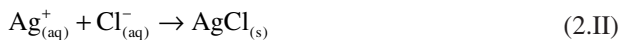
$$v = -\frac{1}{v_A V} \left(\frac{dn_A}{dt}\right) = -\frac{1}{v_B V} \left(\frac{dn_B}{dt}\right) = \frac{1}{v_X V} \left(\frac{dn_X}{dt}\right) = -\frac{1}{v_Y V} \left(\frac{dn_Y}{dt}\right) \quad (2.16)$$

## 2.2 FACTORS THAT INFLUENCE THE VELOCITIES OF REACTIONS

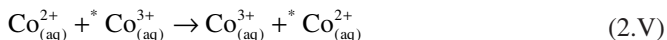
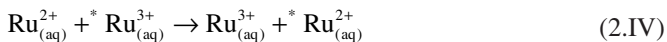
### 2.2.1 Nature of the reagents

The velocities of elementary chemical reactions depend on a great number of factors, in particular the nature of the reactants, concentrations or pressures, temperature, light, catalysts and the solvent used. The great variation observed in reaction velocities will be related first to the nature of the reagents. Many reactions, such as those between oppositely

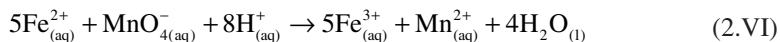
charged ions in aqueous solution, which do not involve breaking chemical bonds are very rapid at room temperature.



However, reactions involving structurally similar reactant molecules such as exchange reactions of electrons between two isotopically labelled transition metal complexes, which also do not involve breaking chemical bonds often show great differences in rates under similar conditions



Reaction (2.IV) is  $10^5$  times faster than reaction (2.V). In contrast, although reactions involving bond breaking and bond formation are generally slow, there are some extremely fast reactions of this type such as the oxidation of iron (II) by permanganate ion in acid solution:



Thus, there appears to be a lack of even qualitative general rules to evaluate the effect of the nature of reactants on the rates of reactions. The success of theoretical calculations of reaction velocities in chemical kinetics without using adjustable parameters has been limited. Even for the simplest reactions in the gas phase, a large amount of computer time is needed with *ab initio* quantum mechanical calculations to obtain detailed and precise information on the potential energy surface of a reaction system, in addition to requiring the calculation of a large number of trajectories before we can calculate the macroscopic velocity of a reaction. For more complex reactions, such calculations are prohibitive in terms of both computer time and money. In practice, it is more common to base the interpretation and prediction of reaction velocities as a function of the nature of reactants on the development of simplified theoretical models that relate some properties of the reactants with the ease with which their bonds can be broken and/or new bonds formed in the products. In Table 2.1 we give typical chemical reactions, with their respective activation energies, and some appropriate parameters that have been used for the theoretical calculation of reaction rates [2].

In this table, we stress the fact that if we keep a series of the parameters constant, it is possible to attribute the change in activation energy, and consequently, the velocity of reaction (eq (1.1)), to the change in a specific parameter. For example, in the reactions (i) and (ii) the increase in the sum of bond lengths in reactants and products leads to an increase in activation energy. With reactions (ii) and (iii), the predominant factor in the decrease in activation energy appears to be the decrease in force constants. Comparison between reactions (iii) and (iv) shows, as we may suspect intuitively, that the most exothermic reaction is the fastest one, from which we can say that the predominant factor in this case is the change in enthalpy of the reaction. However, if we compare reactions (ii) and (v), we find a very significant decrease in activation energy, in contrast to what we would expect from the positive enthalpy change, the increase in bond lengths or the decrease in force constants. In this

**Table 2.1**

Molecular and kinetic parameters of some elementary gas phase reactions

Reaction	$\Delta H^a$ (kJ mol <sup>-1</sup> )	$I_{AB} + I_{BC}$ <sup>b</sup> (Å)	$f_{BC}$ <sup>b</sup> mol <sup>-1</sup> Å <sup>-2</sup> )	$f_{AB}$ <sup>b</sup> mol <sup>-1</sup> Å <sup>-2</sup> )	$I_p^c$ (eV)	$E_A^c$ (eV)	$E_a^d$ (kJ mol <sup>-1</sup> )
(i) $H+H_2 \rightarrow H_2+H$	0	1.482	3439	3439	13.598	0.7542	32
(ii) $CH_3+CH_4 \rightarrow CH_4+CH_3$	0	2.174	3435	3435	9.843	0.08	61
(iii) $C_2H_5+C_2H_6 \rightarrow C_2H_6+C_2H_5$	0	2.188	3348	3348	8.117	-0.26	56
(iv) $CH_3+C_2H_6 \rightarrow CH_4+C_2H_5$	-19	2.181	3348	3435	8.117	0.08	48
(v) $Cl+CH_4 \rightarrow HCl+CH_3$	+8	2.362	3435	3120	12.968	3.614	11

<sup>a</sup>Reaction enthalpy.<sup>b</sup>Sum of the bond lengths of the bonds broken or formed in the course of the reaction, and force constants of these bonds.<sup>c</sup>Ionization energies and electron affinities of the radicals.<sup>d</sup>Experimental activation energies.

case, what appears to be the dominant factor is the difference in electronic structure between the chlorine atom and the methyl radical, represented here by their ionization potentials and electron affinities.

Within this framework, it is useful to define “families of reactions”, in the sense of a series of reactions that occur via the same mechanism and under the same experimental conditions, but where the reactants differ from each other by only small changes in structure, such that they produce only small perturbations in the reaction centre. These small structural changes are normally associated with minor changes in the bonding of substituent groups in the region of the bonds that are broken or being formed during the reaction. Many theoretical models have been suggested for such classes of reactions, leading to empirical correlations between the activation energy and the change in a specific parameter such as reaction enthalpy or electronic or steric parameters.

## 2.2.2 Reactant concentration

Almost all reaction rates depend on the concentration of reagents, while for reversible reactions they are also affected by those of products. The mathematical expression that relates the reaction velocity and the concentration of species present is called the law of reaction velocity, the kinetic law, or most simply, the rate law. Assuming that the reaction being considered involves an elementary process,



the corresponding rate law can be written

$$v = k[A]^a[B]^b \quad (2.17)$$

where the powers  $a$  and  $b$  are known as the partial orders of reaction for components A and B, and the proportionality constant  $k$  is called the specific rate constant for the reaction, or simply the rate constant. This constant is independent of the concentrations of the reactants, but depends on the temperature, pressure and reaction medium. The partial orders can only be identified with the stoichiometric coefficients when we are dealing with an elementary reaction. The rate law of any reaction always has to be determined experimentally. The formulation of this principle is known as the Law of Mass Action, which can be stated that in dilute solutions the velocity of each chemical reaction is proportional to the product of the concentration of reactants, is independent of the concentration of other species and of the presence of any other reactions.

Treating the case of an elementary reversible reaction



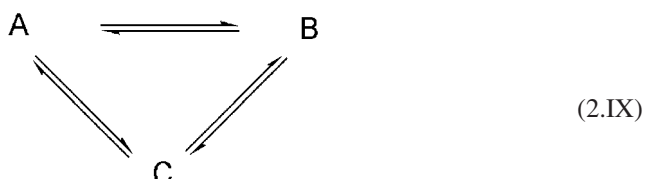
where  $a, b, x$  and  $y$  are whole numbers, this same law indicates that the velocity of the reaction is given by

$$v = k_d [A]^a [B]^b - k_i [X]^x [Y]^y = v_d - v_i \quad (2.18)$$

At equilibrium  $v_d = v_i$ , and since, overall,  $v = 0$  we obtain

$$\left( \frac{k_d}{k_i} \right) = \frac{[X]_{\text{eq}}^x [Y]_{\text{eq}}^y}{[A]_{\text{eq}}^a [B]_{\text{eq}}^b} = K_{\text{eq}} \quad (2.19)$$

where  $K_{\text{eq}}$  is the equilibrium constant for the reaction. From eq. (2.19), we can see that only two of the three constants  $k_d$ ,  $k_i$  and  $K_{\text{eq}}$  are independent. The same reasoning can be applied to more complicated systems such as that described by the following mechanism:



In this cyclic kinetic scheme, there is equilibrium between all the species. As a consequence, we can write the equilibrium constants

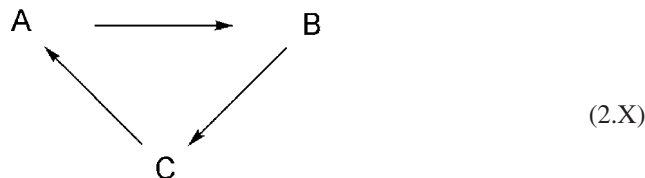
$$\begin{aligned} K_1 &= \frac{k_1}{k_{-1}} = \frac{[B]}{[A]} \\ K_2 &= \frac{k_2}{k_{-2}} = \frac{[C]}{[B]} \\ K_3 &= \frac{k_3}{k_{-3}} = \frac{[A]}{[C]} \end{aligned} \quad (2.20)$$

such that  $K_1 K_2 K_3 = 1$ , from which

$$k_1 k_2 k_3 = k_{-1} k_{-2} k_{-3} \quad (2.21)$$

In this scheme only five of the six rate constants are independent.

At first sight, it may appear strange that the equilibrium constant expression only depends on the stoichiometry of a reaction when it stems from equating the rate laws for the forward and reverse reactions, where these reactions have an empirical character and, except for the case of elementary reactions, the rate expressions cannot be obtained from the overall equation for the chemical reaction. However, this observation has its basis on an important physical principle, the *principle of microscopic reversibility*. This can be stated in the form that in the state of macroscopic equilibrium each elementary process is in equilibrium, and is reversible at the microscopic level. In other words, the mechanism of a reversible reaction is the same in the forward and reverse directions. The mathematical basis of this principle comes from the fact that the equations of motion are symmetrical relative to time inversion, from which a particle which follows a given trajectory in the time from 0 to  $t'$  will follow the identical reverse trajectory in the time from  $t'$  to 0. We can see, in fact, that at equilibrium, the concentrations of reactants and products are constant and do not oscillate about a mean value. Thus, mechanism (2.IX) represents a possible chemical system, which is in agreement with the principle of microscopic reversibility and which will respond promptly to any perturbation from the equilibrium state. The same is not true for mechanism (2.X), where the step for formation of A from B implies an intermediate which is not involved in the formation of B from A, i.e. the mechanism of formation of B from A is different from that for the formation of A from B.



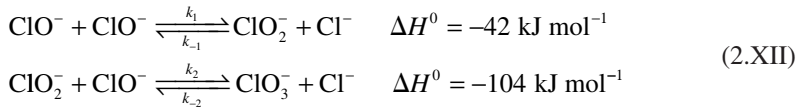
The principle of microscopic reversibility can be applied to the explanation of reaction mechanisms and of rate laws. As an example, we can take the disproportionation of the hypochlorite ion under equilibrium conditions



with the equilibrium constant given by

$$K_{\text{eq}} = \frac{[\text{ClO}_3^-]_{\text{eq}} [\text{Cl}^-]_{\text{eq}}^2}{[\text{ClO}^-]_{\text{eq}}^3} \quad (2.22)$$

and with a reaction mechanism involving the following steps in equilibrium, a slow first step followed by a second fast one



By equating the rates of each elementary process in the forward and reverse direction, we obtain

$$\begin{aligned} k_1 [\text{ClO}^-]_{\text{eq}}^2 &= k_{-1} [\text{ClO}_2^-]_{\text{eq}} [\text{Cl}^-]_{\text{eq}} \\ k_2 [\text{ClO}_2^-]_{\text{eq}} [\text{ClO}^-]_{\text{eq}} &= k_{-2} [\text{ClO}_3^-]_{\text{eq}} [\text{Cl}^-]_{\text{eq}} \end{aligned} \quad (2.23)$$

Eliminating the concentration of the intermediate  $\text{ClO}_2^-$ , which is not present in the expression for the equilibrium constant, by multiplying both these equations, we obtain

$$k_1 [\text{ClO}^-]_{\text{eq}}^2 k_2 [\text{ClO}^-]_{\text{eq}} = k_{-1} [\text{Cl}^-]_{\text{eq}}^2 k_{-2} [\text{ClO}_3^-]_{\text{eq}} \quad (2.24)$$

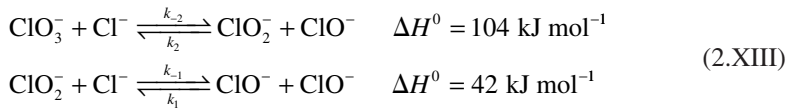
or

$$\frac{k_1 k_2}{k_{-1} k_{-2}} = \frac{[\text{ClO}_3^-]_{\text{eq}} [\text{Cl}^-]_{\text{eq}}^2}{[\text{ClO}^-]_{\text{eq}}^3} \quad (2.25)$$

the expression that gives a relationship between the rate constants, from which we can conclude that for this reaction

$$\frac{k_1 k_2}{k_{-1} k_{-2}} = K_{\text{eq}} \quad (2.26)$$

The equilibrium constant for a reaction arises from the equality of the rates of all the elementary processes. However, it is not possible starting from the rate law for the forward process and the equilibrium constant to obtain the rate law for the reverse process. We will illustrate this with the same reaction. Writing the above reactions in the reverse direction



and considering the values for the change of reaction enthalpies of the elementary processes, it would be expected that the first process would be the slower one, that is, that this will be the rate-determining step of the reaction. The rate law for the reaction written in the direction of eqs. (2.XIII) will then be

$$v_1 = k_{-2} [\text{ClO}_3^-] [\text{Cl}^-] \quad (2.27)$$

Equating the rates of the reaction in the forward and reverse directions, we obtain

$$k_1 [\text{ClO}^-]^2 = k_{-2} [\text{ClO}_3^-][\text{Cl}^-] \quad (2.28)$$

which bears no relationship to the equilibrium constant, or to any power of it, and also does not follow the stoichiometry of the reaction

$$\frac{k_1}{k_{-2}} = \frac{[\text{ClO}_3^-][\text{Cl}^-]}{[\text{ClO}^-]^2} \neq K_{\text{eq}} \quad (2.29)$$

For a system far from equilibrium, if the reverse reaction follows a distinct mechanism from the forward one, common sense tells us that the ratio of concentrations will be different from that given by the rate laws and the equilibrium constant. The mechanisms of reaction in the forward and reverse directions can only be assumed to be the same close to equilibrium. From the above, it is clear that both the rate laws for the reaction must be obtained experimentally. The relationship between the rate laws for reactions far from equilibrium is only equal to the equilibrium constant for elementary reactions, or for systems where the forward and reverse reactions have the same rate-determining step.

As the partial orders of reaction are experimentally determined parameters, they can take any value, and the positive integer values we have presented until now are only specific cases. We will show this with some experimental rate laws. The exchange of iodine atoms between iodate ion and molecular iodine has been studied with radioisotopes



and the following rate law obtained:

$$v = k [\text{I}_2]^{3/5} [\text{IO}_3^-]^{9/5} [\text{H}^+]^{9/5} \quad (2.30)$$

where the partial orders are all fractions. Another example is the following reaction in aqueous solution, which has a negative partial order



$$v = k [\text{I}^-][\text{ClO}^-][\text{OH}^-]^{-1} \quad (2.31)$$

indicating that the reaction rate decreases with increasing pH. These laws also show that the velocity of a reaction can depend on other species apart from the reactants involved in the chemical equation.

Until now, all the rate laws we have given take the general form of eq. (2.17). However, some reactions show very different forms for their rate laws. One example is the formation of hydrogen bromide from bromine and molecular hydrogen



whose rate law is

$$v = \frac{k' [H_2] [Br_2]^{1/2}}{k'' + \frac{[HBr]}{[Br_2]}} \quad (2.32)$$

For this case, it is not possible to define reaction orders, except over limited concentration regions. In the first stages of reaction, when  $[HBr]$  is small, we can make the approximation

$$\frac{[HBr]}{[Br_2]} \ll k'' \quad (2.33)$$

and the previous expression simplifies to

$$v' = k [H_2] [Br_2]^{1/2} \quad (2.34)$$

with  $k = k'/k''$ . In this example, the velocity depends on the concentration of a product of the reaction, such that as the reaction progresses,  $[HBr]$  will increase and towards the end of the reaction we arrive at the situation in which

$$\frac{[HBr]}{[Br_2]} \gg k'' \quad (2.35)$$

Under these conditions, eq. (2.32) reduces to

$$v'' = k' [H_2] [Br_2]^{3/2} [HBr]^{-1} \quad (2.36)$$

Both eqs. (2.34) and (2.36) represent kinetic laws of the general form of eq. (2.17), but the apparent reaction orders will vary with the extent of the reaction such that we cannot strictly talk about reaction orders. For example, the reaction order of bromine changes from 1/2 at the start of the reaction to 3/2 at the end.

This type of kinetic law illustrates two important points that have to be taken into account in the determination of reaction orders. First, a kinetic law is only strictly valid close to the zone where it is studied experimentally; its extrapolation to other concentration regions requires further experimental and theoretical studies. Second, considering the variation in reaction order during a reaction, from this it is important that studies of reaction orders must be limited to periods of relatively small extent of reaction (not  $>10\%$ ), otherwise mean values may be obtained which have no chemical meaning.

Until now, we have only considered chemical reactions in homogeneous systems. However, the study of heterogeneous systems, in which more than one phase is present, are equally important, particularly in the areas of catalysis and corrosion. For example, the oxidation of a metal is faster when its area exposed to the oxidising medium increases. In general, it is seen that the rate of a heterogeneous reaction is directly proportional to the contact area between the reactants,  $S_c$ . Thus, in the rate law (2.17), these reactions are first order relative to  $S_c$ .

### 2.2.3 Temperature

van't Hoff gave the first description of the effect of temperature on the equilibrium constant of a reaction,  $K_{\text{eq}}$ , with the relationship

$$\left( \frac{\partial \ln K_{\text{eq}}}{\partial T} \right)_p = \frac{\Delta H^0}{RT^2} \quad (2.37)$$

where  $\Delta H^0$  is the change in standard enthalpy for the reaction. In contrast to the spirit of the era, in which attempts were made to relate equilibria and rates in terms of molecular motions and Maxwell's distribution law of molecular velocities, the Swedish chemist Arrhenius considered that the effect of temperature on reaction rates is normally too great to be explained simply in terms of its effect on the translational energy of molecules. As an alternative, he proposed that there will be equilibrium between "normal" molecules and "reactive" ones, and that this has the same temperature dependence given by eq. (2.37). It is implicit in this work that the energy difference between molecules is independent of temperature. From this, Arrhenius was able to provide the first adequate description of the relationship between the rate constant and the temperature:

$$k = A \exp\left(-\frac{E_a}{RT}\right) \quad (2.38)$$

where  $A$  is the pre-exponential (or frequency) factor,  $E_a$  the activation energy and  $T$  the absolute temperature. Arrhenius received the Nobel Prize in 1903. However, it was not on the basis of his work on chemical kinetics, and the merits of eq. (2.38) remained controversial for many years.

In the Arrhenius equation the temperature dependence comes basically from the exponential term. However, it should be noted that the pre-exponential factor can also have a weak temperature dependence, and it is more correct to assume that  $A$  is proportional to  $T^m$

$$k = A' T^m \exp\left(-\frac{E_a}{RT}\right) \quad (2.39)$$

where  $A'$  is independent of temperature. Often, the Arrhenius expression (2.38) is used only over a fairly limited temperature range, but eq. (2.39) is able to describe kinetic data over a wider range of temperatures. The units in which  $A$  is expressed are the same as those of the rate constant, while the activation energy is given in the same units as the energy  $R$ , normally in kJ per mole. This leads to the Arrhenius equation in the logarithmic form

$$\ln k = \ln A - \frac{E_a}{R T} \quad (2.40)$$

where the temperature is in Kelvin,  $k$  and  $A$  are now taken, simply, as their numerical values, and the units in eq. (2.38) cancel out.

Assuming that Arrhenius behaviour is followed, for a first-order process a plot of  $\ln(k)$  against  $1/T$  leads to a straight line of slope  $-E_a/R$ . The extrapolation to  $1/T = 0$ , which is

normally significantly outside the temperature range studied and, as such, subject to appreciable errors, gives us  $\ln(A)$ , where  $A$  is given in units ( $\text{time}^{-1}$ ). We must note that when the experimental results are only obtained over a limited temperature range, the accuracy in the values of  $A$  and  $E_a$  will be low.

The rate constants for second-order reactions can be expressed in  $\text{dm}^3 \text{ mol}^{-1} \text{ sec}^{-1}$ , or, if the rate is measured from the change of gas pressure at constant volume, as described in eq. (2.12), in  $(\text{pressure})^{-1}/(\text{time})^{-1}$ . The conversion between units of pressure and those of concentration for gas phase reactions which are not first order, can be obtained from the perfect gas equation, from which, for the general case of a reaction of order  $n$ , the variation in the total gas pressure can be related to the change in the total gas concentration by  $p = cRT$

$$k_c = k_p (RT)^{n-1} \quad (2.41)$$

Thus, from the rate constants given in the units  $(\text{pressure})^{-1}(\text{time})^{-1}$ , to obtain the terms  $A$  and  $E_a$  for reactions other than the first-order case, we must start by converting all the rate constants to be used with expression (2.41) into units of  $(\text{concentration})^{-1}(\text{time})^{-1}$  before we can make an Arrhenius plot. If these values were obtained from logarithmic plots of rate constants given as  $(\text{pressure})^{-1}(\text{time})^{-1}$  against  $1/T$ , we will get different numerical values for  $A$  and  $E_a$ . This is obvious for  $A$ , which, for a second-order process, will be given in terms of  $(\text{pressure})^{-1}(\text{time})^{-1}$ . However, it is equally true for  $E_a$ , and we need to take care to correct for the change in dimensionality to avoid the illusion that the values of activation energy are comparable between the two plots, since they are always given in kilo Joules per mole.

For reactions in solution the values of  $E_a$  typically lie between 40 and 120  $\text{kJ mol}^{-1}$ . As a first approximation, these values correspond to an increase in reaction rate by a factor of 2–5 for every 10 K rise in temperature. The empirical rule often given is that the rate doubles for every 10 K rise in temperature.

## 2.2.4 Light

The effect of light on chemical reactions is well known from the processes of photosynthesis and photography. The general area is known as photochemistry. Normal photosynthesis is a chemical process in which green plants store solar energy through the synthesis of sugars from carbon dioxide and water. This process is catalysed by chlorophyll and requires the presence of light. There are also various types of bacterial photosynthesis, which can use substrates such as  $\text{H}_2\text{S}$  instead of water. However, the basic requirements in terms of light absorption are similar. With the normal photographic process, light absorption leads to the darkening of silver salts through the reduction of  $\text{Ag}^+$  ions to metallic silver.

The action of light on a chemical reaction results essentially from the reactants in the presence of light having the possibility of following a different mechanism that is not possible in the dark. For experimental reasons, the wavelengths ( $\lambda$ ) most commonly used for initiating photochemical processes vary between the ultraviolet (200–250 nm) to the near infrared (750–800 nm). Light at these wavelengths has an energy, which is given by

$$E_{\text{photon}} = h\nu = h \quad (2.42)$$

and corresponds roughly to 600–150 kJ mol<sup>-1</sup>, which is very close to the energies of many chemical bonds. This energy is much greater than the thermal energy at 25 °C, which can be estimated from the mean velocity given by eq. (1.11) following the expression:

$$\frac{1}{2}Ms^2 = \frac{M}{2} \int_0^\infty s^2 f(s) ds = 2M\pi \left( \frac{M}{2\pi RT} \right)^{3/2} \int_0^\infty s^4 \exp\left(-\frac{Ms^2}{2RT}\right) ds = \frac{3}{2}RT \quad (2.43)$$

and is ~3.7 kJ mol<sup>-1</sup>.

In the dark, the electrons in a molecule occupy the lowest energy electronic levels, giving rise to the so-called electronic ground state. When irradiated by light whose wavelength corresponds to the energy difference between the ground state and an electronically excited state, a molecule can absorb a photon and be transformed into this electronically excited state. This is a chemically distinct species, with its own structure, properties and reactivity.

The quantitative description of light absorption by a sample is based on the Beer–Lambert (or, more correctly, Beer–Lambert–Bouger) law. In deriving this law, we consider that incident monochromatic light of intensity  $I_0$  crosses an infinitesimal thickness,  $dl$ , of an absorbing species of concentration  $c$ . The decrease in light intensity,  $dI$ , is proportional to the thickness of the sample, the concentration of the absorbing species and the incident light intensity

$$dI = -acl I_0 dl \quad (2.44)$$

where  $a$  is a proportionality constant which depends on the sample and wavelength. Integrating this expression over the whole optical path of the light in the sample,  $l$ , gives

$$I = I_0 \exp(-acl) \quad (2.45)$$

Expressing the above relationship in the most common form of logarithms to the base 10 gives the normal form of the Beer–Lambert equation

$$I = I_0 10^{-\varepsilon cl} \quad (2.46)$$

where  $\varepsilon$  is the molar absorption coefficient (sometimes referred to as extinction coefficient or molar absorptivity), which normally has the units L mol<sup>-1</sup>cm<sup>-1</sup>. The Beer–Lambert law can also be written as

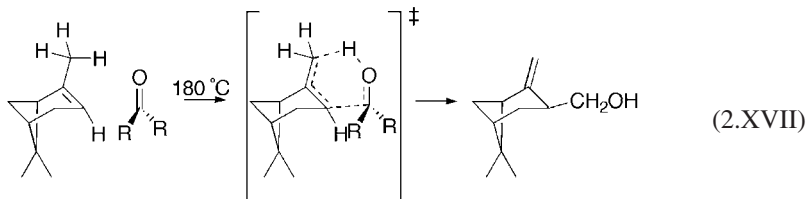
$$A = \log\left(\frac{I_0}{I}\right) = \varepsilon cl \quad (2.47)$$

where  $A$  is the absorbance, a dimensionless parameter.

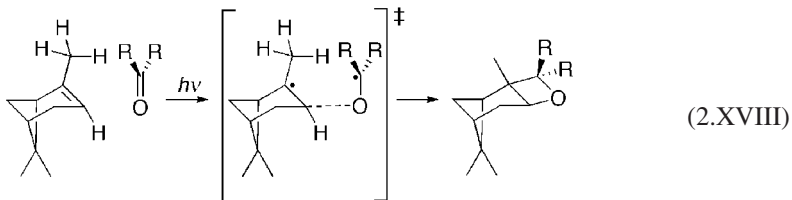
The electronic distribution in the electronic excited state formed by absorption of ultra-violet or visible light is different from that of the ground state, but immediately after light absorption the nuclear configuration is identical to that of the ground state. This is the basis of the Franck–Condon principle. The structural relaxation towards a new nuclear configuration, corresponding to a potential energy minimum in the electronically excited state,

occurs very rapidly, with a rate close to that of a molecular vibration. This new electronically excited isomeric form of the ground state can now undergo new reaction pathways, while its high energy content will also tend to make it more reactive than the ground state. Often, the lifetime of a molecule in its electronically excited state is only a few nanoseconds ( $10^{-9}$  sec) in solution at room temperature. Within this lifetime, the excited molecule can follow various competing routes to lose its excess electronic energy, including re-emitting light and returning to the ground state, reacting exothermically either intra-molecularly or inter-molecularly with another molecule, and thus converting part of its electronic energy into potential energy, or decaying to another more stable electronic state, and eventually to the ground state, dissipating its electronic energy as thermal energy (i.e. heat).

A good example of how light absorption can modify the reactivity of molecules is given by cycloaddition to carbon–carbon double bonds. While the ground state process normally involves the reaction [3]



in the excited state, the reaction which is observed is [4,5]



Increases in reactivity and changes in the mechanism owing to electronic excitation can also be seen in the hydrogen abstraction reactions of ketones. At room temperature, ketones in their ground states do not react with hydrogen atoms bonded to alkanes. However, following light absorption they rapidly abstract hydrogen atoms to produce two radicals



This reactivity has been compared with that of alkoxy radicals [6]



which suggests that light absorption has the effect of breaking the  $\pi$  bonding of the carbonyl group and leaving an unpaired electron on the oxygen atom. This is due to the formation of a so-called n,  $\pi^*$  excited state.

### 2.2.5 Catalysts

Catalysts are substances that although not included in the overall stoichiometric equation of a process, appear in the rate law with a partial order greater than zero. Occasionally, a reaction can undergo autocatalysis when, under the conditions described, a product of the reaction participates in the rate law of this process. Although caution needs to be used with such a definition, from the above a catalyst may increase the rate of a reaction without being consumed during it. The note of caution comes from the fact that in some processes, e.g. Friedel–Crafts alkylations and acylations of aromatic compounds using Lewis acid catalysts, the catalysts are consumed in other steps of the process. Normally, a good catalyst can lead to enormous enhancement in reactions rates even when present in only very small quantities. In any case, the catalyst always has a partial order in the rate law that largely exceeds its stoichiometric coefficient in the overall stoichiometric equation.

It is useful to distinguish between homogeneous catalysis, where reactants, products and catalyst are all in the same phase, and heterogeneous catalyst, where the catalyst is present in a phase different from that of the reactants and products. As an example we can consider the hydrogenation of carbon–carbon double bonds to transform them into single bonds. This can be carried out homogeneously using the Wilkinson catalyst, which is a complex of the transition metal rhodium,  $\text{RhCl}(\text{P}(\text{C}_6\text{H}_5)_3)_3$ , chloro, *tris*(triphenylphosphine)rhodium(I), or heterogeneously, using particularly metallic platinum. This hydrogenation is very important in both the pharmaceutical and food industries, as it leads to the efficient production of saturated products from unsaturated compounds. Partly for his work in developing such homogeneous catalysts through the study of transition metal complexes, Wilkinson received the Nobel Prize in chemistry. A further example of an important industrial catalytic process involves the synthesis of ammonia from nitrogen and hydrogen using metallic iron or other transition metals as heterogeneous catalysts.

Catalysts do not alter the position of equilibrium in a reaction. Their effect, instead, arises from the fact that in their presence a pathway with lower activation energy becomes available to the reactants, as can be seen in Figure 2.1. The uncatalysed route still exists, but this new mechanism becomes kinetically more favourable. As a consequence, in the presence of a catalyst, the form of the rate equation will be changed with the addition of a new term, which becomes more important than the uncatalysed reaction. Returning to the general reaction mechanism (2.VII) and rate law (2.17), the new rate law including the effect of catalysts will take the general form

$$v = k[\text{A}]^a[\text{B}]^b + k_{\text{cat}}[\text{A}]^{a'}[\text{B}]^{b'}[\text{C}]^{c'} \quad (2.48)$$

where C represents the catalyst. When the catalyst is a solid, such as the case of heterogeneous catalysts, its concentration is constant and does not appear as an independent term in this equation. Its effect will be included in the value of  $k_{\text{cat}}$ . As a general rule, to see the effects of catalysis, if the reaction order is unchanged, it is necessary that  $k_{\text{cat}}[\text{C}]^c > 0.1 k$ . As we will discuss in the next section, we should note that while changes in the reaction medium can lead to increases in rate, this phenomenon is not strictly a catalytic process in kinetic terms.

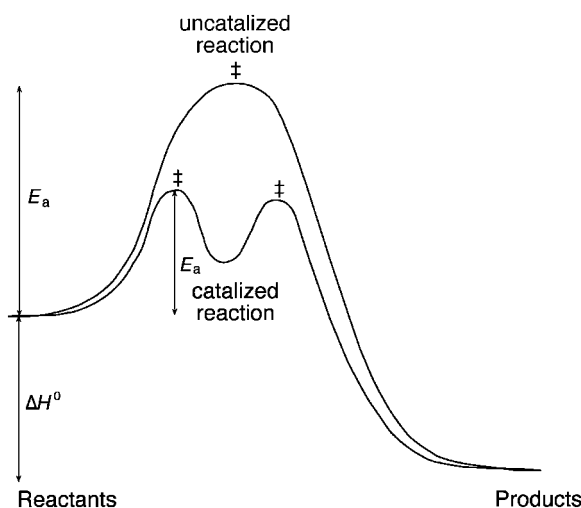


**Figure 2.1** Energy profiles for a catalysed and an uncatalysed reaction showing the appearance of a lower energy pathway in the former case.

## 2.2.6 Reaction medium

More than a century ago, Menschutkin [7] noted that a reaction in solution cannot be separated from the medium in which it occurs. In fact, the effects of solvent on reaction rates can be dramatic. In the reactions studied by Menschutkin, such as



it has been found that the rate increases almost 100,000 times when the solvent is changed from hexane (highly non-polar) to dimethylsulphoxide (very polar and aprotic). This variation is easy to interpret qualitatively, given that charges are created during the reaction, and that these will be stabilised in the presence of a polar solvent. However, the quantitative interpretation of the solvent's effect on the reaction rate is much more difficult. It must be stressed that the effect of the reaction medium can be seen both on the kinetic and thermodynamic properties of the reactions. Ideally, solvent effects on reaction rates should be studied by comparing the same reactions in the gas phase and in solution. However, such a comparison is not always possible experimentally.

Even for systems given in the same units and over the same temperature range the velocities of reactions in solution and gas phase, do not give directly comparable activation energy barriers. For two molecules, A and B, in the gas phase, initially at large distances there is no interaction, but as they approach one another, van der Waals attractive forces become involved at intermediate distances owing to correlations of the motions of the electrons of the two molecules. On even closer approach, an energy barrier is introduced for the reaction as a result of orbital overlap. This effect is even more marked when one of the reactants is an ion. Figure 2.2 shows an energy profile for a gas-phase reaction of this type. It should be noted that the change in entropy in the course of this reaction

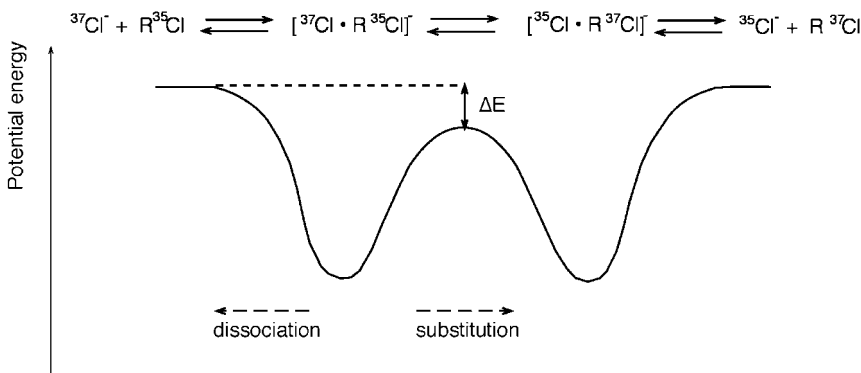


**Figure 2.2** Potential energy profile for a second-order nucleophilic substitution reaction ( $S_N2$ ) in the gas phase. The reaction barrier is 25 kJ mol<sup>-1</sup> below the energy of the separated reactants when  $R = \text{CH}_2\text{CN}$ . The substitution reaction is favoured for total energies less than or equal to that of the reactive channel, while a dissociative pathway ( $S_N1$ ), which is favoured entropically, predominates for higher energies.

tends to counteract the change in potential energy shown in the figure: the formation of a complex leads to a decrease in entropy compared with that of the two isolated molecules, A and B. In solution, it is also necessary to consider the change in entropy and enthalpy associated with solvation of the reagents, transition state and products.

Given the existence of a potential energy minimum between the isolated reactants and the transition state, if it is found that  $\Delta H_f > \Delta H^\ddagger$ , the activation energy for the reaction will be negative although the energy barrier for the reaction could be even bigger than the free energy for the same reaction in solution.

Apart from the effect of solvent on the kinetics of chemical reactions, another significant effect of the reaction medium can come from the ionic strength of solutions. The most important case in which this has to be considered involves the reaction between two ions, A and B, in aqueous solution in the presence of an electrolyte. If A and B have the same charge, there will be an electrostatic repulsion between them, which will inhibit their approach, and, consequently, their reaction rate. The opposite will be true for reactions involving ions with different charges, i.e. reactions between cations and anions. This effect of ionic strength is known as the *primary salt effect*, and, as we will see in Chapter 9, is extremely useful in obtaining information on mechanisms of reactions involving ions in solution.

If the rate law involves the concentration of a species involved in a pre-equilibrium before the rate-determining step of a reaction, then the concentration of this species may depend upon the ionic strength, from which the reaction rate may also show an ionic strength dependence. This effect is known as the *secondary salt effect*. To some extent this effect is an artefact, since it does not really affect the rate constant of the reaction, but changes the concentration of the reactants. The correct rate constant can be determined using the true concentration of the species, calculated using the appropriate equilibrium constant for the pre-equilibrium step determined at the experimental ionic strength.

**REFERENCES**

- [1] H Maskill, *Educ. Chem.* (1984) 122.
- [2] AACC Pais, LG Arnaut, SJ Formosinho, *J. Chem. Soc. Perkin Trans. 2* (1998) 2577.
- [3] JP Bain, *J. Am. Chem. Soc.* 68 (1946) 638.
- [4] E Paterno, G Chieffi, *Gazz. Chim. Ital.* 39 (1909) 3412.
- [5] G Buchi, CG Zuman, ES Lipinsky, *J. Am. Chem. Soc.* 76 (1954) 4327.
- [6] SJ Formosinho, LG Arnaut, *Adv. Photochem.* 16 (1991) 67.
- [7] NA Menschutkin, *Z. Phys. Chem. Neue Folge* 5 (1890) 589.

## – 3 –

# Experimental Methods

---

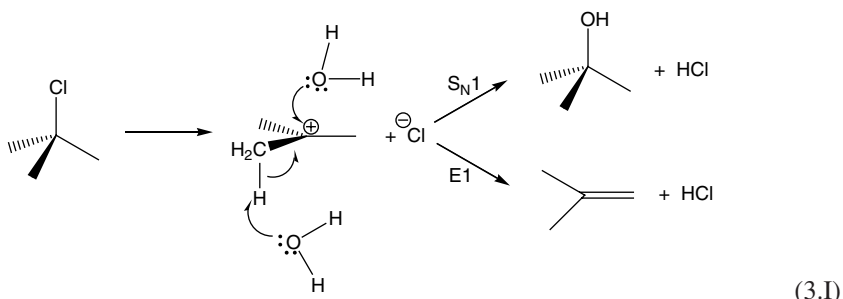
The experimental measurement of a reaction rate requires the use of techniques that allow us to obtain information on the concentration of the species involved for  $N$  reaction times:  $t_1, t_2, t_3 \dots, t_N$ . As the value of  $N$  increases, the description of the time evolution becomes more accurate. It is particularly important to study the early part of a reaction, far from equilibrium, as when there is appreciable reaction, the relatively high concentrations of products means that they can participate in other processes, and, as such, they will make the analysis of the results obtained more difficult. In practice, we need a finite time interval to carry out the measurement of a concentration,  $\Delta t_{\text{obs}}$ . If the reaction is started by mixing two reactants, there will be a dead time before we can make a measurement of the reactant or product concentration. We can consider this time to be the sum of the time interval necessary to mix the reactants,  $\Delta t_{\text{mix}}$ , and the time to obtain a homogeneous distribution of all the chemical species in the solution,  $\Delta t_{\text{hom}}$ . Thus, the total time lapse before we obtain the first measurement of the concentration will be given by the interval  $\Delta t_{\text{obs}} + \Delta t_{\text{mix}} + \Delta t_{\text{hom}}$ . If (as is common) we employ spectroscopic methods to analyse for the reactant or product concentrations and use conventional mixing and homogenisation techniques for the reactant solutions, this time interval is usually between 3 and 5 sec. As it is necessary to record various readings of concentration to describe the velocity of a reaction fully, we should try to ensure that during the first 10 sec of reaction, the concentration of the reactants is reduced by less than half of the initial value. We can observe the evolution of these reactions directly and conventional analytical methods can be employed to monitor the concentration changes. We can note in relation to these analytical measurements that human vision has a somewhat faster time response, with the capacity to distinguish visibly changes occurring with a frequency of  $<10 \text{ sec}^{-1}$ , such that it is easy to see the above reaction directly.

Within certain limits, it is possible to control the rate with which a reaction occurs, for example, through the control of reactant concentrations or temperature. Thus, we can study experimentally a considerable number of reactions over a convenient time scale, using conventional analytical methods [1]. However, a number of other reactions, such as the neutralisation of an acid or the precipitation of a salt, appear to occur “instantaneously”. To study the reaction kinetics of these rapid processes, it is necessary to resort to special techniques. We will discuss these later.

### 3.1 APPLICATION OF CONVENTIONAL TECHNIQUES TO STUDY REACTIONS

#### 3.1.1 First-order reactions

The solvolysis of 2-chloro-2-methylpropane in water occurs by the mechanism



The first step is the rate-determining one for this reaction, and we will follow the velocity of this reaction. In this step, the haloalkane ionises to produce an intermediate species, in this case a carbocation. Subsequently, the carbocation can be attacked by water to give either 2-methylpropanol or 2-methylpropene. The overall reaction is known as unimolecular nucleophilic substitution, S<sub>N</sub>1, when the nucleophilic attack predominates. Alternatively, if after initially forming the same carbocation elimination of a proton occurs to give 2-methylpropene, the process is termed unimolecular elimination, E1. At room temperature, the predominant reaction is S<sub>N</sub>1, but the rate-determining step is the same for both reactions, and both lead to formation of the same amount of HCl. It is not uncommon in chemical kinetics for different pathways to occur via the same intermediate. As the only ionic species formed in either case is HCl, the progress of the reaction can be followed by the increase of the conductance of the solution. If  $\Lambda_0$  is the conductance of the solvent,  $\Lambda$ , the conductance of the solution at time  $t$  and  $\Lambda_\infty$  the final conductance of the solution ( $t = \infty$ ), then

$$[\text{HCl}]_t \propto \Lambda_t - \Lambda_0 \quad (3.1)$$

$$[\text{HCl}]_\infty \propto \Lambda_\infty - \Lambda_0 \quad (3.2)$$

The proportionality constant can be obtained experimentally using the same conductivity cell by measuring the increase in conductivity in the same solvent or in a mixture of solvents owing to the formation of HCl.

#### Experiment 3.1. Experimental determination of the rate constant and reaction order for the solvolysis of 2-chloro-2-methylpropane in ethanol–water mixture [2–4]

*Material.* Stopwatch, thermostat bath, conductivity cell, 1 cm<sup>3</sup> pipette (or syringe), 25 cm<sup>3</sup> pipette, 100 cm<sup>3</sup> measuring cylinder, 250 cm<sup>3</sup> Erlenmeyer flask.

*Experimental procedure.* Prepare a solution of 40% ethanol–water v/v by mixing 40 cm<sup>3</sup> of ethanol with 60 cm<sup>3</sup> of water. Fill an Erlenmeyer flask with 75 cm<sup>3</sup> of this solvent, place

in a thermostat bath at 25 °C and introduce the conductivity cell into the Erlenmeyer flask. When thermal equilibrium with the bath has been reached, prepare a stock solution of 2-chloro-2-methylpropane by adding 0.1 cm<sup>3</sup> of the haloalkane to approximately 10 cm<sup>3</sup> of ethanol. Connect the conductivity bridge and measure the conductivity of the 40% ethanol–water solvent. Inject 0.6 cm<sup>3</sup> of the stock solution of the haloalkane and start the stopwatch. Stir the solution in the conductivity cell continuously until measurements are made. Read the conductivity every 30 sec during the first 5 min, and subsequently every minute until the conductivity no longer changes with time (i.e. the reaction is effectively completed). The stirring should be stopped ~5 sec before each conductivity reading is made. Repeat this experimental procedure using different injected volumes of haloalkane solution, e.g. 1.2–1.8 cm<sup>3</sup>, taking care to wash the electrodes before each new experiment. Make a calibration curve for the conductivity bridge using solutions of HCl (0.5, 1.0 and 2.0 mM) in 40% ethanol–water.

*Results.* Table 3.1 shows typical results obtained by students with this procedure.

From these experimental results, it is possible to plot the changes in HCl concentration with time, as shown in Figure 3.1.

The velocity of this reaction for each time  $t$  can be obtained by tracing tangents to the curve of the variation of concentration with time for the particular time  $t$  of interest. For the time  $t = 0$ , we obtain the initial rate. The plot of initial rate as a function of the initial concentration of haloalkane gives a straight line that passes through the origin. This means

**Table 3.1**

Variation of conductivity with time during the solvolysis of 2-chloro-2-methylpropane in 40% ethanol–water solution

Time (sec)	0.6 cm <sup>3</sup> of haloalkane		1.2 cm <sup>3</sup> of haloalkane		1.8 cm <sup>3</sup> of haloalkane	
	$\Lambda$ (μS)	[HCl] (mM)	$\Lambda$ (μS)	[HCl] (mM)	$\Lambda$ (μS)	[HCl] (mM)
0	39.7	0	40.1	0	40.5	0
30	40.5	0.0157	42.6	0.0377	47.4	0.0880
60	41.4	0.0252	46.8	0.0817	57.4	0.1928
90	42.1	0.0325	51.4	0.1299	66.9	0.2924
120	42.4	0.0356	55.6	0.1739	77.7	0.4055
150	43.6	0.0482	60.0	0.2201	86.2	0.4946
180	44.2	0.0545	64.1	0.2630	92.4	0.5596
210	44.3	0.0555	68.2	0.3059	100.8	0.6476
240	45.6	0.0691	70.5	0.3301	110.1	0.7451
270	46.0	0.0734	74.6	0.3731	115.7	0.8037
300	46.1	0.0744	77.7	0.4055	122.0	0.8698
360	47.3	0.0869	83.2	0.4632	131.6	0.9704
420	47.7	0.0912	88.2	0.5156	140.6	1.0647
480	47.9	0.0933	91.8	0.5533	146.5	1.1265
780	48.4	0.0985	98.6	0.6246	158.6	1.2533
1200	49.1	0.1058	100.4	0.6434	162.0	1.2889
1260	49.2	0.1069	100.4	0.6434	162.0	1.2889
1320	49.2	0.1069	100.5	0.6434	162.5	1.2942
1380	49.3	0.1079	100.5	0.6447	162.7	1.2963
1440	49.4	0.1089	100.8	0.6476	162.9	1.2984

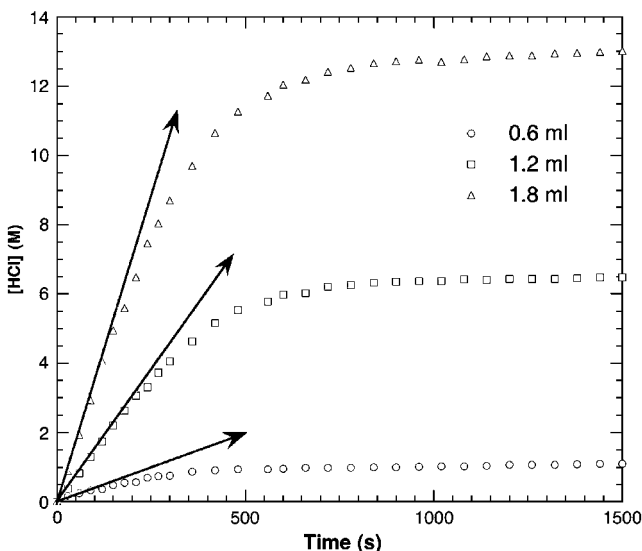
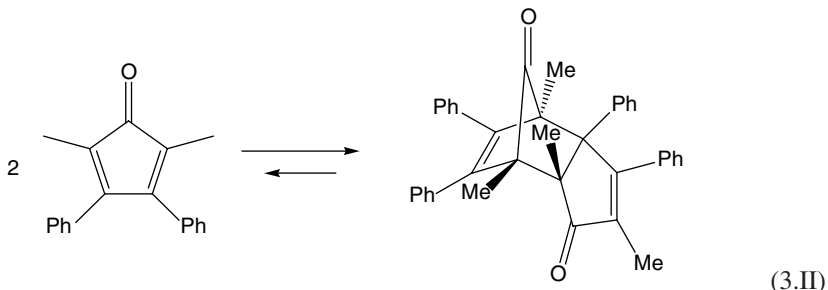


**Figure 3.1** Change in the concentration of HCl with time in the solvolysis of 2-chloro-2-methylpropane in the presence of 40% ethanol–water solution at 20 °C.

that the reaction is first order in terms of the concentration of haloalkane. The rate constant of the reaction can be obtained from the slope of this plot (Figure 3.2). Alternatively, it is possible to use a graph of the logarithm of [HCl] as a function of time to obtain the rate constant of this reaction directly. This is based on the integration of the first-order rate law, as will be discussed in detail in Chapter 4.

### 3.1.2 Second-order reactions

The dimerisation of 2,5-dimethyl-3,4-diphenylcyclopentadienone



can be followed by colorimetry since the monomer is coloured, while the dimer does not absorb in the visible spectral region. The spectrum of the pure monomer is difficult to obtain since the dimerisation proceeds at an appreciable rate at room temperature. Thus, to follow the evolution of the concentration of the monomer with time for this experiment, it

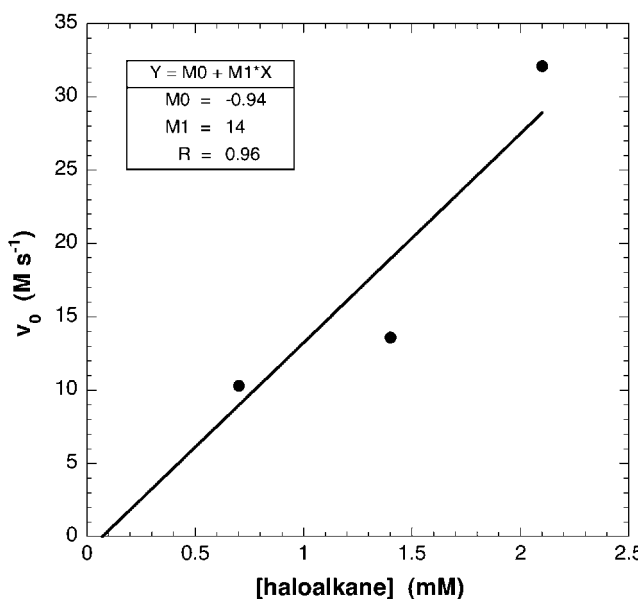


**Figure 3.2** Dependence of the initial rate of solvolysis of 2-chloro-2-methylpropane with initial concentration of the solute in ethanol–water mixture. The slope of the linear plot gives the rate constant  $k = 1.4 \times 10^4 \text{ sec}^{-1}$  at 20 °C.

is necessary to obtain the molar absorption coefficient ( $\varepsilon$ ) of the monomer using data from literature. We note that for a 1 mM solution of the monomer in a 1-cm-pathlength cuvette, the absorbance  $A_{460}$  is 0.225 and by applying the Beer–Lambert law, we can calculate  $\varepsilon$ . The velocity of this reaction is measured by producing the monomer initially by thermolysis of the dimer that is commercially available.

### Experiment 3.2. Experimental determination of the rate constant and reaction order for the dimerisation of 2,5-dimethyl-3,4-diphenylcyclopentadienone in toluene or xylene [5]

*Material.* Stopwatch, colorimeter or spectrometer, water bath, ice, 1 cm glass or plastic cuvettes for visible absorption spectra, 10 cm<sup>3</sup> measuring cylinder, 100 cm<sup>3</sup> Erlenmeyer flask.

*Experimental procedure.* Dissolve approximately 50 mg of the dimer in 10 cm<sup>3</sup> toluene or xylene. Heat the solution in a water bath in a fume cupboard for 10–15 min, until a strongly coloured solution of the monomer is produced. Cool this solution to room temperature in an ice bath. Transfer the solution at room temperature to the cuvette, introduce it in the colorimeter and measure the absorption at 460 nm. When the absorbance of the solution is within the scale of the colorimeter, make the first reading and start the stopwatch. Measure the absorbance every 5 min during the first 1/2 h of the reaction. After this, take readings at longer time intervals until the reaction is completed (~2 h).

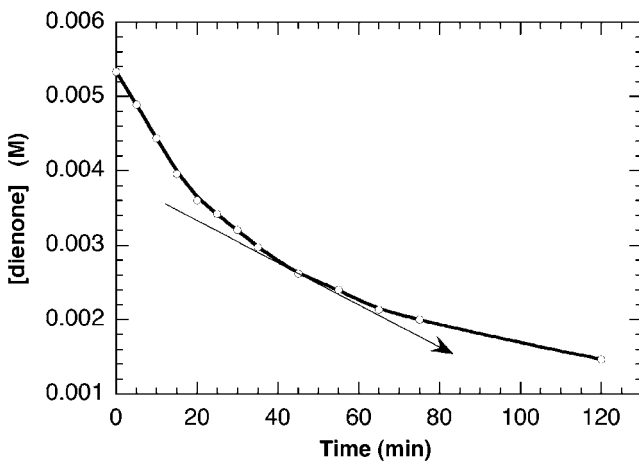
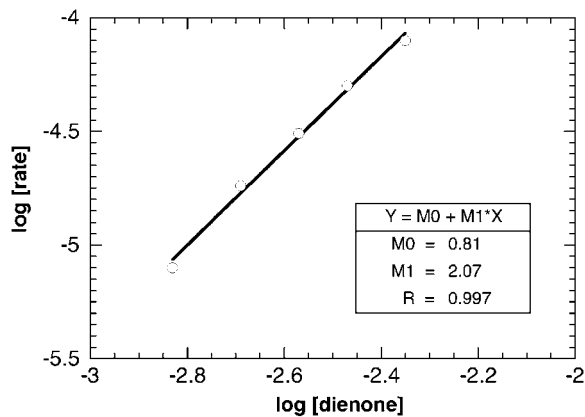
*Results.* Table 3.2 presents typical results obtained by students while following this experimental procedure.

Figure 3.3 presents the variation of concentration of the dienone as a function of time, assuming a molar absorption coefficient of  $\varepsilon = 225 \text{ M}^{-1}\text{cm}^{-1}$ . The velocity of the reaction

**Table 3.2**

Variation of monomer absorbance at 460 nm as a function of reaction time (in minutes)

$t$ (min)	0	5	10	15	20	25	30	35	45	55	65	75	120
$A_{460}$	1.2	1.1	1.0	0.89	0.81	0.77	0.72	0.67	0.59	0.54	0.48	0.45	0.33

**Figure 3.3** Change in concentration of dienone with time.**Figure 3.4** Logarithm of the rate of dimerisation as a function of the logarithm of the concentration of the monomer.

at time  $t$  can be obtained from the slope of the curve corresponding to the point  $t$  on the abscissa. Taking logarithms of eq. (2.8) and noting that the only reactant for this bimolecular process is the monomer, we obtain

$$\log v = \log k + a \log [A] \quad (3.3)$$

from which we can observe that the graph of the logarithm of the rate as a function of the logarithm of the concentration of the monomer (Figure 3.4) is a straight line, whose slope is the order of the reaction in terms of the monomer and whose intercept gives the logarithm of the rate constant. Alternatively, if we assume second-order kinetics in terms of the monomer, we can plot a graph of velocity as a function of [monomer]<sup>2</sup> and observe that we obtain a straight line, which passes through the origin and whose slope is the rate constant. The presentation of integrated laws for second-order reactions will be given in Chapter 4.

### 3.1.3 Complex reactions

Iodination of acetone in water



can be followed by colorimetry since one of the reactants, I<sub>2</sub>, is coloured, while all the other species involved in the reaction are colourless [6]. Alternatively, as we will see later, this reaction is accelerated by the presence of an acid and can be stopped (or quenched) by making the medium more basic. Following this quenching, we can proceed to carry out the analysis of the concentrations of the reactants or products at leisure by titration at any specified reaction time interval.

#### Experiment 3.3. Determination of the rate constant and kinetic order of iodination of acetone in water

*Materials.* Stopwatch, graduated pipettes, burette, volumetric flask, Erlenmeyer flasks.

*Experimental procedure.* Prepare the following in water: 100 cm<sup>3</sup> each of solutions 0.01 M iodine and 1 M in sulfuric acid, 500 cm<sup>3</sup> of an aqueous sodium acetate solution (1M), and 1000 cm<sup>3</sup> of a standardised solution of sodium thiosulfate (0.01 M). As iodine is sparingly soluble in water, the solution of 0.01 M I<sub>2</sub> is prepared by dissolving the appropriate mass of iodine in an aqueous solution of 0.01 M KI. Also prepare a solution of starch indicator in water as follows: mix 1 g of starch and 1 cm<sup>3</sup> of hot water to form a paste, add 1 cm<sup>3</sup> of the 1.0 M H<sub>2</sub>SO<sub>4</sub> solution and 0.1 g NaHSO<sub>3</sub> and finally dilute to 250 cm<sup>3</sup>. To a 250 cm<sup>3</sup> Erlenmeyer flask, add the following quantities of the above solutions:

Solution	CH <sub>3</sub> COCH <sub>3</sub> (ml)	H <sub>2</sub> SO <sub>4</sub> (ml)	H <sub>2</sub> O (ml)
1	20	10	150
2	15	10	155
3	10	10	160
4	20	15	145
5	20	5	155

Add 20 cm<sup>3</sup> of the solution of iodine and start the stopwatch. Withdraw 20 cm<sup>3</sup> aliquots every 5 min and add them to an Erlenmeyer flask containing 10 cm<sup>3</sup> of the sodium acetate solution. Titrate this solution with the standardised solution of sodium thiosulfate, using the starch indicator.

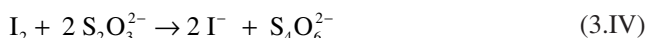


**Table 3.3**

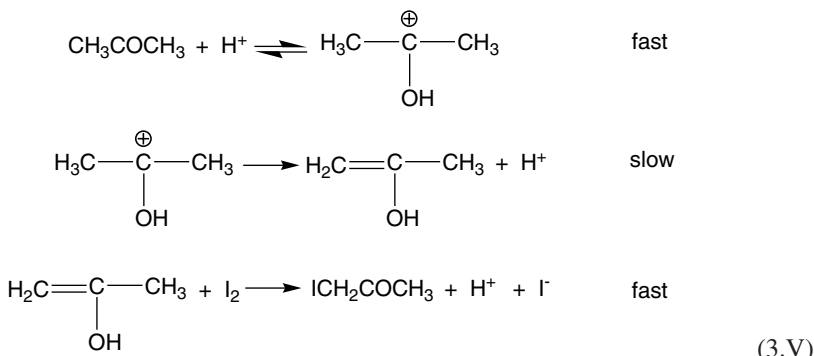
Variation of iodine concentration with time

Time (sec)	Solution 1 [I <sub>2</sub> ] (mM)	Solution 2 [I <sub>2</sub> ] (mM)	Solution 3 [I <sub>2</sub> ] (mM)	Solution 4 [I <sub>2</sub> ] (mM)	Solution 5 [I <sub>2</sub> ] (mM)
300	6.175	5.30	5.60	5.80	5.65
600	4.125	4.70	5.10	4.725	5.275
900	3.25	4.05	4.675	3.275	4.725
1200	2.525	3.425	4.20	2.00	4.40
1500	1.50	2.875	3.875	0.625	4.025
1800	0.875	2.325	3.375	0.25	3.475
2100	0.25	1.65	3.025		3.025
2400		1.075	2.725		2.65

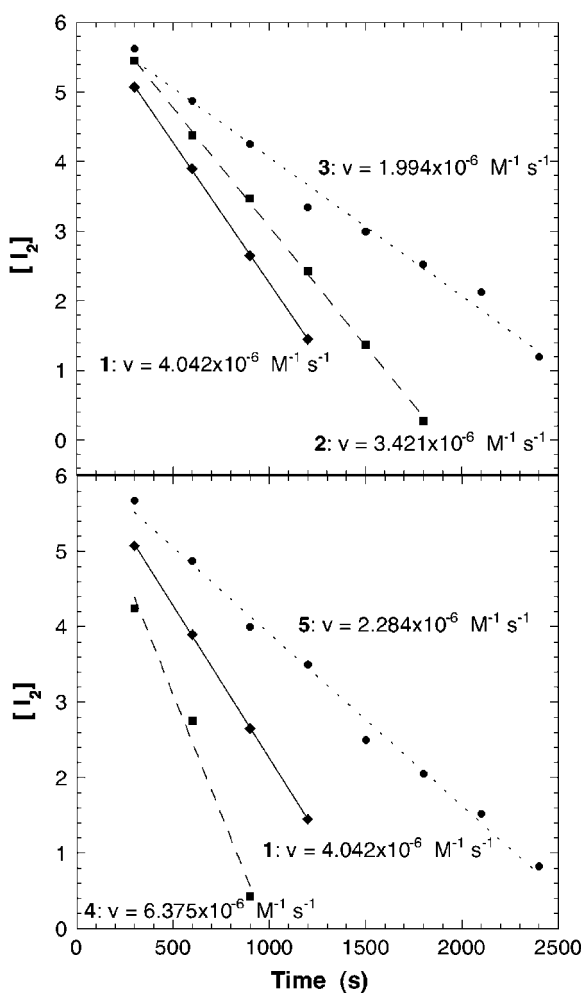
*Results.* By titrating with the standardised solution, calculate the concentration of iodine for each of the kinetic experiment presented in Table 3.3.

Figure 3.5 shows that, for the extent of reaction studied, the iodine concentration varies linearly with time. That is, the velocity of the reaction is constant and independent of the concentration of iodine, i.e. the rate is zero order in terms of the iodine concentration. However, the reaction mechanism is complex, and the participation of I<sub>2</sub> as reactant occurs after the rate-determining step of the reaction. From the slopes of the lines in Figure 3.5 we can obtain the velocities of the reactions,  $v = -d[I_2]/dt$ , for the corresponding concentrations of acid and acetone. The plot of the logarithm of the reaction velocity versus the logarithm of the concentration of acetone has a slope close to one, as does the logarithm of rate versus the logarithm of the H<sup>+</sup> concentration (Figure 3.6). The rate law is thus first order in terms of concentrations of acetone as well as acid. Using the velocities indicated in Figure 3.5 and the orders of reaction, the rate constant of the reaction can now be determined. The mean value obtained for this group of experiments is  $k = 3.1 \times 10^{-5} \text{ M}^{-1}\text{sec}^{-1}$ .

The appearance of H<sup>+</sup> in the rate law, but not in the stoichiometry of the reaction suggests an acid-catalysed step preceding the slowest step in the kinetic scheme. A mechanism that is in agreement with this rate law is



It should be noted that this mechanism requires the presence of two intermediates that have not been detected in this reaction. However, although it is acceptable to propose mechanisms



**Figure 3.5** Variation of the concentration of iodine with time for the five solutions studied in the iodination of acetone.

involving intermediates that are not detected experimentally, evidence should be given to support the existence of these species on the basis of structural, thermochemical and/or kinetic evidence available for related systems.

### 3.1.4 Activation energy

Iodide ion reacts with persulfate to produce iodine and sulfate ion [7,8].



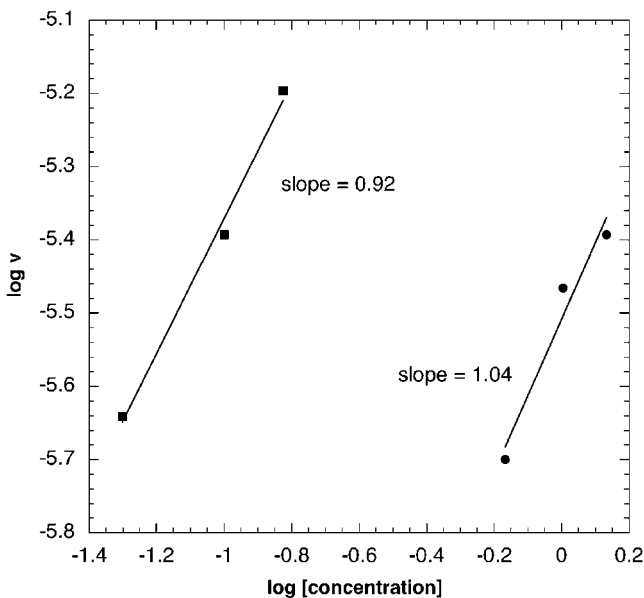


**Figure 3.6** Determination of the reaction orders for acetone (circles) and  $\text{H}^+$  (squares) in the iodination of acetone.

The amount of iodine formed can be determined by titration with thiosulfate in reaction (3.IV) using starch as indicator, since this process as well as the complexation of the iodine produced with iodide ion is fast



The species  $\text{I}_3^-$  forms a complex with starch giving an intense blue colour. Thus, by taking aliquots at various time intervals and determining the iodine concentration by titration, the order and rate of reaction (3.VI) can be determined. Alternatively, instead of taking aliquots, the reaction can be carried out in a single reaction vessel containing the same concentrations of  $\text{I}^-$  and  $\text{S}_2\text{O}_8^{2-}$  ( $y \text{ mol dm}^{-3}$ ), together with a known quantity of  $\text{S}_2\text{O}_3^{2-}$  ( $2x \text{ mol dm}^{-3}$ , where  $2x < y$ ) and starch indicator. Under these conditions, the appearance of the blue colour, owing to the complex formed between  $\text{I}_3^-$  and starch, only occurs when reaction (3.VI) produces more than  $x \text{ mol dm}^{-3}$  of  $\text{I}_2$ . The first  $x \text{ mol dm}^{-3}$  of  $\text{I}_2$  formed by reaction (3.VI) will be consumed by the  $2x \text{ mol dm}^{-3}$  of  $\text{S}_2\text{O}_3^{2-}$  in the reaction flask. This will be followed by reaction (3.IV), and since the rate of this reaction as well as our capacity for seeing the changes is much faster than that of reaction (3.VI), the time that we observe the appearance of the blue colour corresponds to the time of formation of  $x \text{ mol dm}^{-3}$  of  $\text{I}_2$  in reaction (3.VI).

If the initial  $\text{S}_2\text{O}_3^{2-}$  concentration is kept constant for a series of experiments, the time needed to produce the blue colour is a measure of the velocity of the reaction,  $\Delta[\text{I}_2]/\Delta t$ . To

**Table 3.4**

Reaction times at different temperatures						
$T$ (°C)	2	10	20	25	35	40
$T$ (K)	275	283	293	298	308	313
$t_r$ (sec)	79.5	58.5	49.5	36.5	36.0	26.5
$t_r^{-1}$ (sec) <sup>-1</sup>	0.0126	0.017	0.020	0.027	0.028	0.038

be more specific, the reciprocal of the time interval up to the appearance of the blue colour is proportional to the rate of the reaction

$$\frac{1}{t} = c \left[ I^- \right]^a \left[ S_2O_8^{2-} \right]^b \quad (3.4)$$

where  $c$  is a constant proportional to the rate constant of the reaction.

#### Experiment 3.4. Experimental determination of activation energies

*Material.* Stopwatch, thermostat bath, 10 and 1 cm<sup>3</sup> pipettes, 250 cm<sup>3</sup> Erlenmeyer flasks, 250 cm<sup>3</sup> volumetric flasks, thermometer, ice.

*Experimental procedure.* Prepare aqueous solutions of H<sub>2</sub>SO<sub>4</sub> (1.0 M), KI (0.2 M), K<sub>2</sub>S<sub>2</sub>O<sub>8</sub> (0.2 M) and Na<sub>2</sub>S<sub>2</sub>O<sub>3</sub> (0.01 M). Prepare starch indicator as follows: mix 1 g of starch with 1 cm<sup>3</sup> of hot water to form a paste, add 1 cm<sup>3</sup> of the H<sub>2</sub>SO<sub>4</sub> solution and 0.1 g of NaHSO<sub>3</sub>, and, finally, dilute to 250 cm<sup>3</sup>. Transfer to a 100 cm<sup>3</sup> Erlenmeyer flask (solution A) 20 cm<sup>3</sup> of KI and 10 cm<sup>3</sup> of Na<sub>2</sub>S<sub>2</sub>O<sub>3</sub> solutions. Transfer 20 cm<sup>3</sup> of K<sub>2</sub>S<sub>2</sub>O<sub>8</sub> and 1 cm<sup>3</sup> of the starch indicator to another 100 cm<sup>3</sup> Erlenmeyer flask (solution B). Place the two Erlenmeyer flask in a thermostat bath at 20 °C. When the solutions have achieved thermal equilibrium, add the contents of one flask into the other, start the stopwatch and homogenise the mixture. Note the time taken for the appearance of the blue colour. Repeat the experiment at different temperatures.

*Results.* Table 3.4 presents the reaction time obtained for each of the temperature studied.

The logarithmic form of the Arrhenius law (eq. (2.40)) shows that the slope of the plot of ln (1/t<sub>f</sub>) as a function of 1/T is equal to -E<sub>a</sub>/R (Figure 3.7), from which the activation energy can be easily obtained. From the above data, the value E<sub>a</sub> = 56 kJ mol<sup>-1</sup> was obtained. Unfortunately, we cannot apply the same method for the pre-exponential factor, since, in this experiment, we do not determine the rate of the reaction, but quantities that are proportional to it. In addition, Figure 3.7 shows that the pre-exponential factor is obtained by extrapolation over a range far from the experimental results, which will introduce considerable errors. To estimate the pre-exponential factor, we can repeat the kinetic experiment at one temperature using colorimetry or spectroscopy, and from the measured rate constant and calculated activation energy, use eq. (2.38).

#### 3.1.5 Dependence of light intensity

When molecules absorb visible or ultraviolet light, they are transformed from their ground state to the electronically excited states with high-energy contents. At room temperature,

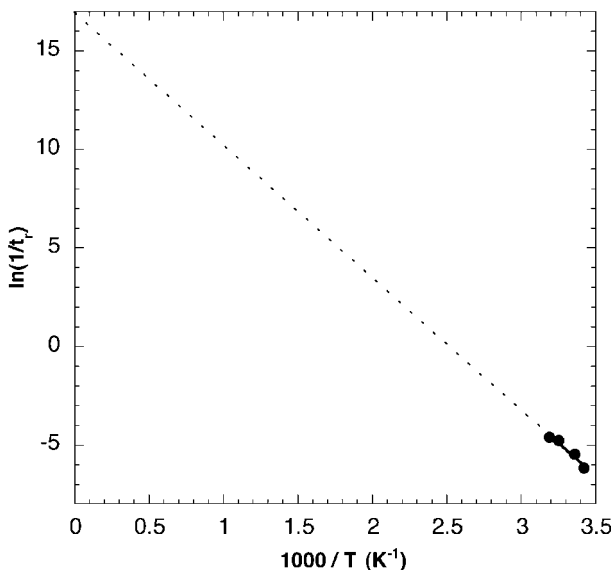
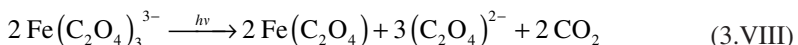


**Figure 3.7** Arrhenius plot for the reaction between iodate and bisulfite ions.

electronically excited molecules have short lifetimes and the study of their reactivity cannot be made simply using conventional analytical methods. However, it is possible to devise and carry out simple experiments that show quantitatively the dependence between the intensity of light absorbed and the quantity of products formed. For example, the ferrioxalate anion when exposed to light of wavelength  $< 590$  nm, decomposes according to the reaction



Such solutions, which are used to measure light intensities, are known as actinometers. At pH *ca.* 3.5, the Fe(II) formed reacts with 1,10-phenanthroline to form the well-known red complex  $[\text{Fe}(\text{phen})_3]^{2+}$  (ferroin), whose molar absorption coefficient at 510 nm is well established ( $\varepsilon = 11100 \text{ cm}^{-1} \text{ M}^{-1}$ ).

### Experiment 3.5. Experimental determination of the effect of light exposure on the photodecomposition of potassium ferrioxalate [9]

*Material.* Stopwatch, colorimeter, 1 cm glass or plastic cuvettes, 1 dm<sup>3</sup> volumetric flask, 250 cm<sup>3</sup> Erlenmeyer flask, 1 cm<sup>3</sup> graduated pipette.

*Experimental procedure.* Prepare potassium ferrioxalate by adding, with stirring, a solution of potassium oxalate (1.5 M) to iron(III) chloride (1.5 M) in the volume ratio 3:1. Recrystallise the precipitate obtained from water, and dry the potassium ferrioxalate crystals obtained and store in the dark. Prepare a 0.006 M solution of this actinometer in a 1 dm<sup>3</sup> flask by dissolving 2.847 g of the crystals obtained in 800 cm<sup>3</sup> water and adding sufficient

2 M sulfuric acid to bring to the 1 dm<sup>3</sup> mark on the flask. This solution absorbs more than 99% of the incident light with  $\lambda > 390$  nm in a 1 cm cell. Irradiate 3 cm<sup>3</sup> of this solution in a 1 cm cuvette at 405 nm in the colorimeter or spectrometer for 30 minutes. At the end of this time, take the cell out of the colorimeter and add 0.5 cm<sup>3</sup> of a solution of sodium acetate (1.8 M) and sulfuric acid (2.16 M) containing 0.1% (m/v) of 1,10-phenanthroline. After 30 min measure the absorbance at 510 nm. Repeat with a reference solution that has been kept in the dark. Convert the difference in absorbance between the irradiated sample and the reference into concentration of Fe<sup>2+</sup> produced in the irradiated solution, knowing that the iron(II)-phenanthroline complex in a 0.1 mM solution in a 1 cm cell has an absorbance of 1.11. Repeat the experiment, irradiating for 45 and 60 min.

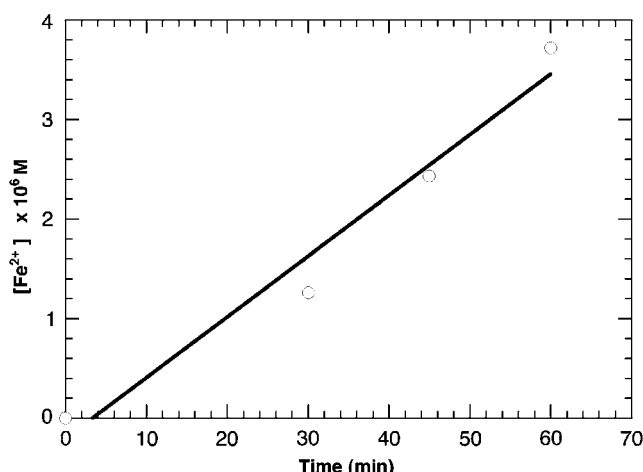
*Results.* Table 3.5 summarises the results obtained.

Figure 3.8 shows [Fe<sup>2+</sup>] as a function of the irradiation time. The quantum yield for formation of iron(II) (that is the ratio of product formed to photons absorbed) when a 0.006 M solution of ferrioxalate is irradiated at 405 nm is 1.14 [10]. This allows us to calculate the intensity of light absorbed by the ferrioxalate solution, which is why this solution is called

**Table 3.5**

Relation between the irradiation time and the concentration of Fe<sup>2+</sup> produced photochemically

Time (min)	Absorbance ( $A$ )	$A - A_0$	[Fe <sup>2+</sup> ] (M)
0	0.0083	0	0
30	0.0223	0.0140	$1.26 \times 10^{-6}$
45	0.0353	0.0270	$2.43 \times 10^{-6}$
60	0.0496	0.0413	$3.72 \times 10^{-6}$



**Figure 3.8** Dependence of the concentration of product formed on the irradiation time.

an actinometer. Assuming that all the incident light is absorbed by the solution, the intensity of this light, in Einstein min<sup>-1</sup>, is given by

$$I = \frac{A_{510}V}{\varepsilon_{510}d\Phi_\lambda t} \quad (3.5)$$

where  $A_{510}$  is the absorbance of the irradiated solution at 510 nm, corrected by the absorbance of the reference solution,  $d$  the optical path of the absorption cell measured in centimetre,  $\varepsilon_{510} = 1.11 \times 10^4 \text{ M}^{-1} \text{ cm}^{-1}$ ,  $\Phi_\lambda$  the quantum yield of production of Fe<sup>2+</sup> at the wavelength ( $\lambda$ ) used in the photolysis,  $t$  the irradiation time and  $V$  the volume in dm<sup>3</sup> of the solution used in the determination of the absorbance. For the experiment shown in Table 3.5,  $V = 3.5 \times 10^{-3} \text{ cm}^3$  and the mean intensity of the incident light is  $1.6 \times 10^{-10}$  Einstein min<sup>-1</sup>, i.e.  $1.5 \times 10^{12}$  photons sec<sup>-1</sup>.

### 3.1.6 Enzyme catalysis

Enzymes are the most efficient and versatile catalysts known. They are able to increase the rates of some reactions by up to 14 orders of magnitude, with a high degree of specificity, such that they can not only distinguish between substrates, but also between two optical isomers of the same substrate. In addition, in biological systems they are normally subject to the regulatory action of cellular metabolites, such that they carry out diverse tasks while maintaining the overall chemical balance relatively constant. The reaction centre in the enzyme where the major chemical processes occur is known as the *active site*. The reactants involved in reactions catalysed by enzymes are known as substrates, and the compounds that increase or decrease the rates of these reactions are known as activators or inhibitors, respectively.

The most relevant parameters that can be obtained from a kinetic study of enzymatic catalysis are the dependence of the velocity of catalysis on the concentration of the substrates, in particular in the early stages of reaction, and the maximum rate at which the enzyme can accelerate the reaction.

A simple experiment in which these parameters can be obtained by conventional experimental methods uses papain as the enzyme and Azocoll as the substrate. Papain is a sulphhydryl protease that can be isolated from the fruit papaya (paw-paw), and which is used for tenderising meat. Azocoll is insoluble ground cowhide to which a red dye has been covalently bonded. When the peptide bonds of the collagen are hydrolysed by the papain, the dye is liberated into the solution and the increase in its concentration as a function of time can be studied spectrophotometrically at 520 nm.

#### Experiment 3.6. Experimental determination of the kinetics of hydrolysis of Azocoll by papain [11]

*Material.* Stopwatch, colorimeter (or spectrometer), 1 cm<sup>3</sup> spectroscopy cuvette, 10 cm<sup>3</sup> measuring cylinder, test tube.

*Experimental procedure.* At room temperature, dissolve an enzyme tablet (Allergan Soflens) in 10 cm<sup>3</sup> of doubly distilled or deionised water. This will give a solution with a

**Table 3.6**

Time evolution of the absorbance ( $A$ ) at 520 nm for various initial concentrations of Azocoll

Time (sec)	$A$ , Azocoll (12.5 mg)	Time (sec)	$A$ , Azocoll (7.1 mg)	Time (sec)	$A$ , Azocoll (4.1 mg)	Time (sec)	$A$ , Azocoll (3.5 mg)
55	0.113	24	0.072	45	0.0520	21	0.031
98	0.206	88	0.173	97	0.144	110	0.144
159	0.392	131	0.268	131	0.247	146	0.299
214	0.639	171	0.412	205	0.320	183	0.340
266	0.856	214	0.567	226	0.464	275	0.567
373	1.22	257	0.763	306	0.701	370	0.722
392	1.38	306	0.928	339	0.814	422	0.918
441	1.42	443	1.38	391	0.907	459	1.01
496	1.62	492	1.57	425	1.06	535	1.11
542	1.71	566	1.72	471	1.16	590	1.22
591	1.80	615	1.80	507	1.31		
				532	1.35		
				602	1.40		

protein concentration of  $\sim 0.5 \text{ mg cm}^{-3}$ . Add 12.5 mg of Azocoll to the spectroscopy cuvette. Add  $2 \text{ cm}^3$  of the enzyme solution to this cell, start the stopwatch and invert the cell to homogenise the solution. Introduce the cell in the colorimeter (or spectrophotometer) and 30 sec later record the first absorbance reading at 520 nm. Invert the cell again, leave for a further 30 sec and read the absorbance. Repeat this procedure for a duration of 10 min. Repeat the experiments with the following amounts of Azocoll: 7.1, 4.1 and 3.4 mg.

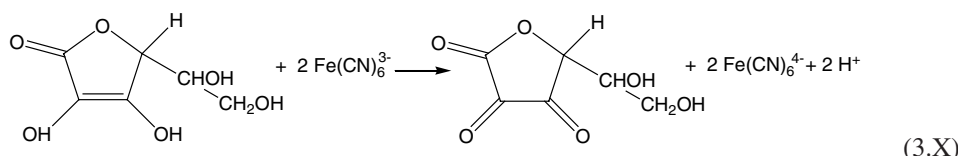
*Results.* Typical results obtained with this procedure are shown in Table 3.6.

Since the variation of absorbance with time is proportional to the reaction velocity, we can estimate quantities proportional to the velocity of the reaction from the tangents of the curves in Figure 3.9 at  $t = 0$ , and follow them as functions of the initial concentration of the substrate (Figure 3.10).

Knowing the molar absorption coefficient of the dye at 520 nm, it is possible, from Figure 3.9, to determine the maximum rate for this catalysis [12].

### 3.1.7 Dependence on ionic strength

Ascorbic acid is oxidised by hexacyanoferrate(III) to produce dehydroascorbic acid



As aqueous solutions of  $[\text{Fe}(\text{CN})_6]^{3-}$  have a maximum absorption at 418 nm with a molar absorption coefficient  $1012 \text{ M}^{-1} \text{ cm}^{-1}$  and the other reactants and products are colourless,

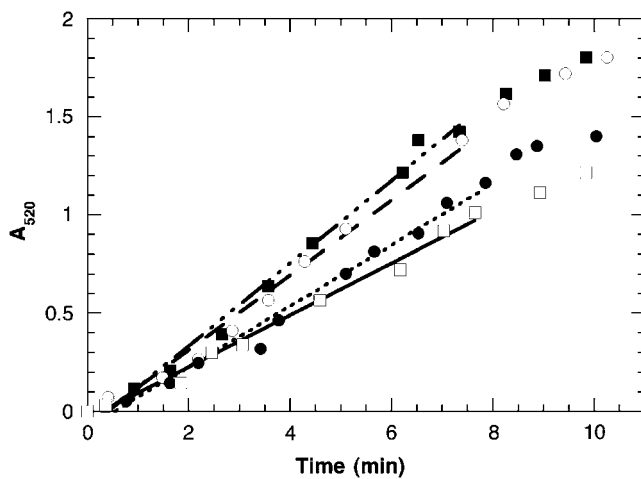


**Figure 3.9** Variation of absorbance with time for the hydrolysis of Azocoll by papain.

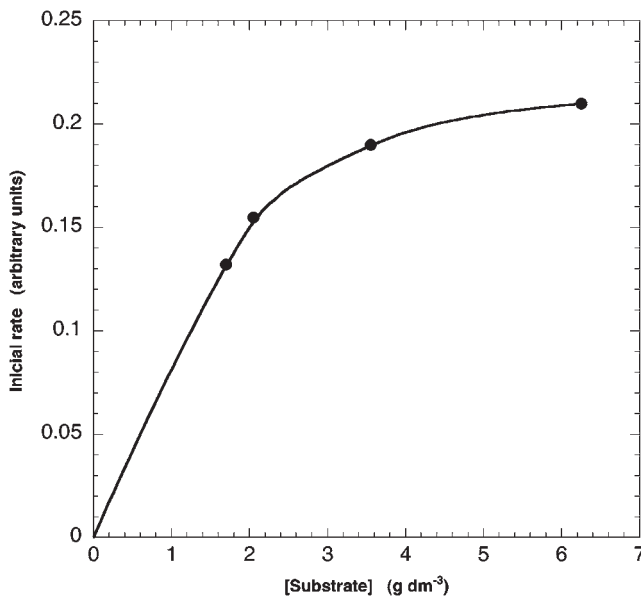


**Figure 3.10** Relative rates as a function of initial concentration of Azocoll.

it is possible to follow the progress of this reaction by visible absorption spectroscopy. The concentration of  $\text{Fe}(\text{CN})_6^{3-}$  at time  $t$  is given by

$$\left[ \text{Fe}(\text{CN})_6^{3-} \right] = \left[ \text{Fe}(\text{CN})_6^{3-} \right]_0 \frac{A}{A_0} \quad (3.6)$$

where  $[Fe(CN)_6^{3-}]_0$  is the initial concentration of hexacyanoferrate(III),  $A_0$  the initial absorbance and  $A$  the absorbance at time  $t$ .

### Experiment 3.7. Experimental determination of the effect of ionic strength [13]

*Material.* Stopwatch, colorimeter or spectrophotometer, 1 cm spectroscopy cuvette, 100 cm<sup>3</sup> volumetric flasks, 25 cm<sup>3</sup> pipettes, 100 cm<sup>3</sup> Erlenmeyer flasks.

*Experimental procedure.* Prepare four solutions of potassium hexacyanoferrate(III) ( $1.0 \times 10^{-3}$  M) in water containing sodium nitrate of different concentrations (e.g. 0.02, 0.05, 0.1 and 0.2 M). Prepare a 0.010 M solution of nitric acid, 0.001% of the disodium salt of EDTA and  $2.5 \times 10^{-4}$  M ascorbic acid. In the preparation of this solution, ascorbic acid must be the last solution to be added. Pipette 25 cm<sup>3</sup> of one of the solutions of  $K_3[Fe(CN)_6]/NaNO_3$  into an Erlenmeyer flask and add 25 cm<sup>3</sup> of the solution of ascorbic acid/nitric acid. Start the stopwatch and shake for a few seconds. Transfer the solution to the cuvette and measure the absorbance at 418 nm every minute for 20 min. To obtain the absorbance corresponding to  $t = 0$ , add 25 cm<sup>3</sup> of water and 25 cm<sup>3</sup> of the solution of  $K_3[Fe(CN)_6]/NaNO_3$  and record the absorbance. Repeat the process for all the solutions over the whole range of NaNO<sub>3</sub> concentrations.

*Results.* Table 3.7 presents the results obtained by students for this experiment.

**Table 3.7**

Effect of sodium nitrate concentration on the kinetics of oxidation of ascorbic acid

Time	$[NaNO_3] = 0.010\text{ M}$		$[NaNO_3] = 0.025\text{ M}$		$[NaNO_3] = 0.050\text{ M}$		$[NaNO_3] = 0.100\text{ M}$	
	$A_{418}$	$[Fe(CN)_6^{3-}]$ ( $10^{-4}\text{ M}$ )						
0	0.434	5.000	0.431	5.000	0.429	5.000	0.427	5.000
1	0.433	4.988	0.430	4.988	0.428	4.988	0.426	4.988
2	0.432	4.977	0.428	4.965	0.426	4.965	0.422	4.941
3	0.431	4.965	0.426	4.942	0.424	4.942	0.418	4.894
4	0.428	4.931	0.424	4.919	0.419	4.883	0.413	4.836
5	0.426	4.908	0.421	4.884	0.416	4.848	0.409	4.789
6	0.425	4.896	0.418	4.849	0.412	4.802	0.405	4.742
7	0.424	4.885	0.416	4.826	0.408	4.755	0.400	4.684
8	0.423	4.873	0.414	4.803	0.405	4.772	0.396	4.637
9	0.422	4.862	0.411	4.768	0.401	4.673	0.391	4.578
10	0.421	4.850	0.409	4.745	0.398	4.638	0.386	4.520
11	0.419	4.827	0.407	4.721	0.395	4.604	0.382	4.473
12	0.417	4.804	0.404	4.687	0.392	4.569	0.377	4.414
13	0.415	4.781	0.401	4.652	0.388	4.522	0.373	4.367
14	0.413	4.758	0.399	4.629	0.385	4.487	0.369	4.321
15	0.412	4.746	0.397	4.605	0.382	4.452	0.365	4.274
16	0.410	4.723	0.395	4.582	0.379	4.417	0.361	4.227
17	0.409	4.712	0.393	4.559	0.375	4.370	0.357	4.180
18	0.407	4.689	0.390	4.524	0.372	4.335	0.353	4.133
19	0.406	4.677	0.387	4.489	0.369	4.300	0.349	4.086
20	0.405	4.666	0.385	4.466	0.366	4.266	0.345	4.040

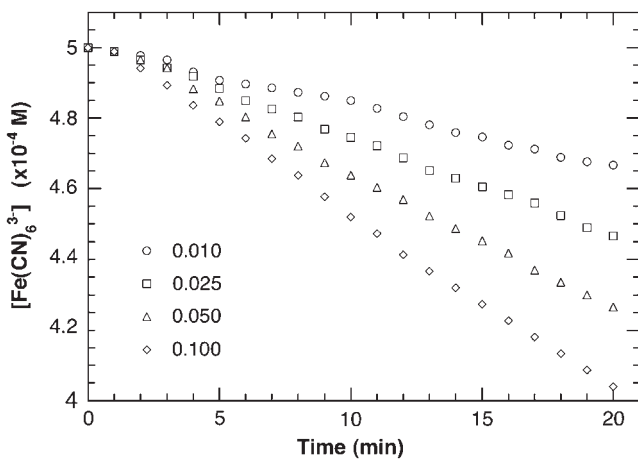
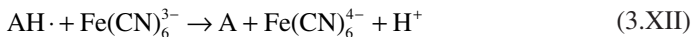


**Figure 3.11** Dependence of the variation in concentration of hexacyanoferrate(III) with time and sodium nitrate concentration.

Figure 3.11 shows that the concentration of  $[\text{Fe}(\text{CN})_6]^{3-}$  decreases more rapidly for solutions containing a higher concentration of  $\text{NaNO}_3$ , that is, the velocity of the reaction increases with the ionic strength. This is what is expected for reactions between two ions of the same charge. One mechanism proposed for the reaction involves initial ionisation of the ascorbic acid ( $\text{AH}_2$ ), which rapidly and reversibly forms an ascorbate anion intermediate ( $\text{AH}^-$ ), which then subsequently transfers an electron to the hexacyanoferrate(III) in the slowest step in the mechanism:



Finally, there is another rapid step in which the ascorbate-free radical ( $\text{AH}\cdot$ ) transfers an electron to the hexacyanoferrate(III) to give dehydroascorbate (A)



### 3.2 APPLICATION OF SPECIAL TECHNIQUES FOR FAST REACTIONS

In conventional kinetic methods in which the reactants are mixed and homogenised by simple addition and shaking, and the progress of the reaction measured by analytical or physical methods, the time of mixing has to be short relative to that of the reaction. For fast reactions, these experimental conditions are not met, so these methods cannot be used. To overcome this problem, various routes can be followed: (i) we can decrease the rate of

the reaction by decreasing the concentration of reagents or the temperature; (ii) we can decrease the time interval of mixing, using flow methods; (iii) we can rapidly perturb the equilibrium, and follow the subsequent chemical changes occurring in the relaxation of the system until the same or a new equilibrium is established; (iv) we can observe the competition between the reaction of interest and another fast process, whose rate is known.

From the experimental point of view, the biggest challenge is to choose the technique which is best adapted to the system that we are trying to study, considering parameters such as the nature of the reactants, rate constants, temperature, solvent, etc. For the reaction under study, it is important to clarify whether this leads to equilibrium between reactants and products, or if it is, effectively, irreversible. In addition, is the product formed stable or not, and what type of reactants, intermediates and products are involved (ions, free radicals, excited states, etc)? The choice of the experimental method will also depend on the order of magnitude expected for the rate constant, the type of solvent used and the analytical techniques available to study reactants, products, etc. In addition, since some of these techniques use rather expensive apparatus, this will also depend upon the availability of the equipment.

### 3.2.1 Flow methods

#### *Continuous flow*

Flow methods were first introduced by Hartridge and Roughton [14] in their study of the reaction between haemoglobin and oxygen. The application of these techniques is fairly general; they have been used to study the kinetics of reactions in liquid and gas phases and reactions with small and large equilibrium constants. The basis of this technique involves the injection of two reactants A and B in a mixing chamber, followed by the determination of their concentration, or that of the products, at a certain distance from the mixing chamber (Figure 3.12). In this continuous flow method, the reactants are injected continuously into the mixing chamber, leading to a profile of concentration of reactants and products along the detection tube, which does not change with time. Knowing the rate of flow, the reaction time can be related to the distance between the mixing chamber and the place where the reactants or products of the reaction are observed by whatever analytical technique is used. Typically, either a spectroscopic or electrochemical technique is used for analysis. For a flow rate of  $10 \text{ m sec}^{-1}$ , a distance of 1 cm corresponds to a reaction time of 1 msec. With the attainment of a stationary state in the concentration of the species involved, the time resolution of the detection method does not generally limit the time resolution of this technique, which normally depends upon only the mixing time. For conventional injection systems involving laminar flow, this is typically about 1 msec. It should be remembered that for all fluids the flow rate and hence the minimum time for mixing will have a limit, since the flow becomes turbulent when the Reynolds number is  $> 2300$ .

$$\text{Re} = \frac{ud\rho}{\eta} > 2300 \quad (3.7)$$

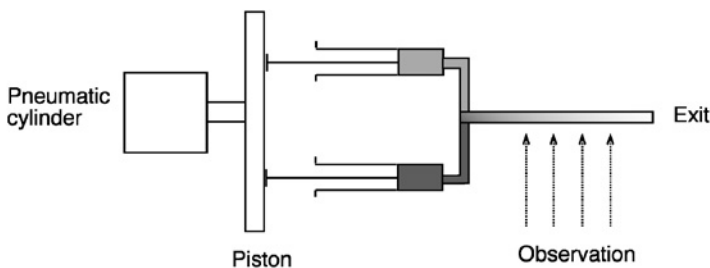


**Figure 3.12** Scheme of an apparatus to measure the kinetics of reactions using continuous flow.

where  $u$  is the flow rate,  $d$  the diameter of the tube,  $\rho$  the density of the reaction medium and  $\eta$  its specific viscosity. Given these limitations, the flow method only enables the study of reactions with half-lives  $>10^{-3}$  sec. In addition, to maintain steady-state conditions throughout the experiment, this technique requires the use of large quantities of reactants.

#### *Stopped flow*

Another common flow technique is the so-called stopped-flow method. This has the advantage of using much smaller amounts of reactants than those in continuous flow. As in the previous method, the solutions containing the reactants are kept in separate syringes, whose pistons are pushed rapidly by the same mechanical system. The reactants are, thus, injected simultaneously into the mixing chamber, where the reaction starts. The whole reaction mixture is then transferred into the observation cell. The flow is interrupted by a stop syringe, which will control the reaction volume studied. This syringe is stopped mechanically by a rigid brake which leads to a rapid slowing of the flow, and which starts the measurement of time for the reaction. The reaction between the well-mixed reactants continues and the changes in the concentrations of reactants and products are followed in real time, normally using spectroscopic methods. The crucial aspect of this technique (Figure 3.13) stems from the fact that small quantities of reactants are mixed rapidly and efficiently, and the kinetics followed electronically using techniques with good time resolution. This technique allows us to follow changes in optical or other properties of solutions with a time resolution in the range of milliseconds to seconds. Figure 3.14 shows a set of results obtained with this method.

### 3.2.2 Relaxation methods

The development of relaxation methods is due principally to Eigen, who was awarded the Nobel Prize for this in 1967. Relaxation methods can be used in the kinetic study of reversible reactions, and are based on the perturbation of a system initially in equilibrium. This perturbation can be induced by rapid variation of any of the parameters that affect the equilibrium constant. These include temperature, pressure, electric field, pH and chemical potential.

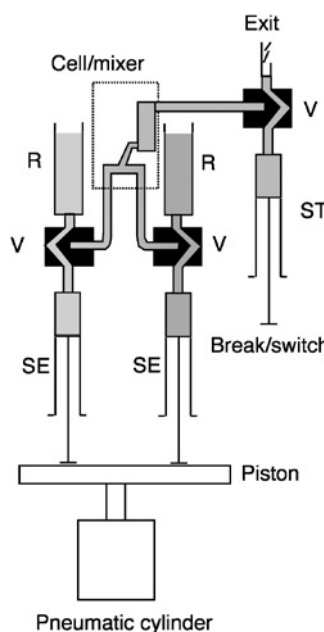


**Figure 3.13** Schematic diagram of an apparatus to measure the kinetics of reactions using stopped flow. The pressure of the pneumatic cylinder controls the rate at which the pistons can be moved to mix the reagents. Detection is made in the mixer/cell, using light absorption or fluorescence emission. R, reactant solution reservoir; V, valve; RS, reactant syringes; SS, stopping syringe.

#### Temperature jump

The most commonly used relaxation technique is based on a temperature jump, using the relationship between temperature and equilibrium constant given by the van't Hoff equation. For efficient perturbation of the equilibrium by this method, the change in the standard enthalpy of solution should be significant. In addition, we need to use a method that heats the system faster than its chemical relaxation time. Normally, this heating is produced by discharge of a high voltage condenser, assuming that the reaction medium does not have a high electrical resistance. This heating method is restricted to solutions in polar solvents of high ionic strength (such as aqueous solutions). The time resolution that can be achieved is around  $10^{-6}$  sec.

Alternatively, it is possible to heat the reaction medium using a high-intensity near-infrared laser pulse (typically,  $>200$  mJ), which will be preferentially absorbed by the solvent—usually in one of its vibrational overtone bands. The time resolution of this technique is limited by the resistance of the cell where the reaction is studied to the high-intensity laser pulse, by the laser pulse and by the relaxation time of the vibrational and rotational states of the solvent in the near-infrared region. For example, for water this relaxation time is  $<10^{-12}$  sec. However, we also have to consider thermal equilibration in the region under study, and, consequently, the time resolution of this technique is of the order of tens of picoseconds.

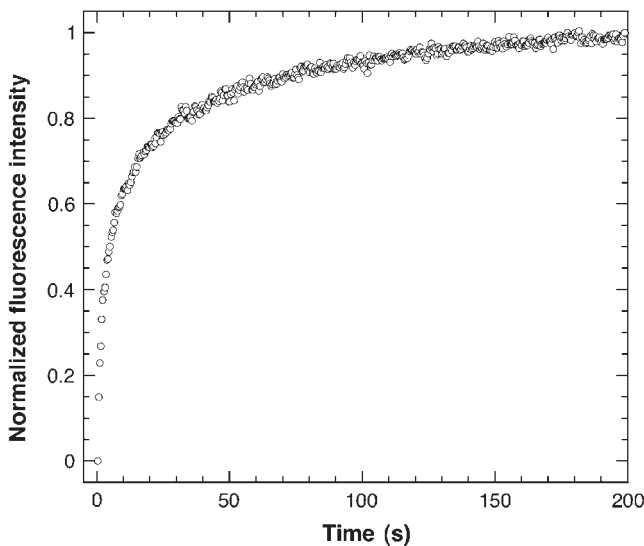


**Figure 3.14** Results obtained by stopped flow for a mixture of bovine serum albumin (BSA) labelled with a fluorescent probe (a rhodamine derivative) with a solution of BSA (without label) and rhodamine green at 35 °C. In the mixture there is energy transfer from the rhodamine green to the labelled protein, when it is irradiated at  $\lambda_{\text{exc}} = 530$  nm. The increase in fluorescence in the labelled protein is followed using  $\lambda_{\text{em}} > 530$  nm. Results were obtained (courtesy of Magda Abreu) in the Coimbra Chemistry Centre using a Hi-Tech SF-61 apparatus.

### Pressure jump

Pressure affects equilibrium constants in a way similar to temperature:

$$\left( \frac{\partial \ln K_{\text{eq}}}{\partial P} \right)_T = -\frac{\Delta V^0}{RT} \quad (3.8)$$

in which the change in molar volume of the reaction is given by  $\Delta V^0 = \sum v_i V_i^0$ , where  $v_i$  is the stoichiometric coefficient and  $V_i^0$  is the partial molar volume of the species  $i$  present in equilibrium in the standard state. The majority of reactions in solution involve changes in volume induced by conformational changes or changes in solvation of the reactants or products, so that they can be affected by change in the pressure. The most common method of inducing a rapid jump in the pressure involves breaking a diaphragm that separates a reaction vessel at atmospheric pressure from one at a much higher pressure. With this, it is possible to increase the pressure by one hundred atmospheres in one hundred microseconds.

### Electric field jumps

Rapid changes in electric field can also be used to perturb chemical equilibria. As high electric fields favour the production of ions from neutral species, it is possible to increase rapidly the dissociation of weak electrolytes. In the most common application of this technique,

a high voltage discharge of a few microseconds' duration is applied and the transient species produced are followed by electrical conductivity measurements.

If the electric field applied is small, dielectric relaxation is obtained. Dielectric relaxation is observed if there is a change in the polarisability of the medium under the influence of an applied electric field. This rule suggests that dielectric relaxation can only be detected in polar media. However, this effect can also be observed in some non-polar materials, since there are contributions to the polarisability owing to collisional effects, i.e. when two non-polar molecules collide, there will be a distortion of the electron clouds and formation of a transient dipole. Dielectric relaxation has a limited application in chemical kinetics, since it reflects the re-orientation of dipoles that occur on a time scale determined by the motions of all the molecules and not specifically those involved in chemical reactions. To obtain chemical information it is necessary to suppress the molecular motions using, for example, rigid matrices as supporting media for the molecules whose reactivity we are trying to study. As such, dielectric relaxation has been used to measure the rate of re-orientation of a whole molecule in simple fluids or the relaxation of segments of polymers.

#### *pH jump*

Acid–base equilibria can be perturbed by a rapid change in the pH of the medium. To induce this change we need to use a species that responds rapidly to a short-duration external stimulus, either transferring a proton to the medium or capturing one from it. Given the extremely high time resolution that can be achieved with pulsed lasers, it is convenient to use these as sources for the external perturbation of the system. To induce the pH jump, we need to introduce into the medium under study a chromophore that has a lesser ionisation constant in its excited state than that in the ground state. Thus, light absorption by the laser pulse will rapidly produce the chromophore excited state which will transfer a proton to the solvent, rapidly increasing the pH of the medium. These conditions are met, for example, by 2-naphthol-6-sulphonate in water, whose  $pK_a$  in the ground state is 9.1, and in the excited state 2, and whose pseudo-first-order rate constant for transferring a proton to water is  $10^9 \text{ sec}^{-1}$ . Using laser pulses with high photon fluxes (*ca.*  $10^{27} \text{ photons cm}^{-2} \text{ sec}^{-1}$ ) it is possible in 10 nsec to increase the  $\text{H}_3\text{O}^+$  concentration with 2-naphthol-6-sulphonate to  $10^{-4} \text{ M}$ , i.e. to decrease the pH of an aqueous solution from pH 7 to  $\sim 4$ .

#### *Ultrasonic absorption*

The observation that a system in chemical equilibrium can absorb ultrasounds dates back to the 1930s. During this period, Bazulin attributed the absorption of ultrasounds by acetic acid to the existence of hydrogen bonds. When an acoustic wave is made to cross a medium, alternate regions of compression and depletion of the particles that comprise it are produced. Eventually, this acoustic wave is attenuated within the space covered, in the same way that an electromagnetic wave is attenuated, because no medium is completely transparent. If species in chemical equilibrium that absorb ultrasound at the frequency used are added to this medium, and if the relaxation for the equilibrium situation is slower than that in the ultrasonic frequency, the regions of compression and depletion will not occur with the same phase or amplitude as the pure solvent. By comparison of the two situations it is possible to obtain the velocity of relaxation of the system in equilibrium. The

time resolution of the system depends upon the frequency of ultrasound used, and can reach  $10^{-11}$  sec.

### 3.2.3 Competition methods

All spectroscopic techniques involve production or deactivation of excited states, normally by the interaction between electromagnetic radiation and molecules. The excited states have finite lifetimes, determined by radiative and non-radiative relaxation to the ground state. Kinetic information can be obtained by comparison of the rates of these processes with those of chemical reactions in competition with them. We will consider two of these processes, involving nuclear spin and electronic excited states. However, the same ideas are applicable to other types of spectroscopic transition.

#### *Nuclear magnetic resonance*

Nuclear magnetic resonance (NMR) is one of the most powerful methods to study the structure and time evolution of species involved in chemical reactions. This spectroscopic method is based on the fact that nuclei with spin (such as  $^1\text{H}$ ) in a magnetic field selectively absorb electromagnetic radiation in the radio frequency region owing to change in the spin orientation. Following this, the excited nuclei can relax to the spin ground state, with emission of energy to the medium. The measurement of these radio frequencies (most commonly given as a chemical shift relative to some reference) and of the rate with which nuclei relax to the ground state constitute the information available by NMR about the molecular structure and dynamics of the sample under study. The energies involved in these nuclear spin transitions are very small and depend upon the magnetic field strength. For example, the  $^1\text{H}$  nucleus in a magnetic field of 4.7 T (Tesla) absorbs radiation of frequency around 200 MHz, which, by the Planck relation  $E = h\nu$  is equivalent to an energy of  $0.08 \text{ J mol}^{-1}$ . As the energy levels involved in these nuclear spin transitions are very close, the probability of relaxation by spontaneous emission to the ground state is very small. Nevertheless, under normal experimental conditions, we do not obtain equal population of the spin levels, which would lead to saturation of the excited state and loss of the resonance signal, because there are non-radiative transitions induced by the fluctuating magnetic field that lead to a loss of this excess energy as thermal energy of the medium. This spin-lattice relaxation has a relaxation time  $T_1$ , known as the longitudinal or spin-lattice relaxation time. Further, when a molecule is subjected to a homogeneous external magnetic field in an NMR experiment, its electrons also respond to this field. If there are unpaired electrons, the magnetic moments of the spins of these electrons are polarised and the magnetic field in the interior of the sample is greater than the applied field. This phenomenon is known as paramagnetism. In contrast, if all the electrons are paired, the external field induces electric currents in the molecule, leading to a polarisation of the electrons in their orbitals, which counteracts the effect of the applied magnetic field. Under these conditions the magnetic field inside the sample is less than the external field, a phenomenon known as diamagnetism. In either case, the local microscopic magnetic environment for the nuclei of these molecules will be different, and when they enter into resonance with the external field, such that different values of applied field will be required, it leads to the

chemical shift in its NMR spectrum. Further effects on the spectra are obtained by the coupling between the nuclear spins of two adjacent nuclei, which leads to splitting of the NMR signals (spin–spin coupling). Apart from these effects, when the oscillating field produced by a nucleus is in phase with that of a neighbour in an identical chemical environment, there can be energy transfer from one nucleus to the other. This leads to deactivation of one of the spin excited states without decreasing the total population of excited states in the process called spin–spin relaxation, given by a relaxation time  $T_2$  known as transversal or spin–spin relaxation time. It is worth noting that all spectroscopic transitions have similar longitudinal and transverse relaxation processes which are responsible for the homogeneous broadening and linewidth of the transitions of isolated molecules, although the experimentally observed spectral linewidths result from inhomogeneous broadening.

A chemical reaction in which there is exchange of one nucleus between two magnetically non-equivalent sites of the reactant can be followed by NMR, provided that the rate of exchange is not so fast relative to  $T_1$  and  $T_2$  that, on the macroscopic scale, we only observe the average of the frequencies of the two sites. Consider a proton NMR experiment in which the difference in resonance frequencies is typically of the order  $10^2$  Hz, corresponding to lifetimes of the order  $10^{-2}$  sec. If the lifetime of the reactant is much longer than this, we will see the NMR signals of both reactant and product without any effect of the exchange, and the NMR experiment corresponds to a conventional kinetic study where we observe the time dependence of the spectra of the reactant and product separately at different phases of the reaction, and so can follow the transformation. However, it is more interesting to study reactions whose rates lie between this limit and that of fast exchange where we see a single signal. In this intermediate case, we see a progressive broadening of the signal as the rate increases, until in the limit the two signals collapse into one, i.e. we are in the fast exchange limit.

From the Heisenberg uncertainty principle, a magnetic nucleus will always give an NMR absorption band with finite width, even if it is not involved in a chemical exchange reaction. The minimum bandwidth can be related to the spin-lattice relaxation time,  $T_1$ , since the mean lifetime of the excited spin state cannot exceed  $T_1$ ,

$$\Delta\nu = \frac{1}{2\pi T_1} \quad (3.9)$$

However, normally the bandwidth at half maximum can be related to the spin–spin relaxation time,  $T_2$ ,

$$\Delta\nu_{1/2} = \frac{1}{\pi T_2} \quad (3.10)$$

In the intermediate chemical exchange condition, the total relaxation frequency is given by the sum of the spin–spin relaxation, as above, together with the relaxation owing to chemical exchange,  $\tau$ , given by,

$$\frac{1}{\tau} = \frac{1}{\tau_A} + \frac{1}{\tau_B} \quad (3.11)$$

where  $\tau_A$  and  $\tau_B$  are the lifetimes of the magnetic nuclei in the magnetically non-equivalent sites A and B, or in other words the reciprocal of their exchange rate constants. In the presence of this exchange, the experimentally observed bandwidth at half maximum will be

$$\Delta v'_{1/2} = \Delta v_{1/2} + \frac{1}{\pi\tau} \quad (3.12)$$

Thus, knowing the value of  $\Delta v_{1/2}$ , which can be obtained by cooling the system such that the exchange becomes slower, and using the value of  $\Delta v'_{1/2}$  obtained experimentally, we can obtain  $\tau$ . If the fractional occupation of the sites is

$$x_A = \frac{\tau_A}{\tau_A + \tau_B} \quad x_B = \frac{\tau_B}{\tau_A + \tau_B} \quad (3.13)$$

we get  $\tau = \chi_A \tau_A = \chi_B \tau_B$ . As was already indicated, the time resolution of the application of the NMR technique is limited by the difference between the resonance frequencies of the magnetic nuclei when the velocity of exchange is very slow, which for protons is not normally  $> 100$  MHz; from this, the lifetime of relaxation processes experimentally accessible must be  $> 10^{-4}$  sec.

In the limit of fast exchange between two species of resonance frequencies  $v_p$  and  $v_d$ ,  $k[\text{reagents}] \gg 2\pi|v_p - v_d|$ , where  $k$  is the exchange rate constant, it is still possible, in certain circumstances, to determine the exchange rate constant. We will consider the case of a process in the presence of a paramagnetic species, which is of particular importance to electron transfer reactions. When the mean lifetimes of a paramagnetic species ( $p$ ) and a diamagnetic one ( $d$ ) are considerably greater than their relaxation times  $T_1$ , the system can be treated as a two-site system. In the particular case of a first-order electron transfer reaction relative to each of the reactants, the mean bandwidth for the mixture of reactants

$$(\Delta v_{1/2})_{dp} = \frac{1}{\pi(T_2)_{dp}} \quad (3.14)$$

where the width at half-height in Hertz for an absorption band of Lorenzian shape, is related to the rate constant for electron exchange.  $k_{\text{ex}}$ , by

$$(\Delta v_{1/2})_{dp} = x_p (\Delta v_{1/2})_p + x_d (\Delta v_{1/2})_d + x_p x_d \frac{4\pi(v_p - v_d)^2}{k_{\text{ex}}([p] + [d])} \quad (3.15)$$

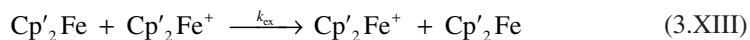
where  $x_p$  and  $x_d$  indicate the mole fractions of the paramagnetic and diamagnetic species, respectively. This expression can be written as

$$k_{\text{ex}} = \frac{4\pi x_p x_d (v_p - v_d)^2}{((\Delta v_{1/2})_{dp} - x_p (\Delta v_{1/2})_p - x_d (\Delta v_{1/2})_d)([p] + [d])} \quad (3.16)$$

from which it can be shown that from the resonance frequencies of the diamagnetic and paramagnetic species and the respective widths at half-height

$$(\Delta v_{1/2})_p = \frac{1}{\pi(T_2)_p} \quad (\Delta v_{1/2})_d = \frac{1}{\pi(T_2)_d} \quad (3.17)$$

and information on the bandwidth measured for the mixture of reactants, we can calculate the rate constant for electron exchange. Figure 3.15 shows some results obtained using the technique of NMR line broadening [15] for the system



where  $\text{Cp}'$  represents the methylated cyclopentadienyl ligand. It should be noted that this technique can be applied because the decamethylferrocinium ion,  $\text{Cp}_2\text{Fe}^+$ , is paramagnetic, with  $v_p = -18667.0$  Hz with  $(\Delta v_{1/2})_p = 274.9$  Hz under the experimental conditions

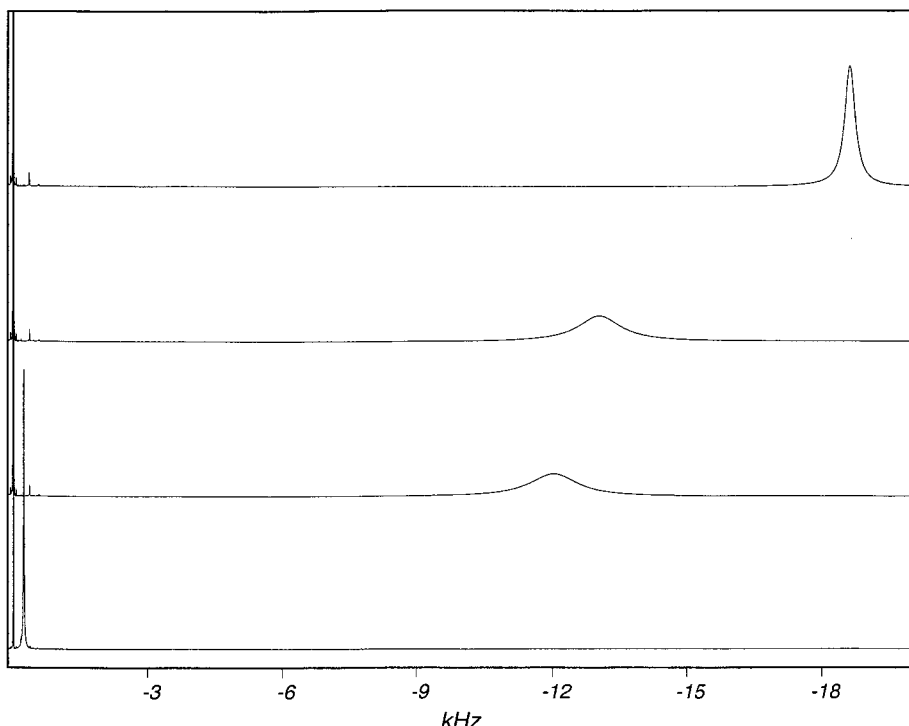


**Figure 3.15** NMR spectra obtained for reaction (3.XIII) for  $\text{Cp}'_2\text{Fe}^+$  (upper spectrum),  $\text{Cp}'_2\text{Fe}$  (lower spectrum, while the intermediate spectra show mixtures of these reactants; obtained on a Varian – Unity 500 MHz NMR spectrometer of the Faculty of Science and Technology, University of Coimbra. (Courtesy of M.I. Silva, J.R. Rodrigues, R. Brito.)

**Table 3.8**

Experimental parameters and rate constants for the self-exchange between decamethylferrocinium hexafluorophosphate and decamethylferrocene in acetone-d<sub>6</sub> at 37 °C

Concentration <sup>a</sup> (mM)	$v_d$ (Hz)	$(\Delta v_{1/2})_{dp}$ (Hz)	$x_p^b$	$x_d^b$	$k_{ex}$ (mol <sup>-1</sup> dm <sup>3</sup> sec) <sup>-1</sup>
38.55	-12,020	1120.4	0.6484	0.3516	$2.80 \times 10^7$
39.09	-12,042	1118.0	0.6496	0.3504	$2.80 \times 10^7$
39.87	-13,068	1042.0	0.7038	0.2962	$2.78 \times 10^7$

<sup>a</sup>Total concentration, [Cp'<sub>2</sub>Fe<sup>+</sup>] + [Cp'<sub>2</sub>Fe].

<sup>b</sup>Mole fraction, calculated from the corresponding chemical shifts:  $x_p = |v_{dp} - v_p| / |v_d - v_p|$  or  $x_d = |v_{dp} - v_d| / |v_d - v_p|$ .

used, while the decamethylferrocene, Cp'<sub>2</sub>Fe, is diamagnetic and, under the same conditions, has  $v_d = 238.4$  Hz with  $(\Delta v_{1/2})_d = 17.3$  Hz.

From the NMR spectra shown in Figure 3.15 it is possible to extract the data presented in Table 3.8 and obtain the exchange rate constants indicated. The exchange rate constant obtained for reaction (3.XIII) is  $k_{ex} = 2.8 \times 10^7$  mol<sup>-1</sup>dm<sup>3</sup>sec<sup>-1</sup> at 37 °C, which is in agreement with the values of  $2.9 \times 10^7$  mol<sup>-1</sup>dm<sup>3</sup>sec<sup>-1</sup> and  $1.8 \times 10^7$  mol<sup>-1</sup>dm<sup>3</sup>sec<sup>-1</sup> determined by Wahl and co-workers [16] at 35 °C and by Weaver *et al.* [17] at 25 °C, respectively.

#### Luminescence quenching

Another technique that is based on competition in the measurement of lifetimes in the absence and presence of chemical reactions is luminescence quenching. Luminescence refers to light emission by electronically excited molecules. When this emission is between states of the same spin multiplicity, it is called fluorescence, while when it is between states of different spin multiplicity, it is termed phosphorescence. The technique of luminescence quenching can be applied to either of these processes, although it is more common with the former. We will only treat explicitly the case of fluorescence quenching. The fluorescence intensity is directly proportional to the number of electronically excited species that emit light in their transition from the electronically excited state to the ground state in the same way that light absorption by the ground state leading to an electronically excited state (A<sup>\*</sup>) is proportional to the concentration of the species in the ground state. The ratio between the number of photons emitted and the number of photons absorbed defines the quantum yield of fluorescence of the system,  $\Phi = I_{em} / I_{abs}$ . In addition to emitting light, the electronically excited state has various other competing pathways available to lose its excitation energy that have been previously mentioned: non-radiative transitions to the ground state or to another state of lower energy with the partial or total conversion of its electronic energy into thermal energy, or chemical reaction with another species:



In the absence of quencher, the quantum yield of emission is

$$\Phi_0 = \frac{k_F}{k_F + k_{nr}} \quad (3.18)$$

In the presence of quencher the quantum yield is reduced due to the presence of an additional competing pathway

$$\Phi = \frac{k_F}{k_F + k_{nr} + k_Q [Q]} \quad (3.19)$$

As the concentration of the quencher is normally much greater than that of the electronically excited species,  $[Q]$  can be treated as a constant. The ratio between the emission quantum yields in the absence and presence of quencher is equal to the ratio between the emission intensities under the same conditions

$$\frac{I_0}{I} = \frac{k_F + k_{nr} + k_Q [Q]}{k_F + k_{nr}} \quad (3.20)$$

This expression is similar to that which will be deduced in the next chapter for the yields of products of parallel first-order (or pseudo-first-order) reactions, such as reactions (3.XIV)–(3.XVI). From the definition of experimental molecular fluorescence lifetimes  $\tau_0 = 1/(k_f + k_{nr})$ , the previous equation reduces to

$$\frac{I_0}{I} = 1 + \tau_0 k_Q [Q] \quad (3.21)$$

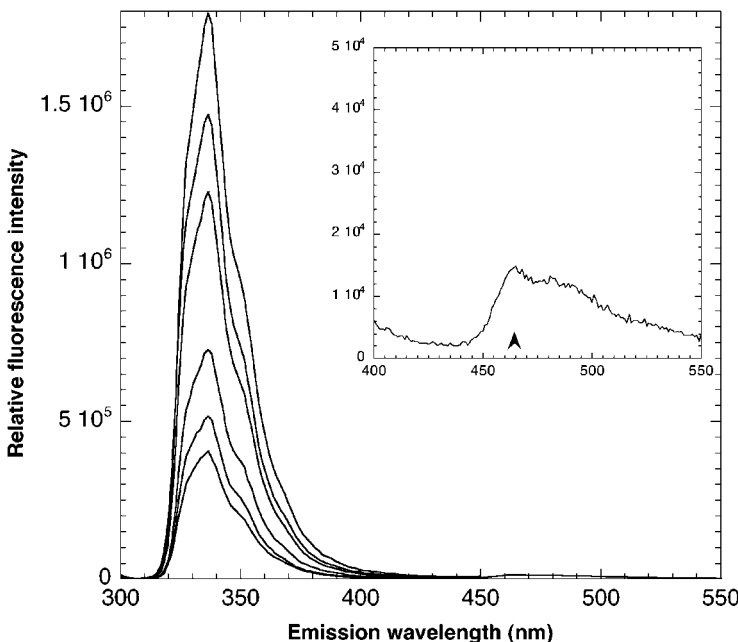
which is the expression obtained in 1919 by Stern and Volmer. Through readings of the fluorescence intensities in the absence of the quencher and the presence of known concentrations of quencher, it is possible to obtain  $k_Q$  knowing  $\tau_0$  or vice versa. This method allows us to obtain rate constants of very fast photochemical reactions, including ones close to or above the diffusion-controlled limits in liquid solution. In Figure 3.16 results are presented for the decrease in naphthalene fluorescence at 337 nm upon increasing the concentration of biacetyl. In this figure we can also see the appearance of biacetyl fluorescence at 470 nm, whose  $S_1$  state is formed by energy transfer.

Figure 3.17 shows the corresponding Stern–Volmer plot obtained for energy transfer from the lowest energy singlet state of naphthalene ( $E_{S1} = 385 \text{ kJ mol}^{-1}$ ) to biacetyl ( $E_{S1} = 267 \text{ kJ mol}^{-1}$ ) [18]. From the slope of the Stern–Volmer plot the product  $k_Q \tau_0 = 268 \text{ M}^{-1}$  is obtained, from which, using the experimental fluorescence lifetime  $\tau_0 = 18.2 \text{ nsec}$  for naphthalene in benzene, we determine  $k_Q = 1.5 \times 10^{10} \text{ M}^{-1} \text{ sec}^{-1}$ .

### 3.2.4 Methods with enhanced time resolution

#### *Flash photolysis*

The development of flash photolysis is due mainly to the work of Norrish and Porter. However, it was the development of the laser in 1960 that allowed this technique to attain



**Figure 3.16** Quenching of fluorescence of a solution of naphthalene (0.01 M) in benzene by biacetyl (<0.01 M). Under these conditions, irradiation at 300 nm leads to negligible light absorption by biacetyl. Results obtained on a SPEX Fluorolog 3 at the Coimbra Chemistry Centre. Accompanying the decrease in the naphthalene emission at 337 nm, an increase is observed in the biacetyl emission at 470 nm. (Courtesy of Marta Piñeiro.)

its full potential. The contributions of Norrish and Porter earned them the Nobel Prize in chemistry in 1967. In fact this technique has great versatility and has been used to study short-lived transients such as radicals, biradicals, electronically excited states, carbenes, exciplexes, radical ions, organic and inorganic species in unstable oxidation states, etc.

The conditions which determine whether flash photolysis can be used to study a given chemical system are: (i) a precursor of the species of kinetic interest has to absorb light (normally from a pulsed laser); (ii) this species is produced on a timescale that is short relative to its lifetime in the system. Current technical developments make it easy to study timescales of nanoseconds for production and analysis of species, and the use of instrumentation with time resolution of picoseconds is already fairly common. In certain specific cases, as we will see in the last part of this chapter, it is possible to study processes on timescales greater than a few femtoseconds. Once the species of interest has been produced, it is necessary to use an appropriate rapid detection method. The most common technique involves transient optical absorption spectroscopy. In addition, luminescence has been frequently used to detect transients, and other methods such as time-resolved resonance Raman spectroscopy and electrical conductivity have provided valuable information in certain cases.

Figure 3.18 shows a set-up for flash photolysis using absorption spectroscopy to detect transients formed on photolysis.

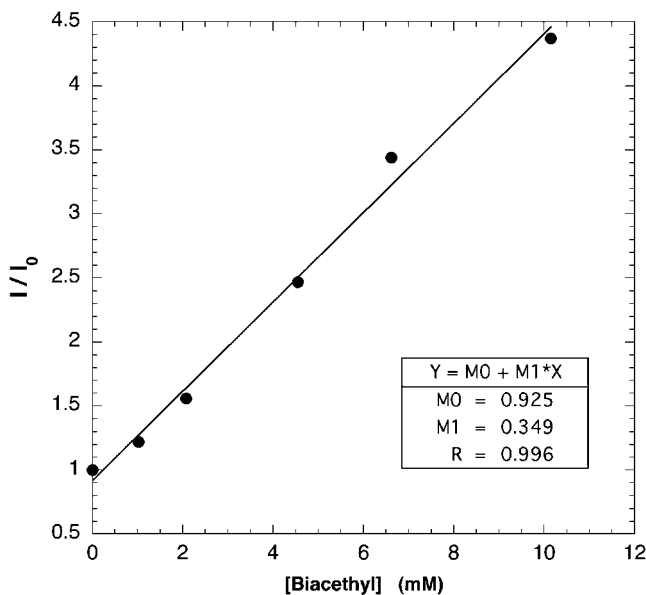


**Figure 3.17** Stern–Volmer plot for energy transfer between naphthalene and biacetyl under the conditions of Figure 3.16.

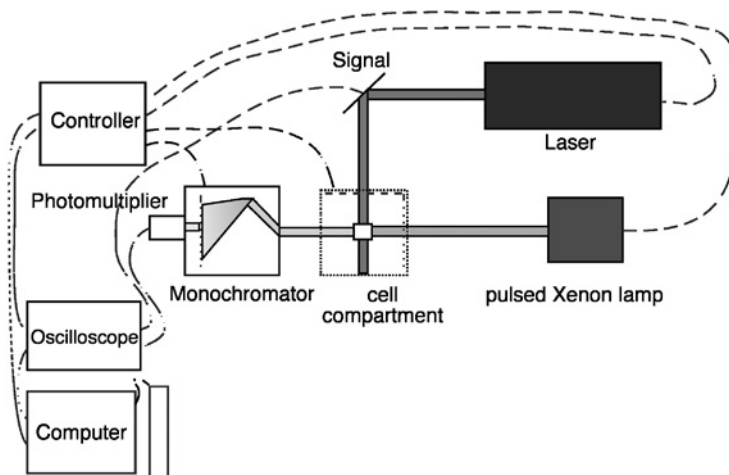


**Figure 3.18** Schematic diagram of a flash photolysis system.

To obtain the decay of a transient, the analysing light is focussed on the sample contained in a cuvette. The initial intensity of the analysing light,  $I_0$ , is detected at the analytical wavelength  $\lambda$  by a photomultiplier. The laser is then discharged. A small part of the laser beam is diverted to a detector that triggers a transient digitiser to start measurement of time and signal acquisition. The rest of the light is absorbed by the sample. The signal

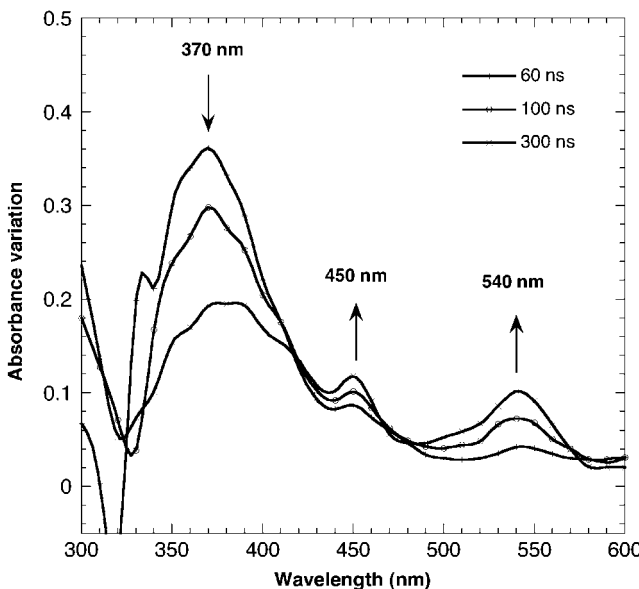


**Figure 3.19** Time-resolved spectra for the system anthraquinone + trimethoxybenzene in acetonitrile, excited at 355 nm, under conditions where the quinone absorbs. The spectra were recorded 60, 100 and 300 nsec after irradiation with the laser pulse. Results obtained on an Applied Photophysics LKS 60 flash photolysis apparatus in the Coimbra Chemistry Centre. (Courtesy of C. Serpa.)

registered by the digitiser is the light intensity of wavelength  $\lambda$  transmitted in the presence of the transient,  $I(\lambda, t)$ , which depends upon time owing to its decay in the reaction of interest. The signal recorded by the digitiser is transferred to the computer and the time profile of the absorbance of the transient at wavelength,  $\lambda$ , is calculated

$$A(\lambda, t) = \log \frac{I_0(\lambda)}{I(\lambda, t)} \quad (3.22)$$

In these experiments the decay curve of transient absorbance at a given wavelength is studied in real time. It is also possible to obtain time-resolved absorption spectra of transients, recording their absorbance at pre-determined times:  $t_1, t_2, \dots, t_n$ .

Figure 3.19 shows transient absorption spectra obtained following excitation of anthraquinone ( $5.1 \times 10^{-4}$  M) at 355 nm in the presence of trimethoxybenzene ( $1.3 \times 10^{-4}$  M). Note the disappearance of the absorption of the triplet state of the anthraquinone at 370 nm, formed following excitation at 355 nm with the 8 nsec laser pulse, with the simultaneous formation of two new bands at 450 and 540 nm.

It is possible to follow the disappearance of the initial intermediates at one analytical wavelength and the formation of new ones at other wavelengths, as can be seen in Figure 3.20. The instrumentation involved requires using a sequence generator for coordination of the various steps which proceed the signal acquisition: triggering the transient

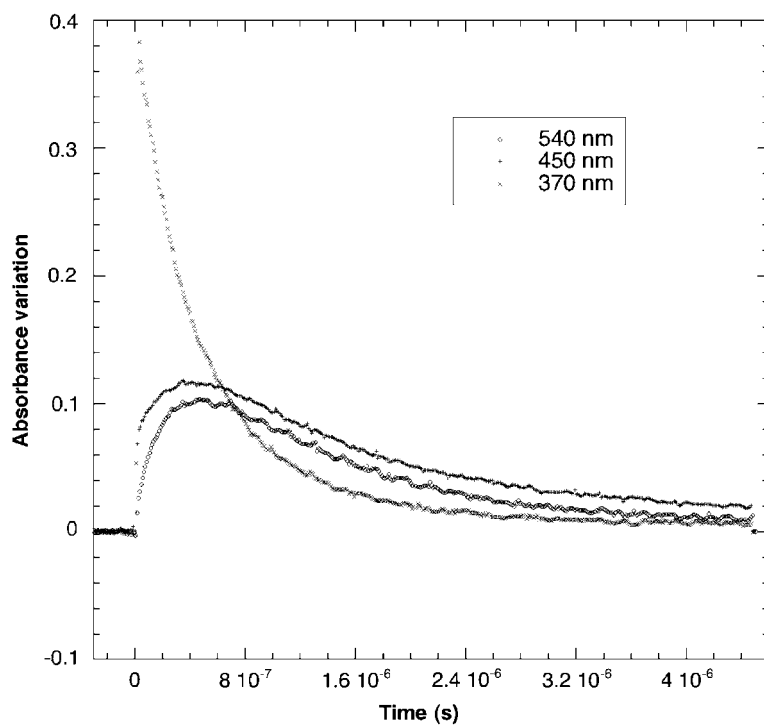


**Figure 3.20** Kinetic traces of signals observed at 370, 450 and 540 nm, corresponding to the anthraquinone triplet state, trimethoxybenzene radical cation and anthraquinone radical anion, respectively. The decay of the triplet state is pseudo-first-order, and has the same lifetime as formation of the radical ions. Subsequently, these compounds decay by slower processes. (Courtesy of C. Serpa.)

digitiser, opening the slits, starting a pulsed analysing lamp (to increase sensitivity), reading  $I_0$ , pulsing the laser, reading  $I(\lambda,t)$  and then closing the slits.

#### Pulse radiolysis

In flash photolysis, transient species are produced by absorption of light, normally from a pulsed laser. This specifically excites the solute. The interaction of high-energy radiation such as X-rays,  $\gamma$ -rays or high-energy electron beams with matter is termed radiation chemistry. High-energy radiation induces ionisation, which can subsequently lead to formation of either free radicals or excited states. Absorption of high-energy radiation is not specific, and will be predominantly by the species present in the greatest amount. For solutions, this is the solvent. Thus, radiation chemistry depends upon the solvent, and provides a route to specifically generate either charged species or excited states, depending upon the solvent used. Pulse radiolysis is the radiation chemistry equivalent of flash photolysis, and provides a valuable complementary technique. Normally, a pulsed beam of high-energy electrons (energies of several MeV) produced by a linear accelerator is used as the radiation source and, as in flash photolysis, transient absorption spectroscopy

is used to characterise reactive intermediates both in terms of their spectra and kinetics. The basic techniques are similar, the main differences stem from the fact that we are considering reactions of solvent-derived transients with solutes, and that, owing to the need for large-scale equipment, there are relatively few places where these experiments can be carried out. However, these are compensated for by the fact that many of the experiments cannot be easily carried out by other fast reaction methods.

As an example, we will consider the characterisation of triplet states of conjugated organic polymers. Pulse radiolysis of aromatic solvents such as benzene produces mainly excited triplet and singlet states in the ratio 3:1. By incorporating an appropriate energy acceptor with high-inter-system crossing yields, it is possible to capture this excitation energy and specifically produce excited triplet states. This species can then act as triplet donor and populate triplet states of other species by energy transfer, even though these may not be readily accessible by photochemical routes because of low yield of inter-system crossing from singlet states.

Figure 3.21 shows the transient spectra observed following pulse radiolysis of an argon-saturated solution of biphenyl (10 mM) and the conjugated polymer MEH-PPV in benzene solution.

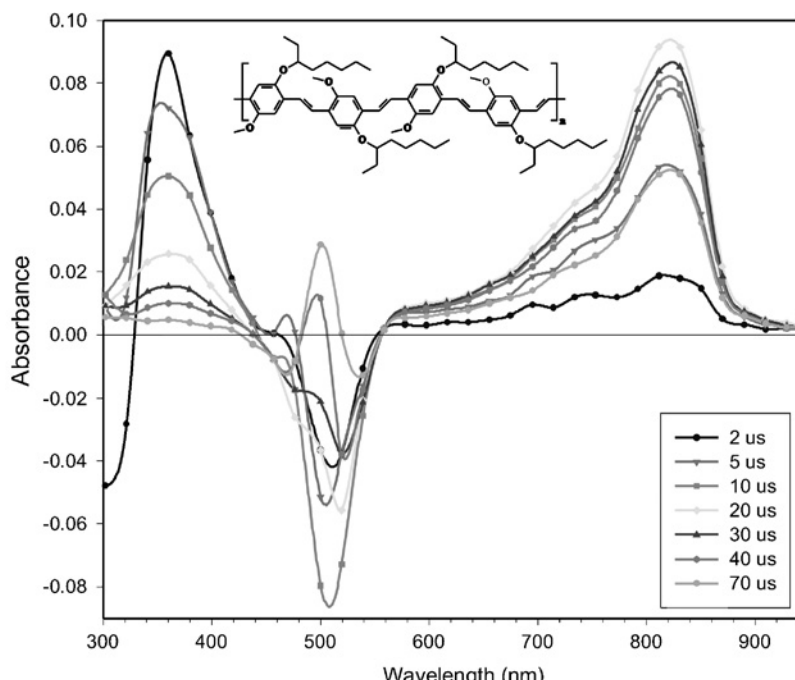


**Figure 3.21** Time evolution of the transient absorption spectra following pulse radiolysis of argon-saturated solutions of MEH-PPV in benzene in the presence of biphenyl sensitiser. Reprinted from AP Monkman, HD Burrows, MG Miguel, I Hamblett, ES Navaratnam, Measurement of the  $S_0-T_1$  energy gap in poly(2-methoxy,5-(2'ethylhexoxy)-*p*-phenylenevinylene), MEH-PPV, by triplet-triplet energy transfer, *Chem. Phys. Lett.* 307 (1999) 303–309. (Copyright 1999, with permission from Elsevier.)

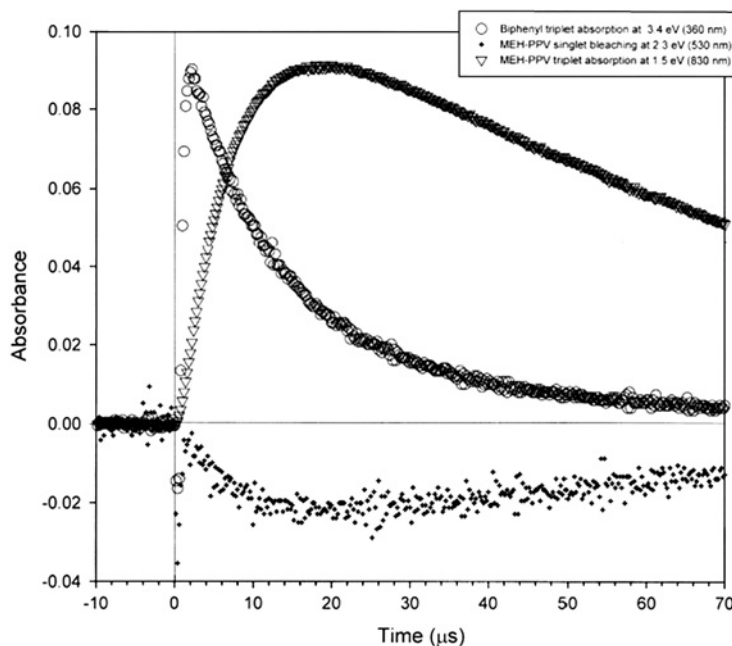
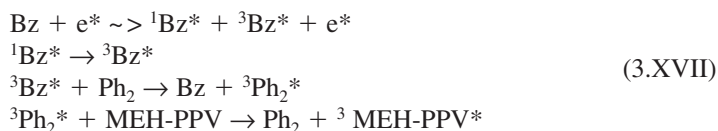


**Figure 3.22** Decay and grow-in of the various spectral features seen in Figure 3.21. Reprinted, with permission, from the same source.

In this experiment, the triplet state of biphenyl is initially formed by energy transfer from the solvent leading to the absorption around 360 nm. This then transfers its triplet energy to the polymer, leading to a new absorption at 830 nm owing to the triplet state of the polymer, and depletion of the ground-state absorption band of the polymer at 530 nm. The overall kinetic scheme is



while the kinetic traces for decay of the biphenyl triplet at 360 nm and formation and decay of the polymer triplet at 830 nm and bleaching at 530 nm are shown in Figure 3.22.

#### *Time-resolved photoacoustic calorimetry*

Time-resolved photoacoustic calorimetry (PAC) is a technique complementary to flash photolysis. In flash photolysis we study transient species through their radiative processes (light absorption or emission) in the wavelength region analysed. In contrast, in photoacoustic calorimetry we study the non-radiative transitions (vibrational relaxation, physical quenching of excited states or chemical reactions), again normally induced by excitation

with a pulsed laser. These transitions correspond to the conversion of absorbed light energy into thermal energy, leading to production of thermal pulses (or heat waves) within the sample. The heat liberated by the transient species is directly proportional to the increase in temperature of the sample [19]

$$H_{\text{ther}} = C_p V_{\text{irr}} \rho \Delta T \quad (3.23)$$

where  $C_p$  is the heat capacity of the solution at constant pressure,  $V_{\text{irr}}$  is the volume irradiated by the laser pulse and  $\rho$  is the density of the solution. At constant volume, the pressure and temperature are related

$$\Delta P = \frac{\alpha}{\kappa_T} \Delta T \quad (3.24)$$

Here,  $\alpha$  is the coefficient of thermal expansion and  $\kappa_T$  is the adiabatic compressibility of the solution. The ratio  $\alpha/\kappa_T$  is also known as the coefficient of thermal pressure or internal pressure of the solvent. From eqs. (3.23) and (3.24) we obtain the transient pressure produced by the conversion of absorbed light into thermal energy

$$\Delta P = \frac{1}{C_p A l \rho} \frac{\alpha}{\kappa_T} H_{\text{ther}} \quad (3.25)$$

where  $A$  is the area of the sample irradiated and  $l$  its thickness. The acoustic wave produced in this process can be detected by coupling a high-frequency transducer to the irradiated sample cell, using the set-up given in Figure 3.23. The transducer or microphone converts the pressure that acts on it into a voltage

$$V_t = c_t \frac{1}{C_p A l \rho} \frac{\alpha}{\kappa_T} H_{\text{ther}} \quad (3.26)$$

where  $c_t$  is an experimental constant.

In photoacoustic experiments, low absorbances must be used for all for solutions to ensure homogeneous light absorption within the sample volume  $V_{\text{irr}}$ . In the first experiment, an acoustic wave is measured for a solution containing a photoacoustic reference material, which converts all the light energy absorbed into thermal energy in a short time compared to the frequency of the transducer. Following this, the acoustic wave of the solution containing the sample under study is measured. This sample must have a lifetime similar to the frequency of the transducer and also the same absorbance as the reference solution at the laser wavelength. Finally, the acoustic wave of the solvent used is determined. This solvent wave is subtracted from those of the reference and the sample.

In Figure 3.24, acoustic waves are shown for a reference and a sample, both corrected for solvent absorption. From the computational analysis of these waves, it is possible to calculate, from the differences in the phase and amplitude, the lifetime of the species under

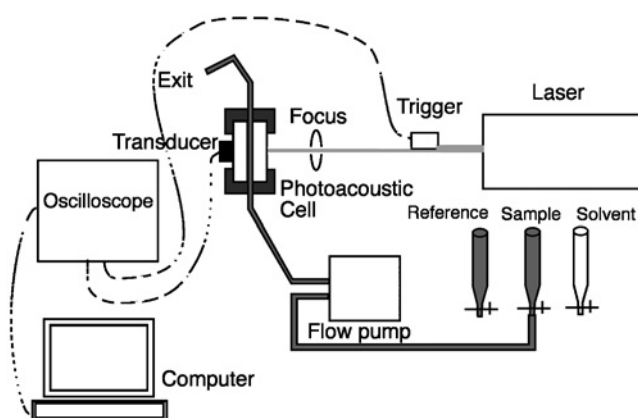


**Figure 3.23** Schematic diagram of an apparatus to study photoacoustic calorimetry, using a front-face configuration.

study together with the enthalpy of the reaction involved. The calculation from this calorimetric data requires the quantum yield of the process involved. The biggest limitation of this technique stems from the fact that it does not allow identification of the transients whose heats of reaction and lifetimes are being measured.

#### *Single photon counting*

The lifetime of a fluorescent species can be determined from the decay of its fluorescence intensity as a function of time. The technique of time-correlated single photon counting (TCSPC), used to determine fluorescence lifetimes, is based on the fact that the probability of time distribution of a single emitted photon follows the statistical distribution of all the photons emitted. If we study a large number of experiments in which we observe only a single photon emitted in each case, the probability distribution for the emission of all the single-photon events provides the distribution of intensity, over time, for all the photons emitted. This method has a high time resolution, allows averaging over many events, and so can be used with relatively weak fluorophores, and allows time resolution in the nanosecond and picosecond range. In addition, the statistical advantage makes this an excellent method for studying multi-exponential or non-exponential processes.

Typically, a TCSPC system has a pulsed excitation source, which could be a pulsed laser, a spark lamp containing a gas (normally N<sub>2</sub> or D<sub>2</sub>) at low pressure (between 0.2 and 1 bar) to which is applied a high voltage (between 4 and 8 kV), or, more recently, light-emitting diodes (nano-LEDs). A typical TCSPC apparatus is shown schematically in Figure 3.25, in which a spark lamp controlled by a thyratron is used, which is the factor that limits the time resolution possible with the set-up. Upon ionisation of the gas in the spark lamp, a short duration pulse of photons is produced. These follow two paths: path (i) passes through a fibre optic connected and is detected by a photomultiplier (FM1), generating an electric signal that is correlated with the excitation pulse. After passing through

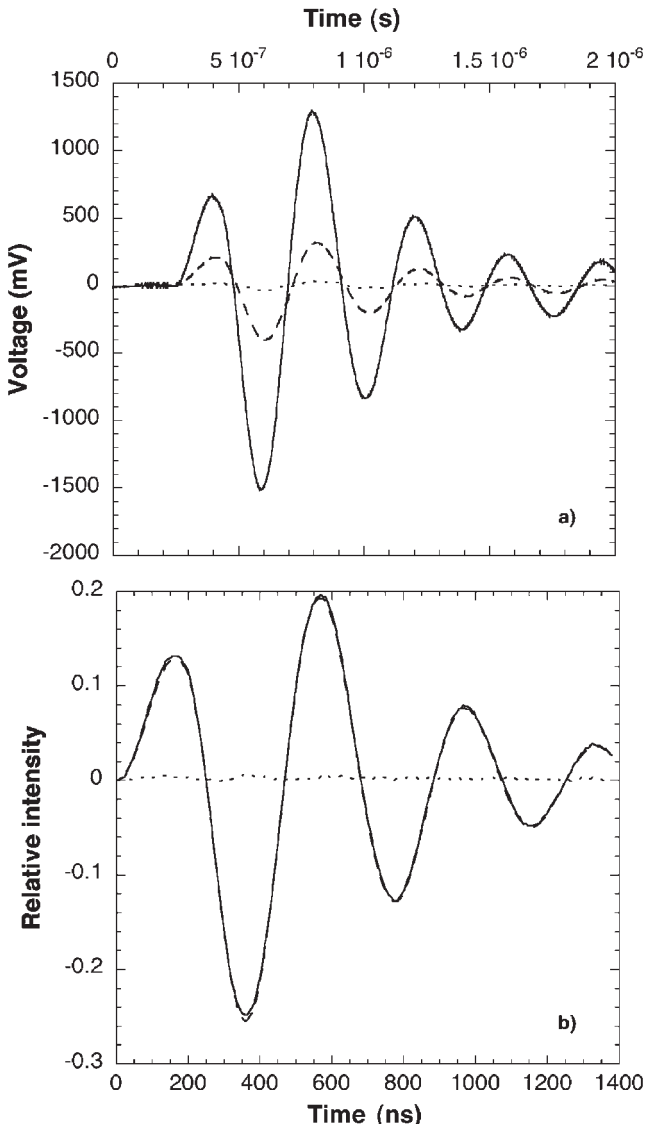


**Figure 3.24** (a) Photoacoustic waves of references (solid line) and sample (dashed line) containing benzophenone and benzhydrol in benzene (dotted line), measured by a 2.25 MHz transducer following excitation by a pulse from a nitrogen laser ( $\lambda_{\text{irr}} = 337$  nm). (b) Comparison between the calculated and experimental waves when two consecutive exponentials are used to describe this process. The dotted line is the difference between the experimental and calculated waves. The first exponential corresponds to the rapid formation of the triplet state of benzophenone, and the second to the abstraction of a hydrogen atom from benzhydrol by benzophenone triplet. Results obtained with the photoacoustic calorimeter in the Coimbra Chemistry Centre. (Courtesy of Monica Barroso.)

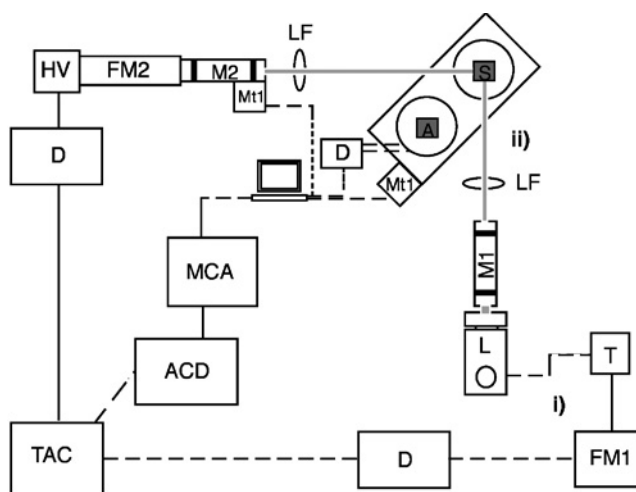
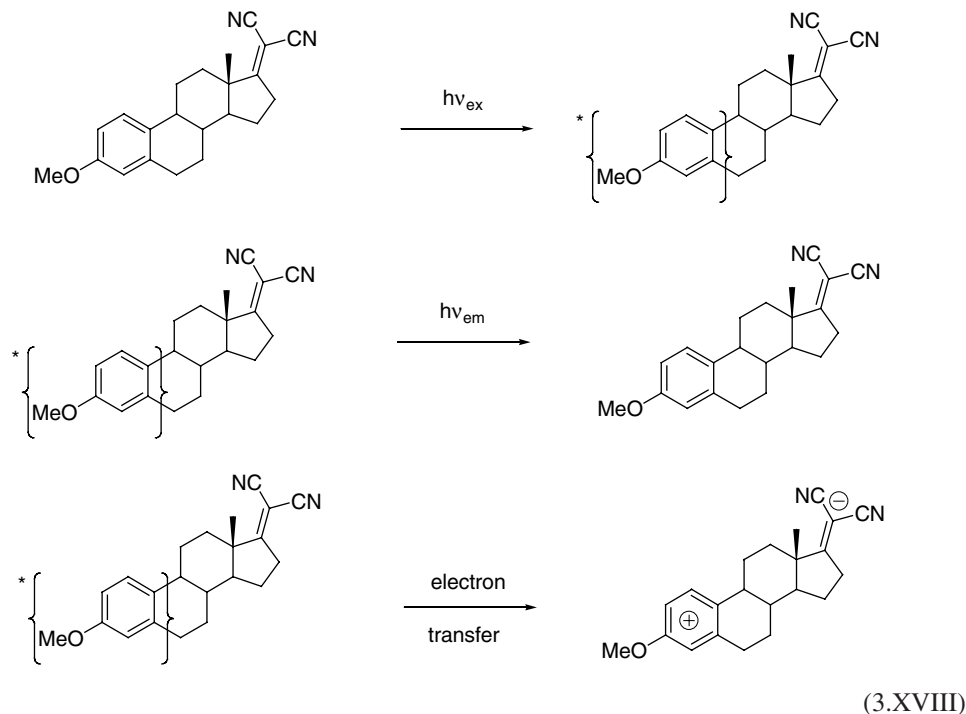


**Figure 3.25** Set-up for the nanosecond TCSPC apparatus in the Coimbra Chemical Centre. D, discriminator; L, lamp; T, thyatron; TAC, time-to-amplitude converter; ADC, analogue-digital converter; MCA, multichannel analyser; FM, photomultiplier; HV, high voltage; Mt, motor; LF, focussing lens; A, sample solution; S, scattering solution; M1 and M2, excitation and emission monochromators; Δ, control unit for motors Mt1 and Mt2 and for cell holder temperature.

the discriminator, this is sent to a time-to-amplitude converter (TAC), which starts the charging of a condenser, thus initiating a voltage ramp that varies linearly with time. This is known as the START channel. The second simultaneous beam (ii) passes through the monochromator M1 to select the appropriate excitation wavelength. This beam then passes alternatively into a scattering solution, to produce the excitation profile, and the sample being analysed. This alternation between the sample and the reference is carried out using a stepping motor driving two sample cell holders fused together alternately into the beam, thus leading to automatic data collection from the two samples. The fluorescence emission or scattering of the lamp profile is observed at 90° by monochromator M2 at a selected wavelength ( $\lambda_{\text{em}}$ ). The emitted photon is detected by photomultiplier FM2 in the STOP channel, producing an electric signal, which, following time discrimination, is sent to the TAC to stop the charging of the condenser. The voltage amplitude measured in the condenser is proportional to the time difference between the START and STOP signals. This pulse generated in the TAC is sent to an analogue to digital converter (ADC), and gives a value corresponding to the time difference between the photon emitted and the excitation pulse. Each count is then stored in the appropriate time channel of a multi-channel analyser (MCA). These signals are distributed and accumulate in the 1024 channels of the MCA, which is interfaced to a computer, and after each cycle of typically 1000 counts, the decay is stored on the computer. A sufficient statistical distribution of counts as a function of channel number is obtained after  $n$  repetitions/cycles (typically 10,000 counts), to allow an accurate analysis of the decay time.

Figure 3.26 shows the application of this technique in the determination of the lifetimes of 3,4-dimethoxybenzene and of the molecule shown in mechanism (3.XVIII).



Note that this molecule has two parts with different functionalities, between which there is photoinduced electron transfer, in addition to the other energy dissipation channels already existing in 3,4-dimethoxybenzene. From the difference in lifetimes between the two molecules, we can determine the rate constant of intra-molecular electron transfer

$$k_{\text{et}} = \frac{1}{\tau_{\text{DA}}} - \frac{1}{\tau_{\text{D}}} \quad (3.27)$$

With the above system, the rate constant of photo-induced electron transfer is  $2.7 \times 10^9 \text{ sec}^{-1}$ . This intra-molecular transfer is expected to occur at the minimum separation between the limits of the aromatic ring and the  $\text{C}=\text{C}(\text{CN})_2$  group, which is about 6.5 Å.

### Femtochemistry

In the first chapter, it was indicated that, intrinsically, the transition state has a virtual existence, since by definition it corresponds to a maximum, at infinitesimally small times, of potential energy on the pathway that separates the reactants and the products. To obtain information on the reaction process, close to the region of the transition state, it is necessary to resort to a technique with an extraordinarily high time resolution. Some idea of this

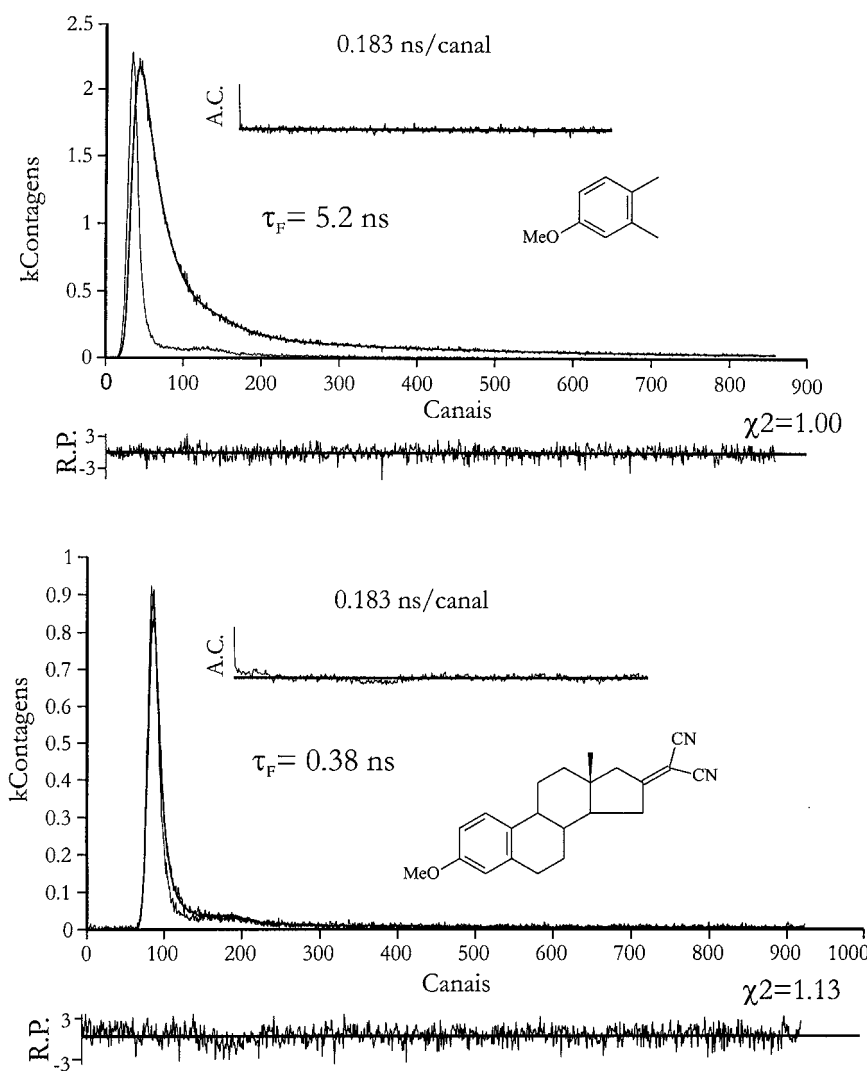


**Figure 3.26** Fluorescence decay of the two molecules studied in acetonitrile. The light trace represents the time profile of the excitation lamp at 281 nm, which is needed for the deconvolution of the signal. In the lower part of each graph, results are shown of the difference between the experimental signal and that calculated from the decay (using the lifetime indicated), convoluted with the lamp signal. Results obtained with the TCSPC system in the Coimbra Chemical Centre. (Courtesy of J. Seixas de Melo.)

time resolution can be obtained by considering that the separation of the fragments of a photo-induced molecular cleavage occurs typically with a velocity  $1000 \text{ m sec}^{-1}$ . Thus, to determine the positions of the fragments when these are separated by 10 pm, which corresponds to 10% of a bond length, it is necessary to make measurements with a time

resolution better than  $10^{-14}$  sec. Although experiments are in progress with attosecond lasers, the most reliable technology currently available produces laser pulses with duration of  $\sim 5\text{--}6$  fsec. This provides possibilities for “transition state spectroscopy”. Many of the pioneering works on the use of lasers in the study of ultrafast events are due to groups, such as those of C.V. Shank at Bell Telephone Laboratories (now ATT). However, the development of femtochemistry to map the reaction coordinate and the spectroscopy of the transition state is mainly due to A. Zewail, who was awarded the Nobel Prize in chemistry for this work in 1999 [20].

A good illustration of the spectroscopy of the transition state is given by the photodissociation of ICN. A low-density beam of ICN molecules is irradiated with a 307 nm laser pulse, exciting the molecules to a repulsive electronic excited state. In this state each molecule dissociates into I and CN. The production of CN can be followed by its fluorescence, induced by an analysing laser pulse at 388.9 nm, which is in resonance at this wavelength with the energy separation between the CN ground state and a fluorescence-excited state. The analysing pulse is delayed relative to the photolysis pulse by variable time intervals, which are controlled by modifying the distance covered by the pulses. This so-called “pump-probe” technique is very commonly used to study ultrafast processes on the picosecond and sub-picosecond time scale. We should remember that with the velocity of light *in vacuo* ( $2.998 \times 10^8$  m sec $^{-1}$ ) light travels about 0.3 mm in a picosecond, and that this distance will depend on the medium used. The intensity of the induced fluorescence of CN is equal to zero until this fragment is separated by  $\sim 600$  nm from the iodine atom. The analysing pulse can be tuned to a slightly longer wavelength, 389.5 nm, to see what happens when the bond is only partially broken. The intensity of the induced fluorescence

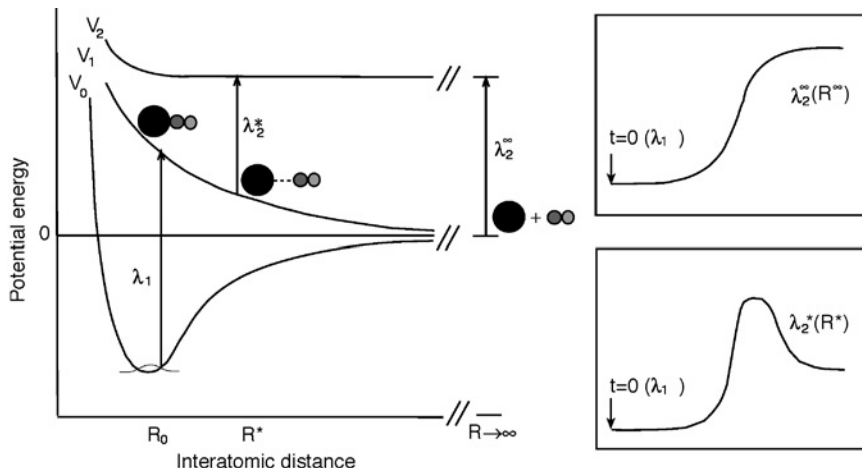


**Figure 3.27** Dissociation of the molecule of ICN by excitation with a  $\lambda_1 = 307$  nm laser pulse, and its analysis in real time by excitation with an analysing pulse of variable wavelength,  $\lambda_2$ , for an emissive state of fragment CN. Detection is made by the intensity of the emission of CN with time, using analysing pulses with different values of  $\lambda_2$ . Values are also shown of the emission expected for analysing pulses that excite the CN fluorescence when this is isolated and when it is still partially bound to the iodine atom [21].

at this longer wavelength pulse increases with time, reaching a maximum and subsequently decaying when the wavelength of the analysing pulse is out of resonance with the fluorescent electronic state (Figure 3.27).

Today, applications of femtochemistry exceed these initial studies in the traditional area of chemical dynamics, and many interesting effects are being observed. The use of femtochemistry is influencing studies with a coherent control of chemical reactions, allowing the cleavage or selective formation of bonds at the molecular level, in addition to providing time-resolved molecular structures resolved by X-ray techniques, energy transfer in photosynthesis, the dynamics of isomerisation and structural rearrangement of rhodopsin in the vision process, etc. Apart from these studies, the appreciable bandwidth associated with 10 fsec pulses, makes it possible to carry out experiments in the time domain, which traditionally were made in the spectral domain.

## REFERENCES

- [1] J Liebermann Jr., *J. Chem. Educ.* **65** (1988) 1067.
- [2] JP Lorimer, TJ Mason, *Educ. Chem.* **21** (1984) 151.
- [3] JP Lorimer, TJ Mason, *Educ. Chem.* **22** (1985) 19.
- [4] A Allen, AJ Haughey, Y Hernandez, S Ireton, *J. Chem. Educ.* **68** (1991) 609.
- [5] HM Weiss, K Touchette, *J. Chem. Educ.* **67** (1990) 707.
- [6] JP Birk, DL Walters, *J. Chem. Educ.* **69** (1992) 585.
- [7] JP Lorimer, TJ Mason, *Educ. Chem.* **23** (1986) 75.
- [8] H Elias, AP Zipp, *J. Chem. Educ.* **65** (1988) 737.
- [9] SL Murov, I Carmichael, GL Hug, *Handbook of Photochemistry*, Marcel Dekker, New York, 1993.
- [10] CG Hatchard, CA Parker, *Proc. Roy. Soc. A* **235** (1956) 518.
- [11] AA Rowe, M Brown, *J. Chem. Educ.* **65** (1988) 548.
- [12] O Moe, R Cornelius, *J. Chem. Educ.* **65** (1988) 137.
- [13] KW Watkins, JA Olson, *J. Chem. Educ.* **57** (1980) 158.
- [14] H Hartridge, FJW Roughton, *Proc. R. Soc. A* **104** (1923) 376.
- [15] DL Jameson, R Anand, *J. Chem. Educ.* **77** (2000) 88.
- [16] ES Yang, M-S Chan, AC Wahl, *J. Phys. Chem.* **84** (1980) 3094.
- [17] RM Nielson, GE McManis, LK Safford, MJ Weaver, *J. Phys. Chem.* **93** (1989) 2152.
- [18] JB Birks, MSSCP Leite, *J. Phys. B* **3** (1970) 417.
- [19] LG Arnaut, RA Caldwell, JE Elbert, LA Melton, *Rev. Sci. Instrum.* **63** (1992) 5381.
- [20] AH Zewail, *Angew. Chem. Int. Ed.* **39** (2000) 2587.
- [21] A Zewail (Ed.) *The Chemical Bond*. Academic Press, San Diego, 1992, p. 223.

This page intentionally left blank

# - 4 -

## Reaction Order and Rate Constants

---

### 4.1 RATES OF ELEMENTARY REACTIONS

The dependence of the rate of a chemical reaction upon the concentration of reactants must be obtained experimentally. For any time instant, the reaction velocity can be calculated from the tangent to the curve of the variation of concentration of reactants or products as a function of time. Since the rate law may change during the course of a reaction, in principle this should be determined experimentally at various times of reaction, either to confirm that it is constant or to identify any changes. However, although this is possible, such a procedure is very time consuming and is not normally used, except for the initial phase of the reaction. The determination of rates of reactions using this method of tangents is known as the differential method of determination of rate laws.

Alternatively, descriptions of the time evolution of concentration can be obtained by mathematical integration of the kinetic laws rather than from the study of the variation of concentration with time. From this, it is possible to predict the concentrations of reactants or products from the initial rate at any instant during the reaction. These can be compared with the experimental results. We should note, however, that there are cases in which the kinetic law is very complex, such that its analytical integration is very difficult or even impossible. In these cases it is still possible to resort to numerical integration.

Although kinetic methods based on differential laws are more exact and more generally applicable, integrated rate laws have the advantage of being more rapid. In addition, in some cases the integrated rate equations can be used to describe the entire course of a chemical reaction.

#### 4.1.1 First-order reactions

We return to the solvolysis of 2-chloro-2-methylpropane in water discussed in Chapter 3 (Section 3.1). The rate-determining step of this reaction is the ionisation of the haloalkane, such that the reaction follows first-order kinetics. Thus, we can write

$$-\frac{d[A]}{dt} = k_1 [A] \quad (4.1)$$

Separating the variables and integrating, using the initial condition that for  $t = 0$ ,  $[A] = [A]_0$ , gives

$$-\int_{[A]_0}^{[A]} \frac{d[A]}{[A]} = k_1 \int_0^t dt \quad (4.2)$$

from which

$$-\ln[A] + \ln[A]_0 = k_1 t \quad (4.3)$$

or

$$\log[A] = -\frac{k_1 t}{2.303} + \log[A]_0 \quad (4.4)$$

These equations show that for a first-order reaction, the logarithm of the concentration is directly proportional to time, and that the proportionality constant is the rate constant. These equations are often given in the exponential form

$$[A] = [A]_0 \exp(-k_1 t) \quad (4.5)$$

Using the relationship

$$[A]_0 = [A] + [B] \quad (4.6)$$

we can describe the variation of product concentration with time

$$[B] = [A]_0 [1 - \exp(-k_1 t)] \quad (4.7)$$

The confirmation of the reaction order is obtained by noting that for a first-order process the rate is directly proportional to the concentration. This dependence can be shown using the initial velocity for various well-defined concentrations. The initial rate for each concentration is obtained from the tangent at time  $t = 0$  of the experimental concentration–time curve. For the solvolysis of 2-chloro-2-methylpropane in water, the initial velocities obtained for different concentrations show a linear dependence on the initial concentration that passes through the origin, with a slope  $k_1$ , confirming that the reaction is first order (see Figure 3.2).

The analysis of the kinetic data following the differential law of eq. (4.1) requires the initial determination of the tangents to the curve of time dependence versus concentration, which can be somewhat subjective, followed by the graph of initial velocity as a function of the initial concentration. The combination of these steps can lead to errors. Alternatively, the same kinetic data can be analysed more quickly and securely using the integrated rate law of eq. (4.3). Figure 4.1 shows that, provided that one is reasonably far from the end of the reaction, the logarithm of the concentration is a linear function of the reaction time. The slope of these plots (using natural logarithms) gives the rate constant. If logarithms to the base 10 are used, they need to be multiplied by  $\ln(10) = 2.303$ . For the set of data shown in Figure 4.1 the slope for the lowest concentration of 2-chloro-2-methylpropane is seen to be much less than those for the other concentrations. This is

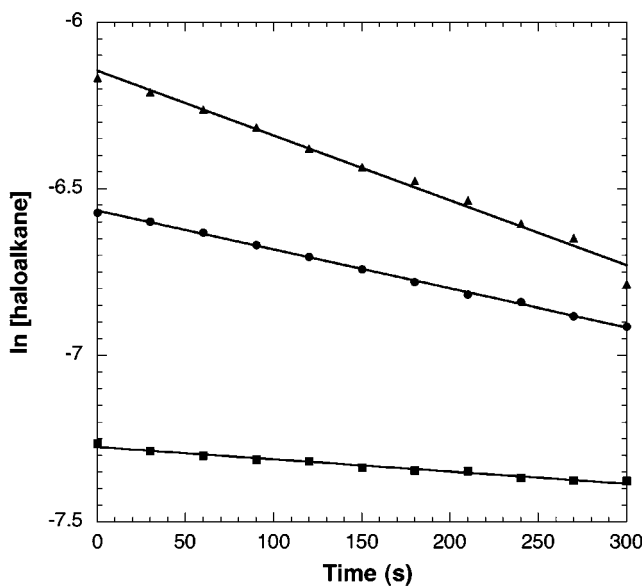


**Figure 4.1** Dependence of the logarithm of the concentration of reactant upon time for the solvolysis of 2-chloro-2-methylpropane.

likely to be caused by experimental error in the measurement of small changes in conductivity at these low concentrations.

Another parameter commonly used to characterise the rates of a first-order reaction is the half-life,  $t_{1/2}$ . For any kinetic process, this is defined as the time taken for the concentration of reactant to be reduced to half its initial value. For a first-order process, we can write from eq. (4.5)

$$\frac{[A]_0/2}{[A]_0} = \exp(-k_1 t_{1/2}) \quad (4.8)$$

from which

$$t_{1/2} = \frac{\ln 2}{k_1} = \frac{0.693}{k_1} \quad (4.9)$$

We can see from the above equation that for a first-order process the half-life does not depend upon the initial concentration. This is seen with the data on the solvolysis of 2-chloro-2-methylpropane in water, where from Table 3.1, the first half-life is about 210 sec, giving a rate constant  $k_1 = 3.3 \times 10^{-3} \text{ sec}^{-1}$ , while for the second half-life, corresponding to the time necessary for the concentration of the reactant to be reduced from  $[A]_0/2$  to  $[A]_0/4$ , the value is virtually identical. Similarly, the half-lives for all steps of this reaction are the same within experimental error. This provides an excellent technique for confirming the reaction order, and, as a working definition, it is normally accepted that if the

integrated rate plot of the logarithm of change in concentration as a function of time is linear for three half-lives (which corresponds to 87.5% of the reaction, and implies that the first three half-lives are identical), the kinetics can be considered to follow good first-order behaviour. One area where the concept of half-lives is commonly used is in the decay of radioactive nuclei. All these reactions follow first-order kinetics.

### 4.1.2 Second-order reactions

Returning to the dimerisation of 2,5-dimethyl-3,4-diphenylcyclopentadienone, discussed in Chapter 3, the second-order rate law in this case is of the type

$$-\frac{d[A]}{dt} = k_2[A]^2 \quad (4.10)$$

Separating the variables, and integrating with the initial conditions that for  $t = 0$ ,  $[A] = [A]_0$ , we get

$$-\int_{[A]_0}^{[A]} \frac{d[A]}{[A]^2} = k_2 \int_0^t dt \quad (4.11)$$

from which

$$\frac{1}{[A]} = k_2 t + \frac{1}{[A]_0} \quad (4.12)$$

The experimental data presented in Chapter 3 allow us to analyse the kinetics of this reaction using the differential law of equation (4.10), and to obtain the dependence of the dienone concentration upon time. To confirm the reaction order, we can take the logarithms of eq. (4.10) to give

$$\log\left(-\frac{d[A]}{dt}\right) = \log(k_2) + 2\log([A]) \quad (4.13)$$

This predicts that a plot of logarithm of rate as a function of logarithm of monomer concentration will give a straight line whose slope gives the order of the reaction (Figure 3.4), while the intercept gives the rate constant. However, since this value is derived from extrapolation over a wide range, which is likely to reduce the precision of the value, it is normally better to obtain the rate constant by plotting rate as a function of [dienone]<sup>2</sup>.

An alternative treatment uses the integrated law, eq. (4.12), to study the kinetics of this reaction. The graph of the reciprocal of concentration as a function of time gives a straight line whose slope is  $k_2$  (Figure 4.2). Again, the integrated rate method is quicker and less subjective than the differential form.

The half-life can also be calculated from eq. (4.12), using

$$\frac{2}{[A]_0} = k_2 t_{1/2} + \frac{1}{[A]_0} \quad (4.14)$$

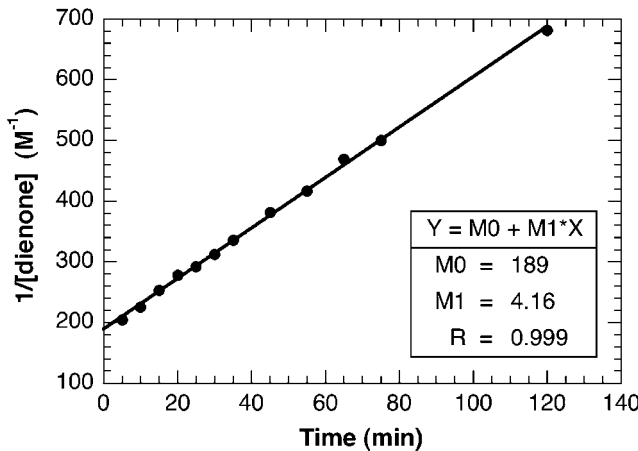


**Figure 4.2** Relationship between the reciprocal of concentration of dienone and time for the reaction of dimerisation of a dienone.

from which

$$t_{1/2} = \frac{1}{k_2 [A]_0} \quad (4.15)$$

The half-life of a reaction of this type depends upon the initial concentration of the reagents.

Another type of second-order reaction involves two different reactants:



from which

$$-\frac{d[A]}{dt} = -\frac{d[B]}{dt} = k_2[A][B] \quad (4.16)$$

Using the condition of mass balance, we obtain

$$\begin{aligned} [A] - [A]_0 &= [B] - [B]_0 \\ [A] - [B] &= [A]_0 - [B]_0 \end{aligned} \quad (4.17)$$

Using, separately, the first and third members, and the second and third members of eq. (4.16), we obtain the two equations [1]:

$$\begin{aligned} \frac{d[A]}{[A]} &= -k_2[B]dt \\ \frac{d[B]}{[B]} &= -k_2[A]dt \end{aligned} \quad (4.18)$$

and subtraction of these then yields

$$\frac{d[A]}{[A]} - \frac{d[B]}{[B]} = k_2 ([A] - [B]) dt \quad (4.19)$$

Using the mass balance eq. (4.17), we can write

$$\frac{d[A]}{[A]} - \frac{d[B]}{[B]} = k_2 ([A]_0 - [B]_0) dt \quad (4.20)$$

which can be integrated from time  $t = 0$  to time  $t$ , to give

$$\ln\left(\frac{[A]}{[A]_0}\right) - \ln\left(\frac{[B]}{[B]_0}\right) = k_2 t ([B]_0 - [A]_0) \quad (4.21)$$

or, rearranging

$$\frac{1}{[A]_0 - [B]_0} \ln\left\{\frac{[B]_0 [A]}{[A]_0 [B]}\right\} = k_2 t \quad (4.22)$$

A plot of  $\log([B]/[A])$  as a function of the time will have a slope of  $([B]_0 - [A]_0)k_2/2.3$ . For the case of second-order reactions in which the initial concentration can be expressed in terms of a single variable,  $[A] = [B] = [A]_0 - x = [B]_0 - x$ . When  $x = 0$  for  $t = 0$ , the integration of eq. (4.16), after substitution for this variable, gives,

$$\frac{x}{[A]_0 ([A]_0 - x)} = k_2 t \quad (4.23)$$

### 4.1.3 Zero-order reactions

Even though concentration of reactants has been given as one of the factors on which reaction rates depend, there are also cases of reactions that are independent of reactant concentration. In this case, the differential rate law is constant

$$-\frac{d[A]}{dt} = k_0 \quad (4.24)$$

On integrating, we obtain

$$[A] = [A]_0 - k_0 t \quad (4.25)$$

Thus, a zero-order reaction gives a linear plot of change in concentration as a function of time, with slope equal to  $-k_0$ . The units of this rate constant are identical to those of the rate (e.g. litres per second). As with other reaction orders, we can determine the half-life, which is given by

$$\frac{[A]_0}{2} = [A]_0 - k_0 t_{1/2} \quad (4.26)$$

where

$$t_{1/2} = \frac{[A]_0}{2k_0} \quad (4.27)$$

Zero-order reactions appear in heterogeneous systems when the surface of a solid phase is saturated with a reactant, but are also seen in certain homogeneous systems.

#### 4.1.4 Third-order reactions

In the same way that differential and integral rates can be defined for first- and second-order reactions, we can also obtain rate laws for third-order reactions of the general type



The differential rate law for this reaction is

$$-\frac{d[A]}{dt} = k_3[A][B][C] \quad (4.28)$$

The integration of this equation can be made using the method of partial fractions, which leads to

$$\begin{aligned} & \frac{1}{([A]_0 - [B]_0)([B]_0 - [C]_0)([C]_0 - [A]_0)} \ln \left( \left( \frac{[A]}{[A]_0} \right)^{[B]_0 - [C]_0} \left( \frac{[B]}{[B]_0} \right)^{[C]_0 - [A]_0} \left( \frac{[C]}{[C]_0} \right)^{[A]_0 - [B]_0} \right) \\ &= k_3 t \end{aligned} \quad (4.29)$$

The use of the expressions (4.28) and (4.29) in the determination of the partial orders of these reactions and their rate constants is not very practicable. As we will discuss later in this chapter, an alternative is to use the so-called isolation method.

However, as previously discussed, third-order reactions involving the simultaneous collision of three molecules are very unlikely in comparison with alternative reaction mechanisms involving a series of elementary second-order steps. A good example of a reaction of this type is the oxidation of vitamin C by hexacyanoferrate(III) discussed in the previous chapter. Although the stoichiometry of this reaction shows the consumption of three molecules of reactants, in reaction (3.X), the mechanism involves a series of simpler steps in which the reaction order is never greater than two, reactions (3.XI) and (3.XII). This is a typical example of a complex reaction whose mechanism involves a sequence of elementary steps. The sum of these steps gives the overall stoichiometry of the reaction. The effect of ionic strength on the kinetics suggests a mechanism with a step involving the reaction between two ions of the same charge. This excludes reaction (3.X) as the rate-determining step in the chemical process.

## 4.2 RATES OF COMPLEX REACTIONS

As seen above, the majority of kinetic processes involves more than one elementary step. However, the fact that a mechanism is in agreement with the kinetic law does not mean that it is the correct mechanism for the reaction. The same kinetic law can, and frequently does, correspond to more than one possible mechanism. A mechanism is always a theoretical hypothesis of how a reaction occurs. We can never prove a mechanism from the kinetic behaviour, but can only eliminate certain hypotheses. A good illustration is given by the gas-phase reaction at 400 °C



studied by Bodenstein in 1894, which was considered to be an elementary process. However, even at this time he recognised that it was difficult to find chemically simple reactions in the gas phase, i.e. reactions whose rates are proportional to the product of the concentrations of reactants raised to integral powers. Reaction (4.III) was presented as an example of an elementary kinetic process in all text books until Sullivan in 1967 detected the presence of free radicals in the system at 350 °C, and proposed an alternative mechanism



where M is an inert gas. In summary, there are a number of important questions needed to test this mechanism. Mechanisms of the reactions are proposed on the basis of the observed kinetic behaviour. Once proposed, a very detailed physical chemical study is necessary before any mechanism can be considered as accepted. It is necessary to confirm the feasibility of all the steps proposed in addition to demonstrating the possible existence of the different intermediates. Because of various experimental difficulties, these tasks are difficult to carry out for the majority of the chemical reactions. In addition to kinetic studies, involving, for example, predictions of the effects of various factors on rates and product distributions, these studies must be complemented by other chemical and physical studies, in particular attempts to try to trap and characterise the intermediates.

Complex reaction mechanisms can conveniently be grouped within the following classification: consecutive reactions, parallel reactions and reversible reactions. Parallel reactions are those in which the same species participates in two or more competitive steps. Consecutive reactions are characterised by the product of the first reaction being a reactant in a subsequent process, leading to formation of the final product. Reversible reactions are those in which the products of the initial reaction can recombine to regenerate the reactant.

As complex reactions follow a reaction mechanism involving various elementary steps, the determination of the corresponding kinetic law involves the solution of a system of differential equations, and the complete analytical solution of these systems is only possible for the simplest cases. In slightly more complicated cases it may still be possible to resolve the system of corresponding differential equations using methods such as Laplace transforms or matrix methods. However, there are systems which cannot be resolved analytically, or whose

analytical solution is so complex that it is not easily applied. In the absence of information on the orders of magnitude of the rate constants involved, the treatment of these kinetic systems is made using numerical methods. These methods allow us to obtain concentrations of the reactants for discrete time intervals, which can then be represented graphically and compared with experimental data to provide an insight into the changes occurring. Further, although the results obtained numerically are inherently approximations, we can estimate and allow for the errors involved, which can be expressed as error limits when compared with experimental data. In some cases, it may also be possible to introduce some changes of a chemical nature in the system to help simplify and analyse these complex systems. For example, if we know the relative magnitudes of some of the rate constants, it may be possible to simplify the system of complex differential equations involved by modifying the initial concentrations of reactants and obtaining a rate equation that can be solved analytically. Finally, when these procedures cannot be used to resolve complex systems of differential equations, it is still possible to use stochastic treatments such as Markov chains or the Monte Carlo method.

#### 4.2.1 Parallel first-order reactions

The simplest parallel reactions involve two competitive first-order steps:



The rate of disappearance of A is given by the differential equation

$$\frac{d[\text{A}]}{dt} = -k_1[\text{A}] - k_2[\text{A}] = k_T[\text{A}] \quad (4.30)$$

where  $k_T = k_1 + k_2$ . Integrating this equation gives

$$[\text{A}] = [\text{A}]_0 e^{-k_T t} = [\text{A}]_0 e^{-(k_1+k_2)t} \quad (4.31)$$

To determine the rate of formation of B, we have

$$\frac{d[\text{B}]}{dt} = k_1[\text{A}] \quad (4.32)$$

and, substituting for [A] using expression (4.31), followed by integration with the condition that for  $t = 0$ ,  $[\text{B}] = 0$ , we obtain

$$[\text{B}] = \frac{k_1[\text{A}]_0}{k_T} \left(1 - e^{-k_T t}\right) \quad (4.33)$$

We can obtain the variation of [C] with time in the same way:

$$[\text{C}] = \frac{k_2[\text{A}]_0}{k_T} \left(1 - e^{-k_T t}\right) \quad (4.34)$$

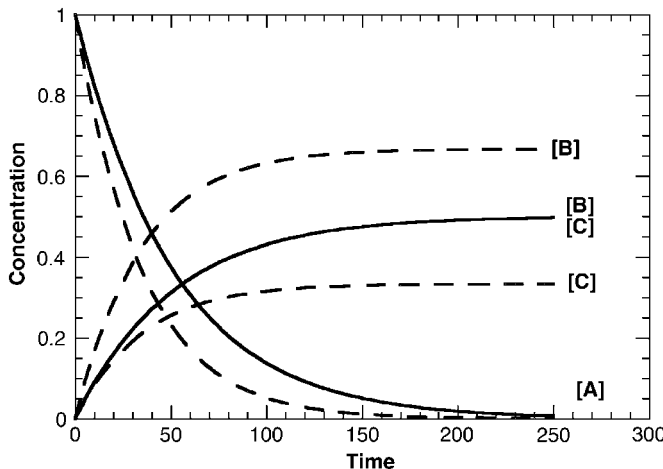


**Figure 4.3** Variation of the concentrations of reactant and final products for parallel first-order reactions. The full lines correspond to the situation in which  $k_1 = k_2$  and the dashed lines correspond to the case in which  $k_1 = 2k_2$ .

From the above two expressions we see immediately that the ratio of the rate constants of parallel first-order reactions is equal to the ratio of yields of the products.

$$\frac{[B]}{[C]} = \frac{k_1}{k_2} \quad (4.35)$$

This quotient is called the branching ratio of the reaction.

Figure 4.3 shows the time evolution of  $[A]$ ,  $[B]$  and  $[C]$  for the cases in which  $k_1 = k_2$  and  $k_1 = 2k_2$ .

This solution can easily be extended to parallel reactions involving more than two processes. If there are  $n$  parallel reactions, then  $k_T = k_1 + k_2 + \dots + k_n$ , and the expression for the disappearance of  $A$  has the same form as eq. (4.30).

## 4.2.2 Consecutive first-order reactions

Another very common kinetic scheme involves a series of first-order reactions, leading first to the formation of an intermediate  $B$ , which subsequently reacts to give the final product



The differential equations describing this sequence of elementary steps are

$$\begin{aligned} \frac{d[A]}{dt} &= -k_1[A] \\ \frac{d[B]}{dt} &= k_1[A] - k_2[B] \\ \frac{d[C]}{dt} &= k_2[B] \end{aligned} \quad (4.36)$$

As we have seen, the integrated rate equation for the disappearance of A is given by

$$[A] = [A]_0 e^{-k_1 t} \quad (4.37)$$

and can be substituted for [A] in the equation describing the variation of [B] with time. After rearranging, this can be written as

$$\frac{d[B]}{dt} + k_2[B] = k_1[A]_0 e^{-k_1 t} \quad (4.38)$$

Multiplying both terms by  $\exp(k_2 t)$ , we obtain [2]

$$e^{k_2 t} \frac{d[B]}{dt} + k_2[B]e^{k_2 t} = k_1[A]_0 e^{(k_2 - k_1)t} \quad (4.39)$$

and as

$$e^{k_2 t} \frac{d[B]}{dt} + k_2[B]e^{k_2 t} = \frac{d([B]e^{k_2 t})}{dt} \quad (4.40)$$

the equation can be written as the differential equation

$$d([B]e^{k_2 t}) = k_1[A]_0 e^{(k_2 - k_1)t} dt \quad (4.41)$$

which, upon integration, leads to

$$[B]e^{k_2 t} = \frac{k_1[A]_0 e^{(k_2 - k_1)t}}{k_2 - k_1} + I \quad (4.42)$$

where the integration constant  $I$  is obtained for the simplest case of  $[B] = 0$  at  $t = 0$ , as

$$I = -\frac{k_1[A]_0}{(k_2 - k_1)} \quad (4.43)$$

Substituting this value for  $I$  in eq. (4.42) and dividing by  $\exp(k_2 t)$ , we obtain the integrated equation for the dependence of [B] upon time:

$$[B] = \frac{k_1[A]_0 (e^{-k_1 t} - e^{-k_2 t})}{k_2 - k_1} \quad (4.44)$$

which is true for the case in which  $k_1 \neq k_2$ . When  $k_1 = k_2$ , we obtain

$$d([B]e^{k_2 t}) = k_1[A]_0 dt \quad (4.45)$$

whose solution is

$$[B] = k_1[A]_0 e^{-k_1 t} t \quad (4.46)$$

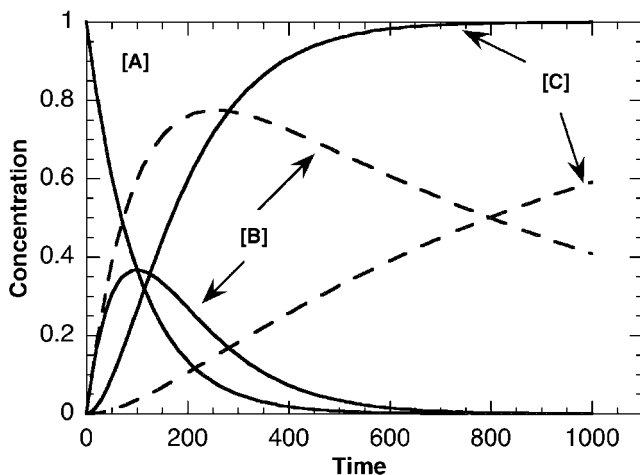


**Figure 4.4** Variation of the concentrations of reactant, intermediate and final product with time for consecutive first-order reactions. The solid line shows the case in which  $k_1 = k_2$ , while the dashed line is for the condition  $k_1 = 10k_2$ .

when  $[B] = 0$  at  $t = 0$ . Figure 4.4 shows the time evolution of the concentrations of reactant, intermediate and final product for the cases in which  $k_1 = k_2$  and  $k_1 = 10k_2$ .

#### 4.2.3 Reversible first-order reactions

The simplest reversible reactions are of the type



The corresponding differential equations for this mechanism are

$$\begin{aligned} -\frac{d[A]}{dt} &= k_f[A] - k_r[B] \\ -\frac{d[B]}{dt} &= k_r[B] - k_f[A] \end{aligned} \quad (4.47)$$

Assuming that at time  $t = 0$  the initial concentrations of the two species are  $[A]_0$  and  $[B]_0$ , we can write the law of conservation of mass for this system:

$$[A]_0 + [B]_0 = [A] + [B] \quad (4.48)$$

and solving in terms of  $[B]$  we obtain

$$[B] = [A]_0 + [B]_0 - [A] \quad (4.49)$$

Substituting  $[B]$  in the differential expression and rearranging, we can write

$$-\frac{d[A]}{dt} = (k_f + k_r) \left\{ \frac{-k_r ([A]_0 + [B]_0)}{(k_f + k_r)} + [A] \right\} \quad (4.50)$$

where

$$\frac{-k_r ([A]_0 + [B]_0)}{(k_f + k_r)} = -m \quad (4.51)$$

is a constant. Thus, the integration

$$\int_{[A]_0}^{[A]} \frac{d[A]}{m - [A]} = (k_f + k_r) \int_0^t dt \quad (4.52)$$

leads to

$$\ln \left( \frac{k_f [A] - k_r [B]}{k_f [A]_0 - k_r [B]_0} \right) = -(k_f + k_r) t \quad (4.53)$$

When equilibrium is reached, the forward and reverse reactions have the same rates. This corresponds to a formulation of the principle of microscopic reversibility. Thus, at equilibrium, the concentrations of reactant and product do not change with time

$$\frac{d[A]_e}{dt} = -\frac{d[B]_e}{dt} = 0 \quad (4.54)$$

i.e.

$$-k_f [A]_e + k_r [B]_e = 0 \quad (4.55)$$

where the subscript refers explicitly to the equilibrium condition. From this, the equilibrium constant is given by

$$\frac{k_f}{k_r} = \frac{[B]_e}{[A]_e} = K_{eq} \quad (4.56)$$

Figure 4.5 shows the evolution of  $[A]$  and  $[B]$  for the cases in which  $k_f = k_r$  and  $k_f = 3 k_r$ .

The same ideas can be applied to reversible reactions that occur in various steps. The principle of microscopic reversibility can help resolve more complicated systems of kinetic equations when the system is in equilibrium.

## 4.3 METHODS FOR SOLVING KINETIC EQUATIONS

### 4.3.1 Laplace transforms

Classical methods of integration are used to solve many of the linear differential equations that describe the kinetic behaviour of chemical reactions. However, the methods of solving

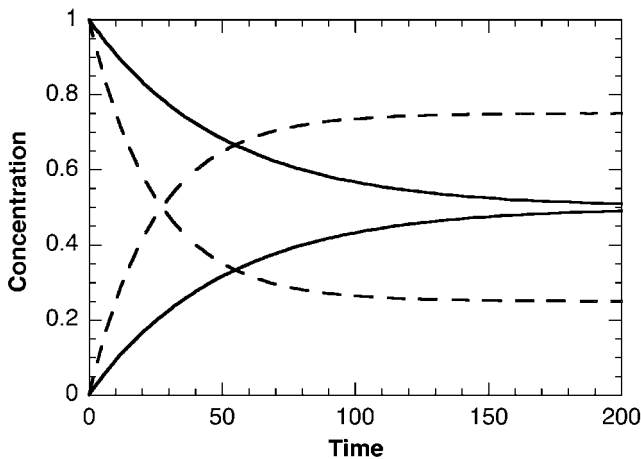


**Figure 4.5** Evolution of the concentrations of the species A and B for a reversible first-order system until equilibrium is reached. The full line indicates the situation in which  $k_f = k_r$  and the dashed line shows the evolution of the system in which  $k_f = 3k_r$ .

these equations can often be very complicated. In contrast, in many cases it is possible to use methods of operational calculus directly to obtain solutions that satisfy a set of given initial conditions without resorting to the manipulation of particular integrals separately or introduction of arbitrary constants. Consequently, operational calculus can be applied profitably to these systems, since it appreciably simplifies and speeds up solution of the appropriate kinetic equations. The principle of integral calculus is based on the introduction of a definite integral, called the transformation integral that is given by the general formula

$$F(p) = \int_a^b f(t) \mathbf{K}(p,t) dt \quad (4.57)$$

where  $F(p)$  is the transformation of  $f(t)$  relative to the *kernel*  $\mathbf{K}(p,t)$ .

A kernel frequently used in chemical kinetics is  $\mathbf{K}(p,t) = e^{-pt}$ . This kernel, integrated between the limits 0 and  $\infty$ , corresponds to the Laplace transform. The great value of this transform stems from the fact that the exponential dependence as a function of time is similar to that encountered in the integrals needed in chemical kinetics, while in the applications of the Laplace transform, with integration between the limits  $t = 0$  and  $t = \infty$ , the transformed function only depends on  $p$ . Thus, the transform  $F(p)$  of the function  $f(t)$  using the Laplace treatment is defined by the integral

$$F(p) = L[f(t)] = \int_0^\infty f(t) e^{-pt} dt \quad (4.58)$$

For the function  $f(t) = a$ , where  $a$  is a constant, its Laplace transform is  $F(p) = a/p$ . If  $L[f(t)] = F(p)$  is the Laplace transform of the function  $f(t)$ , then we say that  $f(t) = L^{-1}[F(p)]$  is the inverse of the Laplace transform of  $F(p)$ .

For example, for the function  $f(t) = \exp(-at)$  in which  $a$  is constant, its Laplace transform is obtained using

$$\begin{aligned} F(p) &= L[e^{-at}] = \int_0^\infty e^{-at} e^{-pt} dt = \int_0^\infty e^{-(a+p)t} dt \\ &= -\frac{1}{a+p} \left[ e^{-(a+p)t} \right]_0^\infty \\ &= \frac{1}{p+a} \end{aligned} \quad (4.59)$$

which is restricted to the condition that  $p > -a$ , for which  $e^{-(a+p)t}$  will be equal to zero and the integral  $L[e^{-at}]$  converges.

The application of Laplace transforms to the analytical solution of complicated differential kinetic laws is simplified significantly on the basis of three of its fundamental properties:

1. The Laplace transform of a linear combination of functions is the same linear combination of the transformed functions. Thus if

$$f(t) = f_1(t) + f_2(t) + \dots + f_n(t) \quad (4.60)$$

then its Laplace transform is

$$L[f(t)] = F_1(p) + F_2(p) + \dots + F_n(p) \quad (4.61)$$

2. The Laplace transform of the derivative of  $f'(t)$ , i.e.  $f'(t)$ , can be easily obtained

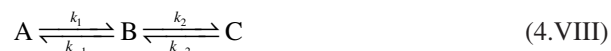
$$\begin{aligned} L[f'(t)] &= \int_0^\infty f'(t) e^{-pt} dt \\ &= f(t) e^{-pt} \Big|_0^\infty + p \int_0^\infty f(t) e^{-pt} dt \\ &= pL[f(t)] - f(0) \end{aligned} \quad (4.62)$$

3. The Laplace transform of an integral of a function  $f(t)$  can be expressed as

$$L\left[\int_0^\infty f(t) dt\right] = \frac{L[f(t)]}{p} \quad (4.63)$$

Using these three properties and tables containing both the Laplace transforms and inverse transforms, it is possible to solve many differential kinetic equations analytically.

As an example of application of Laplace transforms to complex reaction schemes, consider the consecutive first-order reversible reactions



whose corresponding rate equations are

$$\begin{aligned}\frac{d[A]}{dt} &= -k_1[A] + k_{-1}[B] \\ \frac{d[B]}{dt} &= k_1[A] - (k_{-1} + k_2)[B] + k_{-2}[C] \\ \frac{d[C]}{dt} &= k_2[B] - k_{-2}[C]\end{aligned}\quad (4.64)$$

with the initial conditions  $[A] = [A]_0$  and  $[B] = [C] = 0$  at  $t = 0$ . Applying Laplace transforms (eq. (4.62)), and using the mass balance  $[A]_0 = [A] + [B] + [C]$  to eliminate  $[C]$  in the expression of the variation of  $[B]$  with time, we obtain

$$pL[A] - [A]_0 = -k_1 L[A] + k_{-1} L[B] \quad (4.65)$$

$$pL[B] = (k_1 - k_{-2})L[A] - (k_{-1} + k_2 + k_{-2})L[B] + \frac{k_{-2}[A]_0}{p} \quad (4.66)$$

Solving equation (4.65) in the order of  $L[A]$  and introducing the resulting expression into eq. (4.66), we obtain

$$\begin{aligned}L[B] &= \frac{k_1[A]_0(p + k_{-2})}{p[p^2 + (k_1 + k_{-1} + k_2 + k_{-2})p + (k_1k_2 + k_1k_{-2} + k_{-1}k_{-2})]} \\ &= \frac{k_1[A]_0(p + k_{-2})}{p(p + a)(p + b)}\end{aligned}\quad (4.67)$$

where

$$a + b = k_1 + k_{-1} + k_2 + k_{-2} \quad (4.68)$$

and

$$ab = k_1k_2 + k_1k_{-2} + k_{-1}k_{-2} \quad (4.69)$$

We can apply the inverse Laplace transform to the previous equation to obtain the time dependence of the concentration for B. Using the tables of these transforms, we obtain

$$[B] = k_1[A]_0 \left[ \frac{k_{-2}}{ab} + \frac{k_{-2} - a}{a(a - b)} e^{-at} - \frac{k_{-2} - b}{b(a - b)} e^{-bt} \right] \quad (4.70)$$

To obtain  $L[A]$ , we start by solving eq. (4.65) in the order of  $L[B]$ , substitute the value obtained in eq. (4.66) and solve for  $L[A]$

$$L[A] = [A]_0 \left[ \frac{k_{-1}k_{-2} + p(p + c)}{p(p + a)(p + b)} \right] \quad (4.71)$$

where

$$m = k_{-1} + k_2 + k_{-2} \quad (4.72)$$

Applying the inverse transform, we get

$$\begin{aligned} [A] &= [A]_0 \left[ \frac{k_{-1}k_{-2}}{ab} + \frac{k_{-1}k_{-2} - a(m-a)}{a(a-b)} e^{-at} - \frac{k_{-1}k_{-2} - b(m-a)}{b(a-b)} e^{-bt} \right] \\ &= [A]_0 \left[ \frac{k_{-1}k_{-2}}{ab} + \frac{k_{-1}(a-k_2-k_{-2})}{a(a-b)} e^{-at} - \frac{k_{-1}(b-k_2-k_{-2})}{b(a-b)} e^{-bt} \right] \end{aligned} \quad (4.73)$$

The time dependence of the concentration of C can be obtained by introducing eqs. (4.70) and (4.73) into the mass balance expression

$$[C] = k_1 k_2 [A]_0 \left[ \frac{1}{ab} + \frac{1}{a(a-b)} e^{-at} - \frac{1}{b(a-b)} e^{-bt} \right] \quad (4.74)$$

Figure 4.6 presents the concentrations of A, B and C calculated by eqs. (4.70), (4.73) and (4.74), respectively, for the case in which  $k_1 = k_{-1} = 3k_2 = 6k_{-2}$ .

For rate equations that are linear with respect to the reactants, the Laplace transform method allows us to solve the kinetic equations. In the case of non-linear rate laws, these can be made linear by using excess concentrations of certain reactants, leading to pseudo-first-order equations, which can be solved.

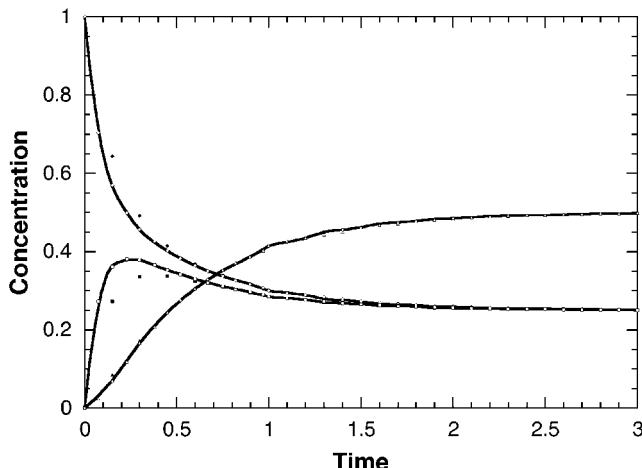


**Figure 4.6** Calculation of the concentrations of the species involved in mechanism (4.VIII) by the method of Laplace transform (lines) and by the fourth-order Runge–Kutta method (points). Two different integration steps were used in the Runge–Kutta method, with the steps of the solid points being twice that of the others. The example presented uses  $k_1 = k_{-1} = 3k_2 = 6k_{-2}$ .

### 4.3.2 Matrix method

Systems involving first-order reversible reactions lead to groups of simultaneous linear differential equations with constant coefficients. These can be solved by using matrix methods, the same mathematical technique frequently encountered in quantum mechanics and vibrational spectroscopy.

For the general case, the concentration of the species  $A_i$  involved in a system of first-order kinetic equations involving  $n$  species is  $[A_i]$ . The set of these equations [3] is

$$\begin{aligned} -\frac{d[A_1]}{dt} &= k_{11}[A_1] + k_{12}[A_2] + \cdots + k_{1n}[A_n] \\ -\frac{d[A_2]}{dt} &= k_{21}[A_1] + k_{22}[A_2] + \cdots + k_{2n}[A_n] \\ &\vdots \\ -\frac{d[A_n]}{dt} &= k_{n1}[A_1] + k_{n2}[A_2] + \cdots + k_{nn}[A_n] \end{aligned} \quad (4.75)$$

which can be expressed in terms of matrices as

$$\begin{bmatrix} -\frac{d[A_1]}{dt} \\ -\frac{d[A_2]}{dt} \\ \vdots \\ -\frac{d[A_n]}{dt} \end{bmatrix} = \begin{bmatrix} k_{11} & k_{12} & \cdots & k_{1n} \\ k_{21} & k_{22} & \cdots & k_{2n} \\ \vdots & & & \\ k_{n1} & k_{n2} & \cdots & k_{nn} \end{bmatrix} \begin{bmatrix} [A_1] \\ [A_2] \\ \vdots \\ [A_n] \end{bmatrix} \quad (4.76)$$

or in the abbreviated form,

$$\frac{d\mathbf{A}}{dt} = \mathbf{KA} \quad (4.77)$$

where  $\mathbf{A}$  is the composition vector and  $\mathbf{K}$  the rate constant matrix. For this problem, in which  $\mathbf{K}$  is an  $n \times n$  matrix, and  $n$  the number of components,  $A_n$ , it is possible to diagonalise  $\mathbf{K}$  and obtain  $n$  linearly independent proper vectors. The solution of the differential eq. (4.77) is similar to the corresponding scalar equation, i.e.

$$\mathbf{A}(t) = \mathbf{A}(0)e^{\mathbf{K}t} \quad (4.78)$$

The matrix  $\exp(\mathbf{K}t)$ , which is designated the transition state matrix, is defined by the expansion of a Taylor series

$$e^{\mathbf{K}t} = \mathbf{U} + \mathbf{K}t + \frac{(\mathbf{K}t)^2}{2!} + \cdots \quad (4.79)$$

where  $\mathbf{U}$  is the unitary matrix of order  $n$ . Eq. (4.77) can be solved by initially calculating successive powers of  $\mathbf{K}$ , followed by the application of eq. (4.79). However, although this

procedure is reasonable, it is very slow. Alternatively, it is possible to reduce the previous infinite series to

$$e^{\mathbf{K}t} = \frac{1}{\Delta} \left[ \Delta_0 \mathbf{U} + \Delta_1 (\mathbf{K}t)^2 + \dots + \Delta_{n-1} (\mathbf{K}t)^{n-1} \right] \quad (4.80)$$

where  $\Delta$  is the Vandermonde determinant

$$\Delta = \det \begin{bmatrix} 1 & \mu_1 & \mu_1^2 & \cdots & \mu_1^{n-1} \\ 1 & \mu_2 & \mu_2^2 & \cdots & \mu_2^{n-1} \\ \vdots & & & & \\ 1 & \mu_n & \mu_n^2 & \cdots & \mu_n^{n-1} \end{bmatrix} \quad (4.81)$$

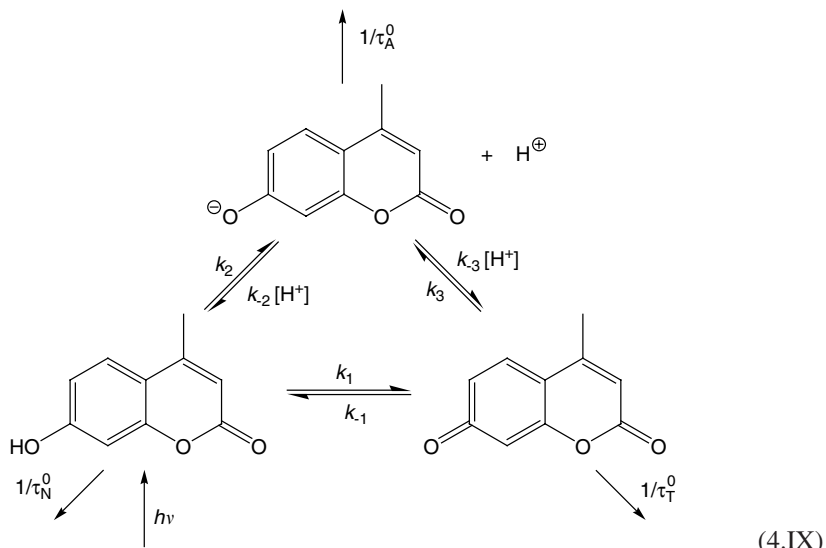
and each  $\Delta_i$  is the determinant obtained from the previous equation substituting  $\mu_1^i, \mu_2^i, \dots, \mu_n^i$  by  $\exp(\mu_1), \exp(\mu_2), \dots, \exp(\mu_n)$ . The values of  $\mu_i$  are related to the proper values of  $\mathbf{K}$  through

$$\mu_i = \lambda_i t, \quad i = 1, 2, \dots, n \quad (4.82)$$

where the proper values are obtained from the equation

$$\det(\mathbf{K} - \lambda \mathbf{U}) = 0 \quad (4.83)$$

The method of matrices has been applied to the solution of reversible equilibria between the excited states of the neutral, anionic and tautomeric forms of 7-hydroxy-4-methylcoumarin [4], which in its most complex form involves equilibria between all the species, as shown in the mechanism below. The values of  $\tau_N^0, \tau_A^0$  and  $\tau_T^0$  refer to the radiative lifetimes of each of the neutral, anionic and tautomeric forms. Absorption of light initially produces the excited state of the neutral form, which then participates in the above scheme. In this kinetic scheme there are nine unknowns: six rate constants and three inverse lifetimes.



which require nine kinetic equations for complete analysis. The differential equations that determine the time dependence of concentrations of the species are

$$\frac{d}{dt} \begin{bmatrix} N^* \\ A^* \\ T^* \end{bmatrix} = \begin{bmatrix} -X & k_{-2}[H^+] & k_{-1} \\ k_2 & -Y & k_3 \\ k_1 & k_{-3}[H^+] & -Z \end{bmatrix} \begin{bmatrix} N^* \\ A^* \\ T^* \end{bmatrix} \quad (4.84)$$

where  $N^*$ ,  $A^*$  and  $T^*$  are the concentrations of N, A and T in the excited state, given by

$$\begin{aligned} X &= k_1 + k_2 + \frac{1}{\tau_N^0} \\ Y &= (k_{-2} + k_{-3})[H^+] + \frac{1}{\tau_A^0} \\ Z &= k_{-1} + k_3 + \frac{1}{\tau_T^0} \end{aligned} \quad (4.85)$$

From the integration of eq. (4.84) we obtain

$$\begin{bmatrix} N^* \\ A^* \\ T^* \end{bmatrix} = \begin{bmatrix} a_{11} & a_{12} & a_{13} \\ a_{21} & a_{22} & a_{23} \\ a_{31} & a_{32} & a_{33} \end{bmatrix} \begin{bmatrix} e^{-\lambda_1 t} \\ e^{-\lambda_2 t} \\ e^{-\lambda_3 t} \end{bmatrix} \quad (4.86)$$

where the proper values  $\lambda_i$  are the reciprocals of the decay lifetimes and the pre-exponential factors  $a_{ij}$  the linear combinations of the proper base of vectors which obey the three initial conditions:

$$\begin{aligned} \sum_{j=1}^3 a_{ij} &= 1, \quad i = 1 \\ \sum_{j=1}^3 a_{ij} &= 0, \quad i = 2, 3 \end{aligned} \quad (4.87)$$

Eq. (4.87) shows the situation where only the reactant  $i = 1$  exists for  $t = 0$ . The nine equations link the values of  $\lambda_j$  and  $a_{ij}$  with the nine unknowns, and can be written in the following form:

$$\begin{bmatrix} -X & k_{-2}[H^+] & k_{-1} \\ k_2 & -Y & k_3 \\ k_1 & k_{-3}[H^+] & -Z \end{bmatrix} = \begin{bmatrix} a_{11} & a_{12} & a_{13} \\ a_{21} & a_{22} & a_{23} \\ a_{31} & a_{32} & a_{33} \end{bmatrix} \begin{bmatrix} -\lambda_1 & 0 & 0 \\ 0 & -\lambda_2 & 0 \\ 0 & 0 & -\lambda_3 \end{bmatrix} \begin{bmatrix} a_{11} & a_{12} & a_{13} \\ a_{21} & a_{22} & a_{23} \\ a_{31} & a_{32} & a_{33} \end{bmatrix}^{-1} \quad (4.88)$$

This equality allows us to determine the rate constants,  $k_i$ , of the system, since we know the values of the pre-exponential factors,  $a_{ij}$ , and the inverse of the decay times,  $\lambda_i$ . Figure 4.7 presents the variations of the concentrations of the various species with time and the values of the kinetic constants determined by this method.

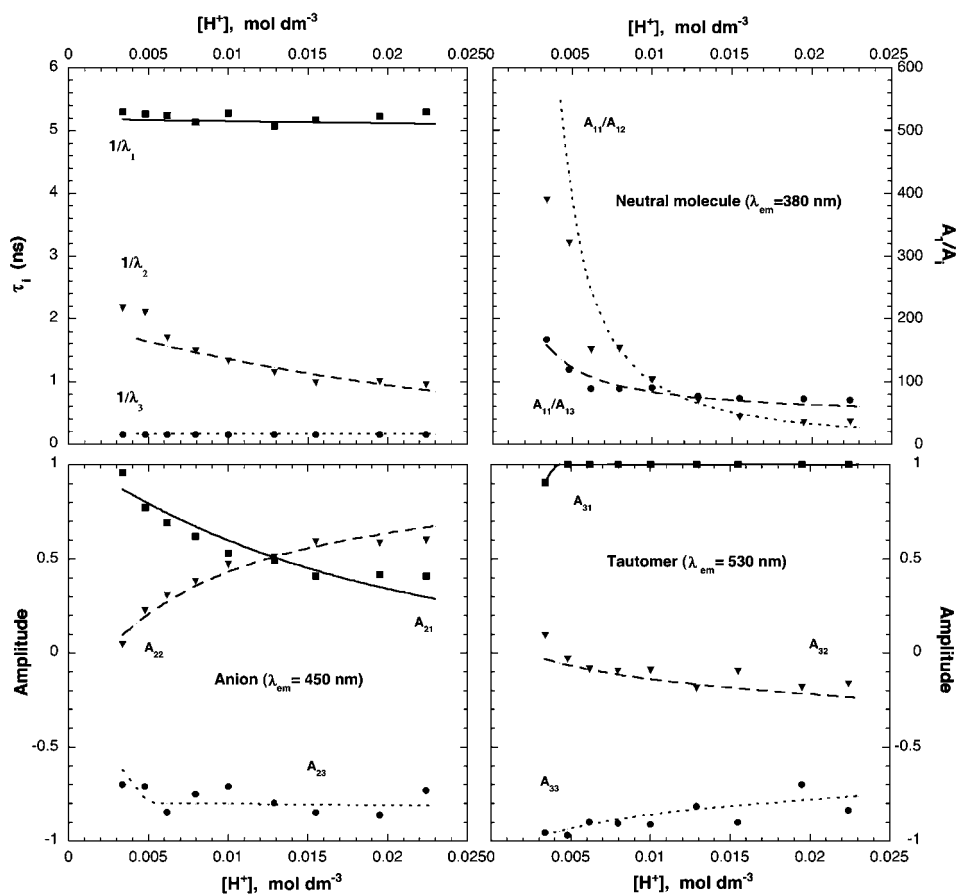


**Figure 4.7** Kinetics of the photokinetic reversible equilibrium among neutral, anionic and tautomeric forms of 7-hydroxy-4-methylcoumarin.

### 4.3.3 Runge–Kutta method

The fourth-order Runge–Kutta method is a numerical method which, when the initial conditions are known (in particular that  $y(t_0) = y_0$ ), allows approximate solutions of differential equations of the type

$$y'(t) = f(t, y) \quad (4.89)$$

where the differential  $dy/dt$  is represented as  $y'$ . For this differential equation, if we divide the time interval  $[t_0, t_n]$  into  $N$  equally spaced sub-intervals of size

$$h = \frac{(t_N - t_0)}{N} \quad (4.90)$$

and each new independent variable increment is approximately equal to

$$t_n = t_0 + nh \quad (4.91)$$

where  $n = 0, 1, 2, \dots, N$ . If  $y(t)$  is continuous and single valued, this can now be expanded relative to the point  $t_0$  using a Taylor series

$$y(t_0 + h) = y(t_0) + f(t_0, y_0)h + f'(t_0, y)\frac{h^2}{2!} + \dots \quad (4.92)$$

When  $h$  is small, higher order terms in  $h$  can be ignored. If we truncate after the term in  $h$  in the Taylor series expansion, we get the method of Euler, where

$$y(t_0 + h) = y(t_0) + hy'(t_0) \quad (4.93)$$

From the value  $y_n$  and its derivative, this process can be continued through various steps to obtain the value of  $y_{n+1}$ .

For a more precise treatment, we can truncate the expansion after the term in  $h^2$ , and obtain the second-order Runge–Kutta method. For this, we need to know the second derivative  $y''(t_0)$ , which can be estimated as a finite difference.

$$y''(t_0) = \frac{\Delta y'}{\Delta t} = \frac{y'(t_0 + h) - y'(t_0)}{h} \quad (4.94)$$

Substituting this expression into the truncated Taylor series, we obtain

$$\begin{aligned} y(t_0 + h) &= y(t_0) + hy'(t_0) + \frac{h^2}{2!} \left( \frac{y'(t_0 + h) - y'(t_0)}{h} \right) \\ &= y(t_0) + \frac{h^2}{2} [y'(t_0 + h) + y'(t_0)] \end{aligned} \quad (4.95)$$

For an even more rigorous treatment, in the third-order method, we keep the terms in the Taylor series until  $h^3$ . For this we need to know the third derivative  $y'''(t_0)$ . The resulting equations are

$$y_{n+1} = y_n + \frac{h}{6} (\Delta Y_1 + 4\Delta Y_3 + \Delta Y_4) \quad (4.96)$$

where

$$\begin{aligned} \Delta Y_1 &= f(t_n, y_n) \\ \Delta Y_2 &= f(t_n + h, y_n + \Delta Y_1) \\ \Delta Y_3 &= f(t_n + h/2, y_n + \Delta Y_1/2) \\ \Delta Y_4 &= f(t_n + h, y_n + \Delta Y_2) \end{aligned} \quad (4.97)$$

Finally, the most common case in chemical kinetics involves the fourth-order Runge–Kutta method, given by the equations

$$y_{n+1} = y_n + \frac{h}{6}(\Delta Y_1 + 2\Delta Y_2 + 2\Delta Y_3 + \Delta Y_4) \quad (4.98)$$

where

$$\begin{aligned}\Delta Y_1 &= f(t_n, y_n) \\ \Delta Y_2 &= f(t_n + h/2, y_n + \Delta Y_1/2) \\ \Delta Y_3 &= f(t_n + h/2, y_n + \Delta Y_2/2) \\ \Delta Y_4 &= f(t_n + h, y_n + \Delta Y_3)\end{aligned}\quad (4.99)$$

The error associated with numerical integration using the Runge–Kutta method of order  $n$  is of the order of magnitude  $h^{n+1}$ , since the terms up to the order  $h^n$  are eliminated in the series expansion. As the error depends on the step size, the temptation is to reduce this by choosing a very small integration step. However, the use of such a small step involves the use of a lot of computer time since it requires a large number of iterations. As each calculation is affected by a rounding-up error, the use of a very small  $h$  introduces a global error determined by the sum of the rounding-up errors, which could be greater than that expected from the order-of-magnitude error associated with the order  $h^{n+1}$ .

As an example of the application of the fourth-order Runge–Kutta method, we will consider the reversible equilibria of mechanism (4.VIII), described by the differential eqs. (4.64). The changes in the concentrations of the species A, B and C are illustrated in Figure 4.6 for two different integration step sizes. Note the difference between the calculated values and the exact ones obtained by the Laplace transform method for calculations using the larger step size. Since we are treating a system that is approaching equilibrium, this difference is conspicuous at the start of these reactions. Care must be exercised in choosing the step size since the choice of a totally inadequate value for it for the rate constants under consideration can lead to completely erroneous results.

#### 4.3.4 Markov chains

The most complex systems of kinetic equations cannot be solved analytically. In addition, when two of the differential equations of these systems describe processes that occur on drastically different timescales, their numerical integration using methods involving finite increments is unstable and unreliable. These methods are inherently deterministic, since their time evolution is continuous and dictated by the system of differential equations. Alternatively, we can apply stochastic methods to determine the rates of these reactions. These methods are based on the probability of a reaction occurring within an ensemble of molecules. This probabilistic formulation is a reflection either of the random nature of the collisions that are responsible for bimolecular reactions or of the random decay of molecules undergoing unimolecular processes. Stochastic methods allow us to study complex reactions without either solving differential equations or supplying closed-form rate equations. The method of Markov chains

is a stochastic one in which the rate constants are considered as probabilities of reaction per unit time [5]. With this method, the microstates of a system change with time such that the probability,  $p_{ij}$ , that the system proceeds from state  $a_i$  at time  $t$  to state  $a_j$  at time  $t + \Delta t$ , depends only on the state  $a_i$  at time  $t$ , and is independent of any states of the system at times before  $t$ . The probability that the state  $a_i$  will be unchanged during the same time interval is  $p_{ii}$ .

For a chemical reaction in which there is a 1:1 relationship in the conversion of reactant to product, the probabilities of transition  $p_{ij}$  can be represented by a square matrix having only positive or zero elements with  $m$  lines or columns, such that the sum of the entries in each line is unity.

$$\sum_{j=1}^m p_{ij} = 1 \quad (4.100)$$

The relation between the representative vector for the reactants considered at time  $t$  and for the products considered at time  $t + \Delta t$  can be expressed as

$$\begin{bmatrix} [A_1]_t & [A_2]_t & \dots & [A_m]_t \end{bmatrix} \begin{bmatrix} p_{11} & p_{12} & \dots & p_{1m} \\ p_{21} & p_{22} & \dots & p_{2m} \\ \vdots & & & \\ p_{m1} & p_{m2} & \dots & p_{mm} \end{bmatrix} = \begin{bmatrix} [A_1]_{t+\Delta t} & [A_2]_{t+\Delta t} & \dots & [A_m]_{t+\Delta t} \end{bmatrix} \quad (4.101)$$

Thus, the concentration of the species  $A_i$  in time  $t + \Delta t$  is given by

$$[A_i]_{t+\Delta t} = p_{1i} [A_1]_t + p_{2i} [A_2]_t + \dots + p_{mi} [A_m]_t \quad (4.102)$$

The values of the probabilities used in the transition matrix are related to the rate constants and to the time interval  $\Delta t$ . For a first-order reaction following eq. (4.1), the first term of the expansion in series of the exponential for one unit of time ( $\Delta t = 1$ ), leads to

$$[A] = [A]_0 (1 - k_1) \quad (4.103)$$

and

$$[A] - [A]_0 = k_1 \quad (4.104)$$

This first term in the expansion only approaches the exact value given by eq. (4.3), if  $k_1 \ll 1$  (i.e. the unit of time). The rate constant can thus be related to the probability with which the molecule  $A_i$  decays within one unit of time,  $p_{1,i}$ , while  $1 - k_1$  is the probability that this molecule remains unchanged during the same period. This relation can be extended to higher order elementary processes, since for sufficiently small time intervals, these kinetic processes can be considered to follow first-order behaviour. In a second-order reaction of the type  $A + B \rightarrow$  products, the probability of disappearance of A per unit time is  $k_2 [B]$  and the probability of A not reacting is  $1 - k_2 [B]$ . For a first-order reaction with  $k_1 = 10^8 \text{ sec}^{-1}$  and  $\Delta t = 10^{-9} \text{ sec}$ , the transition probability is 10%,  $p_{12} = 0.1$ . If the time interval chosen  $\Delta t = 10^{-10} \text{ sec}$ , the transition probability will be only 1%,  $p_{12} = 0.01$ . Using smaller time intervals leads to a linear solution of the kinetic equation that approximates more closely to the exact solution. However, this requires a lengthier calculation to describe the system

at any given time after the start of the reaction, and a compromise has to be made between the precision required and the computation time necessary.

As an example of the use of this treatment to construct a transition matrix, we will take the first-order decomposition reaction



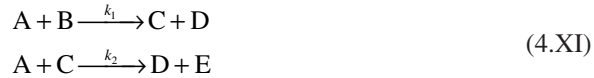
and consider that  $p_1 = k_1\Delta t$ . For the first iteration, the transition matrix will be

$$\begin{bmatrix} [A]_0 & 0 \end{bmatrix} \begin{bmatrix} 1-p_1 & p_1 \\ 0 & 1 \end{bmatrix} = \begin{bmatrix} (1-p_1)[A]_0 & p_1[A]_0 \end{bmatrix} \quad (4.105)$$

where  $[A]_0$  is the initial concentration of the reactant and  $(1-p_1[A]_0)$  its concentration after time interval  $\Delta t$ . The equations of recurrence for the disappearance of A and the formation of B are

$$\begin{aligned} [A]_{t+\Delta t} &= (1-p_1)[A]_t \\ [B]_{t+\Delta t} &= [B]_t + p_1[A]_t \end{aligned} \quad (4.106)$$

The method of Markov chains provides a useful tool for the study of very complex kinetic systems that do not have studied analytical solutions. As an example, consider the competitive-consecutive mechanism [5]



The transition matrix, with  $p_1 = k_1\Delta t$  and  $p_2 = k_2\Delta t$ , can be written

$$\begin{array}{ccccc} A & B & C & D & E \\ \left[ \begin{array}{ccccc} 1-p_1[B]-p_2[C] & 0 & p_1[B]/2 & p_2[C]/2 & (p_1[B]+p_2[C])/2 \\ 0 & 1-p_1[A] & p_1[A]/2 & 0 & p_1[A]/2 \\ 0 & 0 & 1-p_2[A] & p_2[A]/2 & p_2[A]/2 \\ 0 & 0 & 0 & 1 & 0 \\ 0 & 0 & 0 & 0 & 1 \end{array} \right] & & & & (4.107) \end{array}$$

The probability of the formation of C, D and E is multiplied by  $1/2$  since from the stoichiometry of the reaction, two molecules of reactant A are used up to form one molecule of C, D or E. The expressions of recurrence for concentration as a function of time are

$$\begin{aligned} [A]_{t+\Delta t} &= [A]_t (1-p_1[B]_t - p_2[C]_t) \\ [B]_{t+\Delta t} &= [B]_t (1-p_1[A]_t) \\ [C]_{t+\Delta t} &= [A]_t [B]_t + [C]_t (1-p_2[A]_t) \\ [D]_{t+\Delta t} &= p_2[A]_t [C]_t + [D]_t \\ [E]_{t+\Delta t} &= p_1[A]_t [B]_t + p_2[A]_t [C]_t + [E]_t \end{aligned} \quad (4.108)$$

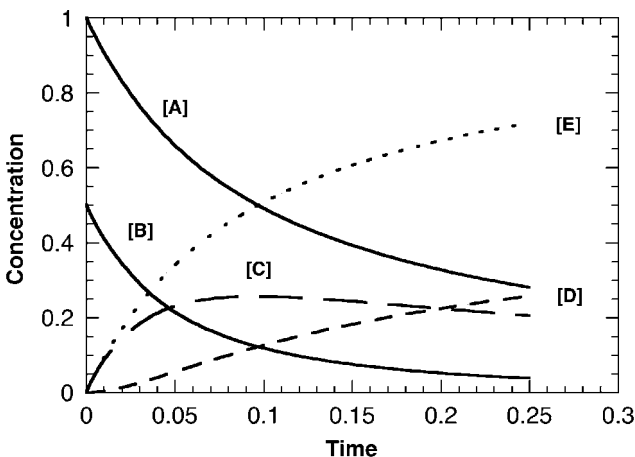


**Figure 4.8** Change in concentrations of reactants and products with time for mechanism (4.XI) calculated using Markov chains for a maximum transition probability of 10%.  $[A]_0 = 1$ ,  $[B]_0 = 0.5$ ,  $[C]_0 = 0$ ,  $[D]_0 = 0$ ,  $[E]_0 = 0$ ,  $k_1 = 20$ ,  $k_2 = 10$ .

The change in the concentrations of A, B, C, D and E with time are shown in Figure 4.8, together with the values of the initial concentrations and rate constants.

This method can also be applied to more complex cases such as flow systems involving spatially inhomogeneous systems and also to oscillating reactions in which the concentrations of the various intermediate species proceed through a number of cycles [6]. An example of an oscillating reaction in a homogeneous system with constant amplitude involves the Lotka type II mechanism [7]



where  $[A]$  is a constant. The transition matrix for this reaction

$$\begin{matrix} & X & Y \\ \begin{bmatrix} 1-p_2[Y]+p_1[A] & p_2[Y] \\ 0 & 1-p_3+p_2[X] \end{bmatrix} & & \end{matrix} \quad (4.109)$$

leads to the following equations for the concentrations of X and Y

$$\begin{aligned} [X]_{t+\Delta t} &= [X]_t (1 - p_2[Y]_t + p_1[A]) \\ [Y]_{t+\Delta t} &= p_2[X]_t [Y]_t + [Y]_t (1 - p_3 + p_2[X]_t) \end{aligned} \quad (4.110)$$

Lotka showed analytically that this system oscillates with a period  $T = 2\pi\sqrt{(k_1 k_2 [A])}$  and that the amplitude depends on the initial concentrations of X and Y. For oscillatory reactions

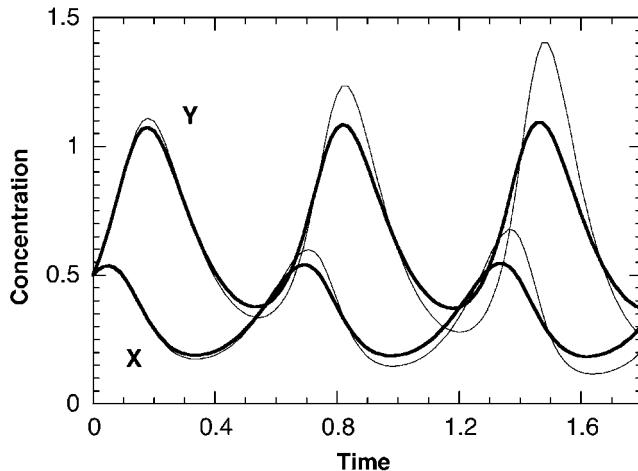


**Figure 4.9** Calculated concentrations of intermediates in a Lotka type II reaction for maximum transition probabilities of 1% (thick line) and 10% (thin line). [X] and [Y] correspond to the smaller and larger amplitudes, respectively.  $[A] = 1$ ,  $[X]_0 = 0.5$ ,  $[Y]_0 = 0.5$ ,  $k_1 = 10$ ,  $k_2 = 15$ ,  $k_3 = 10$ .

of this type the computational error has to be considerably less than 10% because the propagation of errors from one transition to another has the effect that small differences in the oscillation periods ( $\approx 10\%$ ) of X and Y, lead to a marked change in the amplitudes from cycle to cycle (20–30% when the transition probability is 10%). Results of calculations are shown in Figure 4.9 for the cases where transition probabilities of 10% and 1% are used. It is obvious in this case that it is impossible to avoid carrying out a more detailed (and time-consuming) calculation.

#### 4.3.5 Monte Carlo method

The Monte Carlo method is another stochastic procedure for the numerical determination of the change in concentrations of reactants, intermediates or products of a reaction as a function of time. This method can simulate the time evolution of any chemical system.

The major advantage of the Monte Carlo method stems from the fact that its convergence is independent of the dimension of the integral. Let us consider an integral of dimension  $j$

$$I = \int_{x_j} \cdots \int_{x_2} \int_{x_1} F(x) w(x) dx \quad (4.111)$$

where  $F(x)$  is a function of the variables  $x = (x_1, x_2, \dots, x_j)$  and  $w(x)$  is its distribution function. Within the Monte Carlo method, we initially apply a transformation of the type  $x \rightarrow \xi = (\xi_1, \xi_2, \dots, \xi_j)$  to the set of variables, with  $0 \leq \xi_j \leq 1$ . This transforms the above integral into

$$I = \int_0^1 \cdots \int_0^1 F(\xi) w(\xi) J d\xi = \int_0^1 \cdots \int_0^1 F(\xi) d\xi \quad (4.112)$$

where  $J$  represents the Jacobian transform which is equal to  $[w(\xi)]^{-1}$ . Once the values are calculated of  $F$  for  $N$  randomly chosen sets of variables  $(\xi_1, \xi_2, \dots, \xi_j)$ , the value of the integral estimated by the Monte Carlo method,  $I'$ , is given by

$$I \cong I' = \frac{1}{N} \sum_{i=1}^N F(\eta_i) \quad (4.113)$$

where  $\eta_i$  represents the set of the variables  $(\xi_1^i, \xi_2^i, \dots, \xi_j^i)$ . This method has been extensively used in studies of reaction dynamics, where the evolution of a trajectory that leads from the reactants in a given state (electronic, vibrational or rotational) to the products in another state requires the solution of the appropriate differential equations of motion. A minimum of  $10^j$  trajectories for each integral of dimensionality  $j$  is needed to ensure convergence with this type of calculation.

The Monte Carlo method can also be applied to solve the differential equations describing the time evolution of reactants, intermediates and products within a reaction sequence. We start by distributing the reactant molecules within a system of  $N$  coordinates. The molar fraction of each reactant can be considered to be the number of molecules of this reactant distributed over the total number of coordinates. The reaction is simulated by randomly generating numbers between 1 and  $N$ . In a first-order reaction, each time that a number generated corresponds to a coordinate occupied by the reactant, the reaction occurs. The rate constant,  $k_1$ , can be obtained by relating the number of reactive selections  $n_1$  accomplished during a cycle to the reaction time (which is the total number of selections). Each molecule has an equal and constant probability of reacting in time  $\Delta t$  since each position occupied by a molecule has an equal and constant probability,  $p$ , of being selected at random. Thus, if  $m$  is the number of cycles carried out, the simulation of a first-order reaction can be expressed as a function of real time knowing that

$$k_1 \Delta t = p n_1 m \quad (4.114)$$

In a reaction of rate constant  $k_1 = 10^7 \text{ sec}^{-1}$ , if we consider a timescale with units of 1 nsec and 10 events are accomplished in each cycle, the probability of a reaction occurring in each cycle will be  $p = 10^{-3}$ . The description of the time evolution of the system can thus be given in terms of the dependence of the molar fraction as a function of the number of cycles or, using the previous relation and converting the initial molar fraction into the initial concentration, as the variation of concentration with time.

If the reaction is second order, the probability of a molecule occupying a coordinate is independent of another occupying another coordinate. Consequently for each cycle  $m$ , two events must be made, one for each reactant molecule. If a molecule is found in both selections, then the reaction will occur.

Particularly useful applications of the Monte Carlo method include modelling complex oscillatory reactions and studying enzyme catalysis [8,9]. As an example of the latter treatment, we will consider a system involving an initial reversible complex formation between the enzyme and the substrate, accompanied by a reversible step of inhibition of the catalyst

by the product, as described by the scheme



The system of differential equations needed to describe this system is very complex:

$$\begin{aligned}
 \frac{d[S]}{dt} &= -k_1[E][S] + k_{-1}[ES] \\
 \frac{d[E]}{dt} &= -k_1[E][S] + k_{-1}[ES] + k_2[ES] - k_3[E][P] + k_{-3}[EP] \\
 \frac{d[ES]}{dt} &= k_1[E][S] - k_{-1}[ES] - k_2[ES] \\
 \frac{d[P]}{dt} &= k_2[ES] - k_3[E][P] + k_{-3}[EP] \\
 \frac{d[EP]}{dt} &= k_3[E][P] - k_{-3}[EP]
 \end{aligned} \quad (4.115)$$

A further equation is given by the mass balance

$$[E]_0 = [E] + [ES] + [EP] \quad (4.116)$$

where  $[E]_0$  is the initial enzyme concentration. However, the study of this system by the Monte Carlo method avoids having to treat all these equations. Results are presented in Figure 4.10 for a kinetic simulation using as starting point 100 molecules of S and 10 of E.

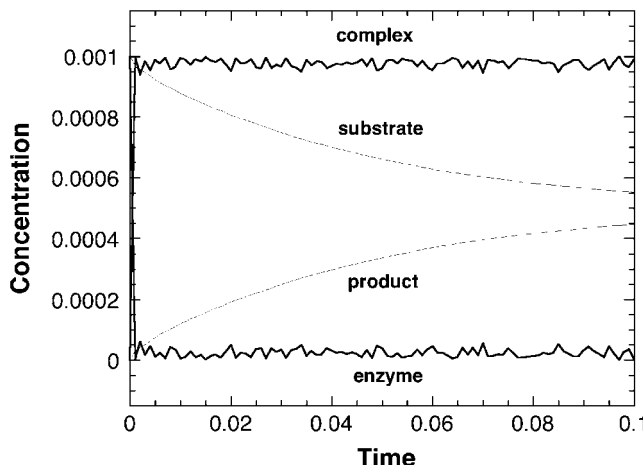


**Figure 4.10** Application of the Monte Carlo method to mechanism (4.XIV).

The simulations accomplished using the Monte Carlo method show oscillations of the order  $N^{-1/2}$ , where  $N$  is the total number of molecules in the simulation. Considering the process at the macroscopic level, it is tempting to assume that the oscillations observed in these simulations are approximations of the continuous behaviour given by the functional and integral expressions. However, events that occur on the molecular scale are discrete. Continuous macroscopic behaviour is only observed since in real chemical systems we normally consider a very large number of molecules. The Monte Carlo method clearly shows that starting from a random microscopic behaviour a deterministic macroscopic behaviour results. We should note that there is currently great interest in studying the dynamic behaviour in these systems at the level of the behaviour of single molecules, using for example, single-molecule fluorescence. These studies are providing important insights into the link between the microscopic and macroscopic behaviour of chemical systems.

## 4.4 SIMPLIFICATION OF KINETIC SCHEMES

In the previous sections, we have discussed methods of solving kinetic equations based upon rigorously formulating all the elementary steps involved in the reaction mechanism in terms of the respective differential equations. In the most complex cases, the solution of the system of these differential equations obtained is possible by the use of approximate numerical methods, leading to an approximate solution to a rigorously formulated kinetic scheme. Alternatively, we can make use of our chemical knowledge of the system, and then make approximations using this knowledge that appreciably simplifies the system of differential equations, such that we can obtain an exact solution of a system that approximately describes the kinetic scheme. In both cases we obtain approximate solutions. With numerical approximations, the precision of the results obtained depends on the amount of the computational time invested. In the case of simplifying the chemical system, the quality of the result depends on how adequately the simplified model describes the real system.

Three types of fundamental simplification can be used: the method of isolation of one of the reactants, the pre-equilibrium approximation and the steady-state approximation. In addition, in many mechanisms it is possible to identify the one step that exercises a pronounced effect on the velocity of the overall reaction. This step is normally termed as the rate-determining step of the reaction, and when it exists, it allows us to obtain very simple relationships for the kinetics of the overall reaction.

### 4.4.1 Isolation method

An elementary reaction involving two or three reactants can, in principle, be treated as a pseudo-first-order reaction using the isolation method. In agreement with this method, if all the reactants except one are in excess, the apparent order of the reaction will be the order relative to the isolated reactant, since the concentrations of the species in excess do not vary appreciably during the reaction. Thus, if a reaction is of order  $a$  relative to A, of order  $b$  relative to B and of order  $c$  relative to C, and if the concentrations of B and C are considerably greater than that of A, experimentally the order of reaction will be  $a$  and the

rate constant will be  $k'$

$$-\frac{d[A]}{dt} = k'[A]^a \quad (4.117)$$

where

$$k' = k_3[B]^b[C]^c \quad (4.118)$$

For the commonest case of  $a = 1$ , eq. (4.117) corresponds to a pseudo-first-order reaction.

The partial orders  $b$  and  $c$  can be obtained by the same process. The application of this method requires some caution, and it is desirable to use other methods to confirm the orders of reaction for the other components, since for complex mechanisms involving various steps, these can be influenced by changes in concentration, leading to different mechanisms under different conditions of “isolation”. In addition, when using a large excess of one of the reagents, if this contains an impurity, the concentration of the impurity under these conditions could be so great that it takes part in the rate law, leading to erroneous and frequently erratic results.

The precision with which this method can be used depends on the experimental conditions used. For example, in an elementary bimolecular reaction in which  $[B] = 100[A]$ , at the end of the first half-life of the reaction, there is only a 0.5% reduction in the initial value of  $[B]$ , while at the end of the reaction, the concentration of B is still 99% of its initial value, and changes of this order of magnitude are not significant within the current methods of analysis. If one of the reactants is  $H^+$  or  $OH^-$ , instead of using an excess of these reactants we can achieve the same effect using a buffer solution that keeps the pH constant throughout the reaction. An alternative method involves keeping one of the reactants in solution in equilibrium with its solid phase, such that even though there is consumption of the reactant, its solution concentration will be constant.

We should note that when one of the reactants is the solvent, its participation in the mechanism of the reaction may not be noticed, since its concentration remains practically constant. The observed rate law for this reaction could, in fact, be a pseudo-first-order one.

#### 4.4.2 Pre-equilibrium approximation

A second-order reaction in equilibrium followed by a first-order one of the type



leads to a kinetic system whose rate of formation of products can be expressed as

$$\frac{d[D]}{dt} = k_2[C] \quad (4.119)$$

but whose analytical solution is complicated. Kinetically, this problem is greatly simplified if  $k_1$  as well as  $k_{-1}$  is significantly larger than  $k_2$ . Under these conditions it is possible

to assume that the formation of C from A and B is in equilibrium, from which [C] can be obtained from the relationship

$$k_1[A][B] = k_{-1}[C] \quad (4.120)$$

knowing that

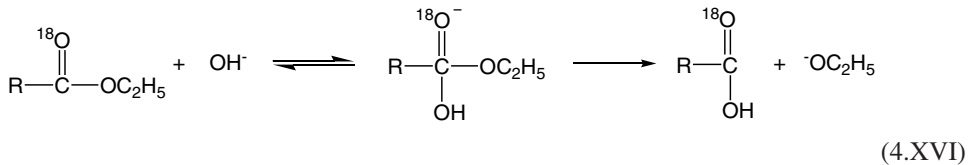
$$K = \frac{k_1}{k_{-1}} \quad (4.121)$$

and substituting  $[C] = K[A][B]$  in the eq. (4.119) to give

$$\frac{d[D]}{dt} = k_2 K[A][B] \quad (4.122)$$

where the rate of this reaction is described by a simple second-order kinetic equation.

A system of the above type is characterised by a rapid pre-equilibrium step. A typical example is given by the base-catalysed hydrolysis of an ester



#### 4.4.3 Steady-state approximation

If in the kinetic scheme



described by the rate laws

$$\begin{aligned} \frac{d[\text{A}]}{dt} &= -k_1[\text{A}] + k_{-1}[\text{B}] \\ \frac{d[\text{B}]}{dt} &= k_1[\text{A}] - (k_{-1} + k_2)[\text{B}] \\ \frac{d[\text{C}]}{dt} &= k_2[\text{B}] \end{aligned} \quad (4.123)$$

the concentration [B] does not vary appreciably with time, i.e. to a first approximation  $d[\text{B}]/dt = 0$ , we can write

$$[\text{B}] = \frac{k_1[\text{A}]}{k_{-1} + k_2} \quad (4.124)$$

which leads to the simple relationship for the rate of disappearance of A or of formation of the product C in the form

$$\frac{d[A]}{dt} = -\frac{d[C]}{dt} = -\frac{k_1 k_2}{k_{-1} + k_2} [A] \quad (4.125)$$

This is known as the steady-state approximation, since the concentration of B is assumed to be constant throughout the reaction. This is valid except at the initial and final stages of many kinetic schemes. Applying the steady-state approximation, the above kinetic scheme is reduced to a first-order rate law, where the observed pseudo-first-order constant is given by  $k_1 k_2 / (k_{-1} + k_2)$ .

It is reasonable that the variation of [B] with time will be small if [B] is also a small quantity. Thus, the condition for application of the steady-state approximation can be given as

$$[B] = \frac{k_1 [A] - \frac{d[B]}{dt}}{k_{-1} + k_2} \quad (4.126)$$

i.e.

$$\frac{d[B]}{dt} \ll k_1 [A] \quad (4.127)$$

At the start of the reaction, when the intermediate B is being formed, the change in its concentration with time is not negligible, and the steady-state approximation does not hold. However, as it is assumed that the concentration of B is small, that is  $[B] \ll [A]$ , we can also formulate the conditions for the application of the steady-state approximation in terms of the rate constants for the formation and decay of B

$$k_{-1} + k_2 \gg k_1 \quad (4.128)$$

Thus, this is valid when the disappearance of the intermediate is faster than its formation. Alternatively, it is useful to consider the validity of the steady-state approximation in terms of free-energy profiles, which are shown in Figure 4.11 for the various situations possible for mechanism (4.XVII) [10]. For profiles (iii), (iv) and (vi) the steady-state approximation is valid because the reactant is more stable than the intermediate, such that the concentration of B will always be less than that of A. Although B is more stable than A in profile (v), it does not form to any appreciable extent because its conversion into products is faster than its rate of formation. However, with profiles (i) and (ii), appreciable concentrations of B will be produced, such that the steady-state approximation is not valid.

One of the most important examples of the application of this approximation is enzyme catalysis [11]. Enzyme catalysis can be described in its simplest form by the scheme



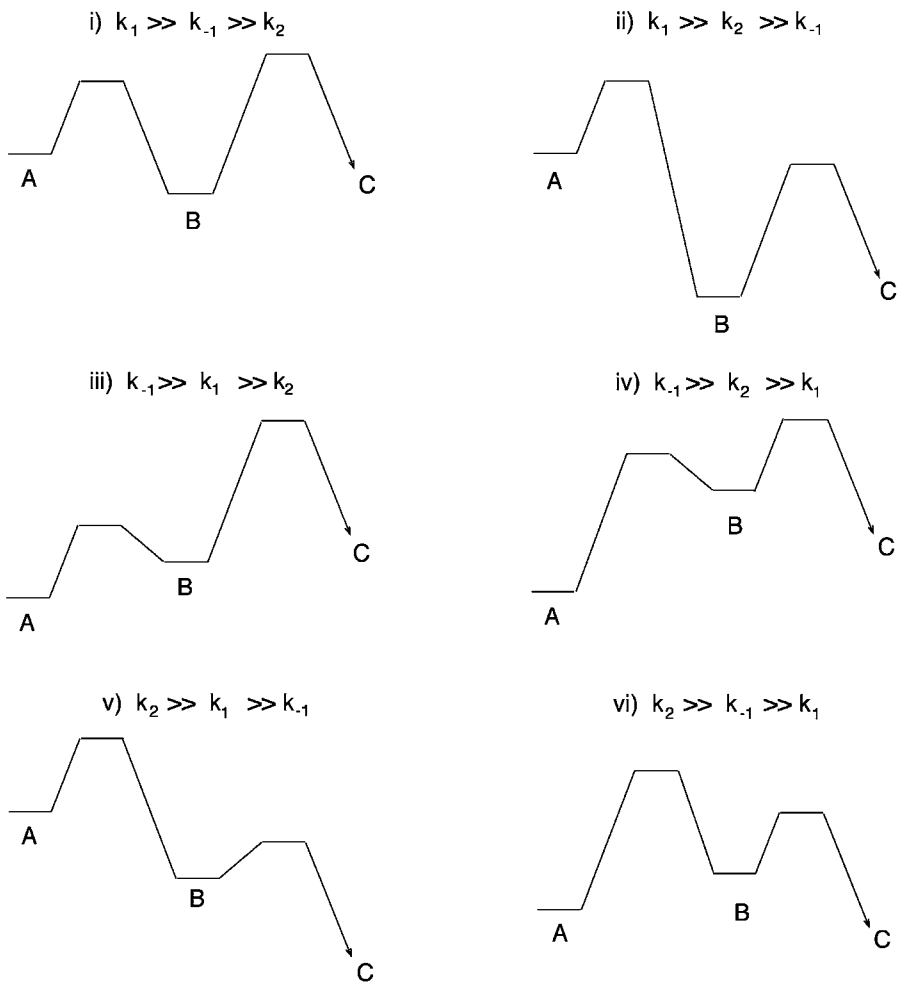


**Figure 4.11** Schematic free-energy profiles illustrating the six possible relationships between the rate constants for mechanism (4.XVII).

where E represents the enzyme, S the substrate and P the catalytic product. Using the steady-state approximation, we obtain

$$\begin{aligned}\frac{d[ES]}{dt} &= k_1 [E][S] - (k_{-1} + k_2)[ES] = 0 \\ [ES] &= \frac{k_1 [E][S]}{k_{-1} + k_2}\end{aligned}\quad (4.129)$$

As the total concentration of enzyme present  $[E]$ , is normally known and can be expressed as

$$[E]_t = [E] + [ES] \quad (4.130)$$

the concentration of the enzyme/substrate complex following the steady-state approximation will be

$$[\text{ES}] = \frac{k_1 [\text{E}]_t [\text{S}]}{k_{-1} + k_2 + k_1 [\text{S}]} \quad (4.131)$$

If we define the rate of reaction in terms of formation of the products,  $v = d[\text{P}]/dt = k_2[\text{ES}]$ , we obtain

$$v = \frac{k_1 k_2 [\text{E}]_t [\text{S}]}{k_{-1} + k_2 + k_1 [\text{S}]} \quad (4.132)$$

which, following Michaelis and Menten, can also be written as

$$v = \frac{V_m [\text{S}]}{K_m + [\text{S}]} \quad (4.133)$$

where  $V_m$  is the maximum velocity and  $K_m$  the Michaelis constant.

$$V_m = k_2 [\text{E}]_t \quad (4.134)$$

and

$$K_m = \frac{k_{-1} + k_2}{k_1} \quad (4.135)$$

The Michaelis–Menten equation can be rewritten to produce linear relationships. For example, Lineweaver–Burke plots are obtained using

$$\frac{1}{v} = \frac{K_m}{V_m [\text{S}]} + \frac{1}{V_m} \quad (4.136)$$

In Figure 4.12, a Lineweaver–Burke plot is shown for the example of enzyme catalysis discussed in Chapter 3.

#### 4.4.4 Rate-determining step of a reaction

For each of the reaction pathways (3.I), (3.V) and (3.XI), discussed in Chapter 3, the slowest step was identified, and was designated the rate-determining step of the reaction. In the general scheme, the subsequent fast steps do not have any influence on the kinetics of the overall reaction: the velocity of formation of the final products cannot exceed the rate of formation of the intermediate produced in the slowest step of the kinetic mechanism [12,13].

It is tempting to associate the slowest step with that which has the highest energy barrier among those involved in the reaction mechanism. However, this is not strictly true for

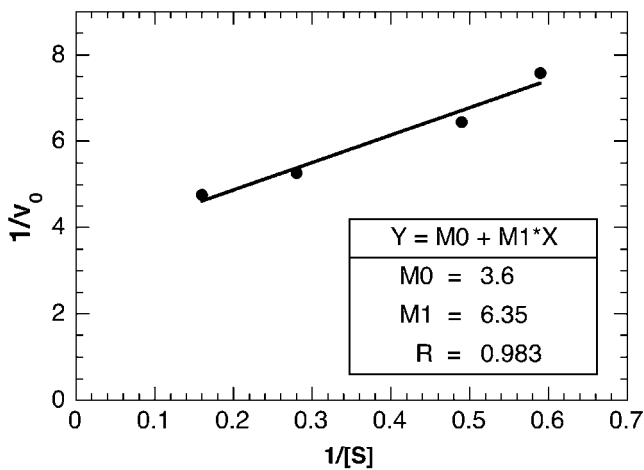


Figure 4.12 Lineweaver–Burke plot for the hydrolysis of Azocoll by papain.

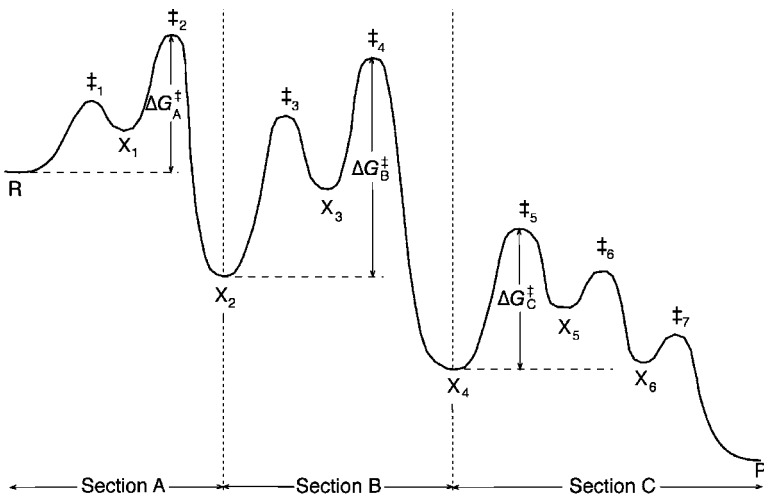
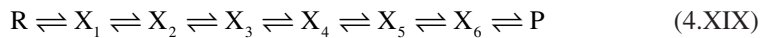


Figure 4.13 Changes in free energy during a reaction that follows mechanism (4.XIX).

reversible reactions, where intermediates that are more stable than the reactants are normally formed. Figure 4.13 shows a complex mechanism of the type



The transition state of the highest energy in this reaction is  $\ddot{\tau}_2$ , but the rate-determining step is not the conversion of  $X_1$  to  $X_2$ . It is convenient to divide the free energy profile into sections to identify the slowest step. The end of each section is determined by the appearance of the first intermediate whose energy is less than that of the intermediate (or initial reactant)

that starts the section. Within each section, it is easy to identify the highest energy transition state. In Figure 4.13, these are  $\ddot{\text{S}}_2$ ,  $\ddot{\text{S}}_4$  and  $\ddot{\text{S}}_5$ . The free energies of activation of these transition states relative to the start of each section are  $\Delta G_{\text{A}}^{\ddagger}$ ,  $\Delta G_{\text{B}}^{\ddagger}$  and  $\Delta G_{\text{C}}^{\ddagger}$ . The largest of them is  $\Delta G_{\text{B}}^{\ddagger}$  and  $\text{X}_2$  is converted into  $\text{X}_4$  more slowly than it is formed from  $\text{R}$ . Thus, the rate-determining step of this reaction is the transformation of  $\text{X}_3$  into  $\text{X}_4$ .

## REFERENCES

- [1] E Levin, JG Eberhart, *J. Chem. Educ.* **66** (1989) 705.
- [2] SC Castillo, SG Micolta, *J. Chem. Educ.* **68** (1991) 179.
- [3] MN Berberan-Santos, JMG Martinho, *J. Chem. Educ.* **67** (1990) 375.
- [4] J Seixas de Melo, AL Maçanita, *Chem. Phys. Lett.* **204** (1993) 556.
- [5] SJ Formosinho, MGM Miguel, *J. Chem. Educ.* **56** (1979) 582.
- [6] SJ Formosinho, *J. Chem. Educ.* **59** (1982) 281.
- [7] AJ Lotka, *J. Am. Chem. Soc.* **42** (1920) 1595.
- [8] MR Kibby, *Nature* **222** (1969) 298.
- [9] DT Gillespie, *J. Phys. Chem.* **81** (1977) 2340.
- [10] R Raines, DE Hansen, *J. Chem. Educ.* **65** (1988) 757.
- [11] O Moe, R Cornelius, *J. Chem. Educ.* **65** (1988) 137.
- [12] JR Murdoch, *J. Chem. Educ.* **58** (1981) 32.
- [13] KJ Laidler, *J. Chem. Educ.* **65** (1988) 250.

This page intentionally left blank

## – 5 –

# Collisions and Molecular Dynamics

---

We can only really say that we understand any physical phenomenon when we can predict it and can calculate both its occurrence and order of magnitude using only fundamental data based on the physical and structural factors involved. This calculation must be based on a theory that relates the forces involved in the observed phenomenon and the experimental measurements on it.

The development of any such scientific theory initially involves experimental observations. Based on this experimental foundation, suppositions or hypotheses are then constructed, which provide reasonable explanations for the observed behaviour and which are able to solve problems (i.e. make predictions) related to it. The success of this is determined by the confirmation of any predictions, the possibility of explaining other related observations and, eventually, by the solution of new problems within the same area. When this process of verification is successful, we obtain one of the “hard core” of scientific laws, which are useful for explanation as well as prediction of experimental observations. However, any theoretical model is an internal representation created within the framework of the world that surrounds us, and as such can never be perfect or complete. A theory is, thus, a set of models associated with various hypotheses that relate, in a causal form, to the real-world systems.

Within scientific theories, in particular those related to chemical kinetics, there is a certain hierarchy. The simplest conceptual structure involves some statistically significant correlation between sets of experimental data, for example, relationships between rate constants of certain reactions and their corresponding equilibrium constants. This is known as an *empirical correlation*. At the opposite extreme, we can find theories that allow us to calculate reaction rate constants using only fundamental constants from the basic laws of physics (such as those given in Appendix I), and, frequently, the Born–Oppenheimer approximation involving separation of nuclear and electron motions. These theories are known as *ab initio* theories, i.e. based on first principles. The term *ab initio*, which to some extent is a misnomer, was first used by Parr to describe processes which had been developed since the beginning within a given research project in his laboratory. In general, the validity of such *ab initio* procedures, as with any scientific theory, can only be shown by comparison with experiments.

Between these limits of empirical correlations and *ab initio* calculations, a large number of theories of chemical kinetics are found with varying degrees of empiricism, which depend upon how many adjustable parameters are needed to fit the calculation to the experimental

data. Although they may lack the theoretical rigour of more fundamental theoretical formulations, these more empirical theories are important since, apart from their historical interest, they often act as pointers for the development of more quantitative theoretical models. These can be directed towards real systems and can help us avoid using highly sophisticated calculations to treat the wrong target. To quote the late John W. Tukey, who made major contributions to statistics, both in industrial and academic areas: “An approximate answer to the right question is worth a great deal more than a precise answer to an approximate question”. It is worth noting that John Tukey’s initial background was chemistry.

At a first glance, an *ab initio* theory would seem to be the most satisfactory way to treat theoretically the chemical kinetics of any system, since this does not need to introduce any experimental data. However, only those systems involving 3–4 atoms in the gas phase can be solved with chemical accuracy ( $\pm 4$  kJ/mol) by this route. For the vast majority of reactions of chemical interest, we need either to introduce major simplifications into the most sophisticated theories so that they can be applied, or to opt for a simpler theory, including empirical parameters, which can be used without *a posteriori* changes to estimate the rate constants. These approaches differ because in the first case, approximations are made when the method is applied, while with the latter approach, the approximations come within the formulation of the theory. In both cases, we hope that we can understand and interpret any discrepancies between the observed and the calculated kinetic data. The approach we use frequently depends upon the nature of the chemical system. The biggest problem is how to interpret any disagreement between experiment and calculation. This could result from experimental error, from wrong approximations when we apply the theory or incorrect assumptions in the theory itself. In the latter case, the theory is wrong and must be rejected. We must try to avoid the tendency of attributing any discrepancies between theoretical prediction and experimental observation to approximations introduced in the application of the theory, rather than to any weakness in the theory itself. The continued use of any obsolete theory past its “sell-by date”, is scientifically incorrect as well as hindering the development of more appropriate models.

As a scientific theory is intended to simulate and help us understand the behaviour of part of or the whole Universe, it should be kept sufficiently simple to be understandable, and its proof should be purely operational. The relevant question should not be whether it is true or false, since this does not have any meaning from a scientific viewpoint. Instead we should ask: “does it work”?

Even so, the answer to this question may not be completely objective. We can discard a theory that contains errors of logic, but a similar decision based upon comparison between theoretical and experimental data depends on how rigorous we want the agreement to be.

Based on these ideas, we will discuss the simple collision theory, which is attractive because of the relationship it provides between the orientation and the energy of the molecules involved in collisions and their reactivity. However, it is not actually satisfactory as a theoretical hypothesis for polyatomic systems, since it cannot be used quantitatively for the calculation of rates of chemical reactions. However, for triatomic systems whose potential energy surfaces (PESs) are well defined, the calculation of trajectories using this approach provides an excellent method for calculating the reaction rates. Thus, we will restrict this type of calculation to simple systems. For polyatomic systems or reactions in

solution, it is totally impracticable and we will make use of other theories to be discussed in the following chapter.

## 5.1 SIMPLE COLLISION THEORY

The simplest model for the rates of chemical reactions assumes that every time there is a bimolecular collision, there is a reaction. From calculations of the frequency of collisions in this system, we can then determine the rate constant.

To calculate the number of collisions per unit time, we need a model for the behaviour of molecules in these systems. The simplest approach involves a system of two gases, A and B, whose molecules behave as hard spheres, which are characterised by impenetrable radii  $r_A$  and  $r_B$ . A collision between A and B occurs when their centres approach within a distance  $d_{AB}$ , such that

$$d_{AB} = r_A + r_B \quad (5.1)$$

If we assume that the molecules of B are fixed and that those of A move with an average velocity  $\bar{v}_A$ , each molecule A sweeps a volume  $\pi d_{AB}^2 \bar{v}_A$  per unit time which contains stationary molecules of B. The area  $\sigma_p = \pi d_{AB}^2$ , is known as the *collision cross section*. If there are  $N_B/V$  molecules of type B per unit volume, the number of collisions of a molecule of type A with the stationary molecules B will be

$$z_{AB} = \frac{\pi d_{AB}^2 \bar{v}_A N_B}{V} \quad (5.2)$$

If the total number of molecules of A per unit volume is  $N_A/V$ , then the total number of collisions of A with B per unit volume is given by

$$Z_{AB} = \frac{\pi d_{AB}^2 \bar{v}_A N_B N_A}{V^2} \quad (5.3)$$

As indicated above, we have assumed that the molecules of B are stationary to obtain the above expression. In practice, Figure 5.1 shows that, for each pair of molecules, A and B, involved in a collisional trajectory, we can define a relative velocity  $v_{AB}$ , which is related to their velocities,  $v_A$  and  $v_B$ , according to

$$v_{AB} = \left( v_A^2 + v_B^2 - 2v_A v_B \cos \theta \right)^{1/2} \quad (5.4)$$

The value of  $\cos \theta$  can vary between  $-1$  and  $1$ . As all values of  $\theta$  between  $0$  and  $360^\circ$  are equally probable, the positive and negative values of  $\cos \theta$  will cancel out, and the mean value will be zero. Thus we obtain

$$\bar{v}_{AB}^2 = \bar{v}_A^2 + \bar{v}_B^2 \quad (5.5)$$

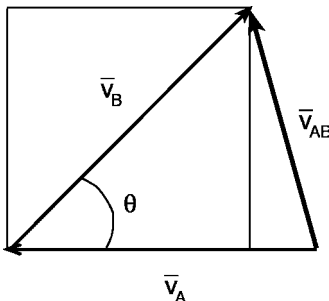


**Figure 5.1** Relative velocities for a collisional trajectory between molecules A and B.

Assuming that the molecular velocities are described by a Maxwell–Boltzmann distribution, the mean velocity of the molecules of a gas A is given by eq. (1.11). Consequently, the relative mean molecular velocity of molecules of types A and B will be

$$\bar{v}_{AB} = \sqrt{\frac{8k_B T}{\pi\mu}} \quad (5.6)$$

where the reduced mass is  $\mu = m_A m_B / (m_A + m_B)$ . Introducing this value for the relative velocity in eq. (5.3), we obtain

$$Z_{AB} = \frac{\pi d_{AB}^2 \bar{v}_{AB} N_B N_A}{V^2} \quad (5.7)$$

If we consider a gas that contains only molecules of type A, the total number of collisions would be

$$Z_{AA} = \frac{1}{2} \frac{\pi 4r_A^2 \bar{v}_{AA} N_A^2}{V^2} \quad (5.8)$$

where the factor  $1/2$  arises because we cannot count the same molecule twice. Since from eq. (5.5), the relative mean velocity of the molecules of a gas can be related to the mean velocity of the molecules,  $\bar{v}_{AA} = \sqrt{2} \bar{v}_A$ , eq. (5.8) can be rewritten as

$$Z_{AA} = \frac{2\sqrt{2}\pi r_A^2 \bar{v}_A N_A^2}{V^2} \quad (5.9)$$

The expressions for the number of collisions per unit time, also known as the collision densities, contain two factors involving the number of molecules per unit volume. These can be expressed in terms of pressures or molar concentrations, giving the rate constant for a bimolecular reaction between molecules of A and B in the experimentally more meaningful form

$$k_{AB} = \sigma_R \bar{v}_{AB} = \pi d_{AB}^2 \sqrt{\frac{8k_B T}{\pi\mu}} \quad (5.10)$$

We can test this collision theory approximation by comparing the value calculated for the elementary reaction



at 870 K with the experimental value,  $k_{\text{exp}} = 1.5 \times 10^2 \text{ dm}^3 \text{ mol}^{-1} \text{ sec}^{-1}$ . From the van der Waals radii of N and O atoms, the reactant bond lengths, and assuming that these behave as hard spheres, we can estimate that  $d_{\text{AB}} = 4 \times 10^{-10} \text{ m}$ . The reduced mass can be calculated from the relative molecular masses of nitrogen dioxide and carbon monoxide

$$\mu = \frac{46 \times 28}{46 + 28} 1.661 \times 10^{-27} = 2.89 \times 10^{-26} \text{ kg} \quad (5.11)$$

where the units conversion factor in the unified atomic mass unit, from which we obtain the relative mean velocity, using the relationship  $1 \text{ J} = 1 \text{ kg m}^2 \text{ sec}^{-2}$ ,

$$\bar{v}_{\text{NO}_2, \text{CO}} = \sqrt{\frac{8 \times 1.38 \times 10^{-23} \times 870}{3.14 \times 2.89 \times 10^{-26}}} = 1.03 \times 10^3 \text{ m sec}^{-1} \quad (5.12)$$

such that we calculate the rate constant to be  $k_{\text{AB}} = 5.17 \times 10^{-16} \text{ m}^3 \text{ molecules}^{-1} \text{ sec}^{-1} = 3.11 \times 10^{11} \text{ dm}^3 \text{ mol}^{-1} \text{ sec}^{-1}$ . We can see from the comparison between the experimental and calculated values that the latter are a factor of at least  $10^9$  greater than the former.

In this simple collision theory, there are two implicit approximations which lead to calculated values that are considerably greater than the experimental ones: (i) not all the collisions occur with a favourable orientation for reaction; (ii) we need a certain amount of energy for the conversion of the reactants into products, and not all the collisions have enough energy to produce this chemical transformation.

The first of these approximations can be corrected for by introducing a geometric factor,  $g \leq 1$ . This can be calculated using the molecular geometries of the reactants and products. In the example of reaction (5.I), it is necessary that in the collision the NO bond is extended and its oxygen atom directly approaches the carbon atom of CO for the reaction to occur (Figure 5.2). When the N–O and C–O bonds are collinear, the chemical transformation results from the stretching of these bonds, since these stretching vibrations are of high frequency and energy. In this model, the geometric factor  $g$  is given by the product of the orientation factor for the CO molecule,  $\frac{1}{2}$ , and that of the  $\text{NO}_2$  molecule, which, as indicated in Figure 5.2, will be approximately  $2/17$ . Therefore, for this reaction,  $g = 1/17$ .

The geometric factor may become much less than unity with increasing complexity of the reaction in the gas phase. In addition, with reactions in solution, we need to consider effects of solvent cage, which allow many collisions to occur during an encounter between the two reactants, such that the effect of the geometric factor becomes more difficult to calculate. However, as we will see, in these systems, too, it is less relevant.

The energetic factor is of fundamental importance in the determination of reaction probabilities and, hence, rate constants. Once more, we start from the Maxwell–Boltzmann distribution (eq. 1.10) to calculate this factor. In practice, in collision theory, we normally

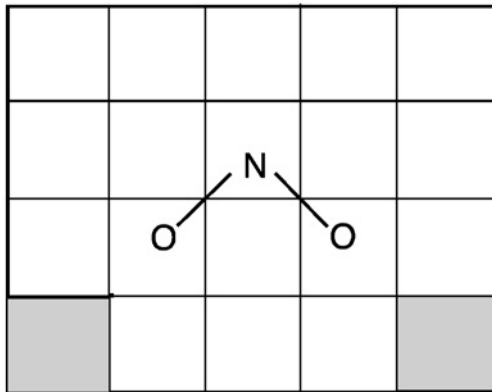


**Figure 5.2** Sketch of the origin of the geometric factor in a collision. The favourable orientations for the attack of the carbon atom of CO are shaded.

use the distribution function of molecular velocities in two dimensions rather than in three.

$$\frac{dN}{N_0} = \frac{m}{k_B T} \exp\left(\frac{-mv^2}{2k_B T}\right) v dv \quad (5.13)$$

Although there is no strong theoretical basis for this decrease in dimensionality, it simplifies the system, and we can rationalise it by considering that at the instant of collision between the two molecules, the velocity vectors have a common point such that they lie within a plane. Thus, the components of the velocities within the two dimensions that define this plane are sufficient to describe an effective collision. The distribution of molecular energies, based on the above equation, is

$$\frac{dN(\varepsilon)}{N_0} = \frac{1}{k_B T} \exp\left(\frac{-\varepsilon}{k_B T}\right) d\varepsilon \quad (5.14)$$

which can be integrated to obtain the fraction of collisions with energy equal to or greater than the critical value,  $\varepsilon_c$ , for the reaction to occur.

$$\begin{aligned} \int_{\varepsilon > \varepsilon_c} \frac{dN(\varepsilon)}{N_0} &= \int_{\varepsilon_c}^{\infty} \frac{1}{k_B T} \exp\left(\frac{-\varepsilon}{k_B T}\right) d\varepsilon \\ &= \exp\left(\frac{-\varepsilon_c}{k_B T}\right) \end{aligned} \quad (5.15)$$

If we include this energetic term and the geometric factor  $g$  in the expression for the rate constant, we obtain the final expression for the rate constant given by the collision theory

that considers only effective collisions.

$$k_{\text{col}} = g\pi d_{\text{AB}}^2 \sqrt{\frac{8k_{\text{B}}T}{\pi\mu}} \exp\left(\frac{-\varepsilon_c}{k_{\text{B}}T}\right) \quad (5.16)$$

This expression bears an obvious resemblance to that of the Arrhenius law. In fact the pre-exponential factor in the latter expression can be identified as

$$A = g\pi d_{\text{AB}}^2 \sqrt{\frac{8RT}{\pi\mu}} \quad (5.17)$$

The activation energy, expressed in molar terms, is given by

$$E_a = \frac{d \ln(k_{\text{col}})}{d(1/RT)} = E_c + \frac{1}{2}RT \quad (5.18)$$

The expressions (5.16)–(5.18) were first applied to bimolecular gas phase reactions by M. Trautz (1916) and W.C. McC. Lewis (1924). The terms in  $d$  and  $\mu$  in eq. (5.17) generally compensate each other, such that, if we exclude the geometric factor  $g$ , in many cases  $\log A = 10.5 \pm 0.5$ , with  $A$  given in  $\text{dm}^3 \text{ mol}^{-1} \text{ sec}^{-1}$ . Steric hindrance, caused by the presence of bulky groups in the positions adjacent to the point of attack, is seen mainly through an increase in the activation energies of reactions and not through a decrease in the frequency of effective collision. Thus, the simple collision theory does not lead to significant correlations between the changes in structures and the calculated values for  $A$ . Some people have refined this theory by defining an entropy of activation for the molecular collisions, leading to

$$A = g\pi d_{\text{AB}}^2 \sqrt{\frac{8RT}{\pi\mu}} \exp(\Delta S^*/R) \quad (5.19)$$

The introduction of this extra term in the expression for the pre-exponential factor may explain values much less than those determined by the frequency of collisions. However, as in most situations it is not easy to calculate this entropy of activation, this new term is only of limited use.

The numerical value of the collision theory value rate constant, previously calculated for the  $\text{NO}_2 + \text{CO}$  reaction ( $3.11 \times 10^{11} \text{ dm}^3 \text{ mol}^{-1} \text{ sec}^{-1}$ ) corresponds to the typical values calculated for the pre-exponential factors of gas-phase bimolecular reactions. Dividing this value by the molar volume of an ideal gas at standard temperature and pressure ( $22.421 \text{ dm}^3 \text{ mol}^{-1}$ ), we obtain a relaxation rate, which is approximately  $(p\tau)^{-1} = 10^{10} \text{ atm}^{-1} \text{ sec}^{-1}$  at 273 K. This implies that the mean free time between collisions of molecules of an ideal gas is 0.1 nsec, and that the corresponding collision frequency is  $\tau_{\text{coll}}^{-1} \approx 10^{10} \text{ sec}^{-1}$ . Some caution must be made in using these values, since molecules interact with a range of velocities and instantaneous inter-molecular distances, such that there is no single collision frequency, but

there is a distribution of time intervals between collisions. This distribution can be given in terms of a Poisson function in  $n$

$$P(n) = e^{-\gamma} \frac{\gamma^n}{n!} \quad (5.20)$$

where the mean value of  $n$  is  $\langle n \rangle = \gamma = T/\tau_{\text{coll}}$ , and  $T$  is the number of collisions per unit time.

The simple collision theory treatment shows the basic elements for a bimolecular rate constant: we need a collision to occur, a certain critical energy has to be exceeded and the particles involved in the collision have to have the correct relative orientations.

## 5.2 COLLISION CROSS SECTION

Instead of assuming hard sphere behaviour, we can refine the collision theory by using cross sections calculated on the basis of microscopic interaction potentials of species A and B during their collision,  $\sigma_R$ . Before we develop the problem for reactive collisions, we will start by treating the simpler situation of an elastic collision between two bodies subjected to a central force, which only leads to scattering.

The collision of these two bodies can be seen by a system of coordinates based on the centre of mass (Figure 5.3). The equations of motion will be determined by the conservation of initial energy,  $E$ , and of angular momentum,  $L$ . As the direction of  $L$  is conserved, the trajectory has to remain in a plane and the equations of motion can be written, in polar coordinates

$$\begin{aligned} L &= \mu v b = \mu r^2 \frac{d\phi}{dt} \\ E &= \frac{1}{2} \mu v^2 = \frac{1}{2} \mu \left( \frac{dr}{dt} \right)^2 + \frac{1}{2} \mu r^2 \left( \frac{d\phi}{dt} \right)^2 + V(r) \\ &= \frac{1}{2} \mu \left( \frac{dr}{dt} \right)^2 + \frac{L^2}{2\mu r^2} + V(r) \end{aligned} \quad (5.21)$$

where  $v$  is the relative incident velocity and  $b$  is the *impact parameter*. Solving these equations, we get

$$d\phi = \frac{L^2}{\mu r^2} dt \quad (5.22)$$

and

$$dr = - \left\{ \frac{2}{\mu} \left[ E - V(r) - \frac{L^2}{2\mu r^2} \right] \right\}^{1/2} dt \quad (5.23)$$

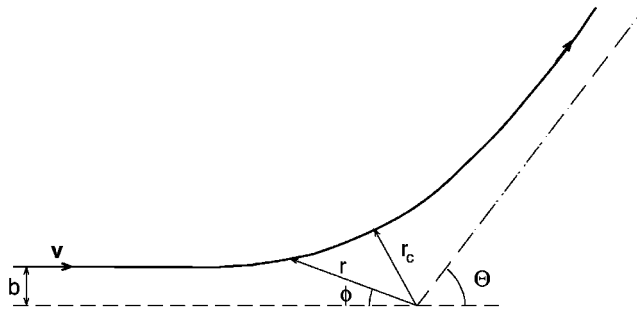


**Figure 5.3** Classical trajectory for velocity  $v$  and impact parameter  $b$ , with deflection angle  $\theta$ , following a system of coordinates based on the centre of mass. The classical turning point is  $r_c$ .

or

$$dt = - \left\{ \frac{2}{\mu} \left[ E - V(r) - \frac{L^2}{2\mu r^2} \right] \right\}^{-1/2} dr \quad (5.24)$$

Now, we can write

$$\begin{aligned} \phi(t) &= \int_{-\infty}^t \left( \frac{L}{\mu r^2} \right) dt \\ &= - \int_{\infty}^r \frac{L/\mu r^2}{\left\{ \frac{2}{\mu} \left[ E - V(r) - \frac{L^2}{2\mu r^2} \right] \right\}^{1/2}} dr \end{aligned} \quad (5.25)$$

and use the relationship  $L = \mu v b = b(2\mu E)^{1/2}$  to obtain

$$\phi(t) = \pm b \int_{\infty}^r \frac{dr}{r^2 \left[ 1 - \frac{b^2}{r^2} - \frac{V(r)}{E} \right]^{1/2}} \quad (5.26)$$

The sign must be chosen to agree with that of the radial velocity: that is positive for the species leaving and negative for those approaching.

For any collision, there will always be a maximum approach distance  $r_c$  for which  $r(t)$  has its minimum value. In this classical turning point all the initial kinetic energy is converted into potential energy. It is convenient to define  $t = 0$  for  $r(t) = r_c$  and  $\phi_{(0)} = \phi_c$ . The complete classical trajectory can be determined by integrating eq. (5.26) from infinity to  $r_c$  and then from  $r_c$  forward. However, it is unnecessary to follow the trajectory

with this detail when we are only observing what happens after the collision. In this case it is sufficient to know the total deflection,  $\Theta$ . As shown in Figure 5.3, this deflection is given by

$$\begin{aligned}\Theta(E, b) &= \pi - 2\phi_c \\ &= \pi - 2b \int_{r_c}^{\infty} \frac{dr}{r^2 \left[ 1 - \frac{b^2}{r^2} - \frac{V(r)}{E} \right]^{1/2}}\end{aligned}\quad (5.27)$$

For us to analyse the behaviour of the angle of deflection as a function of the energy and of the impact parameter, we have to define the potential. In the simplest case of the potential of hard spheres

$$\begin{aligned}V(r) &= 0, \quad r > d_{AB} \\ V(r) &= \infty, \quad r \leq d_{AB}\end{aligned}\quad (5.28)$$

it is obvious that independent of the energy of collision  $r_c = d_{AB}$ . Under these conditions, the integration of eq. (5.27) leads to

$$\begin{aligned}\Theta(E, b) &= \pi - 2b \int_{d_{AB}}^{\infty} \frac{dr}{r^2 \left[ 1 - \frac{b^2}{r^2} - 0 \right]^{1/2}} \\ &= \pi - 2b \int_{d_{AB}}^{\infty} \frac{dr}{r \sqrt{r^2 - b^2}} \\ &= \pi - 2b \left\{ \frac{1}{b} \cos^{-1} \left( \frac{b}{r} \right) \right\}_{r=d_{AB}}^{r=\infty} \\ &= \pi - 2 \left[ \cos^{-1} \left( \frac{b}{\infty} \right) - \cos^{-1} \left( \frac{b}{d_{AB}} \right) \right] \\ &= \pi - \pi + 2 \cos^{-1} \left( \frac{b}{d_{AB}} \right) \\ &= 2 \cos^{-1} \left( \frac{b}{d_{AB}} \right)\end{aligned}\quad (5.29)$$

For impact parameters greater than the hard sphere diameter  $d_{AB}$ , eq. (5.29) requires the reciprocal of the cosine of a number greater than one, which is not possible. For this case,  $\Theta(b) = 0$ . For impact parameters less than  $d_{AB}$ , the value of  $\Theta(b)$  varies between 0 and  $\pi$  (Figure 5.4).

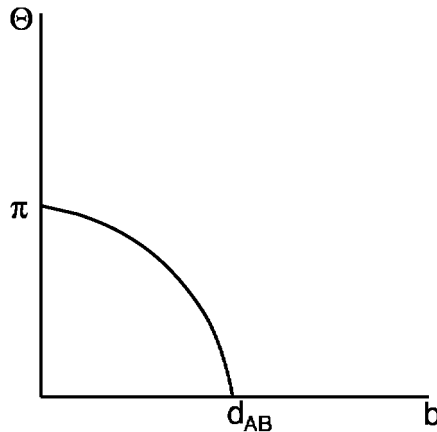


**Figure 5.4** Deflection function  $\Theta(b)$  for the hard sphere potential of diameter  $d_{AB}$ .

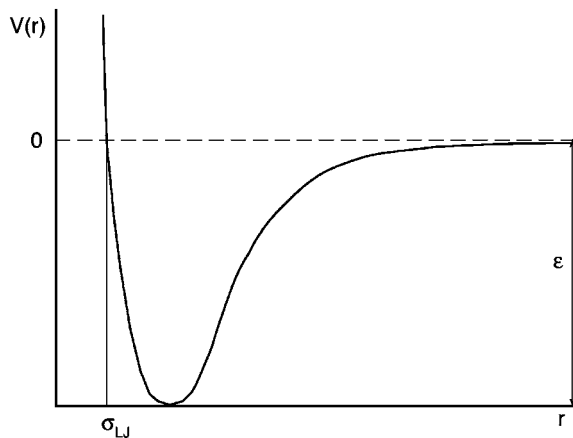


**Figure 5.5** Lennard-Jones potential, showing the minimum at  $r_m = 2^{1/6}/\sigma_{LJ}$  with an energy  $V(r_m) = -\epsilon$ .

A potential energy function that represents the interaction between two bodies in a more realistic form is the Lennard-Jones potential

$$V(r) = 4\epsilon \left[ \left( \frac{\sigma_{LJ}}{r} \right)^{12} - \left( \frac{\sigma_{LJ}}{r} \right)^6 \right] \quad (5.30)$$

shown in Figure 5.5, where the attractive term in  $r$  represents the dispersion forces as well as dipole-dipole and dipole-induced dipole interactions. The purely empirical repulsive part was chosen from adjustment to a wide range of atomic potentials. The deflection function of this potential can be calculated using eq. (5.27). The arithmetical treatment of this

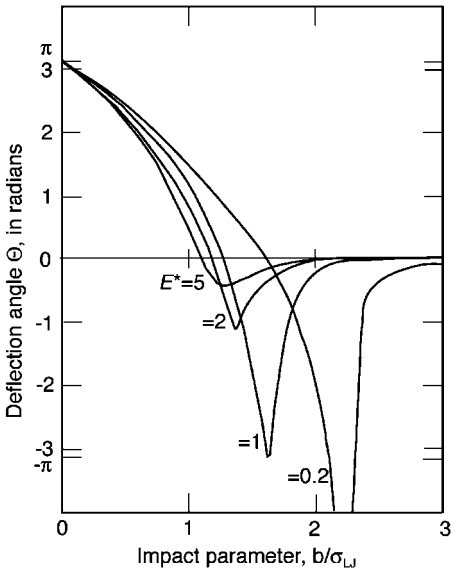


**Figure 5.6** Deflection function  $\Theta(E,b)$  for the Lennard–Jones potential. The minima correspond to the “rainbow” angle discussed in the text.

solution is very complicated. In Figure 5.6, we show only the results in terms of the reduced impact parameter  $b^* = b/\sigma_{\text{LJ}}$  for a range of reduced energies  $E^* = E/\epsilon$ . This figure shows three regions with a different dispersive behaviour.

For collisions that are almost head-on ( $b \rightarrow 0$ ), the deflection function is very similar to that of collision between hard spheres (Figure 5.4), because the impinging particle passes through the attractive part of the potential and is repelled by the wall given by  $r^{-12}$ . This behaviour of specular reflection can be found for scattering with almost all potentials.

For very large-impact parameters, the dispersion is also similar to that for the hard sphere, that is, the impinging particle is hardly scattered in its trajectory. This is due to the rapid decay of the attractive part of the potential to zero. We should note that this limit is reached more rapidly when the energy of the incident particle increases.

In the intermediate region of  $b^*$  and  $E^*$  we find a new behaviour. The deflection angles can take considerably negative values, even less than  $-\pi$ . This results from the strong interaction of the incident particle with the attractive part of the Lennard–Jones potential, as is shown in Figure 5.7.

The above discussion focussed on the trajectory of a single event, specified by an initial energy and an impact parameter. From the practical point of view, although it is possible to accurately define the initial energy in a molecular beam experiment, it is impossible to isolate a single impact parameter. Thus, the experimental results are presented in terms of collision cross sections, as shown in Figure 5.8. In the case of elastic scattering, we can distinguish between the total cross section  $\sigma(E)$  and the differential cross section  $d\sigma/d\Omega$ . This latter parameter is defined as the intensity of scattering per solid

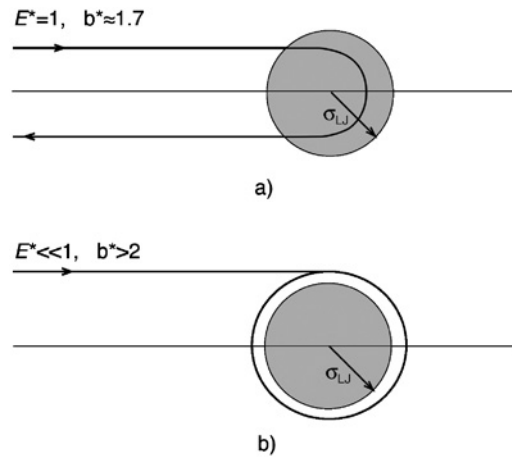


**Figure 5.7** Trajectories in the scattering by a Lennard–Jones potential: (a) “rainbow” scattering,  $\Theta(E,b) = -\pi$ , so called because of the similarity between its mathematical description and that of light scattering in the atmosphere, which leads to the formation of rainbows. (b) Example of a collision captures in an orbit, which may eventually be unstable and lead to separation of the particles.

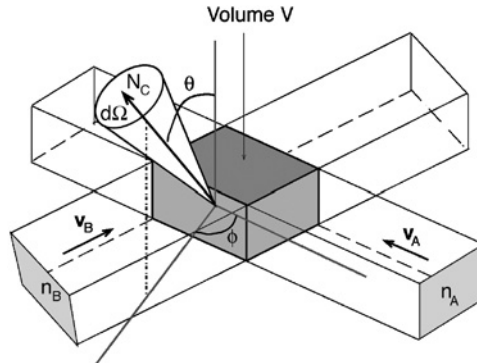


**Figure 5.8** Definition of the scattering process  $A + B \rightarrow C + D$  within laboratory coordinates. The density of the particles A and B is given by  $n_A$  and  $n_B$  in units of number of cubic centimetre;  $\mathbf{v} = |\mathbf{v}_A - \mathbf{v}_B|$  is the relative velocity between the particles A and B; experimentally it is given as number  $dN_c$  of molecules C per unit time which emerge within the solid angle  $d\Omega$  defined by the angles  $\theta$  and  $\phi$  of the centre of scattering,  $d\Omega = \sin \theta d\theta$ ;  $V$  is the volume defined by the intersection of the molecular beams A and B.

angle unit of measurement,  $\theta$ , termed the *dispersion angle*. As it is impossible to distinguish positive and negative deflections,  $\theta$  is given experimentally as the modulus of the magnitude of the deflection  $\theta$  of eq. (5.27) between the limits indicated:

$$\theta = |\Theta|, \quad 0 < \theta < \pi \quad (5.31)$$

Figures 5.4 and 5.5 show that  $\theta(E, b)$  varies continuously with  $b$ . Thus, the trajectories with an impact factor  $b + db$  define an area  $2\pi b db$  and are deflected through a solid angle corresponding to  $2\pi \sin \theta d\theta$ . The differential cross section can now be written as

$$\frac{d\sigma}{d\Omega} = I(\theta, E) = \left| \frac{2\pi b db}{2\pi \sin \theta d\theta} \right| = \left| \frac{b}{\sin \theta \frac{d\theta}{db}} \right| \quad (5.32)$$

and the total elastic section is

$$\sigma(E) = \int \frac{d\sigma}{d\Omega} d\Omega = 2\pi \int_0^\pi I(\theta, E) \sin \theta d\theta \quad (5.33)$$

The use of eqs. (5.27), (5.32) and (5.33) to show the deduction of the cross section from the form of the potential  $V(r)$ , can be easily obtained for the hard-sphere potential case. From eq. (5.29), for all the trajectories for which there is scattering

$$b = d_{AB} \cos\left(\frac{\theta}{2}\right) \quad (5.34)$$

Substituting in eq. (5.32), we obtain  $I(\theta, E) = 1/4 d^2$  and, substituting in eq. (5.33) we get

$$\sigma(E) = 2\pi \int_0^\pi \frac{1}{4} d^2 \sin \theta d\theta = \pi d^2 \quad (5.35)$$

The significance of this result is that the scattering intensity is equal in all directions and is independent of the energy. The total cross section is simply the area of the cross section presented by the sphere. These results could be obtained by various other methods, but show how it is possible to obtain a cross section knowing the potential.

A chemical reaction cannot be described by only two particles interacting. A minimum of three particles is necessary. Unfortunately, for such three-bodied systems it is not possible to obtain analytical solutions and it becomes necessary to use numerical methods. Among these, the Monte Carlo method assumes particular relevance for the calculation of classical trajectories using random sampling.

### 5.3 CALCULATION OF CLASSICAL TRAJECTORIES

By knowing the PES for a chemical reaction it is possible to solve the classical equations of motion for a collision on this surface. In the context of classical mechanics, the movement of particles is described by Newton's second law:

$$\mathbf{F} = \frac{d\mathbf{P}}{dt} = m\mathbf{a} \quad (5.36)$$

where  $\mathbf{F}$  is the force acting on the particle,  $\mathbf{P}$  its linear momentum and  $\mathbf{a}$  the acceleration. In the calculation of trajectories we normally solve the Hamiltonian equations for each coordinate  $Q_j$  and its conjugate momentum  $P_j = m_j dQ_j/dt$ . For a system of  $N$  particles with generalised coordinates  $(q_1, q_2, \dots, q_k)$ , we can establish  $2k$  Hamiltonian equations. When we know the initial state of the system  $(q_1^0, q_2^0, \dots, q_k^0, p_1^0, p_2^0, \dots, p_k^0)$ , its time evolution will be determined through the solution of these  $2k$  first-order differential equations.

The simplest example of a classical trajectory is the collinear collision complex A + BC, for which there are only two independent coordinates: the A–B distance ( $r_1$ ) and the B–C distance ( $r_2$ ). However, even in such a simple system, a complication is introduced by transforming from internal molecular coordinates to Cartesian space. This complication can be appreciated by writing the complete Hamiltonian of the system:

$$\begin{aligned} \mathbf{H} &= T + V \\ &= \frac{1}{2} \frac{m_A m_B}{m_A + m_B} \left( \frac{dr_1}{dt} \right)^2 + \frac{1}{2} \frac{(m_A + m_B)m_C}{m_A + m_B + m_C} \left( \frac{dr_2}{dt} + \frac{m_A}{m_A + m_B} \frac{dr_1}{dt} \right)^2 + V(r_1, r_2) \\ &= \frac{1}{2(m_A + m_B + m_C)} \left[ m_A (m_B + m_C) \left( \frac{dr_1}{dt} \right)^2 + 2m_A m_B \frac{dr_1}{dt} \frac{dr_2}{dt} \right. \\ &\quad \left. + m_C (m_A + m_B) \left( \frac{dr_2}{dt} \right)^2 \right] + V(r_1, r_2). \end{aligned} \quad (5.37)$$

The first term in kinetic energy represents the motion of A relative to B, while the second one represents the motion of AB relative to C. When the equation is expanded, we are left with a cross term,  $dr_1/dt dr_2/dt$ . This term must be eliminated if the movement of any representative point on the PES occurs without friction. It is possible to do this by making a new transformation of the coordinates into a mass-weighted system, which diagonalises the kinetic energy of the system. This transformation is shown in Figure 5.9. The angle between the two coordinate systems [1] is given by

$$\sin\theta = \left[ \frac{m_A m_C}{(m_A + m_B)(m_B + m_C)} \right]^{1/2} \quad (5.38)$$

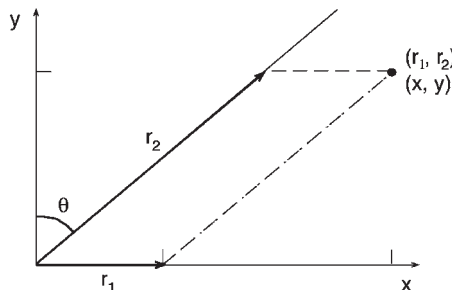


**Figure 5.9** Transformation of Cartesian coordinates into mass-weighted coordinates.

The Hamiltonian then becomes

$$\mathbf{H} = \frac{1}{2} \frac{m_A(m_B + m_C)}{(m_A + m_B + m_C)} \left[ \left( \frac{dx}{dt} \right)^2 + \left( \frac{dy}{dt} \right)^2 \right] + V(r, r_2) \quad (5.39)$$

The calculation of the trajectory for this atom–diatom system requires the specification of 12 initial conditions, even after the separation of the three coordinates of motion by using the centre of mass. The six independent coordinates, together with the six respective conjugates, can be written (using the notation of Figure 5.10)

$$\begin{aligned} Q_1^0 &= R_{BC} \sin \theta \cos \phi & P_1^0 &= -P(\sin \phi \cos \eta - \cos \phi \cos \theta \sin \eta) \\ Q_2^0 &= R_{BC} \sin \theta \sin \phi & P_2^0 &= -P(\cos \phi \cos \eta - \sin \phi \cos \theta \sin \eta) \\ Q_3^0 &= R_{BC} \cos \theta & P_3^0 &= -P \sin \theta \sin \eta \\ Q_4^0 &= 0 & P_4^0 &= 0 \\ Q_5^0 &= b & P_5^0 &= 0 \\ Q_6^0 &= -\sqrt{r^2 - b^2} & P_6^0 &= \mu_{A,BC} v_r^0 \end{aligned} \quad (5.40)$$

where  $P$  is the rotational angular momentum  $J(J+1)h^2/R^2$ , the angles  $\theta$ ,  $\phi$  and  $\eta$  specify the initial orientation of the molecule BC in the space and  $v_r^0$  is the initial relative velocity. The application of the Monte Carlo method to the solution of the Hamiltonian equations of the system corresponds effectively to the calculation of a set of trajectories for which the initial conditions for each of the trajectories will be chosen at random.

The fundamental parameter that is obtained in these calculations is the probability of reaction for any given relative initial velocity (i.e. initial reactive kinetic energy), roto-

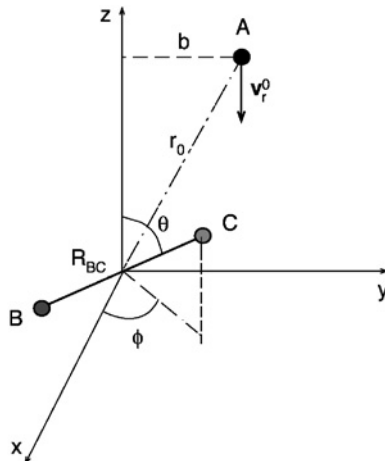


**Figure 5.10** Classic coordinates for an atom diatom collision of the type  $A + BC \rightarrow A + BC$ ;  $\theta$  and  $\phi$  are the angles of the polar spherical coordinates,  $R_{BC}$  the interatomic separation and the angle  $\eta$  specifies the plane of rotation of BC.

vibrational state of BC, impact parameter and orientation. In practice, this probability is defined as the ratio between the number of reactive trajectories and the total number of trajectories

$$P_{v,j}(v_r^0, b, \theta, \phi, R_{BC}, \eta) = \lim_{N \rightarrow \infty} \frac{N_R(v_r^0, b, \theta, \phi, R_{BC}, \eta)}{N_{\text{total}}(v_r^0, b, \theta, \phi, R_{BC}, \eta)} \quad (5.41)$$

which is only statistically correct when a very large number of trajectories have been followed. The reactive cross section, relative to the quantum state of BC, takes the following form:

$$\sigma_{v,j}(v_r^0) = \int_{b=0}^{b_{\max}} \int_{\theta=0}^{\pi} \int_{\phi=0}^{2\pi} \int_{R_{BC}=\rho_-}^{\rho_+} \int_{\eta=0}^{2\pi} P_{v,j}(v_r^0, b, \theta, \phi, R_{BC}, \eta) \\ [H(\eta) d\eta] [G(R_{AB}) dR_{BC}] [\Phi(\phi) d\phi] [\Theta(\theta) d\theta] 2\pi b db \quad (5.42)$$

where  $\rho_-$  and  $\rho_+$  are the interior and exterior turning points of the vibration, respectively,  $G(R_{BC})$  the distribution function for  $R_{BC}$ , which depends on the roto-vibrational state of the molecule and its diatomic potential, and the normalised distribution functions of the angles take the following form:

$$\Theta(\theta) = \frac{1}{2} \sin(\theta) \\ \Phi(\phi) = \frac{1}{2\pi} \\ H(\eta) = \frac{1}{2\pi} \quad (5.43)$$

If we want to make a comparison between these cross sections and the experimental values for the reaction in thermal equilibrium, it is necessary to make first an average over the initial states (reactants) to obtain an expression that gives the rate of appearance of the product in a determined state, and then sum over all the states of the products to obtain the total rate of appearance of products. This procedure constitutes the basis of molecular dynamics. Normally, it is assumed that the molecular velocities are described by a Maxwell–Boltzman distribution, and the specific rate constant is expressed relative to the quantum state of BC not in terms of the initial relative velocity  $v_r^0$ , but in terms of the relative translational energy,  $E_{\text{tr}} = \frac{1}{2}\mu_{A-BC}(v_r^0)^2$ ,

$$k_{v,j} = \left( \frac{2}{k_B T} \right)^{3/2} (\pi \mu_{A-BC})^{-1/2} \int_0^\infty \sigma_{v,j}(E_{\text{tr}}) \exp\left(-\frac{E_{\text{tr}}}{k_B T}\right) E_{\text{tr}} dE_{\text{tr}} \quad (5.44)$$

The total rate constant of the reaction is the average of  $k_{v,j}$  weighted on the basis of the distribution of states ( $v, j$ )

$$k = \sum_v \sum_j F(v, j) k_{v,j} \quad (5.45)$$

where  $F(v,j)$  is the normalised distribution function for the roto-vibrational states of BC

$$F(v,j) = \frac{(2j+1)\exp\left(-\frac{E_{v,j}}{k_B T}\right)}{Q} \quad (5.46)$$

with  $E_{v,j}$  being the energy of the roto-vibrational state  $(v,j)$  and  $Q$  the corresponding roto-vibrational partition function

$$Q = \sum_v \sum_j (2j+1)\exp\left(-\frac{E_{v,j}}{k_B T}\right) \quad (5.47)$$

At the end of each trajectory, this is classified on the basis of the product of collision. However, other properties are equally important for the final statistical analysis, in particular the relative translational energy of the products,

$$E_{\text{tr}} = \frac{1}{2} \mu_{\text{AB-C}} (v_p)^2 \quad (5.48)$$

the scattering angle

$$\cos \theta_{\text{scatt}} = \frac{\mathbf{v}_p \cdot \mathbf{v}_R}{|\mathbf{v}_p| \cdot |\mathbf{v}_R|} \quad (5.49)$$

and the internal states of the products. The velocities indicated above refer to the relative velocities between the centres of mass of products and reactants. The angular momentum  $L$  and the moment of inertia  $I$  can be calculated from the coordinates and from the final momentum. Thus, it is possible to obtain an estimate for the vibrational and rotational energies from the following equations:

$$E_{\text{rot}} = \frac{L^2}{2I} \quad (5.50)$$

$$E_{\text{vib}} = E_{\text{int}} - E_{\text{rot}}$$

Calculations of trajectories provide details on both the state-to-state reactivity ( $k_{v,j}$ ) and the energy distribution (translational, vibrational and rotational) of the products. The comparison between results of these calculations and data from molecular beam experiments allows one to obtain very detailed information on the PES of the reaction system. The most important role of the molecular collision theory is that of identifying the dominant characteristics of a given PES and extracting from these all the possible observable consequences.

The complexity of the classical trajectory method is obvious. As the number of integrals involved increases with the number of atoms in the system, in practice the method is limited to tri- and tetra-atomic systems, always assuming that it is possible to obtain a realistic PES for these systems. Apart from this, the classical trajectory method has two intrinsic limitations: it does not consider either the zero-point energy (ZPE) or quantum mechanical tunnelling.

The ZPE of the reactants comes as one of the immediate consequences of energy quantisation in quantum mechanics. The energy of each vibrational mode is quantised and the ZPE is the quantity of energy of the lowest mode. However, the classical energy distribution is continuous for all degrees of freedom, such that the classical vibrational energy can have values much less than their quantum limit. Thus, even though the reactants are placed in their exact quantum states, during the dynamic evolution of the system the energies of the vibrational modes can decrease below the ZPE and form intermediates or products that violate the quantum restriction. This problem is particularly important for endothermic reactions, where the classical cross section can be much greater than that obtained by exact quantum calculations. A simple method of reducing the problem of the ZPE transformation in a reaction is to exclude trajectories that do not possess an internal energy equal to or greater than the ZPE in the statistical analysis. This procedure can, however, lead to deviations in the initial distributions of the dynamic variables.

The effect of tunnelling concerns the passage of a particle through a barrier of energy greater than its kinetic energy. This means that chemical reactions can occur even though the system lacks sufficient energy to cross the reaction barrier through the minimum energy pathway. The effect of tunnelling is that the classical trajectory method underestimates the rate constant when the energy of the system is close to the classical threshold at which the reaction occurs. Other characteristics of the tunnel effect will be discussed in the next chapter.

The simplicity of the  $\text{H} + \text{H}_2$  system allows us to calculate accurate PESs and use them in molecular dynamics. This system is very well characterised and it is known that there is compensation between the loss of ZPE and tunnelling. The classical trajectories calculated for this system therefore reveal some of the basic aspects of molecular dynamics.

Figure 5.11 allows us to visualise the trajectories in terms of their time evolution while Figure 5.12 shows a comparative analysis between the results of classical trajectories for the system  $\text{H} + \text{H}_2$  and the results obtained by the simple collision theory (assuming hard spheres). In the calculations with the hard-sphere model it is assumed that the probability of reaction  $P_R$  depends on the energy  $E_c$ , which is oriented in the direction in which the movement of the spheres leads to the reaction in agreement with

$$\begin{aligned} P_R(E_c) &= 0 & (E_c < E^*) \\ P_R(E_c) &= 1 & (E_c \geq E^*) \end{aligned} \quad (5.51)$$

where  $E^*$  is the minimum energy necessary for the reaction to occur. Substituting this probability in eq. (5.42), we obtain the reaction cross section for hard spheres.

$$\sigma_R(E) = \int_0^\infty P_R(E(b)) 2\pi b db = \begin{cases} 0 & E < E^* \\ \pi d^2 \left(1 - \frac{E^*}{E}\right) & E \geq E^* \end{cases} \quad (5.52)$$

In spite of the inherent difficulties of calculating PESs for polyatomic systems and the solution of the equations of motion for such surfaces, much effort is being devoted to

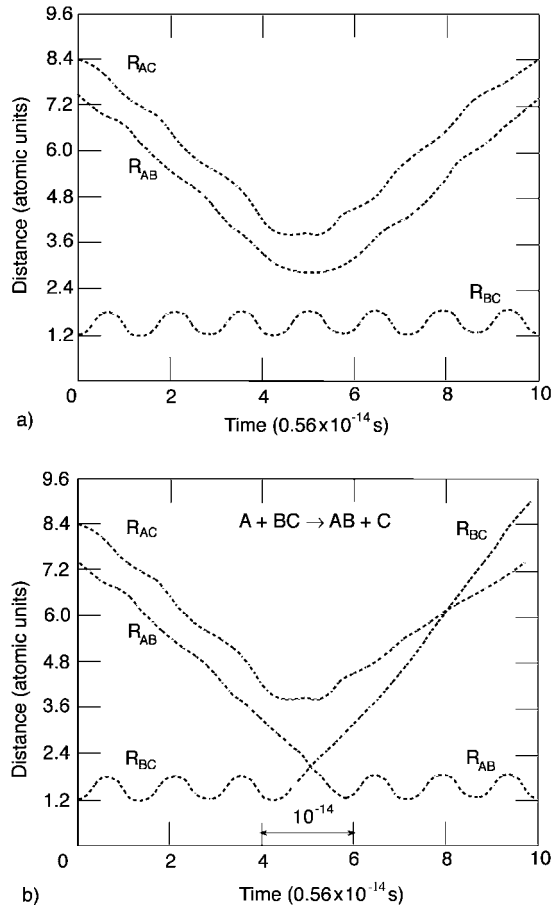
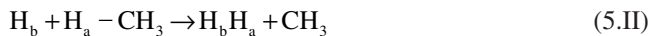


**Figure 5.11** Scattering trajectories ( $J_1 = 0$ ,  $v_1 = 0$ ,  $v_r^0 = 1.32 \times 10^6 \text{ cm sec}^{-1}$ ) represented as changes in interatomic distance with time: (a) Non-reactive trajectory. (b) Reactive trajectory. The difference between the two trajectories appears to be due to a very small difference in the vibrational phase of the molecule BC. The crossing observed in (b) is due to the formation of rotationally excited products ( $J' \approx 5$ ) [2].

extend molecular dynamics studies to such systems. Figure 5.13 shows a PES [3] for the system



and classical trajectories calculated using the program MARINER [4]. One of the images shows a reactive trajectory that passes very close to the saddle-point, while the other shows a non-reactive trajectory, which returns to the reactant valley after being reflected by the barrier.

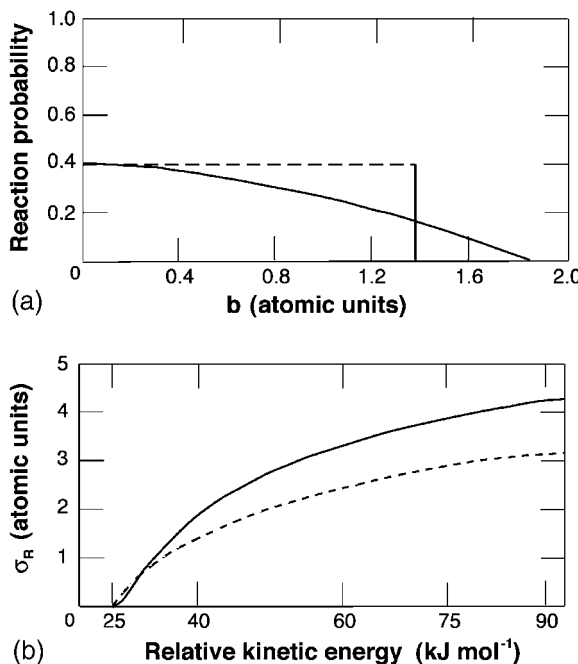
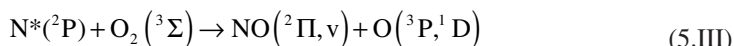


**Figure 5.12** Analysis of classical trajectories on the PES for the system H + H<sub>2</sub>: (a) The dashed line shows the results for simple collision theory using hard spheres with  $b_{\max} = 0.98 \text{ \AA}$  and a steric factor  $g = 0.4$ , while the solid line shows a fit to the empirical function  $P_R^\circ / \cos(\pi b / 2b_{\max})$  that approaches the value calculated for classical trajectories. (b) The solid line indicates the results of classical trajectory calculations and the dashed line that obtained using hard spheres, eq. (5.52) [2].

## 5.4 PES CROSSINGS

The scattering processes we have considered are characterised by taking place on a single electronic PES. Such processes are called adiabatic. However, if there are two electronic PESs, whose energies approach or cross at a particular point in configurational space, it is possible that a trajectory jumps from one PES to the other at this point. Thus, chemical reaction involves a change in electronic PES and the reaction is said to be diabatic (or non-adiabatic). The most common examples of these processes involve electronically excited species, such as in the example



while other cases lead to the separation of an ion pair into atoms



The interaction between PESs in diabatic reactions is shown in Figure 5.14.

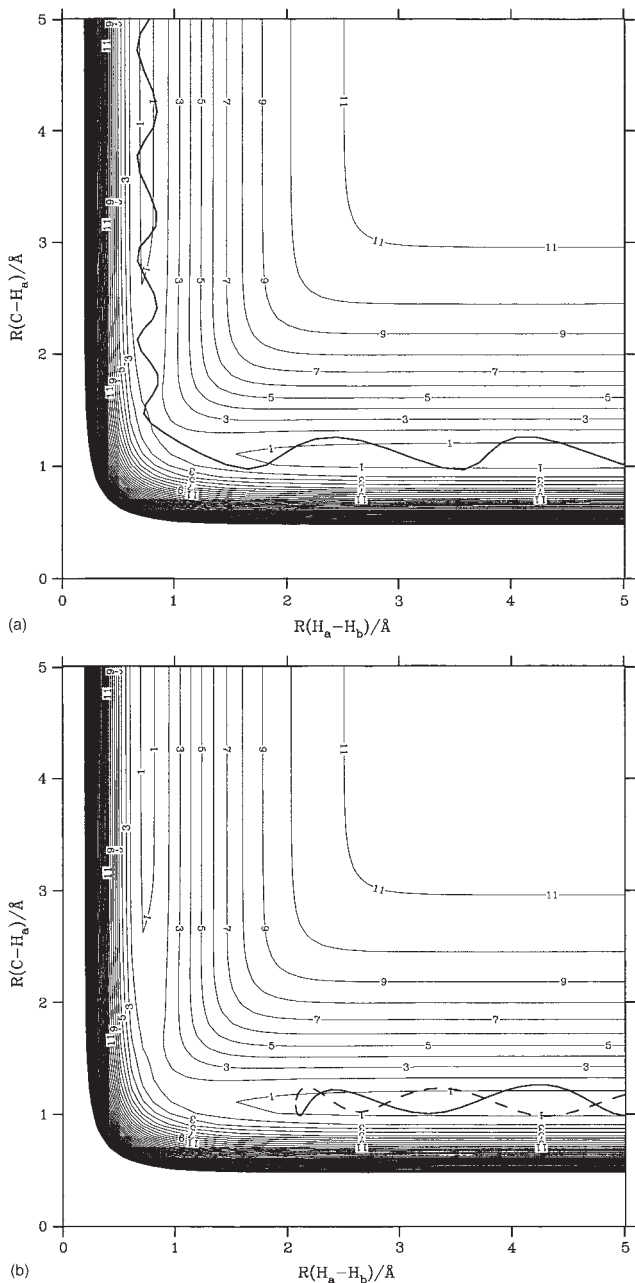


**Figure 5.13** Classical trajectories on the PES indicated by mechanism (5.II). The contours have a separation  $41.84 \text{ kJ mol}^{-1}$ . The top shows a reactive trajectory while the bottom shows a non-reactive one. Trajectory calculations are courtesy of A.A.C.C. Pais.

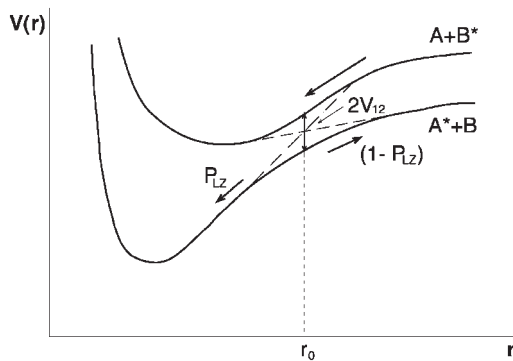


**Figure 5.14** Interaction between two PESs, showing an electronically diabatic trajectory, which crosses the two PESs with a probability  $P_{LZ}$  from the higher energy surface to the lower energy surface, and stays on the lower energy surface with a probability  $(1 - P_{LZ})$  when the reactants separate.

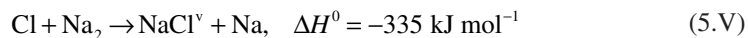
The most simple description for the electronically diabatic processes was formulated independently by Landau and by Zener. Following the model of these authors, the probability of passing from one surface to the other, considered as unidimensional, in the avoided crossing region, is given by

$$P_{LZ} = \exp\left(-\frac{4\pi V_{12}^2}{hv|s_1 - s_2|}\right) \quad (5.53)$$

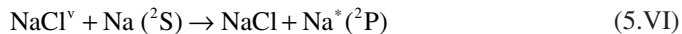
where  $v = dr/dt$  is the velocity at the crossing point  $r_0$ ,  $s_1$  and  $s_2$  the slopes  $dV(r_0)/dr$  of the unperturbed surfaces and  $V_{12}$  half the energetic separation between the two surfaces at the point  $r_0$ .

## 5.5 MOLECULAR DYNAMICS

The first studies on molecular dynamics were made in the early 1930s by Michael Polanyi and co-workers. In these studies, very dilute flames and diffusional flames were used to study the reactions of alkali metals with halogens and halides in the vapour phase. In many cases, chemiluminescence was observed. For example, the reaction



produces a vibrationally excited molecule of sodium chloride ( $\text{NaCl}^v$ ) which transfers its energy to a sodium atom. The vibrational energy content of  $\text{NaCl}^v$  is sufficiently high to produce an electronically excited sodium atom



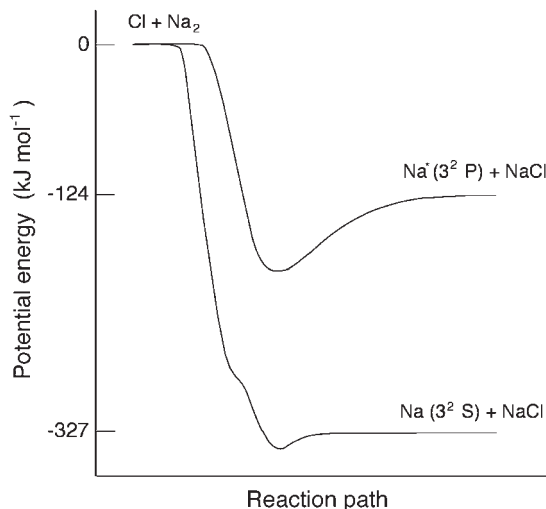


**Figure 5.15** Attractive PES for the system  $\text{Cl} + \text{Na}_2 \rightarrow \text{NaCl} + \text{Na}$  [5].

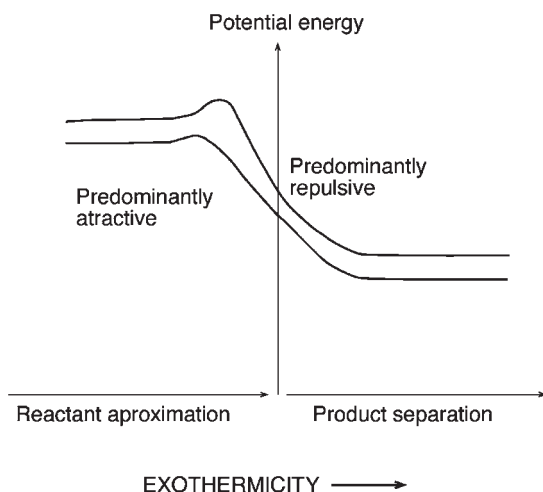


**Figure 5.16** Energy profiles along the reaction coordinate for predominantly attractive and predominantly repulsive PESs, with reactions occurring in the exothermic direction.

which subsequently emits visible light as the well-known orange colour of the sodium D line



Evans and Polanyi put forward the idea that the PES of this system has the shape shown in Figure 5.15. The Na–Na bond is very long (3.1 Å) and the Na–Cl bond is formed by

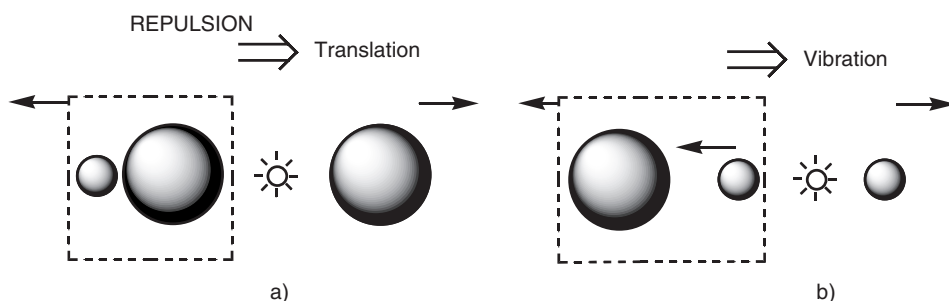


**Figure 5.17** Illustration of two distinct dynamic behaviours on PES involving release of repulsive energy. The size of the spheres shows the relative masses. (a) Schematic for the system  $\text{H} + \text{Cl}_2$ . (b) Schematic for the system  $\text{F} + \text{H}_2$ .

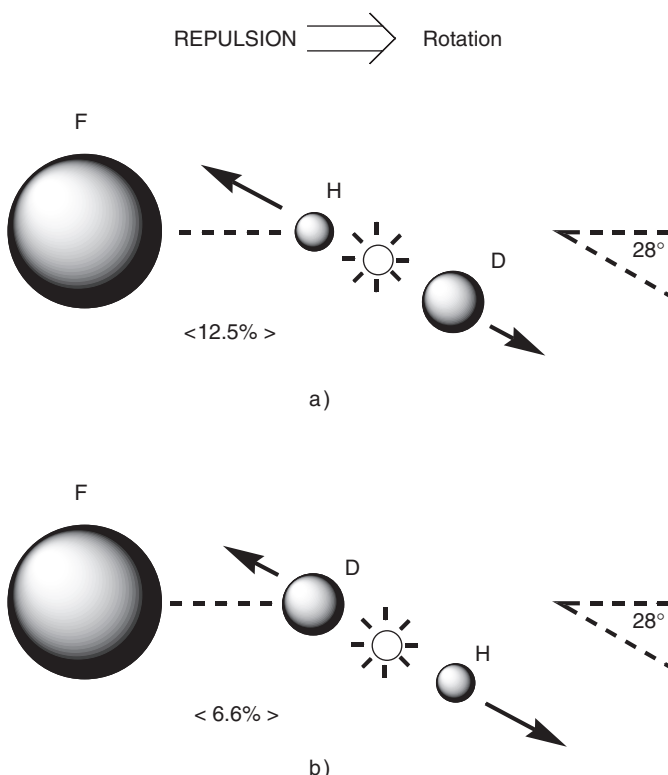


**Figure 5.18** Illustration similar to the previous scheme, but considering the presence of a transition state bent by  $28^\circ$ . The examples shown are appropriate for the reactions (a)  $\text{F} + \text{HD} \rightarrow \text{HF} + \text{D}$  and (b)  $\text{F} + \text{DH} \rightarrow \text{DF} + \text{H}$ . In the second case the conversion of translational into rotational energy has half the efficiency of the first.

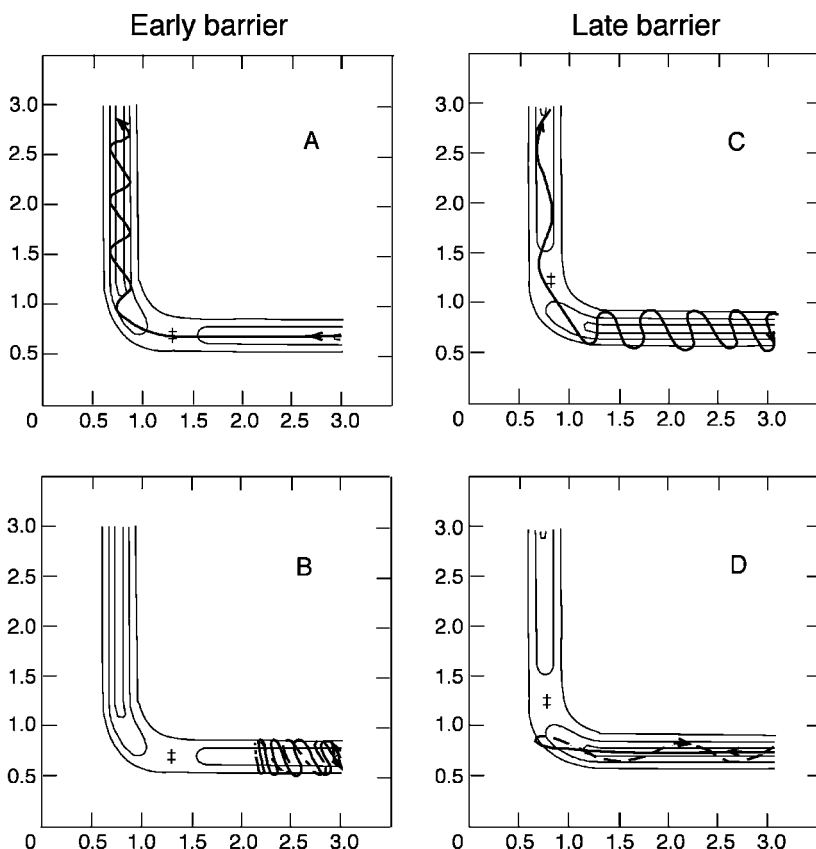


**Figure 5.19** Trajectories showing the effect of energy distribution of the reactants on the reactivity. Translational energy of reactants is effective for crossing an early barrier (A), but ineffective for late barriers (D) on the PES. In contrast, the vibrational energy of the reactants helps cross the late barriers (C), but not the early ones (B).

electron transfer at a distance much greater than the equilibrium length. The  $\text{Na}^+–\text{Cl}^-$  bond that is formed is an ionic bond in which  $\text{Na}^+$ , being a cation, has a very small radius. Following a small barrier ( $1.7 \text{ kJ mol}^{-1}$ ) on entering the PES, much of the exothermicity of the reaction will be liberated as vibrational energy of  $\text{Na}^+–\text{Cl}^-$ . This mechanism explains why 85% of the collisions of Cl and Na result in vibrationally excited NaCl. This type of surface is known as an *attractive* surface.

It was only in the 1960s that the pioneering work of M.G. Evans, M. Polanyi and also of H. Eyring, was extended with the arrival of new techniques, which allowed experimental determination of energies of products, and the introduction of computers capable of effectively solving the equations of motion. Some experimental observations have been rationalised by J.C. Polanyi in terms of localisation of the barrier in

**Table 5.1**

Relative distributions of vibrational, rotational and translational energy of products in gas-phase atom abstraction reactions [9]

	$\Delta E^0/\text{kJ mol}^{-1}$	$V'$	$R'$	$T'$
$\text{F} + \text{H}_2 \rightarrow \text{HF} + \text{H}$	-133.3	0.664	0.083	0.260
$\text{F} + \text{HD} \rightarrow \text{HF} + \text{D}$	-130.0	0.558	0.125	0.287
$\text{F} + \text{DH} \rightarrow \text{DF} + \text{H}$	-137.1	0.626	0.066	0.309
$\text{F} + \text{D}_2 \rightarrow \text{DF} + \text{D}$	-132.9	0.665	0.076	0.259
$\text{Cl} + \text{HBr} \rightarrow \text{HCl} + \text{Br}$	-67	0.5	0.3	0.2
$\text{Cl} + \text{HI} \rightarrow \text{HCl} + \text{I}$	-137	0.68	0.14	0.18
$\text{F} + \text{HCl} \rightarrow \text{HF} + \text{Cl}$	-144	0.56	0.21	0.23
$\text{D} + \text{I}_2$	-158		0.26	
$\text{H} + \text{Br}_2$	-186	0.55	0.04	0.41
$\text{H} + \text{Cl}_2$	-203	0.38	0.08	0.53
$\text{H} + \text{ICl} \rightarrow \text{HCl} + \text{I}$	-219	0.59	0.21	0.20
$\text{H} + \text{BrCl} \rightarrow \text{HCl} + \text{Br}$	-213	0.55	0.09	0.39
$\text{H} + \text{BrCl} \rightarrow \text{HBr} + \text{Cl}$	-148	0.50	0.14	0.36
$\text{H} + \text{ClF} \rightarrow \text{HCl} + \text{F}$	-180	0.47	0.11	0.42
$\text{H} + \text{ClF} \rightarrow \text{HF} + \text{Cl}$	-318	0.68	0.07	0.25
$\text{H} + \text{F}_2$	-429	0.62	0.03	0.33

Note:  $E_{\text{tr}} = 5.0 \text{ kJ mol}^{-1}$  except for  $\text{H} + \text{F}_2$  where  $E_{\text{tr}} = 3.8 \text{ kJ mol}^{-1}$  and for  $\text{F} + \text{H}_2$  and its isotopic variants where  $E_{\text{tr}} = 10 \text{ kJ mol}^{-1}$ .

the PES topography and of the combinations of the masses involved. For example, the reactions



have repulsive PESs (Figure 5.16) because much of the energy is evolved as repulsion between the products. This liberation of repulsive energy produces a marked increase in the relative movements (i.e. translation) of the species when the combination of the masses is  $\text{L} + \text{HH} \rightarrow \text{LH} + \text{H}$  ( $\text{L}$  corresponds to a light atom and  $\text{H}$  a heavy atom), while the same type of energy evolution produces a mainly internal motions (i.e. vibrations) in the products when the combination of masses is  $\text{H} + \text{LL} \rightarrow \text{HL} + \text{L}$ .

This process can be visualised through Figure 5.17 [6,7]. When the two heavy atoms repel, they are deflected with one of them carrying the light atom with it. In contrast, when the two light atoms repel, one of them can leave with a high translational energy, but the other is thrown at high velocity into the heavy atom, producing a high vibrational excitation. Figure 5.17 gives a rough sketch of the events; since in practice the transition state is slightly bent, such that the repulsion applies a torque to the leaving molecule that makes it rotate. This is clearly seen in the reaction  $\text{F} + \text{HD} \rightarrow \text{HF} + \text{D}$  as compared with the process  $\text{F} + \text{DH} \rightarrow \text{DF} + \text{H}$ , since the product HF in the former case has about twice the rotational excitation compared with the product DF (Figure 5.18) [8].

Polanyi showed how the position of the barrier in a collinear PES is related to the way the distribution of energy in the reactants can increase the reactivity. As seen in Figure 5.19, when the barrier is placed at the entrance of the PES, translational energy is much more effective than vibrational energy in making the reactants cross over the barrier to form products. The opposite is true when the barrier occurs in the latter part of the reaction coordinate.

Although these ideas of J. C. Polanyi were well received at the time, and he was awarded the Nobel Prize in chemistry in 1986, it does not appear possible to make generalisations with them for all triatomic systems. For example, the reaction H+F<sub>2</sub> appears to have an anomalous behaviour being highly exothermic, but with particularly small translational energy (Table 5.1).

## REFERENCES

- [1] BH Mahan, *J. Chem. Educ.* **51** (1974) 308.
- [2] M Karplus, RN Porter, RD Sharma, *J. Chem. Phys.* **43** (1965) 3259.
- [3] MJT Jordan, RG Gilbert, *J. Chem. Phys.* **102** (1995) 5669.
- [4] WL Hase, KF Lim, Program package MARINER. K. F. Lim, Department of Chemistry, University of Melbourne, Vic 3052, Australia, Melbourne, 1990.
- [5] M-L Wang, K-L Han, G-Z He, N-Q Lou, *Chem. Phys. Lett.* **284** (1998) 200.
- [6] JC Polanyi, *Acc. Chem. Res.* **5** (1972) 161.
- [7] JC Polanyi, *Science* **236** (1987) 680.
- [8] JC Polanyi, in A. Zewail (Ed.), *The Chemical Bond*, Academic Press, San Diego, 1992, p. 149.
- [9] MR Levy, *Prog. Reaction Kinetics* **10** (1979) 1.

# - 6 -

## **Reactivity in Thermalized Systems**

---

### **6.1 TRANSITION-STATE THEORY**

“The calculation of absolute reaction rates” formulated by Eyring in 1934, was submitted in the form of a scientific paper to the well-known *J. Chem. Phys.* [1]. This paper was rejected by one referee of this journal under the impression that “the method of treatment is unsound and the result incorrect” [2]. Eventually, Eyring’s paper was accepted for publication after Eugene Wigner and Hugh S. Taylor took up the issue with the editor of *J. Chem. Phys.* [3]. Shortly after, M. Polanyi and M. G. Evans also made a significant contribution to this theory, and suggested the term “transition state” to the critical intermediate invoked by the theory for every rate process. Today, this theory is known as the transition-state theory (TST) and has become the paradigm for interpreting the rates of chemical processes and their dependence on temperature, medium, structure and other parameters.

Probably, the most important reason for the initial resistance to TST was the method presented to calculate the pre-exponential factor. Rather than the usual cross section of collision theory, Eyring calculated the pre-exponential factor of the  $\text{H}+\text{H}_2$  reaction from a ratio of partition functions. Although the value given by this method was in good agreement with that from the cross sections, such an agreement was considered “purely accidental”. It is somewhat ironic that in 1941 Eyring and his co-workers, choose to criticise the collision theory precisely for its procedure of calculating the frequency factor [4]. They pointed out that for a reversible reaction



the ratio of the forward and reverse reactions is equal to the equilibrium constant of the system, which, following eq. (5.16), should be written as

$$K = \frac{k_1}{k_2} = e^{-(E_1 - E_2)/RT} \quad (6.1)$$

since the cross sections and reduced masses in the two directions should not differ significantly from each other. The difference between the activation energies for the forward and reverse reactions is equal to  $\Delta H$  and the simple collision theory leads to the

requirement that

$$K = \frac{k_1}{k_2} = e^{-\Delta H/RT} \quad (6.2)$$

which can only be true either at the temperature of absolute zero or if the reaction involves no entropy change. The above equations ignore the steric factors, present in eq. (5.16), which must involve an entropy term. Since the equilibrium constant is  $K=\exp(-\Delta G^0/RT)$ , the collision theory must be modified to include an entropy of activation, as shown in eq. (5.19). Consequently, the collision theory equation should have the form

$$k = \pi d_{AB}^2 \sqrt{\frac{8RT}{\pi\mu}} e^{-\Delta S^\ddagger/RT} e^{-\Delta H^\ddagger/RT} \quad (6.3)$$

where the entropy of activation assimilates the steric factor. This critique by Eyring and co-workers emphasises the fact that it is the free energy of activation, and not the heat of activation, that determines the reaction rate.

### 6.1.1 Classical formulation

The TST, as Eyring's theory is known, is a statistical-mechanical theory to calculate the rate constants of chemical reactions. As a statistical theory it avoids the dynamics of collisions. However, ultimately, TST addresses a dynamical problem: the proper definition of a transition state is essentially dynamic, because this state defines a condition of dynamical instability, with the movement on one side of the transition state having a different character from the movement on the other side. The statistical mechanics aspect of the theory comes from the assumption that thermal equilibrium is maintained all along the reaction coordinate. We will see how this assumption can be employed to simplify the dynamics problem.

Let us define a reaction coordinate  $s$ , joining reactants ( $s < 0$ ) to products ( $s > 0$ ), and a transition state with a fixed value of  $s$ , that is, with one degree of freedom less than a stable molecule (Figure 6.1). It is possible to derive TST from one fundamental assumption: there is a quasi-equilibrium between the transition-state species (formed from the reactants) and the reactants themselves. The quasi-equilibrium state is characterised by the equilibrium between the reactants and the transition-state species, and by the fact that the concentration of these species does not vary with their disappearance to the products. This quasi-equilibrium offers a method to calculate the concentration of transition-state species using chemical equilibrium theories, and the dynamics problem is transformed into an equilibrium problem, with a known solution.

Representing the transition-state species by  $\ddot{\text{:}}$ , the kinetic mechanism



leads to the bimolecular reaction rate

$$v = v^\ddagger [\ddot{\text{:}}] \quad (6.4)$$

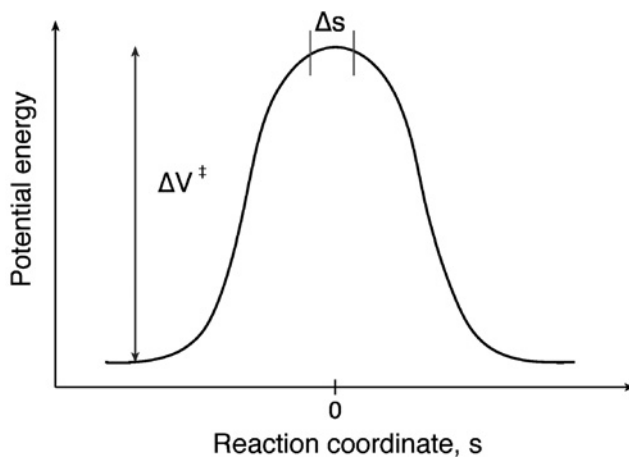


**Figure 6.1** Potential energy curve for a reaction going through a transition state  $\ddot{\text{S}}$  contained in an imaginary potential box with length  $\Delta s$ .

This expression indicates that the number of species transformed into products, per unit time, is the product of their concentration and the frequency of their conversion. The frequency  $v^*$  is the number of times, per unit time, that the transition-state species evolve along the reaction coordinate in the direction of the products. This movement corresponds to the conversion of an internal degree of freedom into a translational degree of freedom. Therefore, the transition state has one degree of freedom less than a normal molecule, because one of these is the reaction coordinate. The movement along this coordinate is that of the relative displacement of two atoms in opposite directions. This frequency can also be represented by the mean velocity of crossing the transition state,  $\bar{v}_q$ , over the length of the transition state at the top of the barrier,  $\Delta s$ . Hence, the above equation can be written as

$$v = \frac{\bar{v}_q}{\Delta s} [\ddot{\text{S}}] \quad (6.5)$$

and the mean velocity can be obtained from the Maxwell–Boltzmann distribution of molecular velocities over one dimension

$$\bar{v}_q = \frac{\int_0^\infty e^{-\sqrt{2m}v_q/k_B T} v_q dv}{\int_{-\infty}^\infty e^{-\sqrt{2m}v_q/k_B T} dv} = \sqrt{\frac{k_B T}{2\pi m}} \quad (6.6)$$

where the limits of integration in the denominator are taken from  $-\infty$  to  $\infty$  to allow for the fact that the complexes are moving in both directions, whereas in the numerator the limits are zero to infinity because it is the mean velocity in the direction of the products that is required. The mass  $m$  is the effective mass of the complex in this movement.

Using the quasi-equilibrium approximation,

$$K^\ddagger = \frac{[\ddagger]}{[A][B]} \quad (6.7)$$

the reaction rate becomes

$$v = \sqrt{\frac{k_B T}{2\pi m}} \frac{1}{\Delta s} K^\ddagger [A][B] \quad (6.8)$$

The calculation of the rate constant is now focussed on the calculation of the quasi-equilibrium constant. Statistical mechanics relate the equilibrium constant with the structures and energies of the reactants and products. These relations are developed in detail in Appendix II. It is shown that the equilibrium constant for the system



can be written in terms of the molar partition functions, per unit volume, of A, B and  $\ddagger$ ,

$$K^\ddagger = \frac{Q_\ddagger}{Q_A Q_B} e^{-\Delta E_0 / RT} \quad (6.9)$$

The partition functions are a measure of the states that are thermally accessible to the molecule at a given temperature. In the equation above, the energetic factor

$$\Delta E_0 = E_0^\ddagger - E_0^A - E_0^B \quad (6.10)$$

is the difference between the zero-point energies (ZPEs) of the transition state and the reactants, per mole, at  $T=0$  K. It is the amount of energy that the reactants must acquire at 0 K to reach the transition state.

As discussed above, one of the vibrational degrees of freedom of  $\ddagger$  in mechanism (6.III) became a translation along the reaction coordinate in mechanism (6.II). This can be factored out of the transition state in mechanism (6.II),  $Q^\ddagger$ , and related to the partition functions of the normal molecule,  $Q_\ddagger$ ,

$$Q_\ddagger = Q_{\text{trans},q} Q^\ddagger \quad (6.11)$$

As will be seen below, the translational partition function along the reaction coordinate has the form

$$Q_{\text{trans},q} = \frac{(2\pi m k_B T)^{1/2} \Delta s}{h} \quad (6.12)$$

and the rate constant can be written, using eq. (6.8)

$$\begin{aligned} k &= \frac{k_B T}{h} K^\ddagger \\ &= \frac{k_B T}{h} \frac{Q_\ddagger}{Q_A Q_B} e^{\Delta E_0 / RT} \end{aligned} \quad (6.13)$$

It is quite remarkable that the combination of the two terms involving the properties of the transition state, namely the velocity of crossing the transition state and the translational partition function along the reaction coordinate, gives the quantity  $k_B T/h$ , which is the same for reactants and reactions of all types. It represents the frequency with which any transition state becomes a product at a given temperature and its value is about  $6 \times 10^{12} \text{ sec}^{-1}$  at 300 K. Additionally, the length  $\Delta s$  representing the transition state at the top of the barrier, is eliminated in this procedure, and there is no obvious restriction on its magnitude. The most interesting achievement of TST is that the calculation of the partition functions of reactants and transition state leads to the reaction rate, provided that the energy term is known.

The constant  $K^\ddagger$  is exactly analogous to any other equilibrium constant, and hence should be related to  $\Delta G^\ddagger$ ,  $\Delta H^\ddagger$  and  $\Delta S^\ddagger$ , the standard free energy, enthalpy and entropy changes, respectively, accompanying the formation of the transition state from the reactants by means of the familiar thermodynamic relationships. In this manner, eq. (6.13) can also be written in the form

$$k = \frac{k_B T}{h} e^{-\frac{\Delta G^\ddagger}{RT}} = \frac{k_B T}{h} e^{\frac{\Delta S^\ddagger}{R}} e^{-\frac{\Delta H^\ddagger}{RT}} \quad (6.14)$$

that satisfies the requirement that the reaction rate is determined by the free energy of activation. This is an improvement over the simple collision theory in that it gives a precise and simple significance to the frequency factor. It must be emphasised that  $\Delta G^\ddagger$ ,  $\Delta H^\ddagger$  and  $\Delta S^\ddagger$  refer to the reactants and transition state in their standard states, although the conventional zero superscript is omitted.

### 6.1.2 Partition functions

Statistical mechanics offers well-established methods to obtain the partition functions of simple systems. In view of their relevance to the calculation of the pre-exponential factor of eq. (6.13), they are briefly reviewed below for translational, rotational and vibrational partition functions. The electronic partition function is assumed here to be identical to the degeneracy of the electronic ground state,  $Q_{\text{elec}} = g_{\text{elec}}$ .

The translational partition function is conveniently derived from the energy levels accessible to a particle of mass  $m$  moving in a potential energy box of length  $l$ . According to the Schrödinger equation for this system, the allowed energy levels are

$$E_n = \frac{n^2 h^2}{8ml^2} \quad (6.15)$$

where  $n$  is the quantum number associated with the energy levels. The one-dimensional partition function is, then,

$$Q_{\text{trans}} = \sum_{n=1}^{\infty} \exp\left(\frac{-n^2 h^2}{8ml^2 k_B T}\right) \quad (6.16)$$

According to the definition of the partition function as a measure of the number of thermally accessible states at a given temperature, there are very large numbers of translational states accessible for molecular systems at typical temperatures because the energetic separation between the translational states is much smaller than the thermal energy,  $\frac{3}{2}k_B T$  from eq. (2.43). Therefore, the summation can be replaced by appropriate integration, with the integral having a standard form

$$\begin{aligned} Q_{\text{trans}} &= \int_0^{\infty} \exp\left(\frac{-n^2 h^2}{8\pi m l^2 k_B T}\right) dn \\ &= \frac{1}{2} \left( \frac{8\pi m l^2 k_B T}{h^2} \right)^{\frac{1}{2}} = \frac{(2\pi m k_B T)^{\frac{1}{2}} l}{h} \end{aligned} \quad (6.17)$$

for each dimension. The translational energy for the three dimensions is

$$E_{\text{trans}} = E_{\text{trans},x} + E_{\text{trans},y} + E_{\text{trans},z} \quad (6.18)$$

and, consequently, the translational partition function for the three dimensions is

$$Q_{\text{trans}} = Q_{\text{trans},x} Q_{\text{trans},y} Q_{\text{trans},z} \quad (6.19)$$

or

$$Q_{\text{trans}} = \left( \frac{2\pi m k_B T}{h^2} \right)^{\frac{3}{2}} V \quad (6.20)$$

where  $V=l^3$ .

The vibrational partition function of a harmonic oscillator has equally spaced energy levels (eq. (1.5)). Representing the separation between the energy levels by  $\varepsilon$ , the vibrational partition function can be written as a geometric progression:

$$\begin{aligned} Q_{\text{vib}} &= 1 + e^{-\varepsilon/k_B T} + e^{-2\varepsilon/k_B T} + \dots = 1 + e^{-\varepsilon/k_B T} + \left(e^{-\varepsilon/k_B T}\right)^2 + \dots \\ &= \frac{1}{1 - e^{-\varepsilon/k_B T}} = \frac{1}{1 - e^{-hv/k_B T}} \end{aligned} \quad (6.21)$$

where we used the relations

$$\begin{aligned} S &= 1 + x + x^2 + \dots \\ xS &= x + x^2 + x^3 + \dots \\ S &= \frac{1}{1-x} \end{aligned} \quad (6.22)$$

The linear, rigid rotor has energy levels given by

$$E_J = \frac{J(J+1)}{2I} \left( \frac{h}{2\pi} \right)^2 \quad (6.23)$$

where  $I = \sum m_i r_i^2$  is the moment of inertia ( $r_i$  is the perpendicular distance between atom  $i$  of mass  $m_i$  and the rotation axis), and  $J=0, 1, 2, \dots$  is the rotational quantum number. The linear, rigid rotor has degenerate energy levels, and the rotational degeneracy is  $2J+1$ . The corresponding rotational partition function is

$$Q_{\text{rot}} = \sum_{J=0}^{\infty} (2J+1) \exp \left[ -\frac{J(J+1)}{2Ik_B T} \left( \frac{h}{2\pi} \right)^2 \right] \quad (6.24)$$

In general, at room temperature, the difference between the rotational energy levels is much smaller than  $k_B T$ . Under these conditions, many rotational levels are occupied and it is reasonable to replace the summation by the integral

$$\begin{aligned} Q_{\text{rot}} &= \int_0^{\infty} (2J+1) \exp \left[ -\frac{J(J+1)}{2Ik_B T} \left( \frac{h}{2\pi} \right)^2 \right] dJ \\ &= \frac{8\pi^2 I k_B T}{h^2} \end{aligned} \quad (6.25)$$

The H<sub>2</sub> molecule is one of the rare exceptions to the conditions formulated above, because its small mass, hence the small moment of inertia, leads to relatively large energetic separations between the energy levels. Given the H–H bond length  $l_{\text{HH}}=0.741 \text{ \AA}$ , we have  $I=4.5 \times 10^{-48} \text{ kg m}^2$  and  $\Delta E_J = 3 \text{ kJ mol}^{-1}$ , whereas at room temperature,  $3/2RT = 3.7 \text{ kJ mol}^{-1}$ .

For a polyatomic molecule with moments of inertia  $I_a$ ,  $I_b$  and  $I_c$  along the principal axis, the rotational partition function is

$$Q_{\text{rot}} = \pi^{1/2} \left( \frac{8\pi^2 I_a k_B T}{h^2} \right)^{1/2} \left( \frac{8\pi^2 I_b k_B T}{h^2} \right)^{1/2} \left( \frac{8\pi^2 I_c k_B T}{h^2} \right)^{1/2} \quad (6.26)$$

### 6.1.3 Absolute rate calculations

Using eq. (6.13), together with eqs. (6.20), (6.21), (6.25) or (6.26), and knowing the ZPE difference between the transition state and the reactants, it is now possible to calculate “absolute” reaction rates. In practice, TST can only be applied if the structure of the transition state and its vibrational levels are also known, because the former is required for the calculation of the rotational partition function of the transition state, and the latter enter the transition-state vibrational partition function. These data and  $\Delta E^0$  can be obtained from *ab initio* calculations or experimental information employed in the making of potential energy surfaces (PESs). The rapid development of computers and software has made it possible to carry out accurate *ab initio* calculations of transition-state properties for many tri-atomic and some tetra-atomic systems in the gas phase. The best-known system is the atom exchange in the H + H<sub>2</sub> system, and the properties of its linear transition state are shown in Table 6.1.

**Table 6.1**

Data from the PES obtained by the double many-bodied expansion (DMBE) method for the linear transition state  $\{\text{H}-\text{H}-\text{H}\}^\ddagger$  [5]

$\Delta V_{\text{cl}}^\ddagger$ (kJ mol $^{-1}$ )	$I_{\text{H}^1\text{H}^2} = I_{\text{H}^2\text{H}^3}^\ddagger$ (Å)	$\bar{v}_{\text{sym}}$ (cm $^{-1}$ )	$\bar{v}_{\text{asym}}$ (cm $^{-1}$ )	$\bar{v}_{\text{bend}}$ (cm $^{-1}$ )	$\Delta V_{\text{ad}}^\ddagger$ (kJ mol $^{-1}$ )
40.4	0.9287	2067	1493i <sup>a</sup>	899	38.2

<sup>a</sup>this is an imaginary frequency

Using the data presented in Appendix III, on the properties of stable molecules, and in Table 6.1, on the linear transition state of the  $\text{H}+\text{H}_2$  reaction, it is possible to calculate the rate constant for this reaction as the product of the partition function ratios

$$k = \frac{k_B T}{h} \left( \frac{Q^\ddagger}{Q_{\text{H}} Q_{\text{H}_2}} \right)_{\text{vib}} \left( \frac{Q^\ddagger}{Q_{\text{H}} Q_{\text{H}_2}} \right)_{\text{rot}} \left( \frac{Q^\ddagger/V}{Q_{\text{H}}/V \ Q_{\text{H}_2}/V} \right)_{\text{trans}} e^{-\Delta E_0/RT} \quad (6.27)$$

that can be calculated separately. The ratio of the translational partition functions at 440 K is

$$\begin{aligned} \left( \frac{Q^\ddagger/V}{Q_{\text{H}}/V \ Q_{\text{H}_2}/V} \right)_{\text{trans}} &= \left( \frac{m_{\text{H}} + m_{\text{H}_2}}{m_{\text{H}} m_{\text{H}_2}} \right)^{3/2} \left( \frac{h^2}{2\pi k_B T} \right)^{3/2} \\ &= (2.683 \times 10^{40} \text{ kg}^{3/2}) (3.900 \times 10^{-71} \text{ kg}^{3/2} \text{ m}^3) \\ &= 1.05 \times 10^{-30} \text{ m}^3 \end{aligned} \quad (6.28)$$

and the ratio of the rotational partition function for the linear transition state is simply given by the ratio of the moments of inertia

$$\begin{aligned} \left( \frac{Q^\ddagger}{Q_{\text{H}_2}} \right)_{\text{rot}} &= \frac{I_{\text{H}^1}^* (I_{\text{H}^1\text{H}^2}^*)^2 + I_{\text{H}^3}^* (I_{\text{H}^2\text{H}^3}^*)^2 - \frac{(m_{\text{H}^1} I_{\text{H}^1\text{H}^2}^* - m_{\text{H}^3} I_{\text{H}^2\text{H}^3}^*)^2}{m_{\text{H}^1} + m_{\text{H}^2} + m_{\text{H}^3}}}{\frac{m_{\text{H}^2} m_{\text{H}^3}}{m_{\text{H}^2} + m_{\text{H}^3}} (I_{\text{H}_2,\text{eq}})^2} \\ &= 6.28 \end{aligned} \quad (6.29)$$

Finally, the ratio of the vibrational partition functions is

$$\begin{aligned} \left( \frac{Q^\ddagger}{Q_{\text{H}_2}} \right)_{\text{vib}} &= \frac{1 - \exp\left(-\frac{h\bar{v}_{\text{H}_2} c}{k_B T}\right)}{\left[1 - \exp\left(-\frac{h\bar{v}_{\text{sym}} c}{k_B T}\right)\right] \left[1 - \exp\left(-\frac{h\bar{v}_{\text{bend}} c}{k_B T}\right)\right]^2} \\ &= 1.12 \end{aligned} \quad (6.30)$$

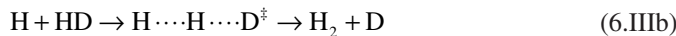
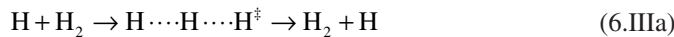
where we considered two degenerate bendings at the transition state, one in the plane, the other in and out of the plane, and the symmetric stretching. The anti-symmetric stretching

has become the reaction coordinate and has an imaginary value. The vibrational frequency of H<sub>2</sub>, employed in the construction of its Morse curve in Appendix III, is  $\bar{v}_{\text{H}_2} = 4400 \text{ cm}^{-1}$ .

The last parameter required for the calculation of the rate constant for the H+H<sub>2</sub> reaction is the energetic factor  $\Delta E_0$ . As mentioned before, it corresponds to the difference between the ZPEs of the transition state and the reactants. In Table 6.1, the classical potential energy difference between transition state and the reactants is represented by  $\Delta V^\ddagger$  and the barrier corrected for the ZPE is represented by  $\Delta V_{\text{ad}}^\ddagger$ . It is often designated as the vibrationally adiabatic barrier and corresponds to  $\Delta E_0$ . The rate constant calculated at 440 K with the universal frequency of TST,  $\Delta V_{\text{ad}}^\ddagger = 38.2 \text{ kJ mol}^{-1}$  and the ratio of the partition functions calculated above is  $1.2 \times 10^6 \text{ dm}^3 \text{ mol}^{-1} \text{ sec}^{-1}$ , fairly close to the experimental value of  $5.7 \times 10^6 \text{ dm}^3 \text{ mol}^{-1} \text{ sec}^{-1}$ .

#### 6.1.4. Statistical factors

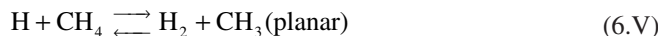
An even better agreement can be obtained considering the role of statistical effects in the transition state. The origin of such effects can be easily understood comparing the reactions



The partition functions for the two reactions are similar. However, the first reaction may result from two possible arrangements of the hydrogen molecule. This is clearer when we number each identical atom of the molecule



In contrast, reaction (6.IIIb) can only occur from one transition-state arrangement, because the other one leads to a different product, HD + H. It is natural that reaction (6.IIIa) is favoured by a statistical factor  $\sigma$  that is twice that of reaction (6.IIIb). The basis for the introduction of such statistical factors relies on the nature of the TST: the reaction rate is determined by the number of species that enter the transition state and do not return to the reactants. A simple method to obtain the statistical factors is to label the identical atoms and count the number of equivalent transition states. For example, the reaction



leads to the labelled species represented in Figure 6.2. The forward reaction leads to four sets of products with different labels, thus  $\sigma_f = 4$ . The reverse reaction also leads to four distinct sets of products, and thus  $\sigma_r = 4$ . The equilibrium constant written as the ratio of forward and reverse reactions agrees with that of equilibrium thermodynamics

$$K_{\text{eq}} = \frac{k_f}{k_r} = \frac{[\text{H}_2][\text{CH}_3]}{[\text{H}][\text{CH}_4]} = \frac{\sigma_f}{\sigma_r} \frac{Q_{\text{H}_2} Q_{\text{CH}_3}}{Q_{\text{H}} Q_{\text{CH}_4}} e^{-\Delta E_0/RT} \quad (6.31)$$

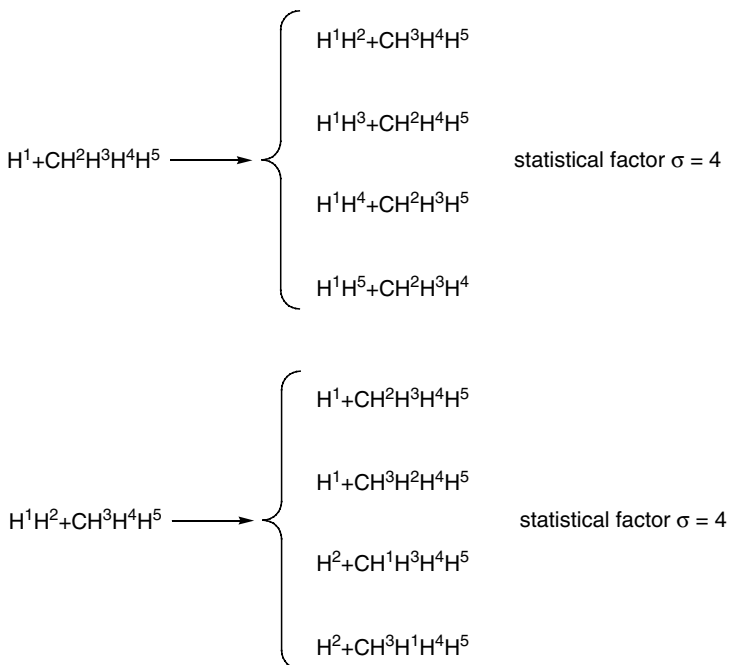


**Figure 6.2** Distinct species present in the reaction  $H + CH_4 \rightarrow H_2 + CH_3$  (planar). The methanes  $CH^2H^3H^4H^5$  and  $CH^3H^2H^4H^5$  as well as  $CH^1H^3H^4H^5$  and  $CH^3H^1H^4H^5$  are enantiomers.

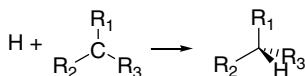


**Figure 6.3** Addition of a hydrogen atom to an asymmetric methyl radical leading to two enantiomers. The statistical factor of the forward reaction is twice that of the reverse reaction.

The use of statistical factors requires extra care when the reaction introduces or removes an asymmetric centre. For example, the addition of a hydrogen atom to an asymmetric methyl radical leads to two enantiomers, because the H atom may bind to either side of the symmetry plane (Figure 6.3). In the forward direction we have  $\sigma_f = 2$ , but in the reverse direction,  $\sigma_r = 1$  and the equilibrium constant is multiplied by a factor of two

$$K_{eq} = \frac{\sigma_f}{\sigma_r} \frac{Q_{CHR_1R_2R_3}}{Q_H Q_{CR_1R_2R_3}} e^{-\Delta E_0/RT} \quad (6.32)$$

The analyses of statistical factors may provide important information on the symmetry of the transition state. For example, the isomerisation of cyclopropane to propene may proceed via a symmetrical or an asymmetrical transition state (Figure 6.4). In the first case,  $\sigma_f = 2$ , whereas in the second case  $\sigma_f = 1$ . The symmetrical transition state corresponds to

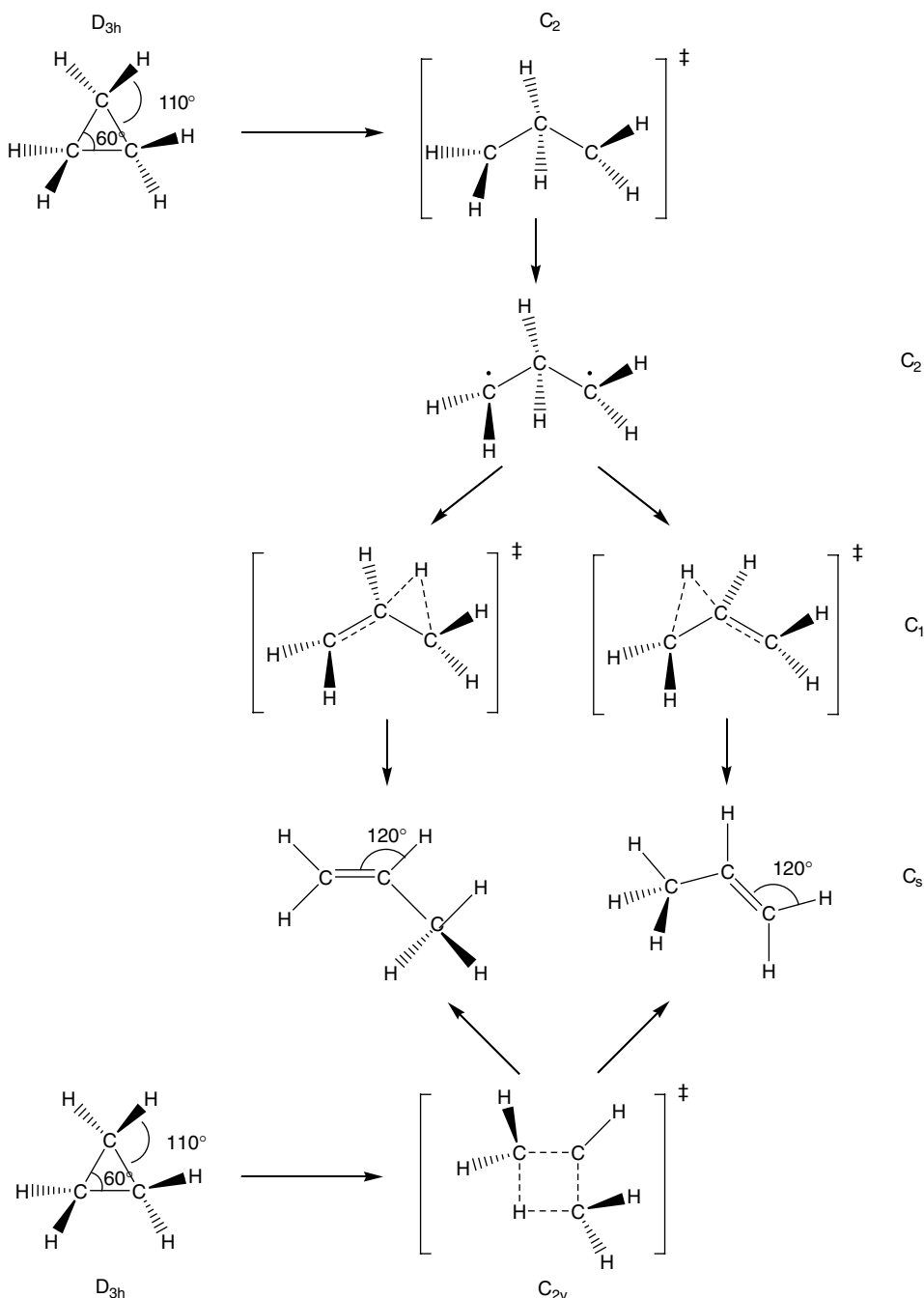


**Figure 6.4** Symmetrical and asymmetrical transition states in the isomerisation of cyclopropane to propene. The symmetrical transition state does not have any physical meaning because it requires the splitting of the reaction path into two paths at the transition state.

the generation of two reaction paths from the same transition state. This cannot happen in a PES, where one transition state can only connect one reactant's valley to one product's valley. Consequently, the symmetrical transition state is unphysical.

The consideration of statistical factors in the TST is a simple and necessary refinement of this theory. When the statistical factor is included, the classical rate constant of TST is expressed as

$$k_{\text{TST}} = \sigma \frac{k_{\text{B}}T}{h} \frac{Q^{\ddagger}}{Q_A Q_{\text{BC}}} e^{-\Delta V_{\text{ad}}^{\ddagger}/RT} \quad (6.33)$$

where explicit mention is made of the fact that the energetic factor is the vibrationally adiabatic barrier,  $\Delta V_{\text{ad}}^{\ddagger}$ . The inclusion of a statistical factor in the rate formulation is not compatible with the inclusion of symmetry numbers in the rotational partition functions. Indeed, such symmetry numbers were not included in our previous calculation of the partition functions. Now that we know that  $\sigma=2$  for the H+H<sub>2</sub> reaction, we can calculate a classical rate of  $2.4 \times 10^6 \text{ dm}^3 \text{ mol}^{-1} \text{ sec}^{-1}$  at 440 K. The calculated rate now approaches the uncertainty of the experimental value,  $5.7 \times 10^6 \text{ dm}^3 \text{ mol}^{-1} \text{ sec}^{-1}$ , but remains too slow.

### 6.1.5 Beyond the classical formulation

Further improvement of TST requires a critical analysis of its fundamental assumptions. The development of this theory was based on the following approximations: (i) the distribution of energy in the reactants and transition state follows the Boltzmann distribution law, (ii) every system that crosses the transition state becomes a product and (iii) the movement along the reaction coordinate is adiabatic and can be described by classical mechanics. Next, we analyse each one of these approximations to identify the conditions in which they fail and see how the theory can be improved in terms of both generality and accuracy.

The quasi-equilibrium assumption, that is the basis for the use of the Boltzmann distribution law, may lose its validity for rapid reactions. In such reactions, the most energetic reactant molecules may disappear very rapidly and the concentration of species at the transition state may be lesser than that for a true equilibrium. In practice, even when  $E_a/RT \approx 1.3$ , as in the Cl+HBr → HCl+Br hydrogen atom abstraction, internal-state non-equilibrium effects are very small [6].

The assumption that the transition state is only crossed once by every reactive system neglects several types of trajectories that the system may follow, as illustrated in Figure 6.5. In fact, the classical TST assumes that the reactive systems can only follow trajectories of type 1, illustrated in this figure. However, trajectories of types 2, 5 and 6 also cross the transition state in the direction of the products, but do not correspond to reactive systems. Furthermore, although trajectories of type 3 are reactive, they cross the transition state twice in the direction of the products, but only contribute once to the actual rate. In general, a trajectory with just the energy necessary to cross the transition state will do so at a region very close to the saddle-point, which is the point of minimum energy separating the

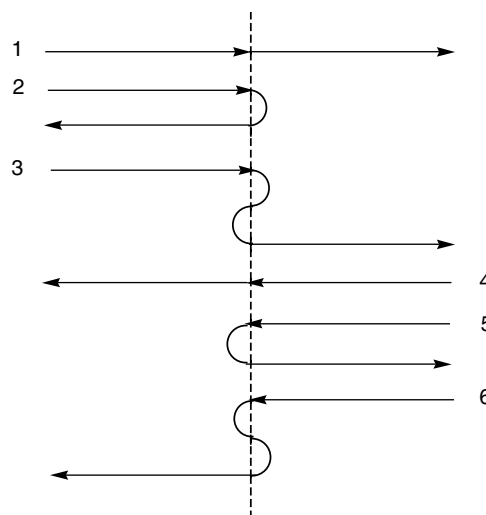


**Figure 6.5** Schematic trajectories illustrating the re-crossing of a transition state. Trajectory 1 corresponds to the situation idealised by TST.

reactants and products in the PES. It is very unlikely that such a trajectory will find a path to return to the reactants and cross the transition state again. However, trajectories with higher energies may deviate appreciably from the minimum energy path connecting the reactants to the transition state and, finally, to the products. Such trajectories have an increased probability of being reflected by the repulsive potential after the transition state, and re-cross it back to the reactants. As the energy of the trajectories increases, the bottleneck of the reaction moves from the saddle-point towards the asymptotic regions of reactants or products where the PES is usually narrower. This behaviour can be rationalised as a competition between the energetic and the entropic factors. The energetic factor is determined by the mean velocity of the trajectories, and favours the localisation of the transition state at the saddle-point. The entropic factor is related to changes in force constants and moments of inertia, and drives the transition state to the more constricted regions of the PES. As the temperature increases, the average energy of the trajectories also increases, and the location of the transition state becomes dominated by the entropic factor, rather than by the energetic factor. These considerations suggest that it is more exact to define a variational transition state, located at the bottleneck that minimizes its re-crossing. This approach was followed by Garrett and Truhlar [7], who used a variational method to locate the transition state. The variational transition state minimises the reactive flux from the reactants to the products. The variational TST (VTST) has met with considerable success, and represents a significant improvement over the classical TST at higher temperatures, where re-crossing effects are more relevant [8]. However, the rates of classical TST are an upper limit of the rates of classical VTST, and this cannot be the reason why the classical TST underestimates the  $\text{H}+\text{H}_2$  reaction rate at 440 K.

The last assumption of the classical TST concerns the adiabaticity of the movement along the reaction coordinate. The term “adiabatic” has been used in many different

instances and requires some explanation. Following the original suggestion by F. London, an (electronically) adiabatic transformation is one in which there is a continuous equilibrium between the electrons and the nuclei, and the whole process takes place on a single PES. This is only possible in the presence of a strong coupling between the reactant and the product states. The opposite of an (electronically) adiabatic process is a non-adiabatic (or diabatic) process that involves a jump from the initial to the final electronic state, that is, it occurs through an abrupt electronic re-arrangement. In addition to the electronic adiabaticity, the TST also assumes that the reactions are vibrationally adiabatic, that is, they occur in the vibrational ground state, with the conservation of the ZPE along the reaction coordinate. To go beyond the vibrational adiabaticity of the classical TST, it is necessary to introduce quantum corrections. Such corrections are very important for systems involving small molecular masses. The introduction of quantum correction in the classical TST leads to hybrid theories, with classical transition states and quantum effects. Such theories are called semi-classical theories.

## 6.2 SEMI-CLASSICAL TREATMENTS

The inclusion of quantum corrections in the reaction coordinate of the TST involves some conceptual and computational difficulties. Conceptually, the precise localisation of the transition state in a PES implies an absolute uncertainty in its conjugated momentum, (eq. (1.8)). This was avoided in the classical derivation of the TST, because the length of the transition state at the top of the barrier,  $\Delta s$  in eq. (6.5), cancelled with the translational partition function along the reaction coordinate in eq. (6.12), and the actual size of the transition state is irrelevant for the calculations.

Eyring adopted an *ad hoc* procedure that has been successful in including quantum effects in TST. First, the classical partition functions are replaced by their quantum analogues. Second, the classical rate is multiplied by a transmission coefficient that takes into account the quantum effects along the reaction coordinate. The quantum partition functions assume that the transition state can be treated as a stable system. The separate quantisation of the reaction coordinate is based on the vibrational adiabaticity assumption, that is, all the other vibrational modes of the reactive system very rapidly adjust to the reaction coordinate and maintain the continuity and smoothness of the PES.

### 6.2.1 Kinetic isotope effects

The quantisation of the vibrational degrees of freedom offers a method of calculating the effect of isotopic substitution on the rate constants, because isotopes differ in their masses, hence in their ZPEs, but not in their electronic potential energies.

Following eqs. (1.2) and (1.5), the ZPE of a molecular vibration is given by

$$E_{v_0} = \frac{1}{2} \hbar \sqrt{\frac{f}{\mu}} \quad (6.34)$$

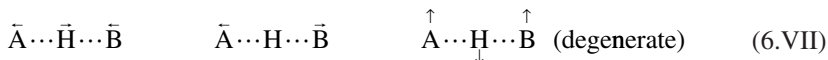
Under the harmonic approximation, and using a force constant of  $2.90 \times 10^3 \text{ kJ mol}^{-1} \text{ \AA}^{-2}$  for a C–H or a C–D bond, the ZPE difference between these two bonds is  $4.7 \text{ kJ mol}^{-1}$ . In the limiting case where they are effectively broken at the transition state, the difference in ZPEs between the C–H and C–D bonds is also their difference in activation energies. Under these circumstances, the ratio of the room-temperature rates involving the breaking of C–H and C–D bonds is  $k_{\text{H}}/k_{\text{D}} = 6.7$ . For higher force constants, such as those of the N–H and O–H bonds, the maximum isotope effect calculated by this minimalist model is even higher. This effect of the ZPE change on the rates of chemical reactions differing by isotopic substitution is named *primary kinetic isotope effect* (KIE).

The naive approximation described above is in conflict with the TST, because the reactive bond is never completely broken at the transition state. The existence of a bonding interaction in  $\text{A}\cdots\text{B}\cdots\text{C}$  is the reason why the transition state can be defined in the first place, and the ZPEs of the C–H or C–D bonds cannot be totally omitted. Thus, the observed KIE should always be smaller than the calculated maximum.

Westheimer [9] pointed out a more consistent method to estimate the maximum KIE in a reaction of the type



from the vibrations of the linear transition state  $\text{A}\cdots\text{H}\cdots\text{B}$ . Neglecting the vibrations of species A and B, we only have to consider the  $3n-5=4$  vibrational modes of the linear transition state. These vibrational modes are the anti-symmetric stretching (which corresponds to the movement along the reaction coordinate), the symmetric stretching (which is perpendicular to the reaction coordinate), and two degenerate bendings (one in the plane and the other in and out of the plane)



Neglecting the contribution of the bendings and considering that the anti-symmetric stretching is, in fact, the translational motion along the reaction coordinate, the ZPE of the transition state is determined only by the symmetric stretching. In a perfectly symmetric transition state,  $\text{B}=\text{A}$ , the symmetric stretching is a synchronous movement of A and B leaving H equally distant from the end atoms, and at rest. The central atom does not move in the symmetric stretching of such a transition state, and the isotopic substitution does not change the symmetric stretching frequency. Consequently, the ZPE of the transition state is the same for the symmetrical transfer of H or D atoms, and Westheimer concluded that the KIE should attain its maximum for symmetrical transfers of H or D atoms (Figure 6.6). Under these approximations, the difference in activation energy between H and D transfers is, again, equal to the ZPE difference of the reactive bonds with H or D.

If the transition state is not perfectly symmetrical, the H atom will be closer to either A or B, and will move with the symmetric stretching. This movement will produce a ZPE difference between the hydrogenated and deuterated species, which will partly offset the ZPE difference of the reactive bonds. Thus, a smaller KIE should be observed when H (or D) is closer to either A or B. In Chapter 7 we will see that in an exothermic reaction the structure of the transition state resembles more closely that of the reactants and in an endothermic

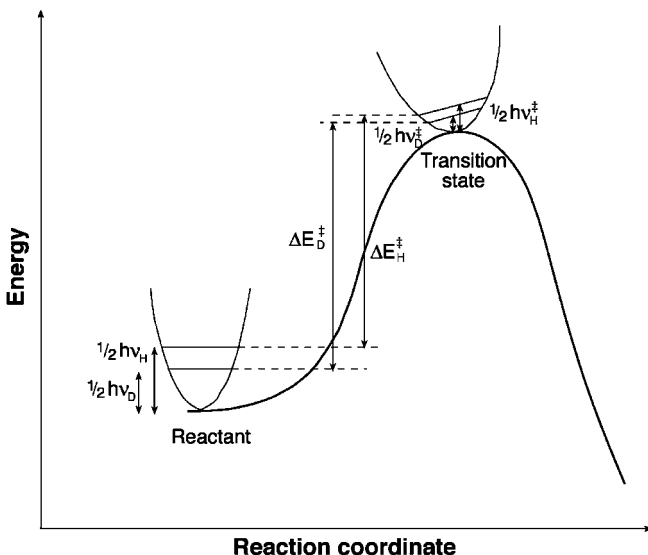


**Figure 6.6** Difference in activation energy due to the difference in ZPE of C–H and C–D bonds, in a symmetrical transition state.

reaction the transition-state structure approaches that of the products. The reasoning presented above leads to the conclusion that in a series of H-atom or proton transfers differing mostly in their reaction energy, the KIE increases from the most exothermic reactions, reaches its maximum for the isothermal reaction and decreases as the reactions become endothermic. Although this discussion was oriented towards the relative position of the central atom, it is clear from eq. (6.34) that the tightness of the bonds also modulates the symmetry of the KIE dependence on the reaction energy.

Westheimer's interpretation of KIE is based on identical pre-exponential factors for H or D transfers, neglects the contribution of the bending vibrations, and assumes that classical mechanics can describe the movement along the reaction coordinate. It is, nevertheless, a useful approximation for mechanistic interpretations of KIE. For example, the observation of a sizeable KIE when a hydrogen atom is replaced by deuterium in a given compound indicates that the bond where the isotopic substitution was made is practically broken in the rate-determining step of the reaction.

It is often possible to observe a KIE even when the bond to the H or D atom is not broken in the course of the reaction. In such cases, we have *secondary KIEs*. Two reasons may concur for the observation of a secondary KIE, and both of them are related to the ZPE differences between the isotopes.

To explain the secondary KIE, we have to go beyond the simple harmonic model for a chemical bond. A more realistic model for a chemical bond is that of a Morse potential

$$V = D_e \left\{ 1 - \exp \left[ -\beta(l - l_{eq}) \right] \right\}^2 \quad (6.35)$$

where  $D_e$  is the electronic dissociation energy,  $l_{eq}$  the equilibrium bond length and  $\beta$  the spectroscopic constant, defined as

$$\beta = \varpi_e \sqrt{\frac{2\pi^2 c \mu}{h D_e}} = 0.01332 \varpi_e \sqrt{\frac{\mu}{D_e}} \quad (6.36)$$

The numerical constant is obtained when the reduced mass of the directly bonded atoms ( $\mu$ ) is expressed in amu,  $D_e$  is in kilojoule per mole, the equilibrium stretching frequency ( $\varpi_e$ ) is per centimetre and  $\beta$  is in per angstrom. The Morse potential reflects the anharmonicity of a chemical bond and reproduces its dissociation energy (Figure 6.7). It is a very convenient potential because the depth of the potential minimum is related to the bond dissociation energies tabulated at 298 K ( $D_{298}^0$ )

$$D_e = D_{298}^0 - 1.5RT + 0.5hc\varpi_e = D_{298}^0 - 1.5RT + 0.00598\varpi_e \quad (6.37)$$

and the equilibrium stretching frequency is related to the infrared stretching frequency

$$\varpi_e = \bar{v} + 0.5hc \frac{(\bar{v})^2}{D_{298}^0 - 1.5RT} = \bar{v} + 0.00598 \frac{(\bar{v})^2}{D_{298}^0 - 1.5RT} \quad (6.38)$$

Thus, all the parameters of this potential can be obtained from experimental data tabulated for many bonds. The term  $1.5RT$  appearing in the above expression accounts for translational

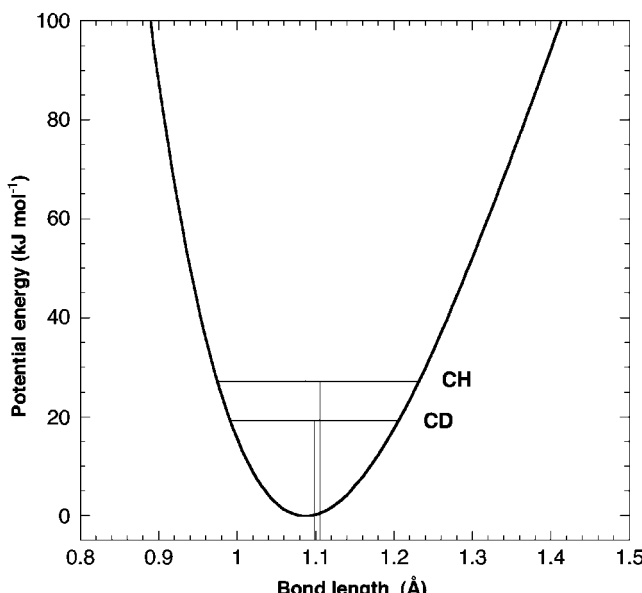


**Figure 6.7** Morse potential of the C–H bond in  $\text{CH}_4$ , with indication of vibrational energy levels.

motion of one additional species when the bond is broken, and should be used with  $T = 298$  K, to be consistent with  $D_{298}^0$ .

The Schrödinger equation has an analytical solution for the Morse potential and gives the following expression for its energy levels

$$E_v = \left( v + \frac{1}{2} \right) hc\omega_e - \left( v + \frac{1}{2} \right)^2 x_e hc\omega_e \quad (6.39)$$

where  $x_e$  is the anharmonicity constant. As shown in Figure 6.7, the fundamental vibrational frequencies of the C–H and C–D bonds correspond to different equilibrium bond lengths. The lighter isotopes have longer equilibrium bond lengths, although they correspond to the same potential energy curve. This leads to two consequences: (i) the longer C–H bond entails that steric effects are more important than with the shorter C–D bond; (ii) with the same electronic nature but a shorter bond, the C–D bond has a higher electron density at C than the C–H bond. In this respect, we can say that deuterium exerts a stronger electron-donating inductive effect than hydrogen. These effects are, nevertheless, very mild, and the secondary KIE,  $k_H/k_D$ , is usually  $<2$  and, in some cases, is even less than unity. In such cases these are named inverse KIEs.

### 6.2.2 Tunnel effect

We have seen that the rate of crossing the transition state leads to the classical factor  $k_B T/h$  in eq. (6.13). In quantum mechanics, we must also consider the possibility that systems with less energy than the barrier height may leak to the product, and also that cases with more energy than the barrier be reflected back to the reactants. For the moment, we will consider only the classical barrier,  $\Delta V^\ddagger$ , without ZPE corrections. We will defer the discussion of tunnelling through the vibrationally adiabatic barrier to a later stage. The classical probability of crossing the barrier,  $P_C(E)$ , in the classical factor

$$\begin{aligned} \frac{k_B T}{h} &= \frac{1}{h} \int_0^\infty dE e^{-E/k_B T} \\ &= \frac{1}{h} \int dE P_C(E) e^{-E/k_B T} \end{aligned} \quad (6.40)$$

must be replaced by the quantum probability,  $P_Q(E)$ . Whereas classically  $P_C(E)=0$  if  $E < \Delta V^\ddagger$  and  $P_C(E)=1$  if  $E \geq \Delta V^\ddagger$ , the solution of the Schrödinger equation for the probability of a particle crossing a barrier gives  $P_Q(E) > 0$  even when  $E < \Delta V^\ddagger$ . The crossing of

**Table 6.2**

de Broglie wavelengths of particles with a kinetic energy of 50 kJ mol<sup>-1</sup>

Particle	e <sup>-</sup>	H	C	Br	C <sub>60</sub>
Mass (amu)	1/1750	1	12	80	720
$\lambda$ (Å)	16.70	0.40	0.12	0.04	0.015

a barrier with a potential energy higher than the kinetic energy of the incident particle is a quantum mechanical phenomenon called the *tunnel effect*.

The origin of the tunnel effect can be found in the wave-particle duality proposed by de Broglie

$$\begin{aligned}\lambda &= \frac{h}{mv} \\ &= \frac{h}{\sqrt{2mE_c}}\end{aligned}\tag{6.41}$$

where  $\lambda$  is the wavelength associated with a particle of mass  $m$ , velocity  $v$  and kinetic energy  $E_c$ . Many chemical reactions have an activation energy *ca* 50 kJ mol<sup>-1</sup>, and we can assume that the reactive systems must have a similar kinetic energy. Using the equation above with  $E_c = 50$  kJ mol<sup>-1</sup>, we calculate the wavelengths of particles such as the electron, hydrogen, carbon or bromine atoms, and the buckminsterfullerene (footballene) molecule ( $C_{60}$ ), shown in Table 6.2. It is evident that the electron has an associated wavelength that is one order of magnitude higher than a typical bond length, and only its wave-like properties will be observed in the course of chemical reactions. The bond length changes that occur as the reactant and product bond lengths extend to their configuration at the transition state are much smaller than the equilibrium bond lengths. The wavelength associated with the hydrogen atom is then similar to the sum of the reactive bond length changes and this atom may also manifest its wave-like properties. It should be noted that the other atoms and molecules have too short associated wavelengths to manifest quantum-mechanical behaviour in the course of chemical reactions, but, under special conditions, even  $C_{60}$  has shown wave-like properties [10].

In quantum mechanics, the wave function that describes the movement along a direction  $x$  of a system with a mass  $m$  and energy  $E$  is

$$\psi(x, t) = \psi(x) \exp(-iEt/\hbar)\tag{6.42}$$

and that wave function must obey the equation of Schrödinger for the system

$$\frac{d^2\psi(x)}{dx^2} + \frac{2m}{\hbar^2} [E - V(x)] \psi(x) = 0\tag{6.43}$$

where  $V(x)$  is the potential that the systems encounter. For some types of potentials it was possible to obtain the exact solutions for the wave function  $V(x)$  that satisfy Schrödinger's equation, and from such solutions it was possible to obtain  $P_Q(E)$ . Independently and almost simultaneously, Brillouin [11], Wentzel [12] and Kramers [13] proposed a method to obtain an approximate solution to eq. (6.43), which gives the permeability of any unidimensional barrier. According to the WKB method, the transmission probability of a particle through a unidimensional barrier is

$$P_Q(E) = \frac{1}{1 + \exp\left\{\frac{2\sqrt{2m}}{\hbar} \int_{x_1}^{x_2} \sqrt{V(x) - E} dx\right\}}\tag{6.44}$$

This equation is rather precise, even for energies close to the barrier maximum,  $\Delta V^\ddagger$ , and it is exact for potential barriers with the shape of an inverted parabola. When  $E$  is much smaller than  $\Delta V^\ddagger$ , a case commonly found in molecular systems, the above expression can be simplified to

$$G(E) = \exp \left\{ -\frac{2\sqrt{2m}}{\hbar} \int_{x_1}^{x_2} \sqrt{V(x) - E} \, dx \right\} \quad (6.45)$$

Eq. (6.45) has analytical solutions for several classes of potential barriers. For example, in the case of a square barrier, Figure 6.8, with a constant potential  $V_{\max}$  over a given interval of the reaction coordinate,  $\Delta x$ , the integral of eq. (6.45) is the area of the square  $[\Delta V^\ddagger - E]^{1/2} \Delta x$ , and the transmission probability becomes

$$G(E) = \exp \left\{ -\frac{2\sqrt{2m}}{\hbar} \sqrt{V_{\max} - E} \Delta x \right\} \quad (6.46)$$

This solution can be applied to the probability of transmission of an electron, through vacuum, from a reduced to an oxidised species, or, in a scanning tunnelling microscopy experiment, the jump of an electron from the surface of the sample to the tip of the probe. In such systems, the electron escapes from the potential well of the donor to the potential well of the acceptor. The ionisation potential of the neutral donor or the work function of the metal gives the energetic factor in eq. (6.46), and the distance between the electron donor and acceptor gives  $\Delta x$ . Thus, eq. (6.46) gives the transmission probability in a non-adiabatic electron transfer reaction.

Another analytical solution can be obtained for the case of the intersection of two parabolae separated by a distance  $\Delta x$  along the reaction coordinate (Figure 6.9). The parabolae are characterised by a square dependence on the displacement from the equilibrium position,

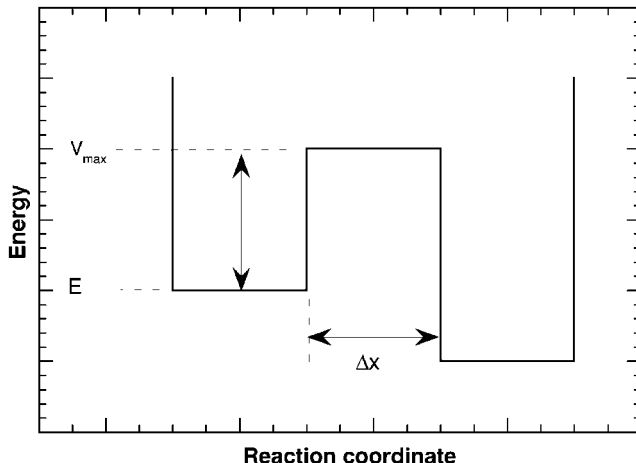


**Figure 6.8** Square potential barrier.

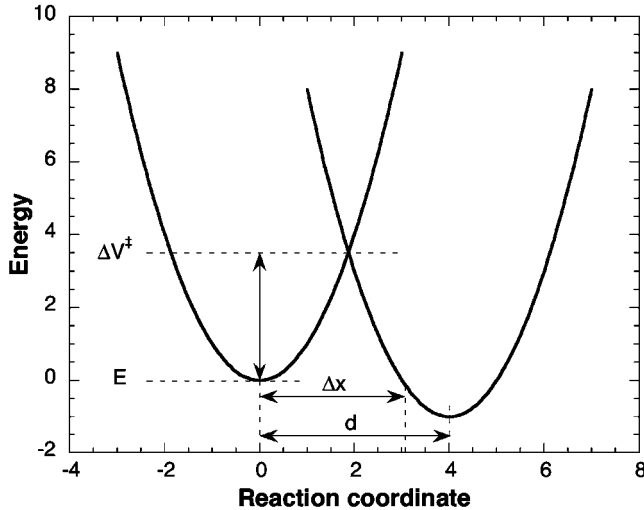


**Figure 6.9** Potential barrier defined by the intersection of two parabolas.

eq. (1.6), and the term  $[V(x)-E]^{1/2}dx$  in eq. (6.45) has the shape of a triangle. The integral is the area of a triangle with a base  $\Delta x$  and a height  $\Delta V^\ddagger$ , and the transmission probability becomes

$$G(E) = \exp\left\{-\frac{\sqrt{2m}}{\hbar}\sqrt{\Delta V^\ddagger - E}\Delta x\right\} \quad (6.47)$$

Finally, a potential barrier that closely approaches the classical reaction path of an atom-transfer reaction and that also has an analytical solution for the transmission probability, is the Eckart barrier [14]

$$\begin{aligned} V(x) &= -\frac{Ay}{1-y} - \frac{By}{(1-y)^2} \\ y &= -\exp\left(\frac{2\pi x}{l}\right) \end{aligned} \quad (6.48)$$

where

$$\begin{aligned} A &= \Delta V^\ddagger - (\Delta V^\ddagger - \Delta V^0) \\ B &= \left[ \sqrt{\Delta V^\ddagger} + \sqrt{\Delta V^\ddagger - \Delta V^0} \right]^2 \\ l &= 2\pi\sqrt{-\frac{2}{f^*}\left[\frac{1}{\sqrt{\Delta V^\ddagger - \Delta V^0}} + \frac{1}{\sqrt{\Delta V^\ddagger}}\right]}^{-1} \end{aligned} \quad (6.49)$$

represented in Figure 6.10. The probability  $G(E)$  of a particle of mass  $\mu$ , moving towards the barrier with an energy  $E$  at  $-\infty$ , to cross the barrier and appear later at  $+\infty$  with an energy  $E$ , has been obtained from the resolution of Schrödinger's equation and has the form

$$G(E) = 1 - \frac{\cosh[2\pi(\alpha - \beta)] + \cosh(2\pi\delta)}{\cosh[2\pi(\alpha + \beta)] + \cosh(2\pi\delta)} \quad (6.50)$$

where

$$\begin{aligned} \alpha &= \frac{1}{2} \sqrt{\frac{E}{C}} \\ \beta &= \frac{1}{2} \sqrt{\frac{E-A}{C}} \\ \delta &= \frac{1}{2} \sqrt{\frac{B-C}{C}} \\ C &= \frac{h^2}{8\mu l} \end{aligned} \quad (6.51)$$

In a real system we do not have one particle with a given energy colliding with the barrier, but many molecules with a Boltzmann distribution of energies at the temperature  $T$ . Thus, for real systems, we have to integrate the transmission probability  $G(E)$  over all the energies

$$\kappa(T) = \exp\left(\frac{\Delta V^\ddagger}{k_B T}\right) \int_0^\infty G(E) \exp\left(-\frac{E}{k_B T}\right) d\left(\frac{E}{k_B T}\right) \quad (6.52)$$

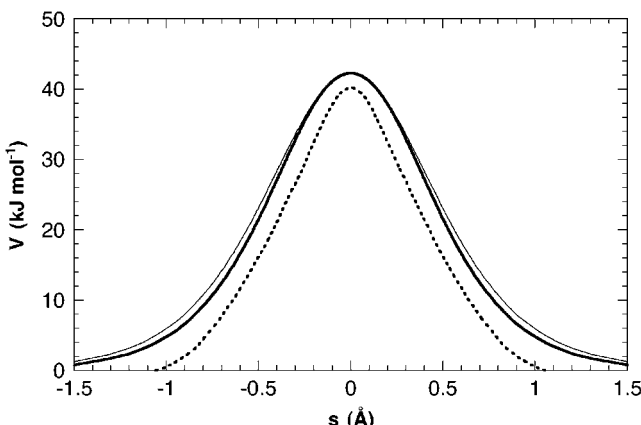


**Figure 6.10** Eckart barrier for the  $\text{H}+\text{H}_2$  reaction (thin line), fitted to the curvature of the reaction path of the ISM (full line). The accurate reaction path by the DMBE PES is shown as a dashed line. For this system,  $\Delta V^0=0$ . The reaction coordinate is defined as  $s=\pm 2^{1/2}(l_{\text{HH}}-l_{\text{HH}}^\ddagger)$ .

to obtain the tunnel correction at the temperature  $T$ . The data required for this calculation are the height of the barrier ( $\Delta V^\ddagger$ ), the reaction energy ( $\Delta V^0$ ), the curvature of the reaction path at the transition state ( $f^\ddagger$ ) and the reduced mass ( $\mu$ ). Using the data in Table 6.1 for the H+H<sub>2</sub> reaction, together with the relation between the frequency and the force constant in eq. (1.2), and the reduced mass

$$\mu = \frac{m_B m_C + m_A m_B}{2(m_A + m_B + m_C)} \quad (6.53)$$

we obtain a tunnelling correction of 3.0 at 440 K, 12 at 300 K and 618 at 200 K. The Eckart barrier permeability tends to overestimate the tunnelling corrections (6.93 and 95.5 at 300 and 200 K, respectively) at lower temperatures for the H+H<sub>2</sub> reaction according to the more sophisticated methods.

Introducing the tunnelling correction in the classical TST equation, we obtain the semi-classical expression

$$k_{\text{scTST}} = \kappa(T) \sigma \frac{k_B T}{h} \frac{Q^\ddagger}{Q_A Q_{BC}} e^{-\Delta V_{\text{ad}}^\ddagger / RT} \quad (6.54)$$

With the tunnelling correction at 440 K calculated from the Eckart barrier permeability discussed above, the semi-classical rate constant is  $7.2 \times 10^6 \text{ dm}^3 \text{ mol}^{-1} \text{ sec}^{-1}$  at this temperature, only slightly higher than the experimental value,  $5.7 \times 10^6 \text{ dm}^3 \text{ mol}^{-1} \text{ sec}^{-1}$ . This excellent agreement shows that absolute rates can be calculated with great accuracy using the TST, provided that the energy and the geometry of the transition state as well as the curvature of the reaction path at this point of the PES are all known.

The unidimensional tunnelling calculations described above presume that movement along the reaction coordinate is electronically and vibrationally adiabatic. In real systems there are two sources of non-adiabatic effects on the reaction coordinate: (i) changes in the frequencies of the internal displacements (perpendicular to the reaction coordinate); (ii) curvilinear effects on the reaction coordinate. Such effects are more pronounced in exothermic reactions, which may lead to vibrationally excited products, and in systems where a light atom is transferred between two heavy atoms (e.g. I-H-I), because the diagonalisation of the kinetic energy in such systems leads to a substantial curvature of the PES.

The most common and meaningful example of the breakdown of the vibrational adiabaticity is the deviation of the tunnelling path relative to the minimum energy path (MEP). Tunnelling occurs preferably along a path displaced towards the concave side of the MEP, which corresponds to the classical turning points for the vibrations perpendicular to the reaction path (Figure 6.11). This path, first described by Marcus and Coltrin [15], contracts the reaction coordinate and leads to a thinner, albeit higher, barrier. Although  $\Delta V^\ddagger$  is larger along this path,  $\Delta x$  is smaller and compensates for the energy factor because it appears as a square root in the exponential decay, eq. (6.45). The Marcus and Coltrin path minimises the exponential dumping of the wave function in the classically forbidden region, and gives the least-action tunnelling correction.

The tunnel effect is the most important correction to the classical TST for reactions involving light particles such as H-atom transfers, proton transfers or hydride transfers. The importance of this correction increases as the temperature is lowered. Traditionally,

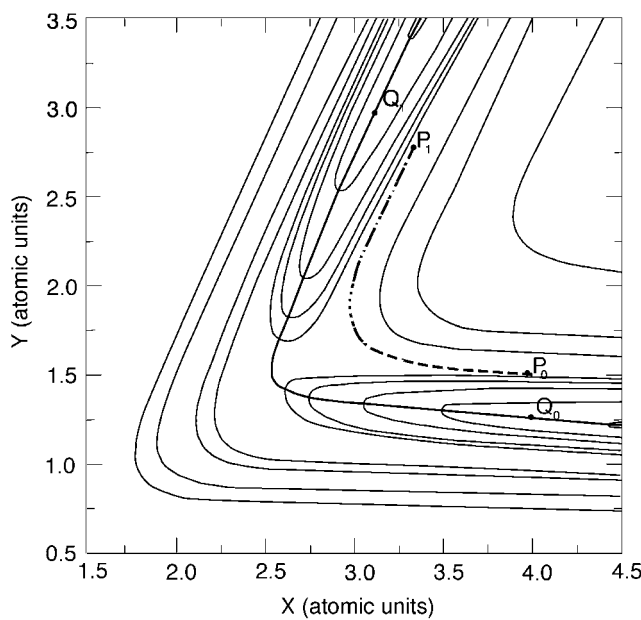


**Figure 6.11** Marcus–Coltrin path (dashed line) and MEP (full line) in a PES for the  $\text{H}+\text{H}_2$  reaction.  $P_0$  and  $P_1$  represent the initial and final points for tunnelling of a trajectory in the Marcus–Coltrin path, respectively;  $Q_0$  and  $Q_1$  have the same meaning, but for the MEP.

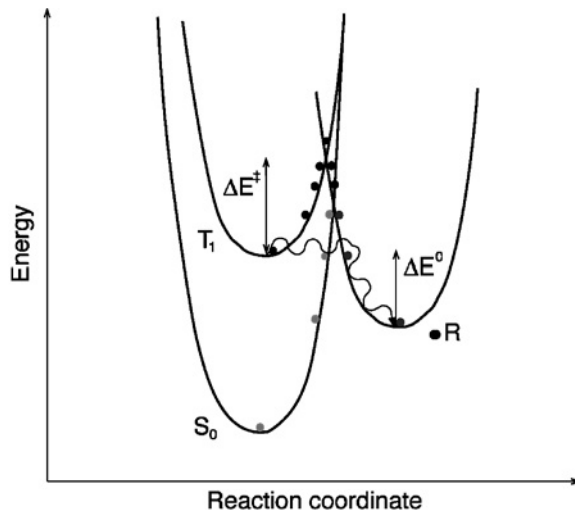


**Figure 6.12** Increase in the reaction quantum yield owing to nuclear tunnelling. Thermal activation takes the system over the barrier and across a funnel from the product surface to the ground-state reactant surface, which may take some system back to the reactants. In contrast, nuclear tunnelling places the reactive systems in a region of the product surface beyond the funnel with the reactants, and the systems cannot return to their original state.

the experimental evidence for nuclear tunnelling in a chemical reaction comes from: (i) sizeable deviations from the Arrhenius law, (ii) isotope-dependent pre-exponential factors, (iii) anomalously high KIE. Additionally, in some photochemical reactions it has been suggested that nuclear tunnelling could lead to higher product quantum yields than thermal activation (Figure 6.12).

### 6.3 INTERSECTING-STATE MODEL

The collision theory and the TST offer methods to calculate the rates of chemical reactions, but both require some information on the PES of the system. The minimum information that they require is the difference in energy between the saddle-point and the reactants, which gives the critical energy necessary for the reaction,  $\varepsilon_c$  in eq. (5.15), or the difference between the ZPEs of the transition state and reactants,  $\Delta E_0$  in eq. (6.13). Just as the simple collision theory can be improved with the calculation of trajectories with a Maxwell–Boltzmann distribution of velocities that explore large regions of the PES, classical TST can also be improved by the inclusion of tunnelling, which requires the knowledge of the PES along the reaction path, or by employing a variational method to optimise the location of the transition state, and which requires an even more detailed knowledge of the PES. Thus, the practical application of these methods depends on our knowledge of the PES. With the currently available *ab initio* methods and using fast computers, it has been possible to obtain PESs with chemical accuracy (better than 1 kcal mol<sup>-1</sup>) for a number of tri-atomic and tetra-atomic systems. However, it remains an enormous challenge to calculate, from first principles, accurate PESs for polyatomic systems without using information on the kinetics of the systems.

Density functional theory (DFT) offers the opportunity to calculate the energies of nuclear configurations of polyatomic systems with an increasing efficiency. “Direct dynamics”, where the energies of the nuclear configurations are calculated as they are reached by a trajectory, promise to bypass the need for a PES in rate calculations. However, chemists need more general and structure-motivated methods to interpret and predict reactivity. Semi-empirical methods may play a significant role in this respect, because they offer a simple, accurate and structure-related approach to chemical reactivity.

The distinctive features of semi-empirical methods are the use of experimental information on reactants and products, and simplified potential models to calculate the transition-state structure and energy. A semi-empirical model that provides useful transition-state data on bond-breaking–bond-forming reactions is the intersecting/interacting state model (ISM) [16,17].

ISM is a unidimensional reactivity model based on the diabatic method originally proposed by Evans and Polanyi [18] and on the conservation of the bond order along the reaction coordinate of the bond-energy–bond-order (BEBO) first proposed by Johnston and Parr [19]. For a reaction of the type



the diabatic method uses the potential curves of the reactive fragments, BC and AB to build the reaction coordinate and, at a later stage, includes the resonance energy between

the two fragments at the transition state. The interesting feature of this method is that it employs the properties of the reactants and products, readily accessible from experiment, to obtain a first approximation for the reaction coordinate. For example, the vertical separation between the reactant and product minima is the reaction energy, and can be easily obtained from the difference of bond dissociation energies of products and reactants, or from the equilibrium constant. However, as illustrated in Figure 6.13, the diabatic method can only be applied if it is possible to calculate the separation of the reactants and products minima along the reaction coordinate,  $d$ .

The success of the method in calculating the horizontal separation  $d$  from the properties of the reactants and products ultimately determines its ability to provide reasonable estimates of the activation energy. According to the ISM, the separation  $d$  is the sum of the reactive bonds' extensions from their equilibrium to their transition-state configurations. For a reaction such as that of mechanism (VIII), this is the sum of the extension of the BC bond with that of the AB bond

$$d = \left| l_{BC}^{\ddagger} - l_{BC,eq} \right| + \left| l_{AB}^{\ddagger} - l_{AB,eq} \right| \quad (6.55)$$

Next, the method requires a relation between the bond extensions and a parameter that can be calculated for any arbitrary bond-breaking–bond-forming reaction. A very interesting relationship involving bond lengths was found by Pauling [20], who showed that they can be related to the corresponding bond orders  $n$ ,

$$l_{n,eq} - l_{s,eq} = -0.6 \log(n) = -a \ln(n) \quad (6.56)$$

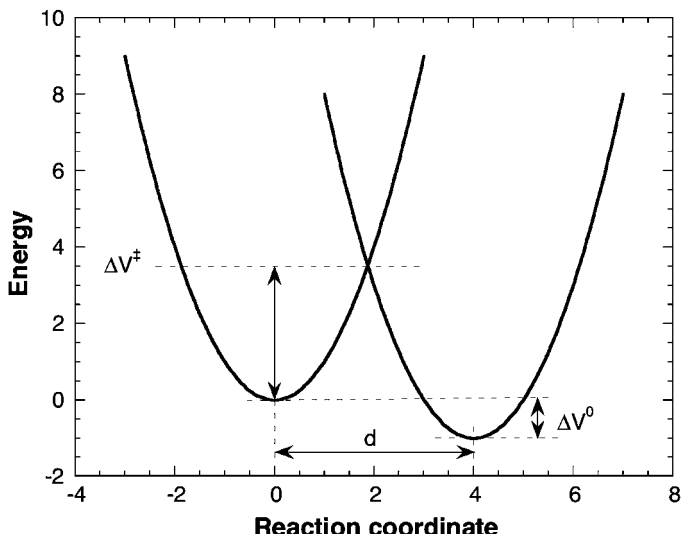


**Figure 6.13** Relationship between the barrier height and the separation between the minima of the potential functions describing the reactant and product fragments along the reaction coordinate.

where  $l_{\text{seq}}$  represents the length of the single bond. This relation is illustrated in Figure 6.14 for CC, NN and OO bonds.

Pauling's equation can be generalised to transition-state configurations, rather than equilibrium ones, using a different scaling

$$\begin{aligned} l_{\text{BC}}^{\ddagger} - l_{\text{BC,eq}} &= -a'(l_{\text{BC,eq}} + l_{\text{AB,eq}}) \ln(n_{\text{BC}}^{\ddagger}) \\ l_{\text{AB}}^{\ddagger} - l_{\text{AB,eq}} &= -a'(l_{\text{BC,eq}} + l_{\text{AB,eq}}) \ln(n_{\text{AB}}^{\ddagger}) \end{aligned} \quad (6.57)$$

where the scaling by  $a'(l_{\text{BC,eq}} + l_{\text{AB,eq}})$  rather than  $a$  is related to the fact that two bonds are involved in the transition state, and that longer bonds will extend more than shorter bonds. The value of the scaling factor  $a'$  will be discussed shortly below, but the generalisation of the Pauling relation allows the method to focus on transition-state bond orders,  $n^{\ddagger}$ , rather than bond extensions.

The calculation of transition-state bond orders is much facilitated by the insightful BEBO method of Johnston and Parr, where the bond order is conserved along the reaction coordinate

$$n_{\text{BC}} + n_{\text{AB}} = 1 \quad (6.58)$$

and defines the reaction coordinate

$$n = n_{\text{AB}} = 1 - n_{\text{BC}} \quad (6.59)$$

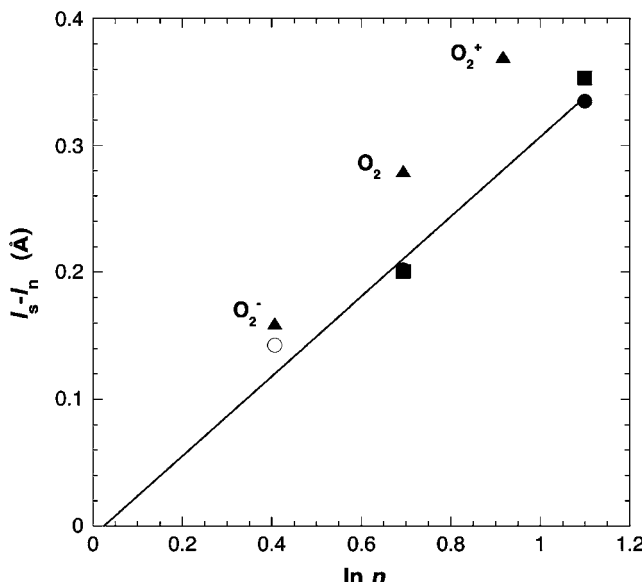


**Figure 6.14** Pauling's relationship between equilibrium bond lengths and bond orders. Circles represent CC bonds and squares represent NN bonds. The  $\text{O}_2$  bond lengths at several oxidation states are relative to  $\text{O}_2^{2-}$  [21]. The open circle represents benzene and was not included in the correlation.

The BEBO method has been quite successful in calculating the activation energies of a large number of atom-transfer reactions, but reveals some difficulties with reactions involving dramatic ZPE differences. For example, it predicts the structure Cl–H–Cl to be a stable molecule rather than a transition state of the Cl + HCl atom exchange. We will not pursue the BEBO method any further, but make use of its definition of the reaction coordinate to express the sum of bond extensions as

$$d = -a' \left( l_{\text{BC,eq}} + l_{\text{AB,eq}} \right) \ln \left[ n^{\ddagger} \left( 1 - n^{\ddagger} \right) \right] \quad (6.60)$$

For a symmetrical reaction, A = C, the transition-state bond order must be  $n^{\ddagger} = 0.5$ , and the bond extensions can be calculated if  $a'$  is known, or vice versa.

### 6.3.1 Activation energies

The simplest method to obtain the scaling factor  $a'$  in eq. (6.60) is purely empirical. Later we will see that the scaling can also be made without using any experimental kinetic information. Representing the energy dependence of the BC and AB bonds on their bond lengths by Morse curves

$$\begin{aligned} V_{\text{BC}} &= D_{\text{e,BC}} \left\{ 1 - \exp \left[ -\beta_{\text{BC}} \left( l_{\text{BC}} - l_{\text{BC,eq}} \right) \right] \right\}^2 \\ V_{\text{AB}} &= D_{\text{e,AB}} \left\{ 1 - \exp \left[ -\beta_{\text{AB}} \left( l_{\text{AB}} - l_{\text{AB,eq}} \right) \right] \right\}^2 + \Delta V^0 \end{aligned} \quad (6.61)$$

where the classical reaction energy is

$$\Delta V^0 = D_{\text{e,BC}} - D_{\text{e,AB}} \quad (6.62)$$

and rewriting the Morse curves to make their relation between bond extension and energy explicit

$$\begin{aligned} l_{\text{BC}} - l_{\text{BC,eq}} &= -\frac{1}{\beta_{\text{BC}}} \ln \left[ 1 - \sqrt{\frac{V_{\text{BC}}}{D_{\text{e,BC}}}} \right] \\ l_{\text{AB}} - l_{\text{AB,eq}} &= -\frac{1}{\beta_{\text{AB}}} \ln \left[ 1 - \sqrt{\frac{(V_{\text{AB}} - \Delta E^0)}{D_{\text{e,AB}}}} \right] \end{aligned} \quad (6.63)$$

we can express  $d$  in terms of the Morse parameters just by recognising that, at the transition state, the energies of BC and AB are identical

$$V_{\text{BC}} \left( l_{\text{BC}}^{\ddagger} \right) = V_{\text{AB}} \left( l_{\text{AB}}^{\ddagger} \right) = \Delta V^{\ddagger} \quad (6.64)$$

which leads to

$$d = -\frac{1}{\beta_{\text{AB}}} \ln \left[ 1 - \sqrt{\frac{(\Delta V^{\ddagger} - \Delta V^0)}{D_{\text{e,AB}}}} \right] - \frac{1}{\beta_{\text{BC}}} \ln \left[ 1 - \sqrt{\frac{\Delta V^{\ddagger}}{D_{\text{e,BC}}}} \right] \quad (6.65)$$

For a symmetrical reaction, the comparison between the equation above and eq. (6.60) yields

$$a' = \frac{\ln \left( 1 - \sqrt{\frac{\Delta V^\ddagger}{D_e}} \right)}{2l_{eq}\beta \ln(0.5)} \quad (6.66)$$

This equation gives the scaling factor for a given barrier and Morse curve parameters of the reactants, which are identical to the products. The choice of the system that will be the reference for the ISM is restricted by the diabatic approximation followed in the derivation of this equation. This approximation does not consider the effect of resonance at the transition state. Thus, it is convenient to use as reference a system where such resonance is expected to be minimal. The obvious choice is the H+H<sub>2</sub> system, in view of its small number of electrons, and relatively high ionisation potentials and low electron affinities of the reactants. Replacing  $\Delta V^\ddagger$  by the experimental  $E_a = 31.8 \text{ kJ mol}^{-1}$ , and using the Morse parameters of the H<sub>2</sub> presented in Appendix III, the above equation gives  $a' = 0.154$ . Historically, the model was scaled to a different set of experimental activation energies and  $a' = 0.156$  was obtained. The difference between these two values is irrelevant. With  $a' = 0.156$  the model gives  $E_a = 32.6 \text{ kJ mol}^{-1}$  for the H+H<sub>2</sub> reaction.

The activation energy calculated with  $a' = 0.156$  accounts for the resonance of the H+H<sub>2</sub> system, but before the ISM can be applied to other systems, it must allow for the difference in resonance between its reference system and those of the others. In this context, resonance is defined as the stabilisation achieved when the electrons can move under the simultaneous influence of more than two nuclei. It is a measure of the electronic delocalisation present in the tri-atomic transition states of the ISM reaction coordinate. The electronic movement is facilitated by low ionisation potentials ( $I_p$ ) and high electron affinities ( $E_A$ ) of the transition-state fragments. In fact, the ionisation potential is defined as the energy necessary to eject an electron from a neutral species and form a mono-positive cation



A low  $I_p$  means a weak attraction between the electron and the nucleus, and makes it easier to share the electron with other nuclei. The electron affinity is defined as the energy necessary to form a mono-negative anion from a neutral species and an electron



A high  $E_A$  corresponds to a more stable anion and a greater ability of the nucleus to interact with an additional electron.

The electron affinity is a measure of the capacity of a molecule or a radical to accept precisely one electron from an electron donor. However, in general, in a transition state we should expect to observe a partial electron delocalisation, rather than a complete electron transfer from A to BC, or from C to AB. The extent to which partial electron transfer contributes to the lowering of the binding energy by maximal flow of electrons, is measured

by the electrophilicity index proposed by Parr

$$m = \frac{-\mu_{el}}{\eta_{el}} = \frac{I_p + E_A}{I_p - E_A} \quad (6.67)$$

which is the ratio between the negative value of the electronic chemical potential,  $\mu_{el} = -(I_p + E_A)/2$ , and the chemical hardness,  $\eta_{el} = (I_p - E_A)/2$ . The electrophilicity index gives the saturation point for electron inflow at the transition state. For very large  $I_p$  or very small  $E_A$ , the electron inflow is negligible and  $m \approx 1$ . This should be the case of the reference system  $H + H_2$ . In contrast,  $m > 1$  reflects an electronic stabilisation of the transition state, much in the same manner as a bond order greater than unity is associated with a stronger bond.

Many other reactivity models have incorporated electronic factors such as the ones mentioned above. A good example is the valence-bond approach to reactivity formulated by Shaik [22], which expresses the barrier height as a fraction of the chemical hardness.

Our confidence that these electronic factors are not just an *ad hoc* scheme to account for the transition-state energy comes from the fact that they are also present in the bond dissociation energies. For example, the bond dissociation energy ( $D_0^{298}$ ) of a C–H bond in  $CH_3NH_2$  is 48 kJ mol<sup>-1</sup> lower than that of  $CH_4$ . Figure 6.15 shows how bond dissociation energies of  $CH_3R$  molecules correlate with the values of  $m$  of the corresponding  $CH_2R$  radicals.

The electrophilicity index of an atom-transfer reaction, mechanism (6.VIII), can be calculated from four different combinations of the ionisation potentials and electron affinities of the atoms or radicals involved in the reaction. Two of them make use of the properties of only one species,  $I_p(A)$  and  $E_A(A)$  or  $I_p(C)$  and  $E_A(C)$ , and the other two involve cross

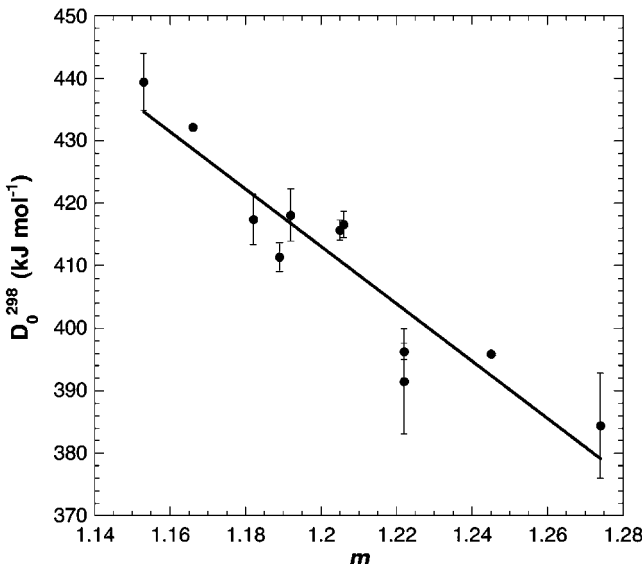


**Figure 6.15** Correlation between the bond dissociation energies of C–H bonds in  $CH_3R$  molecules and the electrophilicity indexes of the corresponding  $CH_2R$  radicals.

terms,  $I_p(A)$  and  $E_A(C)$  or  $I_p(C)$  and  $E_A(A)$ . These latter two cases correspond to charge transfer or polar effects in the transition state. The dominant combination is that which maximises  $m$ , because it produces a greater stabilisation of the transition state. Figure 6.16 illustrates the effect of  $m$  in the stabilisation of the transition-state energy.

With the inclusion of the electrophilicity index, the transition state given by the intersection of the Morse curves in eq. (6.61), can be obtained from

$$\begin{aligned} D_{e,BC} \left\{ 1 - \exp \left[ \frac{a'(l_{AB,eq} + l_{BC,eq})\beta_{BC} \ln(1-n^\ddagger)}{m} \right] \right\}^2 \\ = D_{e,AB} \left\{ 1 - \exp \left[ \frac{a'(l_{AB,eq} + l_{BC,eq})\beta_{AB} \ln(n^\ddagger)}{m} \right] \right\}^2 + \Delta V^0 \quad (6.68) \end{aligned}$$

where the relation between transition-state bond extensions and bond orders, eq. (6.57), has been included. The value of  $n^\ddagger$  that satisfies the above equation must be in the [0,1] interval and is very simple to calculate. All the other parameters involved in the calculations are given by the Morse curves or electronic parameters of the relevant species, and are experimentally accessible for a large number of species. In the special case of a symmetrical reaction, the above expression reduces to

$$\Delta V^\ddagger = D_e \left\{ 1 - \exp \left[ \frac{2a'l_{eq}\beta \ln(0.5)}{m} \right] \right\}^2 \quad (6.69)$$

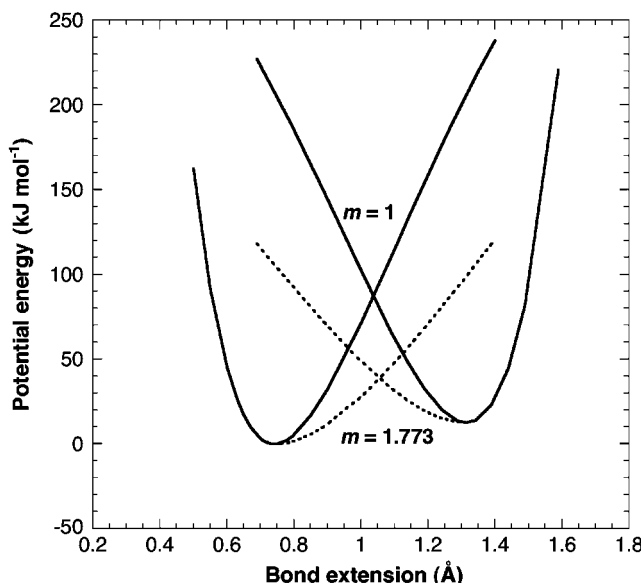


**Figure 6.16** Lowering of the activation owing to an increase in the value of  $m$  at the transition state.

The hydrogen atom-transfer reactions of the type  $R+H_2 \rightarrow RH+H$ , where  $R=H, F, Cl, Br, I, OH, SH, SeH, NH_2, PH_2, AsH_2, CH_3, SiH_3$  and  $GeH_3$ , have been studied in great detail and are an important training set for reactivity models. Table 6.3 compares the activation energies of these reactions with the reaction energy barriers calculated by the ISM using the Morse curve parameters presented in Appendix III and eq. (6.68). The electrophilicity indexes were calculated with the ionisation potentials and electron affinities of Appendix III and eq. (6.67). Given the approximations involved, the agreement between the calculated and the experimental barriers is rather good.

It is very important to define precisely the energy barriers employed in chemical kinetics and explore the relations between them [32]. Figure 6.17 shows the difference, at 0 K, between the purely electronic energy barrier,  $\Delta V^\ddagger$ , defined as the potential energy difference between the classical transition state and the electronic energy of the reactants, and the vibrationally adiabatic barrier,  $\Delta V_{ad}^\ddagger$ , which includes the ZPE difference between the transition state and the reactants. At a given temperature  $T$ , we have to add the thermal energy to the transition state as well as the reactants, using the respective heat capacities, and arrive at the internal energy of activation,  $\Delta U_{T^\ddagger}$ . Furthermore, using the definition of enthalpy,  $H=U+pv$ , a  $\Delta(pv)$  term must be added to the transition state and reactants before we obtain the enthalpy of activation,  $\Delta H^\ddagger$ . For a reaction in the gas phase, assuming ideal gas behaviour,

$$\Delta H^\ddagger = \Delta U^\ddagger + \Delta n_g^\ddagger RT \quad (6.70)$$

where  $\Delta n_g^\ddagger$  is the change in the number of molecules in going from the reactants to the transition state ( $\Delta n_g^\ddagger = -1$  for a bimolecular reaction and  $\Delta n_g^\ddagger = 0$  for a unimolecular reaction).

**Table 6.3**

Calculation of energy barriers by ISM,  $\Delta V^\ddagger$  and experimental activation energies,  $E_a$ , for H-atom transfers in the gas phase

Reaction	ISM		Experimental		Reference
	$m$	$\Delta V^\ddagger$ (kJ mol $^{-1}$ )	$E_a$ (kJ mol $^{-1}$ )	T (K)	
$H+H_2 \rightarrow H_2+H$	1	32.6	31.8	450–750	0 [23]
$H_2+CH_3 \rightarrow H+CH_4$	1	42.7	$46 \pm 2$	300	-5 [24]
$H+SiH_4 \rightarrow H_2+SiH_3$	1.418	8.2	16.0	290–660	-65 [25]
$H+GeH_4 \rightarrow H_2+GeH_3$	1.508	3.2	9.4	210–440	-100 [26]
$H_2+NH_2 \rightarrow H+NH_3$	1.154	32.1	$36 \pm 2$	300	-11 [24]
$H+PH_3 \rightarrow H_2+PH_2$	1.292	6.7	8.7	293–472	-97 [27]
$H+AsH_3 \rightarrow H_2+AsH_2$	1.296	3.7	6.0	294–424	-130 [27]
$H_2+OH \rightarrow H+H_2O$	1.327	8.2	$17 \pm 2$	300	-58 [24]
$H+SH_2 \rightarrow H_2+SH$	1.572	5.7	15	500–1000	-64 [28]
$H_2+F \rightarrow H+HF$	1.679	1.1	$4 \pm 0.4$	300	-132 [24]
$H+HCl \rightarrow H_2+Cl$	1.773	14.4	17.3	298–1190	-13 [29]
$H+HBr \rightarrow H_2+Br$	1.796	2.5	2.6	296–523	-80 [30]
$H+HI \rightarrow H_2+I$	1.828	0.5	2.4	250–373	-150 [31]

*Note:* The reaction energy,  $\Delta E^0$ , contains ZPE corrections for the bond that is broken and the bond that is formed in the course of the reaction.

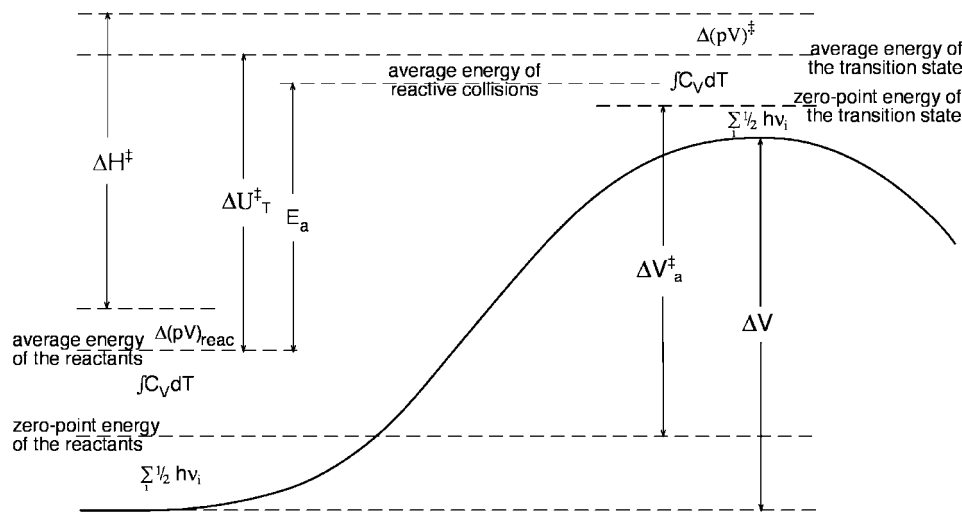


**Figure 6.17** Comparison between the several definitions of the reaction barriers. Tunnelling was not considered, but tends to reduce the observed activation energy.

It should be noted that, given the relation  $d(1/T) = -dT/T^2$ , the activation energy is a phenomenological quantity, defined from [33]

$$\begin{aligned} \frac{d \ln k}{d(1/T)} &= -\frac{E_a}{R} \\ \frac{d \ln k}{dT} &= \frac{E_a}{RT^2} \end{aligned} \quad (6.71)$$

per mole, and does not correspond to any of the barriers defined above. It depends on the range of temperatures experimentally employed. The activation energy in the mid-temperature range is the average total energy (relative translational plus internal energies) of all molecules undergoing reaction minus the average total energy of all the reactant molecules. Additionally, at low temperatures, the tunnel effect is significant and contributes to lower  $E_a$ . This effect is already present in the  $H + H_2$  system and the empirical scaling of the ISM by the activation energy of this system, already accounts for some tunnelling. However, tunnelling is not transferable between different systems and this may contribute to some of the differences between the calculated and experimental barriers in Table 6.3. A more exact estimate of the activation energies must take into account the tunnelling of each system, the ZPE difference between the transition state and reactants, and the heat capacities of the transition state and reactants. This will be addressed later. For the moment, it is interesting to focus on the reactivity patterns revealed by the model.

One of the older reactivity principles relates the activation energy to the reaction enthalpy ( $\Delta H^0$ ). This principle was formulated independently by Bell, and by Evans and Polanyi [34,35]. The Bell–Evans–Polanyi (BEP) relationship is

$$E_a = E_a^0 + \alpha \Delta H^0 \quad (6.72)$$

where  $\alpha$  is constant for a given series of reactions and  $E_a^0$  is the intrinsic barrier, that is, the energy of activation of the reaction of that family for which  $\Delta H^0 = 0$ . If we define a series of reactions as a set of systems with similar modified Morse curves, that is, with similar values for the parameters  $l$ ,  $\beta$  and  $m$ , we may take the  $\text{H} + \text{HCl}$  and  $\text{H} + \text{HBr}$  reactions as examples. Indeed, these reactions obey the BEP relationship: the most exothermic reaction is also that with the lowest activation energy. This reactivity pattern is also present in the ISM: as  $\Delta V^0$  becomes more negative in eq. (6.68), the barrier is lowered.

The definition of similar Morse curves given above includes the parameter  $m$ , and this is why *modified* Morse curves are explicitly mentioned. The reaction series must have a constant value of  $m$ , otherwise large deviations are observed. For example, the reactions  $\text{CH}_3 + \text{H}_2$  and  $\text{H} + \text{HCl}$  have similar reaction energies, but the activation energy of the latter that has the highest  $m$  value is much smaller. The importance of polar or resonance effects has been recognised by other reactivity models, but the ISM integrates this factor in a simple and quantitative manner.

Even when the reaction energies and electrophilicity indexes are similar, the activation energies may be very different. For example, the activation energy of the  $\text{CH}_3 + \text{H}_2$  reaction is 50% higher than that of the  $\text{H} + \text{H}_2$  reaction. Such a difference cannot be related to the reaction energy, because both reactions are nearly isothermal, or to the electronic parameters, because both have  $m \approx 1$ . The only significant difference between the Morse curves of the H–H and C–H bonds is the equilibrium bond length. The C–H bond is 30% longer than the H–H bond. According to eq. (6.69), the ISM predicts that longer bonds lead to higher activation energies. This is also apparent in the calculations presented in Table 6.3. This expectation is corroborated by the activation energy of the  $\text{CH}_3 + \text{CH}_4$  reaction, which is 61 kJ mol<sup>-1</sup> [36].

The activation energies of atom-transfer reactions in the gas phase have been collected and updated in many review articles. At present, the National Institute of Standards and Technology (NIST), maintains a database of the kinetics of such reactions that can be accessed through the site <http://kinetics.nist.gov>. The vast amount of data available can be rationalised using the three reactivity factors underscored by the ISM: the reaction energy  $\Delta E^0$ , the electronic factor  $m$  and the equilibrium bond lengths.

### 6.3.2 Classical rate constants

The most important reactivity observable is the rate constant. The interest in calculating rate constants was already expressed in the development of the collision theory and the TST. Such calculations require a reliable estimate of the reaction barrier, which remains a difficult task for *ab initio* calculations of polyatomic systems. The simplest way to make rate calculations is to use the energy barriers calculated by ISM in eq. (6.54) of the TST. However, in this empirical version of ISM,  $\Delta V^\ddagger$  was obtained from the scaling to the activation energy of a reference system, and differs from the vibrationally adiabatic barrier  $\Delta V_{\text{ad}}^\ddagger$ , used in the TST. An approximate relation between the activation energy and vibrationally adiabatic barrier can be obtained neglecting the tunnel effect and the minor difference between the thermal distribution of the molecules in the transition state and in the

reactants. Deriving the logarithmic form of eq. (6.13) with respect to  $T$  and making it identical to eq. (6.71),

$$\frac{d \ln k}{dT} = \frac{1}{T} + \frac{d \ln K^\ddagger}{dT} = \frac{E_a}{RT^2} \quad (6.73)$$

we obtain, in concentration units,

$$\begin{aligned} E_a &= RT + \Delta U^\ddagger \\ &= RT + \Delta H^\ddagger - p\Delta v^\ddagger \end{aligned} \quad (6.74)$$

where  $\Delta v^\ddagger$  is the difference in volume between the transition state and the reactants.

The heat capacities that distinguish the internal energies from the vibrationally adiabatic energies in Figure 6.17, can be estimated assuming that the temperature is sufficiently high to allow the classical equipartition theorem to accurately calculate the mean translational energies and the mean rotational energies, but sufficiently low to neglect the contribution of the vibrational partition function to the internal energy. For a reaction between an atom and a diatomic molecule going through a linear tri-atomic transition state, such as that of mechanism (6.VIII), the equipartition theorem gives  $C_v^\ddagger = (3/2+1)R$  for the translational and rotational contributions to the transition state, and  $C_v^{A+BC} = (3/2+3/2+1)R$  for the same modes, but for the reactants. Therefore, we have  $\Delta C_v = -3/2R$  and eq. (6.74), becomes

$$\begin{aligned} \Delta V^\ddagger &= RT + \Delta V_{ad}^\ddagger - \frac{3}{2}RT \\ &= \Delta V_{ad}^\ddagger - \frac{1}{2}RT \end{aligned} \quad (6.75)$$

We explicitly use  $\Delta V^\ddagger$  rather than  $E_a$  in the expression above, to emphasise that it was obtained using the ISM approximations for a gas-phase A+BC reaction with a linear tri-atomic transition state, in molar concentration units. Under these approximations, and remembering that the ratio of the vibrational partition functions was assumed to be unity, we obtain a compact expression for the classical transition-state rate constants, eq. (6.33),

$$k_c = \sigma \frac{6.82 \times 10^{10}}{\sqrt{T}} \left( \frac{m_A + m_B + m_C}{m_A(m_B + m_C)} \right)^{3/2} \frac{I_{ABC}}{I_{BC}} \exp\left(-\frac{\Delta V^\ddagger}{RT} - \frac{1}{2}\right) \text{dm}^3 \text{mol}^{-1} \text{sec}^{-1} \quad (6.76)$$

for bimolecular reactions in the gas phase, where the constant is obtained when the atomic masses are expressed in amu and the moments of inertia are

$$I_{ABC} = m_A (l_{AB}^\ddagger)^2 + m_C (l_{BC}^\ddagger)^2 - \frac{(m_A l_{AB}^\ddagger - m_C l_{BC}^\ddagger)^2}{m_A + m_B + m_C} \quad (6.77)$$

and

$$I_{BC} = \frac{m_B m_C}{m_B + m_C} (l_{BC,eq})^2 \quad (6.78)$$

The transition-state moment of inertia can only be calculated with the transition-state bond lengths. This is not a problem because the transition-state bond order,  $n^\ddagger$ , obtained with eq. (6.68), can be employed in eq. (6.57) to yield the transition-state bond extensions. In summary, classical rate constants can be calculated with eqs. (6.57), (6.68), (6.76), (6.77) and (6.78), that only require bond dissociation energies, vibrational frequencies and bond lengths of the reactive bonds, ionization energies and electron affinities of the relevant radicals, and the masses of the atoms involved in the reaction coordinate. A few examples can make these calculations more clear.

The  $\text{H} + \text{H}_2$  atom exchange is symmetrical, thus it is necessary to have  $n^\ddagger = 0.5$ , and we can make use of eq. (6.69), with the appropriate Morse curve parameters on Appendix III, to calculate  $\Delta V^\ddagger = 32.6 \text{ kJ mol}^{-1}$ . With  $n^\ddagger = 0.5$ , eq. (6.57) gives  $I_{\text{HH}}^\ddagger = 0.901 \text{ \AA}$ , and the ratio of the moments of inertia is 5.91. Using these data and  $\sigma=2$  in eq. (6.76), we obtain  $k_c = 5.8 \times 10^6 \text{ dm}^3 \text{ mol}^{-1} \text{ sec}^{-1}$  at 440 K, indistinguishable from the experimental rate of  $5.7 \times 10^6 \text{ dm}^3 \text{ mol}^{-1} \text{ sec}^{-1}$  at this temperature [37,38]. This excellent agreement is biased by the fact that the ISM was scaled by the activation energy of this system, and results from a compensation of factors because a tunnelling correction of 3.0 was previously calculated for this reaction. The scaling by the experimental activation energy is the cause for the empiricism of this version of the ISM. We will see later how that empiricism can be removed. Nevertheless, the empirical ISM may be very useful if it gives accurate rates for other systems.

The  $\text{F} + \text{H}_2$  atom transfer is very asymmetrical and has a large electrophilicity index,  $m = 1.679$ . The solution of eq. (6.68) yields  $n^\ddagger = 0.152$  and  $\Delta V^\ddagger = 1.0 \text{ kJ mol}^{-1}$ , and then eq. (6.57) gives  $I_{\text{HF}}^\ddagger = 0.784 \text{ \AA}$  and  $I_{\text{H}}^\ddagger = 1.404 \text{ \AA}$ . The ratio of the moments of inertia is 22.4 and with  $\sigma=2$ , eq. (6.76) gives  $k_c = 2.9 \times 10^{10} \text{ dm}^3 \text{ mol}^{-1} \text{ sec}^{-1}$  at 300 K. The experimental rate is  $1.5 \times 10^{10} \text{ dm}^3 \text{ mol}^{-1} \text{ sec}^{-1}$  at this temperature [39]. The agreement is excellent because a small barrier is expected to have a small tunnelling correction.

The ISM can also be applied to polyatomic systems, but now the partition function ratio of eq. (6.33) does not simplify into the pre-exponential factor of eq. (6.76). For linear transition states, the ratio of the partition functions for atom+diatomic and atom+polyatomic molecule has the same form

$$\frac{Q^\ddagger}{Q_A Q_{BC}} = \left( \frac{q_v}{q_t} \right)^2 P \quad (6.79)$$

where  $P = (Q_{\text{rot}})^2 / (Q_{\text{trans}})^3$  and  $Q_{\text{trans}}$ ,  $Q_{\text{vib}}$  and  $Q_{\text{rot}}$  are the translational, vibrational and rotational partition functions. The electronic partition functions are equal to the degeneracy of the ground state and are not explicitly considered in this comparison. This formulation gives pre-exponential factors of the order of magnitude of  $10^{10} \text{ mol}^{-1} \text{ dm}^{-3} \text{ sec}^{-1}$  for atom+diatomic and atom+polyatomic molecule systems, in good agreement with the experimental pre-exponential factors. Atom transfers resulting from the attack of diatomic radicals to polyatomic molecules have partition-function ratios of the type  $(1/\theta)^4 P$ , where  $\theta = Q_{\text{rot}}/Q_{\text{vib}}$ , and those involving polyatomic radicals and molecules are of the type  $(1/\theta)^5 P$ . Typical values are  $1 \leq Q_{\text{vib}} \leq 10$  and  $10 \leq Q_{\text{rot}} \leq 100$ , and  $\theta$  may be anywhere from 1 to 100. However, some of the vibrations in polyatomic transition states are very loose vibrations and sometimes even regarded as hindered rotations. Thus,  $\theta$  should be rather close to the

lower limit. Assuming that the value of the rotational partition function is three times that of the vibrational one, we expect that the pre-exponential factor of diatomic + polyatomic systems should be slightly larger than  $10^9$  and that of polyatomic + polyatomic systems should be close to  $5 \times 10^8 \text{ mol}^{-1} \text{ dm}^{-3} \text{ sec}^{-1}$ . Thus, the pre-exponential factors of atom + polyatomic, diatomic + polyatomic and polyatomic + polyatomic systems can be estimated dividing the value obtained for tri-atomic transition states by the factors 1, 9 and 27, respectively, and eq. (6.76) can be generalised to include such systems,

$$k_c = \frac{\sigma}{\theta^j} \frac{6.82 \times 10^{10}}{\sqrt{T}} \left( \frac{m_A + m_B + m_C}{m_A (m_B + m_C)} \right)^{3/2} \frac{I_{ABC}}{I_{BC}} \exp \left( -\frac{\Delta V^\ddagger}{RT} - \frac{1}{2} \right) \text{ dm}^3 \text{ mol}^{-1} \text{ sec}^{-1} \quad (6.80)$$

where  $\theta = 3$ , BC is a polyatomic molecule, and  $j = 0, 2$  or  $3$  when A is an atom, a diatomic radical or a polyatomic radical, respectively.

Using this new approximation we can also use the ISM to calculate the rates of more complex systems, such as the  $\text{CH}_3 + \text{H}_2$  hydrogen atom abstraction. For this system,  $m \approx 1$  and the solution of eq. (6.68) with  $\Delta E^0 = -5 \text{ kJ mol}^{-1}$ , yields  $n^\ddagger = 0.487$  and  $\Delta V^\ddagger = 43.6 \text{ kJ mol}^{-1}$ , and then eq. (6.57) gives  $I_{\text{HH}}^\ddagger = 0.932 \text{ \AA}$  and  $I_{\text{CH}}^\ddagger = 1.292 \text{ \AA}$ . The ratio of the moments of inertia is 20.9,  $\sigma = 2$ ,  $\theta^j = 9$  and eq. (6.80) give  $k_c = 4.8 \times 10^2 \text{ dm}^3 \text{ mol}^{-1} \text{ sec}^{-1}$  at 372 K. The experimental rate is  $2.7 \times 10^2 \text{ dm}^3 \text{ mol}^{-1} \text{ sec}^{-1}$  at this temperature [40], a very good agreement for such a simple method.

Figure 6.18 shows the temperature dependence of the  $\text{H}+\text{H}_2$ ,  $\text{F}+\text{H}_2$  and  $\text{CH}_3+\text{H}_2$  hydrogen abstraction rates. The classical rates tend to underestimate the lower temperature experimental rates, but the general trends are reproduced very well. The empirical ISM has an interesting pedagogical value in chemical kinetics because it makes the calculation of classical atom-transfer rate constants possible with a pocket calculator and provides basic information on the reactants and products.

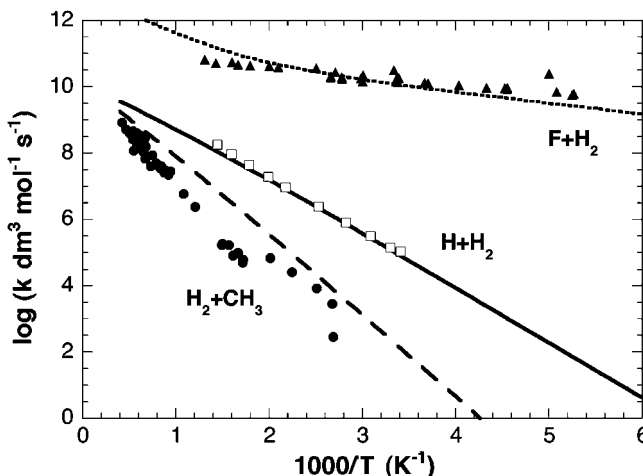


**Figure 6.18** Temperature dependence of the  $\text{H}+\text{H}_2$ ,  $\text{F}+\text{H}_2$  and  $\text{CH}_3+\text{H}_2$  hydrogen abstraction rates, and their comparison with the classical ISM rates.

Although appealing for their simplicity, these classical calculations have two limitations: they cannot explain KIEs and do not include tunnelling corrections. These limitations have been overcome in a more sophisticated formulation, as will be seen below, which additionally removes the empirical scaling of this model to the activation energy of the H + H<sub>2</sub> reaction.

### 6.3.3 Absolute semi-classical rates

The empiricism of the ISM is eliminated using *ab initio* data, rather than experimental data, to obtain the value of  $d$ . The most exact *ab initio* calculations on reactive systems are those of the H + H<sub>2</sub> system. Varandas and co-workers [41] used such *ab initio* calculations to build a DMBE PES, which has the properties presented in Table 1. The *ab initio* sum of bond extensions at the transition state of this surface is  $d = 0.3746 \text{ \AA}$ , and eq. (6.60) with  $n^{\ddagger} = 0.5$  leads to  $a'_{\text{sc}} = 0.182$ . The ISM is now scaled to structural data and does not involve kinetic information. On the other hand, the model now gives classical (electronic) potential energy barriers, free of ZPE or tunnelling corrections, rather than activation energies. They are directly comparable with the classical barriers of *ab initio* calculations, but require a method to calculate ZPE corrections along all the reaction coordinates before they can be employed in the TST to calculate tunnelling corrections and semi-classical rate constants.

The need for an analytical description of the complete reaction coordinate can be satisfied with an interpolation between the energies of the reactants and products, using the continuity of the reaction coordinate  $n$ , following earlier work by Agmon and Levine [42],

$$\begin{aligned} V_{\text{cl}}(n) &= (1-n)V_{\text{BC}}(n) + nV_{\text{AB}}(n) + n\Delta V^0 \\ &= (1-n)D_{\text{e,BC}} \left\{ 1 - \exp \left[ \gamma_{\text{BC}} \ln(1-n) \right] \right\}^2 + nD_{\text{e,AB}} \left\{ 1 - \exp \left[ \gamma_{\text{AB}} \ln(n) \right] \right\}^2 + n\Delta V^0 \\ \gamma_{\text{BC}} &= \frac{a'_{\text{sc}} (l_{\text{BC,eq}} + l_{\text{AB,eq}}) \beta_{\text{BC}}}{m} \\ \gamma_{\text{AB}} &= \frac{a'_{\text{sc}} (l_{\text{BC,eq}} + l_{\text{AB,eq}}) \beta_{\text{AB}}}{m} \end{aligned} \quad (6.81)$$

Equating the first derivative of the classical reaction path, above, to zero gives the location of the classical transition state

$$\begin{aligned} \frac{\partial V_{\text{cl}}(n)}{\partial n} &= -D_{\text{e,BC}} \left[ 1 - \left( 1 - n^{\ddagger} \right)^{\gamma_{\text{BC}}} \right] \left[ 1 - \left( 1 + 2\gamma_{\text{BC}} \right) \left( 1 - n^{\ddagger} \right)^{\gamma_{\text{BC}}} \right] \\ &\quad + D_{\text{e,AB}} \left[ 1 - \left( n^{\ddagger} \right)^{\gamma_{\text{AB}}} \right] \left[ 1 - \left( 1 + 2\gamma_{\text{AB}} \right) \left( n^{\ddagger} \right)^{\gamma_{\text{AB}}} \right] + \Delta V^0 = 0 \end{aligned} \quad (6.82)$$

and eq. (6.81) gives the corresponding classical energy.

Using the parameters of the H<sub>2</sub> Morse curve presented in Appendix III, and knowing that a symmetrical reaction has  $n^{\ddagger} = 0.5$ , we calculate  $\Delta V_{\text{cl}}^{\ddagger} = 42.3 \text{ kJ mol}^{-1}$  for the H + H<sub>2</sub> reaction. The classical reaction barrier for this reaction is 40.4 kJ mol<sup>-1</sup> according to the DMBE PES, Table 6.1, and 41.5 kJ mol<sup>-1</sup> according to the most exact *ab initio* calculations presently available. Table 6.4 presents the classical potential energy barriers calculated with the semi-classical ISM (scISM) and compares them with the classical barriers obtained by the *ab initio* methods. The agreement is quite satisfactory for such simple calculations without adjustable parameters.

The full reaction path given by eq. (6.81) can also be compared with the MEP of the DMBE PES, Figure 6.10, using the distance along the reaction coordinate defined as

$$\begin{aligned} s &= -\sqrt{\left[l_{\text{BC}}(n) - l_{\text{BC}}^{\ddagger}\right]^2 + \left[l_{\text{AB}}(n) - l_{\text{AB}}^{\ddagger}\right]^2}, \quad l_{\text{BC}}(n) \leq l_{\text{BC}}^{\ddagger} \\ s &= +\sqrt{\left[l_{\text{BC}}(n) - l_{\text{BC}}^{\ddagger}\right]^2 + \left[l_{\text{AB}}(n) - l_{\text{AB}}^{\ddagger}\right]^2}, \quad l_{\text{BC}}(n) > l_{\text{BC}}^{\ddagger} \end{aligned} \quad (6.83)$$

The similarity of scISM and DMBE reaction paths suggests that their tunnelling corrections should be similar. The simplest realistic tunnelling correction is that of the Eckart barrier. This barrier can be fitted to the scISM reaction path using its asymptotic limits, the barrier height  $\Delta V_{\text{cl}}^{\ddagger}$  and the curvature of this path at the classical transition state. This latter

**Table 6.4**

Classical potential energy barriers calculated by *ab initio* methods ( $V^{\ddagger}$ ) and by ISM ( $\Delta V_{\text{cl}}^{\ddagger}$ ) [17]

Reaction	Quantum mechanics		scISM	
	$V^{\ddagger} (\text{kJ mol}^{-1})$	$m$		$\Delta V_{\text{cl}}^{\ddagger} (\text{kJ mol}^{-1})$
H+H <sub>2</sub> →H <sub>2</sub> +H	41.5	1		42.3
CH <sub>3</sub> +CH <sub>4</sub> →CH <sub>4</sub> +CH <sub>3</sub>	72.4	1		74.6
C <sub>2</sub> H <sub>5</sub> +C <sub>2</sub> H <sub>6</sub> →C <sub>2</sub> H <sub>6</sub> +C <sub>2</sub> H <sub>5</sub>	64.9	1		76.4
H+CH <sub>4</sub> →H <sub>2</sub> +CH <sub>3</sub>	61.0	1		55.7
O+CH <sub>4</sub> →OH+CH <sub>3</sub>	55.6	1.349		50.0
Cl+CH <sub>4</sub> →HCl+CH <sub>3</sub>	28.9	2.161		28.4
NH <sub>2</sub> +H <sub>2</sub> →NH <sub>3</sub> +H	39.8	1.154		44.2
H+HCl→H <sub>2</sub> +Cl	21.0	1.773		21.7
OH+H <sub>2</sub> →H <sub>2</sub> O+H	23.5	1.327		25.1
H+SH <sub>2</sub> →H <sub>2</sub> +SH	15.1	1.572		15.6
H+SiH <sub>4</sub> →H <sub>2</sub> +SiH <sub>3</sub>	23.2	1.418		21.5
CH <sub>3</sub> +HBr→CH <sub>4</sub> +Br	4.9	2.038		11.0
H+HBr→H <sub>2</sub> +Br	7.9	1.796		10.5
H <sub>2</sub> +CN→H+HCN	15.1	1.793		9.2
H+PH <sub>3</sub> →H <sub>2</sub> +PH <sub>2</sub>	15.1	1.292		18.8
H+GeH <sub>4</sub> →H <sub>2</sub> +GeH <sub>3</sub>	14.8	1.508		14.0
H <sub>2</sub> +CCH→H+HCCH	18.3	1.687		8.6
H <sub>2</sub> +F→H+HF	6.1	1.679		9.2
H+Cl <sub>2</sub> →HCl+Cl	9.4	1.773		7.1
H+F <sub>2</sub> →HF+F	7.5	1.679		0.9

parameter can be obtained from the curvature of the scISM reaction path by making the second derivative of eq. (6.81),

$$\begin{aligned} \frac{d^2V_{\text{cl}}(n)}{dn^2} = & 2\gamma_{\text{BC}} D_{\text{BC}} \left(1 - n^{\ddagger}\right)^{\gamma_{\text{BC}}-1} \left[ (2\gamma_{\text{BC}} + 1) \left(1 - n^{\ddagger}\right)^{\gamma_{\text{BC}}} - \gamma_{\text{BC}} - 1 \right] \\ & + 2\gamma_{\text{AB}} D_{\text{AB}} \left(n^{\ddagger}\right)^{\gamma_{\text{AB}}-1} \left[ (2\gamma_{\text{AB}} + 1) \left(n^{\ddagger}\right)^{\gamma_{\text{AB}}} - \gamma_{\text{AB}} - 1 \right] \end{aligned} \quad (6.84)$$

and multiplying it by  $(dn/ds)^2$ , where

$$\left(\frac{ds}{dn}\right)^2 = \left[\frac{a'_{\text{sc}} (l_{\text{BC}} + l_{\text{AB}})}{m}\right]^2 \left[ \frac{1}{\left(1 - n^{\ddagger}\right)^2} + \frac{1}{\left(n^{\ddagger}\right)^2} \right] \quad (6.85)$$

The curvature of the scISM reaction path at the transition state

$$f^* = \left(\frac{d^2V}{dn^2}\right) \left(\frac{dn}{ds}\right)^2 \quad (6.86)$$

gives the imaginary frequency of the transition state

$$\nu_{\text{asym}} = \frac{1}{2\pi c} \sqrt{\frac{f^*}{\mu}} \quad (6.87)$$

where  $\mu$  is the reduced mass of the anti-symmetric stretch. For a symmetric transition state,  $A = C$ ,  $\mu$  is given by eq. (6.53). Figure 6.10 also shows the Eckart barrier fitted to the scISM reaction path, which is particularly simple for calculating tunnelling corrections.

Unfortunately, the tunnelling correction involves an integral, eq. (6.52), and can only be evaluated numerically. Additionally, the transition rate expression for rate constant, eq. (6.54), requires vibrationally adiabatic barriers, and ZPEs have to be added along the classical reaction path of the ISM.

$$V_{\text{ad}}(n) = V_{\text{cl}}(n) + Z(n) \quad (6.88)$$

where  $Z(n)$  represents the ZPEs along the vibrationally adiabatic path. The procedure for the calculation of  $Z(n)$  is given in Appendix IV and can only be done efficiently using computational methods. The vibrationally adiabatic barrier is the difference between the maximum of eq. (6.88), and the ZPE of the reactants,  $Z_{\text{BC}}$ ,

$$\Delta V_{\text{ad}}^{\ddagger} = V_{\text{ad}}\left(n^{\ddagger}\right) - Z_{\text{BC}} \quad (6.89)$$

Thus, scISM rate constants, given by the procedure described above, are not as easily accessible as their classical counterparts. In contrast, the tunnelling corrections now extend the accuracy of the calculated rates to lower temperatures, and, with the ZPE corrections, provide reasonable estimates of the KIEs. Figure 6.19 illustrates the results obtained for the H+H<sub>2</sub> and H+D<sub>2</sub> systems with the ZPE corrections described in Appendix IV and the tunnelling corrections of an Eckart barrier fitted to the classical path. This figure also presents

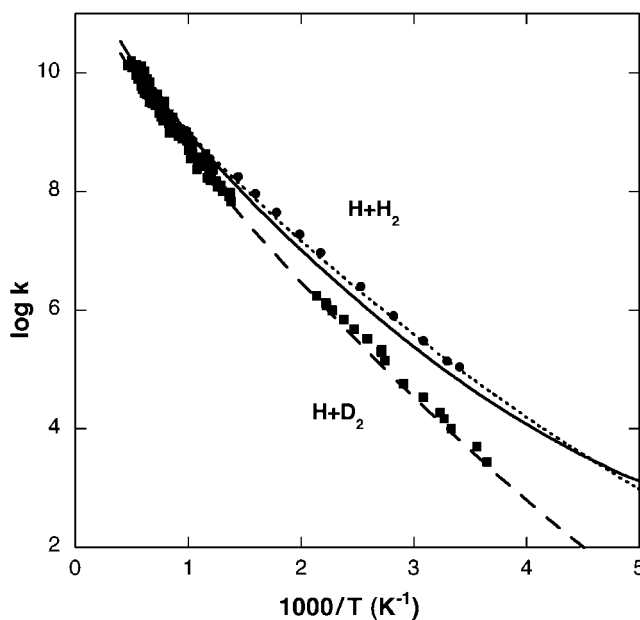


**Figure 6.19** Comparison between the rate constants of the reactions  $\text{H}+\text{H}_2$  and  $\text{H}+\text{D}_2$ , in units of  $\text{mol}^{-1} \text{dm}^{-3} \text{ sec}^{-1}$ , calculated by the scISM with Eckart-barrier tunnelling corrections and by the VTST with least-action tunnelling corrections (dotted lines) with the experimental rates.

the VTST calculations with the DMBE PES and least-action tunnelling corrections, which are presumably the most exact rate calculations within the framework of the TST. More exact calculation using scISM are freely available through the Internet at <http://www.ism.que.pt:8180/ism/>.

#### 6.3.4 Relative rates

An increasing degree of sophistication has taken us to the most exact absolute rate calculations for the simplest reactive system. In chemical kinetics it is often more interesting to relate a given rate constant to others of similar systems, rather than to make a very accurate absolute rate calculation. Such a relation emphasises the factor that dominates the reactivity of a family of reactions, and is particularly useful if the activation energies are expressed as a simple function of that factor. In Section 6.3.1 it was shown that the activation energies of gas-phase atom transfers strongly depend on the reaction energy  $\Delta E^0$ , the electronic factor  $m$ , and the sum of equilibrium bond lengths ( $l_{\text{BC,eq}} + l_{\text{AB,eq}}$ ). In the intuitive concept of a “family of reactions” the equilibrium bond lengths of the reactive bonds do not change appreciably, and the first two parameters should control the reactivity. Thus, it is convenient to express the ISM reaction coordinate explicitly as a function of the thermodynamic parameter

$$G(n) = [-(1-n)\ln(1-n) - n\ln(n)]\Omega + n\Delta G^0 \quad (6.90)$$

where free energies are employed for greater generality and the parameter  $\Omega$  ensures the equivalence between this reaction coordinate and that employed before. It has units of energy and behaves as an intrinsic barrier, that is, the barrier of the symmetric reaction ( $\Delta G^0 = 0$ ,  $n^\ddagger = 0.5$ ) in the family of reactions. This equivalence determines that, for the symmetric reaction,

$$\Omega = \frac{\Delta G^\ddagger}{\ln(2)} \quad (6.91)$$

When the reactants and products are described by Morse curves, the value of  $\Omega$  can be obtained from eq. (6.69). For simplicity, in this section we employ harmonic oscillators, and the barrier is, by analogy with eq. (6.68)

$$\begin{aligned} \Delta G^\ddagger &= \frac{1}{2} f_{BC} \left[ \frac{a' (l_{BC,eq} + l_{AB,eq}) \ln(1 - n^\ddagger)}{m} \right]^2 \\ &= \frac{1}{2} f_{AB} \left[ \frac{a' (l_{BC,eq} + l_{AB,eq}) \ln(n^\ddagger)}{m} \right]^2 + \Delta G^0 \end{aligned} \quad (6.92)$$

Hence, for symmetrical harmonic oscillators,

$$\Omega_0 = 2f_{BC} \left( \frac{a' \ln(2) l_{BC}}{m} \right)^2 \quad (6.93)$$

The location of the transition state for asymmetric reactions is given by the first derivative of eq. (6.90),

$$\frac{\partial G(n)}{\partial n} = \Delta G^0 - \Omega \ln \left( \frac{n^\ddagger}{1 - n^\ddagger} \right) = 0 \quad (6.94)$$

that gives

$$n^\ddagger = \left[ 1 + \exp \left( -\frac{\Delta G^0}{\Omega} \right) \right]^{-1} \quad (6.95)$$

The functional dependence of these parameters can be further simplified using eq. (6.95) together with eqs. (6.57) and (6.59),

$$\begin{aligned} l_{AB}^\ddagger - l_{AB,eq} &= a' (l_{AB,eq} + l_{BC,eq}) \ln \left[ 1 + \exp \left( -\frac{\Delta G^0}{\Omega} \right) \right] \\ l_{BC}^\ddagger - l_{BC,eq} &= -a' (l_{AB,eq} + l_{BC,eq}) \ln \left\{ 1 - \left[ 1 + \exp \left( -\frac{\Delta G^0}{\Omega} \right) \right]^{-1} \right\} \end{aligned} \quad (6.96)$$

to express the sum of bond extensions as

$$d = a' \left( l_{\text{AB,eq}} + l_{\text{BC,eq}} \right) \ln \frac{\left[ 1 + \exp\left(-\Delta G^0 / \Omega\right) \right]}{\left\{ 1 - \left[ 1 + \exp\left(-\Delta G^0 / \Omega\right) \right]^{-1} \right\}} \quad (6.97)$$

that gives, after a Taylor series expansion

$$d = d(0) + \left( \frac{\partial d}{\partial \Delta G^0} \right)_0 \Delta G^0 + \frac{1}{2} \left( \frac{\partial^2 d}{\partial (\Delta G^0)^2} \right) (\Delta G^0)^2 + \dots \quad (6.98)$$

where

$$d(0) = 2a' \left( l_{\text{BC,eq}} + l_{\text{AB,eq}} \right) \ln 2; \quad \frac{\partial d}{\partial \Delta G^0} = 0, \quad \frac{\partial^2 d}{\partial (\Delta G^0)^2} = \frac{a' \left( l_{\text{BC,eq}} + l_{\text{AB,eq}} \right)}{\Omega^2} \quad (6.99)$$

The first three terms of the expansion give

$$d = 2a' \left( l_{\text{BC,eq}} + l_{\text{AB,eq}} \right) \left[ \ln(2) + \left( \frac{\Delta G^0}{2\Omega} \right)^2 \right] \quad (6.100)$$

The simplest way to use this expression is to use the relation expressed by eq. (6.92), and represented in Figure 6.20, to obtain

$$\left( l^* - l_{\text{BC,eq}} \right) = \frac{-f_{\text{AB}} d + \sqrt{f_{\text{AB}}^2 d^2 + (f_{\text{BC}} - f_{\text{AB}})(f_{\text{AB}} d^2 + 2\Delta G^0)}}{(f_{\text{BC}} - f_{\text{AB}})} \quad (6.101)$$

and calculate the free energy of activation from

$$\Delta G^* = \frac{1}{2} f_{\text{BC}} \left[ \frac{l^* - l_{\text{BC,eq}}}{m} \right]^2 \quad (6.102)$$

In earlier empirical applications of the ISM, a different nomenclature was employed, which is related to the present parameters via

$$\begin{aligned} \Lambda &= \Omega \sqrt{m} \\ n^* &= \frac{m}{2} \end{aligned} \quad (6.103)$$

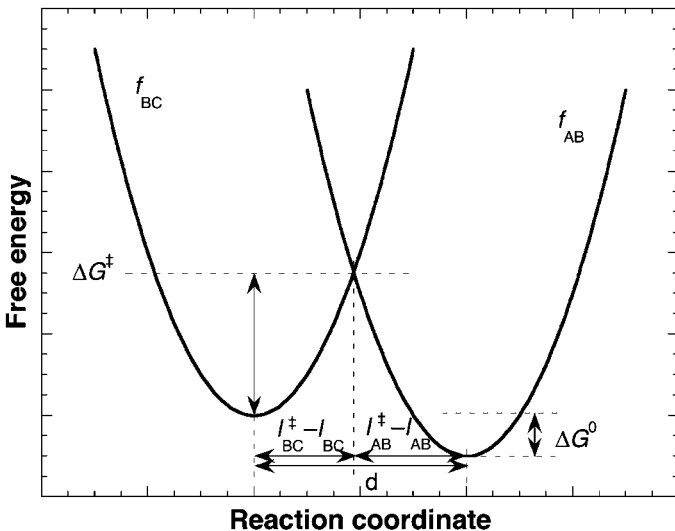


**Figure 6.20** Representation of the reaction coordinate of the Intersecting-State Model using harmonic oscillators for reactant and product bonds.

and eqs. (6.100)–(6.102), respectively, become

$$d_n = \frac{a'(l_{BC,eq} + l_{AB,eq})}{n^{\ddagger}} \left[ \ln(2) + \frac{n^{\ddagger}}{2} \left( \frac{\Delta G^0}{\Lambda} \right)^2 \right] \quad (6.104)$$

$$d_r = \frac{-f_{AB} d_n + \sqrt{f_{AB}^2 d_n^2 + (f_{BC} - f_{AB})(f_{AB} d_n^2 + 2\Delta G^0)}}{(f_{BC} - f_{AB})} \quad (6.105)$$

$$\Delta G^{\ddagger} = \frac{1}{2} f_{BC} d_r^2 \quad (6.106)$$

Both sets of eqs. (6.100)–(6.102) and (6.104)–(6.106) give the same activation free energy, but through a different reactant bond extension,  $d_r = (l^{\ddagger} - l_{BC,eq})/m$ . In principle, for reactions in solution,  $\Omega$  can be estimated from eq. (6.93),  $m$  from eq. (6.67) and the rate constant from eq. (6.14). In practice,  $\Omega$  may differ from  $\Omega_0$ , the solvent may modulate the value of  $m$  and the harmonic approximation tends to overestimate the barrier. As a result, it is better practice to use the set of eqs. (6.104)–(6.106) with  $n^{\ddagger}$  and  $\Lambda$  as the empirical parameters. In this case, such parameters characterise the electronic and thermodynamic dependences of a family of reactions. The parameter  $n^{\ddagger}$  is associated with an increased transition-state bond order, because the electronic stabilisation of a bond can be seen as an increase in its bond order. The parameter  $\Lambda$  is called a “dynamic parameter” because it is related to the dissipation of the reaction energy. This version of the ISM is not employed to analyse a reaction rate *per se*, but it rationalises structure–reactivity and energy–reactivity relationships. As a result, some order emerges from the large amounts of data on chemical reactivity and the relations between reactivity models become clearer.

## REFERENCES

- [1] H Eyring, *J. Chem. Phys.* **2** (1935) 107.
- [2] Editorial Comment, *New J. Chem.* **14** (1990) 257.
- [3] KJ Laidler, MC King, *J. Phys. Chem.* **87** (1983) 2657.
- [4] S Glasstone, KJ Laidler, H Eyring, *The Theory of Rate Processes*, McGraw-Hill, New York, 1941.
- [5] BC Garrett, DG Truhlar, AJC Varandas, NC Blais, *Int. J. Chem. Kin.* **18** (1986) 1065.
- [6] C Lim, DG Truhlar, *J. Phys. Chem.* **89** (1985) 5.
- [7] BC Garrett, DG Truhlar, *J. Phys. Chem.* **83** (1979) 1052.
- [8] DG Truhlar, BC Garrett, *Acc. Chem. Res.* **13** (1980) 440.
- [9] FH Westheimer, *Chem. Rev.* **61** (1961) 265.
- [10] M Arndt, O Nairz, J Vos-Andreae, C Keller, G van der Zouw, A Zeilinger, *Nature* **401** (1999) 680.
- [11] L Brillouin, *J. de Physique* **7** (1926) 353.
- [12] G Wentzel, *Z. Phys.* **38** (1926) 518.
- [13] HA Kramers, *Z. Phys.* **39** (1926) 828.
- [14] C Eckart, *Phys. Rev.* **35** (1930) 1303.
- [15] RA Marcus, ME Coltrin, *J. Chem. Phys.* **67** (1977) 2609.
- [16] AJC Varandas, SJ Formosinho, *J. Chem. Soc., Farad. Trans. 2* **82** (1986) 953.
- [17] LG Arnaut, AAC Pais, SJ Formosinho, M Barroso, *J. Am. Chem. Soc.* **125** (2003) 5236.
- [18] MG Evans, M Polanyi, *Trans. Farad Soc.* **34** (1938) 11.
- [19] HS Johnston, C Parr, *J. Am. Chem. Soc.* **85** (1963) 2544.
- [20] L Pauling, *J. Am. Chem. Soc.* **69** (1947) 542.
- [21] L Vaska, *Acc. Chem. Res.* **9** (1976) 175.
- [22] A Pross, S Shaik, *Acc. Chem. Res.* **16** (1983) 363.
- [23] JA Kerr, in CH Bamford, CFH Tipper (Eds.), *Selected Elementary Reactions*, Elsevier, Amsterdam, 1975, pp. 99–109.
- [24] E Kraka, J Gauss, D Cremer, *J. Chem. Phys.* **99** (1993) 5306.
- [25] A Goumri, W-J Yuan, L Ding, Y Shi, P Marshall, *Chem. Phys.* **177** (1993) 233.
- [26] DF Nava, WA Payne, G Marston, LJ Stief, *J. Geophys. Res.* **98** (1993) 5531.
- [27] NL Arthur, IA Cooper, *J. Chem. Soc., Farad Trans.* **93** (1997) 521.
- [28] M Yoshimura, M Koshi, H Matsui, K Kamiya, H Umeyama, *Chem. Phys. Lett.* **189** (1992) 199.
- [29] GY Adusei, A Fontijn, *J. Phys. Chem.* **97** (1993) 1409.
- [30] PW Seakins, MJ Pilling, *J. Phys. Chem.* **95** (1991) 9878.
- [31] K Lorenz, HG Wagner, R Zellner, *Ber. Bunsenges. Phys. Chem.* **83** (1979) 556.
- [32] PD Pacey, *J. Chem. Educ.* **58** (1981) 612.
- [33] DG Truhlar, *J. Chem. Educ.* **55** (1978) 309.
- [34] RP Bell, *Proc. R. Soc. London A* **154** (1936) 414.
- [35] MG Evans, M Polanyi, *Trans. Faraday Soc.* **32** (1936) 1333.
- [36] LG Arnaut, AAC Pais, SJ Formosinho, *J. Mol. Struct.* **563/564** (2001) 1.
- [37] KA Quickert, DJ Le Roy, *J. Chem. Phys.* **53** (1970) 1325.
- [38] JV Michael, *J. Chem. Phys.* **92** (1990) 3394.
- [39] A Persky, H Kornweitz, *Int. J. Chem. Kinet.* **29** (1997) 67.
- [40] PC Kobrinsky, PD Pacey, *Can. J. Chem.* **52** (1974) 3665.
- [41] AJC Varandas, FB Brown, CA Mead, DG Truhlar, BC Garrett, *J. Chem. Phys.* **86** (1987) 6258.
- [42] N Agmon, RD Levine, *Chem. Phys. Lett.* **52** (1977) 197.

This page intentionally left blank

## — 7 —

# Relationships between Structure and Reactivity

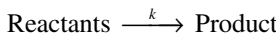
---

### 7.1 QUADRATIC FREE-ENERGY RELATIONSHIPS (QFER)

The view that the ability of molecules to react rests ultimately on their own structural properties has long been dear to chemists. Although the encounter of two molecules triggers unique features which neither molecule possess alone, notably an electron inflow to the reactive bonds up to a point of saturation, the notion that molecules contain all the information necessary to understand their reactivity has proved extremely useful. In the middle of the nineteenth century, Auguste Laurent expressed the idea that “structure determines reactivity and is directly connected with crystalline form” [1]. Chemical reactivity can be understood both as the ability of individual molecules to take part in various chemical reactions as well as the study of rates of such reactions, that is, equilibrium and rate processes. In this textbook, we will focus upon rate constants, conscious that their value for the understanding of chemical reactivity depends largely on our ability to relate them with reaction energies and molecular structure.

Chemical reactivity depends on energy relationships along the reaction coordinate. While some features are specific for particular reactions, others are common to series of reactions, which in some sense constitute a *family of reactions*. Those relations are the ones that allow the establishment of structure-reactivity relationships and can be classified into some broad categories.

It is one of the fundamental assumptions of our chemical knowledge that like substances react similarly and that similar changes in structure produce similar changes in reactivity. This is a qualitative and intuitive notion, which can be addressed in a quantitative way in terms of chemical kinetics; that is in terms of the rate constant  $k$



In an ideal situation one would wish that the changes in  $k$  in a series of chemical reactions would be dominated by the changes in a single structural factor. In such a case, other structural factors do not change along the reaction series, or such changes are not significant. Under such conditions we can say that these processes constitute a reaction family.

Owing to the exponential dependence of the rate upon energy, the rate problem reduces mainly to the determination of the lowest energy barrier that has to be surmounted. The ISM model, which was presented in the previous chapter, points, in general terms, to some structural factors that control the barriers of chemical reactions and as a consequence the rate constants. These relevant factors are (i) *reaction energy*,  $\Delta E^0$ ,  $\Delta H^0$  or  $\Delta G^0$ ; (ii) the *electrophilicity index* of Parr,  $m$ , a measure of the electron inflow to the reactive bonds at the transition state, also characterised as a transition-state bond order  $n^\ddagger$ ; (iii) when the potential energy curves for reactants and products can be represented adequately by harmonic oscillators, the relevant structural parameters are the *force constants* of reactive bonds,  $f_r$  and  $f_p$  in reactants and products, respectively; and (iv) equilibrium *bond-lengths* of reactive bonds,  $l_r$  and  $l_p$  in reactants and products, respectively.

Let us represent the course of reaction (7.I) by the intersection of potential energy curves of the reactant BC and the product AB as



When the potential energy of the molecular species is represented by harmonic oscillators, the common energy of the distended configurations of BC and AB at the transition state is represented by the following expression:

$$\frac{1}{2} f_r x^2 = \frac{1}{2} f_p (d - x)^2 + \Delta E^0 \quad (7.\text{I})$$

where  $x$  is the bond extension of the reactant molecule BC to the transition state, and  $d$  represents the sum of the bond extensions of BC and AB on going to the transition state. In eq. (7.1),  $d - x$  represents the bond extension of the product molecule as illustrated in Figure 7.1. This equation expresses reaction energy in terms of a thermodynamic quantity, the internal energy,  $\Delta E^0$ , rather than in terms of a difference in the potential energies of products and reactants,  $\Delta V^0$ .

Before pursuing further, a word of caution is necessary. Chemical thermodynamics deals with macroscopic observations, but aims to build a bridge between macroscopic variables and events at microscopic level by specifying the composition of the system in molecular terms. Potential energy,  $V$ , is a microscopic variable defined for all configurations of the reacting system. Thus,  $V$  varies in a continuous manner along the progress variable and defines a reaction path. But thermodynamic energies are not continuous functions along this path. They are only valid for stable or metastable states, i.e., for elementary reactions they are only valid for reactants, products and the transition state. Whereas eq. (7.1), defined in terms of  $\Delta V^0$ , possesses a physical meaning for all the points  $0 \leq x \leq d$ , the same mathematical expression defined in terms of  $\Delta E^0$ , or in terms of any other thermodynamic quantity, has no physical meaning for the points interpolated between reactants, transition state and products.

The energy barrier for the prototype reaction, measured with respect to reactants, is expressed by the equation

$$\Delta E^\ddagger = \frac{1}{2} f_r x^2 \quad (7.\text{2})$$

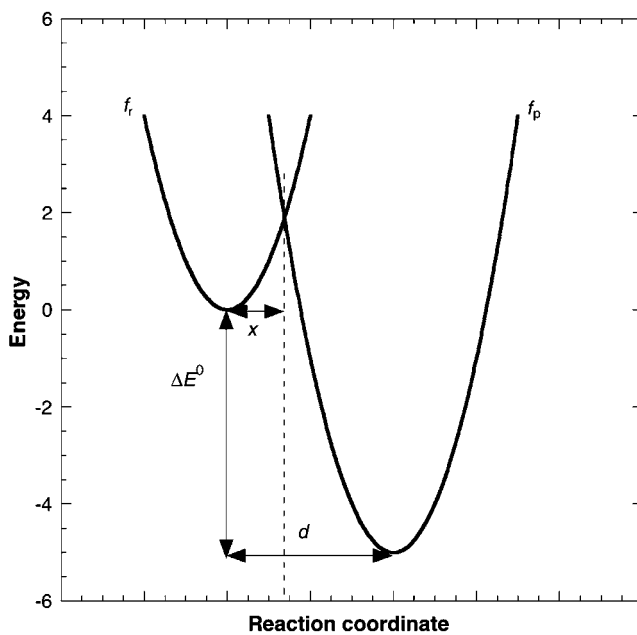


**Figure 7.1** Reaction coordinate of a bond-breaking–bond-forming reaction in terms of intersecting harmonic oscillators. The reaction coordinate  $d$  represents the sum of the reactant and product bond extensions, from equilibrium to transition state configurations.

Under the particular condition of almost equal force constants for reactant and product,  $f=f_r=f_p$ , eq. (7.1) becomes

$$\frac{1}{2}fx^2 = \frac{1}{2}fd^2 - fdx + \frac{1}{2}fx^2 + \Delta E^0 \quad (7.3)$$

Solving this equation for the reactant distension,  $x$ , yields

$$x = \frac{d}{2} + \frac{\Delta E^0}{fd} \quad (7.4)$$

This expression can also take the more convenient form

$$x = \frac{1}{2}d \left( 1 + \frac{2\Delta E^0}{fd^2} \right) \quad (7.5)$$

If we make the substitution of  $x$  in the expression of the energy barrier, eq. (7.2), then we have

$$\Delta E^\ddagger = \Delta E^\ddagger(0) \left( 1 + \frac{\Delta E^0}{4\Delta E^\ddagger(0)} \right)^2 \quad (7.6)$$

where  $\Delta E^\ddagger(0)$  represents the *intrinsic barrier* of reaction (7.I).

$$\Delta E^\ddagger(0) = \frac{1}{8} f d^2 \quad (7.7)$$

The intrinsic barrier represents the barrier of the reaction taking it as an isoenergetic process, that is, with  $\Delta E^0 = 0$ .

In the past, Evans and Polanyi [2] have introduced the concepts of *chemical driving force* and *chemical inertia*. By chemical inertia they meant the work that must be done to produce reaction, partly in breaking BC bond and in placing the atom A sufficiently close to B. In the present formulation this can be represented by the intrinsic barrier,  $\Delta E^\ddagger(0)$ . By chemical driving-force they meant the contribution that the energy of formation of the new bond AB makes towards overcoming the inertia, which is represented by the reaction energy  $\Delta E^0$ . Eq. (7.6) reveals that under certain approximations, one can separate the *thermodynamic contribution*,  $\Delta E^0$ , and the *kinetic contribution*,  $\Delta E^\ddagger(0)$ , for the energy barrier of the reaction  $\Delta E^\ddagger$ . Seminal ideas for such a separation go back to Jean-Auguste Muller in 1886, but the correct quantitative formulation was proposed by Rudolph Marcus [3] in the 1960s.

The sum of bond extensions to the transition state,  $d$ , was given by ISM, in the previous chapter as

$$d = \left[ \frac{a' \ln(2)}{n^\ddagger} + \frac{a'}{2} \left( \frac{\Delta E^0}{\Lambda} \right)^2 \right] (l_r + l_p) \quad (7.8)$$

When the dynamic parameter  $\Lambda$  is, in absolute terms, much greater than the reaction energy,  $\Lambda \gg |\Delta E^0|$ , then  $d$  is independent of the reaction energy. Under such conditions  $d$  has a constant value that is the sum of bond extensions of reactants and products at thermoneutrality,  $d(0)$

$$d(0) = \frac{a' \ln(2)}{n^\ddagger} (l_r + l_p) \quad (7.9)$$

with  $a' = 0.156$ . Under this set of approximations, the separation between the intrinsic and thermodynamic contributions for the energy barrier,  $\Delta E^\ddagger$ , is valid (see eq. (7.6)). Thus, the intrinsic barrier can be expressed in terms of several molecular factors, specifically force constant, transition-state bond order and the sum of the equilibrium bond lengths of reactant and product.

$$\Delta E^\ddagger(0) = \frac{1}{8} f \left[ \frac{0.108}{n^\ddagger} (l_r + l_p) \right]^2 \quad (7.10)$$

Eq. (7.6), known as the equation of Marcus, leads to a quadratic relationship between the barrier of reaction and the reaction energy, which shows up also in the modified form

$$\Delta E^\ddagger = \Delta E^\ddagger(0) + \frac{\Delta E^0}{2} + \frac{(\Delta E^0)^2}{16 \Delta E^\ddagger(0)} \quad (7.11)$$

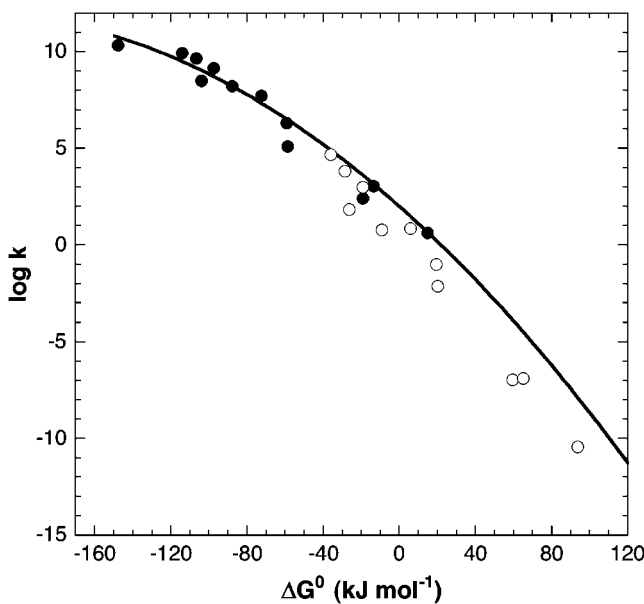


**Figure 7.2** Rate constants of proton transfers from enolate ions and water. The curve represents an application of the Marcus quadratic relationship, with  $\Delta G^\ddagger(0) = 57 \text{ kJ mol}^{-1}$  and  $k_{\text{dif}} = 10^{11} \text{ mol}^{-1} \text{ dm}^3 \text{ sec}^{-1}$ .

For reactions in solution, one tends to use Gibbs energy,  $G$ , instead of internal energy,  $E$ . For this reason, eqs. (7.6) and (7.11) are called (Gibbs) *free-energy relationships*. In this particular case such equations represent *quadratic free-energy relationships* (QFER).

Figure 7.2 illustrates a QFER for the proton-transfer reactions between enolate anions and water molecules [4]. The experimental data can be reproduced by the equation of Marcus with an intrinsic barrier of  $\Delta G^\ddagger(0) = 57 \text{ kJ mol}^{-1}$  and a pre-exponential factor of  $k_{\text{dif}} = 10^{11} \text{ mol}^{-1} \text{ dm}^3 \text{ sec}^{-1}$ . This is a good illustration of a family of reactions which have similar behaviour throughout a very extensive energy range,  $\Delta\Delta G^0 = 200 \text{ kJ mol}^{-1}$  and  $\Delta\Delta G^\ddagger = 85 \text{ kJ mol}^{-1}$  and covering reaction rates over 14 orders of magnitude. Changes in reactivity are controlled entirely by changes in  $\Delta G^0$ . This means that the bonds to be broken and formed, OH and CH, have the same force constants and bond lengths throughout the reaction series and that  $n^\ddagger$  is also constant. This implies that the electrophilicity is quite invariant for the different enolates employed in this study.

## 7.2 LINEAR FREE-ENERGY RELATIONSHIPS (LFER)

Eq. (7.11) can be further simplified if the intrinsic barrier is much higher than the range of reaction energies, such that  $16(\Delta E^\ddagger(0)) \gg (\Delta E^0)^2$ . Inserting this condition into eq. (7.11) leads to

$$\Delta E^\ddagger \approx \Delta E^\ddagger(0) + \frac{\Delta E^0}{2} \quad (7.12)$$

This expression reveals the existence of a linear relation between energy barrier and reaction energy. When expressed in terms of Gibbs energy, this represents a *linear free-energy relationship* (LFER).

The equation of Marcus was developed in 1956 and ISM in 1986. Predictions on the effects of substituents on the rate constants and the equilibrium constants are not due to such developments, but to a rich history of empiricism. Nevertheless, many of those historical paths can now be encompassed by the Marcus equation and ISM.

### 7.2.1 Brönsted equation

In the acid–base reaction (7.II), it appeared reasonable to Brönsted and Pederson that if the rates  $k$  at which proton is removed by a particular basis  $B^-$  were compared for various acids HA



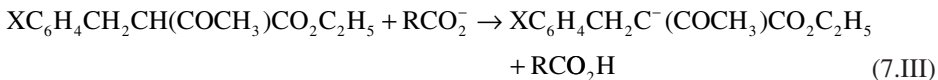
then the base might remove the proton more rapidly from the stronger acids. In fact, relationships between rate of an acid–base reaction and equilibrium have been observed in many cases and frequently obey an equation known as the Brönsted catalysis law

$$k = GK^\alpha \quad (7.13)$$

where  $G$  and  $\alpha$  are empirical constants,  $k$  the rate for reaction (7.II) and  $K$  the acid dissociation equilibrium constant. In logarithmic form, the Brönsted equation can be written as

$$\log k = \alpha \log K + \text{constant} \quad (7.14)$$

The value of  $\alpha$  can be estimated from a plot of the second-order catalytic constant  $\log k$  for the reaction catalysed by the acid HA, against the  $pK_{\text{HA}}$ . Equivalent procedures can also be performed for base catalysed reactions. Figure 7.3 illustrates the application of Brönsted relationship for the proton-transfer reactions [5].



In one set of the reactions, the substituent X of the carbon acid was varied and the same base,  $\text{CH}_3\text{COO}^-$ , was used; this allows one to estimate the Brönsted constant for the acid catalysis,  $\alpha$ . In another set of experiments the base was varied, but the acid was kept constant; this allows the estimation of the Brönsted  $\beta$  parameter for base catalysis.

Taking into consideration the relations between rate constants  $k$  and  $\Delta G^\ddagger$  and equilibrium constants  $K$  and  $\Delta G^0$ ,

$$\begin{aligned} k &= \frac{k_{\text{B}}T}{h} \exp\left(-\frac{\Delta G^\ddagger}{RT}\right) \\ K &= \exp\left(-\frac{\Delta G^0}{RT}\right) \end{aligned} \quad (7.15)$$

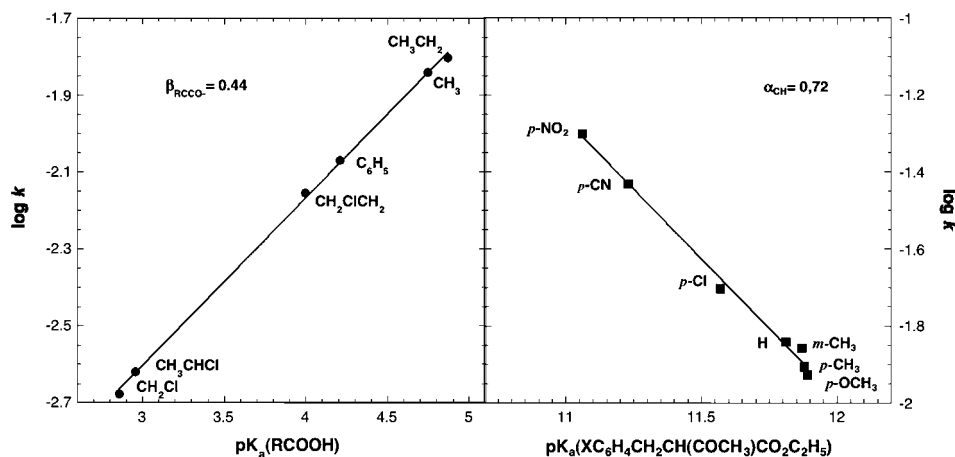


**Figure 7.3** Correlation between the ionisation constants of carboxylic acids  $\text{RCOOH}$  or carbon acids  $\text{R}_3\text{CH}$ , and the second-order rate constant of the reactions in mechanism (7.III).

the Brönsted equation takes the form

$$\Delta G^\ddagger = \alpha \Delta G^0 + \text{constant} \quad (7.16)$$

showing that, at a constant temperature, this equation reflects a LFER.

Following a suggestion of Leffler [6], chemists have tried for a number of years to use the Brönsted coefficient,  $\alpha = \partial(\Delta G^\ddagger)/\partial(\Delta G^0)$ , as a measure of the position of the transition state (TS) along the reaction coordinate, since usually  $0 < \alpha < 1$ , with  $\alpha = 0$  for reactants, and  $\alpha = 1$  for products. As a consequence,  $\alpha = 0.5$  would imply that the transition state is exactly half way between reactants and products.

As illustrated in Figure 7.4 for a thermoneutral reaction,  $\alpha$  is not always a measure of the position of TS. When  $f_r = f_p$  one has for this kind of reaction  $\alpha = 0.5$ , reflecting correctly the position of the transition state. But if  $f_r > f_p$  the transition state is before the measure provided by  $\alpha$ ; if  $f_r < f_p$  the transition state is ahead of the measure of  $\alpha$ .

The Marcus equation, now expressed in terms of Gibbs energy, can be written as

$$\frac{\partial \Delta G^\ddagger}{\partial \Delta G^0} = \frac{1}{2} + \frac{1}{8} \frac{\Delta G^0}{\Delta G^\ddagger(0)} \quad (7.17)$$

This equation does not give full support to the empirical equation of Brönsted, because the relation is a quadratic one, while that of Brönsted is linear, such that under the relevant approximations  $\alpha$  would be constant and always equal to 0.5. ISM, which is more general than the equation of Marcus, accommodates LFER with values of  $\alpha \neq 0.5$  ( $0 < \alpha < 1$ ) when the force constants do not have a common value,  $f_r \neq f_p$ . In empirical terms there are cases with  $\alpha > 1$  and  $< 0$ , but these are anomalous situations which will be discussed later.

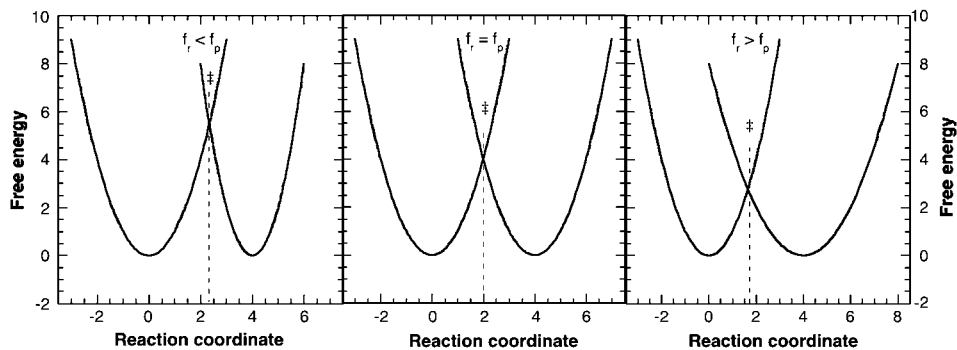


**Figure 7.4** Effect of the force constants of the reactive bonds on the position of the transition state for an isothermal reaction.

on in the Chapter 13, devoted to proton-transfer reactions. Identical considerations are valid for the  $\beta$  coefficients.

### 7.2.2 Bell–Evans–Polanyi equation

In the mid-1930s of the twentieth century, Bell, Evans and Polanyi correlated energies of activation,  $E_a$ , for several reactions in the vapour phase with heats of reaction,  $\Delta H^0$ , according to the following expression:

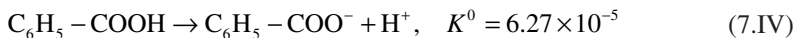
$$E_a = \alpha \Delta H^0 + \text{constant} \quad (7.18)$$

which is also a LFER. The additive constant in this relationship will be taken to assume, according to Rudolph Marcus, the presence of an intrinsic barrier.

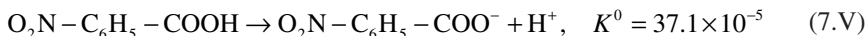
Both free-energy relationships expressed by eqs. (7.6) and (7.18) would imply that reactions which have a strong driving force thermodynamically will also proceed rapidly. However, if we consider this more deeply we will see that such an implication does not hold generally. For example, the energetically favourable oxidation of hydrocarbons in the presence of air may not take place for years, whereas the energetically unfavourable hydration of carbon dioxide takes place in seconds. For elementary reactions, the correct interpretation rests on the values of the intrinsic barriers.

### 7.2.3 Hammett and Taft relationships

In January 1937, Hammett published a paper on the “Effects of structure upon the reactions of benzene derivatives”. Let us consider the dissociation of benzoic acid



Hammett realised that the addition of a substituent in the aromatic ring has a quantitative effect on the dissociation constant  $K$ . For *para*-nitrobenzoic acid the dissociation constant



increases, indicating an increment in the stabilisation of the negative charge generated by dissociation. If the substituent is an ethyl group in *para* position, the opposite effect is observed with respect to the unsubstituted reaction



indicating that the ethyl group destabilises the negative charge generated in dissociation.

Hammett found, for example, that the nitro group has a stabilising effect on other dissociation reactions such as those of phenylacetic acid. He then proposed a quantitative relationship to account for such findings

$$\log K = \log K^0 + \rho\sigma \quad (7.19)$$

The same kind of expression is also valid for the rate constants,  $k$

$$\log k = \log k^0 + \rho\sigma \quad (7.20)$$

$K^0$  and  $k^0$  denotes the corresponding constants for the “parent” or “unsubstituted” compound.

The *substituent constant*  $\sigma$  is a measure of the electronic effect of replacing H by a given substituent (in the *para* or *meta* position) and is, in principle, independent of the nature of reaction. The *reaction constant*  $\rho$  depends on the nature of the reaction, including conditions such as solvent and temperature;  $\rho$  is a measure of the susceptibility of the reaction to the electronic effects of substituents. The reference reaction is the ionisation of unsubstituted benzoic acid in water at 25 °C, with  $\rho = 1$ .

Thus it is clear that just a few values of  $\sigma$  and  $\rho$  can summarise a large body of equilibrium and rate measurements, and can help to predict rate coefficients and equilibrium constants for reactions which have not yet been studied. The *substituent constant*  $\sigma$  is a positive or negative number (Table 7.1, Figure 7.5). For example,  $\sigma_p = 0.71$  for  $-\text{NO}_2$  indicates that this group has an electron-removing effect higher than H-atom, whereas  $\sigma_p = -0.66$  for  $-\text{NH}_2$  indicates that this group has an electron-donating effect stronger than H-atom. Reactions with  $\rho > 0$  are facilitated by electron-removing substituents.

Although the Hammett relationship works well for *meta*- and *para*-substituted aromatic compound, it frequently fails for either *ortho*- aromatic (due to steric effects) or aliphatic compounds, and other scales have been proposed, such as that of Taft.

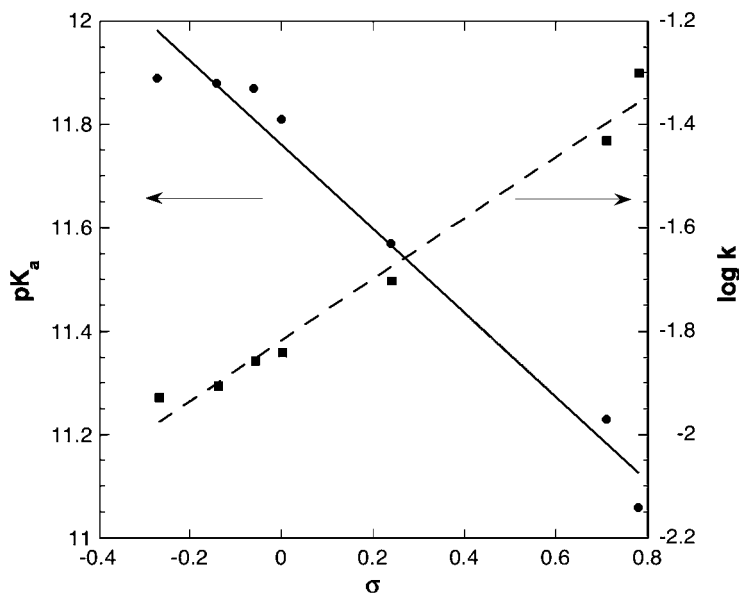
$$\log k - \log k_0 = \rho * \sigma * \quad (7.21)$$

Figure 7.6 compares the performance of the equations of Hammett and Taft with respect to the hydrolysis of ketals that proceed according to mechanism (7.VII) [7].

**Table 7.1**

Hammett ( $\sigma_m$ ,  $\sigma_p$ ) and Taft ( $\sigma^*$ ) coefficients of common substituents in organic molecules

Substituents	$\sigma_m$	$\sigma_p$	$\sigma^*(\text{CH}_2\text{Y})$
$-\text{NH}_2$	-0.16	-0.66	
$-\text{NMe}_2$	-0.10	-0.32	
$-\text{OH}$	0.02	-0.22	0.555
$-\text{OMe}$	0.12	-0.27	0.52
$-\text{OAc}$	0.39	0.31	
$-\text{SMe}$	0.14	0.06	
$-\text{H}$	0	0	
$-\text{Me}$	-0.06	-0.14	-0.10
$-\text{Et}$			-0.10
$-\text{n-Pr}$			-0.13
$-\text{t-Bu}$	-0.09	-0.15	-0.165
$-\text{C}_5\text{H}_5$	0.05	0.05	0.215
$-\text{COMe}$	0.36	0.47	0.60
$-\text{F}$	0.34	0.15	1.1
$-\text{Cl}$	0.37	0.24	1.05
$-\text{Br}$	0.37	0.26	1.00
$-\text{I}$	0.34	0.28	0.85
$-\text{CN}$	0.62	0.71	1.30
$-\text{NO}_2$	0.71	0.78	1.40
$-\text{CF}_3$	0.46	0.53	0.92



**Figure 7.5** Application of the Hammett equation to the reactions following mechanism (7.III).

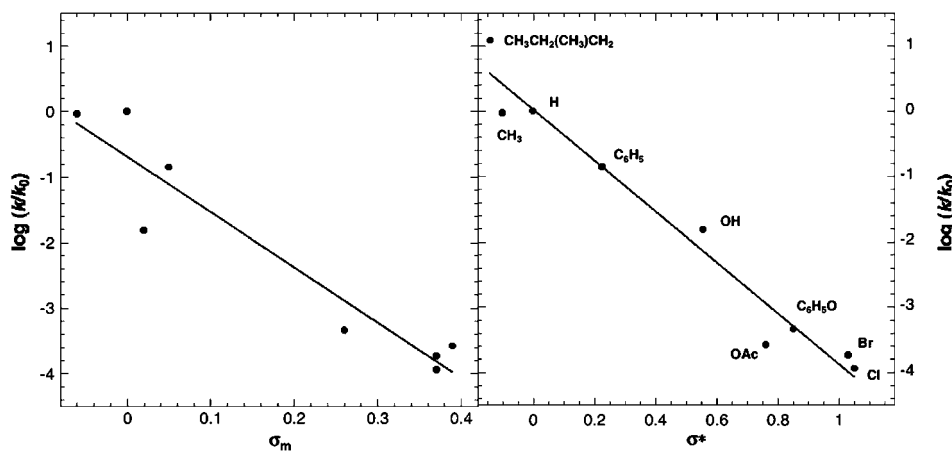
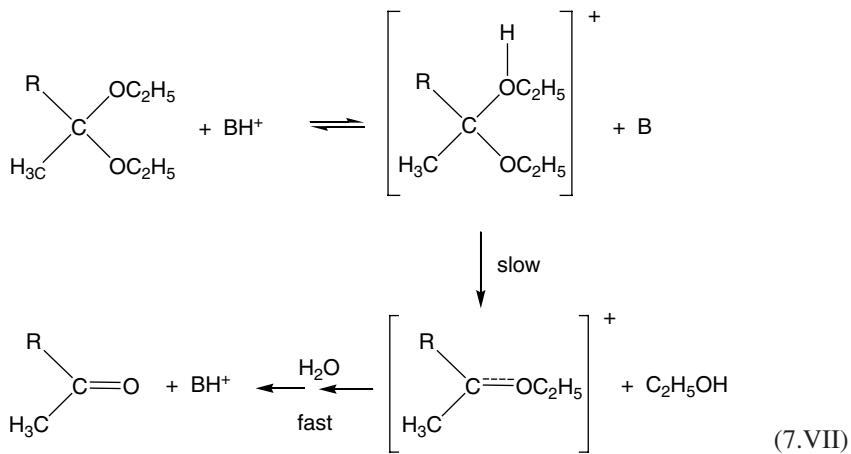


**Figure 7.6** Application of Hammett and Taft equations to the rate of the hydrolysis of ketals that proceed according to mechanism (7.VII).



These empirical correlations call for an explanation, by which we mean a theoretical basis, however profound or modest. From eq. (7.20) we can write

$$\Delta G^{\ddagger 0} = \Delta G_0^{\ddagger 0} - 2.3RT\sigma\rho \quad (7.22)$$

where  $\Delta G_0^{\ddagger 0}$  corresponds to the Gibbs activation energy of the reference reaction. For other homologous reactions, with the same set of substituents, one has

$$\Delta G^{\ddagger 0'} = \Delta G_0^{\ddagger 0'} - 2.3RT\sigma'\rho \quad (7.23)$$

Those two equations can be written in a different form

$$\begin{aligned}\frac{\Delta G^{\ddagger 0}}{\rho} &= \frac{\Delta G_0^{\ddagger 0}}{\rho} - 2.3RT\sigma \\ \frac{\Delta G^{\ddagger 0'}}{\rho'} &= \frac{\Delta G_0^{\ddagger 0'}}{\rho'} - 2.3RT\sigma\end{aligned}\quad (7.24)$$

and if one subtracts the other, we obtain

$$\frac{\Delta G^{\ddagger 0}}{\rho} - \frac{\Delta G^{\ddagger 0'}}{\rho'} = \frac{\Delta G_0^{\ddagger 0}}{\rho} - \frac{\Delta G_0^{\ddagger 0'}}{\rho'} \quad (7.25)$$

We can therefore write a linear equation between the free energies of activation of one set of reactions and those of a corresponding set

$$\Delta G^{\ddagger 0} - \frac{\rho}{\rho'} \Delta G^{\ddagger 0'} = \text{constant} \quad (7.26)$$

where the coefficient  $\rho/\rho'$  has the same value for all reactions in the set. Hammett equations are thus another kind of LFER.

The equations of Hammett and Taft apply reasonably well to Gibbs free energies. One might anticipate that this will also be valid for changes in enthalpies and entropies.

$$\Delta G^\ddagger = \Delta H^\ddagger - T\Delta S^\ddagger \quad (7.27)$$

However, this is not the case. The changes in  $\Delta H^\ddagger$  and in  $\Delta S^\ddagger$  show a considerable scatter when compared with  $\Delta G^\ddagger$ , and there is a compensating effect between  $\Delta H^\ddagger$  and  $\Delta S^\ddagger$ . A substituent group that induces a strong interaction of the solute with solvent molecules and decreases  $\Delta H^\ddagger$ , also decreases  $\Delta S^\ddagger$ . Figure 7.7 illustrates this effect of compensation in the alkaline hydrolysis of ethyl benzoate in water/alcohol and water/dioxane mixtures [8], which can be translated by the linear relationship

$$\delta\Delta H^\ddagger = \beta_{\text{iso}} \delta\Delta S^\ddagger \quad (7.28)$$

when a parameter of the reaction (solvent, substituent, etc.) is changed,

$$\delta\Delta G^\ddagger = \delta\Delta H^\ddagger - T\delta\Delta S^\ddagger = (\beta_{\text{iso}} - T)\delta\Delta S^\ddagger \quad (7.29)$$

The parameter  $\beta_{\text{iso}}$  represents the *isokinetic temperature*, the real or virtual temperature for which all members of the series have the same rate constant (Figure 7.8). Equivalent considerations are also valid for equilibrium constants.

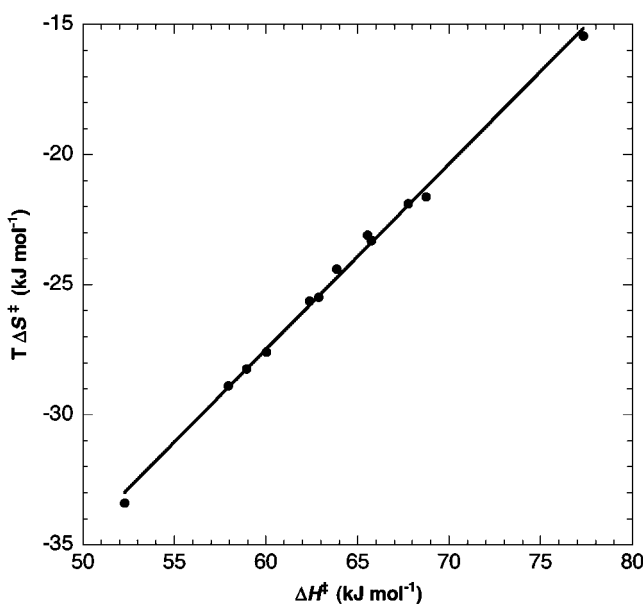


**Figure 7.7** Enthalpy–entropy compensation in the alkaline hydrolysis of ethyl benzoate in water/alcohol and water/dioxane mixtures.

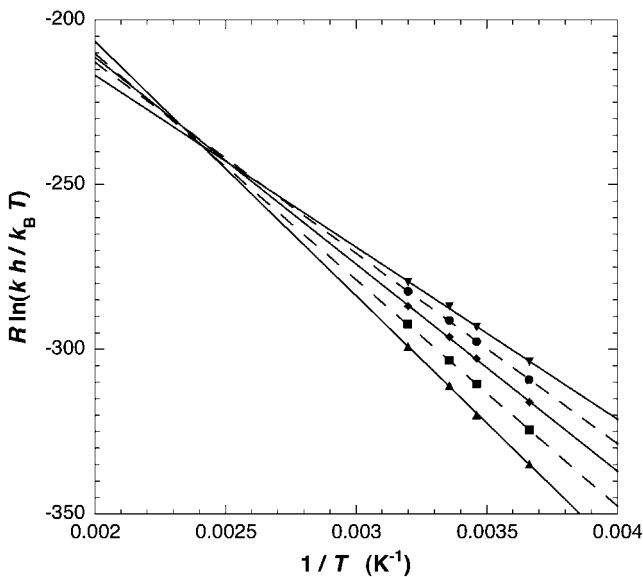


**Figure 7.8** Isokinetic relationship in the alkaline hydrolysis of ethyl benzoate in water/alcohol and water/dioxane mixtures. The enthalpies and entropies of activation of the previous figure were obtained from the slope and intercept of each of the straight lines in this figure.

### 7.3 OTHER KINDS OF RELATIONSHIPS BETWEEN STRUCTURE AND REACTIVITY

#### 7.3.1 The Hammond postulate

The equation of Bell–Evans–Polanyi (see eq. (7.18)) implies that exothermic reactions will have lower barriers than the endothermic ones. The view that a transition state has structural and energy features that are intermediate between those of starting materials and products is due to George Hammond [9], who resurrected the view implied by those three authors in 1955. The aim of Hammond was that of mechanistic interpretations, postulating that the changes in structure of the TS are affected by the manner in which the substituents affect the energies of intermediates on alternate pathways from reactants to products. Since then this assumption has been known as the Hammond postulate.

In an elementary reaction with a significant energy difference between products and reactants, where is the transition state located? The transition state is viewed as changing gradually from reactant-like in highly exergonic reactions, to intermediate in character for ergoneutral reactions, to product-like for endergonic reactions, as illustrated in Figure 7.9. This is expressed quantitatively in a free-energy relationship

$$\Delta\Delta G^\ddagger = \alpha\Delta G_p + (1-\alpha)\Delta G_R \quad (7.30)$$

which relates changes in transition state energy brought about by substituents, to the free energy changes brought about by those same substituents in reactants (R) and products (P). If  $\alpha \approx 0$  then  $\Delta\Delta^\ddagger G \approx \Delta G_R$  and the TS responds to changes in substituents in the same manner as the reactants, a characteristic of exoenergetic elementary steps. The transition state is closer to the reactants and, in consequence, the structural rearrangements to achieve the activated complexes are minimised and the activation barrier is small.

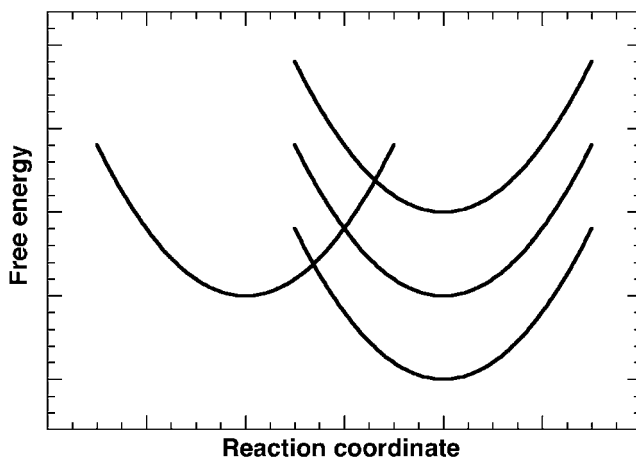


**Figure 7.9** Change in the location of the transition state with the reaction free energy.

Conversely, if  $\alpha \approx 1$  then  $\Delta\Delta^{\ddagger}G \approx \Delta G_p$  and the transition state responds to changes in substituents in a similar fashion to the products, a characteristic of highly endoenergetic elementary reaction. The transition state is closer to the products and its structural features are similar to those of the final materials. Large structural rearrangements are required to attain the transition state and the activation barrier is high.

These considerations are essentially valid when the force constants of reactants and products are similar. However, when  $f_r \gg f_p$  there is a general tendency for the transition state to be closer to reactants, even for endothermic reactions. The inverse is valid, that is when  $f_r \ll f_p$  the transition state has a tendency to be closer to the product configuration.

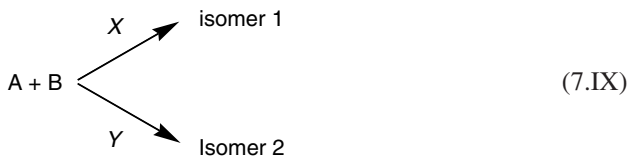
### 7.3.2 The reactivity-selectivity principle (RSP)

Consider the reaction of halogen ( $X_2$ ) with propane



where we represent  $\text{CH}_2\text{XCH}_2\text{CH}_3$  as isomer **1** and  $\text{CH}_3\text{CHXCH}_3$  as isomer **2**. If the  $X_2$  were not selective then the monohalogenated product would be expected to contain 75% of isomer **1** and 25% of **2**, according to the number of positions of primary- and secondary-H. Experimentally it is found that with  $\text{Cl}_2$  at 25 °C, 45% of **1** is produced and 55% of **2**, while with  $\text{Br}_2$  at 125 °C, 5% of **1** and 95% of **2** results. These data are commonly taken to indicate that the less reactive bromine is more selective in the reaction [10].

The question of the relationship between *reactivity* and *selectivity* is usually discussed in terms of the reactivity-selectivity principle (RSP); in a series of related reactions the more reactive species tend to be less selective in their reactivity than less reactive ones. Let us consider two substances A and B that follow the same type of reaction by two different pathways X and Y; for example, one leading to an isomer **1** and the other to an isomer **2**.



The selectivity  $S$  of the reaction is defined as follows:

$$S = \log\left(\frac{k_x}{k_y}\right) \quad (7.31)$$

expression that essentially corresponds to a difference in energy barriers,  $S = \Delta G_Y^{\ddagger} - \Delta G_X^{\ddagger}$ . The two substances A and B that undergo the same kind of reaction, A is more reactive than B. As illustrated in Figure 7.10, the more reactive reactant A is less selective, because it is smaller in difference of energy barriers,  $S(A) = \Delta G_Y^{\ddagger}(A) - \Delta G_X^{\ddagger}(A) < S(B) = \Delta G_Y^{\ddagger}(B) - \Delta G_X^{\ddagger}(B)$ . Following eq. (7.30), it is important to note that  $\alpha$  can also be regarded as a selectivity parameter.

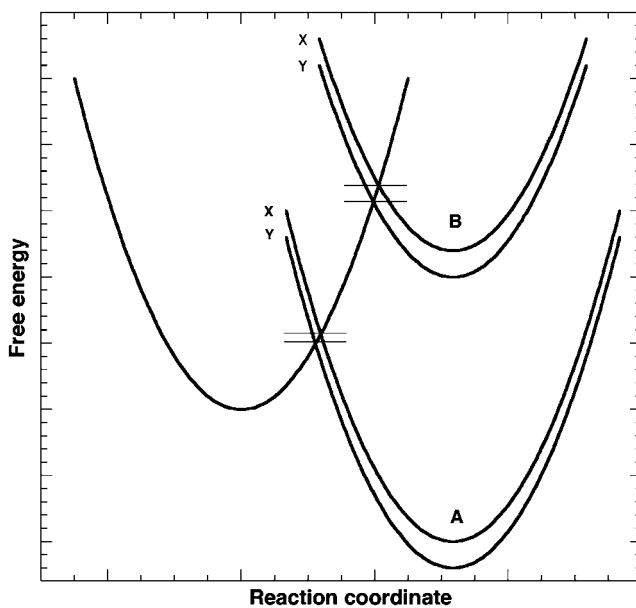


**Figure 7.10** Schematic illustration of the RSP.

**Table 7.2**

Experimental selectivity in the abstraction of hydrogen atoms from alkanes at 350 K

Radical	Primary	Secondary	Tertiary	$\Delta E^0$	$\Delta E^\ddagger$
$\text{Cl}\cdot$ ( $n^\ddagger \approx 1$ )	1	4.3	7.0	0	16
$\text{Br}\cdot$ ( $n^\ddagger \approx 1$ )	1	80	1700	67	75
$\text{CH}_3\cdot$ ( $n^\ddagger = 0.5$ )	1	10	80	-4	73

Table 7.2 presents the selectivity of several radicals ( $\text{R}^\bullet$ ) for H-abstraction from alkanes: primary, secondary and tertiary hydrogen atoms. Selectivity is measured with respect to the reaction



When one compares the selectivity of  $\text{Br}^\bullet$  and  $\text{Cl}^\bullet$ , the more reactive species (Cl) is clearly the less selective one. For example, bromine atoms abstract tertiary H-atoms 1700 times faster than the primary H-atom. By comparison, chlorine radical is only 7 times faster. In fact, the electronic factor  $m$  for those two radicals has almost identical values ( $m$  close to 2) and RSP is obeyed. When changes in reactivity are not due only to changes in reaction energy ( $\Delta E^0$ ,  $\Delta H^0$  or  $\Delta G^0$ ), the postulates of physical organic chemistry are no longer verified. For example,  $\text{Br}^\bullet$  and  $\text{CH}_3\cdot$  have almost the same reactivity with respect to  $\text{CH}_4$ . According to RSP one would expect that both radicals should have identical selectivities for H-atom abstractions. Nevertheless,  $\text{Br}^\bullet$  is much more selective, because the electrophilicity

parameter is also much higher for bromine radical ( $m(\text{Br}) \approx 2$  and  $m(\text{CH}_3) = 1$ ). Owing to an increase in  $m$ , the most reactive species is also the most selective one. Thus basically, the RSP can be expected to apply to reaction series in which  $\Delta G^\ddagger$  is only dependent on  $\Delta G^0$  and not on the electrophilicity parameter  $m$ .

### 7.3.3 Relationships of the electronic effect: equation of Ritchie

Structure–reactivity relationships in chemistry have been dominated by LFER. However, the kinetics of several cation–anion recombinations,



have been described by Calvin Ritchie using the simple empirical relation

$$\log k_{\text{X,C}^+} = \log k_{\text{H}_2\text{O,C}^+} + N_+ \quad (7.32)$$

where  $k_{\text{X,C}^+}$  is the rate of recombination of the nucleophile  $\text{X}^-$  with the cation;  $\text{C}^+$  in a given solvent; and  $k_{\text{H}_2\text{O,C}^+}$  the pseudo-first-order rate constant for the reaction of  $\text{C}^+$  with water in pure form.  $N_+$  is a simple property of the anionic nucleophile and of the solvent. Surprisingly, the last equation has no term describing the normal effect of the reaction energy on the rate constant, i.e., it does not describe a free-energy relationship, in spite of the fact that  $\Delta G^0$  can change by *ca.*  $\delta\Delta G^0 = 30 \text{ kJ mol}^{-1}$ . Figure 7.11 illustrates the application of this equation to cation–anion recombinations [11,12].

A rational for such a relationship can be provided by ISM in terms of a curve-crossing model. One would wish to find the conditions for which the effect of  $\Delta G^0$  on rate constants is minimised and that of  $m$  or  $n^\ddagger$  is maximised. Table 7.3 studies such conditions for harmonic oscillators and reveals that they are verified when  $f_r \ll f_p$  and correlated changes are occurring in the bond lengths. This is precisely the situation with cation–anion recombinations, where the force constants of the cation and anion bonds with the solvent molecules are much weaker and have lower force constants than the normal chemical  $\text{X}-\text{R}$  bond. The nucleophile parameter  $N_+$  is directly proportional to the electronic transition-state bond order,  $n^\ddagger$  (see Figure 7.12).

### 7.3.4 An empirical extension of the Bell–Evans–Polanyi relationship

So far we have considered only the effect of reaction energy and of the electronic electrophilicity parameter on chemical reactivity. ISM implies that other structural factors, such as force constants and bond lengths, can also play a significant role. Although this may be found in very specific cases, it does not have the generality of the factors previously discussed.

The empirical approach continues to be a useful source of knowledge, particular in complex systems such as many of those involved in chemical reactivity. This can be extended to employ powerful statistical methods (chemometrics), such as Partial Least Squares and multivariate analysis, to retrieve useful information and predict system response. It has been shown that activation energies of several atom-transfer reactions can be described

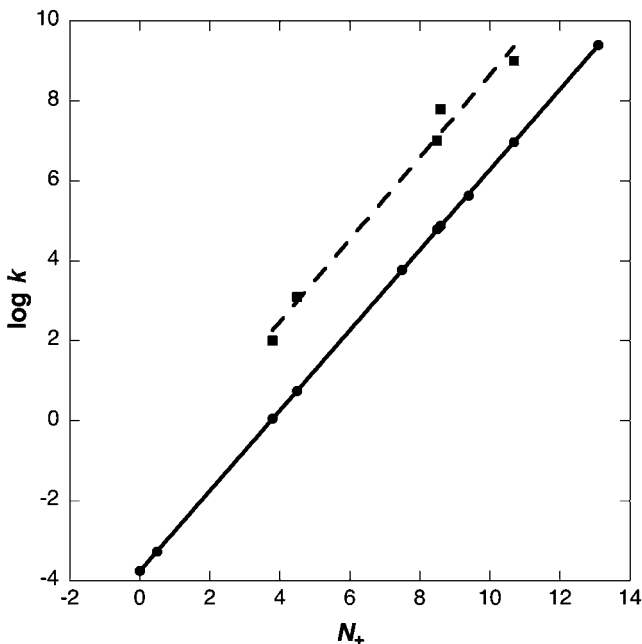


**Figure 7.11** Correlation of cation–anion recombinations by eq. (7.32). Circles: Malachite Green; squares: *p*-tolyl diazonium. The reaction of Malachite Green with water in pure water was taken as the reference and the  $N_+$  scale is defined as the difference between the logarithms of the rate constants of the other Malachite Green reactions and this reference reaction.

**Table 7.3**

Electronic and thermodynamic effects in the reaction barriers as a function of the reactant and product force constants, for  $\Delta G^0=0$ .

$I_r + I_p$ (Å)	$f_r$ (kJ mol <sup>-1</sup> Å <sup>-1</sup> )	$f_p$ (kJ mol <sup>-1</sup> Å <sup>-1</sup> )	$\partial\Delta G^\ddagger/\partial n^\ddagger$	$\partial\Delta G^\ddagger/\partial\Delta G^0$
3	3	3	-628	0.5
4.7 <sup>a</sup>	0.5	3	-518	0.29

<sup>a</sup>The bond length increase is correlated to the force constant decrease using typical values and correlations expressed in the literature

mainly in terms of reaction energy and Parr electrophilicity parameter, according to the expression [14]

$$E_a = A + B\Delta H^0 + Cm^{-3/2} \quad (7.33)$$

where  $A$ ,  $B$  and  $C$  are constants. This expression expands the previous Bell–Evans–Polanyi relationship and shows that the intrinsic barrier has an inverse dependence on  $m$ ; an increase in  $m$  decreases the barrier for the reaction. In this electronically extended Bell–Evans–Polanyi relationship (EBEPR) electronic and reaction energy factors appear now to be dominant for the control of chemical reactivity.

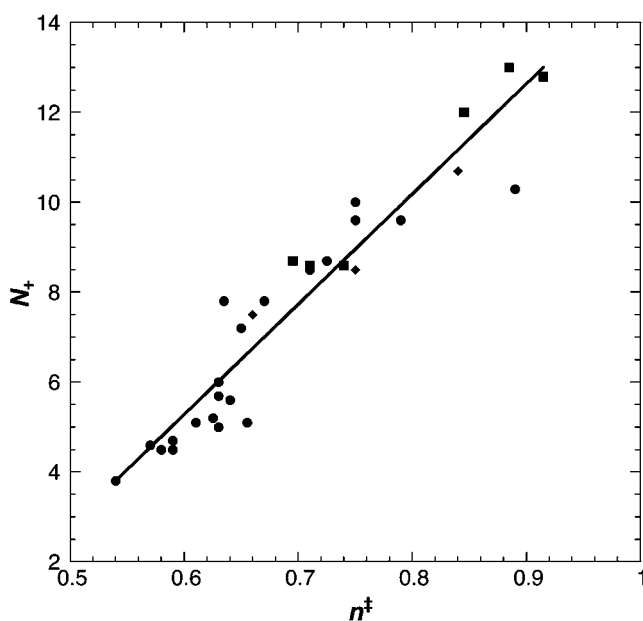


**Figure 7.12** Correlation between Ritchie parameter  $N_+$  for nucleophiles and the transition state bond order  $n^\ddagger$  in cation–anion recombinations. These recombinations were studied in water (circles), dimethylsulphoxide (squares) and methanol (lozenges) [13].

## REFERENCES

- [1] TH Levere, *Ambix* **17** (1970) 112.
- [2] MG Evans, M. Polanyi, *Trans. Faraday Soc.* **34** (1938) 11.
- [3] RA Marcus, *Ann. Rev. Phys. Chem.* **15** (1964) 155.
- [4] J Wirz, *Pure Appl. Chem.* **70** (1998) 2221.
- [5] RP Bell, S Grainger, *J. Chem. Soc. Perkin II* (1976) 1367.
- [6] JE Leffler, *Science* **117** (1953) 340.
- [7] MM Kreevoy, RW Taft, Jr., *J. Am. Chem. Soc.* **77** (1955) 5590.
- [8] RA Fairclough, CN Hinshelwood, *J. Chem. Soc.* (1937) 538.
- [9] GS Hammond, *J. Am. Chem. Soc.* **77** (1955) 334.
- [10] E Buncel, H. Wilson, *J. Chem. Educ.* **64** (1987) 475.
- [11] CD Ritchie, *Acc. Chem. Res.* **5** (1972) 348.
- [12] CD Ritchie, *Can. J. Chem.* **64** (1986) 2239.
- [13] SJ Formosinho, LG Arnaut, *J. Mol. Struct. (Theochem)* **371** (1996) 133.
- [14] M Barroso, JC Pereira, AAC Pais, LG Arnaut, SJ Formosinho, *Mol. Phys.* **104** (2006) 731.

This page intentionally left blank

# - 8 -

## Unimolecular Reactions

---

### 8.1 LINDEMANN-CHRISTIANSEN MECHANISM

In principle, unimolecular reactions should be one of the most conceptually simple reactions in chemistry. However, the history of the understanding of simple decomposition processes, such as



or



has been one of the considerable debate, controversy and complexity, even till our own days. The decomposition of  $\text{N}_2\text{O}_5$ , originally believed to be unimolecular, was eventually shown to occur by a composite mechanism, involving different kinds of radicals, notably  $\text{NO}_2$ ,  $\text{NO}_3$  and  $\text{NO}$ . On another level, one might imagine that even a true elementary reaction such as the decomposition of  $\text{Br}_2$ , although it shows a first-order rate law, cannot possibly have a simple collisional explanation. The reactant molecule must acquire some amount of energy before it decomposes. Obviously, such an amount of energy can be obtained through ultraviolet or visible light of appropriate wavelength (see Chapter 15). But under thermal conditions what is the source of such energy?

In 1919, Perrin proposed that unimolecular gas reactions would acquire the energy for the reaction through the radiation from the walls of the reaction vessels. Later, during a Faraday Society meeting in 1921, Lindemann [1] (later Lord Cherwell) expressed strong opposition to this radiation hypothesis and proposed an activation collision mechanism that was explicitly described in more detail a few days later by Christiansen in his Ph.D. thesis. The mechanism of Lindemann–Christiansen, the basis for all the modern theories of unimolecular reactions [2], considers the formation of a metastable molecule  $\text{A}^*$  having sufficient energy to undergo reaction. The energisation process involves collisions between two molecules of A



The energised molecule may undergo de-energisation by collisions with a normal molecule, or it may undergo a reaction of molecularity equal to one to form products. There are, therefore, three distinct processes in this mechanism with their own rates (i) the rate of energisation is  $k_1[A]^2$ ; (ii)  $A^*$  can be de-energised at a rate  $k_{-1}[A^*][A]$ ; and (iii)  $A^*$  can be converted into products at a rate  $k_2[A^*]$ .

The rate of product formation depends on the  $[A^*]$ , which can be found from a steady approximation for  $A^*$

$$\frac{d[A^*]}{dt} = k_1[A]^2 - k_{-1}[A^*][A] - k_2[A^*] \quad (8.1)$$

From the condition of  $d[A^*]/dt=0$  one obtains

$$[A^*] = \frac{k_1[A]^2}{k_2 + k_{-1}[A]} \quad (8.2)$$

and subsequently

$$v = \frac{d[P]}{dt} = k_2[A^*] = \frac{k_1 k_2 [A]^2}{k_2 + k_{-1}[A]} \quad (8.3)$$

In the vapour phase, at high pressures, one has  $k_{-1}[A^*] \gg k_2$ , and the rate of reaction assumes the more simple form

$$v_\infty = \frac{k_1 k_2}{k_{-1}} [A] \quad (8.4)$$

At high pressures the reaction is a first-order process. Under those conditions, the rate of energisation and de-energisation are relatively fast steps, which can be treated as a fast pre-equilibrium. Thus, the rate determining step is the transformation of  $A^*$  into products.

At low pressures, when  $k_{-1}[A^*] \ll k_2$ , a new expression for the rate of product formation is obtained.

$$v = k_1[A]^2 \quad (8.5)$$

The rate law is second order. At low  $[A]$  de-energisation is much less rapid than the rate at which  $A$  is converted into products. There is no longer equilibrium involving  $A^*$ . The rate of product formation is effectively equal to the rate at which the species  $A^*$  are formed, since now these molecules nearly always become products.

After Lindemann and Christiansen put forward their mechanism, experimental work was carried out to verify if the unimolecular reactions did become second order at sufficiently low pressures. Figure 8.1 illustrates the order of dimethyl ether decomposition in the vapour phase as a function of the addition of a foreign gas. In qualitative terms, the mechanism of Lindemann–Christiansen gives a good account of the experimental observations,

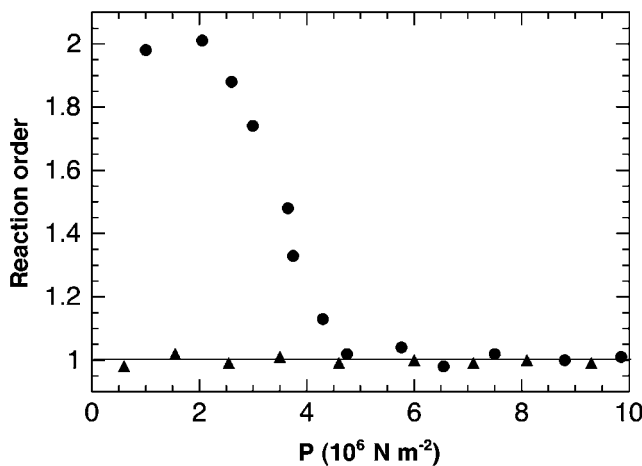


**Figure 8.1** Change in the reaction order in the decomposition of dimethyl ether, in the presence or absence of a foreign gas. Circles: dimethyl ether alone; triangles: dimethyl ether with a large excess of  $\text{H}_2$  or  $\text{N}_2$ .

since the order of the reaction varies from second- to first-order when the overall pressure increases.

In spite of this apparent success, another important aspect of this mechanism is the concentration of A at which one should observe a transition from first- towards second-order kinetics. Defining a rate constant for the first-order process at high pressures,  $k_\infty^1$ ,

$$v = k_\infty^1 [\text{A}] \quad (8.6)$$

eq. (8.4) allows one to write

$$k_\infty^1 = \frac{k_1 k_2}{k_{-1}} \quad (8.7)$$

This rate constant can be estimated experimentally at high pressures. Furthermore, eqs. (8.3) and (8.4) allow the determination of the concentration,  $[\text{A}]_{1/2}$ , at which the rates of de-energisation and product formation are equal

$$k_{-1} [\text{A}^*] [\text{A}]_{1/2} = k_2 [\text{A}^*] \quad (8.8)$$

Under such conditions, the rate is half of the maximum value

$$v_{1/2} = \frac{1}{2} k_2 \frac{k_1}{k_{-1}} [\text{A}]_{1/2} = \frac{1}{2} k_\infty^1 [\text{A}]_{1/2} \quad (8.9)$$

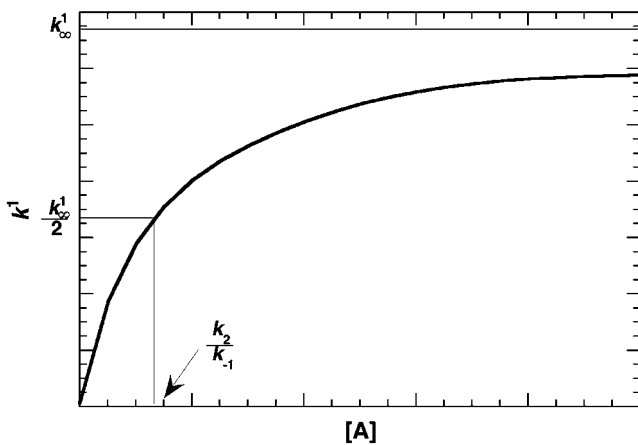


**Figure 8.2** Dependence of the first-order rate coefficient,  $k^1$ , on the concentration of the reactant,  $[A]$ .

A first-order rate coefficient,  $k^1$ , can be defined under any condition by

$$v = k^1 [A] \quad (8.10)$$

Such a coefficient can be studied experimentally as a function of pressure, as shown in Figure 8.2. However, the experimental values of  $[A]_{1/2}$  are always much smaller than those expected from the expression

$$[A]_{1/2} = \frac{k_2}{k_{-1}} = \frac{k_\infty^1}{k_1} \quad (8.11)$$

when  $k_1$  is estimated on the basis of a simple collision theory,  $k_1 = Z_1 e^{-E_1/RT}$ , where  $Z_1$  is the collision frequency and  $E_1$  the activation energy. Thus, a modification must be contemplated to allow  $k_1$  to be much larger than  $Z_1 e^{-E_1/RT}$  and to account for the increase in that discrepancy with the increase in complexity of the reactants, e.g.  $C_3H_6$  versus  $N_2O$  or  $HI$ .

The second difficulty with the Lindemann–Christiansen mechanism becomes apparent when experimental data are plotted in another way

$$\frac{1}{k^1} = \frac{k_{-1}}{k_1 k_2} + \frac{1}{k_1 [A]} \quad (8.12)$$

A plot of  $1/k^1$  against the reciprocal of  $[A]$  should give a straight line. However, deviations from linearity of the kind shown in Figure 8.3 have been found.

## 8.2 HINSHELWOOD'S TREATMENT

The first difficulty of the Lindemann–Christiansen mechanism is associated with the fact that first-order rates are maintained down to lower concentrations than appear to be

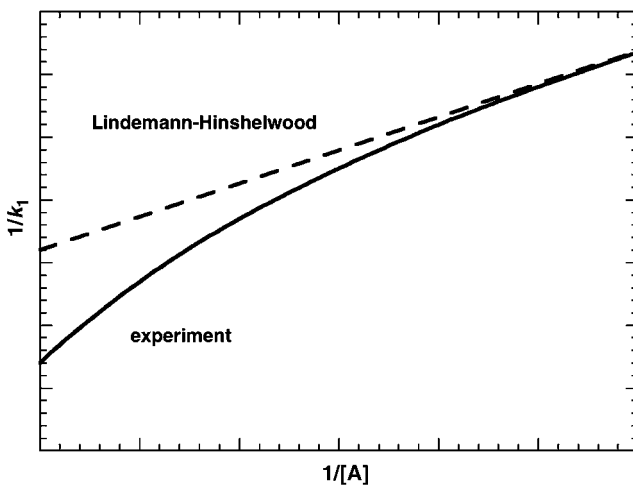


**Figure 8.3** Predicted and observed behaviour when  $1/k^1$  against the reciprocal of  $[A]$ .

permitted by the theory. This difficulty was successfully overcome by Hinshelwood [3], as shown below.

Maxwell and Boltzmann, in their treatment of the distribution of molecular speeds and energies, demonstrated that the fraction of molecules having energies between  $\varepsilon_x$  and  $\varepsilon_x + d\varepsilon_x$  is

$$\frac{dN_x}{N} = \frac{1}{\sqrt{\pi\varepsilon_x k_B T}} \exp\left(-\frac{\varepsilon_x}{k_B T}\right) d\varepsilon_x \quad (8.13)$$

This relationship applies to a molecule moving in the  $x$  direction.

The fraction of molecules,  $f^*$ , that have energies above a certain specified quantity  $\varepsilon^*$  is given by

$$f^* = \frac{1}{\sqrt{\pi k_B T}} \int_{\varepsilon^*}^{\infty} \frac{1}{\sqrt{\varepsilon}} \exp\left(-\frac{\varepsilon}{k_B T}\right) d\varepsilon \quad (8.14)$$

The result of the integration cannot be expressed in a closed form. However, if one considers molecular motions along two directions,  $x$  and  $y$ , the probability of finding the molecule with a translational energy between  $\varepsilon_x$  and  $\varepsilon_x + d\varepsilon_x$  in the  $x$  direction and  $\varepsilon_y$  and  $\varepsilon_y + d\varepsilon_y$  along the  $y$  direction is

$$\frac{dN}{N} = \frac{1}{\pi k_B T \sqrt{\varepsilon_x \varepsilon_y}} \exp\left(-\frac{\varepsilon_x}{k_B T}\right) \exp\left(-\frac{\varepsilon_y}{k_B T}\right) d\varepsilon_x d\varepsilon_y \quad (8.15)$$

Within a kinetic point of view, what is relevant is the total energy of the molecule,  $\varepsilon$ , independent of how this is distributed along the two degrees of motion. With  $\varepsilon = \varepsilon_x + \varepsilon_y$ , we can

estimate the probability of finding the molecule with a total energy between  $\varepsilon$  and  $\varepsilon + d\varepsilon$ . One can obtain such a probability by writing  $\varepsilon_y = \varepsilon - \varepsilon_x$ , and integrating with respect to  $\varepsilon_x$  from 0 to  $\varepsilon$ .

$$\frac{dN}{N} = \frac{1}{\pi k_B T} \int_0^\varepsilon \frac{1}{\sqrt{\varepsilon_x}} \frac{1}{\sqrt{\varepsilon - \varepsilon_x}} \exp\left(-\frac{\varepsilon_x}{k_B T}\right) \exp\left(-\frac{\varepsilon - \varepsilon_x}{k_B T}\right) d\varepsilon_x d\varepsilon \quad (8.16)$$

$$\frac{dN}{N} = \frac{\exp(-\varepsilon/k_B T)}{\pi k_B T} d\varepsilon \int_0^\varepsilon \frac{1}{\sqrt{\varepsilon_x}} \frac{1}{\sqrt{\varepsilon - \varepsilon_x}} d\varepsilon_x \quad (8.17)$$

The value of the integral is  $\pi$ , and the final result takes the simple form

$$\frac{dN}{N} = \frac{1}{k_B T} \exp\left(-\frac{\varepsilon}{k_B T}\right) d\varepsilon \quad (8.18)$$

The fraction of molecules having energy in excess of the critical value  $\varepsilon_0^*$

$$f^* = \frac{1}{k_B T} \int_{\varepsilon_0^*}^{\infty} \exp\left(-\frac{\varepsilon}{k_B T}\right) d\varepsilon \quad (8.19)$$

is obtained by integrating between the limits  $\varepsilon_0^*$  and infinity

$$f^* = \exp\left(-\frac{\varepsilon_0^*}{k_B T}\right) \quad (8.20)$$

Hinshelwood correctly pointed out that the expression  $Z_1 e^{-E_1/RT}$  only applies if the energy is distributed among two degrees of freedom. For some unimolecular reactions, however, the number of internal degrees of freedom,  $s$ , is much greater than two. The activation energy is distributed initially among these  $s$  degrees, and there are many ways in which such a distribution can occur. Under such conditions, Hinshelwood has demonstrated that the fraction of molecules with energy above  $\varepsilon_0^*$  is then given by the expression

$$f^* = \frac{1}{(s-1)!} \left(\frac{\varepsilon_0^*}{k_B T}\right)^{s-1} \exp\left(-\frac{\varepsilon_0^*}{k_B T}\right) \quad (8.21)$$

and the rate constant,  $k_1$ , no longer has an exponential dependence multiplied by simple collision frequency.

$$k_1 = Z_1 \frac{1}{(s-1)!} \left(\frac{\varepsilon_0^*}{k_B T}\right)^{s-1} \exp\left(-\frac{\varepsilon_0^*}{k_B T}\right) \quad (8.22)$$

Thus, a new additional factor is present

$$\frac{1}{(s-1)!} \left( \frac{\varepsilon_0^*}{k_B T} \right)^{s-1} \quad (8.23)$$

that can be greater than unity by many powers of 10, when  $s$  is sufficiently high. For example, with  $s = 5$  and  $\varepsilon_0^*/k_B T = 5$  the factor of eq. (8.23) is 25, but if  $s = 5$  and  $\varepsilon_0^*/k_B T = 10$  the factor is much larger, e.g.,  $1.5 \times 10^4$ .

The activation energy predicted by the formulation of Hinshelwood differs from that predicted by simple collision theory

$$\varepsilon_a = \varepsilon_0^* - \left( s - \frac{3}{2} \right) k_B T \quad (8.24)$$

In spite of the progress that the treatment of Hinshelwood has brought to the field, some difficulties remain. One that persisted was the reciprocal dependence of  $1/k^1$  versus the reciprocal of concentration, which as we have seen is not found at high pressures. However, there are other problems, such as the fact that the number of degrees of freedom required to reproduce experimental data is one-half of the total number of vibrational modes. Also, according to eq. (8.23), one would also expect a strong temperature dependence of the pre-exponential factor, especially for large values of  $s$ . There is no experimental evidence for this prediction.

### 8.3 RICE–RAMPSBERGER–KASSEL–MARCUS (RRKM) TREATMENT

In more advanced treatments of unimolecular reactions, the previous mechanism is modified in order to distinguish *energised* molecules,  $A^*$ , from *activated* molecules,  $A^\ddagger$ . An activated molecule  $A^\ddagger$  is defined as one that is passing directly through the diving part on the product side of the potential-energy surface from the reactants to the products. An energised molecule,  $A^*$  is one that has acquired all the energy it needs to become an activated molecule, but, nevertheless, must undergo vibrations before it does so, and consequently its rate of conversion into  $A^\ddagger$  may depend on the critical energy for the conversion,  $\varepsilon_0^*$ . The mechanism for the general case of the presence of a foreign gas has the following scheme:



The highly energised molecule  $A^*$  has a metastable nature due to reasons associated with the slowness of the internal energy flow or, with the insight provided by the RRKM theory, to an entropy barrier arising from the improbability of concentrating vibrational

energy into a few degrees of freedom prior to reaction. For this new treatment, the rate of conversion into products,  $k_2$ , was found to be

$$k_2 = k^\ddagger \left( \frac{\varepsilon^* - \varepsilon_0^*}{\varepsilon^*} \right)^{s-1} \quad (8.25)$$

where  $\varepsilon^*$  is the amount of energy for the energised species and  $\varepsilon_0^*$  the critical energy value for the conversion into products. This expression is the result of the statistics of a randomly distribution of energy among the various normal modes of vibration. Rice and Ramsperger used classical statistical mechanics, whereas Kassel introduced a quantum treatment in addition to the statistical one. In general, the  $s$  value of the classical formulation that reproduces experimental data ranges between 1/4 and 2/3 of the total number of the normal vibrational modes, but the results from the quantum-mechanical formulation are closer to the total number of modes.

When  $\varepsilon^*$  is sufficiently high, every energised molecule  $A^*$  is essentially an activated species  $A^\ddagger$ , but this conditions depends on the value of  $s$  as shown in Figure 8.4. Figure 8.5 illustrates the application of Lindemann–Christiansen–Hinshelwood, RRK mechanisms to the isomerisation of cyclopropane as a function of pressure [4].

In the limit of high pressures, the theory RRK leads to the limiting high-pressure first-order rate constant of the conventional transition-state theory

$$k_\infty^1 = k^\ddagger \exp\left(-\frac{\varepsilon_0^*}{k_B T}\right) = \frac{k_B T}{h} \frac{Q^\ddagger}{Q_i} \exp\left(-\frac{\varepsilon_0^*}{k_B T}\right) \quad (8.26)$$

where  $Q_i$  and  $Q^\ddagger$  are the partition functions for activated and initial states. Since both partition functions refer to the same molecule, albeit in different configurations, one can expect

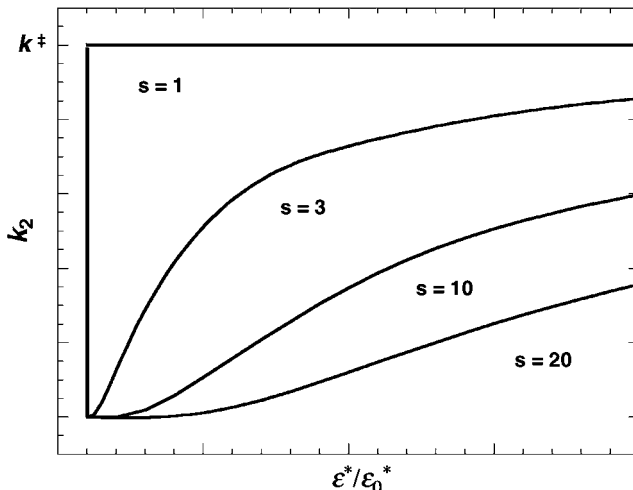


**Figure 8.4** Dependence of  $k_2$  on  $\varepsilon^*/\varepsilon_0^*$  for different values of  $s$ , that is, of the number of degrees of freedom.

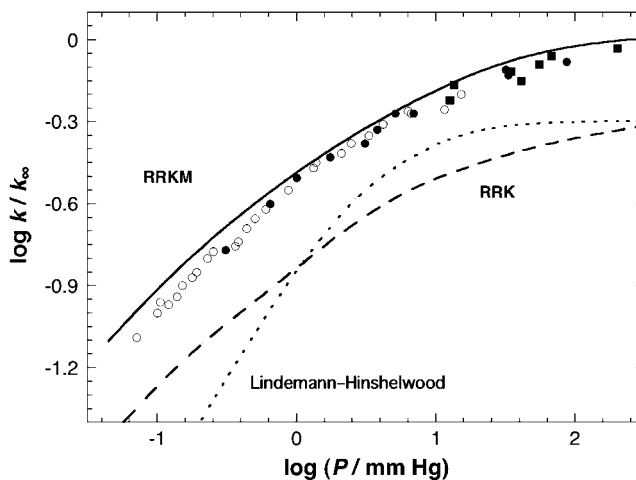


**Figure 8.5** Isomerisation rates of cyclopropane at 765 K, as a function of its pressure. The circles represent experimental data from several authors, and the curves represent the results of calculations with the theories indicated in the plot.

that  $Q_i \approx Q^\ddagger$  and the pre-exponential factor will be close to the average of the normal-mode frequencies, i.e., ca.  $10^{13}$ – $10^{14}$  sec $^{-1}$ . This is found in some reactions, but others present much higher values.

Marcus extended the RRK formalism in such a way that the individual vibrational frequencies of the energised species and activated complexes are considered explicitly [5,6]: account is taken of the way that the rotations and different normal modes of vibration, together with zero-point energies, contribute to the reaction. The energised species possess vibrational energy  $\varepsilon_v^*$  and rotation  $\varepsilon_r^*$ . Along the reaction coordinate, the activated species has a translational energy  $\varepsilon_t^\ddagger$  together with vibrational energies ( $\varepsilon_v^\ddagger$ ), and both contribute to the activation energy,  $\varepsilon^\ddagger$ . Conservation of angular momentum currently requires that the external rotational modes with energy  $\varepsilon_r^\ddagger$  do not contribute for the activation energy,  $\varepsilon^\ddagger$ . These are called *adiabatic modes* and, conversely, the other ones are considered to be the *active modes*. Figure 8.6 illustrates the energy scheme for the RRKM mechanism, while the expression for the rate of conversion into products,  $k_2$ , is

$$k_2(\varepsilon^\ddagger) = \frac{s^\ddagger}{h} \frac{\sum P(\varepsilon_{\text{active}}^*)}{N(\varepsilon_{\text{active}}^*) F_r} \quad (8.27)$$

$s^\ddagger$  is a statistical factor similar to those presented in Section 6.1 and  $\sum P(\varepsilon_{\text{active}}^*)$  the number of vibration-rotational quantum states of the activated molecules, corresponding to all energies up to and including  $\varepsilon_{\text{active}}^\ddagger$ .  $N(\varepsilon_{\text{active}}^*)$  is the density of states having energy between  $\varepsilon^*$  and  $\varepsilon^* + d\varepsilon^*$ , i.e., the number of states per unit energy range. Finally,  $F_r$  is a factor introduced to correct for the fact that rotations may not be the same in the activated molecule as in the energised molecule.

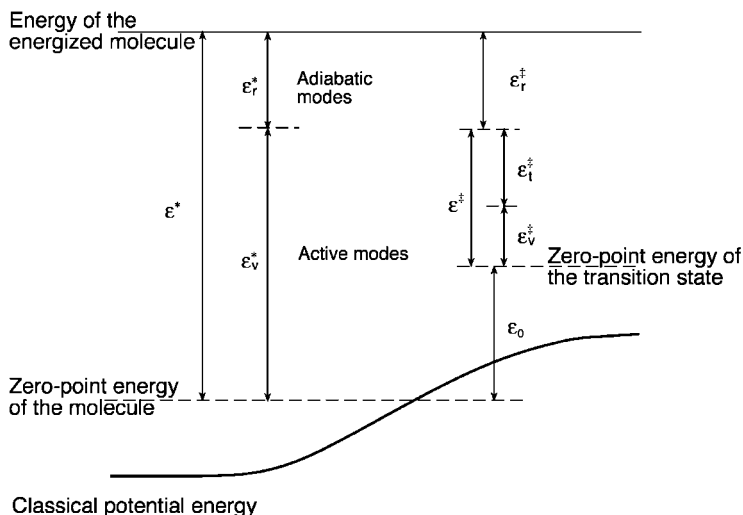


**Figure 8.6** Energy diagram in the RRKM theory.

Under such conditions, pre-exponential factors greater than  $10^{14} \text{ sec}^{-1}$  can be estimated. This is usually interpreted in terms of weakly bonded activated molecules, which have a density of states much higher than the reagents. Figure 8.5 also illustrates the application of RRKM theory to the isomerisation of cyclopropane as a function of pressure. Data were reproduced with a pre-exponential factor of  $A^\infty = 2.82 \times 10^{15} \text{ sec}^{-1}$  and an activation energy  $E_a^\infty = 274 \text{ kJ mol}^{-1}$ .

#### 8.4 LOCAL RANDOM MATRIX THEORY (LRMT)

Efficiencies of energisation and de-energisation are not entirely independent of the nature of molecules. Noble gas and other simple molecules tend to be rather ineffective in transferring energy; complex molecules are more effective. Molecules that are able to react chemically transfer more energy than non-reactive molecules. This finding is interpreted in terms of some distortion of the potential-energy surfaces when there is chemical interaction. These matters are relevant for inter-molecular energy transfer.

Intra-molecular energy transfer is also more complex than the above theories contemplate. RRKM is based on the assumption that when a molecule is energised, the vibrational energy is exchanged rapidly between the normal modes. Details of such modes are relatively unimportant. Progress in this field has revealed, however, that the phenomenological energy flow is much richer than earlier thought and can depend on the local structure of molecular vibrational states. The slowness of energy flow in energised molecules causes substantial deviations from statistical RRKM theory, notably for unimolecular reactions with low reaction barriers.

The harmonic picture of forces in a molecule is a good approximation because nuclei are much heavier than the electron, so the low-energy wave functions for nuclear motion can

be more precisely localised than electron clouds. A pure harmonic system can represent a molecule for kinetics. According to Slater, one waits for classical motions of the modes to be in phase with each other. Reaction occurs when a particular superposition of these modes causes the reaction coordinate to reach the top of the reaction barrier. The anharmonicity of the bonds, however, limits this approach because it allows energy to flow between modes.

However, even for the harmonic level of approximation one can contemplate that certain paths of motion are more facile than others. Such paths follow resonances in which a few quanta in one mode are converted into quanta of other modes, such that the total mode energy is nearly conserved.

Molecules which are not high in symmetry—the vast majority—have many localised normal modes. For ordinary covalently bonded molecules, normal or local modes, supplemented by torsional modes for conformational isomerisations, represent slow varying degrees of freedom and can be used to label privileged quantum states. Figure 8.7 presents a schematic view of the *state space* of a molecule, adapted from the work of Gruebele and Wolynes [7]. Most of the states have excitations in many modes, the so-called *interior states*. Interior states have a rich set of possible non-linear connections, allowing the energy to flow in many ways. If the molecule is sufficiently energised, many of these possible flow paths can be realised. Motion in the interior can be viewed as a sequential hopping to nearby states, limited to states differing by changes of only a few quanta numbers in a few modes. For interior states, the flow to nearby states proceeds first.

The local ways of hopping are quantified through a *local density of states*. This local density is crucial in determining the rate and manner of energy flow in the interior states. It measures the likelihood that a resonance local transfer can occur.

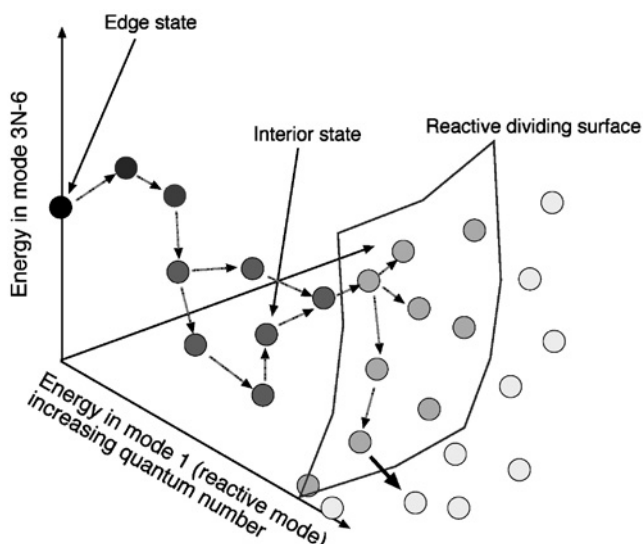


**Figure 8.7** Three of the  $3N-6$  dimensions of the molecular quantum state space. The energy of interior states flows in many ways, as opposed to the edge states. When the energy is localised in a reactive mode, the molecule can directly react as indicated by the thick arrow.

At the periphery of the state space the picture for energy flow is altogether a different one. The so-called *edge states* have nearly all their energy concentrated in a single mode. The direct paths for energy flow from edge states are limited. Instead these states decay by “dynamical tunnelling”, in which intermediate states are never populated but facilitate hopping to energy states that are nearly resonant and which are found in the interior with very different quantum numbers.

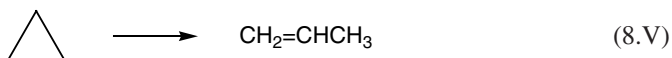
The assumptions of the limits of no randomisation and that of total randomisations are too strong, because either IVR is slow compared to the unimolecular rate for reactions with low-energy barriers and the molecule simply does not have the time to explore all the available phase space before the reaction occurs, or the motion is constrained to a subset of the available phase space. Therefore, real molecules required intermediate pictures between no randomisation and full randomisation. A model that captures this transition from facile energy flow throughout the phase space at high energies to strictly localised energy flow at low excitation is based on the LRMT due to Logan and Wolynes. One of its predictions is that near the intra-molecular vibrational redistribution (IVR) threshold, either a state is very prone to IVR, or it is not. Therefore, LRMT accommodates facts such as that nearly isoenergetic states in propyne molecule could have different IVR properties, depending on how close they are to the edge of the state space; the total density in these cases is nearly identical, but the local densities of states differ. If energy flow is slower than the reaction coordinate vibration itself, the simple RRKM rate will be in error because states depleted by reaction must be repopulated via IVR, and diffusion through the state space becomes rate determining. Such a feature shows up in the pressure dependence of the rates because rate space diffusion is facilitated by collisions.

Freed, Rice and Jortner among others have argued that the density of levels in the state space can be treated as a continuum, allowing the use of the *golden rule* formalism to describe this IVR in the intra-molecular energy transfer processes. Such an approach will be presented later in Chapter 15.

## 8.5 ENERGY BARRIERS IN THE ISOMERISATION OF CYCLOPROPANE

In the early days of the transition-state theory, there was great hope that this theory would allow quantitative predictions of rate constants, although this requires adequate pre-exponential factors and energy barriers for the reactions. The theories previously discussed are essentially concerned with the pre-exponential factors of Arrhenius-type equations. Currently energy barriers for unimolecular reactions are estimated by *ab initio* methods or by density functional theory (DFT). Such quantum-mechanical methods are particularly useful for small systems, but the numerical solution they offer are not easily related to processes of a similar kind.

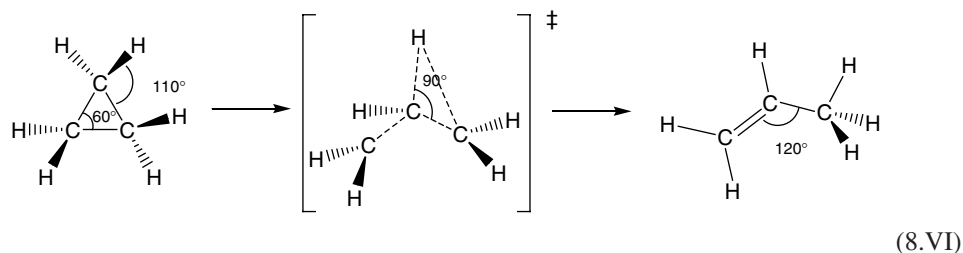
ISM can also be employed to provide some insight for unimolecular reactions. We will consider the case of the isomerisation of cyclopropane to propene.



In the high-pressure region ( $P > 10$  Torr) for the temperature range of 470–520 °C, the rate constant obeys the following expression:

$$k = 1.5 \times 10^{15} \exp\left(-\frac{272}{RT}\right) s^{-1} \quad (8.28)$$

with the energies expressed in kJ mol<sup>-1</sup> and  $\Delta E^0 = -40.5$  kJ mol<sup>-1</sup>. When this unimolecular reaction is considered to follow the mechanism



one recognises that there is breaking of a C–C bond and of a C–H bond and the formation of a new C–H bond and a  $\pi$  carbon–carbon bond. More than one reactive mode is involved in the reactants or in the products, and the reaction coordinate must be a combination of the changes occurring in all the reactive bonds.

Although the concept of reaction coordinate is central to chemical reactivity studies, we must recall that, in the absence of PES information, the definition of “the reaction coordinate” of a given reaction largely remains an educated guess based on chemical intuition. In order to define simple reaction coordinate for a multi-dimensional problem, it is convenient to define an effective force constant,  $f_{\text{eff}}$ , for the stretching of the reactive bonds up to the transition state. When changes in the different reactive bonds define a normal mode of vibration, the current procedure is to define a common force constant, e.g. for a ring, as the arithmetic average of the force constants of the individual bonds. Alternatively, when the reactive modes have local mode behaviour, simple procedure to obtain the effective force constant is to make a vectorial addition of the individual reactive bonds force constants (Figure 8.8).

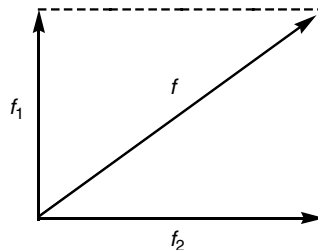


**Figure 8.8** Vectorial addition of two local modes to obtain the effective force constant for a unidimensional reaction coordinate.

We will assume the harmonic approximation for the stretching reactive modes for the isomerisation of cyclopropane. Additionally, we assume that the CCC angle at the transition state is intermediate ( $\theta^\ddagger = 90^\circ$ ) between the value in the reactants ( $60^\circ$ ) and that in the products ( $120^\circ$ ), as illustrated in Scheme 8.VI. If such modes have a local character, with force constants  $f_i$ , the effective force constant is just the result of a vectorial addition as shown in Figure 8.8. Generalising for three bonds, in order to encompass the CH bond perpendicular to the CC bonds, one obtains the following expression:

$$f_{\text{eff}} = \sqrt{f_{\text{CC}}^2 + f_{\text{CC}}^2 + f_{\text{CH}}^2} \quad (8.29)$$

Relying on the values known for the relevant force constants,  $f_{\text{C-C}} = 2.7 \times 10^3 \text{ kJ mol}^{-1} \text{\AA}^{-2}$  and  $f_{\text{C-H}} = 2.9 \times 10^3 \text{ kJ mol}^{-1} \text{\AA}^{-2}$ , eq. (8.29) leads to  $f_{\text{eff}} = 4.8 \times 10^3 \text{ kJ mol}^{-1} \text{\AA}^{-2}$ . For consistency, the effective structural data is estimated as  $l_r + l_p = (2 l_{\text{C-C}} + l_{\text{C-H}})(2/3)$ ; the factor (2/3) is required to impose the equivalent to the sum of two bond lengths. The equilibrium bond length data to be employed is  $l_{\text{C-C}} = 1.54 \text{ \AA}$ ,  $l_{\text{C-H}} = 1.1 \text{ \AA}$ . This leads to  $l_r + l_p = 2.79 \text{ \AA}$ . From eqs. (6.93), (6.103) and (6.106) with  $\Delta E^0 = -40.5 \text{ kJ mol}^{-1}$  and a total bond order at the TS of  $m = 2n^\ddagger = 1$ , one obtains the contribution for the energy barrier due to the reactive stretching modes,  $\Delta E_{\text{stretch}}^\ddagger = 200 \text{ kJ mol}^{-1}$ .

The isomerisation process also requires changes in the bending modes of CCC and CCH. The minimum energy required for harmonic bending motions is

$$\Delta E_{\text{bend}}^\ddagger = \frac{1}{2} f_{\text{CCX}} (\theta^\ddagger - \theta_0)^2 \quad (8.30)$$

where  $\theta_0$  and  $\theta^\ddagger$  are the angles for reactants and transition state, respectively. The estimate of this contribution for the energy barrier is made under thermoneutral conditions, since the exothermicity of the reaction was taken into due account in the stretching contribution for the energy barrier. With the relevant data  $f_{\text{CCC}} = 0.146 \text{ kJ mol}^{-1} \theta^{-2}$ ,  $f_{\text{CCH}} = 0.1 \text{ kJ mol}^{-1} \theta^{-2}$  and for the CCC angle,  $\theta_0 = 60^\circ$  and  $\theta^\ddagger = 90^\circ$ , eq. (8.30) leads to a bending contribution of  $\Delta E_{\text{CCC}}^\ddagger = 66 \text{ kJ mol}^{-1}$  for the changes in the CCC angle. For the CCH angle, one has  $\theta_0 = 110^\circ$  and  $\theta^\ddagger = 90^\circ$ , and the contribution for the energy barrier is  $\Delta E_{\text{CCH}}^\ddagger = 20 \text{ kJ mol}^{-1}$ .

The estimated overall barrier for the isomerisation of cyclopropane is, consequently, the sum of these three contributions,  $\Delta E^\ddagger = 286 \text{ kJ mol}^{-1}$ . It is not so much the close agreement of the estimated barrier with experiment that is important, but the insight which the ISM methodology provides for understanding mechanistic details of this unimolecular reaction.

## REFERENCES

- [1] FA Lindemann, *Trans. Faraday Soc.* **17** (1922) 598.
- [2] MC King, KJ Laidler, *Arch. Hist. Exact. Sci.* **30** (1983) 45.
- [3] CN Hinshelwood, *Proc. Roy. Soc. A* **113** (1927) 230.
- [4] HO Pritchard, RG Sowden, AF Trotman-Dickenson, *Proc. Roy. Soc. A* **217** (1953) 563.
- [5] RA Marcus, *J. Chem. Phys.* **20** (1952) 364.
- [6] GM Wieder, RA Marcus, *J. Chem. Phys.* **37** (1962) 1835.
- [7] M Gruebele, PG Wolynes, *Acc. Chem. Res.* **37** (2004) 261–267.

## - 9 -

# Elementary Reactions in Solution

### 9.1 SOLVENT EFFECTS ON REACTION RATES

With reactions in solution, the solvent is generally present at a much higher concentration than the reactants and its concentration is approximately constant during the course of a reaction. If the solvent is also one of the reactants, as with water in hydrolyses or in the example of recombination of carbocations with water molecules we discussed previously, the order with which the solvent participates in the reaction rate cannot be obtained by kinetic studies in this solvent. To get this, we need kinetic studies with solvent mixtures or isotopically labelled molecules, spectroscopic studies, etc.

In other systems, the solvent only acts as an inert medium where reaction occurs without affecting the mechanism. This appears to be the case of the decomposition of nitrogen pentoxide, in which the pre-exponential factor and the activation energy are very similar in the gas phase and in solvents of various types, as shown in Table 9.1.

A more subtle effect of solvent is seen in the reactions first studied by Menschutkin [1], and which take his name. An example is the reaction



whose rate and equilibrium constants have been studied in a wide range of solvents [2].

The results shown in Table 9.2 indicate that the rate constants decrease by a factor of 140 times on going from acetonitrile to benzene. This solvent effect occurs without any change in mechanism, but what causes it? Note, that there is also an effect in the same solvents on the free energy of reaction,  $\Delta G^\circ$ , which is seen as a decrease in the equilibrium

Table 9.1

Decomposition of  $\text{N}_2\text{O}_5$

Reaction medium	$\log A$ ( $\text{dm}^3 \text{ mol}^{-1} \text{ sec}^{-1}$ )	$E_a$ ( $\text{kJ mol}^{-1}$ )
Gas phase	13.6	103.3
Chloroform	13.7	102.7
Nitromethane	13.5	102.5
Pentachloroethane	14.0	104.6

**Table 9.2**

Effect of solvent on the Menschutkin reaction

Solvent	$\Delta G^\ddagger$ (kJ mol <sup>-1</sup> )	$\Delta G^0$ (kJ mol <sup>-1</sup> )	$n^\ddagger$ <sup>a</sup>	$\beta_{KT}$
Acetonitrile	98.5	-19.0	0.628	0.40
Nitrobenzene	100.0	-14.6	0.628	0.30
Acetone	100.4	-12.1	0.630	0.48
Tetrahydrofurane	105.2	1.9	0.633	0.54
Benzene	110.7	6.1	0.623	0.10

<sup>a</sup>Value which reproduces the activation energy using harmonic oscillators to describe the C–I bond ( $f_{CI} = 1.6 \times 10^3$  kJ mol<sup>-1</sup> Å<sup>-2</sup> and  $l_{CI} = 2.207$  Å) in the reactants and the NC bond ( $f_{NC} = 2.95 \times 10^3$  kJ mol<sup>-1</sup> Å<sup>-2</sup> and  $l_{NC} = 1.472$  Å) in the products.

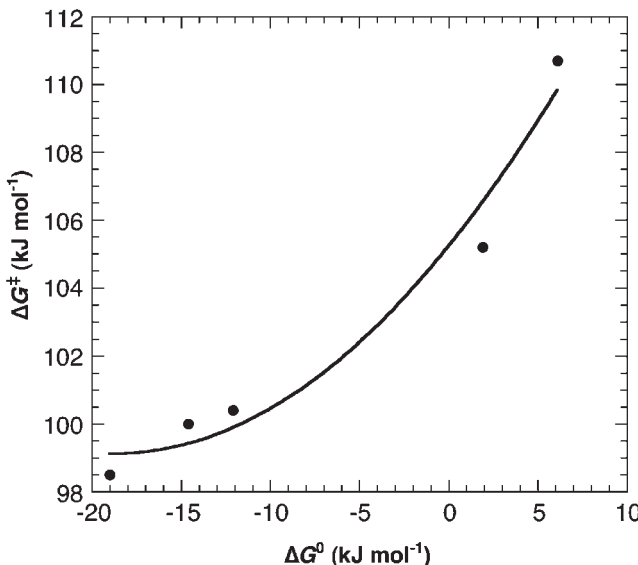


**Figure 9.1** Variation of activation energy with reaction energy, for the Menschutkin reaction (data from Table 9.2).

constant by a factor of  $2.5 \times 10^4$ . However, as shown in Figure 9.1, this does not correspond to a linear correlation between kinetic and thermodynamic parameters.

What seems to be happening is that, though the solvent does produce an effect on  $\Delta G^0$ , at the same time there is a change in the bond order of the transition state,  $n^\ddagger$ . According to Figure 9.2, this can be correlated with the Kamlet–Taft solvent parameter  $\beta_{KT}$ , which is an empirical measure of the capacity of the solvent to coordinate via the donation of a pair of non-bonding electrons, i.e. the solvent acts as a Lewis base.

This effect of the solvent lone pair can be rationalised in terms of attraction by the positive part of the amine dipole, which leads to an increase in  $n^\ddagger$ , due to an increase in electron density in the N–C bond, as indicated diagrammatically in Figure 9.3.

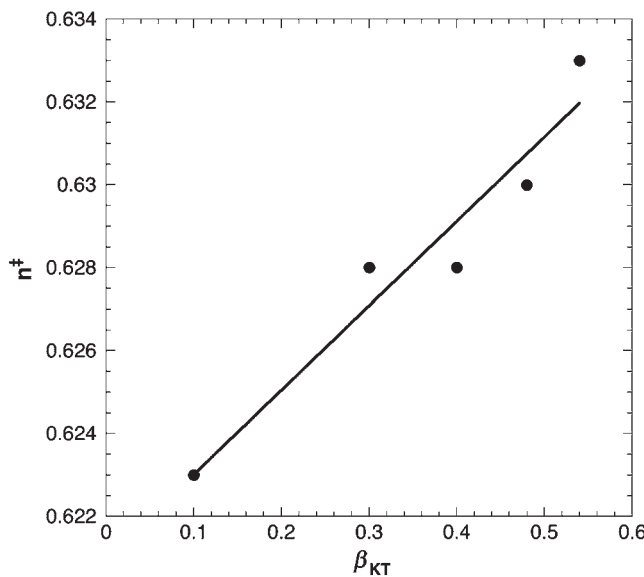


**Figure 9.2** Correlation of transition state bond order ( $n^{\ddagger}$ ) and the Kamlet-Taft  $\beta_{KT}$  parameter for the Menschutkin reaction (data from Table 9.2). The intercept has a value  $n^{\ddagger} = 0.62$ .

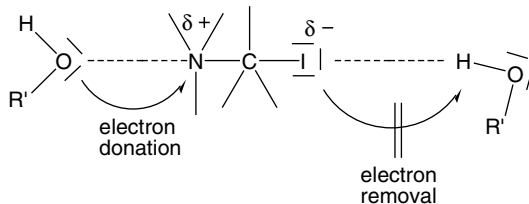


**Figure 9.3** Changes in electron density produced by electron donation and withdrawal by the solvent.

In addition to these limits of a solvent acting as an inert medium or as an active chemical or electronic species in the transition state, we will see a number of other effects of a more physical nature can occur, as will be discussed in the following sections.

## 9.2 EFFECT OF DIFFUSION

With reactions in solution, even when the medium is chemically inert, the solvent will exert an effect as a consequence of it being a condensed phase, with its molecules very close together. As a consequence, the distribution of collisions is much more important than their frequency, which is comparable, but generally 2–3 times greater in liquids than in gases. As seen in a simulation below (Figure 9.4) due to Rabinowitch and

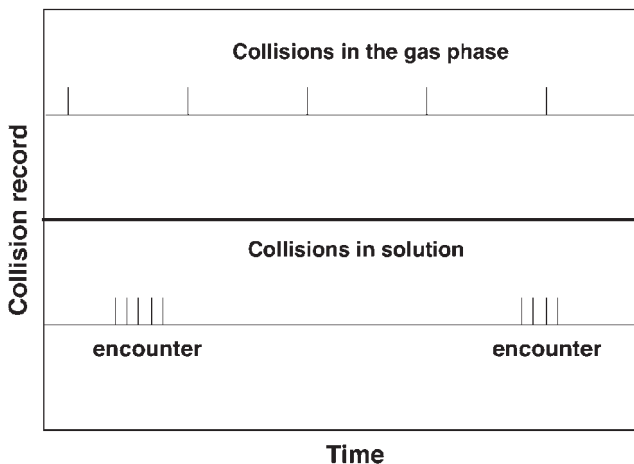
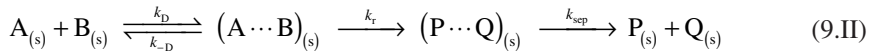


**Figure 9.4** Contrast between collisions in the gas phase and encounters between the same two reactants in the solvent cage in a liquid.

Wood [3], while collisions between molecules in the gas phase are separated by reasonable time intervals; in liquids, collisions occur in groups of rapid sequences, known as encounters.

In each encounter between two reactants, the molecules undergo at least four collisions, until they manage to escape the cage of solvent molecules which surround them. However, the frequency of these encounters is about 100 times lower than that for collisions of the same molecules in the gas phase.

Based on this, a reaction in solution can be broken down into three steps: (1) diffusion of reactants from bulk solution to the collision distance; (2) chemical reaction of the reacting species within the solvent cage; and (3) diffusion of the products from the solvent cage to bulk solution. We can represent these processes in the following kinetic scheme:



The rate of reaction, measured by the decrease in concentration of species A, is given by the expression:

$$-\frac{d[A]}{dt} = k_D [A][B] - k_{-D} [A \cdots B] \quad (9.1)$$

and the formation of the encounter pair or complex,  $(AB)_{(s)}$ , between reactants A and B is

$$\frac{d[A \cdots B]}{dt} = k_D [A][B] - k_{-D} [A \cdots B] - k_r [A \cdots B] \quad (9.2)$$

Assuming steady-state conditions for  $(AB)_s$ ,  $d[(AB)_s]/dt = 0$ , such that from the previous equation

$$[A \cdots B] = \frac{k_D [A][B]}{k_{-D} + k_r} \quad (9.3)$$

Substitution for  $[(AB)_s]$  into eq. (9.1) leads to the reaction rate

$$-\frac{d[A]}{dt} = k_D [A][B] - k_{-D} k_D \frac{[A][B]}{k_{-D} + k_r} \quad (9.4)$$

which, on rearranging, gives

$$-\frac{d[A]}{dt} = \frac{k_r k_D}{k_{-D} + k_r} [A][B] \quad (9.5)$$

Eq. (9.5) shows two limiting conditions in the reaction kinetics,  $k_r \ll k_{-D}$  and  $k_r \gg k_{-D}$ . In the first case, the reaction rate is given by the expression:

$$-\frac{d[A]}{dt} = k_r \frac{k_D}{k_{-D}} [A][B] \quad (9.6)$$

This is the limit of reaction (or activation) control; the rate in solution is controlled by the activation-controlled reaction between the reactants,  $k_r$ . The second limit corresponds to diffusional control, where the rate of reaction is controlled by the rate of diffusion of the reactants,  $k_D$ .

$$-\frac{d[A]}{dt} = k_D [A][B] \quad (9.7)$$

An example of the transition of a process controlled by chemical reaction to one controlled by diffusion is found in the electron transfer between excited aromatic hydrocarbons ( $D^*$ ), and various nitriles A in heptane



The aromatic hydrocarbons are stronger reducing agents when electronically excited than in the ground state, and can donate an electron to a species A. The rate of this electron transfer depends on the ease with which A is reduced, and the reaction follows a linear free-energy relationship. When  $\Delta G^0$  is sufficiently small, such that  $k_r \gg k_{-D}$ , then the reaction is diffusion controlled, with a rate constant which is constant and is independent of the reaction energy. These effects are indicated in Figure 9.5.

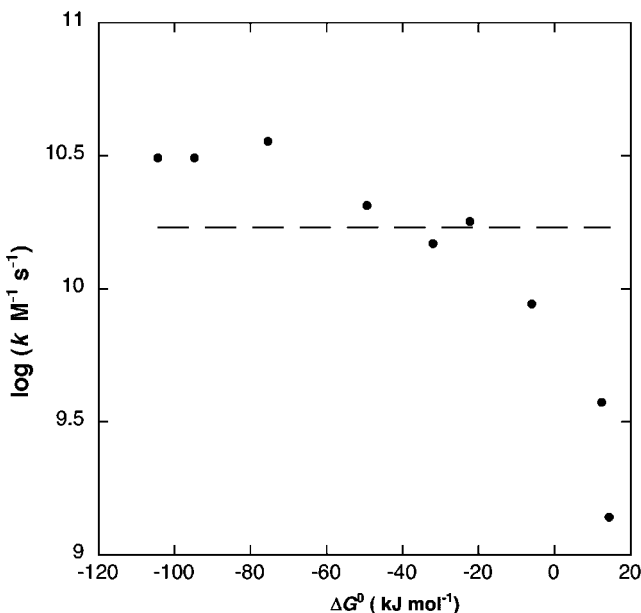
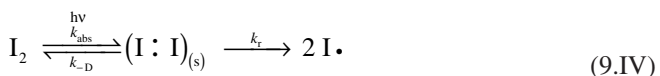


**Figure 9.5** The change from diffusional control to reaction control in electron transfer between electronically excited aromatic hydrocarbons and nitriles in heptane at room temperature. The dashed line is diffusion rate constant calculated with eq. (9.23) using the viscosity of heptane. (Courtesy Carlos Serpa.)

Another example, also involving a photochemical reaction in solution, is the decomposition of molecular iodine and the reverse process of recombination of iodine atoms within the solvent cage.



This is a *primary recombination* process, which can be distinguished from *secondary recombination* reactions, which occur after the two atoms have separated.

The yield of formation of atomic iodine is twice that of disappearance of molecular iodine. Under steady-state conditions for  $(\text{I:I})_{\text{s}}$ , the reaction rate takes the form

$$v = \frac{k_{\text{abs}} k_r}{k_{-D} + k_r} [\text{I}_2] \quad (9.8)$$

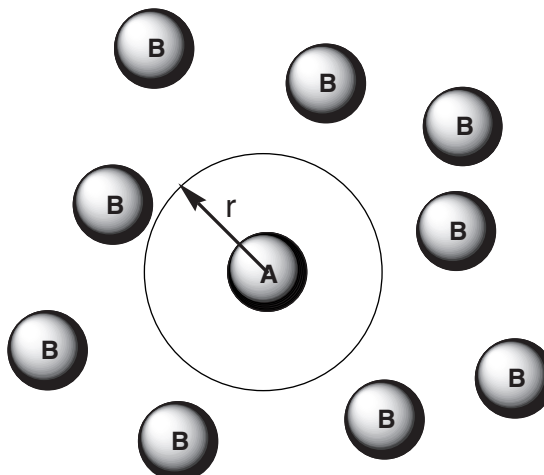
The yield of  $\text{I}_2$  loss is the ratio of the rate of formation of  $2\text{I}$  to the total rate of dissociation of  $(\text{I:I})_{\text{s}}$

$$\phi_{21} = -\phi_{\text{I}_2} = \frac{k_r}{k_{-D} + k_r} \quad (9.9)$$

**Table 9.3**

Yield of decomposition of molecular iodine in a photo-induced reaction

Solvent	$-\phi_{I_2}$	$\eta_s m\rho$
Hexane	0.5	4.0
Carbon tetrachloride	0.11	9.5
Hexachlorobuta-1,3-diene	0.0042	>30

**Figure 9.6** Molecules A in solution surrounded by B.

When the process is diffusion controlled, this yield depends on the solvent viscosity,  $\eta_s$ , and, as we will see shortly, the diffusion constants present an inverse relation with  $\eta_s$ . Data for this reaction are given in Table 9.3. This cage effect becomes more significant when the solvents have a high viscosity, and in this case the highest primary recombination yields are observed. This cage effect is known as the *Franck–Rabinowitch effect*.

To obtain a more detailed understanding of the kinetics of these reactions, we will now see how we can estimate the diffusion constants of reactants.

### 9.3 DIFFUSION CONSTANTS

We will start by considering an uncharged molecule A surrounded by a statistically symmetrical distribution of B molecules (Figure 9.6). The flow,  $J$ , of B molecules in the direction towards A can be considered to be the flow of B molecules which cross a sphere centred on A, with radius  $r$ .

This flow is defined in terms of Fick's first law of diffusion as

$$J \equiv \frac{dn}{dt} = -DA \frac{dc}{dx} \quad (9.10)$$

where  $dn$  represents the number of moles of substance which diffuses across a surface of area  $A$ ,  $D$  the diffusion coefficient and  $dc/dx$  the concentration gradient. For the moment we will consider that molecule A is stationary. The negative sign is due to diffusion being in the direction of lower concentration. The surface of the sphere centred on A, radius  $r$  is  $A = 4\pi r^2$ , such that from eq. (9.10), we have

$$J \equiv \frac{dn_B}{dt} = 4\pi r^2 D_B \frac{dc_B}{dr} \quad (9.11)$$

Here the concentration gradient,  $dc_B/dr$ , takes the increase of the radius as reference, such that the negative sign disappears. Thus, the concentration gradient becomes

$$\frac{dc_B}{dr} = \frac{J_B}{4\pi r^2 D_B} \quad (9.12)$$

Integrating this equation with the limits of concentration of B at the distance  $r$  from A,  $c_{B_0}$ , and the concentration of B in the bulk solution ( $r=\infty$ ), represented as  $[B]$

$$\int_{c_{B_0}}^{[B]} dc_B(r) = \frac{J_B}{4\pi D_B} \int_r^\infty \frac{1}{r^2} dr \quad (9.13)$$

gives

$$c_B \Big|_{c_{B_0}}^{[B]} = -\frac{J_B}{4\pi D_B} \frac{1}{r} \Big|_r^\infty \quad (9.14)$$

which leads to

$$c_{B_0} = -\frac{J_B}{4\pi D_B r} + [B] \quad (9.15)$$

This result is valid for the conditions where A is stationary. However, as in practice this species also diffuses, the equation should be modified to include the two diffusion coefficients

$$c_{B_0} = -\frac{J_B}{4\pi(D_B + D_A)r} + [B] \quad (9.16)$$

When the reaction is totally controlled by diffusion at the microscopic level, B reacts very rapidly with A when they are separated by a critical distance,  $d_{AB}$ . Therefore, when  $r = d_{AB}$  the concentration  $c_{B_0} = 0$ . This is because there is reaction between A and B on every

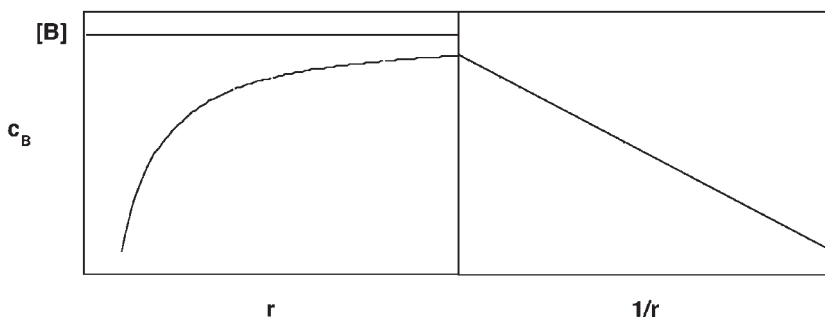


**Figure 9.7** Concentration B as a function of distance from A for a reaction completely controlled by diffusion, following eq. (9.16).

encounter. Therefore, from eq. (9.16), we obtain

$$J_B = 4\pi(D_B + D_A)d_{AB}[B] \quad (9.17)$$

The graph of concentration of B as a function of distance is shown in Figure 9.7.

The rate of reaction involving all molecules of A becomes

$$v = 4\pi(D_B + D_A)d_{AB}[A][B] \quad (9.18)$$

and the diffusion-controlled rate constant is

$$k_D = 4\pi(D_B + D_A)d_{AB} \quad (9.19)$$

The *Système International* (SI) units for  $D_A$  and  $D_B$  are  $\text{m}^2 \text{ sec}^{-1}$ , such that  $k_D$  will have the units  $\text{m}^3 \text{ sec}^{-1}$ . Normally in chemical kinetics we use molar quantities and litres, which requires multiplying  $k_D/\text{m}^3 \text{ sec}^{-1}$  by the Avogadro number  $N_A$  and by  $10^3$  to give

$$k_D = 4\pi 10^3 N_A (D_B + D_A) d_{AB} \quad \text{dm}^3 \text{ mol}^{-1} \text{ sec}^{-1} \quad (9.20)$$

When the diffusion coefficients are not known, we can determine them from the Stokes–Einstein equation

$$D = \frac{k_B T}{6\pi\eta_s r} \quad (9.21)$$

where  $\eta_s$  is the solvent viscosity. The Stokes–Einstein equation is valid when the solute molecules are much bigger than those of the solvent. The sum of the diffusion coefficients is approximately

$$D_A + D_B = \frac{k_B T}{6\pi\eta_s} \left( \frac{1}{r_A} + \frac{1}{r_B} \right) \quad (9.22)$$

And, taking  $d_{AB} = r_A + r_B$ , substitution of eq. (9.22) into eq. (9.20) leads to the diffusion-controlled rate constant

$$k_D = \frac{2k_B T}{3\eta_s} \frac{(r_A + r_B)^2}{r_A r_B} \quad (9.23)$$

If the molecules have the same size (i.e.  $r_A = r_B$ ), we obtain

$$k_D = \frac{8k_B T}{3\eta_s} \quad (9.24)$$

The rate constant  $k_{-D}$  is the reciprocal of the time in which A and B remain as nearest neighbours, which, in the absence of any specific interactions between A and B will be

$$k_{-D} = \frac{6(D_A + D_B)}{d_{AB}^2} \quad (9.25)$$

When the reactions are controlled by diffusion, the rate will be proportional to the reciprocal of the solvent viscosity, as shown by eqs. (9.7) and (9.24), and Table 9.4. The typical activation energy of diffusion in solution is fairly small, *ca.* 15 kJ mol<sup>-1</sup>. Figure 9.8 shows an Arrhenius plot of one of the systems in Figure 9.5 under the diffusion-controlled regime, but measured in isopropyl ether. The experimental activation energy for this system in this solvent is 11 kJ mol<sup>-1</sup>, and is entirely due to the temperature dependence of the viscosity.

**Table 9.4**

Diffusion controlled rate constants calculated from eq. (9.24) and viscosities for some common solvents at 25 °C

Solvent	Viscosity <sup>a</sup> ( $\eta$ ) (mPa sec)	$k_{\text{diff}}^b$ (M <sup>-1</sup> sec <sup>-1</sup> )
Carbon dioxide	0.0577 <sup>c</sup>	$1.2 \times 10^{11}$
Diethyl ether	0.222	$3.0 \times 10^{10}$
Hexane	0.294	$2.2 \times 10^{10}$
Acetone	0.316	$2.1 \times 10^{10}$
Toluene	0.558	$1.2 \times 10^{10}$
Decane	0.861	$7.7 \times 10^9$
Water	0.890	$7.4 \times 10^9$
Ethanol	1.083	$6.1 \times 10^9$
Propan-2-ol	2.044	$3.2 \times 10^9$
Ethylene glycol	19.9 <sup>d</sup>	$3.3 \times 10^8$
Glycerol	945	$7.0 \times 10^6$

<sup>a</sup>From *Handbook of Chemistry and Physics*. 59th Edn. (ed. RC Weast), CRC Press, West Palm Beach, FA, 1979.

<sup>b</sup>Using viscosities in mPa sec, it is necessary to multiply by 10<sup>6</sup> to get values in M<sup>-1</sup> sec<sup>-1</sup>.

<sup>c</sup>At 35 °C and 10 MPa, in the supercritical phase, from <http://webbook.nist.gov/>.

<sup>d</sup>At 20 °C.

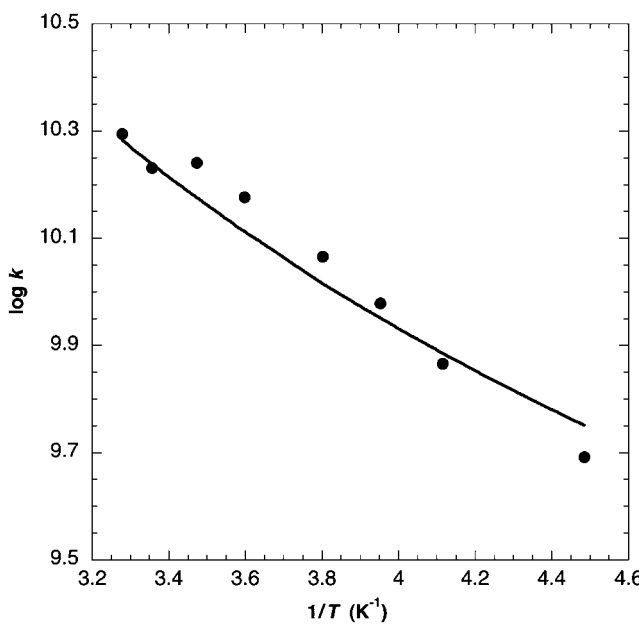


**Figure 9.8** Temperature dependence of electron transfer between electronically excited naphthalene and fumaronitrile in isopropyl ether. The line is the diffusion rate constant calculated at the different temperatures. (Courtesy Paulo Gomes.)

Although from eq. (9.23) the diffusion-controlled constant,  $k_D$ , depends on the size of molecules, according to

$$\frac{(r_A + r_B)^2}{r_A r_B} = 2 + \frac{r_A}{r_B} + \frac{r_B}{r_A} \quad (9.26)$$

With the normal range of sizes of molecules of interest, this only shows a modest change with  $r_A/r_B$ . For example, the ratio of eq. (9.26) will be 4.5 for  $r_A/r_B = 2$  and 4.0 with  $r_A/r_B = 1$ . However, dramatic effects can be seen when one of the species is a polymer, and the other is a small molecule. For example, with the case given in Chapter 3 of triplet energy transfer in benzene from biphenyl to the polymer MEH-PPV, of molecular weight  $1.5 \times 10^6$ , the experimental rate constant is  $1.97 \times 10^{11} \text{ dm}^3 \text{ mol}^{-1} \text{ sec}^{-1}$  [4], which can be compared with the normal diffusion controlled rate constant in benzene at 25 °C ( $1.1 \times 10^{10} \text{ dm}^3 \text{ mol}^{-1} \text{ sec}^{-1}$ ) [5]. Using eq. (9.23) and reasonable estimates for the polymer and biphenyl size, we can calculate a value  $k_D = 1.2 \times 10^{11} \text{ dm}^3 \text{ mol}^{-1} \text{ sec}^{-1}$  for this system.

For reactions between species of similar size in water at 25 °C, eq. (9.24) leads to a value of the diffusion-controlled rate constant for neutral species of  $7 \times 10^9 \text{ dm}^3 \text{ mol}^{-1} \text{ sec}^{-1}$ . This is probably an underestimate, and in Table 9.5, some experimental rate constants are given for diffusion-controlled reactions in water.

**Table 9.5**

Experimental rate constants for some typical diffusion controlled reactions in aqueous solutions<sup>a</sup>

Reaction	$k$ ( $10^9 \text{ M}^{-1}\text{sec}^{-1}$ )
$\text{H}^\cdot + \text{H}^\cdot \rightarrow \text{H}_2$	7.75
$\text{H}^\cdot + \cdot\text{OH} \rightarrow \text{H}_2\text{O}$	7.0
$\cdot\text{OH} + \cdot\text{OH} \rightarrow \text{H}_2\text{O}_2$	5.5
$\cdot\text{OH} + \text{OH}^- \rightarrow \text{O}^{3-} + \text{H}_2\text{O}$	13
$\text{H}^\cdot + \text{O}_2 \rightarrow \text{HO}_2^\cdot$	21
$\text{H}^\cdot + \text{Fe}(\text{CN})_6^{3-} \rightarrow \text{H}^+ + \text{Fe}(\text{CN})_6^{4-}$	6.3
$\text{C}_6\text{H}_6$ (benzene) + $\cdot\text{OH} \rightarrow \text{C}_6\text{H}_6\text{OH}^\cdot$	7.8

<sup>a</sup>Data selected from ref. [6].

**Table 9.6**

Rate constants for reactions of hydrated electrons ( $e_{\text{aq}}^-$ ) with charged and uncharged species in aqueous solution<sup>a</sup>

Reaction	$k$ ( $10^{10} \text{ M}^{-1}\text{sec}^{-1}$ )
$e_{\text{aq}}^- + \text{H} \rightarrow \text{H}_2 + \text{OH}^-$	2.5
$e_{\text{aq}}^- + e_{\text{aq}}^- \rightarrow \text{H}_2 + 2\text{OH}^-$	0.55
$e_{\text{aq}}^- + \text{OH}^\cdot \rightarrow \text{OH}^-$	3.0
$e_{\text{aq}}^- + \text{H}^+ \rightarrow \text{H}^\cdot$	2.3
$e_{\text{aq}}^- + \text{O}_2 \rightarrow \text{O}_2^{2-}$	1.9
$e_{\text{aq}}^- + \text{O}_2^{2-} \rightarrow \text{O}_2^{2-}$	1.3
$e_{\text{aq}}^- + \text{Ag}^+ \rightarrow \text{Ag}(0)$	3.7
$e_{\text{aq}}^- + \text{Cu}^{2+} \rightarrow \text{Cu}^+$	3.3
$e_{\text{aq}}^- + \text{UO}_2^{2+} \rightarrow \text{UO}_2^+$	1.7
$e_{\text{aq}}^- + \text{Co}(\text{NH}_3)_6^{3+} \rightarrow \text{Co}(\text{NH}_3)_6^{2+}$	8.8
$e_{\text{aq}}^- + \text{Au}(\text{CN})_2^- \rightarrow \text{Au}(0) + 2\text{CN}^-$	0.35
$e_{\text{aq}}^- + \text{Al}(\text{OH})_4^{2-} \rightarrow \text{Al}(\text{OH})_4^{2-}$	0.00055
$e_{\text{aq}}^- + \text{Fe}(\text{CN})_6^{3-} \rightarrow \text{Fe}(\text{CN})_6^{4-}$	0.31
$e_{\text{aq}}^- + \text{C}_6\text{H}_6$ (benzene) $\rightarrow \text{C}_6\text{H}_7^\cdot$	0.0009
$e_{\text{aq}}^- + \text{coenzyme B12} \rightarrow \text{reduced form}$	3.2

<sup>a</sup>Data selected from ref. [6].

For reactions between species of charge  $Z_1e$  and  $Z_2e$ , eq. (9.24) needs to be modified to allow for the electrostatic attraction or repulsion between ions

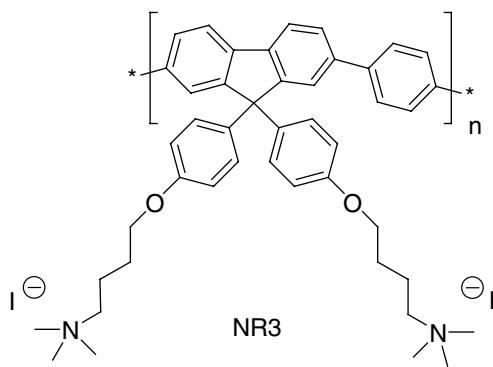
$$k_D = \frac{8k_B T}{3\eta_s} \frac{\delta}{\exp(\delta) - 1} \quad (9.27)$$

with

$$\delta = \frac{Z_A Z_B e^2}{4\pi \epsilon k_B T d_{AB}} \quad (9.28)$$

where  $\epsilon$  is the relative permittivity of the solvent. This equation shows that reactions between oppositely charged species will have diffusion-controlled rate constants greater than those for uncharged neutral molecules. For example, with  $Z_1 Z_2 = -2$  in water, rate constants are about 3 times faster than those involving uncharged species. In contrast, with ions of the same charge, the diffusion-controlled rate constants will be less than with neutral molecules; for  $Z_1 Z_2 = 2$  in water,  $k_D(\text{ions})/k_D(\text{neutral molecules}) \approx 1/5$ . Some typical values for reaction of hydrated electrons with charged species are given in Table 9.6.

A particularly dramatic example of the effect of charge on diffusion-controlled reaction is seen with the conjugated polyelectrolyte NR3 and the solvated electron,



where the rate constant is  $5.4 \times 10^{12} \text{ dm}^3 \text{ mol}^{-1} \text{ sec}^{-1}$ . From this, the charge NR3 is calculated to be +13, which is in reasonable agreement with that expected from the size of the polymer, assuming complete ionisation.

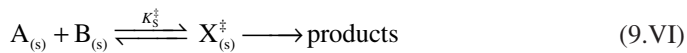
We should note that for very fast reactions produced by either photoexcitation or high-energy radiation, the initial distribution of reactants is not homogeneous, and that the diffusional rate constants are time dependent.

## 9.4 REACTION CONTROL

With reactions in solution which are not controlled by diffusion, similar chemical considerations are involved to those given earlier, and again we resort to TST. However, because of problems, in particular, of standard states and activities, there are difficulties in formulation of partition functions for species solution. The best way of applying TST in this case involves the thermodynamic formulation of CTST (Conventional Transition State Theory). Within this, the reaction rate is directly proportional to the concentration of the activated complexes.

$$v = \frac{k_B T}{h} [X^*] \quad (9.29)$$

For a bimolecular reaction



the activation equilibrium constant is given by the expression

$$K_s^{\ddagger} = \frac{\gamma_{\ddagger} [X^{\ddagger}]}{\gamma_A [A] \gamma_B [B]} \quad (9.30)$$

in which  $\gamma_A$  and  $\gamma_B$  are the activity coefficients for the reactants and  $\gamma_{\ddagger}$  for the activated complex. Substituting eq. (9.30) into eq. (9.29) gives

$$v = \frac{k_B T}{h} K_s^{\ddagger} \frac{\gamma_A \gamma_B}{\gamma_{\ddagger}} [A][B] \quad (9.31)$$

from which, the rate constant will be

$$k_s = \frac{k_B T}{h} K_s^{\ddagger} \frac{\gamma_A \gamma_B}{\gamma_{\ddagger}} \quad (9.32)$$

The activity coefficient of the transition state  $\gamma_{\ddagger}$  enters into the expressions for the reaction rate and rate constant since the concentration of activated complexes comes from the activation equilibrium constant. If the reaction rate depends on the activity of the transition state,  $a_{\ddagger} = \gamma_{\ddagger}[X^{\ddagger}]$ , then the overall rate of reaction will depend on the activity coefficients of the reactants.

As with ideal gases in the gas phase the activity coefficients are equal to one, we get

$$k_g = \frac{k_B T}{h} K_g^{\ddagger} \quad (9.33)$$

and

$$k_s = k_g \frac{\gamma_A \gamma_B}{\gamma_{\ddagger}} \quad (9.34)$$

When rate constants are equal in the gas phase and solution, this implies  $(\gamma_A \gamma_B)/\gamma_{\ddagger} = 1$ . For unimolecular reactions where this is true, such as the decomposition of  $N_2O_5$ , this is due to the structures of the activated complexes being similar in the two media. However, in the closely related case of decomposition of nitric acid, the reaction rate is significantly lower in solution than in the gas phase, probably as a result of complexation between the reactant and solvent.

We will compare now the behaviour in two different solvents. The activity coefficients are based on a convenient standard state, usually infinite dilution of the solutes. With this reference state, the rate constant is given by

$$k_0 = \frac{k_B T}{h} K_0^{\ddagger} \quad (9.35)$$

Applying CTST for first-order reactions, with

$$E_a = \Delta H^{\ddagger 0} + RT \quad (9.36)$$

and

$$k = \frac{k_B T}{h} \exp\left(\frac{\Delta S^{\ddagger 0}}{R}\right) \exp\left(-\frac{E_a - RT}{RT}\right) \quad (9.37)$$

or

$$k = e \frac{k_B T}{h} e^{S\Delta^0 t/R} e^{-E_a/RT} \quad (9.38)$$

The estimation of various activation entropies for non-polar molecules in solution showed that the pre-exponential factors are about 3 times greater than in the gas phase. This is close to the ratios of the collision frequencies in the two media.

#### 9.4.1 Internal pressure

Attractive forces between molecules vary inversely with the intermolecular separation,  $r$ , with a dependence  $r^{-6}$ , such that their magnitude is appreciable when distances are close to molecular diameters. This is true for liquids, and such cohesion forces are responsible for many of the properties of this state of matter. Cohesion forces are also present in the gas phase and are responsible for the van der Waals ( $a/V^2$ ) correction to the *internal pressure*.

However, in liquids, repulsive forces also operate at short intermolecular distances to balance the attractive, cohesive intermolecular forces. This leads to

$$P_i dV = \left( \frac{\partial E}{\partial V} \right)_T dV \quad (9.39)$$

or

$$P_i = \left( \frac{\partial E}{\partial V} \right)_T \quad (9.40)$$

From these equations, an internal pressure  $P_i$  can be defined in terms of its effect on the internal energy of the liquid. For any substance, we can show

$$\left( \frac{\partial E}{\partial V} \right)_T = T \left( \frac{\partial P}{\partial T} \right)_V - P \quad (9.41)$$

in which  $P$  is the *external pressure*, and given that this is, in general, much less the internal pressure. So we can also write

$$P_i = T \left( \frac{\partial P}{\partial T} \right)_V \quad (9.42)$$

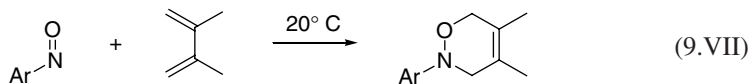
The internal pressure can be estimated experimentally by studying the increase in pressure with the temperature. If we take  $\alpha$  as the coefficient of thermal expansion of the liquid and  $\beta$  its compressibility coefficient, given by

$$\left( \frac{\partial P}{\partial T} \right)_V = \left( \frac{\partial P}{\partial V} \right)_T \left( \frac{\partial V}{\partial T} \right)_P \quad (9.43)$$

then

$$P_i = T \frac{\alpha}{\beta} \quad (9.44)$$

The solvent internal pressure can induce changes in the reaction kinetics when specific solvent–solute interactions are weak, and the activation volumes involved, which we will discuss later, are substantial. An example involves the kinetics of the Diels–Alder reaction between 4-bromonitrosobenzene and 2,3-dimethylbutadiene in solutions of various inorganic perchlorates in acetone [7]



where rates correlate linearly with the effective internal pressure of the solutions (Figure 9.9). Here, the increase in the effective internal pressure depends on the nature of the cation [8].

Hildebrand and Scott developed expressions for the activity coefficients of non-electrolytes in terms of molar volumes,  $V_x$ , and energies of vaporisation,  $L_x$ . These are related to average internal pressure through

$$P_{i,x} = \frac{L_x}{V_x} \quad (9.45)$$

If we take  $k_0$  as the rate constant under ideal conditions, we can write the expression for a bimolecular reaction between A and B

$$\ln k = \ln k_0 + \frac{V_A}{RT} \left( \sqrt{P_{i,s}} - \sqrt{P_{i,A}} \right)^2 + \frac{V_B}{RT} \left( \sqrt{P_{i,s}} - \sqrt{P_{i,B}} \right)^2 - \frac{V_{\ddagger}}{RT} \left( \sqrt{P_{i,s}} - \sqrt{P_{i,\ddagger}} \right)^2 \quad (9.46)$$

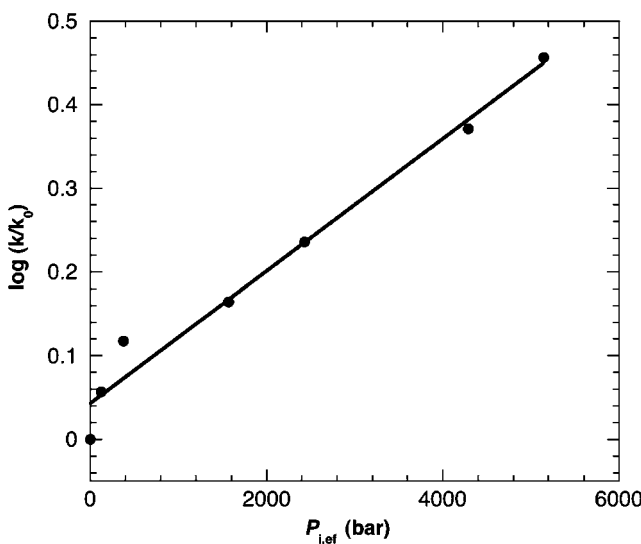


**Figure 9.9** Dependence of the kinetics of reaction 9.VII on the effective internal pressure in acetone solutions of inorganic perchlorates.

in which  $P_{i,A}$  and  $P_{i,B}$  are the internal pressures of the solutes,  $P_{i,\ddagger}$  is that of the activated complex,  $P_{i,s}$  that of the solvent, while  $V_A$  and  $V_B$  are the molar volumes of the solutes and  $V_{\ddagger}$  that of the activated complex, all taken in the liquid phase. We assume that the internal pressure of the activated complex will be intermediate between that of reactants and products.

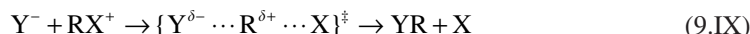
From eq. (9.46), we see that when the internal pressures of A, B and the transition state are similar, the solvent behaves as ideal and  $k \approx k_0$ . However, when  $P_{i,\ddagger}$  is greater than  $P_{i,s}$  and different from that of the solutes, the term  $(P_{i,s}^{1/2} - P_{i,\ddagger}^{1/2})^2$  will be dominant, and  $k$  will be smaller than under ideal conditions. In contrast, if the internal pressure of the solvent is similar to that of the activated complex, but markedly different from those of the reactants, the internal pressure terms of these will be dominant in eq. (9.46), and  $k$  will be greater in solution than under ideal conditions.

With these ideas, in the Menschutkin reaction:



the activated complexes are partially ionised and will be more strongly solvated than the reactants in a polar solvent, such as nitrobenzene. This lowers the activity coefficient  $\gamma_{\ddagger}$  more than  $\gamma_A$  and  $\gamma_B$ , such that, from eq. (9.32), the rate will be greater than under ideal conditions.

However, if we consider the case



the activated complex is less solvated than the reactants, such that  $\gamma_{\ddagger} > \gamma_A \gamma_B$ , and the rate will be lower than under ideal conditions.

### 9.4.2 Reactions between ions

We will base our discussion of reactions between ions in solution on the effects of electrostatic interactions between species of charges  $Z_A e$  and  $Z_B e$  in a solvent of dielectric constant,  $\epsilon$ . Initially we consider the ions at an infinite distance, and then calculate the energy needed to bring them together to a contact distance,  $d_{AB}$ , forming the double sphere as shown in Figure 9.10.

When the ions are separated by a distance  $r$ , the force  $f$  between them is given by Coulomb's law

$$f = \frac{Z_A Z_B e^2}{4\pi\epsilon_0 \epsilon r^2} \quad (9.47)$$

where  $\epsilon_0$  is the permittivity of vacuum ( $\epsilon_0 = 8.854 \times 10^{-12} \text{ C}^2 \text{ N}^{-1} \text{ m}^{-2}$ , one of the basic quantities for all electrostatic equations using SI units). The work is done when the ions approach through a separation distance  $dr$  will be

$$dw = -\frac{Z_A Z_B e^2}{4\pi\epsilon_0 \epsilon r^2} dr \quad (9.48)$$

Integrating between the limits of the initial position and the contact distance

$$w = - \int_{\infty}^{d_{AB}} \frac{Z_A Z_B e^2}{4\pi\epsilon_0 \epsilon r^2} dr \quad (9.49)$$

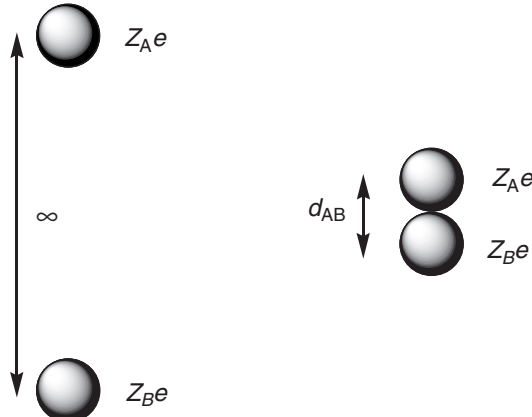


**Figure 9.10** Approach of two ions to a contact distance.

gives

$$w = \frac{Z_A Z_B e^2}{4\pi\epsilon_0 \epsilon d_{AB}} \quad (9.50)$$

The work  $w$  is positive if the charges of the ions are the same and negative if they are different.

This work corresponds to the contribution of the electrostatic interactions when the two ions form an activated complex to the free energy of activation,  $\Delta G_{es}^{\ddagger 0}$ . Multiplying by Avogadro's constant gives this in molar quantities

$$\Delta G_{es}^{\ddagger 0} = \frac{N_A Z_A Z_B e^2}{4\pi\epsilon_0 \epsilon d_{AB}} \quad (9.51)$$

The free energy of activation  $\Delta G^{\ddagger 0}$  is the sum of the contributions which are not due to electrostatic effects,  $\Delta G_{nes}^{\ddagger 0}$ , with the electrostatic contribution

$$\Delta G^{\ddagger 0} = \Delta G_{nes}^{\ddagger 0} + \frac{N_A Z_A Z_B e^2}{4\pi\epsilon_0 \epsilon d_{AB}} \quad (9.52)$$

Using CTST, the expression for the rate constant is

$$k = \frac{k_B T}{h} \exp\left(-\frac{\Delta G^{\ddagger 0}}{RT}\right) = \frac{k_B T}{h} \exp\left(-\frac{\Delta G_{nes}^{\ddagger 0}}{RT}\right) \exp\left(-\frac{Z_A Z_B e^2}{4\pi\epsilon_0 \epsilon d_{AB} k_B T}\right) \quad (9.53)$$

where  $R/N_A = k_B$ , the Boltzmann constant. In logarithmic form

$$\ln k = \ln \frac{k_B T}{h} - \frac{\Delta G_{nes}^{\ddagger 0}}{RT} - \frac{Z_A Z_B e^2}{4\pi\epsilon_0 \epsilon d_{AB} k_B T} \quad (9.54)$$

which is more conveniently given as

$$\ln k = \ln k_0 - \frac{Z_A Z_B e^2}{4\pi\epsilon_0 \epsilon d_{AB} k_B T} \quad (9.55)$$

where  $k_0$  is the rate constant for a medium of infinite dielectric constant.

Eq. (9.55) predicts that if we study a reaction in various solvents,  $\ln k$  will vary linearly with  $1/\epsilon$ . The slope of such a plot,  $Z_A Z_B e^2 / (4\pi\epsilon_0 d_{AB} k_B T)$  allows us to estimate the contact distance between the ions. Figure 9.11 shows this type of study for the reaction between  $\text{BrCH}_2\text{CO}_2^-$  and  $\text{S}_2\text{O}_3^{2-}$ , from which we can calculate  $d_{AB} = 5.1 \text{ \AA}$ .

For reactions between ions, eq. (9.52) allows us to estimate the electrostatic contribution to the entropy of activation,  $\Delta S_{es}^{\ddagger 0}$ , given that

$$S = \left( \frac{\partial G}{\partial T} \right)_P \quad (9.56)$$

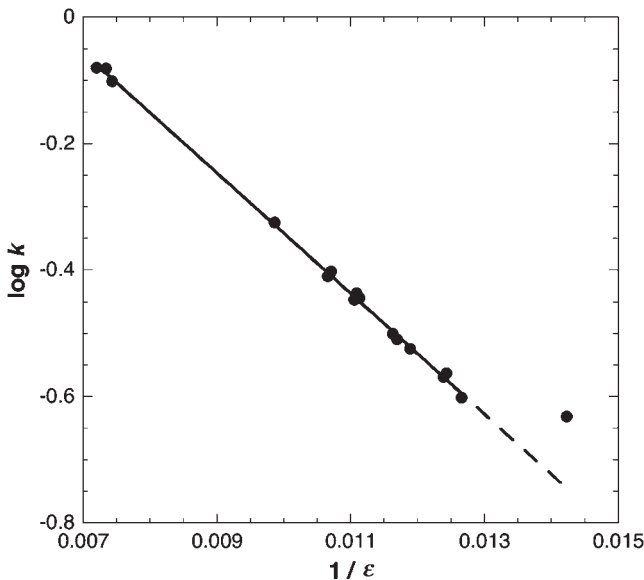


**Figure 9.11** Study of the dependence of rate constant on solvent dielectric constant for the reaction between  $\text{BrCH}_2\text{CO}_2^-$  and  $\text{S}_2\text{O}_3^{2-}$  [9].

From eqs. (9.52) and (9.56) we obtain

$$\Delta S_{\text{es}}^{\ddagger 0} = -\frac{N_A Z_A Z_B e^2}{4\pi\epsilon_0 d_{AB}} \left( \frac{\partial (1/\epsilon)}{\partial T} \right)_P \quad (9.57)$$

which can be expressed as

$$\Delta S_{\text{es}}^{\ddagger 0} = +\frac{N_A Z_A Z_B e^2}{4\pi\epsilon_0 d_{AB}\epsilon^2} \left( \frac{\partial \epsilon}{\partial T} \right)_P \quad (9.58)$$

or

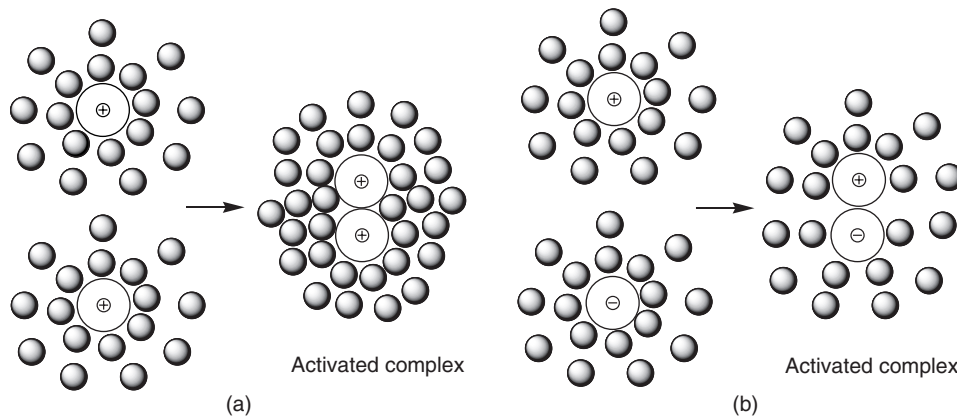
$$\Delta S_{\text{es}}^{\ddagger 0} = +\frac{N_A Z_A Z_B e^2}{4\pi\epsilon_0 d_{AB}\epsilon} \left( \frac{\partial \ln \epsilon}{\partial T} \right)_P \quad (9.59)$$

For aqueous solutions,  $\epsilon = 78.5$  and  $(\partial \ln \epsilon / \partial T)_P = -0.0046 \text{ K}^{-1}$ , and taking a typical value  $d_{AB} = 2 \text{ \AA}$ , we obtain

$$\Delta S_{\text{es}}^{\ddagger 0} \approx -40 Z_A Z_B \text{ J K}^{-1} \text{ mol}^{-1} \quad (9.60)$$

**Table 9.7**Some predicted and observed pre-exponential factors and entropies of activation<sup>a</sup>

Reactants	Experimental		Estimated	
	$A$ (dm <sup>3</sup> mol <sup>-1</sup> sec <sup>-1</sup> )	$\Delta S^{\ddagger 0}$ (J K <sup>-1</sup> mol <sup>-1</sup> )	$A$ (dm <sup>3</sup> mol <sup>-1</sup> sec <sup>-1</sup> )	$\Delta S^{\ddagger 0}$ (J K <sup>-1</sup> mol <sup>-1</sup> )
$\text{Cr}(\text{H}_2\text{O})_6^{3+} + \text{CNS}^-$	$\approx 10^{19}$	$\approx 126$	$10^{19}$	126
$\text{Co}(\text{NH}_3)_5\text{Br}^{2+} + \text{OH}^-$	$5 \times 10^{17}$	92	$10^{17}$	84
$\text{CH}_2\text{BrCOOCH}_3 + \text{S}_2\text{O}_3^{2-}$	$1 \times 10^{14}$	25	$10^{13}$	0
$\text{CH}_2\text{ClCOO}^- + \text{OH}^-$	$6 \times 10^{10}$	-50	$10^{11}$	-42
$\text{ClO}^- + \text{ClO}_2^-$	$9 \times 10^8$	-84	$10^{11}$	-42
$\text{CH}_2\text{BrCOO}^- + \text{S}_2\text{O}_3^{2-}$	$1 \times 10^9$	-71	$10^9$	-84
$\text{Co}(\text{NH}_3)_5\text{Br}^{2+} + \text{Hg}^{2+}$	$1 \times 10^8$	-100	$10^5$	-167
$\text{S}_2\text{O}_4^{2-} + \text{S}_2\text{O}_4^{2-}$	$2 \times 10^4$	-167	$10^5$	-167
$\text{S}_2\text{O}_3^{2-} + \text{S}_2\text{O}_3^{2-}$	$2 \times 10^6$	-126	$10^5$	-167

<sup>a</sup>From refs. [10,11].**Figure 9.12** Model of electrostriction: (a) The approach of two ions with the same charge leads to an increase in the electrostriction of the solvent. (b) The approach of oppositely charged ions decreases the electrostriction of the solvent.

This is interesting, because it shows us that the pre-exponential factor,  $A \propto \exp(\Delta S_{\text{es}}^{\ddagger 0}/R)$ , changes by a factor of 100 for each change of one unit in the product,  $Z_A Z_B$ .

The results in Table 9.7 are qualitatively in agreement with this prediction, although there are some quantitative differences, probably due to the sum of reactant radii being different from  $d_{AB} = 2 \text{ \AA}$ .

The physical basis of this effect is shown schematically in Figure 9.12a for the case of two positively charged ions. Each ion is surrounded by a certain number of solvent molecules. With ions of the same charge, when the activated complex is formed, the charge increases, which results in the attraction of more solvent molecules (Figure 9.12a). This

restriction in the motion of solvent molecules in the activated complex, relative to the reactants, leads to a decrease in the entropy of activation  $\Delta S^{\ddagger 0}$  and, hence, the pre-exponential factor. The restriction of the movements of the solvent molecules becomes greater with increasing charge of the ions. This effect is known as *electrostriction* or *solvent bonding*. Note that the dependence with the reciprocal of  $\epsilon$  expressed by eq. (9.59), which is more important than the change in  $(\partial \ln \epsilon / \partial T)_P$ , which means that the effect of the electrostriction on the activation entropy will be more significant in solvents of low polarity. In polar solvents, the high value of  $\epsilon$  rapidly attenuates any effect due to the charges of the ions and electrostriction only has a small effect on the pre-exponential factor or activation entropy.

With oppositely charged ions (Figure 9.12b), electrical charge decreases when the activated complex is formed. Therefore, there is a decrease in the electrostriction, and there are fewer molecules of solvent in the activated complex. This leads to an increase in the entropy of activation and the pre-exponential factor. These will be much greater than typical values of uncharged species, (e.g.  $A = 10^{13} \text{ mol}^{-1} \text{ dm}^3 \text{ sec}^{-1}$ ).

### 9.4.3 Effect of ionic strength

Ionic strength,  $I$ , is a measure of the concentration of electrically charged species in solution

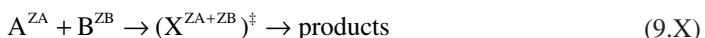
$$I = \frac{1}{2} \sum_i c_i Z_i^2 \quad (9.61)$$

in which  $c_i$  is the concentration of ion  $i$  of charge  $Z_i$ . In a solution in which the ionic strength is not zero, the interactions involved between many ions have rather different effects from those between pairs of ions we have just considered. For solutions of relatively low ionic strength, the activity coefficient of an ion can be estimated by the Debye–Hückel theory. This uses a model with each ion surrounded by an atmosphere of ions of the same charge, but which is opposite to that of the central ion. The ionic atmosphere lowers the chemical potential of the central ion by neutralising its charge. If A and B have charges of the same sign, a high ionic strength favours the formation of encounter pairs having a higher charge and, consequently, increases the rate of reaction. The Debye–Hückel theory expression for the activity coefficient is

$$\log \gamma_i = -AZ_i^2 \sqrt{I} \quad (9.62)$$

The parameter  $A$  in water at 25 °C has the value  $A = 0.51 \text{ mol}^{-1/2} \text{ dm}^{3/2}$ .

For a reaction of the type



eq. (9.32) gives the expression for the rate constant

$$k = k_0 \frac{\gamma_A \gamma_B}{\gamma_\ddagger} \quad (9.63)$$

relative to the value in an ideal medium,  $k_0$ ,

$$\log k = \log k_0 + \log \gamma_A + \log \gamma_B - \log \gamma_{\pm} \quad (9.64)$$

Introducing activity coefficients from eq. (9.62) we get

$$\log k = \log k_0 - A \left[ Z_A^2 + Z_B^2 - (Z_A + Z_B)^2 \right] \sqrt{I} \quad (9.65)$$

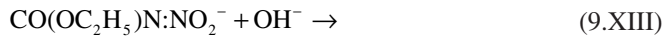
which can be written as

$$\log k = \log k_0 + 2AZ_A Z_B \sqrt{I} \quad (9.66)$$

Using the numerical value of  $A$  for aqueous solutions at 25 °C, this becomes

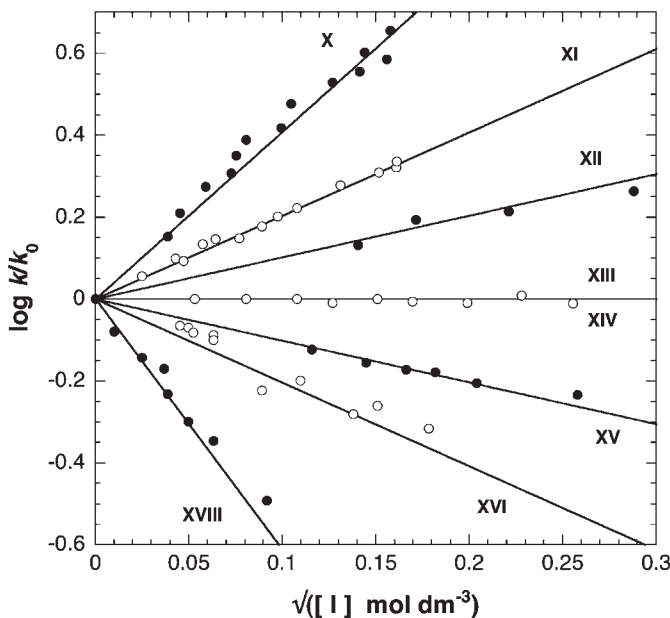
$$\log \frac{k}{k_0} \approx 1.02 Z_A Z_B \sqrt{I} \quad (\text{mol dm}^{-3})^{1/2} \quad (9.67)$$

Figure 9.13 shows the confirmation of these predictions of ionic strength effects in solution for the following group of reactions between ions [10,11]:



The increase in  $I$  increases the rate constant for reactions between ions of the same charge and decreases it when the ions are oppositely charged. This kinetic effect of addition of a salt to the solutions, when the salt is not involved in the reaction, was studied in detail by Brönsted [12] and Bjerrum [13] and the expression, which it represents, is known as the *Brönsted–Bjerrum equation*.

For reactions in which one of the species is neutral, ionic strength should not have any effect. In practice, there are often small effects of changing ionic strength when reactions are catalysed by acids or bases. These are known as secondary salt effects, and are due to effects of ionic strength on acid–base equilibria.



**Figure 9.13** Effect of ionic strength on the kinetics of ionic reactions in aqueous solutions. Reactions (9.XI–9.XVIII) are given in the text. Slopes are equal to  $1.02 Z_A Z_B$ .

#### 9.4.4 Effect of hydrostatic pressure

Because the rates of reaction are much less sensitive to the effect of pressure than of temperature, studies of the effects of external pressure for reactions in solution are more difficult to carry out, and need pressures of several thousand atmospheres (kilobars). However, they do yield important information on the transition state, which helps understanding mechanisms. The theory of pressure effects was initially formulated by van't Hoff in terms of the effect of pressure on equilibrium constants

$$\left( \frac{\partial \ln K_c}{\partial P} \right)_T = -\frac{\Delta V^0}{RT} \quad (9.68)$$

where  $\Delta V^0$  is the change in the standard volume, which is the difference between the standard volumes of the products and the reactants

$$\Delta V^0 = V_p - V_r \quad (9.69)$$

If  $V_{\ddagger}$  is volume of the activated complex, then

$$\Delta V^0 = (V_{\ddagger} - V_r) - (V_{\ddagger} - V_p) \quad (9.70)$$

Since for an elementary reaction

$$K_c = \frac{k_1}{k_{-1}} \quad (9.71)$$

we get the relationship

$$\left( \frac{\partial \ln k_1}{\partial P} \right)_T - \left( \frac{\partial \ln k_{-1}}{\partial P} \right)_T = -\frac{\Delta V_1^{\ddagger 0}}{RT} + \frac{\Delta V_{-1}^{\ddagger 0}}{RT} \quad (9.72)$$

where  $\Delta V_1^{\ddagger 0}$  is the change in the standard volume in the forward direction and  $\Delta V_{-1}^{\ddagger 0}$  for the reverse reaction. These quantities are known as the *volumes of activation*.

The simplest way of separating this into the effects on the forward and back reactions is

$$\left( \frac{\partial \ln k_1}{\partial P} \right)_T = -\frac{\Delta V_1^{\ddagger 0}}{RT} \quad (9.73)$$

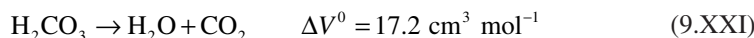
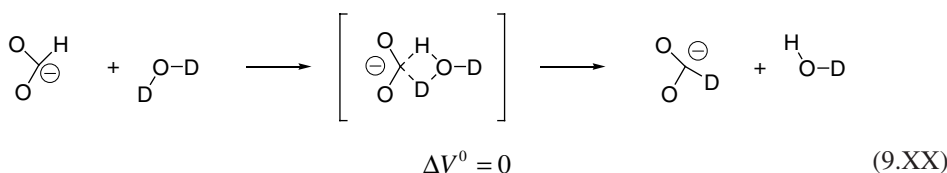
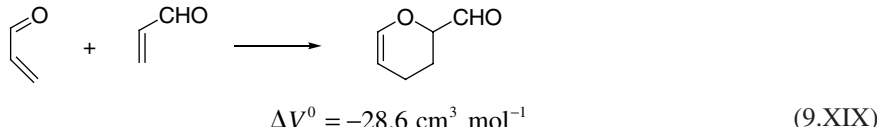
and

$$\left( \frac{\partial \ln k_{-1}}{\partial P} \right)_T = -\frac{\Delta V_{-1}^{\ddagger 0}}{RT} \quad (9.74)$$

In terms of volumes of activation, we can write

$$\ln k = \ln k_0 - \frac{\Delta V^{\ddagger 0}}{RT} P \quad (9.75)$$

in which  $k_0$  is the rate constant for zero hydrostatic pressure (in practice usually taken as atmospheric pressure). A study of the change in  $\ln k$  with pressure,  $P$ , will give a linear relationship, whose slope,  $\Delta V^{\ddagger 0}/RT$ , allows us to determine the volume of activation of the reaction [14]. Figure 9.14 gives data from studies of the effect of pressure on the reactions



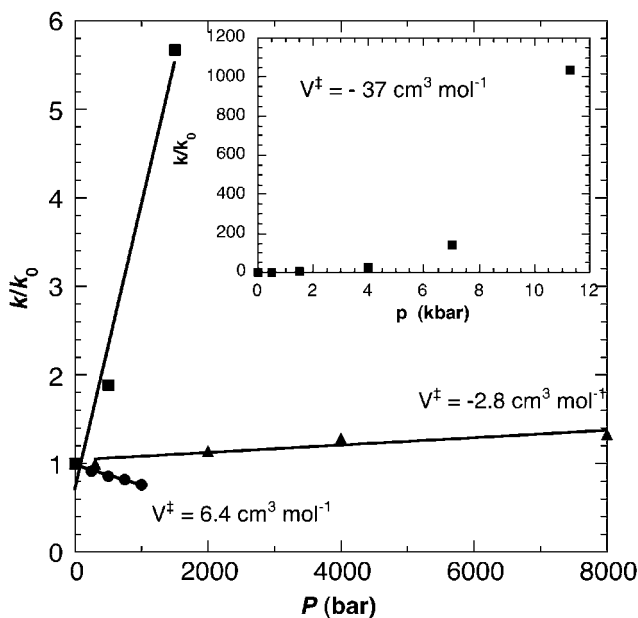


**Figure 9.14** Effect of external pressure on the kinetics of reactions (9.XIX) (squares) [15], (9.XX) (triangles) [16] and (9.XXI) (circles) [17].

In interpreting volumes of activation, we need to consider both structural variations in reactants and activated complexes and also contributions due to the solvent. For a reaction in the gas phase, such as



in which M is an inert or non-reactive molecule, the structural effects due to the involvement of M lead to  $\Delta V^\ddagger > 0$ , or for the reverse reaction  $\Delta V^\ddagger < 0$ . With reactions in solution, with neutral species  $\Delta V^\ddagger$  is dominated by structural effects, while for reactions between ions in general the effects of solvent dominate. In agreement with the model of electrostriction (Figure 9.10), for ions of the same sign, it is predicted that there will be a decrease in both  $\Delta V^\ddagger$  and  $\Delta S^\ddagger$ . For oppositely charged ions, we expect an increase in  $\Delta V^\ddagger$  and  $\Delta S^\ddagger$ .

Table 9.8 presents some values for  $\Delta V^\ddagger$  for water exchange reactions involving hydrated metal ions. Two extreme types of mechanisms that are considered are, an *associative mechanism* in which the central ion increases the coordination number in the activated complex

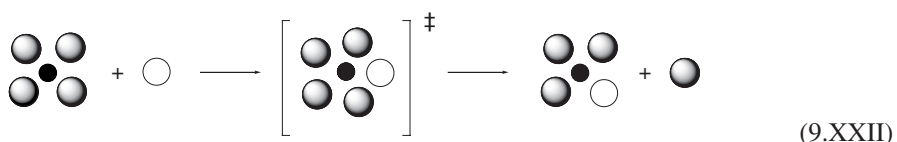
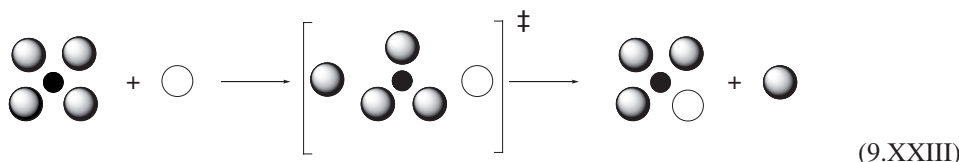


**Table 9.8**

Volumes and entropies of activation for water exchange reactions of metal cations

	$\Delta V^\ddagger$ (cm <sup>3</sup> mol <sup>-1</sup> )	$\Delta S^\ddagger$ (J mol <sup>-1</sup> K <sup>-1</sup> )
Ni <sup>2+</sup> <sub>(aq)</sub>	+7.7	+32
Co <sup>2+</sup> <sub>(aq)</sub>	+6.1	+21
V <sup>3+</sup> <sub>(aq)</sub>	-10.0	-67
Cr <sup>3+</sup> <sub>(aq)</sub>	-9.3	+20
Fe <sup>2+</sup> <sub>(aq)</sub>	+3.8	-
Fe <sup>3+</sup> <sub>(aq)</sub>	-5.4	+12

and a *dissociative* one, in which in the transition state shows a decrease in metal coordination



For an associative mechanism the change in the volume of activation is

$$\Delta V_A^\ddagger = [V^\ddagger(\text{solvated ion})] - [V^\ddagger(\text{solvated ion} + V_{H_2O})] \approx -10 \text{ cm}^3 \text{ mol}^{-1} \quad (9.76)$$

Knowing that the molar volume of water is 10 cm<sup>3</sup> mol<sup>-1</sup>, and assuming that the molar volumes of the hydrated ions and complexes are approximately equal, a value of  $\Delta V_A^{\ddagger 0} = -10 \text{ cm}^3 \text{ mol}^{-1}$  can be estimated for a purely associative mechanism of water exchange. Similarly, for the dissociative case we have

$$\Delta V_D^\ddagger = [V^\ddagger(\text{solvated ion}) + 2V_{H_2O}] - [V^\ddagger(\text{solvated ion} + V_{H_2O})] \approx 10 \text{ cm}^3 \text{ mol}^{-1} \quad (9.77)$$

## REFERENCES

- [1] NA Menschutkin, *Z. Phys. Chem. Neue Folge* **5** (1890) 589.
- [2] T Matsui, N Tokura, *Bull. Chem. Soc. Jpn.* **43** (1970) 1751.
- [3] E Rabinowitch, WC Wood, *Trans. Faraday Soc.* **32** (1936) 1381.
- [4] HD Burrows, J Seixas de Melo, C Serpa, LG Arnaut, MG Miguel, AP Monkman, I Hamblett, S Navaratnam, *Chem. Phys.* **285** (2002) 3.
- [5] SL Murov, I Carmichael, GL Hug, *Handbook of Photochemistry*, Marcel Dekker, New York, 1993.

- [6] GV Buxton, CL Greenstock, WP Helman, AB Ross, *J. Phys. Chem. Ref. Data* **17** (1988) 513.
- [7] G Faita, PP Righetti, *Tetrahedron* **51** (1995) 9091.
- [8] A Kumar, *J. Org. Chem.* **59** (1994) 4612.
- [9] KJ Laidler, *Chemical Kinetics*, HarperCollins, New York, 1987.
- [10] CT Burris, KJ Laidler, *Trans. Faraday Soc.* **15** (1955) 1497.
- [11] DTY Chen, KJ Laidler, *Can. J. Chem.* **37** (1959) 599.
- [12] JN Brönsted, *Z. Phys. Chem.* **102** (1922) 169.
- [13] N Bjerrum, *Z. Phys. Chem.* **108** (1924) 1924.
- [14] R van Eldik, T Asano, W Le Noble, *Chem. Rev.* **89** (1989) 549.
- [15] J Rimmelin, G Jenner, H Abdi-Oskoui, *Bull. Soc. Chim. Fr.* (1977) 341.
- [16] SD Hamann, M Linton, *Aust. J. Chem.* **30** (1977) 1883.
- [17] R van Eldik, DA Palmer, *J. Solution Chem.* **11** (1982) 340.

# – 10 –

## Reactions on Surfaces

---

Several reactions of industrial interest occur at inconveniently slow rates in the absence of a catalyst, but can be accelerated considerably by the solid surface of a metal. These include the Haber process for the synthesis of ammonia, the cracking of petroleum, the Fischer–Tropsch synthesis and others. Originally, it was thought that the main effect of the solid catalyst was presenting the reactants at considerably higher local concentrations than in the gas phase. However, this is not generally true, since in some cases, different surfaces cause a substance to react in different ways. We will analyse some of these.

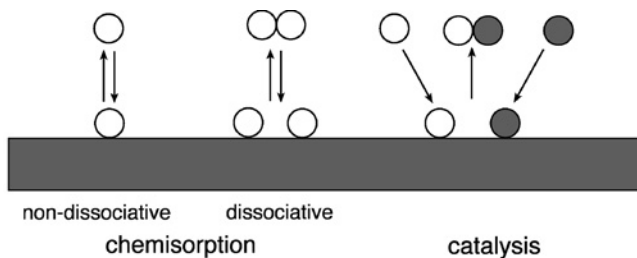
As illustrated in Figure 10.1, a surface reaction may be regarded as requiring five consecutive steps:

- (i) diffusion of the reactant molecules to the surface;
- (ii) adsorption of the gases on the surface;
- (iii) reaction of the adsorbed reactants on the surface;
- (iv) desorption of the products formed;
- (v) diffusion of the desorbed products into the main body of the gas phase.

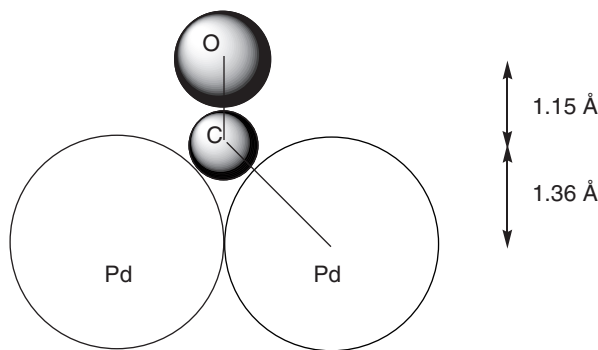
### 10.1 ADSORPTION

A fundamental understanding of the great diversity of chemistry occurring at surfaces requires familiarity with the molecule–surface interaction. Two main types of adsorption may be distinguished. One is relatively weak and arises mainly through van der Waals interactions, with heats of adsorption  $\Delta H_{\text{ad}}^0$  typically in the range from  $-20$  to  $-30 \text{ kJ mol}^{-1}$ . This is called *physical adsorption*, or physisorption. Physical adsorption equilibria are usually established very rapidly, except when limited by gaseous diffusion. The other type of adsorption is of a much stronger nature, typically with  $\Delta H_{\text{ad}}^0$  in the range from  $-50$  to  $-400 \text{ kJ mol}^{-1}$ . When the molecules are bound to a surface, chemical bonds can be established between the adsorbed molecule and the surface in the so-called *chemisorption*. A relevant example is the adsorption of carbon monoxide (CO) molecules on a palladium surface. As illustrated in Figure 10.2, the CO molecules are bonded to the metal through the carbon atom, with a Pd–C bond length of  $1.93 \text{ \AA}$ , a Pd–CO vibrational frequency of  $236 \text{ cm}^{-1}$  and  $\Delta H_{\text{ad}}^0 = -150 \text{ kJ mol}^{-1}$ .

Another good example showing that chemisorbed molecules possess structures and chemical properties substantially different from those of the isolated species is benzene



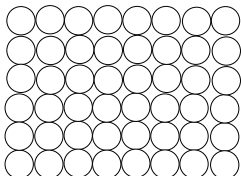
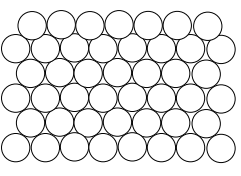
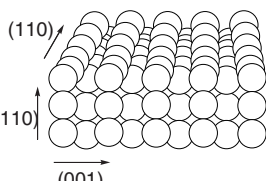
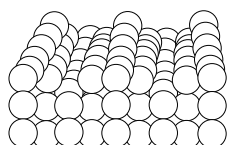
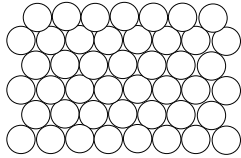
**Figure 10.1** Reactive processes at the surface of a solid.



**Figure 10.2** Adsorption of a CO molecule onto the surface of palladium. For simplicity, only two palladium atoms on the surface are illustrated in this scheme.

(C<sub>6</sub>H<sub>6</sub>) adsorbed on Pt(111). The aromaticity of adsorbed C<sub>6</sub>H<sub>6</sub> is somewhat reduced, the planar and six-fold symmetries of the molecule are broken as the H atoms distort away from surface, and the carbon–carbon bonds have alternating lengths [1]. At the same time, adsorbate binding causes changes in the substrate geometry, leading to surface reconstruction. Until about 1970 there was little direct evidence as to the detailed structure of surfaces. Now, several surface analysis techniques such as HREELS (high-resolution electron energy loss spectroscopy), XPS (X-ray and ultraviolet photoemission spectroscopy), LEED (low-energy electron diffraction), FIM (field-ion microscopy), STM (scanning tunnelling microscopy) are available that provide information at the molecular level of molecule–surface interactions. Figure 10.3 illustrates cases of Pt surface reconstructions occurring in the presence of CO.

Molecules that dissociate upon adsorption can act as intermediates in surface–catalysed chemical reactions. A good example is the catalytic formation of biphenyl (C<sub>6</sub>H<sub>5</sub>–C<sub>6</sub>H<sub>5</sub>) from adsorption of iodobenzene on metal surfaces. The reaction has been studied on well-defined single-crystal surfaces in vacuum. With the Cu(111) surface, the reaction proceeds via a number of steps. First, iodobenzene adsorbs to the copper surface, dissociating above 180 K to form surface-bound iodine atoms (an *adatom*, i.e. adsorbed atom) and phenyl intermediates. Subsequently, between 180 and 300 K, phenyl moieties diffuse on the surface, while above 300 K they react to form biphenyl, which subsequently desorbs upon its

	1x1 surface	reconstructed surface
(100)		 hex
(110)		 1x2
(111)		

**Figure 10.3** Structural models of the three low-index planes of Pt surfaces. Of the three, only the closed-packed Pt(111) surface is stable in its bulk-like  $1\times 1$  termination, while the more open (100) and (110) surfaces reconstruct into a quasi-hexagonal (hex) and a  $1\times 2$  “missing-row” geometry, respectively. Certain adsorbates such as CO can reversibly lift these reconstructions [2].

formation between 300 and 400 K. Finally, removal of iodine as CuI occurs at temperatures *ca.* 950 K. The role of the surface in this reaction is two-fold. The surface creates the  $C_6H_5$  intermediates via dissociation of iodobenzene. Additionally, the phenyl species on the surface experience inter-molecular forces, resulting in the formation of loosely bound complexes bringing the phenyl radicals into close proximity, leading to the correct orientation for eventual biphenyl formation [3]. A schematic view of an example of activated chemisorption with dissociation is illustrated in Figure 10.4 [4].

The surface of a solid material, even of a well-defined crystalline metal, is not entirely uniform. Some of the main features of a solid surface are illustrated in Figure 10.5. There are various kinds of surface sites. These include atoms in *terraces*, atoms at *steps*, atoms at *kinks* and *adatoms*, which project out of the surface. Atoms in terraces have several neighbouring atoms, whereas adatoms have none. On most surfaces there are a few adatoms, together with many more atoms in different surface sites until the limit of surface densities *ca*  $10^{14}-10^{15}$  atoms  $cm^{-2}$  of those atoms in terraces is reached. The various

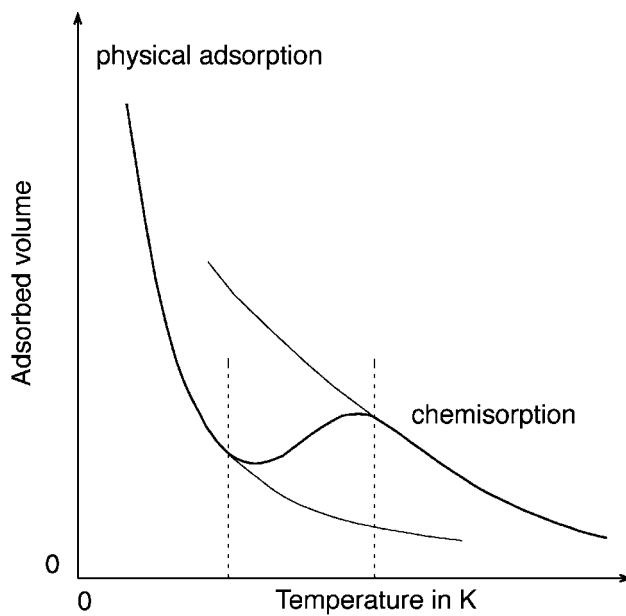
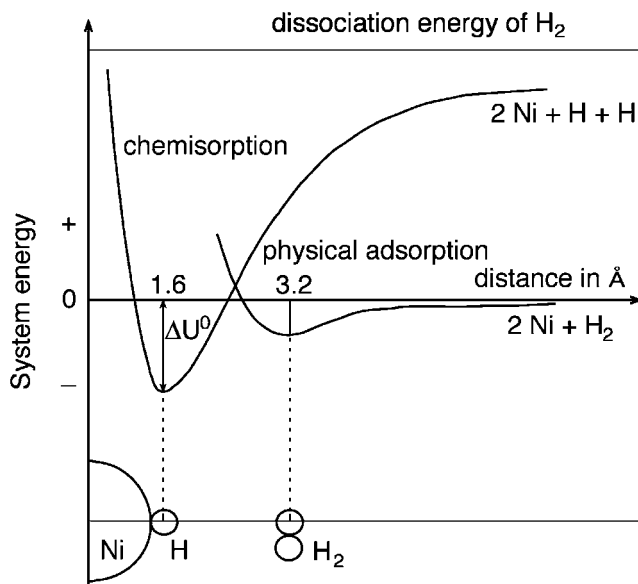


**Figure 10.4** Upper panel: potential energy curves for physisorption and chemisorption. Lower panel: adsorption isobars illustrating the presence of the two types of adsorption, one involving stronger binding forces than the other.

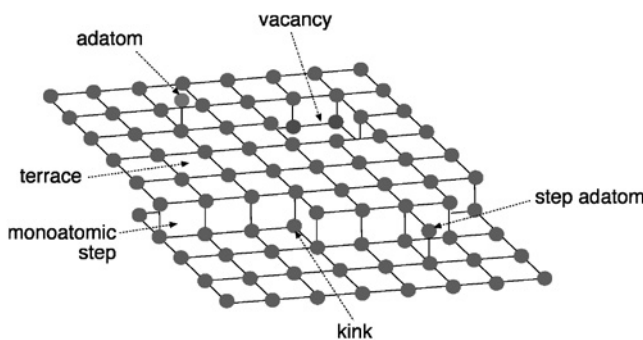


**Figure 10.5** Types of structures and defects found at the surfaces of metals.

types of surface atoms differ very markedly in their properties, and in particular their ability to chemisorb and to catalyse chemical reactions.

Benzene, for example, adsorbed on Pt(111) surface binds more strongly at defect sites and at step edges. The STM images of adsorbed C<sub>6</sub>H<sub>6</sub> display three distinct molecular shapes that are attributed to the C<sub>6</sub>H<sub>6</sub> bonds at different types of surface sites. In one of these, the C<sub>6</sub>H<sub>6</sub> molecule appears as a protrusion on the surface, with a three-fold symmetry and a central depression. Additionally, three small but pronounced depressions appear symmetrically about the periphery of the molecule. These depressions indicate that the perturbation of the surface electronic structure or local density of states is significantly larger than the molecule, extending up to 6–10 Å away from the centre of the C<sub>6</sub>H<sub>6</sub> molecule.

On Cu(111), C<sub>6</sub>H<sub>6</sub> interacts weakly with the surface forming disordered monolayers, while it desorbs from terrace sites at <250 K. The C<sub>6</sub>H<sub>6</sub> molecules present a high mobility on terraces and at 77 K they can be observed by STM only when bound at step edges or in clusters with high coverage. Benzene can act as a nucleophile and thus donate electrons to the surface. Consequently, it has a higher affinity for binding at the upper step edges where the electron density is smoothed. The filled surface electronic-state density is decreased above step edges, while it is increased near the lower edges of the steps (the so-called Smoluchowski effect).

In contrast, tetracyanoquinonedimethane (TCNQ) is a strong electrophile and is known to form charge-transfer complexes with copper. TCNQ is thus expected to perturb the electronic structure of the surface strongly. Whereas C<sub>6</sub>H<sub>6</sub> was observed to bind preferentially at the electron-poor region above step edges, TCNQ, which is an electron acceptor, binds at electron-rich sites such as the bottom of the steps.

Electronic effects on surfaces can generate preferential adsorption sites, as illustrated for step edges. However, a necessary condition for this to occur on surfaces is the availability of free charge as well as states for the free charge to occupy. The closed-packed (111) surfaces allow for a greater orbital overlap of the surface atoms. This greater electron freedom leads to a two-dimensional free-electron gas confined to the surface. However, such surface states do not exist for the (110) and (100) surfaces. Studies on C<sub>6</sub>H<sub>6</sub> adsorbed on Ag(110) reveals that the terraces and the (001) steps remain completely free of molecules.

## 10.2 ADSORPTION ISOTHERMS

### 10.2.1 Langmuir isotherm

The simplest situation for the mechanism of adsorption is to consider that gas atoms or molecules occupy single sites on the surface and are not dissociated. The process can be represented by



Langmuir employed a kinetic approach to derive the isotherm under such ideal conditions [5]. Let  $\theta$  be the fraction of surface that is covered;  $1-\theta$  will then be the fraction that is not covered. The rate of adsorption,  $v_{\text{ad}}$ , will then be that for the bimolecular process between the reactant, A, and an active site of the surface,

$$v_{\text{ad}} = k_{\text{ad}} [\text{A}] (1-\theta) \quad (10.1)$$

Here  $k_{\text{ad}}$  is the rate constant of adsorption. Such a rate law assumes that  $k_{\text{ad}}$  is independent of  $\theta$ , i.e. that  $\Delta H^0_{\text{ad}}$  is independent of  $\theta$ . The rate of desorption,  $v_{\text{-ad}}$ , will be that for the unimolecular dissociation process with the concentration at surface equivalent to the coverage  $\theta$ ,

$$v_{\text{-ad}} = k_{\text{-ad}} \theta \quad (10.2)$$

At equilibrium these rates are equal such that

$$k_{\text{ad}} [\text{A}] (1-\theta) = k_{\text{-ad}} \theta \quad (10.3)$$

or

$$\frac{k_{\text{ad}} [\text{A}]}{k_{\text{-ad}}} = \frac{\theta}{1-\theta} \quad (10.4)$$

If we represent the equilibrium constant for the adsorption process by  $K = k_{\text{ad}}/k_{\text{-ad}}$ , we can express the coverage as

$$\theta = \frac{K [\text{A}]}{1 + K [\text{A}]} \quad (10.5)$$

The variation of  $\theta$  with  $[\text{A}]$ , known as the Langmuir adsorption isotherm (eq. (10.5)), is shown in Figure 10.6a. Eq. (10.5) represents an isotherm since  $K$  is dependent on temperature, such that the curves of Figure 10.6 must be determined at a constant  $T$ . At sufficiently low concentrations (or pressures),  $K [\text{A}]$  is small in comparison with unity, and  $\theta$  is then proportional to  $[\text{A}]$ .

The bare fraction of surface is given by

$$1-\theta = \frac{1}{1 + K [\text{A}]} \quad (10.6)$$

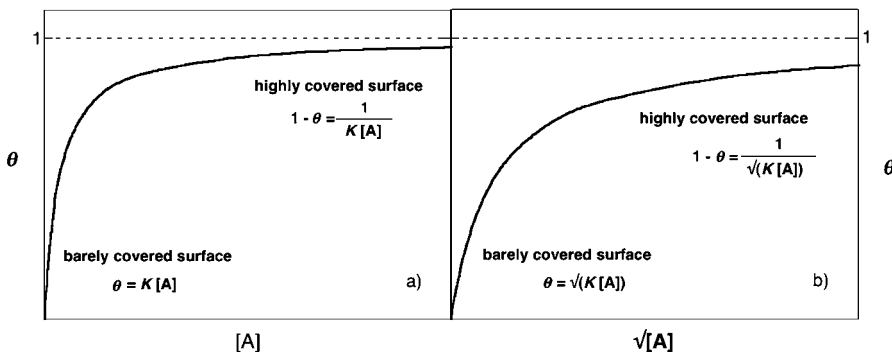


**Figure 10.6** Langmuir isotherms, without dissociation (a), and with dissociation (b).

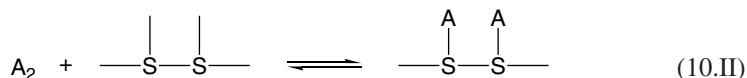
and at sufficiently high concentrations this will be given by

$$1 - \theta \approx \frac{1}{K[A]} \quad (10.7)$$

A distinctive feature of this isotherm is that the surface becomes saturated ( $\theta \approx 1$ ) with adsorbed molecules at high concentrations of  $A$ .

### 10.2.2 Adsorption with dissociation

In certain cases there is evidence that the process of adsorption is accompanied by the dissociation of the molecule on the surface, as shown in mechanism (10.II)



Since the process of adsorption can be viewed as a reaction between a gas molecule  $A_2$  and two reaction sites, the rate of adsorption will be

$$v_{ad} = k_{ad} [A_2] (1 - \theta)^2 \quad (10.8)$$

The desorption process involves a bimolecular reaction between two adsorbed atoms, and the rate is

$$v_{-ad} = k_{-ad} \theta^2 \quad (10.9)$$

At equilibrium these rates are equal and therefore

$$\frac{\theta}{1 - \theta} = \left( \frac{k_{ad} [A_2]}{k_{-ad}} \right)^{1/2} \quad (10.10)$$

So one can write

$$\theta = \frac{\sqrt{K[A_2]}}{1 + \sqrt{K[A_2]}} \quad (10.11)$$

At low concentrations of  $A_2$ ,  $\theta$  is proportional to  $[A_2]^{1/2}$ . This can then be written as

$$1 - \theta = \frac{1}{1 + \sqrt{K[A_2]}} \quad (10.12)$$

such that at high concentrations,  $K^{1/2} [A_2]^{1/2} \gg 1$ , the fraction of the bare surface is inversely proportional to the square root of the concentration or pressure. Figure 10.6b illustrates the Langmuir isotherm with dissociation.

### 10.2.3 Competitive adsorption

When two substances A and B adsorb on the same surface and compete for the same sites, inhibition can occur. Let the fraction of coverage by substance A be represented by  $\theta_A$  and that for B by  $\theta_B$ . The uncovered fraction is  $(1 - \theta_A - \theta_B)$ . If both species are adsorbed without dissociation, the rate of adsorption of A will be

$$v_{ad}^A = k_{ad}^A [A](1 - \theta_A - \theta_B) \quad (10.13)$$

and an equivalent expression will be given for B. The corresponding rates of desorption are

$$v_{-ad}^A = k_{-ad}^A \theta_A \quad (10.14)$$

and similarly an equivalent expression for B can be written. At equilibrium, the rates of adsorption and desorption for each substance are equal and consequently we can write

$$\frac{\theta_A}{1 - \theta_A - \theta_B} = K_A [A] \quad (10.15)$$

and

$$\frac{\theta_B}{1 - \theta_A - \theta_B} = K_B [B] \quad (10.16)$$

Here,  $K_A = k_{ad}^A / k_{-ad}^A$  and  $K_B = k_{ad}^B / k_{-ad}^B$ . Solving the two eqs. (10.15) and (10.16) for the surface coverages leads to

$$\theta_A = \frac{K_A [A]}{1 + K_A [A] + K_B [B]} \quad (10.17)$$

$$\theta_B = \frac{K_B [B]}{1 + K_A [A] + K_B [B]} \quad (10.18)$$

Eq. (10.17) shows that the coverage of A,  $\theta_A$ , diminishes when there is an increase in [B]; the opposite is true for  $\theta_B$  when there is an increase in [A]. This competition exists because A and B are competing for a limited number of active sites, hence the term competitive adsorption. There is evidence that sometimes two substances are adsorbed on two different sets of adsorption sites, for example, at steps and at terraces, and in such cases there is no such competition.

## 10.3 KINETICS ON SURFACES

### 10.3.1 Unimolecular surface reactions

Surface reactions that involve a single molecule can be classified as unimolecular reactions. When the adsorption follows a Langmuir isotherm, the rate of reaction,  $v$ , will be proportional to the surface coverage,  $\theta$ , and can be written as

$$v = k\theta = \frac{kK[A]}{1 + K[A]} \quad (10.19)$$

where  $k$  is the rate constant. At high concentrations of the reactant,  $K[A] \gg 1$ , the rate of reaction is constant,

$$v = k \quad (10.20)$$

since all the active sites are occupied with adsorbed molecules. This is a zero-order reaction. At low concentrations, however, the rate law is

$$v = kK[A] \quad (10.21)$$

and we are dealing with a first-order process.

The decomposition of  $\text{NH}_3$  on a surface of platinum follows this kind of behaviour. One of the reaction products,  $\text{H}_2$ , poisons the catalyst. From eq. (10.20) the surface coverage can be expressed by

$$\theta = \frac{K_A[A]}{1 + K_A[A] + K_I[I]} \quad (10.22)$$

where I represents the *inhibitor* and  $K_I$  is the adsorption constant for the same. The rate of the reaction is given by

$$v = \frac{kK_A[A]}{1 + K_A[A] + K_I[I]} \quad (10.23)$$

When  $K_I[I] \gg 1 + K[A]$  the rate law simplifies to the form

$$v = \frac{kK_A[A]}{K_I[I]} \quad (10.24)$$

This behaviour arises from the fact that since the surface is covered sparsely by A, the coverage is proportional to [A]. However, under these conditions the surface is almost fully covered by the inhibitor, I, and as a consequence the bare fraction is inversely proportional to [I].

The rate law for the decomposition of ammonia is  $v = k [\text{NH}_3]/[\text{H}_2]$ . Since hydrogen is a product of the reaction, there is progressive inhibition as the reaction proceeds.

### 10.3.2 Activation energies of unimolecular surface reactions

The dependence of the rate constant of eq. (10.19) on the temperature should take the form of the Arrhenius equation,

$$\frac{d \ln k}{dT} = \frac{E_2}{RT^2} \quad (10.25)$$

where  $E_2$  is the activation energy corresponding to the reaction of the adsorbed species, i.e. to



The temperature dependence of the equilibrium constant  $K$  will follow the van't Hoff relationship

$$\frac{d \ln K}{dT} = \frac{\Delta U^0}{RT^2} \quad (10.26)$$

Here  $\Delta U^0$  is the standard molar internal energy change in the adsorption process. At low pressures, since the rate of reaction is  $v = kK[A]$ , the overall rate constant for this process is simply

$$k^1 = kK \quad (10.27)$$

and it follows that

$$\frac{d \ln v}{dT} = \frac{d \ln k^1}{dT} = \frac{d \ln k}{dT} + \frac{d \ln K}{dT} \quad (10.28)$$

or, in equivalent terms,

$$\frac{d \ln k^1}{dT} = \frac{E_2 + \Delta U^0}{RT^2} \quad (10.29)$$

The apparent activation energy,  $E_a$ , for this first-order reaction is thus

$$E_a = E_2 + \Delta U^0 \quad (10.30)$$

At high concentrations of the reactant, the rate follows eq. (10.20), and the observed activation energy is simply

$$E_a = E_2 \quad (10.31)$$

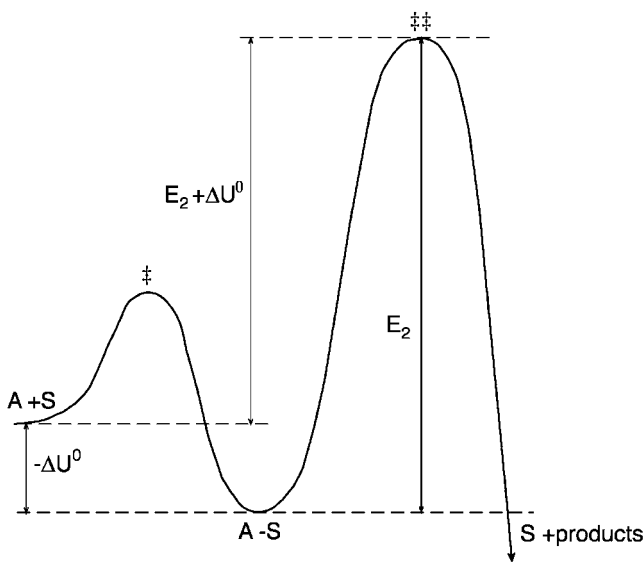


**Figure 10.7** Energy diagram for a unimolecular surface reaction.

The energy diagram for a unimolecular surface reaction of Figure 10.7 reveals that initially the reactant has to surmount a small energy barrier, but stays adsorbed in a well, either to be converted into products or to revert somewhat more easily to the desorbed condition.

At low concentrations, the majority of the molecules are not adsorbed, such that they have to surmount the energy barrier,  $E_2 + \Delta U^0$  ( $\Delta U^0 < 0$ ). However, at high concentrations, equilibrium favours the adsorbed molecules and the barrier to be surmounted is even higher,  $E_2$ .

When there is inhibition, according to eq. (10.24),

$$\frac{d \ln K_I}{dT} = \frac{\Delta U_I^0}{RT^2} \quad (10.32)$$

and the apparent activation energy is thus

$$E_a = E_2 + \Delta U_A^0 - \Delta U_I^0 \quad (10.33)$$

which is greater than  $E_2 = \Delta U_A^0$  for the uninhibited reaction since  $\Delta U_I^0$  is negative. The reason for this increase in activation energy is that a molecule of the inhibitor must be desorbed (an endothermic process) when a reactant molecule is adsorbed and undergoes reaction.

### 10.3.3 Reaction between two adsorbed molecules

For a surface bimolecular reaction to occur, the reactants or intermediates must have enough energy, usually through thermal activation, to surmount an activation barrier.

Additionally, the reactants or intermediates must be in close proximity to react, while for molecular (as opposed to atomic) species, the relative orientation can also be critical. The frequency with which all of these conditions are met determines the reaction rate.

For a surface reaction between two reactants A and B, there are two distinct mechanisms: Langmuir–Hinshelwood and Rideal–Eley. In the former mechanism, the reaction occurs between A and B when both are adsorbed on the surface. In the latter, the reaction occurs between an adsorbed molecule and a molecule in the gas phase. These mechanisms may be distinguished on the basis of the corresponding kinetic equations.

The rate of reaction of the Langmuir–Hinshelwood mechanism is proportional to the fractions of the molecules of A and B that are adsorbed,

$$v = k\theta_A \theta_B \quad (10.34)$$

These fractions are given by eqs. (10.17) and (10.18), such that the rate is therefore

$$v = \frac{k K_A K_B [A][B]}{(1 + K_A [A] + K_B [B])^2} \quad (10.35)$$

Figure 10.8 illustrates the variation of the rate of reaction as a function of [A], keeping [B] constant. The rate first increases in a manner proportional to [A], then passes through a maximum and subsequently decreases. The decline in the rate at high [A] can be explained in terms of the displacement of one of the reactants, B, when the concentration of A increases.

Eq. (10.35) can be employed for the study of special cases such as the regime of sparsely covered surface at low concentrations of both reactants ( $K_A[A] + K_B[B] \ll 1$ ), the case when one of the reactant is very weakly adsorbed, ( $K_A[A] \ll 1 + K_B[B]$ ) or strongly adsorbed ( $K_B[B] \gg 1$ ), etc. For the latter situation the rate is

$$v = \frac{k K_A [A]}{K_B [B]} \quad (10.36)$$

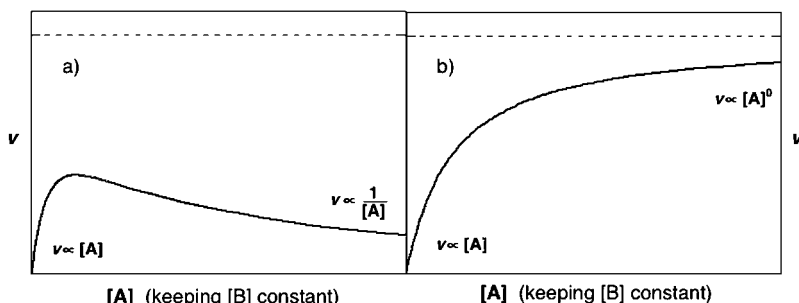


**Figure 10.8** Surface bimolecular reaction rate as a function of one of the reactants. (a) Langmuir–Hinshelwood mechanism; (b) Rideal–Eley mechanism.

The activation energies can be established under the experimental conditions for which eq. (10.35) is valid,

$$E_a = E_2 + \Delta U_A^0 + \Delta U_B^0 \quad (10.37)$$

and under the conditions of the validity of eq. (10.36),

$$E_a = E_2 + \Delta U_A^0 - \Delta U_B^0 \quad (10.38)$$

These two examples reveal that, within the same mechanism, the observed activation energy is strongly dependent upon the experimental conditions of surface coverage.

#### 10.3.4 Reaction between a molecule in the gas phase and an adsorbed molecule

When the reaction follows the Rideal–Eley mechanism, where reactant A is in the gas phase and B is adsorbed, the rate is given by

$$v = k\theta_B [A] \quad (10.39)$$

or

$$v = \frac{kK_B[A][B]}{1 + K_A[A] + K_B[B]} \quad (10.40)$$

The rate of reaction declines with an increase in [A], because reactant A occupies sites that are no longer available for B. Figure 10.8b displays the variation of the rate with [A], keeping [B] constant. The rate no longer passes through a maximum in contrast to its behaviour in the Langmuir–Hinshelwood mechanism.

### 10.4 TRANSITION-STATE THEORY FOR REACTIONS ON SURFACES

#### 10.4.1 Unimolecular reactions

The statistical mechanical formulation of the transition-state theory (TST) can also be applied to the kinetics of reactions on surfaces. Let us consider the following reaction:



The equilibrium between the activated complex and the reactant can be expressed by the equation

$$\frac{c_\ddagger}{c_g c_s} = \frac{Q_\ddagger}{Q_g Q_s} \exp\left(-\frac{\epsilon_0}{k_B T}\right) \quad (10.41)$$

Here  $c_g$  represents the concentration of the reactant in the gas phase,  $c_g = N_g/V$  where  $N_g$  is the number of molecules in the gas phase and  $V$  the volume of the gas;  $c_{ad}$  the concentration of adsorbed molecules in molecules per unit area,  $c_{ad} = N_{ad}/S$  and  $S$  is the area of the surface;  $c_s$  the concentration of bare sites per unit area,  $c_s = N_s/S$ , where  $N_s$  is the number of sites at adsorption equilibrium;  $c_{\ddagger}$  the concentration per unit area of activated complexes,  $c_{\ddagger} = N_{\ddagger}/S$  where  $N_{\ddagger}$  is the number of activated complexes. The partition functions  $Q_{\ddagger}$  and  $Q_s$  are for unit area and  $Q_g$  for unit volume. The energy  $\varepsilon_0$  represents the molecular energy of activation at absolute zero.

The rate of reaction is estimated in terms of the product of the frequency of transformation,  $v_{\ddagger}$ , of the activated complexes and the concentration of the same complexes,  $v = v_{\ddagger} c_{\ddagger}$ . As previously discussed, one of the vibrational factors in the partition function corresponds to a very loose vibration expressed usually by  $k_B T/h\nu$ , where  $\nu$  is its vibrational frequency. If we define a new partition function that lacks the contribution of such loose vibration,  $Q_{\ddagger} = Q^{\ddagger}(k_B T/h)$ , the rate of the reaction is given by

$$v = c_g c_s \frac{k_B T}{h} \frac{Q^{\ddagger}}{Q_g Q_s} \exp\left(-\frac{\varepsilon_0}{k_B T}\right) \quad (10.42)$$

The value of the partition function  $Q^{\ddagger}$  may be taken as unity,  $Q^{\ddagger} = 1$ , since the activated state consists of a molecule immobilised on the surface.

Two limiting cases of eq. (10.42) are of interest. The first is that of a sparsely covered surface. The concentration of bare surface sites  $c_s$  is approximately equal to  $L_s$  the total number of sites per unit area of completely bare surface. Under such conditions,  $c_s$  is approximately independent of  $c_g$ , such that the rate is directly proportional to  $c_g$ . Therefore, we are dealing with a first-order process,

$$v = c_g L_s \frac{k_B T}{h} \frac{Q^{\ddagger}}{Q_g Q_s} \exp\left(-\frac{\varepsilon_0}{k_B T}\right) \quad (10.43)$$

The second limiting case involves the surface covered almost completely by the adsorbed molecules. The concentration of active sites  $c_s$  can be estimated from the isotherm equation, now written as

$$\frac{c_{ad}}{c_s} = c_g \frac{Q_{ad}}{Q_g Q_s} \exp\left(-\frac{\varepsilon}{k_B T}\right) \quad (10.44)$$

where  $\varepsilon$  represents the adsorption energy, which is the difference between the zero-point energy (ZPE) of the adsorbed and the free molecule. Substituting this equation in the rate expression, we obtain

$$v = c_{ad} \frac{k_B T}{h} \frac{Q^{\ddagger}}{Q_{ad}} \exp\left(-\frac{\varepsilon_0 - \varepsilon}{k_B T}\right) \quad (10.45)$$

When the surface is almost completely covered by the adsorbed molecules,  $c_{ad}$  may be considered to be constant, and the rate is independent of the pressure of the reactant. The kinetics are therefore zero order.

The partition function of the adsorbed species involves only vibrational factors, because the adsorbed molecules do not possess translation or rotational degrees of freedom. For the vibrational partition function we can assume  $Q_{\text{ad}} \approx 1$ , and since  $Q^{\ddagger} = 1$ , the expression for the rate will be

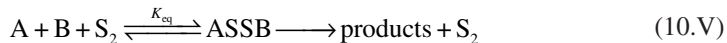
$$v = c_{\text{ad}} \frac{k_B T}{h} \exp\left(-\frac{E_0}{RT}\right) \quad (10.46)$$

where  $E_0$  is the molar activation energy at 0 K.

Eq. (10.46) can be employed to estimate the rate of the catalysed decomposition of  $\text{NH}_3$  on a tungsten surface under zero-order conditions at 904 K. The experimental activation energy is known,  $E_0 = 159 \text{ kJ mol}^{-1}$ . Employing typical values for a smooth surface of  $10^{15}$  atoms  $\text{cm}^{-2}$  gives  $c_{\text{ad}} \approx L_s = 10^{15} \text{ cm}^{-2}$ . The estimated reaction rate is  $4 \times 10^{17} \text{ cm}^{-2} \text{ sec}^{-1}$  at 904 K, which should be compared with the experimental value of  $8 \times 10^{18} \text{ cm}^{-2} \text{ sec}^{-1}$ . The cross section of a molecule is  $\pi r^2$ , and can be estimated using a typical radius of  $r = 1.5 \text{ \AA}$ . When the entire surface of a catalyst is covered with a monolayer of adsorbed molecules, one molecule per active site, the number of covered sites is the reciprocal of the cross section, thus  $L_s = 10^{15} \text{ cm}^{-2} = 10^{19} \text{ m}^{-2}$ . With this  $L_s$  value and the thermal frequency factor  $k_B T/h = 10^{13} \text{ sec}^{-1}$ , the pre-exponential factor typical for a unimolecular reaction on a surface is  $10^{28} \text{ cm}^{-2} \text{ sec}^{-1}$ .

### 10.4.2 Bimolecular reactions

Let us assume that a reaction on a surface follows the Lindemann–Hinshelwood mechanism



$\text{S}_2$  represents an active dual site. The rate of reaction is then given by

$$v = c_g c'_g c_{\text{S}_2} \frac{k_B T}{h} \frac{Q^{\ddagger}}{Q_g Q'_g Q_{\text{S}_2}} \exp\left(-\frac{E_0}{k_B T}\right) \quad (10.47)$$

where  $c_g$  and  $c'_g$  are the molecular concentrations of A and B, respectively, in the gas phase,  $Q_g/V$  and  $Q'_g/V$  are the corresponding partition functions per unit volume,  $c_{\text{S}_2}$  is the concentration of the dual sites where the species A and B can be adsorbed in contiguous positions.

The concentration of bare dual sites is related to the concentration of bare single sites. Each single site has a certain number of available adjacent sites. For a random distribution this is  $s(1-\theta)$  where  $s$  is the coordination number of the surface and  $(1-\theta)$  represents the bare surface which is available to adsorb the reactant species. Thus the concentration of dual sites is given by

$$c_{\text{S}_2} = \frac{c_s s (1-\theta)}{2} \quad (10.48)$$

If the number of dual sites was evaluated by counting  $s$  for each single site, the result would be  $sc_s$ , but in such a procedure each pair is counted twice: one as a central site, the other as an adjacent one. In eq. (10.48) the division by two takes this fact into account.

If the concentration of covered single sites is  $c_{\text{ad}}$ ,  $\theta$  is then given by

$$\theta = \frac{c_{\text{ad}}}{c_{\text{ad}} + c_s} \quad (10.49)$$

taking into consideration eq. (10.48), the concentration of bare dual sites is

$$c_{S_2} = \frac{sc_s^2}{2(c_{\text{ad}} + c_s)} \quad (10.50)$$

or

$$c_{S_2} = \frac{sc_s^2}{2L_s} \quad (10.51)$$

where  $L_s = c_{\text{ad}} + c_s$  is the total concentration of single sites per unit area when the surface is completely bare. By introducing eq. (10.51) into eq. (10.47) we obtain

$$v = \frac{1}{2} s \frac{c_g c_g' c_s^2}{L_s} \frac{k_B T}{h} \frac{Q^\ddagger}{Q_g Q_g' Q_s} \exp\left(-\frac{\epsilon_0}{k_B T}\right) \quad (10.52)$$

This equation may be presented in a more general form using the equilibrium expressions for the adsorption of A and B

$$K = \frac{c_{\text{ad}}}{c_g c_s} \quad (10.53)$$

$$K' = \frac{c'_{\text{ad}}}{c_g c_s} \quad (10.54)$$

where  $c_{\text{ad}}$  and  $c'_{\text{ad}}$  are the concentrations of adsorbed A and B, respectively, by unit area. Since in addition

$$c_{\text{ad}} + c'_{\text{ad}} + c_s = L_s \quad (10.55)$$

from eqs. (10.53) and (10.54) one obtains

$$c_s = \frac{L_s}{1 + Kc_g + K'c'_g} \quad (10.56)$$

Inserting this expression into eq. (10.52) gives

$$v = \frac{1}{2} s \frac{c_g c'_g L_s}{(1 + Kc_g + K'c'_g)^2} \frac{k_B T}{h} \frac{Q^\ddagger}{Q_g Q'_g Q_s} \exp\left(-\frac{\epsilon_0}{k_B T}\right) \quad (10.57)$$

as a general rate expression for a bimolecular reaction on a surface.

When the surface is covered sparsely,  $Kc_g + K'c'_g \ll 1$ , and as a consequence the rate equation becomes

$$v = \frac{1}{2} sc_g c'_g L_s \frac{k_B T}{h} \frac{Q^\ddagger}{Q_g Q'_g Q_s} \exp\left(-\frac{\epsilon_0}{k_B T}\right) \quad (10.58)$$

This type of expression can be applied quantitatively for the catalysed reaction of NO and O<sub>2</sub> on a glass surface. The reaction is second order and the rate at 85 K follows the expression

$$v = 9.4 \times 10^{-27} c_{NO} c_{O_2} \exp\left(-\frac{E_0}{RT}\right) \text{ cm}^4 \text{ sec}^{-1} \quad (10.59)$$

Eq. (10.58) with  $Q^\ddagger/Q_s = 1$ ,  $L_s = 10^{15} \text{ cm}^{-2}$  and a coordination number  $s = 4$  leads to a pre-exponential factor of  $15 \times 10^{-27} \text{ cm}^4 \text{ sec}^{-1}$ , in good agreement with the experimental data.

Without resorting to the calculation of the partition functions, the equations presented above can provide order of magnitude values of the pre-exponential factor,  $(1/2)sL_s(k_B T/h)(1/Q_g Q'_g)$ , using the orders of magnitude of the partition functions for the different types of motion involved, given in Chapter 6 (partition functions: translation,  $Q_{\text{trans}} = 10^{25} - 10^{26} \text{ cm}^{-3}$ ; rotation of a linear molecule,  $Q_{\text{rot}} = 10 - 10^2$ , and a non-linear molecule,  $Q_{\text{rot}} = 10^4 - 10^5$ , vibration,  $Q_{\text{vib}} = 1 - 10$ ). As the temperature is not very high, let us assume that  $Q_{\text{vib}} = 1$  for both the reactants and take the geometric mean values for  $Q_{\text{trans}}$  and  $Q_{\text{rot}}$ . Under these assumptions we obtain a pre-exponential factor of  $10^{-26} \text{ cm}^4 \text{ sec}^{-1}$  that is not far from the experimental value.

When one of the reactants is strongly adsorbed, we can have  $Kc_g \gg 1 + K'c'_g$  and as a consequence the rate is

$$v = \frac{1}{2} s \frac{L_s}{K^2} \frac{c'_g}{c_g} \frac{k_B T}{h} \frac{Q^\ddagger}{Q_g Q'_g Q_s} \exp\left(-\frac{\epsilon_0}{k_B T}\right) \quad (10.60)$$

We can express the equilibrium constant  $K$  in terms of the partition functions as

$$v = \frac{1}{2} s L_s \frac{c'_g}{c_g} \frac{k_B T}{h} \frac{Q^\ddagger Q_g Q_s}{Q'_g Q_{\text{ad}}^2} \exp\left(-\frac{\epsilon_0 + 2\epsilon}{k_B T}\right) \quad (10.61)$$

The activation energy is greater by  $2\epsilon$  than the value for a sparsely covered surface; the underlying reason is that two molecules of A must be adsorbed before the activated complex is formed.

This equation is valid for the reaction between CO and O<sub>2</sub> on a platinum surface. At 527 K the empirical rate was found to be [6]

$$v = 7.1 \times 10^{-14} \frac{c_{O_2}}{c_{CO}} \text{ cm}^{-2} \text{ sec}^{-1} \quad (10.62)$$

with an activation energy of 139 kJ mol<sup>-1</sup>. The rate estimated by the TST (eq. (10.61)) is  $4.3 \times 10^{-14} \text{ cm}^{-2} \text{ sec}^{-1}$ , once again in good agreement with the experimental data.

## 10.5 MODEL SYSTEMS

### 10.5.1 Langmuir–Hinshelwood mechanism

The catalytic oxidation of CO on a Pt surface has been extensively studied in view of its relevance to automotive gas pollution. Moreover, its relative simplicity motivated its extensive use as a model system for heterogeneous catalysis. Molecular beam studies of the catalytic oxidation of CO on the plane (111) on platinum indicate that the reaction follows a Langmuir–Hinshelwood mechanism [2],



where  $\text{O}_{\text{ad}}$  represents the adatoms of atomic oxygen. The energy diagram for the reaction can be constructed on the basis of experimental data, as illustrated in Figure 10.9 [7,8]. The energy barrier for the reaction of the  $\text{CO}_{\text{ad}}$  and  $\text{O}_{\text{ad}}$  adsorbed species is  $\Delta E^\ddagger = 105 \text{ kJ mol}^{-1}$  and the reaction energy is  $\Delta E^0 = -40.5 \text{ kJ mol}^{-1}$ .

The reactive components of the catalytic oxidation of CO on a Pt surface are the adsorbed O and CO. A very fast chemical reaction occurs between  $\text{O}_{\text{ad}}$  and  $\text{CO}_{\text{ad}}$  in neighbouring adsorption sites of the surface, followed by the immediate release of the  $\text{CO}_2$  produced. Oxygen atoms on a Pt(111) surface tend to occupy sites of the highest available coordination, which in the case of Pt(111) correspond to three-fold sites. There are two different three-fold hollow sites per primitive unit cell, one of which is a hexagonally close-packed (hcp) site and the other is a face-centred cubic (fcc) site. At  $\theta = 0.25$ , which is about the saturating coverage on the Pt(111) surface, oxygen films have a  $p(2 \times 2)$  structure. This

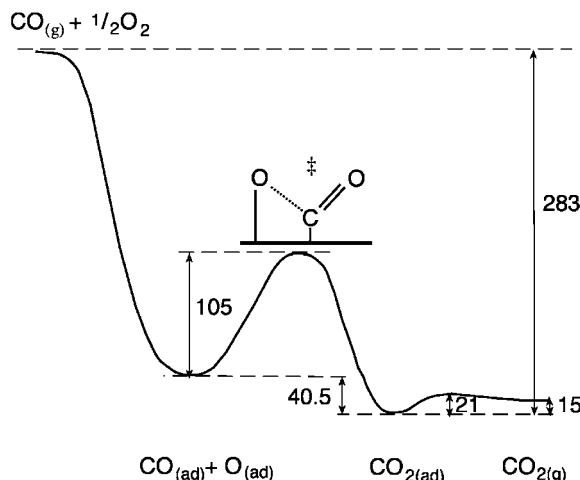


**Figure 10.9** Potential energy diagram for the catalytic oxidation of CO on a Pt(111) surface. Energies are in kJ/mol.

structure is very stable and can be observed at temperatures up to 350 K [9]. However, at low temperatures, the well-ordered p(2×2) structure of chemisorbed oxygen film can be obtained only after annealing at room temperature [10]. To form the p(2×2) structure of adsorbed oxygen and of O–CO co-adsorbed layers, oxygen atoms must have a certain mobility, sufficient for ordering the film. This feature is also essential for the reaction with the co-adsorbed CO molecule. To activate the oxidation of CO, the temperature is increased to 220–300 K, depending on the film structure. It is believed that only activated oxygen atoms can react with the CO molecules [10].

Two crucial events in the reaction pathways have been suggested: (i) the adsorbed O atom must be activated from the initial hollow chemisorption site and (ii) the CO molecule has to approach the  $O_{ad}$  atom in the correct orientation. Petrova and Yakovkin [11] have employed a Monte Carlo simulation to further elucidate the CO and O co-adsorption and reaction on Pt(111). In the dissociative chemisorption of the  $O_2$  molecule, precursor states (extrinsic and intrinsic) play an important role. These intermediate states can be qualitatively described in terms of capturing the molecule into a potential well near the surface, and therefore may be related to temporal molecular physisorption. Being captured in this extrinsic precursor state, the  $O_2$  molecule may be placed above a vacant site at the surface, that is, in the intrinsic precursor state. Then the  $O_2$  molecule can dissociate, with the chemisorption of the two atoms in two neighbouring sites, or, alternatively, can be desorbed from the precursor state. Relative probabilities control the kinetics of the net adsorption. Dissociation of  $O_2$  molecules occurs at temperatures above 150 K. The O atoms thus produced occupy the three-fold sites. One half of the three-fold sites corresponds to the hcp-type and the other to the fcc-type. However, these sites should be distinguished with regard to the binding energy. The calculations show that fcc-sites are favoured by *ca.* 45–48 kJ mol<sup>-1</sup> with respect to the hcp-sites (Figure 10.10). This feature leads to pronounced difference of activation barriers for surface diffusion from the fcc to the hcp-site. As a result, at the temperatures of 200–300 K, most of the oxygen atoms must occupy the fcc adsorption sites. After each adsorption attempt, O atoms can jump into an adjacent three-fold site. In other words, the adsorption of atoms at the lattice sites is followed by their rearrangement through surface diffusion. Ordering of the film is achieved by many jumps, the probabilities of which are controlled by lateral interaction and the diffusion barriers. Monte Carlo simulation predicts the correct value of saturating oxygen coverage,  $\theta=0.25$ . This value relates to conditions of sufficient mobility of O atoms. Further, at low temperatures, formation of the film structure can be hindered because of formation of domains, which leads to freezing of the film.

For catalysed reactions on metal surfaces, Zhang and Hu [12] proposed that the reaction barrier is given by

$$E_a = E_O + E_{CO} + E_{surf} + E_m \quad (10.63)$$

where  $E_a$  is the reaction barrier,  $E_O$  and  $E_{CO}$  are the energies required to activate  $O_{ad}$  and CO, respectively, from the initial state to the transition state,  $E_{surf}$  the energy associated with surface relaxation during the reaction and  $E_m$  a mixing term that includes the  $O_{ad}$ –CO bond formation energy and an energy due to bond competition.

The catalytic oxidation of CO on Pt(111) appears to be dominated by the  $E_O$  contribution. The barrier for the reaction probably originates from the strong bonding of the O

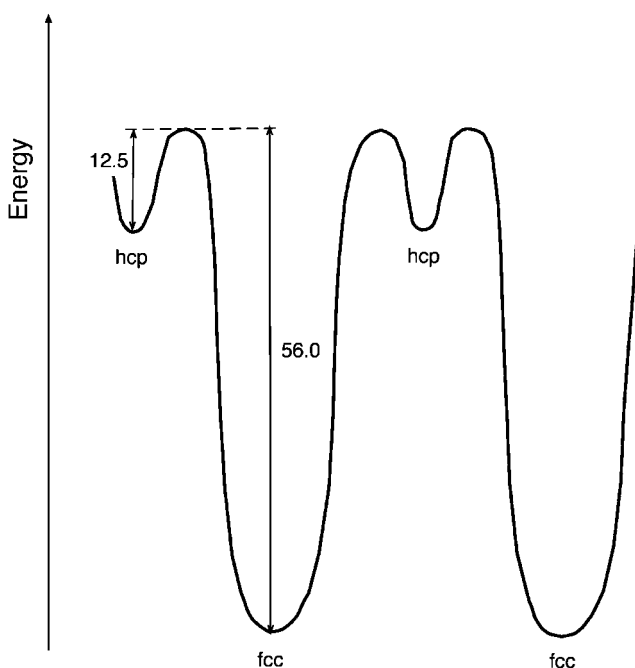
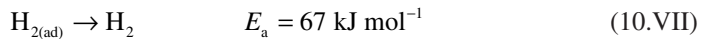


**Figure 10.10** Energy diagram of the three-fold fcc and hcp sites on a Pt(111) surface, with indication of the relative energies in kJ/mol [11].

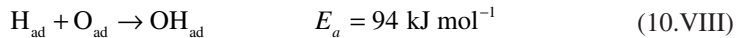
atoms with the surface. Currently, one assumes that the three-fold hcp sites, where the bonds of the  $O_{ad}$  atoms to the Pt(111) surface are substantially weaker, are the active sites for the reaction. According to Figure 10.10, the activation energy for the reaction is thus 60 kJ mol<sup>-1</sup>.

### 10.5.2 Eley–Rideal mechanism

Reaction of gas-phase atomic hydrogen with dissociatively chemisorbed oxygen on Ru(001) can be taken as a model reaction for the Eley–Rideal mechanism. The Langmuir–Hinshelwood reaction between co-adsorbed hydrogen  $H_{ad}$  and  $O_{ad}$  atoms does not occur on the Ru(001) surface. The reason for this is simple. The activation energy for recombinative desorption of molecular hydrogen



is approximately 27 kJ mol<sup>-1</sup> less than that for the reaction



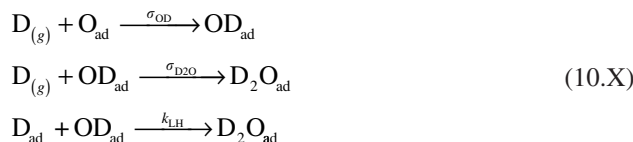
Therefore the reaction occurs between the hydrogen molecules (or atoms) in the vapour phase and the adsorbed oxygen atoms.

The reaction



on Ru(001) is estimated to be exothermic by approximately 230–270 kJ mol<sup>-1</sup> (depending on the exact value of the Ru–OH) and is expected to have only a small barrier [13].

Weinberg reports studies with an ordered p(1×2) oxygen adatom overlayer corresponding to a fractional area of  $\theta_{\text{O}}=0.5$ . The metal surface was bombarded with deuterium atoms with a flux  $\Xi_{\text{D}}=1.2\times10^{13}$  cm<sup>-2</sup> sec<sup>-1</sup>. D and H atoms produce identical results within experimental uncertainties. The elementary reactions taken into consideration were



where  $\sigma$  represents the reaction cross section, and  $k_{\text{LH}}$  is the competing Langmuir–Hinshelwood reaction rate coefficient that is negligible under the surface temperature of 90 K employed in the experiments. According to this mechanism, in general terms we can write

$$\begin{aligned} \frac{d\theta_{\text{O}}}{dt} &= -\sigma_{\text{OD}}\Xi_{\text{D}}\theta_{\text{O}} \\ \frac{d\theta_{\text{OD}}}{dt} &= -\sigma_{\text{OD}}\Xi_{\text{D}}\theta_{\text{O}} - \sigma_{\text{D}_2\text{O}}\Xi_{\text{D}}\theta_{\text{OD}} - k_{\text{LH}}\theta_{\text{D}}\theta_{\text{OD}} \\ \frac{d\theta_{\text{D}_2\text{O}}}{dt} &= \sigma_{\text{D}_2\text{O}}\Xi_{\text{D}}\theta_{\text{OD}} + k_{\text{LH}}\theta_{\text{D}}\theta_{\text{OD}} \end{aligned} \quad (10.64)$$

On neglecting the terms involving  $k_{\text{LH}}$ , and based on the surface coverage of water on Ru(001), Weinberg reported cross-section values of  $\sigma_{\text{OD}}=6.8\times10^{-17}$  cm<sup>2</sup> and  $\sigma_{\text{D}_2\text{O}}=2.2\times10^{-15}$  cm<sup>2</sup>. The product water remains adsorbed at the reaction temperature and acts as an inhibitor of the direct reaction when  $\theta_{\text{D}_2\text{O}}>0.3$ .

## REFERENCES

- [1] S Lehwald, H Ibach, JE Demuth, *Surf. Sci.* **78** (1978) 577–590.
- [2] R Imbihl, G Ertl, *Chem. Rev.* **95** (1995) 697.
- [3] ECH Sykes, P Han, SA Kandel, KF Kelly, GS McCarty, PS Weiss, *Acc. Chem. Res.* **36** (2003) 945–953.
- [4] B Frémaux, *Éléments de Cinétique et de Catalyse, Technique et Documentation*, Lavoisier, Paris, 1989.
- [5] I Langmuir, *J. Am. Chem. Soc.* **38** (1916) 2221.

- [6] I Langmuir, *Trans. Farad. Soc.* **17** (1922) 621.
- [7] G Ertl, PR Norton, J Rustig, *Phys. Rev. Lett.* **49** (1982) 177.
- [8] MJ Hei, HB Chen, YJ Lin, YZ Lin, G Wei, DW Liao, *Surf. Sci.* **417** (1998) 82.
- [9] PR Norton, JA Davies, TE Jackman, *Surf. Sci. Lett.* **122** (1982) L593.
- [10] J Yoshinobu, M Kawai, *J. Chem. Phys.* **103** (1995) 3220.
- [11] NV Petrova, IN Yakovkin, *Surf. Sci.* **578** (2005) 162.
- [12] CJ Zhang, P Hu, *J. Am. Chem. Soc.* **123** (2001) 1166.
- [13] WH Weinberg, *Acc. Chem. Res.* **29** (1996) 479.

# – 11 –

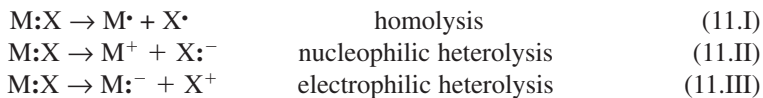
## Substitution Reactions

---

### 11.1 MECHANISMS OF SUBSTITUTION REACTIONS

A substitution reaction is characterised by the replacement of a molecule (or ion) from the coordination shell of a reactive centre by another molecule (or ion) from the reaction medium, irrespective of whether it is a gas or a liquid. During the substitution the bond between the ligand and the reactive centre is broken, while a new bond is formed between that centre and the new species entering the coordination shell. In 1933, Christopher (later Sir Christopher) Ingold with Patel [1,2] introduced a classification for substitution reactions on carbon atoms that was subsequently popularised by Ingold and E. D. Hughes. This classification is based on the type of bond breaking between the leaving group and the reactive centre, which can be either homolytic or heterolytic. In homolytic reactions the two electrons of the chemical bond are separated, with one remaining in the reactive centre, while the other goes to the leaving group. This leads to the chemistry of systems with unpaired electrons, commonly referred to as free radicals, which will be addressed in Chapter 12. In heterolytic reactions the electron removal or addition to the reactive centre occurs in pairs. This is the chemistry of diamagnetic charged species, i.e. cations and anions.

In the latter case, a subdivision of this classification is made by considering the site of the electron pair after the heterolytic scission. When the electron pair remains in the reactive centre, it is named electrophilic heterolysis and when it accompanies the leaving group, it is called nucleophilic heterolysis.



“Nucleophilic substitution” is now the commonly accepted designation of a substitution reaction by a nucleophilic reactant, and is usually represented by  $S_N$  followed by a number that represents the molecularity of the reaction. For example, bimolecular nucleophilic substitution is represented as  $S_N2$ , whereas first-order nucleophilic substitution is described as  $S_N1$ . Similarly, for electrophilic heterolysis, the processes are described as  $S_E2$  and  $S_E1$  reactions, while for the homolytic reactions, they are referred to as  $S_H2$  and  $S_H1$  reactions. As we will see shortly, these may be considered as the limits in a spectrum of reaction mechanisms.

Nucleophilic substitution reactions are one of the most important classes of reactions in organic chemistry. In particular, S<sub>N</sub>2 reactions are among the most extensively studied chemical processes in solution and in the gas phase, both theoretically and experimentally. The history of the study of these reactions closely parallels (and is sometimes responsible for) the development of concepts such as structure–reactivity relationships, linear free-energy relationships, steric inhibition, kinetics as a probe of mechanism, stereochemistry as a probe of mechanism and solvent effects.

## 11.2 S<sub>N</sub>2 AND S<sub>N</sub>1 REACTIONS

A nucleophilic substitution reaction

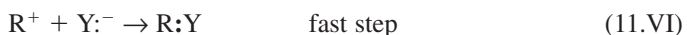
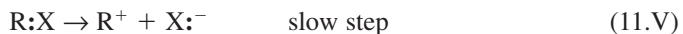


may occur as a concerted R–X bond-breaking and R–Y bond-making process, where Y<sup>−</sup> is the nucleophilic reagent and X the leaving group. The reaction rate of this elementary reaction is

$$v = k_2 [\text{RX}] [\text{Y}^-] \quad (11.1)$$

where  $k_2$  is a bimolecular rate constant, usually expressed in units of M<sup>−1</sup> sec<sup>−1</sup>. This reaction is described as an S<sub>N</sub>2 reaction.

Ingold and co-workers also considered another reaction mechanism, where the rate-limiting step is the heterolytic dissociation of the RX substrate



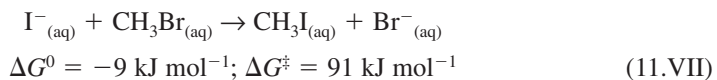
The reaction rate is now determined by the rate of the slow step, heterolytic dissociation of the C–X bond,

$$v = k_1 [\text{RX}] \quad (11.2)$$

where  $k_1$  is a first-order rate constant.

The difference between S<sub>N</sub>2 and S<sub>N</sub>1 reactions can be rationalised by the reaction energy profiles shown in Figure 11.1. The nucleophilic substitutions of bromomethane and of tertiary butyl bromide in aqueous solution illustrate some of the factors that determine the size of the energy barriers and the stability of the intermediate in these mechanisms.

The nucleophilic substitution of bromomethane by iodine



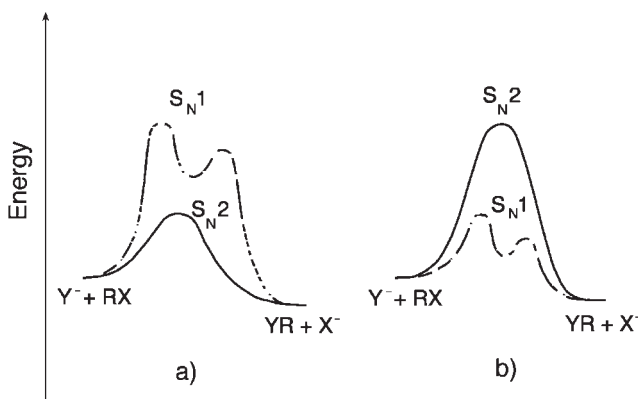
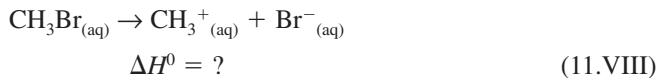


**Figure 11.1** Energy profiles characterising S<sub>N</sub>2 and S<sub>N</sub>1 reactions: (a) Reaction proceeding through the S<sub>N</sub>2 mechanism. (b) Reaction proceeding through the S<sub>N</sub>1 mechanism.

can be decomposed in a thermodynamic cycle to obtain the enthalpy of the first step, the heterolytic cleavage



using the data from the literature [3,4], in kJ/mol,

$\text{CH}_3\text{Br}_{(\text{aq})} \rightarrow \text{CH}_3\text{Br}_{(\text{g})} + \text{water}$	$-\Delta H_{\text{hyd}}(\text{CH}_3\text{Br}) = 10$
$\text{CH}_3\text{Br}_{(\text{g})} \rightarrow \text{CH}_3^{\bullet}_{(\text{g})} + \text{Br}^{\bullet}_{(\text{g})}$	$D_e(\text{C}-\text{Br}) = 293$
$\text{Br}^{\bullet}_{(\text{g})} + \text{e}^-_{(\text{g})} \rightarrow \text{Br}^-_{(\text{g})}$	$E_A(\text{Br}) = -324$
$\text{Br}^-_{(\text{g})} + \text{water} \rightarrow \text{Br}^-_{(\text{aq})}$	$\Delta H_{\text{hyd}}(\text{Br}^-) = -293$
$\text{CH}_3^{\bullet}_{(\text{g})} \rightarrow \text{CH}_3^+_{(\text{g})} + \text{e}^-_{(\text{g})}$	$I_p(\text{CH}_3) = 949$
$\text{CH}_3^+_{(\text{g})} + \text{water} \rightarrow \text{CH}_3^+_{(\text{aq})}$	$\Delta H_{\text{hyd}}(\text{CH}_3^-) = -271$
<hr/>	
$\text{CH}_3\text{Br}_{(\text{aq})} \rightarrow \text{CH}_3^+_{(\text{aq})} + \text{Br}^-_{(\text{aq})}$	$\Delta H^0 = 360 \text{ kJ mol}^{-1}$

A more accurate estimate for the enthalpy of the heterolytic cleavage of CH<sub>3</sub>Br must include an electrostatic term for the stabilisation of the (CH<sub>3</sub><sup>+</sup>Br<sup>-</sup>) ion pair. However, the stabilisation for a 2.5 Å charge separation in water ( $\epsilon = 78.5$ ) is only  $-10.5 \text{ kJ mol}^{-1}$ , and does not change the fact that the enthalpy for the heterolytic bond cleavage is much higher than the activation free energy of reaction (11.VII). Thus, the barrier of the S<sub>N</sub>1 mechanism is much higher than that observed for the reaction, showing that it must proceed through the alternative S<sub>N</sub>2 mechanism.

However, estimation of the enthalpy of dissociation of tertiary butyl bromide in water

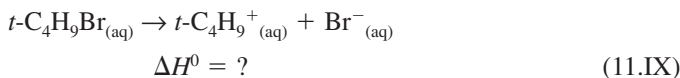


**Table 11.1**

Comparison of the energies of the steps in the thermodynamic cycle for the heterolytic dissociation of CH<sub>3</sub>Br and *t*-C<sub>4</sub>H<sub>9</sub>Br in water

Steps	CH <sub>3</sub> Br (kJ mol <sup>-1</sup> )	<i>t</i> -C <sub>4</sub> H <sub>9</sub> Br (kJ mol <sup>-1</sup> )	ΔH(CH <sub>3</sub> Br) – ΔH( <i>t</i> -C <sub>4</sub> H <sub>9</sub> Br) (kJ mol <sup>-1</sup> )
–ΔH <sub>hidr</sub> (RX)	10	10	0
D <sub>e</sub> (C–Br)	293	263	30
E <sub>A</sub> (Br)	–324	–324	0
ΔH <sub>hyd</sub> (Br <sup>–</sup> )	–293	–293	0
I <sub>P</sub> (R <sup>·</sup> )	949	716	233
ΔH <sub>hyd</sub> (R <sup>+</sup> )	–271	–220	51

leads to strikingly different results. The same thermodynamic cycle, using identical data sources,

<i>t</i> -C <sub>4</sub> H <sub>9</sub> Br <sub>(aq)</sub> → <i>t</i> -C <sub>4</sub> H <sub>9</sub> Br <sub>(g)</sub> + water	–ΔH <sub>hyd</sub> (CH <sub>3</sub> Br) = 10
<i>t</i> -C <sub>4</sub> H <sub>9</sub> Br <sub>(g)</sub> → <i>t</i> -C <sub>4</sub> H <sub>9</sub> <sup>·</sup> <sub>(g)</sub> + Br <sup>–</sup> <sub>(g)</sub>	D <sub>e</sub> (C–Br) = 263
Br <sup>–</sup> <sub>(g)</sub> + e <sup>–</sup> <sub>(g)</sub> → Br <sup>–</sup> <sub>(g)</sub>	E <sub>A</sub> (Br) = –324
Br <sup>–</sup> <sub>(g)</sub> + water → Br <sup>–</sup> <sub>(aq)</sub>	ΔH <sub>hyd</sub> (Br <sup>–</sup> ) = –293
<i>t</i> -C <sub>4</sub> H <sub>9</sub> <sup>·</sup> <sub>(g)</sub> → <i>t</i> -C <sub>4</sub> H <sub>9</sub> <sup>+</sup> <sub>(g)</sub> + e <sup>–</sup> <sub>(g)</sub>	I <sub>P</sub> (CH <sub>3</sub> ) = 716
<i>t</i> -C <sub>4</sub> H <sub>9</sub> <sup>+</sup> <sub>(g)</sub> + water → <i>t</i> -C <sub>4</sub> H <sub>9</sub> <sup>+</sup> <sub>(aq)</sub>	ΔH <sub>hyd</sub> (CH <sub>3</sub> <sup>–</sup> ) = –220
<i>t</i> -C <sub>4</sub> H <sub>9</sub> Br <sub>(aq)</sub> → <i>t</i> -C <sub>4</sub> H <sub>9</sub> <sup>+</sup> <sub>(aq)</sub> + Br <sup>–</sup> <sub>(aq)</sub>	ΔH <sup>0</sup> = 150 kJ mol <sup>–1</sup>

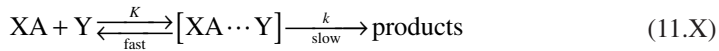
shows that the enthalpy of this heterolytic dissociation is 200 kJ mol<sup>–1</sup> lower than that of the bromomethane heterolytic dissociation. The dramatic stabilisation of the (*t*-C<sub>4</sub>H<sub>9</sub><sup>+</sup> Br<sup>–</sup>) ion pair offers an alternative to the S<sub>N</sub>2 mechanism. The rate of reaction (11.IX) was studied in 80% ethanol and ΔG<sup>‡</sup> = 91 kJ mol<sup>–1</sup> was obtained at 55 °C. An approximate estimate for the enthalpy of this reaction in 80% ethanol is ΔH<sup>0</sup> ≈ 110 kJ mol<sup>–1</sup>, including the ion-pair stabilisation. If we consider that the entropy change is relatively unimportant, this compares reasonably well with the experimental ΔG<sup>‡</sup> and strongly suggests that this reaction follows the S<sub>N</sub>1 mechanism.

The comparison between the contributions to the thermodynamic cycle is presented, step-by-step, in Table 11.1. This comparison assigns most of the difference between the enthalpies of reactions (11.VIII) and (11.IX) to the ionisation potentials of the radical R<sup>·</sup>. Minor contributions also come from the hydration of the R<sup>+</sup> carbocation and from the C–X bond dissociation energy. The factor that controls the mechanism of nucleophilic substitution appears then to be I<sub>P</sub>(R<sup>·</sup>). A low I<sub>P</sub>(R<sup>·</sup>) favours the S<sub>N</sub>1 mechanism because it lowers the enthalpy of its rate-determining step, while a high I<sub>P</sub>(R<sup>·</sup>) favours the S<sub>N</sub>2 mechanism.

### 11.3 LANGFORD–GRAY CLASSIFICATION

The mechanisms of substitution reactions at carbon atoms lead to a direct relation between the order of the reaction and its molecularity. This may cause the impression that S<sub>N</sub>1 and

$S_N2$  mechanisms encompass all possible substitution reaction mechanisms. However, the most general case is



and the reaction rate can be obtained using the same kinetic analysis presented for enzyme catalysis, eq. (4.133). Writing  $k_1 = k_{-1}K$ , dividing both the numerator and denominator by  $k_{-1}$ , and assuming that  $k_2/k_{-1} \ll 1$ , gives

$$-\frac{d[XA]}{dt} = \frac{kK[XA][Y]}{1 + K[Y]} \quad (11.3)$$

independent of the nature of the interaction in the  $XA \cdots Y$  species (ion-pair, solvation or complexation). When  $K[Y] \gg 1$ , the rate law becomes

$$v = k[XA] \quad (11.4)$$

and one can, apparently, consider that the reactant Y is not present in the transition state (TS) of the rate-determining step. This is misleading and does not contribute to the correct understanding of the reaction mechanism. Under these conditions, the reaction order is not a good criterion for the molecularity of the reaction, and  $S_N1$  and  $S_N2$  mechanisms should be regarded as limiting cases.

Langford and Gray presented another classification for the mechanism of substitution reactions that is particularly appropriate for metal complexes [5], but also englobes the classification of Ingold and co-workers for organic substitutions. This classification makes a distinction between the stoichiometric mechanism and the activation mechanism. The stoichiometric mechanism concerns the nature of the intermediate. It distinguishes between:

- (i) An *associative* mechanism (A), where an intermediate has a higher coordination number than that of the reactants.
- (ii) A *dissociative* mechanism (D), where an intermediate has a lower coordination number than that of the reactants.
- (iii) An *interchange* mechanism (I), where the bond-breaking–bond-making processes occur in a previously formed aggregate.

The activation mechanism is related to the nature of the activation step. It distinguishes between:

- (i) *Dissociative* activation, identified by the subscript d, when the TS of the rate-determining step does not have an interaction between the reactive centre and the entering group.
- (ii) *Associative* activation, identified by the subscript a, when the TS of the rate-determining step has an interaction between the reactive centre and the entering group.

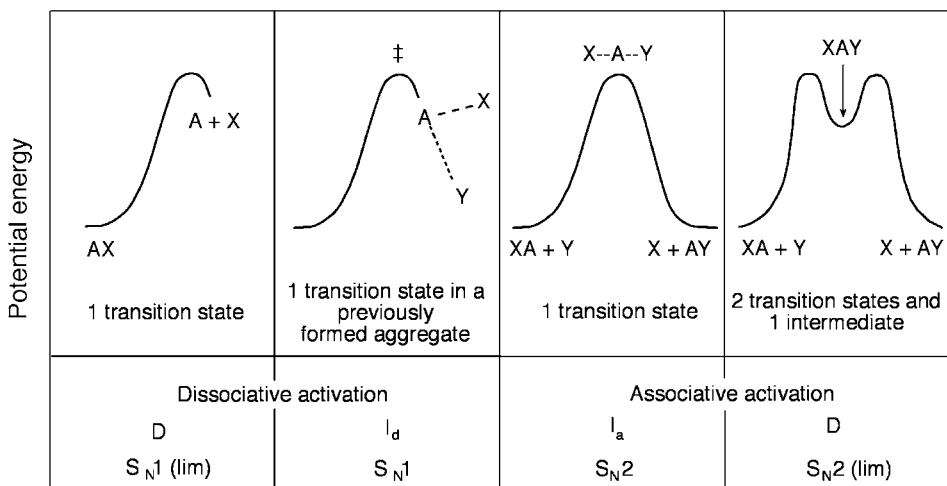
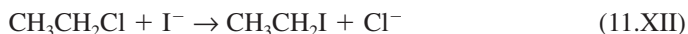


**Figure 11.2** Relationship between the mechanisms of substitution reactions and their energy profiles, and the classifications of Hughes–Ingold and Langford–Gray.

Figure 11.2 presents the relation between the classification of Ingold–Hughes and that of Langford–Gray. An example of a dissociative mechanism, D, which corresponds to the S<sub>N</sub>1 mechanism in the classification of Ingold–Hughes, is reaction (11.VII) and



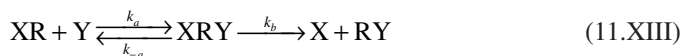
An example of an interchange mechanism, I, which is essentially an S<sub>N</sub>2 mechanism, is the reaction



that can be more exactly classified as I<sub>a</sub>.

The transition between an I<sub>a</sub> mechanism and an associative mechanism occurs when a single TS is replaced by one intermediate and two TSs. In one of these TSs the bond making is more advanced than the bond breaking, whereas in the other, the converse is true. Figure 11.3 illustrates the energy profiles for associative mechanisms.

The associative mechanism can also be illustrated by the kinetic mechanism



which leads to the reaction rate

$$-\frac{d[XR]}{dt} = \frac{k_a k_b}{k_{-a} + k_b} [XR][Y] = k_2 [XR][Y] \quad (11.5)$$

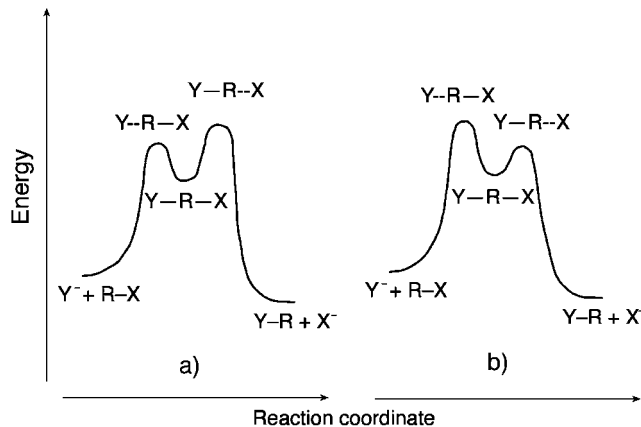


**Figure 11.3** Energy profiles for the associative mechanism of substitution reactions, A in the Langford–Gray classification, showing the relation between the intermediate and the two TSs: (a) The bond-breaking TS has higher energy. (b) The bond-making TS has higher energy.

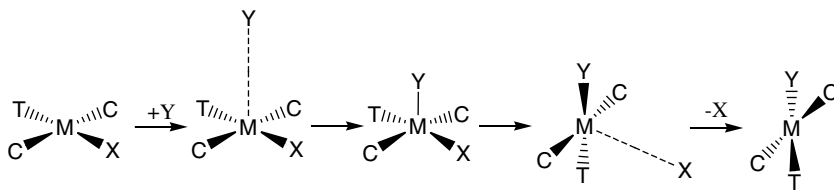


**Figure 11.4** Nucleophilic substitution in a complex with a square planar geometry proceeding through a TS with a trigonal bipyramidal geometry.

where

$$k_2 = \frac{k_a k_b}{k_{-a} + k_b} \quad (11.6)$$

This rate law has two limiting cases. If  $k_{-a} \gg k_b$  then

$$k_2 = \frac{k_a k_b}{k_{-a}} \quad (11.7)$$

and if  $k_b \gg k_{-a}$  then

$$k_2 = k_a \quad (11.8)$$

Good examples of the associative mechanism are substitution reactions in complexes with a square planar geometry, which proceed via a trigonal bipyramidal geometry, as shown in Figure 11.4.

### 11.4 SYMMETRICAL METHYL GROUP TRANSFERS IN THE GAS-PHASE

The high ionisation potential of the  $\text{CH}_3\cdot$  radical makes methyl group transfers undergo the  $\text{S}_{\text{N}}2$  mechanism



This class of reactions has been extensively studied, both experimentally and using *ab initio* methods and is one of the archetypal reactions of physical organic chemistry. Table 11.2 shows that the gas-phase internal barriers ( $\Delta E_i^\ddagger$ ) of symmetrical methyl group transfers are strongly dependent on the nature of the reactants. Additionally, the rates of the asymmetric reactions may change by ten orders of magnitude with the polarity of the solvent [6].

It is convenient to start considering the study of methyl transfers with the reactions in the gas phase, which are free from solvent effects. However, there is a price to be paid for this simplification. In the gas phase these reactions proceed through the formation of a precursor ion–dipole complex in the absence of a barrier, followed by the actual methyl transfers and the formation of a successor ion–dipole complex, and the subsequent separation of the final products [9, 10].



Figure 11.5 represents the energy changes involved in this mechanism for the case of the  $\text{Cl}:\text{-} + \text{CH}_3\text{Cl} \rightarrow \text{ClCH}_3 + \text{Cl}:\text{-}$  reaction using the data from Ziegler and co-workers [11].

Table 11.2 uncovers a very interesting relation between  $\Delta E_i^\ddagger$  and the position of the entering or leaving group in the Periodic Table. There is a trend towards lower internal barriers along the rows of the periodic table and also along the columns, although this latter trend is much less pronounced. These trends are correlated with the stabilisation energy ( $\Delta E_c$ ) of the ion–dipole complex. The formation of the ion–dipole complexes is associated with a decrease in the entropy of the systems, and compensates for the decrease in entropy

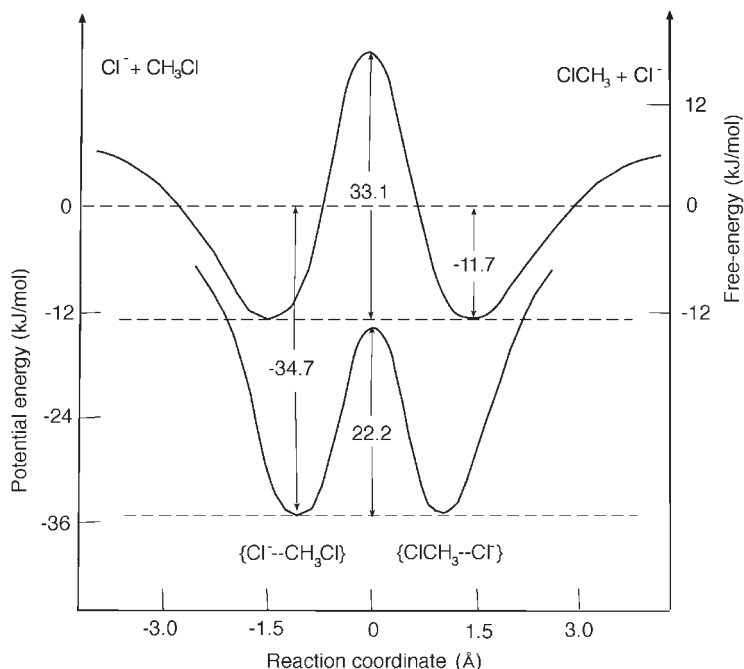
**Table 11.2**

Complexation energies (in  $\text{kJ mol}^{-1}$ ) of ion–molecule complexes (upper row) and central barriers (lower row) of gas-phase identity methyl transfer reactions of the type:  $\text{X}:\text{-} + \text{CH}_3\text{X}$  ( $\text{X} = \text{CH}_3\text{CH}_2$ ,  $\text{CH}_3\text{NH}$ ,  $\text{CH}_3\text{O}$ ,  $\text{F}$ ,  $\text{CH}_3\text{SiH}_2$ ,  $\text{CH}_3\text{PH}$ ,  $\text{CH}_3\text{S}$ ,  $\text{Cl}$ ,  $\text{CH}_3\text{GeH}_2$ ,  $\text{CH}_3\text{AsH}$ ,  $\text{CH}_3\text{Se}$ ,  $\text{Br}$ ,  $\text{CH}_3\text{SnH}_2$ ,  $\text{CH}_3\text{SbH}$ ,  $\text{CH}_3\text{Te}$ ,  $\text{I}$ ).

C	187 <sup>a)</sup>	N	123 <sup>a)</sup>	O	81.6 <sup>a)</sup>	F	-57.2 <sup>b)</sup> 55.6 <sup>b)</sup>
Si	192 <sup>a)</sup>	P	125 <sup>a)</sup>	S	91.6 <sup>a)</sup>	Cl	-44.1 <sup>b)</sup> 56.9 <sup>b)</sup>
Ge	159 <sup>a)</sup>	As	103 <sup>a)</sup>	Se	74.5 <sup>a)</sup>	Br	-42.0 <sup>b)</sup> 46.2 <sup>b)</sup>
Sn	128 <sup>a)</sup>	Sb	82.4 <sup>a)</sup>	Te	60.0 <sup>a)</sup>	I	40.2 <sup>a)</sup>

<sup>a)</sup>Hoz *et al.* [7].

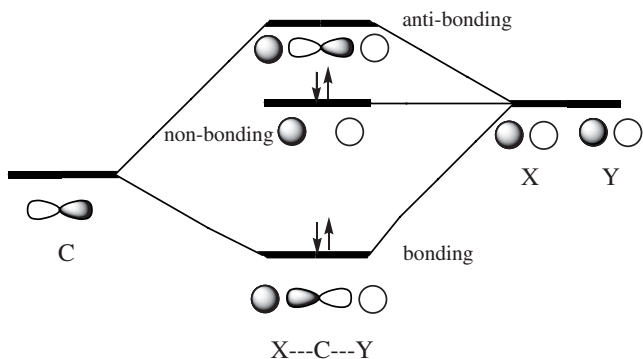
<sup>b)</sup>Parthiban *et al.* [8].



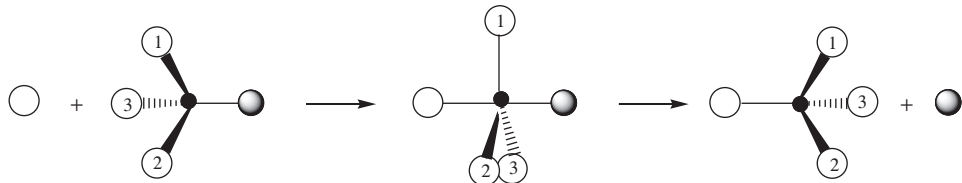
**Figure 11.5** Energy profiles of the gas-phase  $\text{Cl}^- + \text{CH}_3\text{Cl} \rightarrow \text{ClCH}_3 + \text{Cl}^-$  reaction. The upper line corresponds to the free-energy changes at 300 K and the lower line represents the classical potential energy.

also expected for the TSs. For example, the entropy change upon formation of the ion–dipole complex from the separated reactions in the  $\text{Cl}^- + \text{CH}_3\text{Cl}$  methyl exchange is  $-64.0 \pm 4.2 \text{ J K}^{-1} \text{ mol}^{-1}$  [10]. Thus, when free-energy changes are calculated, the thermodynamic stabilisation of the complexes decreases significantly, but the internal (free-energy) barriers remain very high. For this reaction, the calculated entropy changes for the formation at 300 K of the complex and of the TS are  $-76.6$  and  $-104.6 \text{ J K}^{-1} \text{ mol}^{-1}$ , respectively, and the internal free-energy barrier is only  $10.9 \text{ kJ mol}^{-1}$  higher than the classical internal barrier [11].

The traditional interpretation of  $S_N2$  reactions considers that the ten valence electrons of reaction (11.XIV) are accommodated in a trigonal bipyramidal TS where the entering (Y) and leaving (X) groups occupy axial positions and the central carbon atom has an  $\text{sp}^2$  hybridisation with the spectator (H) ligands in the equatorial positions. The  $\sigma$  bonds with the hydrogen atoms are maintained by the  $\text{sp}^2$ -hybridised carbon atom, and the axial  $p_z$  orbital of the carbon atom interacts with the p orbitals of  $\sigma$  symmetry ( $p_z$ ) of X and Y. Figure 11.6 illustrates this interaction, and the resulting bonding, non-bonding and anti-bonding orbitals. The four electrons left out of the C–H bonds occupy the bonding and non-bonding orbitals. The total bond order is unity and is maintained along the reaction coordinate.



**Figure 11.6** Molecular orbital diagram of an  $S_N2$  reaction, illustrating the interaction between the central carbon atom and the axial ligands of the trigonal bipyramidal TS. This is also an  $I_a$  mechanism.



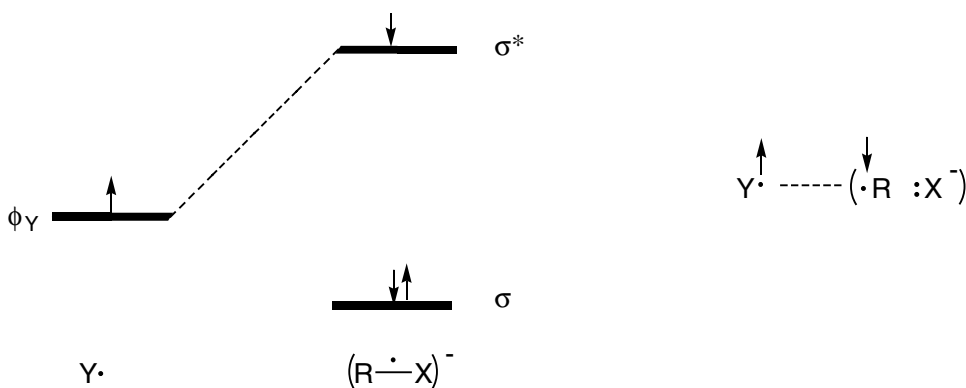
**Figure 11.7** Inversion of configuration at the carbon atom following an  $S_N2$  (or an  $I_a$ ) reaction.

Figure 11.6 also shows that for energetic and symmetry reasons the highest occupied molecular orbital (HOMO) is mostly localised in the X and Y groups. This leaves the carbon atom with an eight-electron valence shell and the attack on the tetrahedral carbon is directed towards a facial attack, with the entering group occupying the opposite position to the leaving group. The result is an inversion of configuration at the carbon atom, as illustrated in Figure 11.7.

This traditional view explains the inversion of configuration observed experimentally in methyl transfers. However, it gives no leads to the motifs of the internal barriers reported in Table 11.2. Moreover, this view does not capture the driving force for the reaction: how is it possible that the C–X bond breaks if all the electrons have bonding or non-bonding character?

## 11.5 STATE CORRELATION DIAGRAMS OF PROSS AND SHAIK

Pross and Shaik developed a model based on the valence-bond configurations of the reactive bonds that offers a conceptual understanding of the energy variations along the reaction coordinate of  $S_N2$  reactions [12]. The key feature of this model is the representation of the reactants and products by valence-bond wave functions  $\Psi_R$  and  $\Psi_P$ , respectively, and the recognition that they are incorporated into well-defined excited states of the products



**Figure 11.8** Molecular orbital and valence bond representations of the ground-state reactants in  $S_N2$  reactions.

and reactants. The only excited states considered in this work are charge-transfer states in which the nucleophiles ( $\text{Y}^-$  and  $\text{X}^-$ ) transfer one single electron to their respective substrates ( $\text{R}-\text{X}$  and  $\text{Y}-\text{R}$ ). The choice of the charge-transfer excited states is motivated by their correlation with the ground-state reactants or products. For example, the  $\text{Y}^{\cdot-}(\text{R}-\text{X}^-)$  charge-transfer state can either be described by the molecular-orbital or valence-bond representations shown in Figure 11.8. According to the molecular-orbital representation, this charge-transfer state contains a  $\phi_{\text{Y}}-\sigma^*$  bond pair, indicated by the dashed line, which accounts for one inter-molecular bond between the  $\text{Y}^-$  and  $\text{R}-\text{X}$  reactants. This is also the interaction that promotes the cleavage of the  $\text{R}-\text{X}$  bond. The electronic distribution of this charge-transfer state contains that of the products  $(\text{Y}-\text{R}): \text{X}^-$ , but in the geometry of the reactants. Therefore  $\text{Y}^{\cdot-}(\text{R}-\text{X}^-)$  qualifies as a unique excited state that will correlate with the ground state of the products,  $(\text{Y}-\text{R}): \text{X}^-$ .

More insight into the nature of the  $\text{Y}^{\cdot-}(\text{R}-\text{X}^-)$  charge-transfer state is given by the valence-bond representation of Figure 11.9. It emphasises the fact that this excited state mirrors the electronic distribution of the ground-state products,  $(\text{Y}-\text{R}): \text{X}^-$ , at the reactants' geometry. As the geometry is varied along the reaction coordinate,  $\text{Y}^{\cdot-}(\text{R}-\text{X}^-)$  will be gradually stabilised and will eventually correlate with  $(\text{Y}-\text{R}): \text{X}^-$ , as illustrated in Figure 11.9 [13]. Analogous arguments apply to the  $\text{Y}^- (\text{R}-\text{X}) \rightarrow (\text{Y}-\text{R})^{\cdot-} \text{X}$  correlation line in this Figure. The energy gaps in Figure 11.9 are the vertical electron transfer energies,  $I_p(\text{Y}^-) - E_A(\text{RX})$  and  $I_p(\text{X}^-) - E_A(\text{RY})$ , where  $I_p$  and  $E_A$  are the ionisation potentials and electron affinities, respectively. They reflect the essence of the electronic reshuffle in  $S_N2$  reactions, where a single electron shift is concomitant with the bond-breaking–bond-forming process. It follows that the barrier for the reaction can be expressed as a fraction ( $f$ ) of the vertical electron transfer energy, from which the crossing avoidance ( $B$ ) has been subtracted,

$$\Delta^{\ddagger}E = f[I_p(\text{Y}^-) - E_A(\text{RX})] - B \quad (11.9)$$

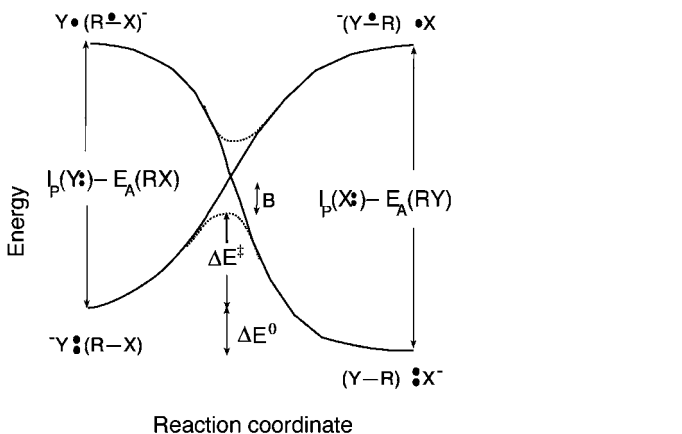


**Figure 11.9** Shaik and Pross state correlation diagram for  $S_N2$  reactions.

Eq. (11.9) contains the physical essence of the activation process. The energy of activation arises from the molecular distortions that must attend the single electron shift ( $Y \rightarrow X$ ) characterising the  $S_N2$  reaction. The only manner by which such a shift can take place is when an energy equality between  $Y^-$  ( $R-X$ ) and  $Y^{\bullet}$  ( $R-X^-$ ) is attained. Since these two states are initially separated by an energy  $I_p(Y^-) - E_A(RX)$ , their crossing must be achieved at the expense of molecular distortions that stabilise  $Y^{\bullet}$  ( $R-X^-$ ) and simultaneously destabilise  $Y^-$  ( $R-X$ ). The activation energy will then reflect the size of the vertical electron transfer energy and the resistance to molecular distortions, with the latter parameter being reflected by the value of  $f$ .

The value of the curvature factor  $f$  depends on the energy curve employed to derive eq. (11.9). For example, when straight lines are employed to connect the appropriate states of a symmetrical reaction, then  $f = 0.5$ . In contrast, if two identical parabolas are employed, then  $f = 0.25$ . In this case, a Marcusian-type expression is obtained, where the energy gap  $I_p(Y^-) - E_A(RX)$  replaces the reorganisation energy  $\lambda$  in the Marcus expression. Shaik associated the value of  $f$  to the extent of the “extra delocalisation” of the bonding odd electrons in the charge-transfer states. The extra delocalisation of the odd electrons causes a sluggish descent of the charge-transfer states towards their intersection point, and increases the  $f$  factor [13].

The state correlation diagrams of Pross and Shaik provide a very interesting insight into the nature of the reaction coordinate of  $S_N2$  reactions. However, they cannot be used for quantitative estimates of the reaction rates. In fact, the simplest expectation from eq. (11.9), a correlation between the energy gap and the energy barrier, is not verified (Figure 11.10). More recently, Shaik and Shurki reproduced the intrinsic barriers of the halide series in calculations where the resonance term  $B$  was assumed to be dependent on the HOMO-LUMO orbital splitting and on the charge distribution at the TS [14]. The success of the Shaik–Pross state correlation diagram in predicting correctly the barriers of

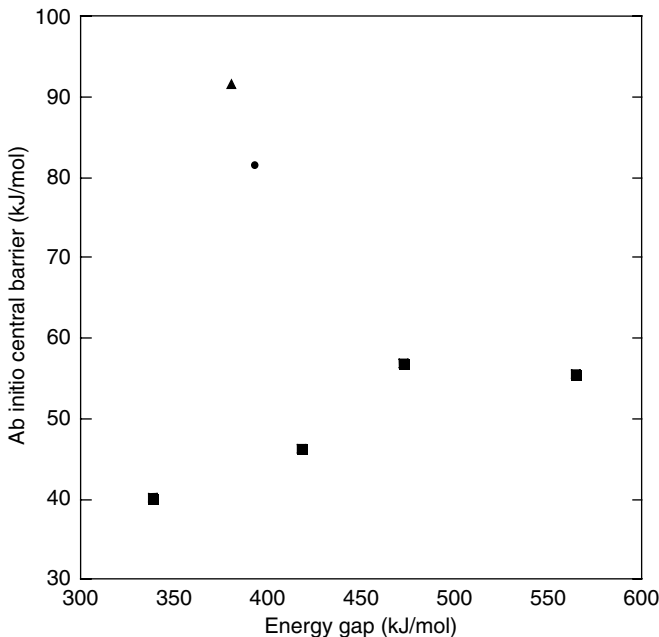


**Figure 11.10** Correlation between the energy gap  $[I_p(\text{Y}) - E_{\text{A}}(\text{RX})]$  and the central barrier of methyl transfers in the gas phase. The energy gap values were taken from Table 2 of Ref. [13], and the central barriers are from Table 11.2. (Squares: X = halogen atom; circles: X =  $\text{CH}_3\text{O}$ ; triangle: X =  $\text{CH}_3\text{S}$ .)

halide–methyl halide  $\text{S}_{\text{N}}2$  identity reactions cannot be, at the moment, reduced to a simple, easy-to-use model or explanation [7].

## 11.6 INTERSECTING-STATE MODEL

The formalism of the intersecting-state model (ISM) previously applied to atom-transfer reactions in Chapter 6, can also be employed to interpret the trends observed in central barriers of gas-phase identity methyl transfer reactions [15]. The symmetry of such reactions offers the opportunity to use the simplest version of ISM. For harmonic oscillators and symmetric reactions, eq. (6.92) gives

$$\Delta V^* = 2 \frac{f}{m^2} \left[ a' l_{\text{xc}} \ln(2) \right]^2 \quad (11.10)$$

where  $a' = 0.183$ , the electrophilicity index of Parr is

$$m = \frac{I_{\text{p}} + E_{\text{A}}}{I_{\text{p}} - E_{\text{A}}} \quad (11.11)$$

and the force constant is

$$f = 2D_e\beta^2 \quad (11.12)$$

with the spectroscopic constant  $\beta$  related to electronic dissociation energy of the  $\text{CH}_3\text{-X}$  bond, to the vibrational energy and to the reduced mass

$$\beta = \varpi_e \sqrt{\frac{2\pi^2 c \mu}{h D_e}} = 0.01332 \varpi_e \sqrt{\frac{\mu}{D_e}} \quad (11.13)$$

where the numerical value applied corresponds to the case when the masses are expressed in amu, the frequencies in per centimetre and energies in kJ/mol.

The data on the ionisation potentials ( $I_p$ ) and electron affinities ( $E_A$ ) of X and on the  $\text{CH}_3\text{-X}$  bonds dissociation energies, bond lengths and vibrational frequencies of the systems represented in Table 11.2 can be found in Tables 1 and 3 of Appendix III [15]. Unfortunately, the values of  $I_p$  and  $E_A$  are not readily available for all the systems of Table 11.2. Nevertheless,

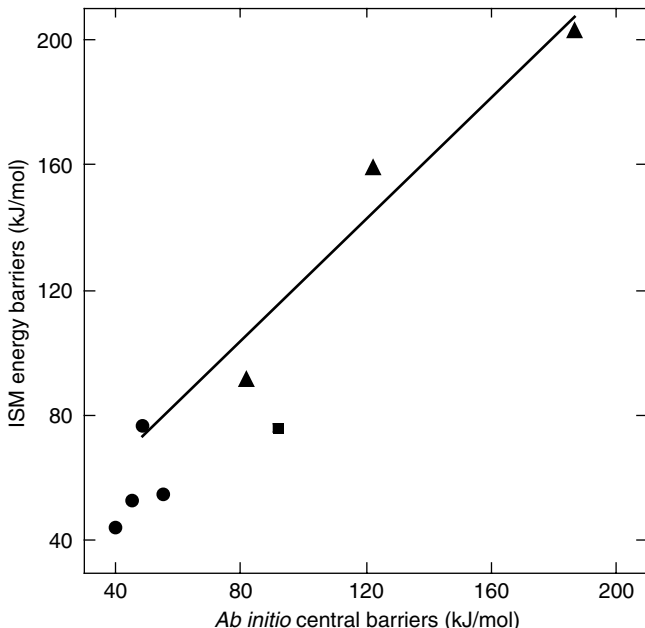


**Figure 11.11** Correlation between the central barriers of *ab initio* calculations given in Table 11.2, and the barriers of the ISM calculations under the harmonic approximation. (Squares: X = halogen atom; circles: X =  $\text{CH}_3\text{CH}_2$ ,  $\text{CH}_3\text{NH}$ ,  $\text{CH}_3\text{O}$ ; triangle:  $\text{CH}_3\text{S}$ . The line is the correlation between the barriers of the second row of the Periodic Table.)

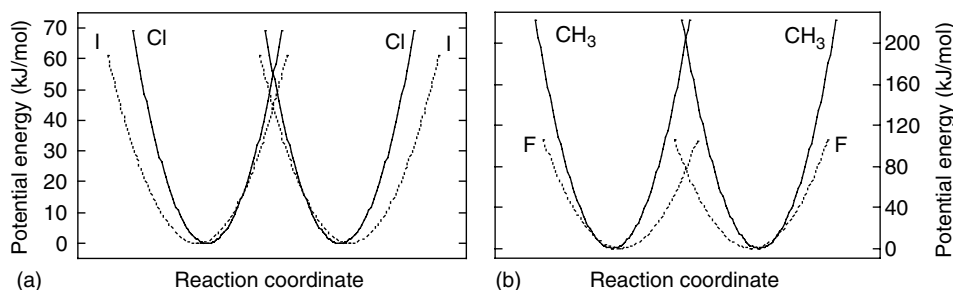


**Figure 11.12** (a) Compensation between decreases in force constants and increases in bond lengths. (b) Effect of the electrophilicity index  $m$  on the TS, schematically represented by the division of the force constant by  $m^2$ .

Figure 11.11 presents the results obtained for a larger set of data than Figure 11.10, and shows that the ISM presents a good account of the central barriers in the gas phase. More importantly, these simple calculations reproduce the trends of the *ab initio* barriers: the central barriers change modestly along the last column and dramatically along the second row of the Periodic Table.

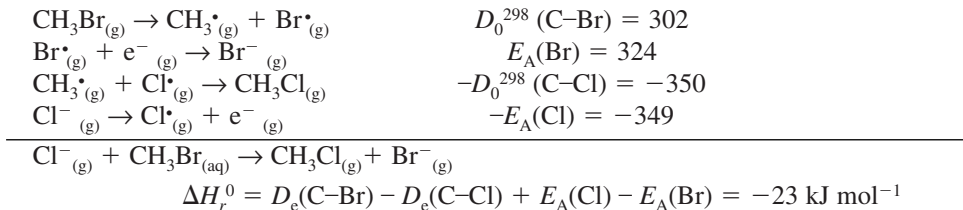
The relative constancy of the central barrier within a column of the Periodic Table has a simple explanation in the framework of the ISM. As the atomic number increases along the series of halogens, the X–C bond lengths increase ( $1.351$ ,  $1.764$ ,  $1.951$  and  $2.027$  Å), the corresponding force constants decrease ( $2950$ ,  $1740$ ,  $1410$  and  $1130$   $\text{kJ mol}^{-1} \text{\AA}^{-1}$ ), while the electrophilicity indices remain approximately constant ( $1.493$ ,  $1.773$ ,  $1.796$  and  $1.828$ ). Eq. (11.10) shows that, for a constant  $m$ , the decrease in  $f_{\text{XC}}$  is compensated by the increase in  $l_{\text{XC}}$  and the barriers remains approximately constant [15]. This compensation is illustrated in Figure 11.12.

The ISM also accommodates the decrease in central barrier along the second row of the Periodic Table. In this case the decrease in  $l_{\text{XC}}$  ( $1.512$ ,  $1.474$ ,  $1.404$  and  $1.351$  Å) is not accompanied by a systematic trend in the corresponding force constants ( $2450$ ,  $3110$ ,  $2610$  and  $2950$   $\text{kJ mol}^{-1} \text{\AA}^{-1}$ ), and the relative reactivity is dominated by the increase in  $m$  ( $0.938$ ,  $1.163$ ,  $1.343$  and  $1.493$ ). Figure 11.12 offers a simple view of the effect of  $m$  on the energy barrier, by dividing  $f_{\text{XC}}$  by  $m^2$ . It should always be remembered that this is only a schematic view, because the force constants near the minima are given by the spectroscopic properties of the bonds, while the full effect of  $m$  is only manifested at the TS.

The beauty of this explanation undoubtedly lies in its straightforwardness and simplicity. Moreover, similar trends have been calculated for the transfer of the  $\text{N}(\text{CH}_3)_2$  group [16] and confirmed by other authors [17], in support of the reactivity factors described above. At this level of simplicity the ISM cannot provide a complete explanation for all the observations, and its success is probably due to a compensation of errors. For example, the central barriers tend to be underestimated when Morse curves, rather than harmonic oscillators, are employed in the calculations. The harmonic oscillators compensate for the original scaling of the ISM to the  $\text{H}+\text{H}_2$  atom abstraction.

### 11.7 CROSS-REACTIONS IN METHYL GROUP TRANSFERS IN THE GAS PHASE

The reaction energy of a cross-reaction can be obtained from the difference in bond dissociation energies and electron affinities of the two reaction partners. For example,



However, this is not the directly relevant reaction energy for the central barrier, because the energetic separation between the minima of the precursor and successor complexes may not correspond to the energetic separation between the isolated reactants and the products. For the case of the reaction illustrated above, the complexation energies of  $\text{Cl}^{-}\cdots\text{CH}_3\text{Br}$  and  $\text{Br}^{-}\cdots\text{CH}_3\text{Cl}$  are 52 and 46  $\text{kJ mol}^{-1}$ , respectively, and the energetic separation between the complexes is only 6  $\text{kJ mol}^{-1}$  less exothermic than  $\Delta H_r^0$ . When the difference between complexation energies is small, as in the case of alkylhalide–halide ions [10,18], it is legitimate to expect that the global free energy of the reaction is reflected by the central barrier, and that the free-energy relationships discussed in Chapter 7 may apply. This is approximately the case for the cross-reactions between halide ions such as  $\text{Cl}^{-}/\text{CH}_3\text{Br}$ ,  $\text{F}^{-}/\text{CH}_3\text{Cl}$  and  $\text{F}^{-}/\text{CH}_3\text{Br}$ , where the reaction exothermicity increases from  $-23$ , to  $-147$ , and to  $-171 \text{ kJ mol}^{-1}$ , with a concomitant decrease of the central barrier from 36, to 12, and to 3  $\text{kJ mol}^{-1}$ . The ISM calculations using the harmonic approximation and the global reaction energy reproduce these barriers relatively well, giving 43.0, 24.6 and 20.6  $\text{kJ mol}^{-1}$ , respectively, when the average value of  $m$  of the halogens involved is employed.

The success of this approach to gas-phase methyl transfers is very limited. For example, Figure 11.13 illustrates the reaction energy profile of the  $\text{F}^{-} + \text{CH}_3\text{SH}$  methyl transfer and shows that the overall reaction is exothermic,  $\Delta H_r^0 = -48 \text{ kJ mol}^{-1}$ , but the central barrier is placed between the two minima corresponding to ion–molecule complexes whose endothermic conversion requires  $\Delta V_{\text{ad}}^0 = 75 \text{ kJ mol}^{-1}$  [19]. Although the reaction energy, measured for the separated products to the separated reactants, is moderately exothermic, the actual reaction involves a precursor and successor complex that must be regarded as the reaction intermediates. The conversion between these two intermediates is an elementary reaction, and is endothermic because the electrostatic stabilisation in the  $\text{F}^{-} + \text{CH}_3\text{SH}$  complex is stronger than in the  $\text{HS}^{-} + \text{CH}_3\text{F}$  complex. The barrier calculated for the elementary reaction is high,  $\Delta V_{\text{ad}}^{\ddagger} = 166 \text{ kJ mol}^{-1}$  [19], as expected for an endothermic reaction, but the energy of the TS is only 18  $\text{kJ mol}^{-1}$  above that of the separated reactants.

There are several lessons to be learnt from this example. First, free-energy relationships can only be applied to elementary reactions, otherwise they will fail or fortuitously give the correct results owing to compensation of factors. Second, the presence of a stable intermediate may reduce the experimental activation energy, and may even lead to a negative

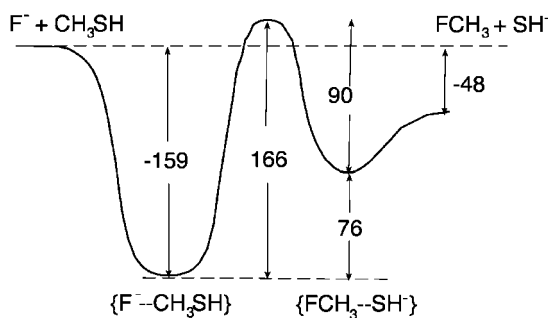


**Figure 11.13** Reaction energy profile of the  $\text{F}^- + \text{CH}_3\text{SH}$  methyl transfer in the gas phase. The energies were obtained by *ab initio* methods by Schaefer and co-workers, and include zero-point energy (ZPE) corrections [19].

activation energy, but that does not mean that high-energy barriers do not exist along the reaction path in the conversion between the intermediates. Finally, the presence of two complexes separated by a barrier suggests that their conversion resembles that of a unimolecular reaction and that the experimental data corresponding to this mechanism should be evaluated with the RRKM theory. In fact, RRKM calculations have been remarkably successful in describing the kinetics of three-bodied ion–molecule association reactions [20], but non-statistical behaviour, where the vibrational energy is not rapidly and randomly distributed among the vibrational modes, is also known [21].

The mechanistic complexity of  $\text{S}_{\text{N}}2$  reactions is removed in aqueous solutions. The solvation of the attacking nucleophile reduces the energy of the reactants below that of the complex, and the reaction occurs in a single step, with concerted bond breaking and bond making.

## 11.8 SOLVENT EFFECTS IN METHYL GROUP TRANSFERS

The rate constant for the symmetrical methyl transfer between  $\text{I}^-$  and  $\text{CH}_3\text{I}$  varies with change of solvent, and has values at 298 K (in  $\text{M}^{-1} \text{ sec}^{-1}$ ) ranging from  $5.1 \times 10^{-4}$  in water to  $3.2 \times 10^{-3}$  in methanol and 8.0 in acetone, and is expected to exceed  $10^9$  in the gas phase [22]. This change in the rate is clearly related to the polarity of the solvent. Another way of looking at this effect is to consider the free energies of activation,  $\Delta G^\ddagger$ , in the different media (Table 11.3; [22]). It is important to emphasise that the energy data in solution are not (adiabatic or electronic) potential energies, but free energies. Such free energies are estimated from the rate constants using the pre-exponential factor of the transition state theory (TST) in its thermodynamic formulations,  $k_{\text{B}}T/h$ . They are not directly comparable with the potential energies presented for gas-phase reactions, which do not include entropy changes. Fortunately, the entropy changes along the reaction path of the  $\text{Cl}^- + \text{CH}_3\text{Cl}$  have been calculated with high accuracy by *ab initio* methods [11], and provide a term for comparison.

**Table 11.3**

Energies of activation for symmetrical exchange reactions in different media, in  $\text{kJ mol}^{-1}$ .

Reaction	$\Delta G^\ddagger$ (water)	$\Delta G^\ddagger$ (methanol)	$\Delta G^\ddagger$ (dimethylformamide (DMF))	$\Delta G^\ddagger$ (acetone)	$\Delta V_{\text{cl}}^\ddagger$ (gas) <sup>a</sup>	$\Delta G^\ddagger$ (gas) <sup>b</sup>
$\text{F}^- + \text{CH}_3\text{F}$	133				56	
$\text{Cl}^- + \text{CH}_3\text{Cl}$	111	118	95	91	57	65
$\text{Br}^- + \text{CH}_3\text{Br}$	99	96	77	71	42	
$\text{I}^- + \text{CH}_3\text{I}$	97	88	67	68	40	
$\text{OH}^- + \text{CH}_3\text{OH}$	175					

Note: From Ref. [22] unless otherwise noted.

<sup>a</sup>Central barriers from Ref. [7], without (ZPE) corrections.

<sup>b</sup>Central free-energy barrier, obtained from the ZPE-corrected (G3 method) central barrier with the addition of the calculated (DFT method) entropy changes upon formation of ion-dipole complex, and TS, from the separated reactants, from Ref. [11].

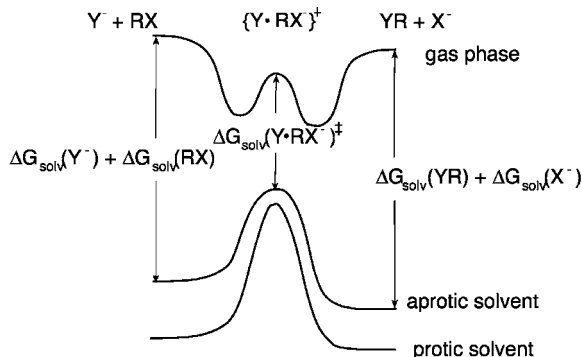


**Figure 11.14** Solvent effect on the energy profiles of methyl transfer reactions.

The effect of the solvent on methyl group transfers is illustrated in Figure 11.14. In Figure 11.5 we had already shown that the consideration of entropy changes reduces the energy difference between the reactants and the precursor complex, as well as between the products and the successor complex. Now, we also have to consider that the ionic nature of the reactants and products facilitates their solvation to higher degree than in these complexes. As a result, in a sufficiently polar solvent such as water, these complexes disappear from the reaction coordinate, and the methyl group transfer becomes an elementary reaction.

The TS is of lower polarity than the reactants and the products. Thus, in polar solvents, it rises in energy with respect to the reactants, and to a higher degree than the precursor and the successor complexes. This can be verified for the  $\text{Cl}^- + \text{CH}_3\text{Cl}$  reaction, where the internal free-energy barrier in the gas phase is smaller than the free-energy barrier in solution. For identity transfers, where  $\Delta G^0 = 0$ , the changes in solvation energy are relatively independent of the nature of the reactants, and the reactivity trends observed for gas-phase reactions are also observed in solution. In fact, from  $\text{Cl}^- + \text{CH}_3\text{Cl}$  to  $\text{I}^- + \text{CH}_3\text{I}$  there is a

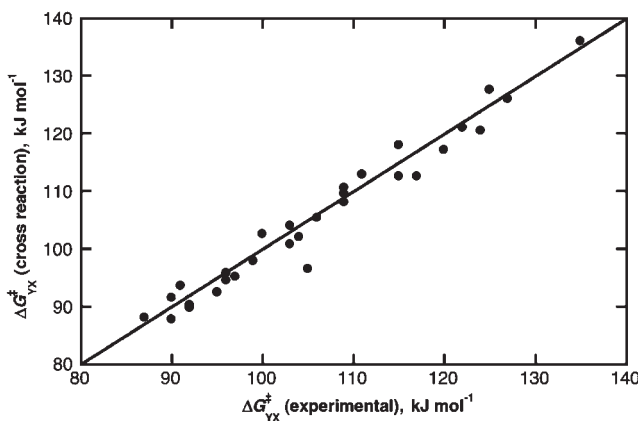


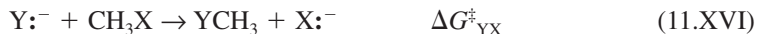
**Figure 11.15** Comparison between the activation free energies calculated by the cross-reaction scheme and the experimental values, using data from Albery and Kreevoy [22].

ca 20% decrease in the free-energy barrier, similar to that calculated for  $\Delta V_{\text{el}}^{\ddagger}$  in the gas phase. Also, the free energy of activation of the  $\text{OH}^- + \text{CH}_3\text{OH}$  exchange in water is much higher than the self-exchanges involving halide ions, a trend also observed in the gas phase. The recognition of the same reactivity patterns in symmetrical methyl transfers in the gas phase and in solution, suggests that the explanation offered by the ISM for such patterns in the gas phase is also applicable to solution. However, a quantitative account of the free-energy barriers in solution requires a different scaling factor,  $a'_{\text{sol}} > a'_{\text{gas}}$ .

The comparison between gas phase and solution becomes more convoluted when cross-reactions are considered. For example, the rate of the  $\text{Cl}^- + \text{CH}_3\text{Br}$  reaction, at 298 K (in  $\text{M}^{-1} \text{ sec}^{-1}$ ), decreases from  $8 \times 10^9$  in the gas phase, to 0.4 in DMF,  $6 \times 10^{-6}$  in methanol, and reaches  $5 \times 10^{-6}$  in water [23]. We have seen that this reaction is exothermic in the gas phase. The difference in free energies of formation in aqueous solution, at 298 K in kJ/mol, of  $\text{CH}_3\text{Cl}$  (-57) and  $\text{CH}_3\text{Br}$  (-24), almost compensates those of  $\text{Cl}^-$  (-131) and  $\text{Br}^-$  (-104), and the exothermicity of this reaction in aqueous solution,  $\Delta G^0 = -6 \text{ kJ mol}^{-1}$ , is comparable with the value given previously for the gas phase [22]. Clearly, the minor decrease in exothermicity for the gas phase to solution cannot justify the 15 orders of magnitude change in the methyl transfer rate. This reactivity difference must also be related to the differential solvation of the TS and the reactants.

In addition to the striking difference in absolute rates in different media, there are differences and reversals in relative rates. For instance, the halogen nucleophilic order is changed from  $\text{F}^- > \text{Cl}^- > \text{Br}^- > \text{I}^-$  in the gas phase and polar aprotic solvents such as acetone and DMF, to  $\text{I}^- > \text{Br}^- > \text{Cl}^- > \text{F}^-$  in protic solvents such as methanol and water [23]. This difference can also be understood in terms of differential solvation of the TS and the reactants. The enthalpies of transfer from dimethylsulphoxide (polar aprotic solvent) to methanol are, at 298 K in kJ/mol,  $\text{Cl}^-$  (-10.4),  $\text{Br}^-$  (-0.4), and  $\text{I}^-$  (11.3). The increase in the relative solvation of the smaller halides in methanol is enough to reverse their order of reactivity, since the solvation of the TSs is not as sensitive to solvent changes as the solvation of the reactant anions [23].

The fact that methyl transfers in water are elementary reactions suggests that they should be a better ground to test the applicability of free-energy relationships in S<sub>N</sub>2 reactions. Albery and Kreevoy made an extensive study of such reactions and attempted to interpret their free-energy dependence using the Marcus cross-reaction scheme. According to the Marcus cross-relation, the free energy of activation of the cross-reaction



is related to the free energies of activation of the symmetrical exchanges



according to the expression

$$\Delta G_{\text{YX}}^\ddagger = \Delta G_{\text{YX}}^{\ddagger 0} \left( 1 + \frac{\Delta G_{\text{YX}}^0}{4 \Delta G_{\text{YX}}^{\ddagger 0}} \right)^2 \quad (11.14)$$

where

$$\Delta G_{\text{YX}}^{\ddagger 0} = \frac{1}{2} (\Delta G_{\text{XX}}^\ddagger + \Delta G_{\text{YY}}^\ddagger) \quad (11.15)$$

Albery and Kreevoy studied methyl transfers having the ions PhSO<sub>3</sub><sup>-</sup>, NO<sub>3</sub><sup>-</sup>, F<sup>-</sup>, Cl<sup>-</sup>, Br<sup>-</sup>, I<sup>-</sup>, CN<sup>-</sup>, OH<sup>-</sup> as nucleophiles as well as leaving groups. They also considered the substitution by the water molecule, which is involved in the hydrolysis of halogenomethanes. In the absence of information in most of the identity exchange reactions, they fitted the values of ΔG<sup>‡</sup><sub>XX</sub> and ΔG<sup>‡</sup><sub>YY</sub>, to obtain the best agreement with ΔG<sup>‡</sup><sub>YX</sub>, given the experimental reaction free energies, ΔG<sup>0</sup><sub>YX</sub>. Some of the activation energies included in Table 11.3 were in fact obtained by this method. Figure 11.15 shows that the activation free energies calculated with the cross-relation are in good agreement with the experimental cross-reaction activation free energies. Such a good agreement is not totally expected because Marcus originally proposed the cross-reaction scheme for electron-transfer reactions, where the reaction coordinate involves the two reactants and the two products. In S<sub>N</sub>2 reactions this scheme is equivalent to saying that the properties of the C-X bond in the reactants and of the C-Y bond in the product are similar to the average of the C-X and C-Y bond properties. The assumption that the free-energy dependence is quadratic rather than linear is also reasonably followed in the exothermicity range of 200 kJ mol<sup>-1</sup> covered by the systems selected by Albery and Kreevoy.

The calculation of the rates of these elementary reactions in aqueous solution using the ISM poses a new problem. This method calculates the electronic parameter, *m* in eq. (11.11), from the gas-phase ionisation energies and electron affinities, which may not be adequate for reactions in aqueous solution. In fact, it is not the actual *I*<sub>P</sub> and *E*<sub>A</sub> in aqueous solution that is relevant, but their changes due to differential solvation. The simplest way to circumvent this problem is to rescale the method by using an empirical value of *a'*, fitted to

yield the best agreement with the rates of methyl transfers in aqueous solution. The result is a decrease in the value of  $m$ , because a higher barrier requires a lower  $m$ . Additionally, in the spirit of the cross-relation, the electronic parameter of the cross-reaction,  $m_{YX}$ , is taken as the average of the values of  $m$  for the identity relations,  $m_{YX} = (m_{XX} + m_{YY})/2$ .

The activation energy is determined by the energy of the crossing between the reactant and product potential energy curves,

$$V_{CX} = V_{CY} + V_0 \quad (11.16)$$

where  $V_0$  is the reaction energy. When the reactant C–X and the product C–Y bond are represented by harmonic oscillators, we have

$$\begin{aligned} V_{CX} &= \frac{1}{2} f_{CX} \left[ \frac{a_w' (l_{CX} + l_{CY}) \ln(1-n)}{m_{YX}} \right]^2 \\ V_{CY} &= \frac{1}{2} f_{CY} \left[ \frac{a_w' (l_{CX} + l_{CY}) \ln(n)}{m_{YX}} \right]^2 \end{aligned} \quad (11.17)$$

where the value of  $n$  that satisfies the equality of eq. (11.16) is the TS bond order,  $n^\ddagger$ .

The pre-exponential factor can be calculated by the methods described in Chapter 6. In practice, when  $Y = F^-, Cl^-, Br^-, I^-, CN^-$  or  $OH^-$ , the value of the pre-exponential factor

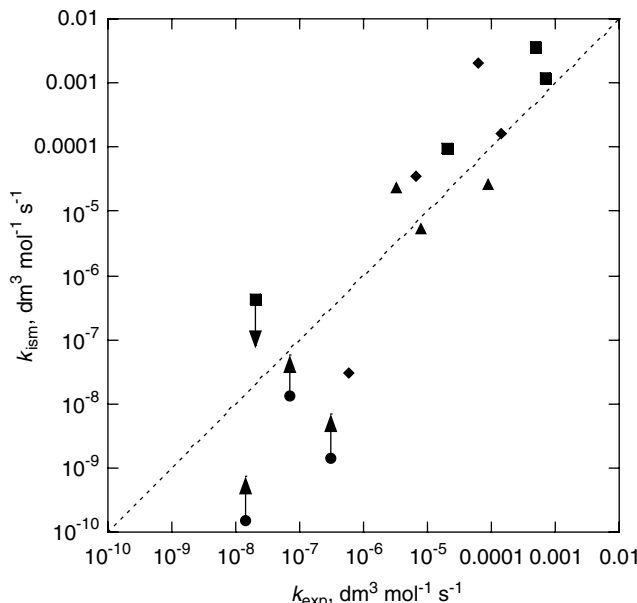


**Figure 11.16** Comparison between the ISM and experimental rate constants in methyl transfers. (Circles:  $F^- + CH_3X$ , squares:  $I^- + CH_3X$ , lozenges:  $OH^- + CH_3X$ , triangles:  $Cl^-$  or  $Br^- + CH_3X$ : in all cases,  $X = F, Cl, Br, I$ .)

is  $(8 \pm 5) \times 10^9 \text{ dm}^3 \text{ mol}^{-1} \text{ sec}^{-1}$ , and the changes in reactivity are mainly determined by the changes in the activation energy. Figure 11.16 compares the experimental rates constants at 25 °C [24,25], with the rate constants calculated with  $a_w' = 0.23$ , the values of  $V_0$  given by Albery and Kreevoy, and the bond dissociation energies, bond lengths and vibrational frequencies presented in Tables 1 and 2 of Appendix III. This value of  $a_w'$  is 26% larger than the value employed for the same reaction in the gas phase. In view of the approximations involved in this simple calculation, the agreement between the calculated and the experimental rates can be considered to be good. An example of such approximations is the estimate of the reaction free energy of the  $\text{I}^- + \text{CH}_3\text{F}$  by Albery and Kreevoy,  $\Delta G^0 = -5 \text{ kJ mol}^{-1}$ . It is 8 kJ mol<sup>-1</sup> lower than that obtained from the ratio of the forward and reverse reactions measured by Moelwyn-Hughes [24]. This error, tentatively assigned to the free energy of formation of  $\text{F}^-$  or  $\text{CH}_3\text{F}$  in aqueous solution, makes the  $\text{I}^- + \text{CH}_3\text{F}$  reaction exothermic rather than endothermic. The arrows in Figure 11.16 illustrate how this error propagates into the rate constants of the reactions where  $\text{F}^-$  is the nucleophile.

## REFERENCES

- [1] ED Hughes, CK Ingold, CS Patel, *J. Chem. Soc.* (1933) 526.
- [2] CK Ingold, *Structure and Mechanism in Organic Chemistry*, Cornell University Press, Ithaca, NY, 1969.
- [3] RG Pearson, *J. Am. Chem. Soc.* **108** (1986) 6109.
- [4] RC Weast (Ed.), *CRC Handbook of Chemistry and Physics*, CRC Press, Boca Raton, FL, 1983.
- [5] CH Langford, HB Gray, *Ligand Substitution Processes*, Benjamin, Nova Iorque, 1965.
- [6] S Wolfe, DJ Mitchell, MT Bowers, *J. Am. Chem. Soc.* **103** (1981) 7694.
- [7] S Hoz, H Basch, JL Wolk, T Hoz, E Rozental, *J. Am. Chem. Soc.* **121** (1999) 7724.
- [8] S Parthiban, G De Oliveira, JML Martin, *J. Phys. Chem. A* **105** (2001) 895.
- [9] ST Gravel, MT Bowers, *J. Am. Chem. Soc.* **113** (1991) 9696.
- [10] RC Dougherty, JD Roberts, *Org. Mass Spectrom.* **8** (1974) 81.
- [11] S-Y Yang, P Fleurat-Lessard, I Hristov, T Ziegler, *J. Phys. Chem. A* **108** (2004) 9461.
- [12] SS Shaik, A Pross, *J. Am. Chem. Soc.* **104** (1982) 2708.
- [13] SS Shaik, *Prog. Phys. Org. Chem.* **15** (1985) 197.
- [14] SS Shaik, A Shurki, *Angew. Chem. Int. Ed.* **38** (1999) 586.
- [15] LG Arnaut, AAC Pais, SJ Formosinho, *J. Mol. Struct.* **563/564** (2001) 1.
- [16] R Yi, H Basch, S Hoz, *J. Org. Chem.* **67** (2002) 5891.
- [17] E Uggerud, *Chem. Eur. J.* **12** (2006) 1127.
- [18] C Li, P Ross, JE Szulejko, TB McMahon, *J. Am. Chem. Soc.* **118** (1996) 9360.
- [19] JM Gonzales, RS Cox III, ST Brown, WD Allen, HF Schaefer III, *J. Phys. Chem. A* **105** (2001) 11327.
- [20] BD Wladkowski, KF Lim, WD Allen, JI Brauman, *J. Am. Chem. Soc.* **114** (1992) 9136.
- [21] L Sun, K Song, WL Hase, *Science* **296** (2002) 875.
- [22] J Albery, MM Kreevoy, *Adv. Phys. Org. Chem.* **16** (1978) 87.
- [23] WN Olmstead, JI Brauman, *J. Am. Chem. Soc.* **99** (1977) 4219.
- [24] EA Moelwyn-Hughes, *The Chemical Statics and Kinetics of Solutions*, Academic Press, London, 1971.
- [25] AJ Parker, *Chem. Rev.* **69** (1969) 1.

# – 12 –

## Chain Reactions

---

Open shell atoms and other molecular species that act as *free radicals* play a special role as intermediates in reaction mechanisms. Because they have incomplete electron shells they are usually highly reactive, even with stable molecules at ordinary temperatures. The concentrations of such free radicals in these reaction systems are usually low and the application of the *steady-state hypothesis* to them is valid.

In *chain reactions* free radicals bring about chemical processes such as abstraction when they react with a molecule, producing new atoms and radicals, which can then bring about further reactions. Figure 12.1 displays a sequence of steps for chain reactions involving halogens and molecular hydrogen: (i) *initiation* step which produces the chain carriers, R<sub>i</sub>; (ii) *propagation* steps in which chain carriers recycle and thus catalyse the conversion of reactants, Q, to products; (iii) *termination* steps which remove the intermediates [1].

### 12.1 HYDROGEN-BROMINE REACTION

The mechanism for the reaction between Br<sub>2</sub> and H<sub>2</sub> was proposed in 1916 independently by Christiansen [2], Herzfeld [3,4] and Polanyi [5]. The basic steps are

- |      |                                |                   |
|------|--------------------------------|-------------------|
| (1)  | Br <sub>2</sub> → 2Br          | initiation        |
| (2)  | Br + H <sub>2</sub> → HBr + H  | chain propagation |
| (3)  | H + Br <sub>2</sub> → HBr + Br | chain propagation |
| (-1) | 2Br → Br <sub>2</sub>          | termination       |
| (-2) | H + HBr → H <sub>2</sub> + Br  | termination       |
- (12.I)

This mechanism has an initiation step (1) one termination step (-1) and a pair of propagation steps (2) and (3). There is an additional step of termination (-2), which accounts for the inhibition by HBr seen experimentally.

As shown in Table 12.1 the rates of the propagation steps are much greater than those of the initiation or the termination processes, which have negligible contributions to the overall rate. In the propagation steps, atoms are formed and consumed. One needs to obtain expressions for their concentrations, which is most frequently done through the steady-state hypothesis.

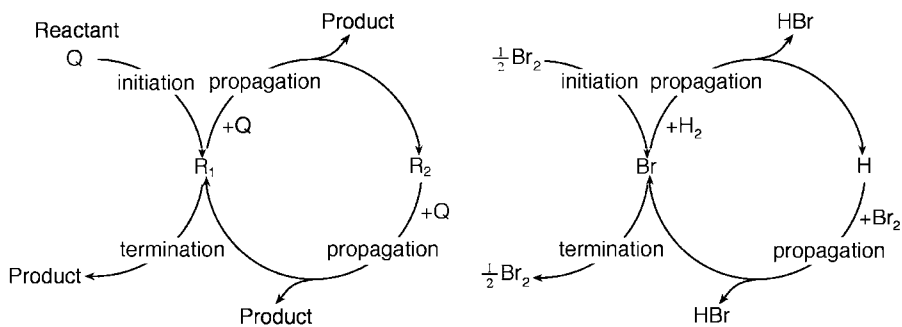


**Figure 12.1** Reaction between halogens and molecular hydrogen.

**Table 12.1**

Experimental rate constants for the different elementary steps of the reaction between  $\text{H}_2 + \text{Br}_2$ , at 1 atm, 500 K and  $[\text{M}] \approx 0.025 \text{ M}$

Reaction	Step	$k$ ( $\text{dm}^3 \text{ mol}^{-1} \text{ sec}^{-1}$ )	Step no.
$\text{Br}_2 + \text{M} \rightarrow 2\text{Br} + \text{M}$	Initiation	$3.8 \times 10^{-8} [\text{M}]$	(1)
$2\text{Br} + \text{M} \rightarrow \text{Br}_2 + \text{M}$	Termination	$4.2 \times 10^{-13} [\text{M}]$	(-1)
$\text{Br} + \text{H}_2 \rightarrow \text{HBr} + \text{H}$	Propagation	960	(2)
$\text{H} + \text{HBr} \rightarrow \text{H}_2 + \text{Br}$	Inhibition	$7.2 \times 10^9$	(-2)
$\text{H} + \text{Br}_2 \rightarrow \text{HBr} + \text{Br}$	Propagation	$9.6 \times 10^{10}$	(3)

As we have seen for the reaction between  $\text{Br}_2$  and  $\text{H}_2$ , once a mechanism is postulated for a chain reaction, the sequential nature of the different steps, in closed cycles, leads to some repetition of the rate laws in the differential equations established for each atom or radical. This means that mathematical simplifications, involving addition or subtraction, can be introduced into these equations.

By applying the steady-state hypothesis to the two intermediates  $\text{Br}$  and  $\text{H}$ , both of which are present at very low concentrations, we can write

$$\frac{d[\text{H}]}{dt} = k_2 [\text{Br}][\text{H}_2] - k_3 [\text{H}][\text{Br}_2] - k_{-2} [\text{H}][\text{HBr}] = 0 \quad (12.1)$$

$$\frac{d[\text{Br}]}{dt} = 2k_1 [\text{Br}_2] - k_2 [\text{Br}][\text{H}_2] + k_3 [\text{H}][\text{Br}_2] + k_{-2} [\text{H}][\text{HBr}] - 2k_{-1} [\text{Br}]^2 = 0 \quad (12.2)$$

By adding these two equations, a solution for  $[\text{Br}]$  is obtained

$$2k_1 [\text{Br}_2] - 2k_{-1} [\text{Br}]^2 = 0 \quad (12.3)$$

and therefore

$$[\text{Br}] = \left( \frac{k_1}{k_{-1}} \right)^{\frac{1}{2}} [\text{Br}_2]^{\frac{1}{2}} \quad (12.4)$$

Substituting  $[Br]$  in eq. (12.1) gives

$$k_2 \left( \frac{k_1}{k_{-1}} \right)^{1/2} [Br_2]^{1/2} [H_2] - k_3 [H][Br_2] - k_{-2} [H][HBr] = 0 \quad (12.5)$$

which can be rearranged mathematically to give

$$[H] = \frac{k_2 \left( \frac{k_1}{k_{-1}} \right)^{1/2} [Br_2]^{1/2} [H_2]}{k_3 [Br_2] + k_{-2} [HBr]} \quad (12.6)$$

The rate of reaction, in terms of the disappearance of  $H_2$ , is

$$v = \frac{d[H_2]}{dt} = k_2 [Br][H_2] - k_{-2} [H][HBr] \quad (12.7)$$

Subtracting this expression from eq. (12.1) leads to

$$v = k_3 [H][Br_2] \quad (12.8)$$

Rewriting eq. (12.6) in the light of eq. (12.8) we have the expression for the rate of reaction

$$v = \frac{k_3 k_2 \left( \frac{k_1}{k_{-1}} \right)^{1/2} [Br_2]^{3/2} [H_2]}{k_3 [Br_2] + k_{-2} [HBr]} \quad (12.9)$$

or

$$v = \frac{k_2 \left( \frac{k_1}{k_{-1}} \right)^{1/2} [Br_2]^{1/2} [H_2]}{1 + \left( \frac{k_{-2} [HBr]}{k_3 [Br_2]} \right)} \quad (12.10)$$

This is in good agreement with the empirical rate law [6]

$$v = \frac{k [Br_2]^{1/2} [H_2]}{1 + m \frac{[HBr]}{[Br_2]}} \quad (12.11)$$

where  $k$  and  $m$  are constants; the value of  $m$  is *ca.* 10 and is virtually independent of temperature. The circumstance that  $Br_2$  and  $HBr$  are both in competition for the  $H$  atoms accounts for the fact that the inhibitory effect of  $HBr$  decreases with an increase of  $[Br_2]$ . This provides a good rationale for the appearance of  $[HBr]/[Br_2]$  in the denominator of the rate law.

This mechanism has a unique feature for chain reactions. The  $[Br]$  is identical to the equilibrium concentration,  $Br_2 \rightleftharpoons 2Br$  ( $\Delta H^0 = 194 \text{ kJ mol}^{-1}$ ). In contrast, for example, in

**Table 12.2**

Activation energies, in kilojoule per mole, for the elementary reactions between halogens and hydrogen, at 500 K

Reaction	Cl	Br	I
(1) $\text{X}_2 \rightarrow 2\text{X}$	245	195	154
(-1) $2\text{X} \rightarrow \text{X}_2$	0	0	0
(2) $\text{X} + \text{H}_2 \rightarrow \text{HX} + \text{H}$	18.8	72.5	135.5
(-2) $\text{H} + \text{HX} \rightarrow \text{H}_2 + \text{X}$	14.6	3.0	5.5
(3) $\text{H} + \text{X}_2 \rightarrow \text{HX} + \text{X}$	2.9	2.4	2.3
(4) $\text{X}_2 + \text{H}_2 \rightarrow 2\text{HX}$	170	178	205
$E_a = E_2 + (\frac{1}{2})(E_1 - E_{-1})$	141	170	213
$E_4 - E_a$	29	8	-8

the decomposition reaction of ethane,  $[\text{C}_2\text{H}_5]$  is much higher than the concentration of the equilibrium  $\text{C}_2\text{H}_6 \rightleftharpoons \text{C}_2\text{H}_5 + \text{H}$  ( $\Delta H^0 = 410 \text{ kJ mol}^{-1}$ ), since the initiation of the decomposition of ethane is much more endothermic than the equivalent step for bromine. The circumstance that  $[\text{Br}]$  is an equilibrium concentration implies that the overall rate of reaction is independent of the presence of any catalyst or of a foreign body, M, present in the activation or in the deactivation steps of bromine,  $\text{Br}_2 + \text{M} \rightleftharpoons 2\text{Br} + \text{M}$ .

Eq. (12.10) reveals that at the beginning of the reaction, when  $[\text{HBr}]$  is low, the following rate law is valid

$$v = k_2 \left( \frac{k_1}{k_{-1}} \right)^{1/2} [\text{Br}_2]^{1/2} [\text{H}_2] \quad (12.12)$$

Under such conditions the activation energy is

$$E_a = E_2 + \frac{1}{2}(E_1 - E_{-1}) \quad (12.13)$$

As will be discussed in Section 12.4, the activation energies of the different elementary steps of the mechanism calculated through the intersecting-state model (ISM), and displayed in Table 12.2, give a value of  $E_a$  ( $E_a = 170 \text{ kJ mol}^{-1}$ ) extremely close to that reported by Laidler for this reaction,  $E_a = 168 \text{ kJ mol}^{-1}$  [7].

## 12.2 REACTION BETWEEN MOLECULAR HYDROGEN AND CHLORINE

The thermal and photochemical reactions between molecular hydrogen and chlorine show some resemblance to the hydrogen–bromine reactions, but the mechanisms are more complex. Since it is easier to understand its main features, we will consider first the photochemical reaction. The mechanism has to account for the profound effect of oxygen

on the rates [8],

- (1)  $\text{Cl}_2 + h\nu \rightarrow 2\text{Cl}$
  - (2)  $\text{Cl} + \text{H}_2 \rightarrow \text{HCl} + \text{H}$
  - (3)  $\text{H} + \text{Cl}_2 \rightarrow \text{HCl} + \text{Cl}$
  - (4)  $\text{H} + \text{O}_2 \rightarrow \text{HO}_2$
  - (5)  $\text{Cl} + \text{O}_2 \rightarrow \text{ClO}_2$
  - (6)  $\text{Cl} + \text{X} \rightarrow \text{ClX}$
- (12.II)

where X is a species capable of removing the chlorine atoms. The chain ending step  $2\text{Cl} \rightarrow \text{Cl}_2$  is not taken into consideration, because the chlorine radicals are removed more effectively by reactions (5) and (6). In fact, since chlorine recombination is a second-order process with respect to Cl, the rate is very low when  $[\text{Cl}]$  is low, which is the general case within the present mechanism.

The concentration of chlorine atoms  $[\text{Cl}]$  in this mechanism is much lower than that of  $[\text{Br}]$  in the  $\text{H}_2/\text{Br}_2$  reaction. This is a direct consequence of the lower activation energy of  $\text{Cl} + \text{H}_2 \rightarrow \text{HCl} + \text{H}$  when compared with  $E_a$  of  $\text{Br} + \text{H}_2 \rightarrow \text{HBr} + \text{H}$ , as will be discussed in Section 12.4.

The rate of Cl formation in step (1) is  $2I$ , where I is the intensity of the absorbed light in appropriate units, because two radicals are formed for each absorbed photon. This rate has the following expression:

$$\frac{d[\text{Cl}]}{dt} = 2I - k_2 [\text{Cl}][\text{H}_2] + k_3 [\text{H}][\text{Cl}_2] - k_5 [\text{Cl}][\text{O}_2] - k_6 [\text{Cl}][\text{X}] = 0 \quad (12.14)$$

Under stationary conditions for H atom we have

$$\frac{d[\text{H}]}{dt} = k_2 [\text{Cl}][\text{H}_2] - k_3 [\text{H}][\text{Cl}_2] - k_4 [\text{H}][\text{O}_2] = 0 \quad (12.15)$$

from which it follows that

$$[\text{Cl}] = \frac{k_3 [\text{H}][\text{Cl}_2] + k_4 [\text{H}][\text{O}_2]}{k_2 [\text{H}_2]} \quad (12.16)$$

Introduction of this expression into eq. (12.14), neglecting the small quadratic term in  $[\text{O}_2]$ , leads to

$$[\text{H}] = \frac{2Ik_2 [\text{H}_2]}{k_3 k_6 [\text{Cl}_2][\text{X}] + [\text{O}_2](k_2 k_4 [\text{H}_2] + k_3 k_5 [\text{Cl}_2] + k_4 k_6 [\text{X}])} \quad (12.17)$$

The rate of formation of the product HCl is then

$$v = \frac{d[\text{HCl}]}{dt} = k_2 [\text{Cl}][\text{H}_2] + k_3 [\text{H}][\text{Cl}_2] \quad (12.18)$$

Subtraction of eq. (12.15) from eq. (12.18) leads to an expression for the rate law for the  $\text{H}_2/\text{Cl}_2$  photochemical reaction that can be inserted into eq. (12.17) to give

$$v = \frac{2Ik_2k_3[\text{H}_2][\text{Cl}_2]}{k_3k_6[\text{Cl}_2][\text{X}] + [\text{O}_2](k_2k_4[\text{H}_2] + k_3k_5[\text{Cl}_2] + k_4k_6[\text{X}])} \quad (12.19)$$

The thermal reaction has some additional complications owing to the fact that the decomposition of  $\text{Cl}_2$  can take place on the surface of the reaction vessels. The rate law assumes the general form

$$\frac{d[\text{HCl}]}{dt} = \frac{k'[\text{H}_2][\text{Cl}_2]^2}{m'[\text{Cl}_2] + [\text{O}_2]([\text{H}_2] + n'[\text{Cl}_2])} \quad (12.20)$$

Here  $k$ ,  $m'$  and  $n'$  are constants. This expression can be rationalised in terms of a preferential termination step on the surface vessel. This is no longer valid in the presence of  $\text{O}_2$ .

### 12.3 REACTION BETWEEN MOLECULAR HYDROGEN AND IODINE

The reaction between  $\text{H}_2$  and  $\text{I}_2$  was extensively studied by Bodenstein [9–11] at the end of the nineteenth century. For many years it was considered to be a true bimolecular reaction. However, in 1959, Sullivan showed the presence of free radicals in the system above 600 K, leading to the proposed mechanism [12–14]

- (1)  $\text{I}_2 \rightarrow 2\text{I}$
  - (2)  $\text{I} + \text{H}_2 \rightarrow \text{HI} + \text{H}$
  - (3)  $\text{H} + \text{I}_2 \rightarrow \text{HI} + \text{I}$
- (12.III)

i.e. a chain reaction. Once the intermediate  $\text{HI}$  is formed, it can be deactivated through the reverse process of step (2). In addition, it is also plausible that there is the formation of a linear transition state  $\{\text{I}\dots\text{H}\dots\text{H}\dots\text{I}\}^\ddagger$ , which relates  $\text{I}$  and  $\text{H}_2\text{I}$  with the products,  $\text{HI}$ . The following mechanism includes the formation of intermediates of this type

- (1)  $\text{I}_2 \rightleftharpoons 2\text{I}$  (fast)
  - (2)  $\text{I} + \text{H}_2 \rightleftharpoons \text{H}_2\text{I}$  (fast)
  - (3)  $\text{H} + \text{H}_2\text{I} \rightleftharpoons 2\text{HI}$  (slow)
- (12.IV)

where the rate-determining step is step (3) and thus

$$v = k_3[\text{I}][\text{H}_2\text{I}] \quad (12.21)$$

Inserting the expressions for  $[\text{I}]$  and  $[\text{H}_2\text{I}]$ , obtained from the equilibrium processes (1) and (2), one gets

$$v = k[\text{H}_2][\text{I}_2] \quad (12.22)$$

Here,  $k = k_3 K_2 / K_1$ . This mechanism, together with mechanism (12.III) and a few others, all appear to make contributions to the overall reaction. Another process that is almost certainly involved proceeds via the elementary step  $I_2 + H_2 \rightarrow 2HI$ , which proceeds via a transition state with a trapezoidal configuration.

This illustrates that a single reaction can often occur by more than one mechanism proceeding simultaneously. In general there is no unique mechanism corresponding to a given empirical law, although under certain experimental conditions one may be dominant.

## 12.4 CALCULATION OF ENERGY BARRIERS FOR ELEMENTARY STEPS IN HYDROGEN–HALOGEN REACTIONS

The calculation of the energy barriers for the elementary reactions between X and  $H_2$ , H and  $HX$  and H and  $X_2$ , which are involved in the mechanisms 12.I–12.III has been presented in Chapter 6. Using the ISM formalism and the structural parameters of Appendix III, data have been calculated for chlorine, bromine and iodine and are presented in Table 12.2.

The calculation of the energy barrier for the elementary reaction between molecular halogens and hydrogen,



presents some new challenges for a formal treatment, because one has to deal with the simultaneous breaking and formation of two chemical bonds. Figure 12.2 presents a transition state with a trapezoidal geometry for this kind of reaction.

The extension of each reactive bond from its equilibrium length up to the transition state can be estimated through a generalisation of eq. (6.57)

$$\begin{aligned} l_{AB}^{\ddagger} - l_{AB} &= -a'(l_{AB} + l_{CD} + l_{AC} + l_{BD}) \ln(n_{AB}^{\ddagger}) \\ l_{CD}^{\ddagger} - l_{CD} &= -a'(l_{AB} + l_{CD} + l_{AC} + l_{BD}) \ln(n_{CD}^{\ddagger}) \\ l_{AC}^{\ddagger} - l_{AC} &= -a'(l_{AB} + l_{CD} + l_{AC} + l_{BD}) \ln(n_{AC}^{\ddagger}) \\ l_{BD}^{\ddagger} - l_{BD} &= -a'(l_{AB} + l_{CD} + l_{AC} + l_{BD}) \ln(n_{BD}^{\ddagger}) \end{aligned} \quad (12.23)$$

Here one considers the sum of four equilibrium bond lengths, since this is the number of the reactive bonds in the transition state.

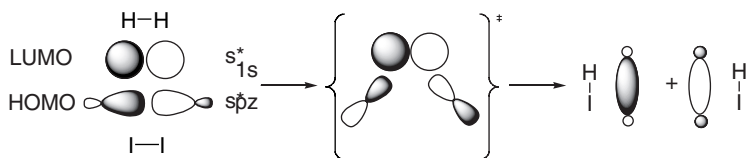


**Figure 12.2** Reaction coordinate of reaction (12.V), illustrating the changes in the frontier orbitals.

Making the assumption that the bond-forming–bond-breaking processes have a concerted nature, we can use the bond order of any one of the formed bonds as the reaction coordinate. As a consequence we can write

$$n = n_{\text{AC}} = n_{\text{BD}} = 1 - n_{\text{AB}} = 1 - n_{\text{CD}} \quad (12.24)$$

The variation of the classical potential energy along the reaction coordinate can be obtained through generalisation of eq. (6.81) for the case of four reactive bonds, each one described by a Morse curve

$$V_{\text{MEP}}(n) = (1-n)(V_{\text{AB}} + V_{\text{CD}}) + n(V_{\text{AC}} + V_{\text{BD}}) + n\Delta V^0 \quad (12.25)$$

where

$$\Delta V^0 = (D_{\text{AB}} + D_{\text{CD}}) - (D_{\text{AC}} + D_{\text{BD}}) \quad (12.26)$$

The modified functional form for each of the molecules of reactants and products is

$$V_{\text{AB}} = D_{\text{AB}} \left\{ 1 - \exp \left[ -\beta_{\text{AB}} (l - l_{\text{AB}})/m \right] \right\}^2 \quad (12.27)$$

In the same fashion, the electrophilicity index of the same molecules is obtained as given earlier (see eq. (6.67))

$$m = \frac{I_p + E_A}{I_p - E_A} \quad (12.28)$$

Since the electron affinities of the atomic halogens are higher and the ionisation energies are lower than the corresponding values for H<sub>2</sub>, the value of *m* is determined by the electronic properties of the atomic halogen species (see Appendix III).

The expression in eq. (12.25) can be calculated for all the values of *n* between 0 and 1, employing the Morse curve parameters for X<sub>2</sub>, H<sub>2</sub> and HX and the ionisation potentials and electronic affinities of X. The structural and electronic data required for the calculations are also given in Appendix III. The maximum value of *m* allows one to estimate the classical potential energy barriers for the molecular reactions (12.V), without the use of any adjustable parameters. The results are compiled in Table 12.2.

The energy barrier for the reactions X<sub>2</sub>→2X is simply taken as the dissociation energy of the molecular species. Morse curves use potential energies at 0 K; hence we subtract the zero-point energy (ZPE) values from *D<sub>e</sub>* and add ( $\frac{3}{2}$ )RT to account for the differences in heat capacities between two atoms and a diatomic molecule. The final result is also given for each reaction in Table 12.2.

We consider that the association processes 2X→X<sub>2</sub> with atoms have no activation barrier, as illustrated in Figure 12.3. With more complex species such as free radicals where the translational energy can be converted into energy of some internal modes, the de-energisation of X<sub>2</sub>\* can occur without the need for termolecular collisions with a foreign body (such as an inert gas, M).

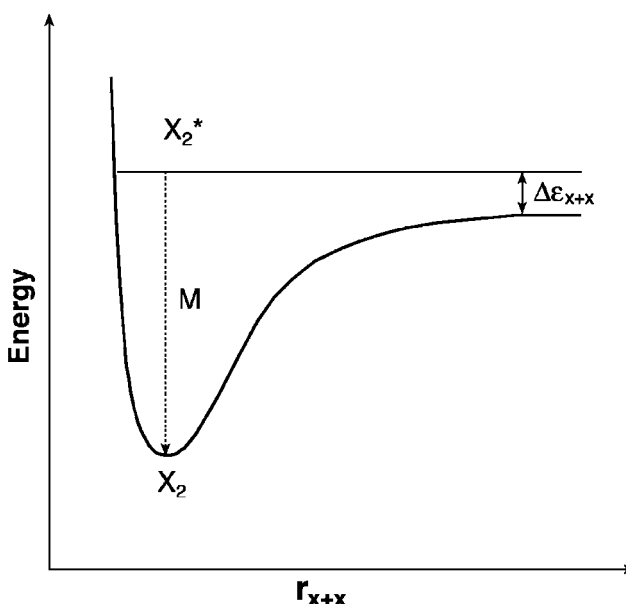


**Figure 12.3** Potential energy curve for the recombination between atoms;  $\Delta\epsilon_{x+x}$  is the kinetic energy of the collision between the atoms, and M represents a molecule that deactivates the vibrational energy of  $X_2^*$ .

## 12.5 COMPARISON OF THE MECHANISMS OF THE HYDROGEN–HALOGEN REACTIONS

Although chlorine, bromine and iodine are homologous, there are significant differences in the way they react with hydrogen. The first main difference is:

(i) *The reaction between H<sub>2</sub> and I<sub>2</sub> is largely a molecular reaction whereas the others are almost entirely chain reactions.* If the reaction between H<sub>2</sub> and I<sub>2</sub> were entirely a chain reaction (eq. (12.13)) analogous to that for the H<sub>2</sub>/Br<sub>2</sub> reaction, the activation energy would be given by eq. (12.13). To understand what is really happening, it is necessary to compare the activation energies of the chain reaction with those of the molecular process. With the data given in Table 12.2 we have

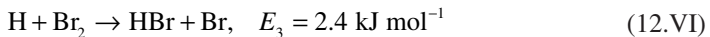
$$E_a(H_2/I_2)_{ch} = 135.5 + (154 - 0)/2 = 212.5 \text{ kJ mol}^{-1} \quad (12.29)$$

However, we have estimated a lower energy barrier for the molecular process, 205 kJ mol<sup>-1</sup>. Therefore, the molecular process occurs more rapidly.

In contrast, for the H<sub>2</sub>/Br<sub>2</sub> and H<sub>2</sub>/Cl<sub>2</sub> reactions, which have much lower E<sub>a</sub>, the chain reaction mechanisms have much lower activation energies than the molecular process (see Table 12.2).

Although the comparison established between the activation energies, E<sub>a</sub>, and the classical potential-energy barrier of the molecular process, V<sub>4</sub>, only provides a simple qualitative analysis of the relative reactivities of the different systems, it does fulfil the present objectives.

(ii) In the  $H_2/Br_2$  reaction there is a significant inhibition by the product,  $HBr$ ; in the  $H_2/Cl_2$  reaction there is no noticeable inhibition by  $HCl$ . The activation energies of the relevant elementary processes

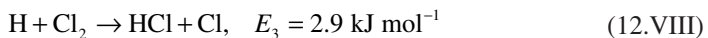


and



are low and extremely close; consequently, both reactions have high and comparable rates. In such a situation,  $Br_2$  and  $HBr$  compete for the  $H$ -atoms, with the product  $HBr$  having a very small advantage at high temperatures owing to a higher pre-exponential factor.

The homologous processes with chlorine



and

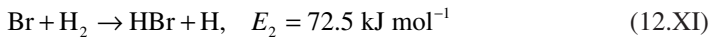


have very different activation energies. The reaction with the product  $HCl$  is *ca* 100 times slower at 300 K and, consequently, is unable to compete with the reagent,  $Cl_2$ , for the hydrogen atoms.

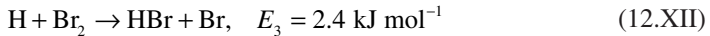
(iii) The rate of the thermal  $H_2/Br_2$  reaction is proportional to  $[Br_2]^{1/2}$ . For the  $H_2/Cl_2$ , the reaction rate is proportional to  $[Cl_2]$ . The termination step that dominates in the  $H_2/Br_2$  reaction is



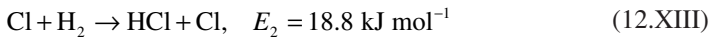
because  $[Br]$  is relatively high owing to the very low rate for the removal of bromine atoms through the reaction with molecular hydrogen



as a consequence of its relatively high activation energy. In contrast, the formation of bromine atoms through the step



is a very fast process. Thus, we have both fast formation of bromine atoms and slow removal of the same species, such that  $[Br]$  is high. This contrasts markedly with the  $H_2/Cl_2$  system,



Here the chlorine ( $Cl$ ) atoms are removed much more rapidly than the  $Br$  atoms in the earlier case, and  $[Cl]$  is around nine orders of magnitude lower than  $[Br]$ . Under such

circumstances, the rate of bimolecular Cl–Cl recombination will be an extremely slow process.

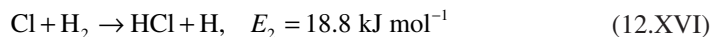
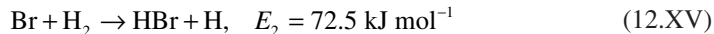
(iv) *The chain lengths for the reaction H<sub>2</sub>/Cl<sub>2</sub> are much greater than for the case with H<sub>2</sub>/Br<sub>2</sub>.* The length of a chain reaction,  $\gamma$ , can be defined as the average number of times the closed cycle of reactions, comprised of the chain-propagation steps, is repeated. Thus,  $\gamma$  is given by the ratio of two rates: the rate of the overall reaction divided by that of the initiation step,  $\gamma = v/v_i$ . In the absence of the product HBr, from eq. (12.12) one can write

$$\gamma = \frac{k_2 \left( \frac{k_1}{k_{-1}} \right)^{1/2} [H_2][Br_2]^{1/2}}{k_1 [Br_2]} \quad (12.30)$$

and thus

$$\gamma = k_2 \left( \frac{1}{k_1 k_{-1}} \right)^{1/2} [H_2][Br_2]^{-1/2} \quad (12.31)$$

The *chain length*  $\gamma$  is directly proportional to  $k_2$  for the H<sub>2</sub>/Br<sub>2</sub> as well as the H<sub>2</sub>/Cl<sub>2</sub> reactions. If we compare the activation energies of the two elementary steps



one immediately realises that  $k_2(H_2/Cl_2) \gg k_2(H_2/Br_2)$  and consequently,  $\gamma(H_2/Cl_2) \gg \gamma(H_2/Br_2)$ .

This comparative study in a family of complex reactions illustrates the levels of complexity of the field of chemical kinetics. Even with such homologous species, minor differences in activation energies may modify drastically the reaction mechanisms of the reacting systems. Simple models, such as the ISM, that provide estimates of  $E_a$  from structural and electronic parameters, help to rationalise such complex kinetic behaviour.

## 12.6 PYROLYSIS OF HYDROCARBONS

A linear chain reaction is one in which chain carriers react with no net gain in the number of carriers. Although the rate laws obtained can be as complex as those seen earlier for the reaction between H<sub>2</sub> and Br<sub>2</sub>, this is not necessarily the case. The thermal decomposition of hydrocarbons in the gas phase involves homolytic bond cleavage at the weakest chemical bond to produce two free radicals. In general, free radicals lead to chain reactions. However, the rate laws are often simple as was shown in 1934 by Rice and Herzfeld [15].

### 12.6.1 Pyrolysis of ethane

The mechanism proposed by Rice and Herzfeld for the pyrolysis of ethane is as follows:

- (1)  $\text{C}_2\text{H}_6 \rightarrow 2\text{CH}_3$  initiation step
  - (2)  $\text{CH}_3 + \text{C}_2\text{H}_6 \rightarrow \text{CH}_4 + \text{C}_2\text{H}_5$  initiation step
  - (3)  $\text{C}_2\text{H}_5 \rightarrow \text{C}_2\text{H}_4 + \text{H}$  propagation step
  - (4)  $\text{H} + \text{C}_2\text{H}_6 \rightarrow \text{H}_2 + \text{C}_2\text{H}_5$  propagation step
  - (5)  $\text{H} + \text{C}_2\text{H}_5 \rightarrow \text{C}_2\text{H}_6$  termination step
- (12.XVII)

The chain carriers are the radicals  $\text{C}_2\text{H}_5$  and  $\text{H}$ . The free radical  $\text{CH}_3$  does not propagate the chain reaction, since it is formed in step (1), deactivates in step (2), and is not to be regenerated. The stationary conditions for  $\text{CH}_3$ ,  $\text{C}_2\text{H}_5$  and  $\text{H}$  lead to the following set of differential equations:

$$2k_1[\text{C}_2\text{H}_6] - k_2[\text{CH}_3][\text{C}_2\text{H}_6] = 0 \quad (12.32)$$

$$k_2[\text{CH}_3][\text{C}_2\text{H}_6] - k_3[\text{C}_2\text{H}_5] + k_4[\text{H}][\text{C}_2\text{H}_6] - k_5[\text{H}][\text{C}_2\text{H}_5] = 0 \quad (12.33)$$

$$k_3[\text{C}_2\text{H}_5] - k_4[\text{H}][\text{C}_2\text{H}_6] - k_5[\text{H}][\text{C}_2\text{H}_5] = 0 \quad (12.34)$$

Adding these three equations we obtain

$$2k_1[\text{C}_2\text{H}_6] - 2k_5[\text{H}][\text{C}_2\text{H}_5] = 0 \quad (12.35)$$

from which the concentration of hydrogen atoms is

$$[\text{H}] = \frac{k_1[\text{C}_2\text{H}_6]}{k_5[\text{C}_2\text{H}_5]} \quad (12.36)$$

This expression can be inserted into eq. (12.34), leading, after some mathematical rearrangement, to

$$k_3k_5[\text{C}_2\text{H}_5]^2 - k_1k_5[\text{C}_2\text{H}_6][\text{C}_2\text{H}_5] - k_1k_4[\text{C}_2\text{H}_6]^2 = 0 \quad (12.37)$$

The general solution of this quadratic equation is

$$[\text{C}_2\text{H}_5] = \left\{ \frac{k_1}{2k_3} + \left[ \left( \frac{k_1}{2k_3} \right)^2 + \left( \frac{k_1k_4}{k_3k_5} \right) \right]^{1/2} \right\} [\text{C}_2\text{H}_6] \quad (12.38)$$

The constant  $k_1$  is very small since the initiation reaction has a very high activation energy. The terms involving  $k_1/2k_3$  are therefore very small in comparison with  $k_1k_4/k_3k_5$  and therefore

$$[\text{C}_2\text{H}_5] = \left( \frac{k_1k_4}{k_3k_5} \right)^{1/2} [\text{C}_2\text{H}_6] \quad (12.39)$$

The rate of production of ethene is

$$\frac{d[C_2H_4]}{dt} = k_3 [C_2H_5] \quad (12.40)$$

or

$$v = \left( \frac{k_1 k_3 k_4}{k_5} \right)^{1/2} [C_2H_6] \quad (12.41)$$

The reaction is thus first order. Inserting the corresponding Arrhenius expressions for the individual rate constants leads to

$$v = \left[ \frac{A_1 \exp\left(-E_1/RT\right) A_3 \exp\left(-E_3/RT\right) A_4 \exp\left(-E_4/RT\right)}{A_5 \exp\left(-E_5/RT\right)} \right]^{1/2} [C_2H_6] \quad (12.42)$$

or

$$v = \left( \frac{A_1 A_3 A_4}{A_5} \right)^{1/2} \exp\left(-\frac{E_1 + E_3 + E_4 - E_5}{2RT}\right) [C_2H_6] \quad (12.43)$$

The activation energy for the overall reaction is

$$E_a = \frac{1}{2}(E_1 + E_3 + E_4 - E_5) \quad (12.44)$$

Since  $E_3$  and  $E_4$  are much smaller than  $E_1$ , the activation energy of the reaction is much lower than that of the initiating step,  $E_1 = 360 \text{ kJ mol}^{-1}$ .

The chain length is given by

$$\gamma = \frac{v}{v_i} = \frac{\left( \frac{k_1 k_3 k_4}{k_5} \right)^{1/2} [C_2H_6]}{k_1 [C_2H_6]} \quad (12.45)$$

or

$$\gamma = \left( \frac{k_3 k_4}{k_1 k_5} \right)^{1/2} \quad (12.46)$$

Since  $k_1$  is very small, the chain length is often very large.

Although the above mechanism explains the first-order dependence, other termination steps have been suggested such as



that account for the production of a small amount of butane. However, a mechanism with steps (1), (2), (3), (4), (5a) and (5b) should lead to a rate law of order  $\frac{1}{2}$ . Therefore, to explain the experimental kinetic behaviour, a second-order initiation reaction was proposed,



However, evidence has been presented that the production of methane, in small amounts, shows a first-order dependence and this indicates that the initiation reaction is first order. A complete, satisfactory solution of the mechanism is still lacking.

### 12.6.2 Pyrolysis of acetic aldehyde

The Rice–Herzfeld mechanism for the decomposition of acetaldehyde involves the following steps:

- (1)  $\text{CH}_3\text{CHO} \rightarrow \text{CH}_3 + \text{CHO}$
- (2)  $\text{CH}_3 + \text{CH}_3\text{CHO} \rightarrow \text{CH}_4 + \text{CH}_3\text{CO}$  (12.XVIII)
- (3)  $\text{CH}_3\text{CO} \rightarrow \text{CH}_3 + \text{CO}$
- (4)  $2\text{CH}_3 \rightarrow \text{C}_2\text{H}_6$

The radical CHO gives other decomposition products that will not be considered here. Applying the steady-state condition we obtain

$$k_1[\text{CH}_3\text{CHO}] - k_2[\text{CH}_3][\text{CH}_3\text{CHO}] + k_3[\text{CH}_3\text{CO}] - 2k_4[\text{CH}_3]^2 = 0 \quad (12.47)$$

and for the  $\text{CH}_3\text{CO}$  radicals

$$k_2[\text{CH}_3][\text{CH}_3\text{CHO}] - k_3[\text{CH}_3\text{CO}] = 0 \quad (12.48)$$

Addition of these equations gives

$$k_1[\text{CH}_3\text{CHO}] - 2k_4[\text{CH}_3]^2 = 0 \quad (12.49)$$

which can be rearranged to

$$[\text{CH}_3] = \left( \frac{k_1}{2k_4} \right)^{1/2} [\text{CH}_3\text{CHO}]^{1/2} \quad (12.50)$$

The rate of formation of methane is

$$\frac{d[\text{CH}_4]}{dt} = k_2[\text{CH}_3][\text{CH}_3\text{CHO}] \quad (12.51)$$

$$\frac{d[\text{CH}_4]}{dt} = k_2 \left( \frac{k_1}{2k_4} \right)^{1/2} [\text{CH}_3\text{CHO}]^{3/2} \quad (12.52)$$

The mechanism explains correctly the three-halves order. The overall activation energy is

$$E_a = E_2 + \frac{1}{2}(E_1 - E_4) \quad (12.53)$$

which is again usually much lower than  $E_1$ .

The chain length is given by

$$\gamma = k_2 (k_1 2k_4)^{-1/2} [\text{CH}_3\text{CHO}]^{1/2} \quad (12.54)$$

and depends on the concentration of the reactant.

To obtain a  $\frac{3}{2}$  order the initiation step can be a first-order process, but the termination step requires the combination of the same two radicals. If in the same mechanism instead of step (4) we have the reaction



as the termination step, the rate law becomes

$$\frac{d[\text{CO}]}{dt} = k_3 \left( \frac{k_1}{2k_4} \right)^{1/2} [\text{CH}_3\text{CHO}]^{1/2} \quad (12.55)$$

### 12.6.3 Goldfinger–Letort–Niclause rules

The above examples show that the order of the overall reaction depends on the manner in which the chains are broken as well as the nature of the radicals. Goldfinger, Letort and Niclause [16] have treated this problem in a systematic manner by distinguishing between two types of radicals:

- (i) Radicals that are involved in second-order propagation steps; these are referred to as  $\beta$  radicals. In the above cases the H and  $\text{CH}_3$  radicals are examples of this type.
- (ii) Radicals that are involved in first-order reactions in the propagation steps; these are referred to as  $\mu$  radicals. The radicals  $\text{C}_2\text{H}_5$  and  $\text{CH}_3\text{CO}$  are of this type.

The order of the overall reaction depends on the kinetic type of the radicals which carry the chains and on the presence or absence of a third body M in the termination steps. The presence of a foreign body reduces the overall order by  $\frac{1}{2}$ . Table 12.3 displays the overall orders of reactions for thermal decompositions of hydrocarbons. The same order,  $n$ , can also be estimated through the expression

$$n = \frac{i + \rho_1 + \rho_2 - t}{2} \quad (12.56)$$

Here  $i$  is the order of the initiation step and  $\rho_i$  the orders of the propagation steps:  $\rho = 1$  for the  $\mu$  radicals and  $\rho = 2$  for the  $\beta$  radicals;  $t$  the order of the termination step. For example, for the decomposition of ethane we have  $i = 1$ ,  $\rho_1 = 1$ ,  $\rho_2 = 2$  and  $t = 2$  and thus  $n = 1$ .

**Table 12.3**

Reaction orders for chain reactions in the pyrolysis of hydrocarbons

First-order initiation		Second-order initiation		Reaction order
Simple termination	Termination with third body	Simple termination	Termination with third body	
$\beta\beta$		$\beta\beta$		2
$\beta\mu$	$\beta\beta M$	$\beta\mu$	$\beta\beta M$	3/2
$\mu\mu$	$\beta\mu M$	$\mu\mu$	$\beta\mu M$	1
	$\mu\mu M$		$\mu\mu M$	1/2
				0

## 12.7 EXPLOSIVE REACTIONS

The gas-phase reactions between oxygen and various substances such as hydrogen, carbon monoxide and phosphorus have a special characteristic: under certain conditions of temperature,  $T$ , and pressure,  $P$ , they occur normally, but a slight change in  $T$  or  $P$  may cause the mixture to explode. An explosion is a sudden and violent release of energy, in general associated with emission of light, a violent burst and a large release of heat. Often there is a sudden pressure change, and one speaks of a *detonation*. Detonations have typical speeds of 2 km/sec, while detonations for military purposes may have speeds of 6 to 8 km/sec. The manner in which a detonation travels through a gas mixture was first investigated by Dixon [17]. Later Chapman [18], based on such results, developed a theory of gaseous detonations. We are going to study the reaction between  $H_2$  and  $O_2$  as an example of this behaviour.

### 12.7.1 Combustion between hydrogen and oxygen

A stoichiometric mixture of the two gases explodes spontaneously at any pressure above 600 °C. Below about 460 °C there is no explosion at any pressure, unless a spark passes through the gaseous mixture or a flame is introduced into it. Between 460 and 600 °C, however, a stoichiometric mixture explodes spontaneously at certain pressures but not at others, as displayed in Figure 12.4. In this figure there are three limits of explosion as a function of pressure. The first one occurs at very low pressures, around  $10^{-3}$  atm (260 Pa); a second one in the range of  $10^{-1}$  atm and, finally, a third limit of explosion at higher pressures at ca 10 atm.

To explain the kinetic behaviour of such systems Semenov [19,20] and Hinshelwood and Thompson [21,22] have proposed the concept of *branching chains*. When a pair of ordinary propagation steps occurs, there is no change in the number of chain carriers. When a branching chain occurs, however, there is an increase in the number of carriers. Let us consider the pair of reactions:



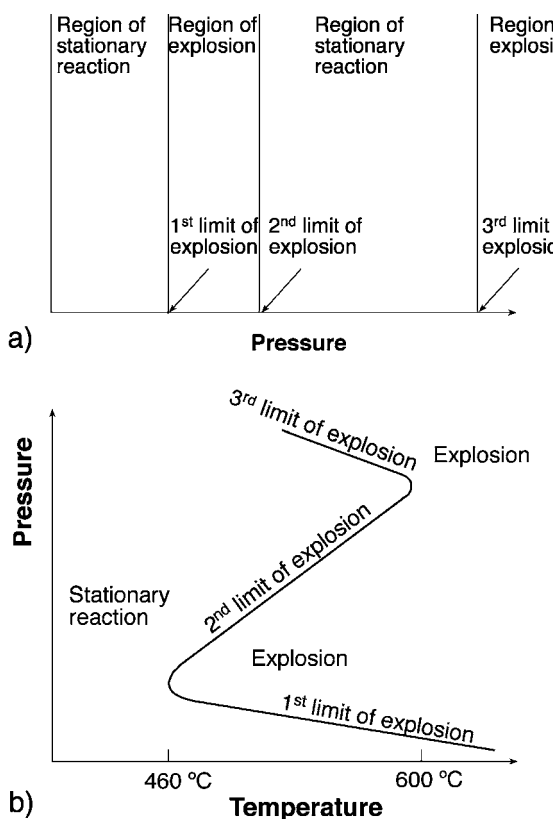


**Figure 12.4** (a) Regions of stationary and explosive reactions for a typical combustion in the gas phase such as the hydrogen/oxygen reactions. (b) Change in the limits of explosion with the temperature: the temperatures indicated correspond to the stoichiometric mixture  $2\text{H}_2 + \text{O}_2$ .

In both cases, two chain carriers have been formed from one. When the two reactions are added together the net result is



so that the H atom is regenerated, but has produced two OH radicals which can undergo further reactions. When such chain branching happens, the number of atoms and free radicals can increase rapidly in the system (see Table 12.4), and an explosion may result.

Suppose the steps (1) and (2) are associated with step (3)



in the formation of water molecules. Each time the pair of reactions (1) and (2) occurs, reaction (3) occurs twice, so that the overall reaction is



**Table 12.4**

Increase in the number of reactive species in the branching chain reaction between H atoms and H<sub>2</sub>O molecules

Number of cycles	Number of H atoms reacting	Number of H atoms produced	Number of H <sub>2</sub> O formed
1	1	3	2
2	3	9	6
3	9	27	18
4	27	81	54
10	19 683	59 049	39 366
20	$1.16 \times 10^9$	$3.49 \times 10^9$	$2.32 \times 10^9$
30	$6.9 \times 10^{13}$	$2.05 \times 10^{14}$	$1.4 \times 10^{14}$
49	$4.1 \times 10^{18}$	$1.2 \times 10^{19}$	$8.1 \times 10^{18}$
50	$2.4 \times 10^{23}$	$7.2 \times 10^{23}$	$4.8 \times 10^{23}$

Thus, in the first cycle of reactions, one H atom produces 3H atoms together with two molecules of water. The numbers produced in subsequent cycles are shown in Table 12.4. After 50 cycles the number of H radicals and water molecules is of the order of the Avogadro constant. The reactions are very fast, and 50 cycles can occur in a fraction of a second.

In more general terms, a branching chain reaction, with initiation and termination steps, can be considered with reference to the following mechanism:

- (1)  $\rightarrow R$  initiation step (rate  $r_i$ )
  - (2)  $R \rightarrow \alpha R$  branching chain ( $\alpha > 1$ , generally  $\alpha \approx 2$ )
  - (3)  $R + Q \rightarrow Z + R$  propagation step
  - (4)  $R \rightarrow$  termination step
- (12.XXIII)

Here, no distinction is made between the different kinds of radicals, R; Q represents a reactant and Z a product. The termination step can be the ending of the chain at a surface or in the gas phase. The rates of the four reactions are:

$$\begin{aligned}
 (1) \quad r_i &= \frac{d[R]}{dt} \\
 (2) \quad r_b &= k'_b [R] = \frac{1}{\alpha-1} \frac{d[R]}{dt} \\
 (3) \quad r_p &= k'_p [R] \\
 (4) \quad r_t &= k'_t [R] = -\frac{d[R]}{dt}
 \end{aligned} \tag{12.57}$$

where  $r_b$  and  $r_t$  are rates of first-order processes with respect to the active radicals and the rate constants  $k'_b$  and  $k'_t$  are usually functions of the concentrations of other reactants. The

net rate of the formation of radicals is independent of the rate of the propagation step and can be written as

$$\frac{d[R]}{dt} = r_i + r_b (\alpha - 1) - r_t \quad (12.58)$$

or

$$\frac{d[R]}{dt} = r_i + \{k'_b (\alpha - 1) - k'_t\}[R] \quad (12.59)$$

If one defines a *net branching factor*,  $\phi$ , in terms of the expression

$$\phi = k'_b (\alpha - 1) - k'_t \quad (12.60)$$

then eq. (12.59) can be written in the form

$$\frac{d[R]}{dt} = r_i + \phi[R] \quad (12.61)$$

which shows that the rate of radical formation follows a first-order law. If the net branching factor is  $\phi < 0$ , a stationary condition can be found for  $[R]$ ,  $[R]_{ss} = r_i / |\phi|$ . Under such conditions the branching chain behaves as a normal chain reaction, because there is no significant net accumulation of active radicals; the termination step dominates over the branching step.

However, if  $\phi > 0$  (see Figure 12.5),  $[R]$  increases exponentially and approaches infinity at large values of  $t$ ,

$$[R] = \frac{r_i}{\phi} [\exp(\phi t) - 1] \quad (12.62)$$

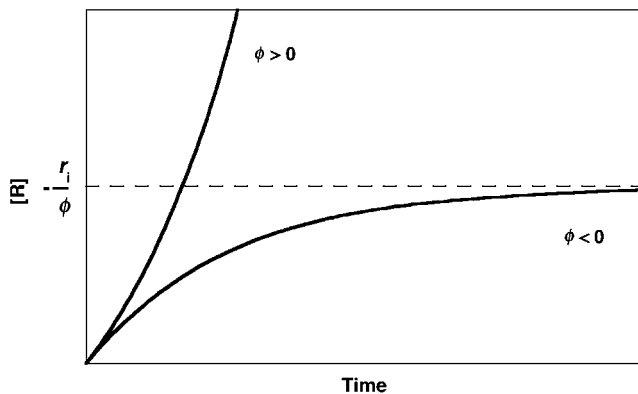


**Figure 12.5** Increase in the concentration of the radical that propagates the chain reaction  $[R]$ , for different values of the net branching factor,  $\phi$ .

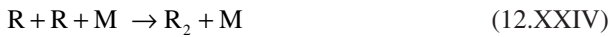
Then the rate of reaction will be

$$v = k_p' [R] = \frac{r_i k_p'}{\phi} [\exp(\phi t) - 1] \quad (12.63)$$

After the initial instants, the rate increases exponentially with time. The branching processes dominate the termination process; there is an autocatalytic effect which leads eventually to an explosion. The primary cause of such an explosion is the increase in active chain carriers, and not the increase in temperature that is also present in an exothermic reaction. The rate of reaction tends to infinity, but above a certain limit the reaction develops the characteristics of the explosive reactions.

In the gas phase there are two explosion limits. At low pressures the reaction has a low rate with  $\phi < 0$ . At low pressure the removal of the radicals occurs primarily at the surface of the vessel. However, at a certain temperature, an increase in pressure reduces the rate at which radicals can reach the walls of the vessel, reducing  $k_t$ . Such a decrease occurs up to a certain pressure  $p_1$  for which we arrive at the condition  $\phi = 0$ . Thus, one reaches the first explosion limit.

At much higher pressures,  $p \gg p_1$ , the termination step occurs in the gas phase, with sufficient efficiency so that  $\phi < 0$ . Lowering this pressure, a new decrease in  $k_t$  occurs since the termination step is a kind of a third-order process,



and, thus,  $\phi > 0$ . At a pressure  $p_u$  ( $p_u > p_1$ ) we reach once again the condition  $\phi = 0$ , and hence the second explosion limit. Keeping the temperature constant, between  $p_u$  and  $p_1$  is the condition  $\phi > 0$  and the reaction is always explosive (see Figure 12.5). Above  $p_u$  is the condition  $\phi < 0$  and the combustion occurs in a smooth manner till one reaches a third explosion limit whose origin is discussed in the next section.

### 12.7.2 Thermal explosions

A thermal explosion is one where the primary cause is the auto-catalysis produced by the self-heating effect of the reaction mixtures. For an exothermic reaction the heat evolved during the course of the reaction raises the temperature of the reacting mixtures, thereby accelerating the reaction rates, leading to further heating and further reaction, until an explosion occurs. Such a thermal reaction stabilises when the rate of generation of heat is compensated by thermal dissipation through thermal convection and conductivity or by radiation.

The rate of production of a certain amount of heat,  $Q_R$ , in a system of volume  $V$  and with a reaction rate,  $v$ , is given by

$$Q_R = -Vv|\Delta H| \quad (12.64)$$

where  $-|\Delta H|$  represents the change of the enthalpy of the reaction. If we assume for simplicity that the rate law has the form

$$v = kC^x \quad (12.65)$$

where  $C$  is the concentration of the reactant,  $x$  the order of the reaction and  $k$  the rate constant, which follows the Arrhenius expression

$$k = A \exp\left(-\frac{E_a}{RT}\right) \quad (12.66)$$

under such conditions we obtain

$$Q_R = -VC^x A \exp\left(-\frac{E_a}{RT}\right) |\Delta H| \quad (12.67)$$

Let us assume that the rate of the dissipation of heat follows the empirical law of Newton,

$$Q_C = Sh(T - T_{ext}) \quad (12.68)$$

Here  $T$  is the temperature of the gaseous mixture,  $T_{ext}$  the temperature of the surroundings,  $S$  the surface of the vessel and  $h$  the thermal coefficient per unit area of the reaction vessel.

Figure 12.6 illustrates three possible conditions for  $Q_R$  at three concentrations of the reagent,  $C_1 > C_c > C_2$ . At  $C_2$  the system is at a temperature  $T_s$  where the rate of generation of heat is higher than that of heat dissipation,  $Q_R > Q_C$ . The temperature of the system rises

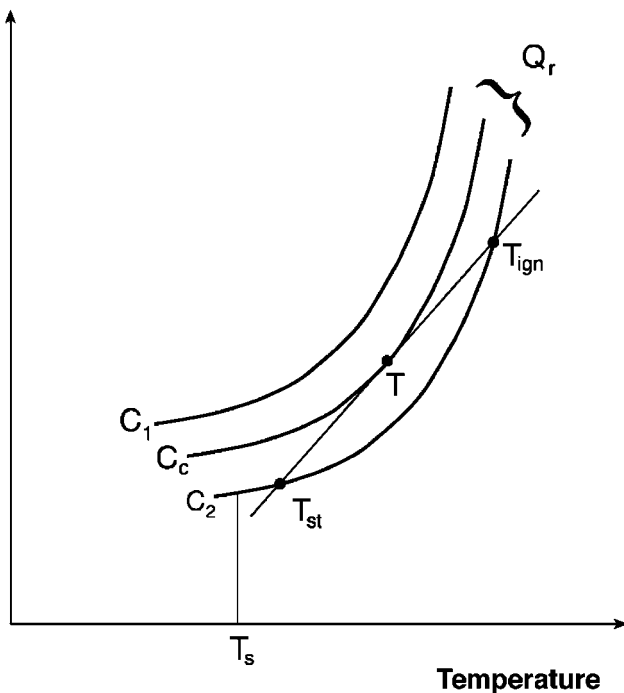


**Figure 12.6** Variation of  $Q_R$  with the temperature for three concentration values.

up to  $T_{\text{st}}$  where  $Q_R = Q_C$ . Around this temperature the system reveals some stability to small perturbations. When the system is heated to a temperature well above  $T_{\text{st}}$  the rate of cooling is higher compared to the rate of heat production and the temperature drops down to  $T_{\text{st}}$ . However, when the system is heated to the temperature of ignition,  $T_{\text{ign}}$ , it is no longer stable because  $Q_R > Q_C$  always.

There is a critical concentration,  $C_C$ , where the temperature of ignition and that of stationary conditions have the same value, and then

$$Q_C = Q_R \quad (12.69)$$

or

$$\frac{dQ_C}{dt} = \frac{dQ_R}{dt} \quad (12.70)$$

Hence

$$\frac{RT_C^2}{E_a} = T_C - T_{\text{ext}} \quad (12.71)$$

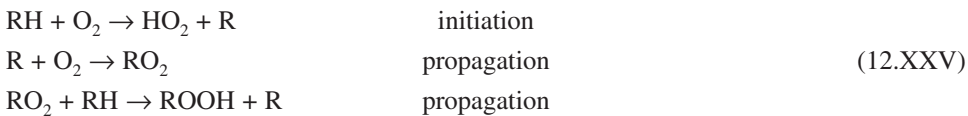
and from this equation we obtain

$$Sh(T_C - T_{\text{ext}}) = -VC_C^n A \exp\left(-\frac{E_a}{RT}\right) |\Delta H| \quad (12.72)$$

Above such a limiting condition one reaches the limit of thermal explosion. This corresponds to the third explosion limit of the reaction  $O_2/2H_2$ . The explosions in the reactive system  $Cl_2/H_2$  are also primarily of a thermal nature, because the chain is not a branching one and owing to the high activation energy,  $E_a = 141 \text{ kJ mol}^{-1}$ , the rate of formation of the chain carriers is sufficiently low to be the source of any isothermal explosion.

### 12.7.3 Combustion of hydrocarbons

The combustion of hydrocarbons has some features in common with reactions such as that between hydrogen and oxygen, in that explosion occurs between certain limits of temperature and pressure. But the mechanism involves what Semenov [19,20] has designated as *degenerated branching*. This type of branching is brought about by some intermediate which has a relatively long lifetime compared with the ordinary free radicals. Let us take as example the combustion of hydrocarbon RH,



In the vapour phase, below 100 °C, the hydroperoxides ROOH are the only products for many oxidation reactions of hydrocarbons. These hydroperoxides can decompose into new

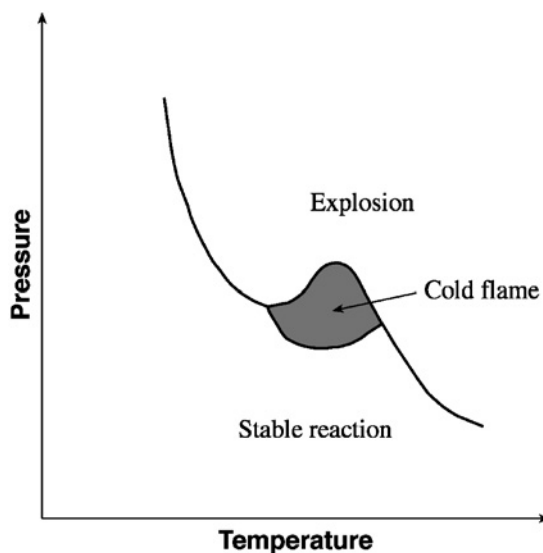


**Figure 12.7** Illustration of the temperature and pressure conditions necessary to obtain a cold flame.

branching chain carriers in reactions that are much slower than the above ones.



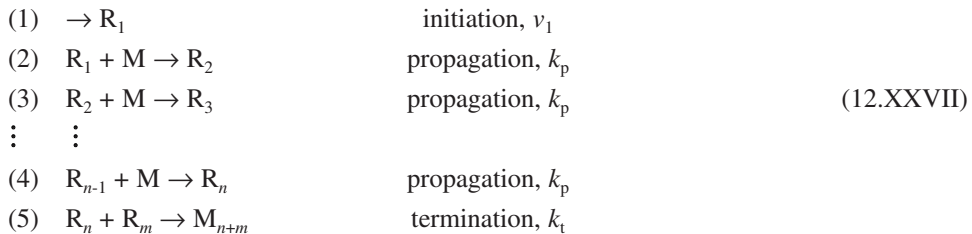
Thus these oxidation reactions present quite substantial *induction periods*, periods of time needed for free radicals such as RO and HO to reach some concentration values.

During the first instants of the reaction  $\phi < 0$  and the oxidation reaction is a slow process. For high temperatures  $\phi$  is high,  $\phi \gg 0$ , and the combustion process is accompanied by ordinary *hot flames*. However, under certain conditions (see Figure 12.7) the so-called *cold flames* are also observed. Several of these blue flames are associated with sharp temperature increases (*ca.* 100 °C) and the corresponding rate acceleration. Nevertheless, quenching processes do occur before the reaction is complete. Not much reactant is consumed during the passage of a cold flame. As a consequence, the net branching factor  $\phi$  must change sign during these pulses, so that only a degenerated explosion occurs. A full explanation of these reactions in the cold-flame regions is still awaited.

## 12.8 POLYMERISATION REACTIONS

Gas-phase polymerisations occur by composite mechanisms that may be of a molecular type or of a radical type. In liquid solutions and emulsions, again both ionic and radical polymerisation mechanisms are important, depending upon whether one is dealing with condensation or addition polymerisation. In this section we will consider the formation of macromolecules  $M_n$  made by a repetition of a certain number of identical monomers M by

a free-radical mechanism, as follows:



where  $R_1$  is a radical that initiates the polymerisation and  $R_n$  is a radical  $R_1$  linked to a chain of  $(n-1)$  monomers. All the propagation steps are considered to have the same rate constant  $k_p$ ; the termination step has a rate constant  $k_t$ .

The steady-state condition for species  $R_1$  leads to

$$v_i - k_p [R_1][M] - k_t [R_1]([R_1] + [R_2] + \dots + [R_n]) = 0 \quad (12.73)$$

The termination step considers the removal of radical  $R_1$  by reaction with  $R_1, R_2, \dots, R_n$  and this leads to

$$v_i - k_p [R_1][M] - k_t [R_1] \sum_1^n [R_n] = 0 \quad (12.74)$$

Similarly, for  $R_2$ , one has

$$k_p [R_1][M] - k_p [R_2][M] - k_t [R_2] \sum_1^n [R_n] = 0 \quad (12.75)$$

while for  $R_n$  the expression is

$$k_p [R_{n-1}][M] - k_p [R_n][M] - k_t [R_n] \sum_1^n [R_n] = 0 \quad (12.76)$$

The sum of all such equations simply states that the rate of initiation is equal to the sum of the rates of all the termination steps

$$v_i - k_t \left( \sum_1^n [R_n] \right)^2 = 0 \quad (12.77)$$

or

$$\sum_1^n [R_n] = \left( \frac{v_i}{k_t} \right)^{1/2} \quad (12.78)$$

The rate of consumption of monomer is

$$-\frac{d[M]}{dt} = k_p [M] \sum_1^n [R_n] \quad (12.79)$$

which reduces to

$$-\frac{d[M]}{dt} = k_p \left( \frac{v_i}{k_t} \right)^{1/2} [M] \quad (12.80)$$

This is a set of general equations that can be made explicit for different kinds of mechanisms. For example, if the initiation step is a second-order process,

$$v_i = k_i [M]^2 \quad (12.81)$$

then from eq. (12.80) we get

$$-\frac{d[M]}{dt} = k_p \left( \frac{k_i}{k_t} \right)^{1/2} [M]^2 \quad (12.82)$$

If initiation has a photochemical nature, then

$$v = I \quad (12.83)$$

where  $I$  is the intensity of the absorbed light, and subsequently, the rate of monomer consumption can be written as

$$-\frac{d[M]}{dt} = k_p \left( \frac{I}{k_t} \right)^{1/2} [M] \quad (12.84)$$

If the initiation step involves catalysis, where Cat represents the catalyst, then

$$v_i = k_i [Cat][M] \quad (12.85)$$

and

$$-\frac{d[M]}{dt} = k_p \left( \frac{k_i}{k_t} \right)^{1/2} [M]^{3/2} [Cat]^{1/2} \quad (12.86)$$

The length of the chain is given by the general expression

$$\gamma = -\frac{d[M]/dt}{v_i} \quad (12.87)$$

which for a second-order initiation step (eq. (12.81)) leads to

$$\gamma = \frac{k_p \left( \frac{k_i}{k_t} \right)^{1/2} [M]^2}{k_i [M]} \quad (12.88)$$

or

$$\gamma = k_p \left( \frac{1}{k_i k_t} \right)^{1/2} [M] \quad (12.89)$$

## REFERENCES

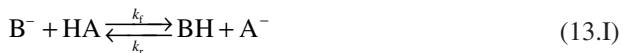
- [1] MG Neuman, *J. Chem. Educ.* **63** (1986) 684.
- [2] JA Christiansen, *Vidensk. Selsk. Mat.-Fys. Medd.* **1** (1919) 14.
- [3] KF Herzfeld, *Z. Elektrochem.* **25** (1919) 301.
- [4] KF Herzfeld, *Ann. Phys.* **59** (1919) 635.
- [5] M Polanyi, *Z. Elektrochem.* **26** (1920) 50.
- [6] M Bodenstein, SC Lind, *Z. Phys. Chem.* **57** (1907) 108.
- [7] KJ Laidler, *Chemical Kinetics*, HarperCollins, New York, 1987.
- [8] M Bodenstein, W Unger, *Z. Phys. Chem. B* **11** (1930) 253.
- [9] M Bodenstein, *Z. Phys. Chem.* **13** (1894) 56.
- [10] M Bodenstein, *Z. Phys. Chem.* **22** (1897) 23.
- [11] M Bodenstein, *Z. Phys. Chem.* **29** (1899) 295.
- [12] JH Sullivan, *J. Chem. Phys.* **30** (1959) 1291.
- [13] JH Sullivan, *J. Chem. Phys.* **36** (1962) 1925.
- [14] JH Sullivan, *J. Chem. Phys.* **39** (1963) 300.
- [15] FO Rice, KF Herzfeld, *J. Am. Chem. Soc.* **56** (1934) 284.
- [16] P Goldfinger, M Letort, M Niclause, Contribution à l'étude de la structure moléculaire, *Liège V. Henri Commemorative Volume* (1948) 283.
- [17] HB Dixon, *Philos. Trans.* **175** (1884) 617.
- [18] DL Chapman, *Philos. Mag.* **47** (1899) 90.
- [19] NN Semenov, *Z. Phys.* **46** (1927) 109.
- [20] NN Semenov, *Chemical Kinetics and Chain Reactions*, Clarendon Press, Oxford, 1935.
- [21] CN Hinshelwood, HW Thompson, *Proc. R. Soc. London* **118** (1928) 171.
- [22] CN Hinshelwood, HW Thompson, *Kinetics of Chemical Change in Gaseous Systems*, Clarendon Press, Oxford, 1933.

## – 13 –

# Acid–Base Catalysis and Proton-Transfer Reactions

---

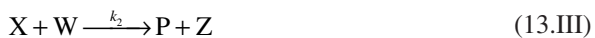
Proton-transfer (PT) reactions lie at the heart of the mechanistic definition of what is an acid and what is a base in the concept initially proposed by Brönsted. Remember that, according to Brönsted, an acid is a molecular entity capable of donating a proton, and a base is another molecular entity with a tendency to accept that proton. The equilibrium



represents the transfer of a proton from an acid HA to a base  $B^-$ , or, for the reverse reaction, the transfer of a proton from the conjugate base  $A^-$  (of the AH acid), to the conjugate acid BH (of the  $B^-$  base). Such reactions are present in catalysis by acids or bases in solution, and are also particularly relevant in enzyme catalysed processes in biological systems.

### 13.1 GENERAL CATALYTIC MECHANISMS

Following Laidler [1], we first consider a mechanism that is sufficiently general to encompass most homogeneous catalysis. Designating the catalyst as C and the substrate as S (that is the reactant subject to the catalytic reaction), the mechanism can be written



where X and Y represent intermediates, one of which (X) reacts with another substance (W), to yield the final product (P) and an additional substance (Z), which may subsequently react, but which is not involved in kinetically significant reactions. For simplicity, we will consider that only the first step is reversible. This is also equivalent to the case where the products are rapidly removed from the reaction.

### 13.1.1 Fast pre-equilibrium: Arrhenius intermediates

When the first step of the mechanism, step (13.II), is a fast equilibrium, the intermediate X is in equilibrium with the reactants, and corresponds to Arrhenius's concept of an equilibrium intermediate. This step leads to

$$\frac{[X][Y]}{[C][S]} = \frac{k_1}{k_{-1}} = K \quad (13.1)$$

In this expression, the concentrations of C and S, [C] and [S], are their equilibrium concentrations and not their initial concentrations. For initial concentrations,  $[C]_0$  and  $[S]_0$ , we can write

$$[C]_0 = [C] + [X] \quad (13.2)$$

$$[S]_0 = [S] + [X] \quad (13.3)$$

Introducing these expressions in eq. (13.1), we obtain

$$\frac{[X][Y]}{([C]_0 - [X])([S]_0 - [X])} = K \quad (13.4)$$

which is a quadratic equation in X. The reaction rate, expressed in terms of the formation of the product P in step (13.III), is given by

$$v = k_2[X][W] \quad (13.5)$$

The intermediate X can be eliminated from this expression using eq. (13.4).

It is often more useful to consider the relative concentrations of the catalyst and substrate and obtain limiting cases for the rate law, rather than carry out all the algebra with the quadratic equation. Because [X] cannot be larger than  $[C]_0$ , we can obtain a first limiting case when the initial concentration of the substrate is relatively high,  $[S]_0 \gg [C]_0$ , and, consequently,  $[S]_0 - [X] \approx [S]_0$ . Under this approximation eq. (13.4) becomes

$$\frac{[X][Y]}{([C]_0 - [X])[S]_0} = K \quad (13.6)$$

or

$$[X] = \frac{K[C]_0[S]_0}{K[S]_0 + [Y]} \quad (13.7)$$

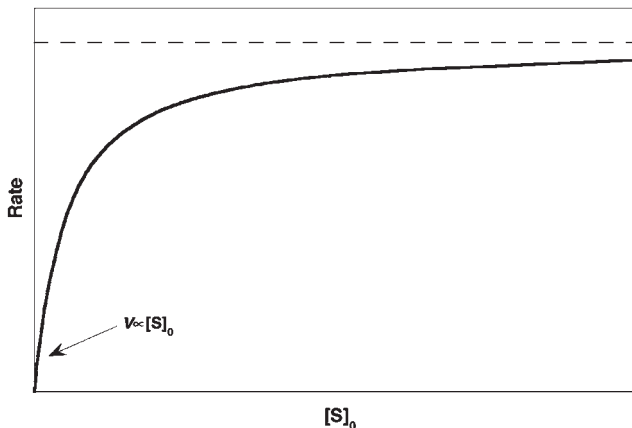


**Figure 13.1** Rate of a catalysed reaction as a function of the initial concentration of substrate,  $[S]_0$ , observed when  $[S]_0 \gg [C]_0$ .

and the rate law can be written as

$$v = \frac{k_2 K [C]_0 [S]_0 [W]}{K [S]_0 + [Y]} \quad (13.8)$$

This expression shows that the reaction rate changes with  $[S]_0$ , as illustrated in Figure 13.1. For low substrate concentration, the rate resembles a first-order process with respect to the substrate. However, for higher substrate concentrations, the rate may attain a plateau and become independent of the substrate concentration, just like a zero-order reaction with respect to S. As long as  $[S]_0 \gg [C]_0$ , the reaction rate is first order with respect to the catalyst.

We have seen this behaviour before in Chapter 10 in single-substrate reactions on the surface of solids, and will discuss it again in Chapter 14 in the context of enzyme catalysis. For both cases of surface reactions and enzyme catalysis, the species Y and W do not exist and eq. (13.8) becomes

$$v = \frac{k_2 K [C]_0 [S]_0}{K [S]_0 + 1} \quad (13.9)$$

this equation is equivalent to eq. (10.19) of surface reactions, which is defined per unit area, and to the Michaelis–Menten equation of enzyme catalysis, eq. (4.133).

Another limiting case is obtained when the catalyst is in excess relative to the substrate,  $[C]_0 \gg [S]_0$ , and eq. (13.4) becomes

$$\frac{[X][Y]}{[C]_0 ([S]_0 - [X])} = K \quad (13.10)$$

leading to

$$v = \frac{k_2 K [C]_0 [S]_0 [W]}{K [C]_0 + [Y]} \quad (13.11)$$

Now the reaction is always first order with respect to the substrate, independent of  $[S]$ , provided that  $[S]_0 \ll [C]_0$ , but the partial order with respect to the catalyst may vary between zero and unity.

Additionally, when  $K[C]_0$  is much greater than  $[Y]$ , the rate of reaction is simply given by

$$v = k_2 [S]_0 [W] \quad (13.12)$$

and the activation energy is

$$E_a = E_2 \quad (13.13)$$

where  $E_a$  is the activation energy of reaction (13.III).

The activation energies associated with the rates expressed by eqs. (13.8) and (13.11) can also be obtained when only a very small quantity of the substrate S is present. In such cases, the rate of reaction is

$$v = k_2 \frac{k_1}{k_{-1}} [C]_0 [S]_0 [W] [Y]^{-1} \quad (13.14)$$

and the activation energy becomes

$$E_a = E_1 + E_2 - E_{-1} \quad (13.15)$$

where  $E_1$  and  $E_{-1}$  represent the activation energy of reaction (13.II) and its reverse, respectively.

### 13.1.2 Steady-state conditions: van't Hoff intermediates

If  $k_2[W] \gg k_{-1}[Y]$  in mechanism (13.II–13.III), then  $[X]$  is small and the steady-state approximation can be applied to this mechanism. Laidler called X under these conditions a van't Hoff intermediate. The energy profiles corresponding to Arrhenius and van't Hoff intermediates are illustrated in Figure 13.2.

Under steady-state conditions,  $[X]$  does not change appreciably with time

$$\frac{d[X]}{dt} = k_1 [C][S] - k_{-1} [X][Y] - k_2 [X][W] = 0 \quad (13.16)$$

Replacing eqs. (13.2) and (13.3) in this expression gives

$$k_1 ([C]_0 - [X]) ([S]_0 - [X]) - k_{-1} [X][Y] - k_2 [X][W] = 0 \quad (13.17)$$

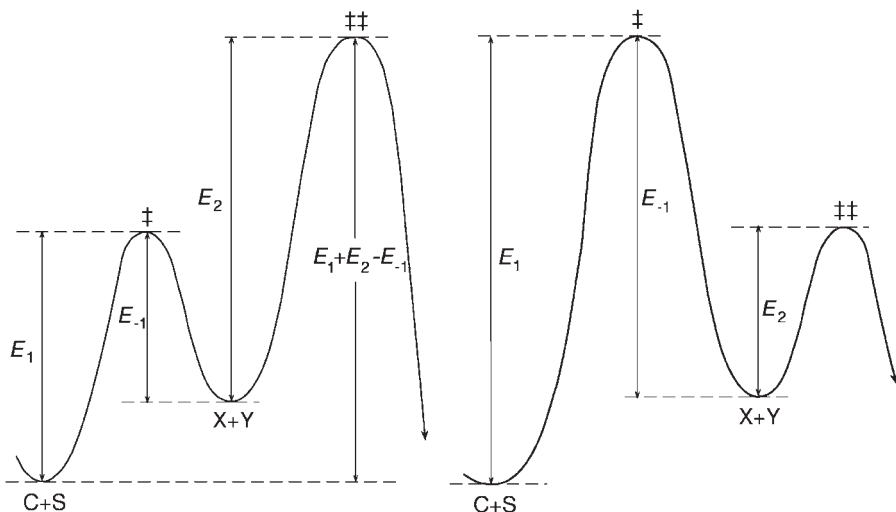


**Figure 13.2** Potential-energy profiles for catalysed reactions. (a) The rate-determining step is the second step, occurring after the formation of an Arrhenius intermediate. (b) The rate-determining step is the first step, which leads to a van't Hoff intermediate.

The low concentration of X justifies ignoring the quadratic term in [X], and leads to

$$[X] = \frac{k_1 [C]_0 [S]_0}{k_1 ([C]_0 + [S]_0) + k_{-1} [Y] + k_2 [W]} \quad (13.18)$$

The rate is therefore

$$v = \frac{k_1 k_2 [C]_0 [S]_0 [W]}{k_1 ([C]_0 + [S]_0) + k_{-1} [Y] + k_2 [W]} \quad (13.19)$$

As mentioned before, Y and W do not exist in surface and enzyme catalysis, and eq. (13.19) simplifies to

$$v = \frac{k_1 k_2 [C]_0 [S]_0}{k_1 ([C]_0 + [S]_0) + k_{-1} + k_2} \quad (13.20)$$

At high catalyst concentrations, eq. (13.19) reduces to eq. (13.12), and the activation energy is given by eq. (13.13). For low substrate and catalyst concentrations, eq. (13.20) becomes

$$v = \frac{k_1 k_2}{k_{-1} + k_2} [C]_0 [S]_0 \quad (13.21)$$

The Arrhenius equation, and consequently the definition of activation energy, does not apply to this system, except if  $k_2 \gg k_{-1}$  or  $k_{-1} \gg k_2$ . In the first case,

$$v = k_1 [C]_0 [S]_0 \quad (13.22)$$

and the activation energy is

$$E_a = E_i \quad (13.23)$$

In the second case,

$$v = \frac{k_1 k_2}{k_{-1}} [C]_0 [S]_0 \quad (13.24)$$

and the activation energy is that of eq. (13.15).

## 13.2 GENERAL AND SPECIFIC ACID–BASE CATALYSIS

Arrhenius and Ostwald played very important roles in the early studies on acid–base catalysis, one century ago. Arrhenius contributed to the definition of acids and bases, and established the dependence between the rate constants and the temperature. Additionally, he also formulated an electrolytic theory of dissociation that ultimately led to him receiving the 1903 Nobel Prize in Chemistry. Ostwald proposed useful definitions of catalysis and classifications of catalysts, but he was unable to develop a satisfactory theory of these effects. This is not surprising, in view of the very limited knowledge of the mechanisms of catalysis at his time, and of the lack of understanding of how molecular properties can influence the rates of reactions. Nevertheless, his seminal work on catalysis was rewarded by him receiving the 1909 Nobel Prize in Chemistry.

Ostwald recognised that a catalysed reaction proceeds by an alternative reaction pathway, made possible by the addition of a new species. For a process that in the absence of catalysts proceeds with a rate constant  $k_0$ , the general acid–base catalysed reaction follows the rate expression:

$$v = (k_0 + k_{H^+} [H^+] + k_{OH^-} [OH^-] + k_{HA} [HA] + k_{A^-} [A^-]) [S] \quad (13.25)$$

involving the sum of the rates for all the alternative pathways. In this expression,  $k_{H^+}$  and  $k_{OH^-}$  are the rate constants for catalysis by proton and hydroxide ion, and  $k_{HA}$  and  $k_{A^-}$  are the catalytic rate constants for the acid HA and the base  $A^-$ . In aqueous solutions the proton is strongly hydrated and, as will be discussed below, it is not present in the form of the free  $H^+$  ion. However, for simplicity, except where required to illustrate PT to water, we will continue to use the representation  $H^+$  for the proton in the equations, and will also continue to represent the hydroxide ion,  $OH^-$ .

Eq. (13.25) indicates that the reaction is catalysed by an acid, HA, or a base,  $A^-$ , present in the solution, in addition to catalysis by  $H^+$  and  $OH^-$ . We refer to catalysis in the former

case (by HA and A<sup>-</sup>) as general acid–base catalysis. However, in many catalytic mechanisms, particularly in aqueous solutions, only H<sup>+</sup> and OH<sup>-</sup> significantly influence the rate of the reaction. In this case we are in the presence of specific acid–base catalysis.

In the general catalytic mechanism represented by (13.II) and (13.III), an acid catalysis corresponds to replacing X by SH<sup>+</sup>, the catalyst C by the acid AH and Y by that catalyst without a proton. In the second step, SH<sup>+</sup> transfers a proton to the species, W, for example a water molecule, and gives the product P



This example, where W is a solvent molecule, corresponds to a protolytic transfer. When W is the conjugate base of the catalyst, W=A<sup>-</sup>, the mechanism is called prototropic. Table 13.1 presents the four possible combinations for acid and base catalysis that correspond to the possible identities of species involved in the general catalytic mechanism.

The mechanism of each of the four possible combinations may involve an Arrhenius or a van't Hoff intermediate. This leads to eight possible mechanisms, schematically presented in Table 13.2. Each of these mechanisms can be developed using either the pre-equilibrium or the steady-state approximation to arrive at the corresponding rate law. The lessons that can be learnt from the treatment of these mechanisms are also indicated in Table 13.2; some mechanisms lead exclusively to specific acid or base catalysis, while others lead to general acid or base catalysis. Furthermore, the specific catalysis is associated with the existence of a limiting rate, that is the rate that will not increase indefinitely with the H<sup>+</sup>, or OH<sup>-</sup>, concentration, but attain a limiting value equal to  $k_2[\text{S}]_0$ .

For specific acid–base catalysis at low pH, eq. (13.25) simplifies to

$$v = (k_0 + k_{\text{H}^+} [\text{H}^+])[\text{S}] \quad (13.26)$$

As the pH increases, the participation of the hydroxide ion in the catalysis becomes increasingly important, and the reaction rate for specific acid–base catalysis becomes

$$v = (k_0 + k_{\text{H}^+} [\text{H}^+] + k_{\text{OH}^-} [\text{OH}^-])[\text{S}] \quad (13.27)$$

**Table 13.1**

Nature of the reacting species in general acid–base catalysis in aqueous solutions

Catalysis	C	Y	W	Z
Acid	HA	A <sup>-</sup>	H <sub>2</sub> O	H <sub>3</sub> O <sup>+</sup>
Acid	H <sub>2</sub> O	OH <sup>-</sup>	B	BH <sup>+</sup>
Base	B	BH <sup>+</sup>	H <sub>2</sub> O	OH <sup>-</sup>
Base	H <sub>2</sub> O	H <sub>3</sub> O <sup>+</sup>	HA	A <sup>-</sup>

**Table 13.2**

Summary of mechanisms for acid–base catalysis

Acid catalysis	Arrhenius intermediates	van't Hoff intermediates
$\text{H}^+$ transferred to solvent	$k_2 \ll k_{-1} [\text{B}]$	$k_2 \gg k_{-1} [\text{B}], k_2 \gg k_1 [\text{BH}^+]$
$\text{BH}^+ + \text{S} \rightleftharpoons \text{SH}^+ + \text{B}$	Specific $\text{H}^+$ catalysis	General catalysis
$\text{SH}^+ + \text{H}_2\text{O} \longrightarrow \text{P} + \text{H}_3\text{O}^+$	With limiting rate	No limiting rate
$\text{H}^+$ transferred to solute	$k_2 \ll k_{-1}$	$k_2 \gg k_{-1}$
$\text{BH}^+ + \text{S} \rightleftharpoons \text{SH}^+ + \text{B}$	General catalysis	General catalysis
$\text{SH}^+ + \text{B} \longrightarrow \text{P} + \text{BH}^+$	No limiting rate	No limiting rate
$\text{H}^+$ transferred from solvent	$k_2 \ll k_{-1} [\text{BH}^+]$	$k_2 \gg k_{-1} [\text{BH}^+], k_2 \gg k_1 [\text{B}]$
$\text{B} + \text{SH} \rightleftharpoons \text{S}^- + \text{BH}^+$	Specific $\text{OH}^-$ catalysis	General catalysis
$\text{S}^- + \text{H}_2\text{O} \longrightarrow \text{P} + \text{OH}^-$	With limiting rate	No limiting rate
$\text{H}^+$ transferred from solute	$k_2 \ll k_{-1}$	$k_2 \gg k_{-1}$
$\text{B} + \text{SH} \rightleftharpoons \text{S}^- + \text{BH}^+$	General catalysis	General catalysis
$\text{S}^- + \text{BH}^+ \longrightarrow \text{P} + \text{B}$	No limiting rate	No limiting rate

It is convenient to define a pseudo-first-order rate constant

$$k_\Psi = \frac{v}{[\text{S}]_T} \quad (13.28)$$

where  $[\text{S}]_T$  is the total concentration of the substrate, and express the reaction rate constant in terms of

$$k_\Psi = k_0 + k_{\text{H}^+} [\text{H}^+] + k_{\text{OH}^-} [\text{OH}^-] \quad (13.29)$$

In aqueous solutions, the equilibrium



where  $[\text{H}^+][\text{OH}^-] = K_w$ , leads to

$$k_\Psi = k_0 + k_{\text{H}^+} [\text{H}^+] + \frac{k_{\text{OH}^-} K_w}{[\text{H}^+]} \quad (13.30)$$

Usually, it is possible to consider a region of sufficiently low pH where the catalysis is dominated by the  $\text{H}^+$  ion, and eq. (13.30) simplifies to

$$k_\Psi = k_{\text{H}^+} [\text{H}^+] \quad (13.31)$$

or

$$\log k_\Psi = \log k_{\text{H}^+} - \text{pH} \quad (13.32)$$

It may also be possible to find a region of sufficiently high pH where the catalysis is dominated by the  $\text{OH}^-$  ion, and eq. (13.30) becomes

$$k_\Psi = \frac{k_{\text{OH}^-} K_w}{[\text{H}^+]} \quad (13.33)$$

or

$$\log k_\Psi = \log k_{\text{OH}^-} - \text{p}K_w + \text{pH} \quad (13.34)$$

Another special case is that of a small spontaneous reaction, in the absence of catalysis, that is,  $k_0 \ll (K_w k_{\text{H}^+} k_{\text{OH}^-})^{1/2}$ , and the rate of reaction as a function of the pH goes through a minimum. The value of that minimum can be obtained differentiating eq. (13.30):

$$\frac{dk_\Psi}{d[\text{H}^+]} = k_{\text{H}^+} - \frac{k_{\text{OH}^-} K_w}{[\text{H}^+]^2} \quad (13.35)$$

equating the derivative to zero and expressing the  $\text{H}^+$  concentration as

$$[\text{H}^+]_{\min} = \sqrt{\frac{k_{\text{OH}^-} K_w}{k_{\text{H}^+}}} \quad (13.36)$$

This expression allowed Wijs [2,3], at the end of the 19th century, to measure the catalytic rate constants for the hydrolysis of ethyl acetate at low and high pHs and obtain the ionic product of water,  $K_w$ .

### 13.3 MECHANISTIC INTERPRETATION OF THE pH DEPENDENCE OF THE RATES

The above discussion shows that the dependence of the reaction rate upon the pH contains very important information on the reaction mechanism. Each rate must be measured at constant pH, which usually involves measuring it in a buffer solution. In addition, usually an inert salt is added to maintain ionic strength constant to avoid the salt effects discussed in Chapter 9. In fact, experimentally, the rates are measured at different buffer concentrations, keeping the pH and the ionic strength constant. Under these conditions, and for a constant substrate concentration, there is a linear dependence between the rate and the buffer concentration, as illustrated in Figure 13.3. Extrapolating to zero buffer concentration, one obtains the rate for a constant pH. When general acid–base catalysis is present,

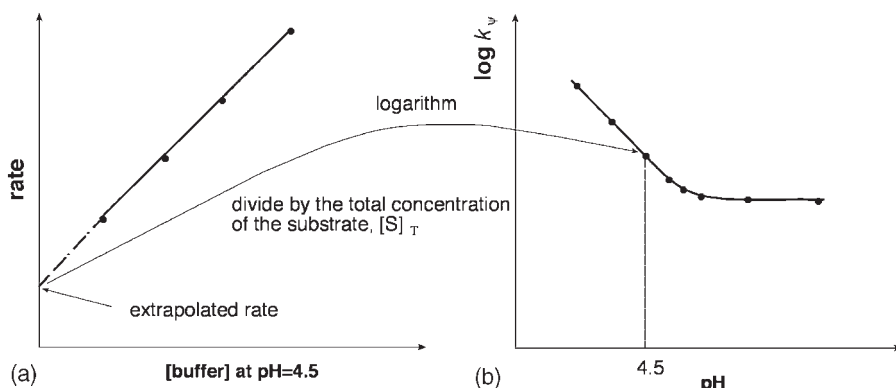


**Figure 13.3** Representation of the method employed to obtain the pH dependence of the pseudo-first-order rates ( $k_\psi$ ) as a function of the pH. (a) Rates measured for different buffer concentrations at pH 4.5. (b) Pseudo-first-order rates at different pHs.

the rate depends on the nature of the buffer, and the extrapolation gives different rates for different buffers. Such cases of general acid–base catalysis will be discussed in the next section. Here, we focus on the mechanistic interpretation of the pseudo-first-order rate constants measured as a function of the pH in aqueous solutions.

There are 5 fundamental types of pH dependence, and they are illustrated in Figure 13.4 by the dependence of the logarithm of the rate as a function of pH (to a first approximation, the negative of the logarithm of the hydrogen ion concentration) [4]. The experimentally observed pH dependences can be divided in sections that correspond to these fundamental types. Types (a), (b) and (c) correspond to reactions that are catalysed by  $\text{H}^+$ , not catalysed, and catalysed by  $\text{OH}^-$ , respectively. The catalysis by  $\text{H}^+$  is described by eq. (13.32), which explains the origin of the slope  $-1$ , corresponding to a linear dependence of rate upon hydrogen ion concentration. The absence of significant acid–base catalysis occurs when  $k_0$  dominates all the other terms in the right-hand side of eq. (13.30), and leads to a rate that is independent of the pH of the solution. The catalysis by  $\text{OH}^-$  is described by eq. (13.34), which shows the origin of the slope  $+1$ . The other two types, (d) and (e), correspond to cases where the rate constant decreases, case (d), or stops increasing, case (e), after a certain pH. These cases cannot correspond to a change in mechanism because such a change is always associated with the predominance of a competitive reaction, after a certain pH, and that necessarily leads to an increase in the rate. This is not the case, because the bends followed by the downward trend of the curves represented in (d) and (e) reflect a decrease in the rates after a given pH. Thus, each of these curves with a downward trend must be associated with a single mechanism. There are two alternative mechanisms that may lead to such breaks followed by downward trends; the presence of a fast pre-equilibrium or a change in the rate-determining step.

In the case of a mechanism of acid catalysis involving a fast pre-equilibrium



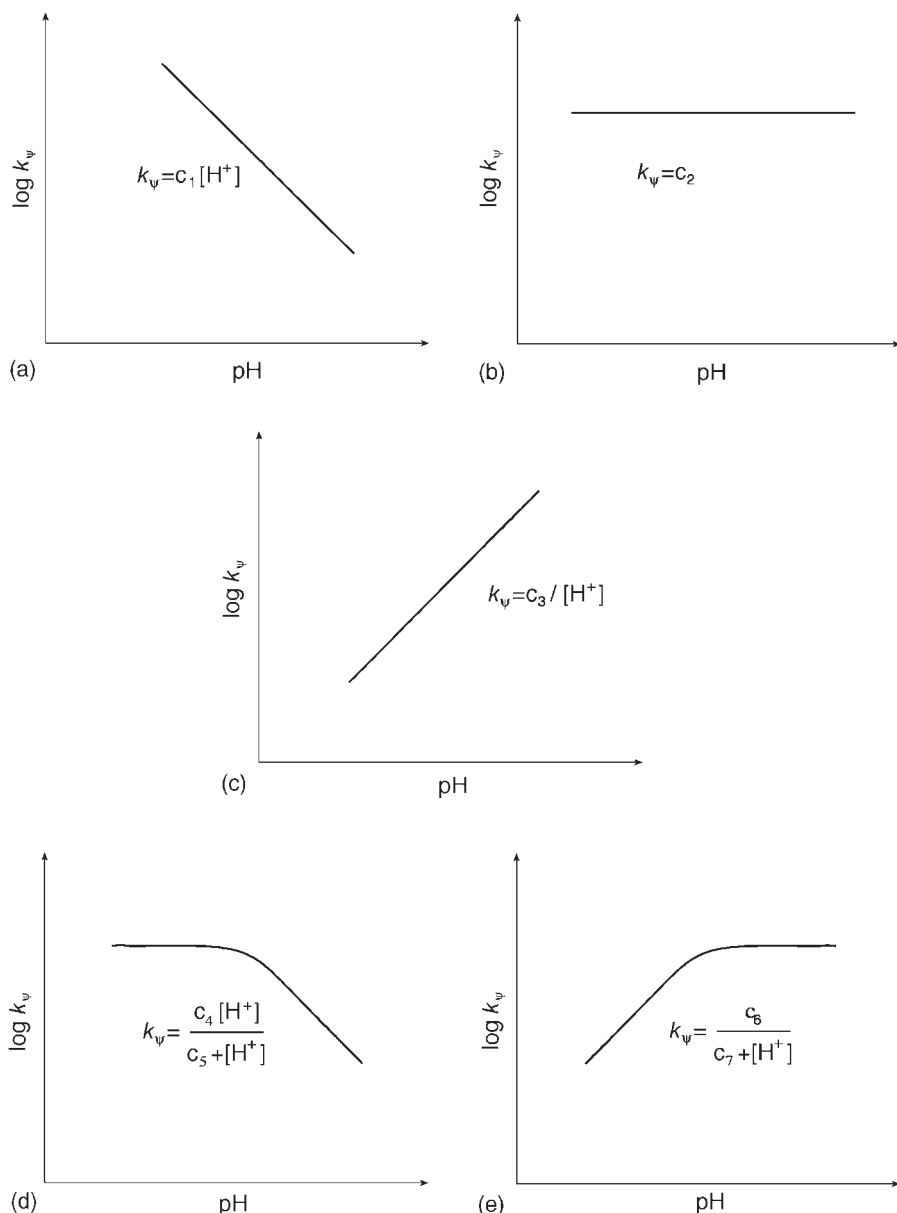


**Figure 13.4** Fundamental curves representing the dependence of the logarithm of the pseudo-first-order rate of acid-base catalysis on the pH of the solution, without involving a change in the reaction mechanism.

where the acidity constant is  $K_a = k_{-1}/k_1$ , it is convenient to express the rate constant in terms of the fraction of protonated substrate

$$f_{\text{SH}} = \frac{[\text{SH}^+]}{[\text{SH}^+] + [\text{S}]} = \frac{[\text{H}^+]}{K_a + [\text{H}^+]} \quad (13.37)$$

because  $[\text{SH}^+] = f_{\text{SH}}[\text{S}]_T$  and the rate constant is  $v = k_2[\text{SH}^+] = k_2 f_{\text{SH}}[\text{S}]_T$ . Using these relations and eq. (13.28), gives

$$k_\Psi = k_2 f_{\text{SH}} = \frac{k_2 [\text{H}^+]}{K_a + [\text{H}^+]} \quad (13.38)$$

This expression is equivalent to

$$k_\Psi = \frac{c_4 [\text{H}^+]}{c_5 + [\text{H}^+]} \quad (13.39)$$

where  $c_4$  and  $c_5$  are constants, which is the equation of the curve represented in Figure 13.4d.

In contrast, the rate constant of a mechanism of base catalysis involving a fast pre-equilibrium



where the acidity constant is  $K_a = k_1/k_{-1}$ , is conveniently expressed in terms of the fraction of un-protonated substrate

$$f_s = \frac{[\text{S}]}{[\text{SH}^+] + [\text{S}]} = \frac{K_a}{K_a + [\text{H}^+]} \quad (13.40)$$

because

$$k_\Psi = k_2 f_s = \frac{k_2 K_a}{K_a + [\text{H}^+]} \quad (13.41)$$

and has a clear analogy with the mathematical expression of the curve represented in Figure 13.4e

$$k_\Psi = \frac{c_6}{c_7 + [\text{H}^+]} \quad (13.42)$$

where  $c_6$  and  $c_7$  are constants.

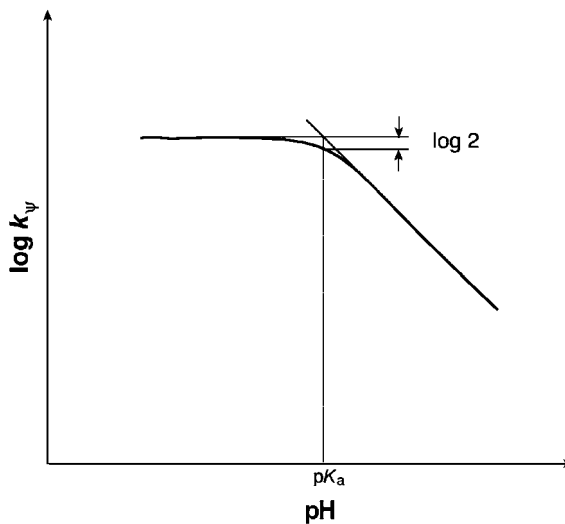


**Figure 13.5** Estimation of the  $K_a$  for deprotonation of a substrate from the dependence of its pseudo-first-order rate constant on the pH of the solution.

It is interesting to note that in curves (d) and (e) of Figure 13.4, the two segments of the curve intersect at  $K_a = [H^+]$ , and the  $K_a$  of the substrate is given by the pH at that intersection (Figure 13.5). At this pH,  $k_\psi = k_2/2$ .

There are other mechanisms that also lead to mathematical expressions identical to eqs. (13.39) or (13.42). Such mechanisms are kinetically indistinguishable, and require additional information to decide which actually applies to the reaction. For example, the mechanism



where X is a van't Hoff intermediate, has a first step that is independent of the pH followed by a second step where the reaction rate increases with the pH. For sufficiently acidic solutions, the second step is slow and becomes rate determining. However, for basic solutions, the second step is fast and the rate is determined by the first step, which is independent of the pH. Thus, we can expect to find pH dependences such as that in Figure 13.4e. This can be verified using the steady-state approximation to find the concentration of the van't Hoff intermediate, and then replace it in the rate law. The result is

$$k_\psi = \frac{k_1 k_2 [\text{OH}^-]}{k_{-1} + k_2 [\text{OH}^-]} = \frac{k_1 k_2 K_w / [\text{H}^+]}{k_{-1} + k_2 K_w / [\text{H}^+]} = \frac{(k_1 k_2 / k_{-1}) K_w}{(k_2 k_w / k_{-1}) + [\text{H}^+]} \quad (13.43)$$

Another mechanism of this type is



that gives the pseudo-first-order rate constant

$$k_\psi = \frac{k_1 k_2 [\text{H}^+]}{k_{-1} + k_2 [\text{H}^+]} = \frac{k_1 [\text{H}^+]}{\frac{k_{-1}}{k_2} + [\text{H}^+]} \quad (13.44)$$

which is mathematically equivalent to eq. (13.39). Note that the change in the rate-determining step exemplified by mechanisms (13.VIII) and (13.IX) requires the presence of an intermediate and, conversely, a change in the rate-determining step suggests the presence of an intermediate.

The distinction between mechanisms (13.VII) and (13.VIII), or between mechanisms (13.VI) and (13.IX), cannot be made exclusively on the grounds of their kinetic behaviour. However, the presence, or absence, of a substituent with a  $pK_a$  that may correspond to the pH where the slope of the curve changes, as indicated in Figure 13.5, may help to assign the correct mechanism.

The most important conclusion of this discussion is that only the observation of a curve with a bend followed by an upward trend reveals a change in mechanism with a change in pH (Figure 13.6). Such a curve indicates that, at a certain pH, the rate constant becomes higher than expected, and that a new mechanism has been triggered by the change in pH. Consequently, the number of independent terms that describe the rate of a reaction as a function of the pH is equal to the number of upward bends plus one. Each one of these

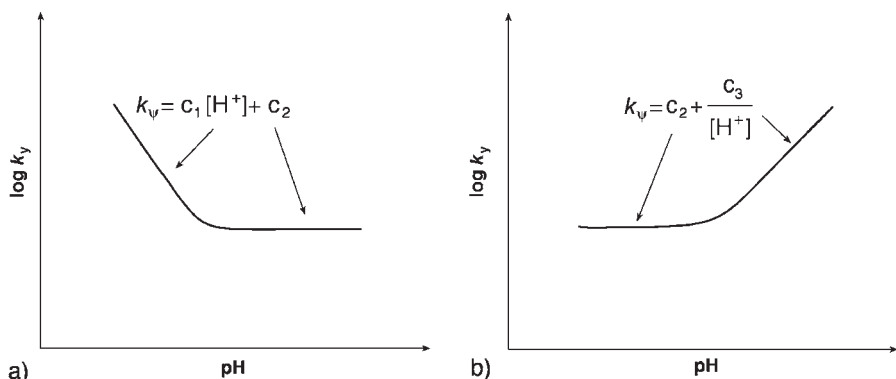


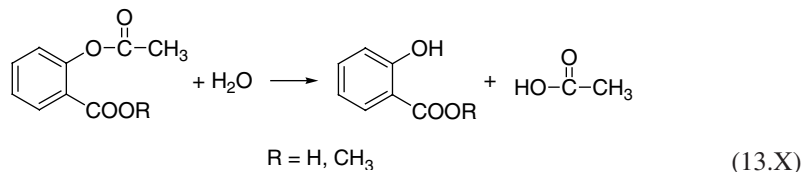
**Figure 13.6** Examples of the dependence of the pseudo-first-order rate of acid–base catalysis on the pH of the solution with upward curvature, which require a change in the reaction mechanism with the pH.

terms can be expressed in the form of the fundamental curves of Figure 13.4. Each independent term of the rate equation corresponds to a different mechanism and its predominance can be observed in a specific pH range.

Very complex pH-rate profiles can be interpreted using a sequence of five steps [4]:

- (i) Divide the pH-rate profile into regions separated by upward curvature.
  - (ii) Note each pH value at which a downward curvature occurs, and evaluate whether the substrate may have a group, which may undergo acid-base dissociation at this value. If so, postulate that the downward bend corresponds to substrate dissociation. If not, postulate that it corresponds to a change in the rate-determining step.
  - (iii) Use the empirical equations of Figure 13.4 to represent the pH dependence in each region. Multiply each term less than two pH units to the left (lower pH) of a  $pK_a$  by  $f_{SH}$ , and all terms less than two pH units to the right (higher pH) of that  $pK_a$  by  $f_s$ .
  - (iv) Fit the empirical rate law to the data.
  - (v) Propose a mechanism consistent with the rate law to each region of the pH-rate profile.

The application of this sequence of steps is conveniently illustrated by the hydrolysis of aspirin and its methyl ester,



which exhibit the pH-rate profiles illustrated in Figure 13.7. Figure 13.7b represents the idealised profiles, which identify more clearly the regions separated by upward curvatures.

The pH-rate profile of the methyl ester of aspirin has three regions, with slopes  $-1$ , zero and  $+1$ , and the molecule does not contain ionisable groups. By analogy with Figure 13.4, the pseudo-first-order rate constant must have the form

$$k_\Psi = c_1 \left[ \text{H}^+ \right] + c_2 + \frac{c_3}{\left[ \text{H}^+ \right]} \quad (13.45)$$

Region a must be an acid catalysis, and its mechanism can be written as



where E represents the methyl ester of aspirin and a water molecule was explicitly included because it is an hydrolysis reaction. The corresponding rate law in this region is

$$k_{\Psi} = k_1 [\text{H}_2\text{O}] [\text{H}^+] \quad (13.46)$$

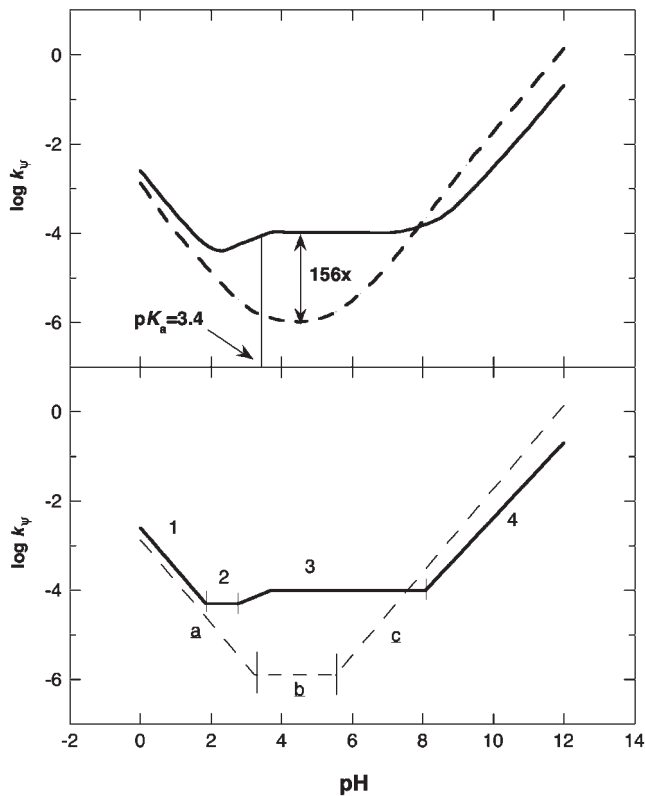


**Figure 13.7** (a) The pH-rate profiles of aspirin (full line) and its methyl ester (dashed line). (b) Idealised profiles with the identification, by number in aspirin and by letters in its methyl ester, of the different regions that correspond to different terms of the rate law.

Region b does not involve acid–base catalysis and its mechanism must be



with the rate law

$$k_\Psi = k_2 [\text{H}_2\text{O}] \quad (13.47)$$

Finally, region c is the region of base catalysis, and its mechanism can be written as



expressed by the rate law

$$k_\Psi = k_3 [\text{OH}^-] = k_3 \frac{K_w}{[\text{H}^+]} \quad (13.48)$$

The pH-rate profile of aspirin is more complex, with four regions, and involves a molecule with an ionisable group, the carboxylic acid group. The downward curvature of region 3 may correspond to the titration of this group because the pH of the intersection between the two arms of this region is typical of an aromatic carboxylic acid,  $pK_a = 3.4$ . Additionally, region 2 is less than 2 pH units from the postulated  $pK_a$  and its rate law must be multiplied by  $f_{SH}$ . On the other hand, region 4 does not have to be multiplied by  $f_S$  because it is more than 2 pH units from that  $pK_a$ . Putting together all the contributions to the rate laws yields:

$$k_\Psi = c_1 \left[ H^+ \right] + \frac{c_2 \left[ H^+ \right]}{K_a + \left[ H^+ \right]} + \frac{c_3 K_a}{K_a + \left[ H^+ \right]} + \frac{c_4}{\left[ H^+ \right]} \quad (13.49)$$

This rate law can be fitted to the experimental pH-rate profile very well using the following parameters:  $c_1 = 2.8 \times 10^{-3} \text{ M}^{-1} \text{ min}^{-1}$ ,  $c_2 = 1.89 \times 10^{-5} \text{ min}^{-1}$ ,  $c_3 = 1.55 \times 10^{-4} \text{ min}^{-1}$ ,  $c_4 = 19.7 \text{ M}^{-1} \text{ min}^{-1}$ , and  $K_a = 4.17 \times 10^{-4} \text{ M}$ .

In region 1, aspirin is predominantly in the protonated form (SH) and the mechanism of hydrolysis in this region is



The corresponding rate law is given by eq. (13.46). In region 2, aspirin remains in the protonated form and the un-catalysed hydrolysis follows the mechanism



with the rate law

$$k_\Psi = k_2 f_{SH} [\text{H}_2\text{O}] = \frac{k_2 \left[ H^+ \right] [\text{H}_2\text{O}]}{K_a + \left[ H^+ \right]} \quad (13.50)$$

The value of  $k_2$  for aspirin is about 20 times greater than for its methyl ester. This suggests a special role for the carboxylic acid group, which may be formulated in terms of intra-molecular acid catalysis (Figure 13.8a).

The mechanism of region 3 may be expressed as the attack of a water molecule on the aspirin anion



for which the rate law is

$$k_\Psi = k_3 f_S [\text{H}_2\text{O}] = \frac{k_3 K_a [\text{H}_2\text{O}]}{K_a + \left[ H^+ \right]} \quad (13.51)$$

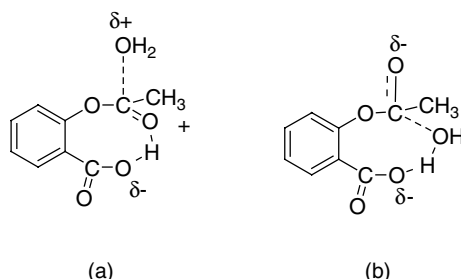


**Figure 13.8** (a) Intra-molecular acid catalysis by the carboxylic acid group of aspirin. (b) Intra-molecular base catalysis by the carboxylate group of aspirin.

The rate constant for this reaction is 156 times larger than that of the analogous reaction in the methyl ester of aspirin and suggests a special role for the carboxylate group of aspirin. A molecular structure for the postulated intra-molecular base catalysis is presented in Figure 13.8b. There are other kinetically indistinguishable mechanisms that are possible for regions 2 and 3. The distinction between such mechanisms requires additional information of the system, such as isotope effects comparing behaviour in water and D<sub>2</sub>O, or studies of substituent effects using related compounds.

Finally, region 4 suggests the mechanism



with the rate law

$$k_\Psi = k_4 [\text{OH}^-] = k_4 \frac{K_w}{[\text{H}^+]} \quad (13.52)$$

This procedure leads to mechanisms of specific acid–base catalysis that are compatible with the kinetic data. However, it should always be remembered that kinetically indistinguishable mechanisms may exist and that the proposal of a mechanism should always be based on all the information available for the system, and not only the kinetic data.

### 13.4 CATALYTIC ACTIVITY AND ACID–BASE STRENGTH

The search for relationships between molecular structure and chemical reactivity, presented in Chapter 7, was instrumental for the development of chemical kinetics in the beginning of the twentieth century. One of the early successes in this area was the relationship suggested by Brønsted and Pedersen for the acid catalysis,



according to which the catalytic constant of an acid HA is related to the acid dissociation constant  $K_{\text{HA}}$ , by [5]

$$k_f = G_f (K_{\text{AH}})^\alpha \quad (13.53)$$

where  $G_f$  is a constant that depends on the temperature, medium and substrate, whereas  $\alpha$  is a parameter that remains constant for the same type of acid. This parameter is called the Brönsted coefficient for acid catalysis. The reverse reaction in mechanism (13.XVIII) can be regarded as a base catalysis, where  $\text{A}^-$  is the base catalyst. For this reaction a similar relationship applies

$$k_r = G_r \left( \frac{1}{K_{\text{AH}}} \right)^\beta \quad (13.54)$$

and  $\beta$  is the Brönsted coefficient for base catalysis.

Brönsted relationships can only be observed for a limited range of acid dissociation constants  $K_{\text{HA}}$ , because as they become larger the reaction eventually becomes diffusion controlled and  $\alpha$  must tend to be zero. On the other hand, given the equilibrium constant  $K_{\text{eq}} = (k_f/k_r)$ , when  $\alpha=0$  the reaction rate for the reverse reaction must vary inversely with  $K_{\text{eq}}$  and, consequently, be proportional to  $(K_{\text{HA}})^{-1}$ . Then,  $\beta=1$ . In general, the sum of the Brönsted coefficients must be equal to unity

$$\alpha + \beta = 1 \quad (13.55)$$

When the acid has more than one equivalent proton that can be transferred and the conjugate base has more than one equivalent basic site to be protonated, the above equations can be generalised to

$$\frac{k_f}{p} = G_f \left( \frac{q}{p} K_{\text{AH}} \right)^\alpha \quad (13.56)$$

$$\frac{k_r}{q} = G_r \left( \frac{p}{q} \frac{1}{K_{\text{AH}}} \right)^\beta \quad (13.57)$$

where  $p$  is the number of equivalent dissociable protons and  $q$  the number of equivalent basic sites in the conjugate base. These relations have the same nature as the statistical correction for equivalent hydrogen atoms discussed in Chapter 6.

Figure 13.9 illustrates the reversible abstraction of a proton of 2,2',4,4'-tetrannitrophenylmethane by a series of bases in 50% water–50% dimethylsulfoxide, where this acid has a dissociation constant of  $K_a^{\text{CH}} = 0.90$ , and that may proceed by general acid–base catalysis [6]. The general expression for the rate constant of this reaction is, according to eq. (13.25),

$$k_{\text{obs}} = k_p^{\text{H}_2\text{O}} + k_p^{\text{OH}} [\text{OH}^-] + k_p^{\text{B}} [\text{B}^-] + k_{-p}^{\text{H}} [\text{H}^+] + k_{-p}^{\text{BH}} [\text{BH}] + k_{-p}^{\text{H}_2\text{C}} \quad (13.58)$$

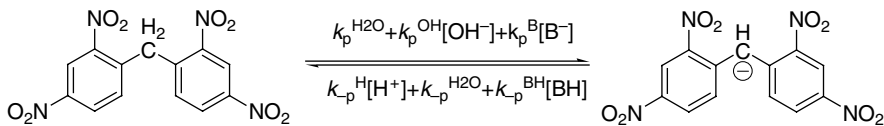


**Figure 13.9** Reversible abstraction of a proton of 2,2',4,4'-tetranitrophenylmethane in 50% water—dimethylsulphoxide at 25 °C.

This reaction can be studied under conditions where some of the terms of the general equation can be neglected. For example, in the presence of an excess of  $\text{OH}^-$ , eq. (13.58) reduces to

$$k_{\text{obs}} = k_p^{\text{OH}} [\text{OH}^-] + k_{-p}^{\text{H}_2\text{O}} \quad (13.59)$$

and a plot of  $k_{\text{obs}}$  as a function of  $[\text{OH}^-]$  is linear. In this case,  $k_p^{\text{OH}}$  can be obtained from the slope ( $k_p^{\text{OH}} = 46.6 \text{ M}^{-1} \text{ sec}^{-1}$ ) and  $k_{-p}^{\text{H}_2\text{O}}$  is given by the intercept or by  $k_{-p}^{\text{H}_2\text{O}} = k_p^{\text{OH}}/K_p^{\text{OH}}$  ( $k_{-p}^{\text{H}_2\text{O}} = 3.31 \times 10^{-4} \text{ sec}^{-1}$ ), where  $K_p^{\text{OH}}$  is the equilibrium constant for the system represented in Figure 13.9 in the absence of a buffer solution and at high pH. In contrast, in HCl solutions, eq. (13.58) becomes

$$k_{\text{obs}} = k_{-p}^{\text{H}} [\text{H}^+] \quad (13.60)$$

and  $k_{-p}^{\text{H}} = 1.75 \times 10^4 \text{ M}^{-1} \text{ sec}^{-1}$  has been measured. From the relation  $k_p^{\text{H}_2\text{O}} = k_{-p}^{\text{H}} K_a^{\text{CH}}/K^{\text{H}_2\text{O}}$ , where  $K^{\text{H}_2\text{O}} = -1.44$  ( $[\text{H}_2\text{O}] = 27.5 \text{ M}$ ) in this medium,  $k_p^{\text{H}_2\text{O}} = 7.92 \times 10^{-9} \text{ M}^{-1} \text{ sec}^{-1}$ .

The values of  $k_{-p}^{\text{BH}}$  and  $k_p^{\text{B}}$  can be measured in experiments run at different values of the ratio  $[\text{BH}]/[\text{B}^-]$ . For buffers with  $\text{pH} < 5$ , eq. (13.58) simplifies to

$$k_{\text{obs}} = k_{-p}^{\text{H}} [\text{H}^+] + k_{-p}^{\text{BH}} [\text{BH}] \quad (13.61)$$

and the rate constant for the general acid catalysis is given by the slope of the plot of  $k_{\text{obs}}$  as a function of  $[\text{BH}]$ . Several parallel lines of this type are obtained when the experiments are done at different pH values. In the case of phenol and methoxyphenol buffers, the slope of  $k_{\text{obs}}$  as a function of  $[\text{BH}]$  depends on the pH, as illustrated in Figure 13.10. In this case eq. (13.58) becomes

$$k_{\text{obs}} = k_p^{\text{B}} [\text{B}^-] + k_{-p}^{\text{BH}} [\text{BH}] \quad (13.62)$$

because  $k_p^{\text{OH}}[\text{OH}^-]$  and  $k_{-p}^{\text{H}_2\text{O}}$  are negligible, as shown by the intercepts of Figure 13.10. The rate constants  $k_{-p}^{\text{BH}}$  and  $k_p^{\text{B}}$  can be obtained from experiments at different values of the  $[\text{BH}]/[\text{B}^-]$  ratio. Table 13.3 presents the rate constants for general acid and base catalysis for the systems represented in Figure 13.9 when the catalysts are phenols. Figure 13.11 illustrates the Brønsted plots for the base catalysis of the ionisation reaction and for the acid catalysis of the re-protonation reaction. The sum of the experimental Brønsted coefficients is only slightly in excess of unity.

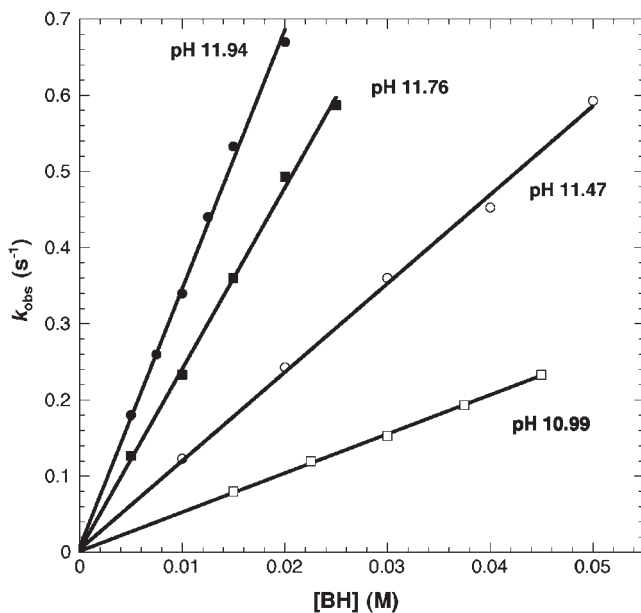


**Figure 13.10** pH and buffer concentration effect on the PT rates of 2,2',4,4'-tetrinitrophenylmethane in 50% water—dimethylsulphoxide at 25 °C.

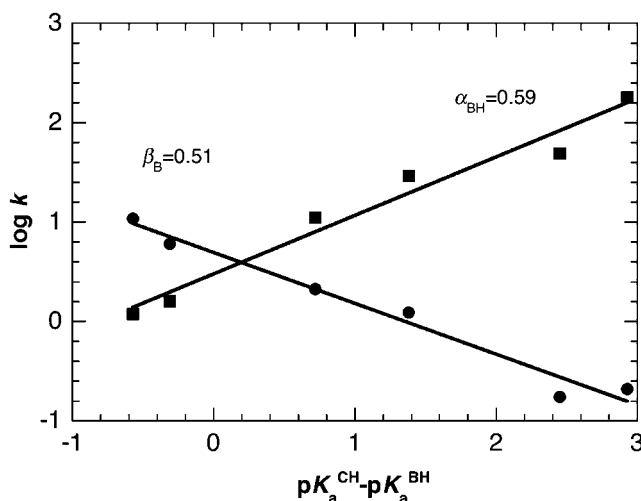


**Figure 13.11** Brønsted plots for the base catalysis (circles) and acid catalysis (squares) of 2, 2', 4, 4'-tetrinitrophenylmethane PT in 50% water—dimethylsulphoxide at 25 °C.

**Table 13.3**

Rate constants for the acid and base catalysis of PT in 2,2',4,4'-tetranitrophenylmethane in 50% water—dimethylsulphoxide at 25 °C ( $pK_a^{\text{CH}} = 10.90$ )

Buffer (acid form)	$pK_a^{\text{BH}}$	$k_{-\text{p}}^{\text{BH}} (\text{M}^{-1} \text{ sec}^{-1})$	$k_{\text{p}}^{\text{B}} (\text{M}^{-1} \text{ sec}^{-1})$
2-Cyanophenol	7.97	180	0.21
4-Cyanophenol	8.45	49.1	0.174
2-Bromophenol	9.52	29.4	1.23
4-Chlorophenol	10.18	11.13	2.13
Phenol	11.21	1.62	6.05
4-Methoxyphenol	11.47	1.20	10.87

### 13.5 SALT EFFECTS

The addition of 0.1 M lithium perchlorate increases the ionisation rate of a sulfonic acid ester by a factor of  $10^5$  when the reaction takes place in a non-polar solvent. The empirical relation between the rate and the salt concentration is

$$k = k_0 + b[\text{salt}] \quad (13.63)$$

where  $k_0$  is the rate constant in the absence of salt and  $b$  a constant that depends on the nature of the salt. This remarkably high salt effect is due to the formation of ion-pairs. In polar solvents, the salt effect is usually much lower.

In acid–base catalysis it is convenient to distinguish between a primary salt effect and a secondary salt effect. The primary effect is related to the dependence of the rate constant on the activity coefficients of the species entering the rate law

$$\nu = k_0 [\text{A}][\text{B}] \frac{\gamma_A \gamma_B}{\gamma_{\ddagger}} \quad (13.64)$$

As the addition of a salt changes the activity coefficient  $\gamma$ , it also changes the reaction rate. This effect was discussed in Chapter 9 and was expressed in eq. (9.67).

The secondary effect is related to the changes introduced by the salt in the ionisation constant of a weak acid HB,

$$K_{\text{HB}} = \frac{[\text{H}^+][\text{B}^-]}{[\text{HB}]} \frac{\gamma_{\text{H}^+} \gamma_{\text{B}^-}}{\gamma_{\text{AB}}} \quad (13.65)$$

where  $K_{\text{HB}}$  is the true dissociation constant of the acid. The addition of a salt changes the ionic strength, hence the activity coefficients, and the concentrations of HB and  $\text{H}^+$ . Some examples of positive secondary salt effects are illustrated in Table 13.4. They refer to an increase in  $[\text{H}^+]$ , and decrease in [HB], with addition of salt. Different effects are expected for charged acids or bases. For strong acids and bases the secondary salt effects are negligible.

**Table 13.4**

Secondary salt effects on the decomposition of diazoacetic ester in 0.05 M acetic acid, at 15 °C

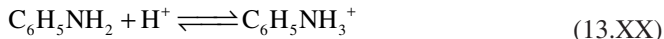
[KNO <sub>3</sub> ] (mol dm <sup>-3</sup> )	[H <sup>+</sup> ] (10 <sup>-4</sup> mol dm <sup>-3</sup> )	<i>k</i> (min <sup>-1</sup> )
0.00	9.53	1.27
0.02	10.3	1.37
0.10	10.9	1.46

## 13.6 ACIDITY FUNCTIONS

The simplest relationship between rate constants and the pH, which is an acidity function, was illustrated in Figure 13.4. However, the concept of pH is in general only valid in the region 0 < pH < 14. For very concentrated acid solutions, these relationships break down and alternative acidity functions have been proposed. The first to meet with some success was proposed by Hammett and Deyrup [7] and was based on equilibria of the type



found in anilines.



The equilibrium constant of such reactions is

$$K = \frac{[\text{BH}^+]}{[\text{H}^+][\text{B}]} \frac{\gamma_{\text{BH}^+}}{\gamma_{\text{B}} \gamma_{\text{H}^+}} \quad (13.66)$$

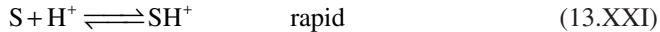
and may also be written as

$$\log K - \log \frac{[\text{BH}^+]}{[\text{B}]} = -\log \left( a_{\text{H}^+} \frac{\gamma_{\text{B}}}{\gamma_{\text{BH}^+}} \right) \quad (13.67)$$

If [BH<sup>+</sup>] and [B] can be distinguished spectroscopically, as is the case for the anilines, and if *K* can be measured in more dilute solutions, then all the quantities in the left-hand side of eq. (13.67) are experimentally accessible. The right-hand side, where *a*<sub>H<sup>+</sup></sub> is the activity of H<sup>+</sup>, is defined as the acidity function *H*<sub>0</sub>

$$H_0 \equiv -\log \left( a_{\text{H}^+} \frac{\gamma_{\text{B}}}{\gamma_{\text{BH}^+}} \right) \quad (13.68)$$

This acidity function can be measured in any acidic solution by introducing a suitable indicator and measuring the concentration of  $[BH^+]$  and  $[B]$ . For example, the mechanism



where the second step is the rate-determining step,

$$v = k^\ddagger \left[ (SH^+)^\ddagger \right] \quad (13.69)$$

and the transition states are in quasi-equilibrium with the species  $SH^+$

$$K_s^\ddagger = \frac{a_\ddagger}{a_{SH^+}} = \frac{\left[ (SH^+)^\ddagger \right] \gamma_\ddagger}{\left[ SH^+ \right] \gamma_{SH^+}} \quad (13.70)$$

where  $a_\ddagger$  and  $\gamma_\ddagger$  are the activity and activity coefficient of the activated complex, respectively, leads to the rate

$$v = k^\ddagger K_s^\ddagger [SH^+] \frac{\gamma_{SH^+}}{\gamma_\ddagger} \quad (13.71)$$

This rate law can be expressed in terms of the reactant concentrations using the pre-equilibrium approximation:

$$\frac{a_{SH^+}}{a_S a_{H^+}} = \frac{[SH^+]}{[S]} \frac{\gamma_{SH^+}}{\gamma_S \gamma_{H^+}} = K_s \quad (13.72)$$

that yields

$$v = k^\ddagger K_s^\ddagger K_s \frac{\gamma_S}{\gamma_\ddagger} a_{H^+} [S] \quad (13.73)$$

The first-order rate constant

$$k = k^\ddagger K_s^\ddagger K_s \frac{\gamma_S}{\gamma_\ddagger} a_{H^+} \quad (13.74)$$

can be written in logarithmic terms as

$$\log k = \log(k^\ddagger K_s^\ddagger K_s) + \log \left( \frac{\gamma_S}{\gamma_\ddagger} a_{H^+} \right) \quad (13.75)$$

**Table 13.5**Hydrolysis of  $\beta$ -propiolactone in concentrated perchloric acid solution [8]

$[\text{HClO}_4]$ (mol dm $^{-3}$ )	$k(10^{-3} \text{ min}^{-1})$	$-\log_{10} k (\text{min}^{-1})$	$-H_0$
1.83	3.65	2.44	0.58
2.60	5.38	2.27	0.94
4.53	32.2	1.49	1.84
5.36	69.9	1.16	2.28

to emphasise the similarity between the last term and the acidity function  $H_0$ . Accordingly, there must be a linear correlation between  $\log(k)$  and  $H_0$ , with a slope of  $-1$ . The hydrolysis of  $\beta$ -propiolactone in concentrated acid solution presents this type of behaviour, as illustrated in Table 13.5.

Just as with pH, the function  $H_0$  is a logarithmic function. It is convenient to define its anti-logarithm as

$$H_0 = -\log h_0 \quad (13.76)$$

where  $h_0$  is equal to the activity of  $\text{H}^+$  in diluted aqueous solution.

### 13.7 HYDRATED PROTON MOBILITY IN WATER

The proton in water, represented above by  $\text{H}^+$  or  $\text{H}_3\text{O}^+$ , is strongly hydrated. Eigen argued that the symmetrical distribution of the excess positive charge among the 3 protons in the hydronium ion allows for the formation of very stable hydrogen bonds to 3 neighbouring  $\text{H}_2\text{O}$  molecules and the complex ion  $\text{H}_3\text{O}^+(\text{H}_2\text{O})_3$  should be remarkably stable and observable in aqueous solution. Direct evidence for the existence of the “Eigen ion” in solution was obtained in the X-ray and neutron scattering studies of Triolo and Narten [9], who measured a nearest-neighbour oxygen–oxygen distance of  $l_{\text{OO}}(\text{H}_3\text{O}^+\cdots\text{OH}_2) = 2.52 \text{ \AA}$ . This is much shorter than the near-neighbour  $\text{H}_2\text{O}\cdots\text{OH}_2$  distance in the tetrahedral network of pure water,  $l_{\text{OO}} = 2.85 \text{ \AA}$ , also measured by these authors. Although the enthalpy of the hydrogen bond in liquid water is known rather precisely,  $10.6 \pm 0.4 \text{ kJ mol}^{-1}$  [10], the strength of the H-bonds in the Eigen ion is not known but must be greater than this because shorter H-bonds distances correspond to stronger H-bonds. For example, the calculated gas-phase O–O distance of  $\text{H}_5\text{O}_2^+$  is  $l_{\text{OO}} = 2.38 \text{ \AA}$  [11] and its experimental H-bond enthalpy is  $133 \text{ kJ mol}^{-1}$  [12]. A good estimate for the strength of the H-bond in the Eigen ion can be obtained with the Lippincott–Schroeder [13] potential. This potential, presented in detail in Appendix V, gives a quantitative relation between H-bond strengths, distances and frequencies. A comparison between H-bond lengths and strengths is presented in Figure 13.12.

For low degrees of hydration, Zundel proposed that the  $(\text{H}_2\text{O}-\text{H}^+\cdots\text{OH}_2)$  ion should also be relatively stable. In fact, the X-ray and neutron diffraction measurements of Kameda

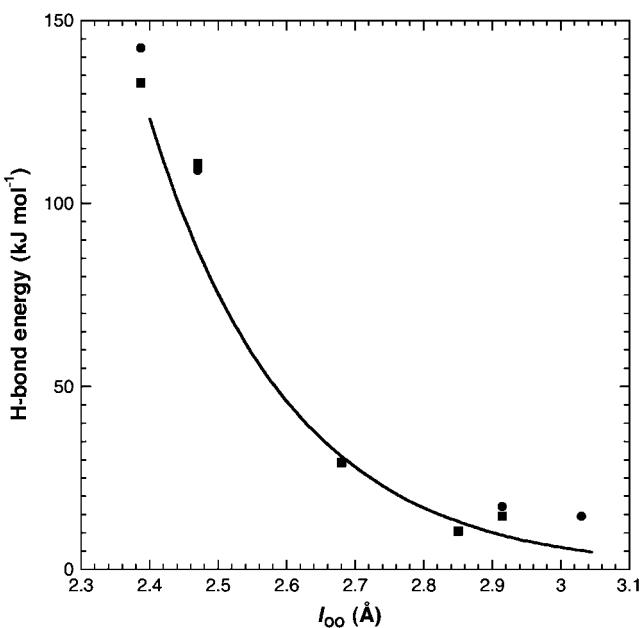


**Figure 13.12** Relation between the H-bond lengths and strengths involving oxygen acids and bases. The circles are classical potential energies from *ab initio* calculations, the squares are experimental H-bond enthalpies and the line is the relation given by the Lippincott–Schroeder potential described in Appendix V.

and co-workers on aqueous 21% HCl solutions, revealed the existence of a species with a nearest-neighbour O···O distance of  $2.37 \pm 0.02$  Å, consistent with the Zundel ion. This is an exceptionally short distance, comparable with that obtained by *ab initio* calculations for this ion in the gas phase. According to the Lippincott–Schroeder potential, the H-bond strength of the Eigen ion is  $33 \text{ kJ mol}^{-1}$  and that of the Zundel ion is  $92 \text{ kJ mol}^{-1}$ . In spite of this difference, the Eigen ion is the predominant species in dilute acid solutions, because it involves 3 hydrogen bonds. Other theoretical and experimental data also indicate that the Eigen ion is slightly more stable than the Zundel ion in dilute acid solutions, by *ca.*  $3 \text{ kJ mol}^{-1}$  [14].

The identification of both Eigen and Zundel ions in acidic solutions helps to understand the anomalously high mobility of protons in liquid water, which is approximately 5 times that of ions of similar size to  $\text{H}_3\text{O}^+$ . An early explanation for this high mobility is known as the Grotthuss mechanism. This involves a proton shuttling between successive water molecules, such that rather than involving the transport of the larger  $\text{H}_3\text{O}^+$  species, protons move by a relay in the H-bonded water network. This picture must be refined to accommodate the very fast dynamics of the aqueous proton transport, which approach 1 ps [15]. The proton changes positions between H-bonded oxygen atoms nearly  $10^{12}$  times every second, equivalent to vibration in a shallow potential well. The current view on this process is that the Zundel ion is almost always an intermediate in the conversion between

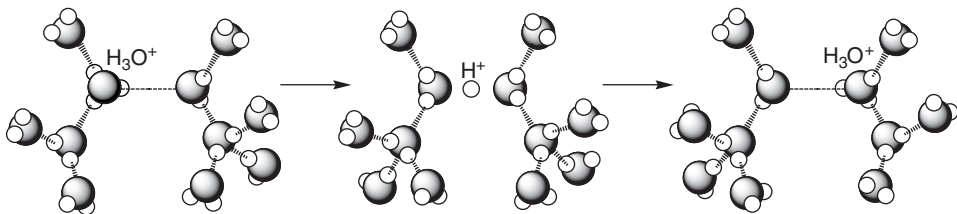
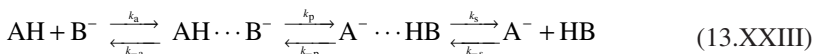


**Figure 13.13** From left to right, a proton in an Eigen ion migrates to form a Zundel ion, and then proceed to form another Eigen ion. Only the hydration shell of the lower water molecules is shown.

two Eigen ions. This process is illustrated in Figure 13.13 and should be associated with a very small barrier. The actual rate-determining step may be a change in the second hydration layer, and proton mobility is facilitated by cooperative many-molecule effects [16,17].

The very small barrier associated with the transfer of the proton in water is a consequence of the strong hydrogen bonds involved. This is not exclusive to the excess proton in water. When AH and B<sup>-</sup> in reaction (13.I) can form H-bonds stronger than 4 kJ mol<sup>-1</sup>, the barrier for PT is significantly reduced and the PT rate is significantly enhanced at room temperature. This is always the case for PT between oxygen, nitrogen and halogen acid and bases. In such cases, the mechanism for PT between strong acids and bases involves hydrogen-bonded intermediates. According to the mechanism proposed by Eigen [18], we have to consider a precursor and a successor complex along the reaction coordinate



The hydrogen bond involves an incipient PT because it corresponds to an advancement of the PT coordinate with respect to the separated reactants. Using the bond order of the product bond as the reaction coordinate, it changes from 0 in the reactants, to  $n_{\text{H}\cdots\text{B}}$  in the precursor complex, to  $n_{\text{H}\cdots\text{B}}^{\ddagger}$  in the transition state, to  $n_{\text{A}\cdots\text{H}}$  in the successor complex and finally to 1 in the products. Using the definition of the bond order given by the ISM in Chapter 6, which relates bond orders to bond extensions, and given the relation between bond lengths and bond strengths shown in Figure 13.12, it is not surprising that ISM and the LS potential give an approximately linear relation between the bond order in the H-bonded complex AH $\cdots$ B and the corresponding H-bond strength (Figure 13.14). When the bond strength exceeds 140 kJ mol<sup>-1</sup>,  $n_{\text{H}\cdots\text{B}}$  reaches 0.5. At this point, the barrier for the PT disappears and the proton is symmetrically placed between A and B. This is the case of the FHF<sup>-</sup> ion, that is formed in water with an association constant of 4 M<sup>-1</sup> [19], and in the gas phase is a symmetrical ion with an H-bond enthalpy of 203 kJ mol<sup>-1</sup>, the highest ever measured. The high stability of this species is likely to be one of the reasons that, in contrast to the other hydrohalic acids (HI pK<sub>a</sub> -9; HBr pK<sub>a</sub> -8, HCl pK<sub>a</sub> -6.1), HF is a weak acid in water (pK<sub>a</sub> 3.18).

The three steps of mechanism (13.XXIII) correspond to the diffusion of the reactants in solution until an H-bonded complex is formed, followed by the PT step between precursor

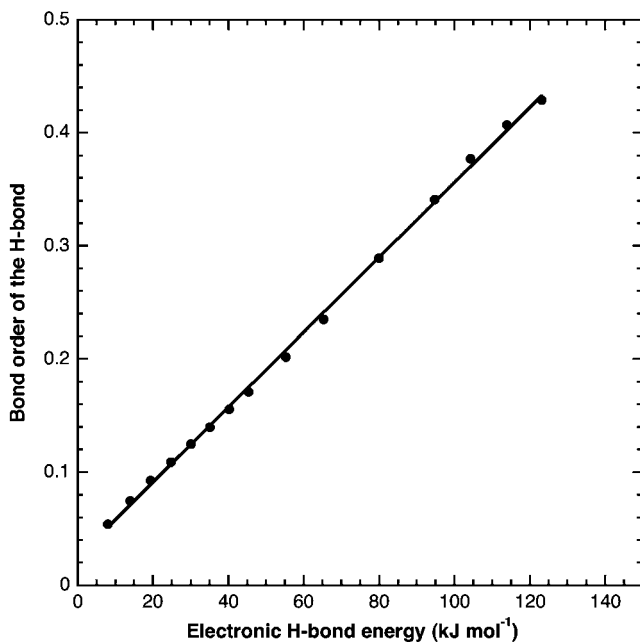


**Figure 13.14** Relation between hydrogen bond orders ( $n_{\text{H}\cdots\text{O}}$ ) and electronic H-bond energies ( $D_{\text{e(OHO)}}$ ), according to the LS potential and ISM.

and successor complexes, and the diffusion of the products to their equilibrium separations. The rate constant for the forward transfer is

$$v = k_f [\text{AH}][\text{B}^-] \quad (13.77)$$

and the forward rate constant can be expressed in terms of the actual rate constants of the three steps using the steady-state approximation for the concentration of the two complexes.

$$k_f = \frac{k_a k_p k_s}{k_p k_s + k_{-a} k_s + k_{-p} k_a} \quad (13.78)$$

Similarly, for the reverse rate constant

$$v = k_r [\text{A}^-][\text{HB}] \quad (13.79)$$

the reverse rate constant can also be expressed within the same approximation as

$$k_r = \frac{k_{-a} k_{-p} k_{-s}}{k_p k_s + k_{-a} k_s + k_{-p} k_{-a}} \quad (13.80)$$

**Table 13.6**

Brönsted coefficients for PT reactions

Catalysis	Catalyst (changing along the series)	Substrate (constant along the series)	Brönsted coefficient	
			Forward	Reverse
Acid	$\text{HA}_i$	$\text{B}^-$	$\alpha_A$	$\beta_A$
Base	$\text{B}_{-i}$	$\text{HA}$	$\beta_B$	$\alpha_B$

In acid catalysis, the nature of AH changes while the substrate  $\text{B}^-$  is maintained constant. The Brönsted coefficient for the forward process is  $\alpha_A$  and for the reverse process it is  $\beta_A$ . In base catalysis,  $\text{B}^-$  varies while AH remains constant along the reaction series; now  $\beta_B$  is the Brönsted coefficient in the forward direction and the  $\alpha_B$  coefficient for the reverse direction. Table 13.6 summarises these relationships.

Acids centred on oxygen, nitrogen and halogen atoms have rapid PT,  $k_p \gg k_a, k_s$ . Additionally, for exothermic forward reactions,  $k_p > k_{-p}$ . When these conditions are met, eqs. (13.78) and (13.80) simplify to

$$\begin{aligned} k_f &= k_a \\ k_r &= \frac{k_{-s}}{k_s} \frac{k_{-p}}{k_p} k_a \end{aligned} \quad (13.81)$$

and the forward rate constant is independent of the acidity of AH and of the basicity of  $\text{B}^-$ , that is,  $\alpha_A = 0$  and  $\beta_B = 0$ . In this case there is no catalysis by the acid AH, or by the base  $\text{B}^-$ , and the value of  $k_f$  approaches that of the diffusion rate constant, *ca.*  $10^{10} \text{ dm}^3 \text{ mol}^{-1} \text{ sec}^{-1}$  in aqueous solution. For the reverse reaction, the rate constant  $k_r$  depends on the acidity constant of the acid and is directly proportional to  $-\Delta pK = -(pK_{\text{HA}} - pK_{\text{HB}})$ , because  $(k_{-p}/k_p) = (pK_{\text{HB}} - pK_{\text{HA}})$ . Although there is no acid catalysis in the forward direction, in the reverse direction there is base catalysis and the Brönsted coefficient which will affect  $k_r$  is  $\beta_A = 1$ . This behaviour is illustrated in Figure 13.15.

Another limiting condition for eqs. (13.78) and (13.80) is  $k_p \gg k_a, k_s$ , but  $k_p < k_{-p}$ . In this case, the forward PT is an endothermic process. The rate constants are simplified to

$$\begin{aligned} k_f &= \frac{k_a}{k_{-a}} \frac{k_p}{k_{-p}} k_s \\ k_r &= k_{-s} \end{aligned} \quad (13.82)$$

The forward rate constant depends on the equilibrium constant of the PT, and  $k_f$  is directly proportional to  $(pK_{\text{HA}} - pK_{\text{HB}})$ . The consequences are similar to those discussed above for the first limiting condition: forward direction, acid catalysis gives  $\alpha_A = 1$  and base catalysis gives  $\beta_B = 1$ . The reverse reaction is diffusion controlled and is not catalysed.

In summary, when the barrier for PT is small in the forward direction, the exothermic rate constants are diffusion controlled and catalysis is not observed. On the other hand, the

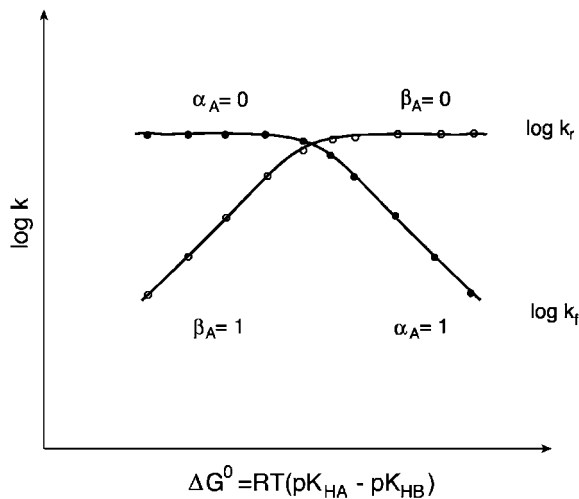


**Figure 13.15** Eigen plots for the acid–base catalysis of strong acids following mechanism (13.XXIII). In acid catalysis in the forward direction, HA is the catalyst and varies along the reaction series, while the substrate B<sup>-</sup> is kept constant. In the forward direction, the change in HA gives the Brønsted coefficient  $\alpha_A$  for acid catalysis, and for the reverse direction the change in A<sup>-</sup> gives the Brønsted coefficient  $\beta_B$  for base catalysis.

barriers in the reverse direction are high and increase in the same fashion as their endothermicity. The rates vary in the same proportion as the pH (specific acid catalysis) or the pOH (specific base catalysis).

A third limiting condition occurs when  $k_p < k_{-a}$  and  $k_{-p} < k_s$ . The rate determining step is now the transfer of the proton, and

$$\begin{aligned} k_f &= \frac{k_a}{k_{-a}} k_p \\ k_r &= \frac{k_{-s}}{k_s} k_{-p} \end{aligned} \quad (13.83)$$

This condition is often met in carbon acids. In this case, it is possible to observe general acid–base catalysis and the values of  $\alpha$  and  $\beta$  are in between 0 and 1.

### 13.8 PROTON-TRANSFER RATES IN SOLUTION

The protolysis of acids of similar strength spans an extraordinary range of reaction rates. For example, the rate of the acid catalysed dedeuteration of azulene-1-d ( $pK_a = -1.76$ ) is  $0.45 \text{ M}^{-1} \text{ sec}^{-1}$  [20], whereas the deprotonation rate of electronically excited 5-cyano-1-naphthol ( $pK_a = -2.8$ ) is  $1.3 \times 10^{11} \text{ sec}^{-1}$  [21], when both of them are measured in water ( $pK_a = -1.74$ ). The nature of the reactants also has a profound effect on the kinetic isotope

effects (KIE). For example, the deprotonation of toluene ( $pK_a = 41.2$ ) by cesium cyclohexylamine ( $pK_a = 41.6$ ) in cyclohexylamide has  $k_H/k_D = 11$  [22], whereas for the deprotonation of 5-cyano-1-naphthol in water  $k_H/k_D$  is only 1.6 [21].

The free-energy dependence of many PT rates follows the Brönsted relationship described above, but the success of this free-energy linear relationship is unexpected. In principle, it should not be valid over a large range of acidity constants, because the Brönsted coefficient for acid catalysis should vary dramatically from  $\alpha_A = 0$  to  $= 1$  when the reaction becomes endothermic, as shown in Figure 13.15, where acid–base catalysis is not observed. This was assigned to the small size of the barrier for the forward PT, but an explanation for the size of the barriers based on molecular structure of the reactants is still lacking.

In the remainder of this chapter, the rates of PT reactions in solution are quantitatively related to the molecular structures of the reactants and to their hydrogen-bonding ability. This relation uses the ISM, previously employed to calculate the rates of atom transfers and  $S_N2$  reactions, thus providing a general account of the rates of the most important bond-breaking–bond-making reactions. In the next chapter, the principles applied to these reactions in gas phase and in solution are also applied to some cases of enzyme catalysis.

### 13.8.1 Classical PT rates

The most important difference between the application of ISM to H-atom transfers in the gas phase and PT in solution is the calculation of the reaction energy. In the first case, the classical potential energy of the H-atom transfer,  $\Delta V^0$ , is obtained as the difference between the classical potential energies of the HA bond in the reactants and the HB bond in the products. Then the vibrationally adiabatic potential energy is obtained by adding the difference in zero point-energies between reactants and products. For PT in solution the reaction free energy is directly obtained from the difference in acidity constants.

$$\Delta G^0 = -RT \left[ 2.303pK_{BH} + \ln\left(\frac{p_B}{q_B}\right) - 2.303pK_{AH} - \ln\left(\frac{p_A}{q_A}\right) \right] \quad (13.84)$$

The reaction free energy is simple to obtain experimentally for most PTs of interest. However, its decomposition in enthalpy and entropy contributions requires the measurement of acidity constants as a function of temperature. The entropies of reaction are not usually known, but, for the calculation of PT rates, the participation of the entropy in the reaction coordinate can be limited to the determination of the partition functions. In the simplest approximation, it can be assumed that the ratio of the transition state versus reactant vibrational partition functions is close to unity. Ignoring tunnelling corrections and vibrational frequency changes along the reaction coordinate, the classical rate for PT is, following eq. (6.80)

$$k_{cl} = \sigma \left( \frac{1}{3} \right)^3 \frac{6.82 \times 10^{10}}{\sqrt{T}} \left( \frac{m_A + m_B + m_C}{m_A (m_B + m_C)} \right)^{3/2} \frac{I_{BHA}}{I_{HA}} \exp\left(-\frac{\Delta V_{cl}^\ddagger}{RT}\right) \quad (13.85)$$

where  $\sigma$  is a statistical factor ( $\sigma = p_A q_B$ ), the scaling factor  $(1/3)^3$  was obtained from the typical ratio of vibrational to rotational partition functions in polyatomic systems, and the value of the constant gives the rate in units of  $M^{-1} \text{ sec}^{-1}$  when the masses are expressed in atomic mass units. The moment of inertia of the reactants is

$$I_{\text{HA}} = \frac{m_{\text{H}} m_{\text{A}}}{m_{\text{H}} + m_{\text{A}}} \left( l_{\text{HA,eq}} \right)^2 \quad (13.86)$$

and that of the transition state is

$$I_{\text{BHA}} = m_{\text{B}} \left( l_{\text{HB}}^{\ddagger} \right)^2 + m_{\text{A}} \left( l_{\text{HA}}^{\ddagger} \right)^2 - \frac{\left( m_{\text{B}} l_{\text{HB}}^{\ddagger} - m_{\text{A}} l_{\text{HA}}^{\ddagger} \right)^2}{m_{\text{B}} + m_{\text{H}} + m_{\text{A}}} \approx m_{\text{B}} \left( l_{\text{HB}}^{\ddagger} \right)^2 + m_{\text{A}} \left( l_{\text{HA}}^{\ddagger} \right)^2 \quad (13.87)$$

These equations have a simple solution for nearly symmetrical reactions, when  $\Delta V^0 \approx 0$  and  $n^{\ddagger} \approx 0.5$ . In this case, following ISM, the transition state bond lengths are given by

$$\begin{aligned} l_{\text{HA}}^{\ddagger} &= l_{\text{HA,eq}} - a'_{\text{sc}} \left( l_{\text{HA,eq}} + l_{\text{HB,eq}} \right) \ln(0.5) \\ l_{\text{HB}}^{\ddagger} &= l_{\text{HB,eq}} - a'_{\text{sc}} \left( l_{\text{HA,eq}} + l_{\text{HB,eq}} \right) \ln(0.5) \end{aligned} \quad (13.88)$$

and the classical energy barrier is

$$\begin{aligned} \Delta V_{\text{cl}} &= D_{\text{e,HA}} \left\{ 1 - \exp \left[ \beta_{\text{HA}} a'_{\text{sc}} \left( 2l_{\text{HA,eq}} \right) \ln(0.5) / m \right] \right\}^2 \\ &= D_{\text{e,HB}} \left\{ 1 - \exp \left[ \beta_{\text{HB}} a'_{\text{sc}} \left( 2l_{\text{HB,eq}} \right) \ln(0.5) / m \right] \right\}^2 \end{aligned} \quad (13.89)$$

where the electronic dissociation energy ( $D_{\text{e,HA}}$ ,  $D_{\text{e,HB}}$ ), spectroscopic constant ( $\beta_{\text{HA}}$ ,  $\beta_{\text{HB}}$ ) and equilibrium bond length ( $l_{\text{HA,eq}}$ ,  $l_{\text{HB,eq}}$ ) are readily available from bond dissociation energies, vibrational frequencies and structural data. Some examples are given in Table 13.7. The “universal” constant of ISM,  $a'_{\text{sc}} = 0.182$ , and the electrophilicity index of Parr

$$m = \frac{I_{\text{P}} + E_{\text{A}}}{I_{\text{P}} - E_{\text{A}}} \quad (13.90)$$

complete all the data required to calculate the  $\Delta V_{\text{cl}}^*$ , provided that the ionisation potential ( $I_{\text{P}}$ ) and the electron affinity ( $E_{\text{A}}$ ) of B (or A) are also known.

This simple method to calculate classical rates is conveniently illustrated by the deprotonation of the conjugated acid of azulene in aqueous solution, mechanism (13.XXIV). In the absence of data on the radical ion of azulene, we take the ionisation potential and electron affinity of the molecule,  $I_{\text{P}} = 7.42 \text{ eV}$  and  $E_{\text{A}} = 0.79 \text{ eV}$ , to calculate  $m = 1.238$ . The  $D_{\text{e,HA}}$ ,  $\beta_{\text{HA}}$  and  $l_{\text{HA,eq}}$  values of the two acidic C–H bonds of azulene can be taken from those of benzene. Using these parameters and eq. (13.89), we obtain  $\Delta V_{\text{cl}}^* = 56.1 \text{ kJ mol}^{-1}$ . With  $D_{\text{e,HA}}$ ,  $\beta_{\text{HA}}$  and  $l_{\text{HA,eq}}$  values of water a similar calculation gives  $\Delta V_{\text{cl}}^* = 61.5 \text{ kJ mol}^{-1}$ . The model is very forgiving, provided that a consistent set of data are employed. Using

**Table 13.7**

Bond lengths, bond dissociation energies, vibrational frequencies of the molecules and ionisation potentials and electron affinities of the radicals employed in the calculation of the energy barriers of PT reactions<sup>a</sup>

	$l_{\text{eq}}(\text{\AA})$	$D_e(\text{kJ mol}^{-1})$	$\beta(\text{\AA}^{-1})$	$I_p(\text{eV})$	$E_A(\text{eV})$
$\text{C}_6\text{H}_6$	1.101	488.7	1.8415	8.32	1.096
$\text{CH}_3\text{C}_6\text{H}_5$	1.111	390.4	1.9894 <sup>b</sup>	7.242	0.912
$\text{CH}_3\text{COCH}_3$	1.103	425.9	1.9005	9.703 <sup>c</sup>	1.76 <sup>d</sup>
$\text{CH}_3\text{NO}_2$	1.088	64.6	2.5447	11.08 <sup>c</sup>	0.50 <sup>c</sup>
$\text{CH}_3\text{NH}_2$	1.010	270.3	2.1717		
$\text{H}_2\text{O}$	0.9575	517.1	2.1697	13.017	1.8277
$\text{CH}_3\text{COOH}$	0.97	461.5	2.2581	10.65 <sup>c</sup>	3.29 <sup>d</sup>
$\text{C}_6\text{H}_5\text{OH}$	0.956	381.2	2.5617	8.56	2.253

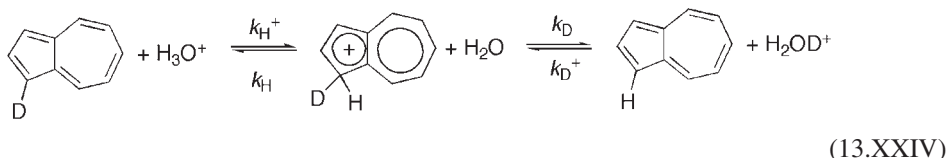
<sup>a</sup>Boldface letters indicate where the radical is centred after the bond to the hydrogen atom is broken; bond lengths and bond dissociation energies from ref. [23]; ionisation potentials and electron affinities from webbook.nist.gov, except where noted.

<sup>b</sup>Zavitsas [24].

<sup>c</sup>For the molecule.

<sup>d</sup>Pearson [25].

$\Delta V_{\text{cl}}^{\ddagger}=58.6 \text{ kJ mol}^{-1}$ , the classical rate is  $1.5 \times 10^{-2} \text{ M}^{-1} \text{ sec}^{-1}$ . Table 13.8 compares this and other calculated rates with the corresponding experimental data.



The approximate calculation of classical PT barriers in H-bonded systems is slightly more complicated, because hydrogen bonding reduces the PT barrier. As mentioned earlier, the H-bond corresponds to a progress along the PT reaction coordinate. This is taken into account by replacing  $n^{\ddagger}$  by  $(n^{\ddagger} - n_{\text{H}\cdots\text{B}})$ , where  $n_{\text{H}\cdots\text{B}}$  is the bond order associated with the hydrogen bond. The ISM classical barrier is now

$$\Delta V_{\text{cl}}^{\ddagger} = \left[ 1 - (n^{\ddagger} - n_{\text{H}\cdots\text{B}}) \right] D_{\text{e,HA}} \left\{ 1 - \exp \left[ \beta_{\text{HA}} a'_{\text{sc}} (2l_{\text{HA,eq}}) \ln (1 - n^{\ddagger} + n_{\text{H}\cdots\text{B}}) / m \right] \right\}^2 + (n^{\ddagger} - n_{\text{H}\cdots\text{B}}) D_{\text{e,HB}} \left\{ 1 - \exp \left[ \beta_{\text{HB}} a'_{\text{sc}} (2l_{\text{HB,eq}}) \ln (n^{\ddagger} - n_{\text{H}\cdots\text{B}}) / m \right] \right\}^2 \quad (13.91)$$

The bond order associated with the H-bond is given by the LS potential, provided the H-bond strength or length is known. The simplest method to obtain  $n_{\text{H}\cdots\text{B}}$  is to use the linear correlation between this parameter and the H-bond strength illustrated in Figure 13.14 for oxygen acids and bases,  $n_{\text{H}\cdots\text{B}} \approx 0.0253 + 0.0033 D_{\text{e(AHB)}}$ . For energies below 50 kJ mol<sup>-1</sup>, a good linear correlation is also found with the vibrationally adiabatic H-bond energies,  $n_{\text{H}\cdots\text{B}} = 0.0427 + 0.0039 D_{0(\text{AHB})}$ .

**Table 13.8**

Parameters employed in the ISM reaction coordinate of  $\text{AH} + \text{B}^- \rightarrow \text{A}^- + \text{HB}$ , and corresponding ISM classical ( $k_{\text{cl}}$ ) and semiclassical ( $k_{\text{sc}}$ ) rates<sup>a</sup>

$\text{AH, p}K_{\text{a}}$	$\text{HB, p}K_{\text{a}}$	Reactant model	Product model	$m$	$D_{0(\text{AHB})}$ (kJ mol $^{-1}$ )	$k_{\text{cl}}$	$k_{\text{sc}}$	$k_{\text{exp}}$
$\text{H}_3\text{O}^+, -1.74$	Azulene $\text{H}^+$ , -1.76	$\text{C}_6\text{H}_6$	$\text{H}_2\text{O}$	1.238	—;—	$1.5 \times 10^{-2}$	1.2	$1.5^b$
$5\text{CN1N}^*, -2.8$	$\text{H}_3\text{O}^+, -1.74$	$\text{C}_6\text{H}_6\text{OH}$	$\text{H}_2\text{O}$	2.574	8; 17	$5.2 \times 10^9$	$1.7 \times 10^{11}$	$1.3 \times 10^{11c}$
Nitromethane, 10.22	Water, 15.74	$\text{CH}_3\text{NO}_2$	$\text{H}_2\text{O}$	1.095	—;—	$8.8 \times 10^{-2}$	6.5	$9.2^d$
Acetylacetone, 9.0	Water, 15.74	$\text{CH}_3\text{COCH}_3$	$\text{H}_2\text{O}$	1.443	—;—	$1.4 \times 10^1$	$6.0 \times 10^3$	$2 \times 10^{4e}$
Acetic acid, 4.76	Propionic acid, 4.88	$\text{CH}_3\text{COOH}$	$\text{CH}_3\text{COOH}$	1.894	17; 17	$4.0 \times 10^6$	$1.3 \times 10^9$	$3.9 \times 10^{8f}$
Toluene, 41.2	Li <i>c</i> -hexylamide, 41.6	$\text{C}_6\text{H}_5\text{CH}_3$	$\text{CH}_3\text{NH}_2$	1 <sup>g</sup>	—;—	$7.5 \times 10^{-4}$	$1.1 \times 10^{-2}$	$6.3 \times 10^{-2h}$

<sup>a</sup>Rates at 25 °C per equivalent proton in M $^{-1}$  sec $^{-1}$ , except for italicised rates, which are in sec $^{-1}$ .

<sup>b</sup>Gruen and Long [20].

<sup>c</sup>Pines and co-workers [21].

<sup>d</sup>Bell and Goodall [26].

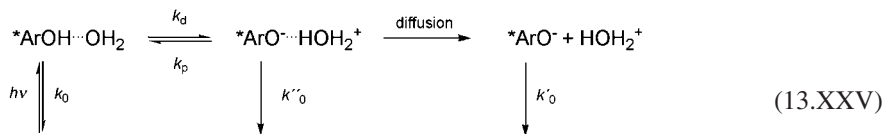
<sup>e</sup>At 12 °C, [18].

<sup>f</sup>Rates at 20 °C, [27].

<sup>g</sup>For H bonded to sp $^3$  carbon atoms the standard value of unity is always employed by ISM.

<sup>h</sup>Streitwieser, Jr. [22].

The procedure to calculate the barrier for PT in an H-bonded system is conveniently illustrated with the excited-state deprotonation of 5-cyano-1-naphthol (5CN1N) in water, mechanism (13.XXV). The H-bond energies of precursor and successor complexes are 8 and 17 kJ mol<sup>-1</sup>, respectively. We will use  $D_{0(\text{AHB})} = 12.5 \text{ kJ mol}^{-1}$  to have the symmetry required by the simplified formulation. This gives  $n_{\text{H}\cdots\text{B}} = 0.0915$ . The excited-state  $I_p$  is the ground state  $I_p$  minus the excited state energy ( $E_e$ ). Using  $I_p(\text{C}_6\text{H}_5\text{O}) = 8.56 \text{ eV}$  and  $E_e(5\text{CN1N}) = 3.444 \text{ eV}$ , together with  $E_A(\text{C}_6\text{H}_5\text{O}) = 2.253 \text{ eV}$ , we obtain  $m = 2.574$ . With the  $D_e$ ,  $l_{\text{eq}}$  and  $\beta$  values of the O-H bonds in naphthol and water, eq. (13.91) gives  $\Delta V_{\text{cl}}^\ddagger = 6.3 + 11.3 = 17.6 \text{ kJ mol}^{-1}$ .



The transfer of a proton in an H-bonded system corresponds to the movement of the proton along its hydrogen bond. This movement is limited by the frequency of approach between the A and B atoms in the H-bonded precursor complex, which is the H-bond vibrational frequency,  $\bar{v}_{AB}$ . It is related to the H-bond distance and strength through the LS potential. For an H-bond strength of 12.5 kJ mol<sup>-1</sup> between oxygen atoms, this frequency is  $\bar{v}_{AB} = 236 \text{ cm}^{-1}$ . The PT is now a first-order reaction and the classical rate constant expressed in terms of this vibrational frequency is

$$k_{\text{cl}} = K_c c \bar{v} \exp\left(-\frac{\Delta V_{\text{cl}}^\ddagger}{RT}\right) \quad (13.92)$$

where  $K_c$  represents the fraction of acid species H-bonded to the base. For 5CN1N in aqueous solution all acid species are H-bonded to water,  $K_c = 1$ , and  $k_{\text{cl}} = 5.9 \times 10^9 \text{ sec}^{-1}$  at 298 K. The comparison with the experimental rate is presented in Table 13.8.

The classical rates necessarily underestimate the experimental rates because the zero-point energy corrections reduce the barrier by 5–10 kJ mol<sup>-1</sup> (a factor of 5–30 at room temperature) and tunnelling further increases the rates by another factor of 5–10 at room temperature. Thus, the symmetrical classical rates are one to two orders of magnitude too small. The underestimate of  $k_{\text{cl}}$  is more severe in exothermic reactions, because the reaction energy was not taken into account in these very simple calculations. The systems presented in Table 13.8 confirm this expectation.

Although the simple calculations using a classical model tend to underestimate the rates, classical ISM does explain the 11 orders of magnitude difference between the excited-state deprotonation of 5CN1N and the acid catalysed de deuteration of azulene without adjustable parameters. According to ISM, the molecular factors that control the rates of nearly isothermal PT are the electrophilicity index  $m$  and the hydrogen-bonding ability. Low values of  $m$  ( $m \rightarrow 1$ ) correspond to “hard molecules” [28], and lead to high barriers. Electronic excitation increases the value of  $m$ , leads to “softer” acids and faster reactions. Strong hydrogen bonds appreciably decrease the barriers and correspond to “normal”, or rapidly reacting acids.

### 13.8.2 Semiclassical absolute rates

The similarity between classical calculations of atom and PT rates can be extended to the semiclassical calculations. The methods employed for the semiclassical calculations are those of Section 6.3.3. They require zero-point energy corrections along the reaction coordinate, as well as tunnelling corrections. Such corrections can only be done efficiently with the aid of a computer program. However, the calculations remain so simple that can be done using programs freely available over the Internet [29]. Representative semiclassical rate constants are presented in Table 13.8 [30]. As expected, they are a significant improvement over the classical calculations. Additionally, with the aid of a computer, the rates of asymmetrical systems are easily calculated and the free-energy dependence of the rates can be explored.

Figure 13.16 shows the free-energy dependence calculated for the protonation of aromatic hydrocarbons, such as azulene discussed above, and for the excited-state PT from aromatic alcohols, such as 5CN1N also discussed above. The calculations employed the parameters of azulene and water, for the first family of reactions, and of naphthol and water, for the second family of reactions, and only the reaction free energy was changed within each series of reactions. The calculated and experimental free-energy dependence are in excellent agreement and illustrate the change from a Brønsted-type of relationship for the aromatic hydrocarbons, to an Eigen-type of relationship for the excited naphthols.

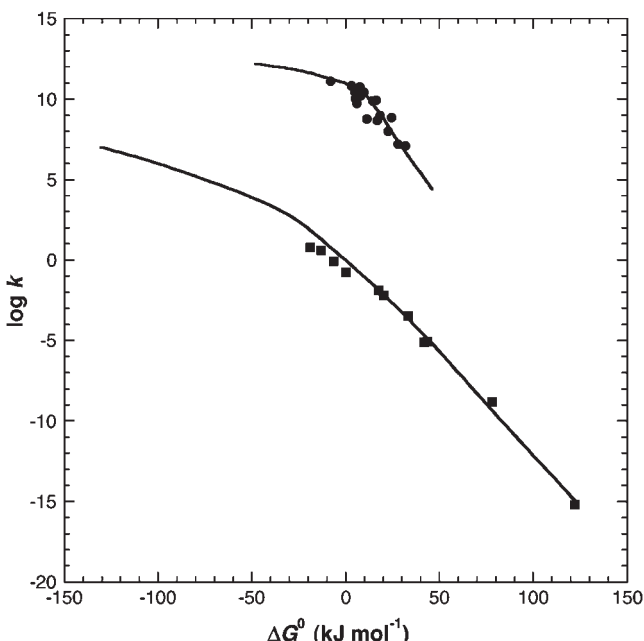


**Figure 13.16** Free-energy relationships in the protonation of aromatic hydrocarbons and methoxybenzenes (squares) and in the excited-state PT from aromatic naphthols (circles), in water.

The dramatic increase in the curvature of the free-energy dependence is closely associated with the increase in electrophilicity index. A value of  $m$  close to unity leads to a free-energy dependence that looks linear over a wide range of free energies, whereas a large value of  $m$  leads to a strong dependence of the free energy for endothermic reactions, changing rapidly to nearly free-energy independent rates for exothermic reactions. The Brönsted- and Eigen-type of free-energy dependences can also be related to the size of the “intrinsic barriers” of each family of reactions. With low values of  $m$ , the Brönsted plots correspond to high “intrinsic barriers”, and the location of the transition state changes slowly with the free-energy originating “constant” Brönsted coefficients for acid and base catalysis. On the other hand, the large values of  $m$  give the low barriers characteristic of the Eigen plots, and the location of the transition state changes from very close to the structure of the successor complex to that of the precursor complex, as the reaction free energy changes from slightly positive to slightly negative.

One of the most interesting features of the semiclassical calculations is their ability to predict and rationalise KIE. The most significant isotope effects arise from the replacement of the proton by a deuteron. As shown in Figure 6.6, this replacement increases the zero-point energy difference between the transition state and the reactants when the bond to proton, or deuteron, is partially broken at the transition state. Assuming identical pre-exponential factors for proton and deuteron transfers and neglecting all changes in the bending vibrational frequencies along the reaction coordinate, Westheimer predicted a maximum KIE for symmetrical transfers, where the symmetric stretching at the transition state is independent of the mass of the central atom [31]. Figure 13.17 shows the ratio between the rates of proton ( $k_H$ ) and deuteron ( $k_D$ ) transfer as a function of the reaction free energy of nitroalkane ionisations to bases such as  $\text{H}_2\text{O}$ ,  $\text{OH}^-$ ,  $\text{RCOO}^-$  or  $\text{PhO}^-$  [32–35], and of excited-state PT of naphthols to water [36,37]. These systems were selected for the structural homogeneity of the reactants in each family of reactions. The experimental data do not follow very closely Westheimer’s postulate. The maximum KIE of PT between carbon and oxygen atoms is displaced towards the endothermic reactions, and an opposite asymmetry is observed in the transfer between oxygen atoms. Moreover, the maximum KIE in the nitroalkane ionisation exceeds  $k_H/k_D = 6.7$ , that is the value expected from the difference in the zero-point energies of C–H and C–D bonds,  $4.7 \text{ kJ mol}^{-1}$ . An opposite anomaly is observed in the transfer between oxygen atom, where the experimental KIE is much lower than  $k_H/k_D = 7.9$ , calculated from the zero-point energy differences of O–H and O–D bonds,  $5.1 \text{ kJ mol}^{-1}$ .

The semiclassical calculations using the ISM–LS reaction coordinate and TST with tunnelling corrections but otherwise identical pre-exponential factors for proton and deuteron transfers are in good agreement with the experimental data of Figure 13.17. The success of these calculations comes from the incorporation of the tunnelling corrections and, in the case of excited naphthols, hydrogen bonding. The tunnelling correction for a PT in a nitroalkane with  $\Delta G^0 = 0$  is 14, whereas for a deuteron transfer in this system it is only 4. Thus, the tunnelling correction contributes with a factor of 3.5 to the KIE, and the calculated KIE is “only” 8 because the difference in zero-point energies is  $2 \text{ kJ mol}^{-1}$ , rather than the maximum value of  $4.7 \text{ kJ mol}^{-1}$ . The asymmetry of the KIE as a function of the reaction free energy is due to asymmetry of the reactive bonds: a C–H is broken and an O–H bond is formed. The excited-state PT of the naphthols is not symmetrical either. The

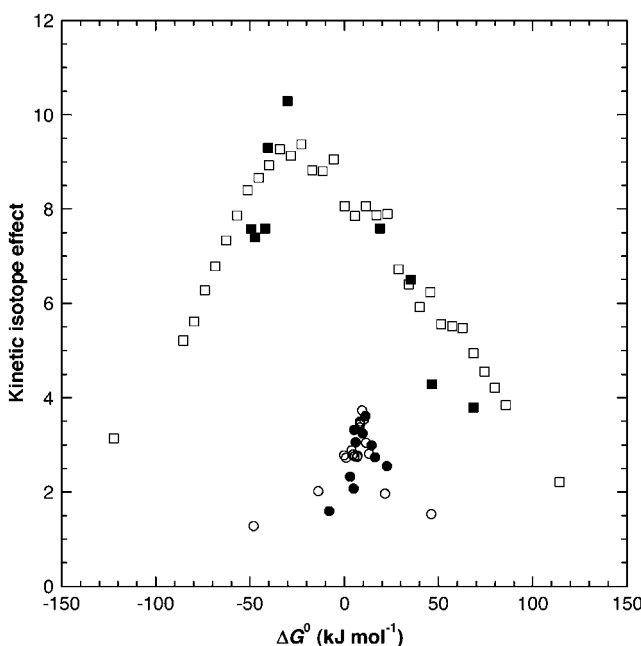


**Figure 13.17** KIE in the ionisation of nitroalkanes to water, hydroxide and carboxylate ions (squares), and in the excited-state PT of naphthols to water (circles). ISM–LC/scTST calculations (open symbols) employed the data for nitromethane or excited naphthols and water.

hydrogen bond formed between the ionic products is stronger than that formed between the neutral reactants, and the maximum KIE now occurs in the endothermic reactions. The hydrogen bond is also responsible for the progress of the reactants along the reaction coordinate and for a further reduction in zero-point energies differences between proton and deuteron transfers. The calculated vibrationally adiabatic barriers differ only by 0.8 kJ mol for a naphthol ionisation with  $\Delta G^0 = 0$ , which contribute with a factor of 1.4 to the KIE at 298 K. The low barriers of these reactions give small tunnelling corrections at this temperature, 2.5 for the proton and 1.5 for the deuteron, and the calculated KIE is only 2.3.

## REFERENCES

- [1] KJ Laidler, *Chemical Kinetics*, HarperCollins, New York, 1987.
- [2] JJA Wijs, *Z. Phys. Chem.* **11** (1893) 492.
- [3] JJA Wijs, *Z. Phys. Chem.* **12** (1893) 415.
- [4] GM Loudon, *J. Chem. Educ.* **68** (1991) 973–983.
- [5] JN Brönsted, KL Pederson, *Z. Phys. Chem.* **108** (1924) 185.
- [6] F Terrier, J Lelievre, A-P Chatrousse, P Farrell, *J. Chem. Soc. Perkin 2* (1985) 1479.
- [7] LP Hammett, AJ Deyrup, *J. Am. Chem. Soc.* **54** (1932) 2721.
- [8] LA Long, M Purcham, *J. Am. Chem. Soc.* **72** (1950) 3267.
- [9] R Triolo, AH Narten, *J. Chem. Phys.* **63** (1975) 3624–3631.

- [10] DM Carey, GM Korenowski, *J. Chem. Phys.* **108** (1998) 2669–2675.
- [11] P Salvador, M Duran, JJ Dannenberg, *J. Phys. Chem. A* **106** (2002) 6883–6889.
- [12] M Meot-Ner (Mautner), CV Speller, *J. Phys. Chem.* **90** (1986) 6618–6624.
- [13] ER Lippincott, R Schroeder, *J. Chem. Phys.* **23** (1955) 1099–1106.
- [14] N Agmon, *Isr. J. Chem.* **39** (1999) 493–502.
- [15] Z Luz, S Meiboom, *J. Am. Chem. Soc.* **86** (1964) 4768–4769.
- [16] D Marx, ME Tuckerman, J Hutter, M Parrinello, *Nature* **397** (1999) 601.
- [17] H Lapid, N Agmon, MK Petersen, GA Voth, *J. Chem. Phys.* **122** (2005) 014506.
- [18] M Eigen, *Ang. Chem. Int. Ed. Engl.* **3** (1964) 1.
- [19] RL Scott, *J. Phys. Chem.* **75** (1971) 3843–3845.
- [20] LC Gruen, FA Long, *J. Am. Chem. Soc.* **89** (1967) 1287–1291.
- [21] E Pines, D Pines, T Barak, B-Z Magnes, LM Tolbert, JE Haubrich, *Ber. Bunsenges. Phys. Chem.* **102** (1998) 511–517.
- [22] A Streitwieser, Jr., PH Owens, G Sonnichsen, WK Smith, GR Ziegler, HM Niemeyer, TL Kruger, *J. Am. Chem. Soc.* **95** (1973) 4254.
- [23] DR Lide *Handbook of Chemistry and Physics*, CRC Press Inc., 2001.
- [24] AA Zavitsas, *J. Am. Chem. Soc.* **94** (1972) 2779–2789.
- [25] RG Pearson, *J. Am. Chem. Soc.* **108** (1986) 6109.
- [26] RP Bell, DM Goodall, *Proc. Roy. Soc. London A* **294** (1966) 273–297.
- [27] M-L Ahrens, G Maass, *Angew. Chem. Int. Ed.* **7** (1968) 818–819.
- [28] RG Pearson, *Acc. Chem. Res.* **26** (1993) 250–255.
- [29] LG Arnaut, M Barroso, D Oliveira *ISM\_APT*, University of Coimbra, Coimbra, 2006.
- [30] M Barroso, LG Arnaut, SJ Formosinho, *J. Phys. Chem. A.*, in press.
- [31] FH Westheimer, *Chem. Rev.* **61** (1961) 265.
- [32] RP Bell, JE Crooks, *Proc. Roy. Soc. London A* **286** (1965) 285.
- [33] DJ Barnes, RP Bell, *Proc. Roy. Soc. London A* **318** (1970) 421–440.
- [34] FG Bordwell, WJ Boyle, Jr. *J. Am. Chem. Soc.* **97** (1975) 3447–3452.
- [35] M Amin, WH Saunders, Jr. *J. Phys. Org. Chem.* **6** (1993) 393–398.
- [36] LG Arnaut, SJ Formosinho, *J. Photochem. Photobiol. A: Chem.* **75** (1993) 1–20.
- [37] M Barroso, L Arnaut, SJ Formosinho, *J. Photochem. Photobiol. A: Chem.* **154** (2002) 13–21.

This page intentionally left blank

## **—14—**

# **Enzymatic Catalysis**

---

Enzymes are the best catalysts known. They mediate a vast array of chemical transformations in all living organisms and do so very efficiently under mild conditions. Most enzymatic mechanisms of catalysis have ample precedents in organic catalytic reactions. Yet reactions that are very fast in the presence of enzymes, become extremely slow in their absence, and some have half-lives approaching the age of the Earth. For example, the half-life for the spontaneous decarboxylation of amino acids is 1100 million years, but in the presence of arginine decarboxylase, the rate constant of the catalysed reaction is in the vicinity of  $100\text{--}1000 \text{ sec}^{-1}$  [1]. This, as many other enzyme-catalysed reactions, demonstrates the excellent kinetic efficiency of these catalysts. In general, enzymes produce rate enhancements that range from  $10^7$ -fold to  $10^{19}$ -fold.

In addition to their efficiency, enzymes are also remarkable for their specificity. Each enzyme usually catalyses one specific reaction, and sometimes, only one specific reactant, called substrate, is converted into products. For example, succinate dehydrogenase is an enzyme that exclusively catalyses the oxidation of succinic acid, and not any other carboxylic acid. One of the other important aspects of enzyme catalysis is their stereospecificity. For example, proteases only hydrolyse the derivatives of L-amino acids and not the corresponding D-amino acids. This can be extremely valuable in understanding enzyme mechanisms. At the other extreme, are the enzymes that catalyse families of reactions, such as the esterases, which are enzymes that catalyse the hydrolysis of esters independent of the molecular groups attached to the ester linkage.

### **14.1 TERMINOLOGY**

All known enzymes are proteins. They are made of covalently linked amino acids residues that form very long, unbranched chains. The amino acid residues are consecutively numbered, starting from the N-terminus. The DNA code specifies the amino acid sequence of the proteins, but before they can carry out their functions, in particular as enzymes, they must take on a particular shape or a “fold”. This usually results from relatively weak non-covalent interactions such as hydrogen bonding, electrostatic attractions or repulsions and hydrophobic interactions. In addition, some cross-linking may occur owing to S–S bonding involving cystine residues. At temperatures above 60–70 °C, most proteins denature, that

is, over a relatively narrow temperature range their native structure unfolds in a cooperative manner, and they become inactive.

The specificity of an enzyme is closely related to the three-dimensional arrangement of its amino acid residues, the tertiary structure. The polypeptide chain follows a complicated path that is unique to each protein. In the complex structure of a protein, it is possible to identify regularities associated with the local conformation of its backbone, its secondary structure. A frequently encountered regularity is a right-handed  $\alpha$ -helix of the polypeptide conformation that enables conformational changes and favourable hydrogen-bonding patterns. Another common regularity is the  $\beta$ -pleated sheet, which corresponds to favourable hydrogen bonding between adjacent polypeptide chains, rather than within one chain as in the  $\alpha$ -helix.

An enzyme's tertiary structure strictly defines the geometry and charge distribution around a substrate-binding site. This site is largely preformed, waiting for the substrate to bind, but also exhibits at least some degree of induced fit upon binding of the substrate. The lock-and-key hypothesis, formulated by Emil Fischer in 1894, captures the essence of the enzyme specificity for its substrate: the enzyme is like a lock with a complementary geometry to that of the substrate, which is the key. The binding of the substrate to the enzyme is due to hydrogen bonding, electrostatic and van der Waals interactions (Figure 14.1). The active sites correspond to 10–20% of the total volume of the enzyme.

In addition to the backbone, involving the amino acid residues, many enzymes are strongly associated with small molecules or transition metal ions, called cofactors. Sometimes the cofactors are organic molecules transiently associated with a given enzyme, but in other cases they are permanently associated with their protein. In both cases, these organic molecules are known as coenzymes, but when they are permanently associated, they are called prosthetic groups. For example, the haem prosthetic group of haemoglobin is tightly bound to its protein through extensive hydrophobic and hydrogen-bonding interactions, together with a covalent bond between the haem  $\text{Fe}^{2+}$  ion and the imidazole group of a histidine residue of the protein.

A catalytically active enzyme–cofactor complex is called a holoenzyme. When the cofactor can be separated from the enzyme, for example using dialysis, the enzymatically inactive protein is referred to as an apoenzyme.

Enzymes are classified and named according to the nature of the chemical reactions they catalyse. The six major classes of reactions that enzymes catalyse are (with the enzyme

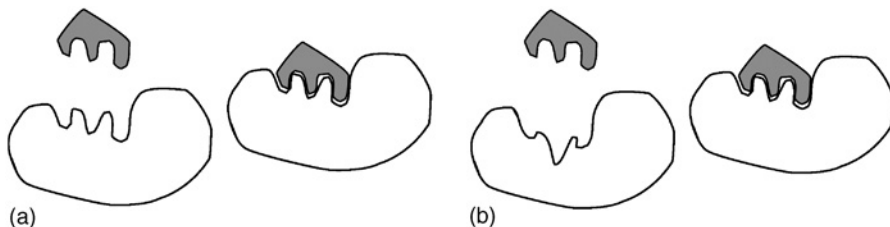


**Figure 14.1** Binding of a substrate to the active site of an enzyme, owing to the favourable interaction with the functional groups present in the active site: (a) lock-and-key hypothesis, where the shape of the active site is complementary to that of the substrate; (b) induced fit model, where the complementarity of the shapes is induced by the interactions between the enzyme and the substrate.

classification in parentheses): oxidation–reduction reactions (oxidoreductases), transfer of functional groups (transferases), hydrolysis reactions (hydrolases), group elimination to form double bonds (lyases), isomerisation (isomerase) and bond formation coupled with ATP hydrolysis (ligases). There are sub-classes and sub-sub-classes within these classes, and systematic names have been given to minimise ambiguity, but for the purpose of the study of enzyme kinetics, it is not necessary to go into these details.

## 14.2 MICHAELIS–MENTEN EQUATION

In 1902, Adrian Brown proposed an explanation for the rate of hydrolysis of sucrose to glucose and fructose catalysed by the yeast enzyme  $\beta$ -fructofuranosidase, based on the formation of a complex between the enzyme and its substrate [2]. Today, the mechanism involving such an intermediate is expressed as



where E and S represent the enzyme and the substrate, respectively, ES is the enzyme–substrate complex and P the final product. In 1913, Leonor Michaelis and Maude Menten [3] proposed a simple equation to describe the kinetics of this mechanism on the basis of the steady-state approximation for the complex ES,

$$k_1 [\text{E}][\text{S}] - k_{-1} [\text{ES}] - k_2 [\text{ES}] = 0 \quad (14.1)$$

In general, the concentrations of free enzyme and of the enzyme–substrate complex are not known, but the total concentration of enzyme is equal to its initial concentration,  $[\text{E}]_0$ , and

$$[\text{E}]_0 = [\text{E}] + [\text{ES}] \quad (14.2)$$

The value of  $[\text{E}]$  can be eliminated from the above two equations to give

$$k_1 ([\text{E}]_0 - [\text{ES}])[\text{S}] - (k_{-1} + k_2)[\text{ES}] = 0 \quad (14.3)$$

or

$$[\text{ES}] = \frac{k_1 [\text{E}]_0 [\text{S}]}{k_{-1} + k_2 + k_1 [\text{S}]} \quad (14.4)$$

Following the definition of reaction rate

$$v = k_2 [\text{ES}] \quad (14.5)$$

and substituting for  $[\text{ES}]$  gives the reaction rate in terms of the initial enzyme concentration and the concentration of the substrate

$$v = \frac{k_1 k_2 [E]_0 [S]}{k_{-1} + k_2 + k_1 [S]} \quad (14.6)$$

This can be presented in a more convenient form dividing the numerator and the denominator of the fraction by  $k_1$ ,

$$v = \frac{\frac{k_2 [E]_0 [S]}{k_{-1} + k_2 + [S]}}{k_1} \quad (14.7)$$

and representing the ratio of rate constants by the Michaelis constant

$$K_M = \frac{k_{-1} + k_2}{k_1} \quad (14.8)$$

$K_M$  represents the dissociation constant of the enzyme–substrate complex when  $k_{-1} \gg k_2$ . Low values of  $K_M$  thus correspond to strong enzyme–substrate complexes.

The reaction rate in terms of the Michaelis constant, is

$$v = \frac{k_2 [E]_0 [S]}{K_M + [S]} \quad (14.9)$$

When the concentration of the substrate is sufficiently small,  $[S] \ll K_M$  and the reaction rate is first order with respect to the substrate

$$v = \frac{k_2}{K_M} [E]_0 [S] \quad (14.10)$$

For high substrate concentrations,  $[S] \gg K_M$  and the reaction rate is zero order with respect to the substrate

$$v = k_2 [E]_0 \quad (14.11)$$

The enzyme is saturated and an increase in  $[S]$  is not reflected in the effects on the reaction rate. This behaviour resembles that of surface catalysis on solids described in Chapter 11. Figure 14.2 represents the initial rate of enzyme catalysis as a function of substrate concentration.

Eq. (14.9) can be represented in another form, using the maximum rate  $V_{\max}$  that occurs for very high substrate concentrations, when the enzyme is saturated, that is, it is entirely in the ES form. This is the reaction rate expressed by eq. (14.11), which can also be written as

$$V_{\max} = k_2 [E]_0 \quad (14.12)$$

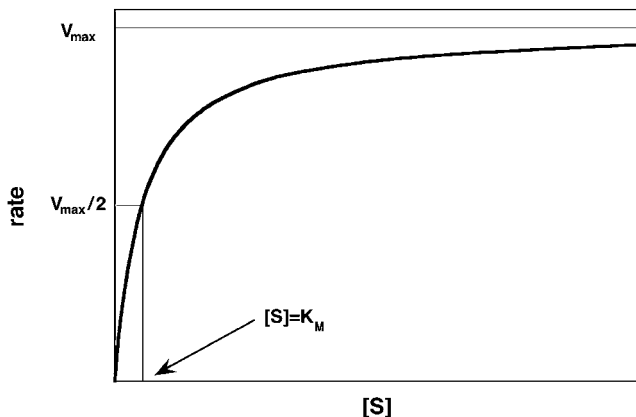


**Figure 14.2** Dependence of the initial reaction rate of a simple Michaelis–Menten scheme on the substrate concentration.

The Michaelis–Menten equation uses both  $K_M$  and  $V_{\max}$  to simplify the expression of the reaction rate of this mechanism

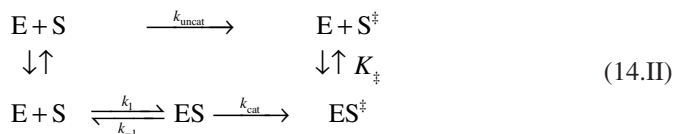
$$v = \frac{V_{\max} [S]}{K_M + [S]} \quad (14.13)$$

This expression gives another meaning to the Michaelis constant. When  $K_M = [S]$  then  $v = V_{\max}/2$ . Using these parameters, it is also useful to define the catalytic constant of an enzyme as

$$k_{\text{cat}} = \frac{V_{\max}}{[E]_0} \quad (14.14)$$

This quantity is also known as the turnover number of an enzyme because it is the number of reaction processes (turnovers) that each active site catalyses per unit time. For the Michaelis–Menten mechanism it is obvious from eq. (14.12) that  $k_{\text{cat}} = k_2$ . However, for more complex mechanisms,  $k_{\text{cat}}$  may be a function of several rate constants.

The ratio  $k_{\text{cat}}/K_M$  in the Michaelis–Menten mechanism represents the apparent second-order rate constant, which can be taken as a measure of the efficiency of the catalysis. When divided by the rate constant for the uncatalysed reaction in water,  $k_{\text{uncat}}$  this defines the efficiency of enzyme catalysis,  $(k_{\text{cat}}/K_M)/k_{\text{uncat}}$ . The efficiency is formally the equilibrium constant for the conversion of the transition state of the uncatalysed reaction in water and the enzyme in water into the transition state of the enzyme–substrate complex,



Prior to the development of rapid methods for data treatment, Hans Lineweaver and Dean Burk proposed a simple method using the reciprocals of eq. (14.13) to obtain experimentally the values of  $V_{\max}$  and  $K_M$  [4],

$$\frac{1}{v} = \frac{K_M}{V_{\max}[S]} + \frac{1}{V_{\max}} \quad (14.15)$$

and their work has become, rather unexpectedly, the most cited work in biochemistry. The double-reciprocal plot, illustrated in Figure 14.3, shows that enzyme catalysis following the Michaelis–Menten mechanism gives a linear dependence of  $1/v$  as a function of  $1/[S]$ , with an extrapolated intercept of  $-1/K_M$  and a slope of  $K_M/V_{\max}$ .

Most experimental measurements involve relatively high  $[S]$ . A better separation between the experimental points can be achieved using Eadie plots, which results from

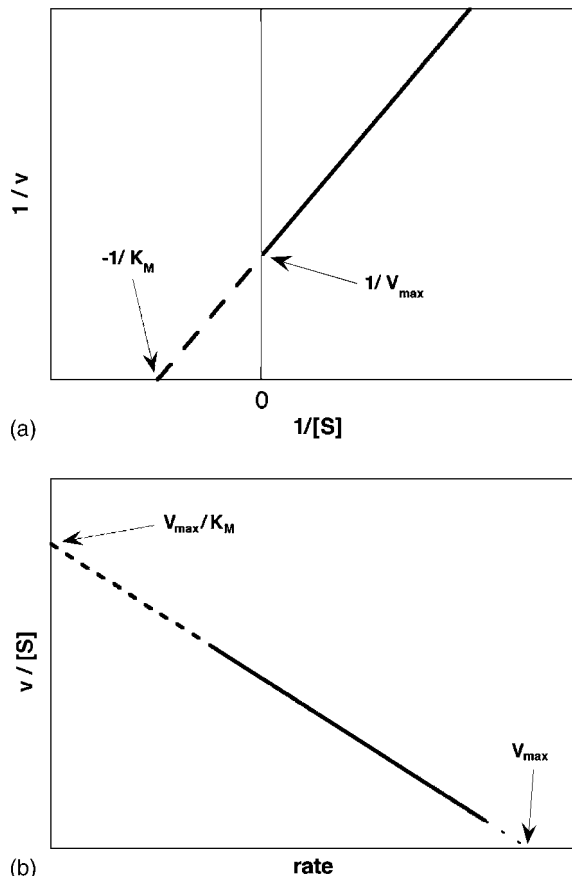


**Figure 14.3** (a) Lineweaver–Burk plot. (b) Eadie plot.

another mathematical rearrangement of eq. (14.13),

$$vK_M + v[S] = V_{\max}[S] \quad (14.16)$$

or

$$\frac{v}{[S]}K_M + v = V_{\max} \quad (14.17)$$

and finally

$$\frac{v}{[S]} = -\frac{1}{K_M}v + \frac{V_{\max}}{K_M} \quad (14.18)$$

Eadie plots represent  $v/[S]$  as a function of the reaction rate itself. The plot is also linear for a Michaelis–Menten mechanism, but the slope is  $-1/K_M$  and the intercept at the origin is  $V_{\max}/K_M$ , as illustrated in Figure 14.3. Although, where the quality of the experimental data permits, with the development of efficient computer software packages, the Eadie, Lineweaver–Burk and related treatments should be considered as starting points for more sophisticated treatments of data within the Michaelis–Menten scheme, these simple plots are still widely used.

Steady-state studies cannot give the values of the three rate constants,  $k_1$ ,  $k_{-1}$  and  $k_2$ . Only using techniques with fast time resolution, such as the stopped-flow technique, is it possible to study experimentally the initial moments of enzyme catalysis. As shown in Figure 14.4, there is an induction period, given by

$$\tau = \frac{1}{k_{-1} + k_2 + k_1 [S]_0} \quad (14.19)$$

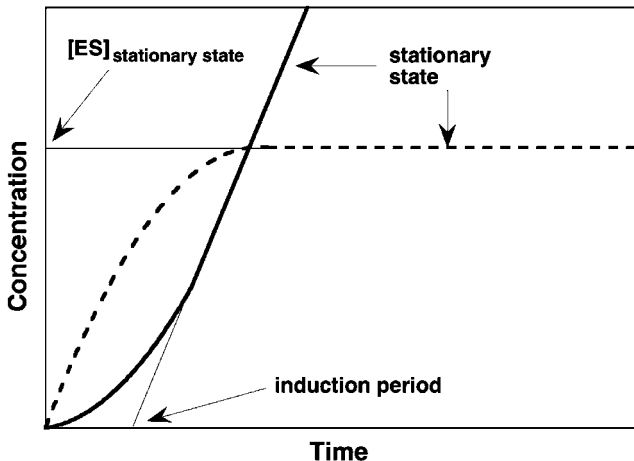


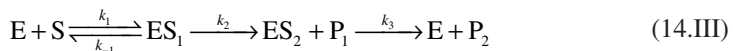
**Figure 14.4** Variations in the initial concentration of the enzyme–substrate complex (dashed line) and concentration of the reaction product (full line) for a reaction following the Michaelis–Menten mechanism.

where  $[S]_0$  is the initial concentration of the substrate, when steady-state conditions do not apply. Measuring  $\tau$  as a function of  $[S]_0$  gives the values of  $k_1$  and  $(k_{-1} + k_2)$ . Associating these values with the value of  $K_M$ , obtained under steady-state conditions, it is thus possible to obtain all the rate constants for the elementary steps of the Michaelis–Menten mechanism.

### 14.3 MECHANISMS WITH TWO ENZYME–SUBSTRATE COMPLEXES

Sometimes the mechanism of enzyme catalysis involves more than one enzyme–substrate complex. A representative example is chymotrypsin, one of the most-studied enzymes. Chymotrypsin can act as an esterase and a protease, because the chemical mechanisms of ester and amide hydrolases are almost identical. The catalytic mechanism when chymotrypsin acts as a serine protease involves the following steps:

First, chymotrypsin binds the polypeptide substrate to form the Michaelis complex. The substrate is held in the correct configuration for the subsequent reaction by non-covalent interactions. In the rate-determining step, it is suggested that there is a nucleophilic attack of the serine in position 195 of chymotrypsin (Ser195) on the carbonyl group of the peptide to form a tetrahedral intermediate. In this process, the imidazole ring of histidine in position 75 (His75) accepts a proton forming an imidazolium ion. Next, the tetrahedral intermediate decomposes to form the acyl-enzyme intermediate, under the driving force of proton donation from N3 of His75. The amine product, which is the new N-terminal portion of the cleaved polypeptide chain, is released from the protein and replaced by a water molecule from the solvent. The acyl-enzyme intermediate is now subject to nucleophilic attack by water and a second tetrahedral intermediate is formed. Finally, the deacylation of this intermediate leads to the release of the resulting product with a free carboxylate group, which is the new C-terminal portion of the cleaved polypeptide chain, and the active enzyme is regenerated. These steps are illustrated in Figure 14.5, adapted from Voet and Voet [5], and the kinetics can be schematically represented by the mechanism



where  $P_1$  and  $P_2$  are the amine and carboxylate products, respectively, and  $ES_1$  and  $ES_2$  represent the Michaelis complex and the acyl-enzyme intermediate, respectively. Applying the steady-state approximation to both complexes  $ES_1$  and  $ES_2$ , it is possible to show that the reaction rate still obeys Michaelis–Menten kinetics, eq. (14.13), but now

$$K_M = \frac{k_3(k_{-1} + k_2)}{k_1(k_2 + k_3)} \quad (14.20)$$

and

$$V_{\max} = \frac{k_2 k_3 [E]_0}{k_2 + k_3} \quad (14.21)$$

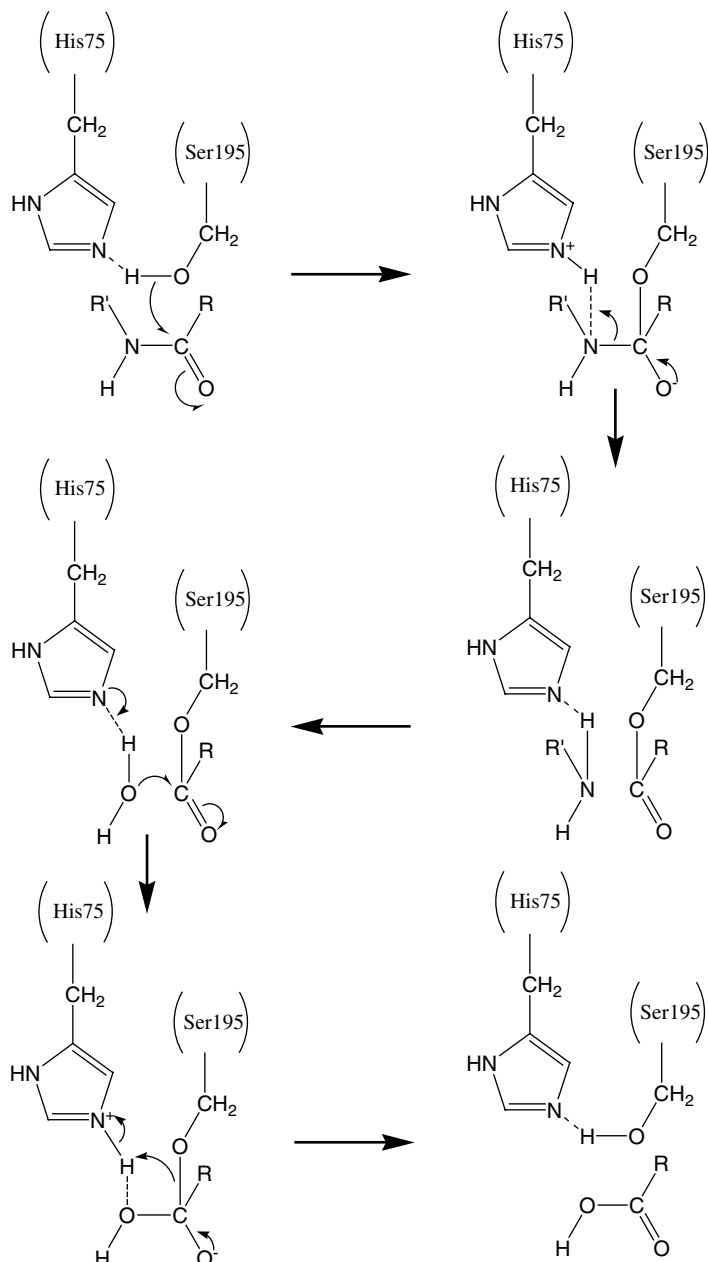
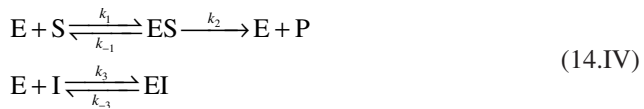


**Figure 14.5** Steps involved in the catalytic mechanism of serine proteases, represented by chymotrypsin.

## 14.4 INHIBITION OF ENZYMES

The efficiency of an enzyme can be reduced or can even become negligible in the presence of certain substances, known as inhibitors. Many inhibitors have structural resemblances with the substrates and compete with them for the formation of complexes with the enzyme. This is the case of the inactivation of cytochrome *c* oxidase by the cyanide ion, which blocks the mitochondrial electron-transport chain to oxygen. Similarly, the inactivation of the succinate dehydrogenase by malonate involves its inhibition of the conversion of succinate to fumarate in the citric acid cycle. In the latter case, the mechanism for competitive inhibition is



where *S* is the succinate ( $\text{^-OOCCH}_2\text{CH}_2\text{COO}^-$ ) and *I* is the malonate ( $\text{^-OOCCH}_2\text{COO}^-$ ). Assuming that the inhibitor binds reversibly to the enzyme and is in rapid equilibrium,

$$K_I = \frac{[E][I]}{[EI]} \quad (14.22)$$

and using the definition of the Michaelis constant, eq. (14.8), together with the steady-state approximation for the ES complex, eq. (14.1), gives

$$[E] = \frac{K_M [ES]}{[S]} \quad (14.23)$$

When the concentrations of the enzyme-inhibitor complex and of the free enzyme, which can be obtained from eqs. (14.22) and (14.23), are substituted in the expression for the conservation of the total enzyme concentration

$$[E]_0 = [ES] + [EI] + [E] \quad (14.24)$$

the following equation is obtained:

$$[E]_0 = [ES] \left\{ \frac{K_M}{[S]} \left( 1 + \frac{[I]}{K_I} \right) + 1 \right\} \quad (14.25)$$

which can be solved for [ES]

$$[ES] = \frac{[E]_0 [S]}{K_M \left( 1 + \frac{[I]}{K_I} \right) + [S]} \quad (14.26)$$

so that the initial reaction rate defined by eq. (14.5), is expressed as

$$v = \frac{k_2 [E]_0 [S]}{K_M \left( 1 + \frac{[I]}{K_I} \right) + [S]} \quad (14.27)$$

or

$$v = \frac{V_{\max} [S]}{K + [S]} \quad (14.28)$$

where

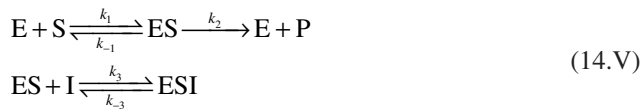
$$K = K_M \left( 1 + \frac{[I]}{K_I} \right) \quad (14.29)$$

The corresponding Lineweaver–Burk plot has the form

$$\frac{1}{v} = \frac{1}{V_{\max}} + \frac{K_M}{V_{\max}} \left( 1 + \frac{[I]}{K_I} \right) \frac{1}{[S]} \quad (14.30)$$

This shows that in competitive catalysis the maximum rate  $V_{\max}$  is not changed. Rather, the presence of I has the effect of making  $[S]$  appear more dilute than it actually is, and the effect of the inhibitor can be overcome for sufficiently high substrate concentrations.

In uncompetitive inhibition, the inhibitor binds to the enzyme, but not to its active site, and an ESI complex can be formed.



where now

$$K_I = \frac{[ESI]}{[ES][I]} \quad (14.31)$$

When the binding of the inhibitor in this complex changes the conformation of the active site, as illustrated in Figure 14.6, such changes produce a decrease in the  $V_{\max}$ . The corresponding double-reciprocal plot is

$$\frac{1}{v} = \frac{1}{V_{\max}} \left( 1 + \frac{[I]}{K_I} \right) + \frac{K_M}{V_{\max}} \frac{1}{[S]} \quad (14.32)$$

However, now the lines have the same slope,  $K_M/V_{\max}$ .

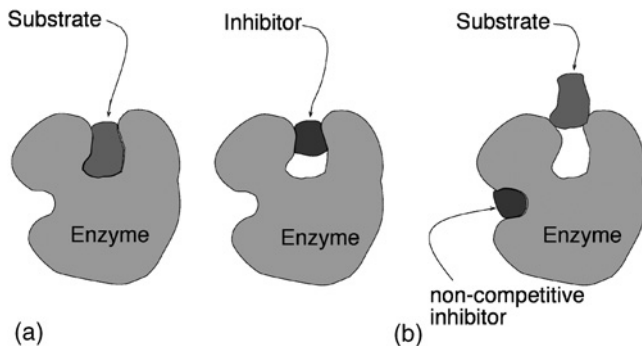


**Figure 14.6** Changes in the active site of an enzyme resulting from its binding to an inhibitor in: (a) competitive inhibition, where the active site is blocked; (b) uncompetitive inhibition inducing conformational changes in the active site.

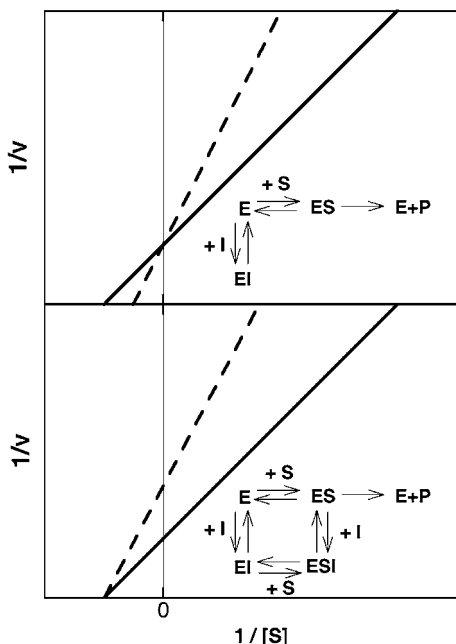


**Figure 14.7** Steady-state kinetics of competitive inhibition (upper plot) and of uncompetitive inhibition (lower plot). In the competitive inhibition the slope increases by a factor of  $(1 + [I]/K_i)$  with respect to the absence of competition (full line). In the uncompetitive inhibition the maximum rate is divided by that same factor.

Competitive and uncompetitive inhibitions can be kinetically distinguished under steady-state conditions. Figure 14.7 shows that in competitive inhibition the change in  $[I]$  does not change  $V_{max}$ , whereas in the case of mixed (competitive and uncompetitive) inhibition illustrated in the same figure, an increase in  $[I]$  decreases  $V_{max}$ .

### 14.5 EFFECTS OF pH

Most proteins, including enzymes, are only effective within a narrow pH range, typically from 5 to 9. The pH effect in the rates of enzyme catalysis, illustrated in Figure 14.8, gives rise to a bell-shaped dependence with a maximum close to pH 7.4, the physiological pH. This is due to the presence of ionisable groups in the amino acid chain, namely  $\text{-NH}_3^+$  and  $\text{-CO}_2\text{H}$ , which must be in appropriate ionisation states in the vicinity of the active site for enzyme catalysis to be observed. Michaelis interpreted the pH effects on the basis of the mechanism

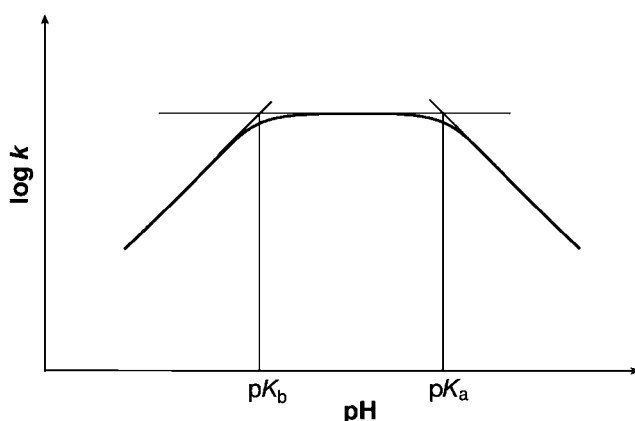
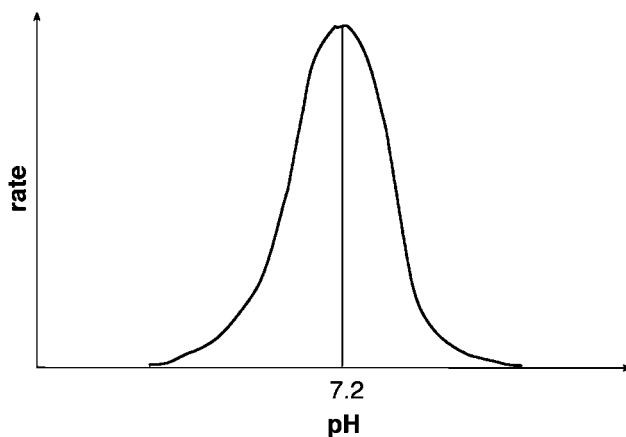
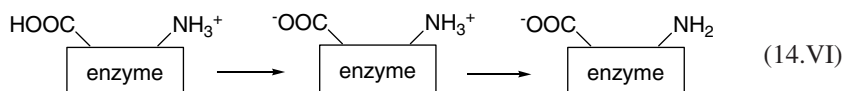
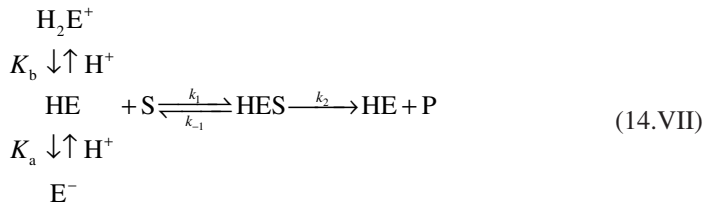


**Figure 14.8** (a) The effect of pH on the initial rate of a reaction catalysed by an enzyme. (b) Profile of the pH dependence of the catalytic constant of an enzyme.

where the zwitterion was considered the active form. The concentration of the zwitterion goes through a maximum as a function of the pH, and its actual position depends on the acidity constants of these two groups. The simplest situation is represented by the mechanism



Assuming that the steady-state approximation applies to the concentration of the HES complex, the reaction rate is

$$v = \frac{k_2 [\text{E}]_0 [\text{S}]}{K_M \left( 1 + \frac{K_a}{[\text{H}^+]^{+}} \frac{[\text{H}^+]}{K_b} \right) + [\text{S}]} \tag{14.33}$$

Note that at any given pH, eq. (14.33) behaves as a simple Michaelis–Menten equation.

For low substrate concentrations and at low pH values,  $([\text{H}^+]/K_b) \gg (K_a/[\text{H}^+])$  and the above equation is simplified to

$$v = \frac{K_b k_2 [\text{E}]_0 [\text{S}]}{K_M [\text{H}^+]} \tag{14.34}$$

or

$$\log v = \text{constant} - \log [\text{H}^+] = \text{constant} + \text{pH} \tag{14.35}$$

At high pH, the corresponding equation is

$$v = \frac{k_2 [\text{E}]_0 [\text{S}] [\text{H}^+]}{K_M K_a} \tag{14.36}$$

and

$$\log v = \text{constant} + \log [\text{H}^+] = \text{constant} - \text{pH} \tag{14.37}$$

The slope of the plots of  $\log (v)$  as a function of the pH changes from  $-1$  to  $+1$ . The maximum of this function occurs at  $(\text{p}K_a + \text{p}K_b)/2$ . Typical  $\text{p}K_s$  found in enzymes are 4 for the  $\text{RCOO}_2\text{H}$  group in Asp or Glu residues, 6 for histidine and 10 for the  $\text{RNH}_3^+$  group of lysine. However, the  $\text{p}K_a$  of a given acid–base group in a protein residue may vary by several pH units from its expected value as a consequence of the electrostatic influence of the

nearby charged groups and the polarity of its environment. It is interesting to note that this simple approach to the pH dependence of enzymatic activity is consistent with a maximum efficiency at pH *ca* 7 for enzymes with RCOO<sub>2</sub>H and RNH<sub>3</sub><sup>+</sup> groups in the vicinity of the active site.

## 14.6 TEMPERATURE EFFECTS

As mentioned before, at temperatures above 60 °C most enzymes lose their tertiary structure and, consequently, become inactive. The denaturation of proteins and DNA at high temperatures is the fundamental mechanism by which bacteria in boiling water are killed. However, a few bacteria are fit to live at relatively high temperatures. A good example is the bacterium *Thermus aquaticus*, first identified in the Lower Geyser Basin of the Yellowstone hot springs, a habitat where the temperature ranges from 50 to 80 °C. This thermophilic bacterium produces a DNA polymerase enzyme that is widely used to replicate DNA in high-temperature polymerase chain reactions.

With thermophilic enzymes, the study of catalysis as a function of temperature has often demonstrated the biphasic Arrhenius behaviour, with an increased enthalpy of activation at lower temperatures, assigned to an increase in protein rigidity [6]. However, in general, at temperatures below 60 °C, a temperature increase leads to an increase in the rate of the enzyme-catalysed reaction, often in agreement with the Arrhenius equation. As a consequence, the activity of enzymes as a function of the temperature goes through a maximum, and the study of the temperature dependence of enzyme activity must be carried out at relatively low temperatures.

For lower substrate concentrations, the reaction rate from eq. (14.9) is

$$v = \frac{k_2}{K_M} [E]_0 [S] \quad (14.38)$$

or

$$v = \frac{k_1 k_2}{k_{-1} + k_2} [E]_0 [S] \quad (14.39)$$

The corresponding temperature dependence is relatively complicated, but becomes more informative when  $k_{-1} \gg k_2$ , that is, for a fast equilibrium between the substrate and the enzyme. Under these conditions, the reaction rate can be written as

$$v = \frac{k_1 k_2}{k_{-1}} [E]_0 [S] \quad (14.40)$$

and the global activation energy has contributions from the activation energies of the three elementary reactions

$$E_a = E_{a1} + E_{a2} - E_{a-1} \quad (14.41)$$

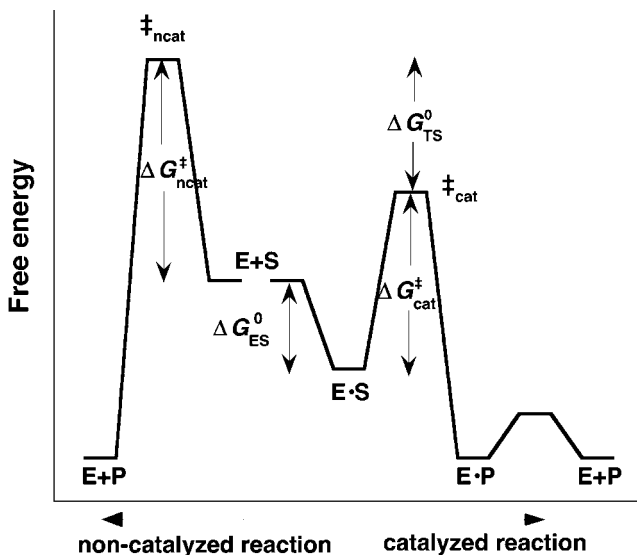


**Figure 14.9** Free-energy profiles for an enzyme-catalysed reaction controlled by the formation of the product (from centre to right) and for a non-catalysed reaction (from centre to left). The reaction path going through the formation of the ES complex is the minimum-energy path.

In typical enzyme catalysis, the rate-determining step is the second step, as illustrated in Figure 14.9. The alternative,  $k_{-1} \ll k_2$ , would correspond to a reaction kinetically controlled by the formation of the enzyme–substrate complex, rather than by the product formation.

For higher substrate concentrations, the reaction rate attains its maximum,  $V_{\max} = k_2[E]_0$ . The study of the reaction rate as a function of the temperature under these conditions gives directly the activation energy for the transformation of the ES complex into products,  $E_{a2}$ .

The enthalpies of activation of enzyme-catalysed reactions are typically *ca* 45 kJ mol<sup>-1</sup> and the corresponding  $T\Delta S^\ddagger$  values are concentrated around -20 kJ mol<sup>-1</sup> [7]. These values combine to give rate constants of the catalysed reaction of the order of 100–1000 sec<sup>-1</sup>, as mentioned earlier. The extraordinary rate enhancements achieved in the presence of enzymes are mainly related to the decrease in  $\Delta H^\ddagger$  with respect to the uncatalysed reactions. The key to the understanding of enzyme catalysis is in the explanation for the energetic stabilisation of their transition states of the catalysed reactions.

## 14.7 MOLECULAR MODELS FOR ENZYME CATALYSIS

Over half a century ago, Pauling [8] formulated the hypothesis that “enzymes are molecules that are complementary in structure to the activated complexes (transition states) of the reactions that they catalyse”. This view of enzyme catalysis was highly influential and was corroborated by the first structural characterisations of enzyme active sites, which occurred many years later. Today, it is widely recognised that enzyme catalysis involves very specialised molecular recognition, and that this accounts for a major part of the

efficiency of enzyme catalysis. Molecular recognition is due to the complementarities of non-covalent forces. The active site of the enzyme stabilises the transition state through desolvation, electrostatic forces, van der Waals forces, proximity (entropy trap), steric effects and other mechanisms. Additionally, molecular recognition is enforced by partially covalent interactions such as hydrogen bonding and general acid–base catalysis. All these forces contribute to high enzyme–substrate association constants. Similar effects also contribute to other host–guest interactions such as cyclodextrins binding organic guests or drug–receptor interactions.

The most recent addition to our understanding of the factors that contribute to enzyme proficiency is the establishment of the limits of molecular recognition. Using the idea of entropy–enthalpy compensation, the binding free energies achieved by non-covalent and partially covalent forces are usually below  $65\text{ kJ mol}^{-1}$  [9]. This sets the maximum of  $10^{11}\text{ M}^{-1}$  for the efficiency of enzyme catalysis. It is an extraordinarily large number, but not quite enough for all the rate enhancements observed in the presence of enzymes. Houk proposed that the maximum efficiency is only achieved when direct covalent bonding between the enzyme or cofactor and the reacting substrate is involved in the reaction mechanism. This is the case of the acyl-enzyme intermediate involved in the catalytic mechanism of serine proteases (Figure 14.5). In covalent catalysis, the enzyme actually reacts with the substrate, for example, through electrophilic or nucleophilic reactions.

The free-energy changes in enzyme-catalysed and uncatalysed reactions can be compared using the free-energy profile of Figure 14.9. According to this figure

$$\Delta G_{\text{ncat}}^{\ddagger} + \Delta G_{\text{ES}}^0 = \Delta G_{\text{cat}}^{\ddagger} + \Delta G_{\ddagger}^0 \quad (14.42)$$

where  $\Delta G_{\text{ES}}^0$  is the free-energy change in the formation of the enzyme–substrate complex by the forces of molecular recognition, and  $\Delta G_{\text{ncat}}^{\ddagger}$  and  $\Delta G_{\text{cat}}^{\ddagger}$  are the free energies of activation of the non-catalysed and catalysed reactions, respectively. The efficiency of the catalysis comes from the value of  $\Delta G_{\ddagger}^0$ .

The role played by the factors that contribute to enzyme efficiency has been investigated using simple molecular models. A convenient method to study the role of proximity is to use intra-molecular models. In this context, it is useful to define the effective molarity (EM) as the (first-order) rate constant for the intra-molecular reaction divided by the (second-order) rate constant for the equivalent inter-molecular process. The EM is nominally the concentration of the equivalent external catalyst needed to make the inter-molecular rate match that of the intra-molecular reaction [10]. An example of intra-molecular acid catalysis was presented in Figure 13.8a, in the context of the hydrolysis of aspirin.

In aspirin, the acid catalysis is enhanced by the presence of an intra-molecular hydrogen bond. The H-bond in the salicylate anion is worth  $17\text{--}21\text{ kJ mol}^{-1}$ , and raises the  $\text{p}K_a$  of the phenolic OH to 13. Other molecular models showed that EMs for intra-molecular general acid–base catalysis can be at least  $10^4\text{ M}$ , if favourable intra-molecular H-bonds are formed [10]. This is also the factor that separates the typical pre-exponential factor of a bimolecular reaction in solution,  $10^9\text{ M}^{-1}\text{ sec}^{-1}$ , from that of an intra-molecular reaction between the hydrogen-bonded reactants,  $10^{13}\text{ sec}^{-1}$ . The basis for this change has been discussed in the context of the intersecting-state model (ISM) applications to proton transfers

(eqs. (13.85) and (13.92)). The EM can exceed this value because another factor contributes to accelerate the intra-molecular rate: the strength of the H-bond. A hydrogen bond of energy  $17 \text{ kJ mol}^{-1}$  corresponds to 20% advance of the bond order along the reaction coordinate (Figure 13.14). Using the data for phenol in Table 13.7 ( $m = 1.714$ ), eq. (13.91) gives a  $5 \text{ kJ mol}^{-1}$  decrease in  $\Delta V_{\text{cl}}^{\ddagger}$ , relative to the same system in the absence of the H-bond. This gives a factor of 50 in the rate constant at room temperature, and increases the EM to  $5 \times 10^5 \text{ M}$ . Proximity effects, including enhanced hydrogen bonding, are indeed a considerably important part of the non-covalent and partially covalent forces that contribute to enzyme catalysis, but the role of the other factors is equally important and requires further investigation.

Another good group of molecular models for self-assembly in enzyme catalysis involves the cyclodextrins. This designation covers a class of  $\alpha$ - $\delta$ -glucose oligomers with a hydrophobic cavity surrounded by OH groups on the upper and lower edges (Figure 14.10). The hydrophobic pocket favours desolvation and proximity, since it provides a trap

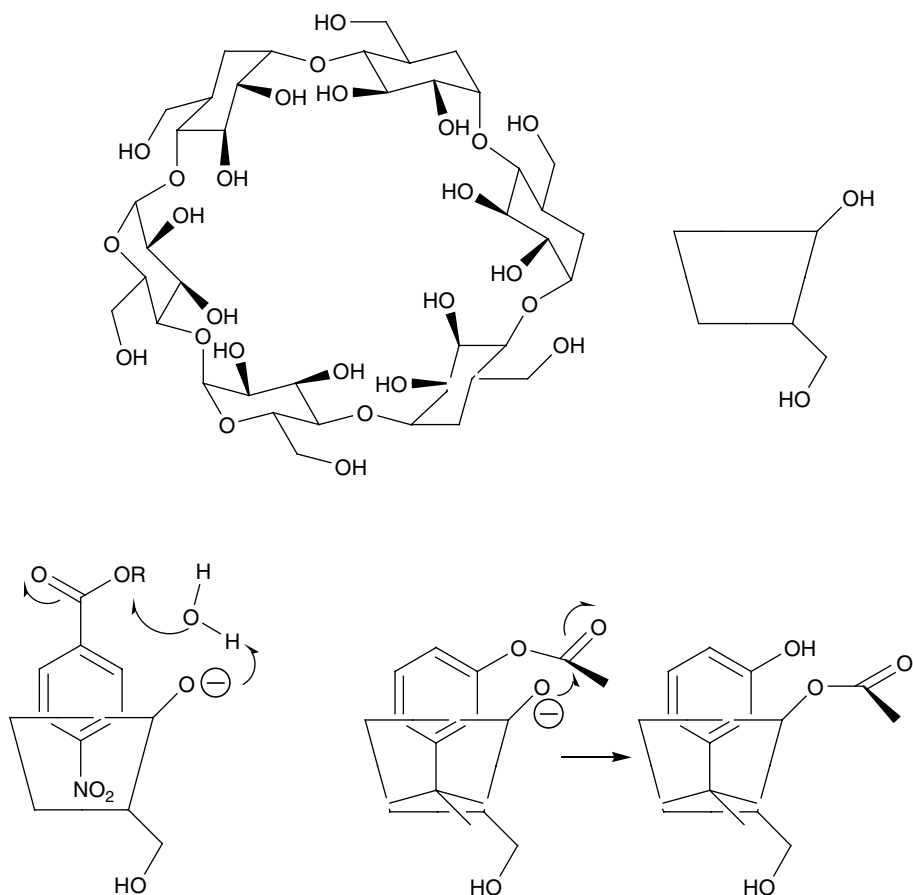


**Figure 14.10** Molecular models for enzyme catalysis based on cyclodextrins.

**Table 14.1**

Energetic stabilisation of an ion-pair ( $q_1=1$ ,  $q_2=-1$ ) at a distance  $d_{AB}=2.7 \text{ \AA}$ , as a function of the dielectric constant of the medium

$\epsilon$	$\Delta (\Delta G^0) (\text{kJ mol}^{-1})$
4.8	106.7
15	34.2
30	17.1
40	12.8
78.5	6.5
$\infty$	0

for the less-polar moieties of the substrate. Additionally, cyclodextrins lower the local dielectric constant ( $\epsilon$ ) and may enhance the roles of hydrogen bonding and electrostatic forces. For example, the rates of acylation reactions are accelerated in the presence of cyclodextrins [11]. This is quite analogous to the first step of the catalytic cycle of serine proteases, discussed above.

The strength of the hydrogen bonds increases as the static dielectric constant decreases, and this effect is particularly notable when charged species are involved [12]. Additionally, the electrostatic interaction between two atomic charges on the donor and acceptor atoms,  $q_1$  and  $q_2$ , has a reciprocal dependence upon both their distance  $d_{AB}$  and  $\epsilon$ , eq. (9.50),

$$E = \frac{q_1 q_2 e^2}{4\pi\epsilon_0 \epsilon d_{AB}} \quad (14.43)$$

where  $\epsilon_0$  is the vacuum permittivity. The dielectric constant at the surface of a protein, where many polar groups can be found, is *ca* 30–40. In the most hydrophobic regions of the protein, this value drops to a value closer to that of chloroform (4.8). In the active site of an enzyme it is assumed that  $\epsilon \approx 15$  [13]. The energetic stabilisation calculated for an ion-pair at a distance of 2.7 Å is presented in Table 14.1 for several values of  $\epsilon$ . To see these effects in action, it is necessary to study specific enzymatic catalysis.

## 14.8 ISOMERISATION OF DIHYDROXYACETONE PHOSPHATE TO GLYCERALDEHYDE 3-PHOSPHATE CATALYSED BY TRIOSE-PHOSPHATE

A representative example of how enzymes stabilise reactive intermediates is the loss of a proton from the  $\alpha$ -position of a carbonyl compound, a rate-limiting step in carbon–carbon bond formations and racemisations, which proceeds via an unstable enol or enolate intermediate. A particularly interesting illustrative case is that of triose-phosphate isomerase (TIM) and how it catalyses the isomerisation between dihydroxyacetone phosphate (DHAP) and glyceraldehyde 3-phosphate (GAP) (Figure 14.11). The uphill direction from DHAP to GAP is essential for optimal throughput in the glycolytic pathway, since only GAP can proceed further along this pathway. Thus, the TIM reaction ensures efficient

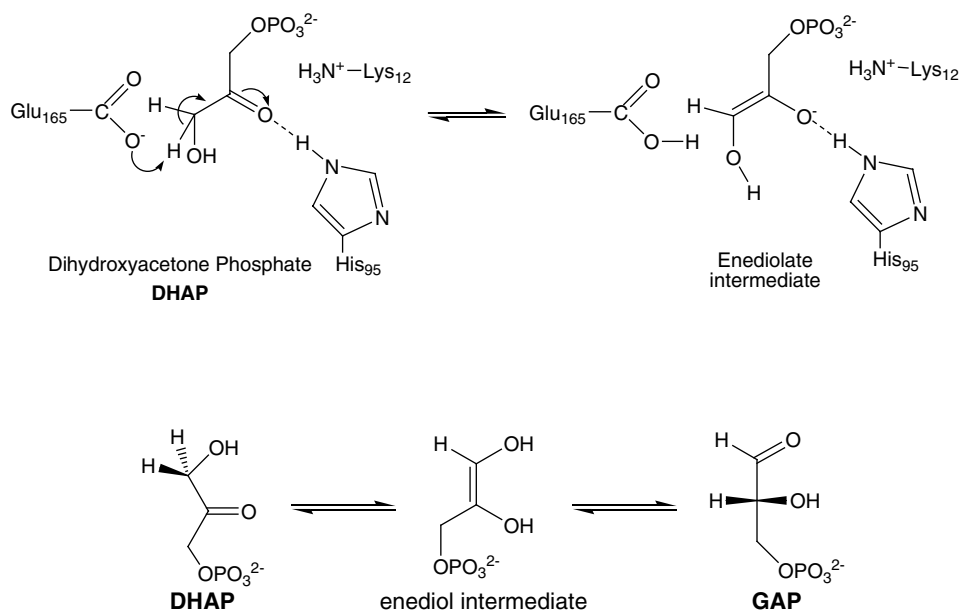


**Figure 14.11** Isomerisation of DHAP to GAP catalysed by TIM.

catabolism of all the six carbons in glucose. The TIM is at a branch point in sugar metabolism, from which various biodegradative pathways emanate. Consequently, there is a strong evolutionary pressure for efficient catalysis by the enzyme under *in vivo* conditions. Viscosity-dependence studies have established that TIM is diffusion-controlled, that is, the rate of the reaction is limited by the diffusion of the substrate and product to and from the active site, and all the purely chemical steps are faster [14].

The key chemical step is a proton transfer where the general base catalyst is Glu165 ( $pK_a^{\text{Glu165}} = 6$ ) [15]. The nature of the (enediol or enediolate) intermediates in this type of reaction remains a subject of lively debate. The  $pK_a^K$  of DHAP has not been measured, but from the similarity in the rate constants for hydroxide-catalysed elimination of DHAP ( $0.56 \text{ M}^{-1} \text{ sec}^{-1}$  at  $37^\circ\text{C}$  [16]) and hydroxide-catalysed deprotonation of acetone ( $0.22 \text{ M}^{-1} \text{ sec}^{-1}$  at  $25^\circ\text{C}$  [17]), it was deduced that both reactions proceeded through an enediolate intermediate, and that DHAP ionising at carbon-3 should have an acidity constant slightly lower than that of acetone,  $pK_a^K(\text{acetone}) = 19$ . The reaction energy estimated from the  $\Delta pK_a$  ( $\Delta G^0 = 75 \text{ kJ mol}^{-1}$ ) is not compatible with the high turnover number of the TIM-catalysed isomerisation of DHAP ( $k_{\text{cat}} = 1300 \text{ sec}^{-1}$  [16]), which suggests that  $\Delta G^\ddagger = 54 \text{ kJ mol}^{-1}$ .

The explanation by Gerlt and Gassman [15,18] of electrophilic catalysis extends the model of enzyme catalysis beyond the classical view that rate enhancements result because they provide a better fit for the intermediate than for the substrate. Proton abstraction by the general base catalyst was assumed to be concerted with the protonation of the carbonyl group by an acidic (electrophilic) catalyst, the His95, generating an enediol. According to this view, it is not the exact nature of the “enolate intermediate” that is relevant for the stabilisation of the intermediate, but its ability to establish “short, strong hydrogen bonds” to

the electrophilic catalyst. According to Gerlt and Gassman, such bonds could stabilise the intermediate by 29–33 kJ mol<sup>-1</sup>. A more dramatic stabilisation of 40–80 kJ mol<sup>-1</sup> owing to the formation of “low-barrier hydrogen bonds” in enzyme–intermediate complexes was proposed by Cleland and Kreevoy [19] and by Frey and co-workers [20]. Such proposals met with considerable criticism [21,22], because H-bonds of this strength are usually typical of charged groups in the gas phase. Fersht and co-workers [23] showed that the differential stabilisation of charged versus uncharged H-bond donors or acceptors in proteins is typically of the order of 13 kJ mol<sup>-1</sup>. As DHAP is converted into the enediolate intermediate, a negative charge accumulates in this oxygen atom and leads to a very strong interaction with the adjacent RNH<sub>3</sub><sup>+</sup> group of Lys12. The QM/MM calculations of Cui and Karplus [24] show that the presence of Lys12 merely 3.0 Å from the carbonyl group of DHAP [25], leads to a 73.6 kJ mol<sup>-1</sup> stabilisation of the intermediate. This is a realistic distance, because the transition-state analogue phosphoglycolohydroxamate of the DHAP interconversion to GAP, forms a complex with TIM where the N $\zeta$  of Lys12 is 2.797–2.84 Å from the O<sup>2</sup> of PGH [24]. A distance of 2.68 Å between the N $\zeta$  of the Lis13 residue of *Leishmania mexicana* TIM and the carbonyl oxygen of 2-phosphoglycolate, another transition-state analogue, has also been measured [26].

Simple electrostatics, eq. (14.43), gives a stabilisation energy of 34.2 kJ mol<sup>-1</sup> for two opposing charges at a 2.7 Å separation in a medium of  $\epsilon = 15$  (Table 14.1). This is the electrostatic stabilisation energy expected for the charged oxygen atom of the intermediate in the presence of the Lys12 residue. Adding the 13 kJ mol<sup>-1</sup> differential stabilisation of charged versus uncharged H-bond donors or acceptors, and subtracting the total stabilisation from the free energy associated to the  $\Delta pK_a$  of DHAP and Glu-165, the endergonicity of the proton transfer in the enzyme drops to  $\Delta G^0 = 29$  kJ mol<sup>-1</sup>. Cui and Karplus arrived at  $\Delta G^0 = 26$  kJ mol<sup>-1</sup>.

The transition-state theory (TST) rate calculations using the reaction path of the ISM, discussed in the previous chapter for proton-transfer reactions, assume that the reactions in enzymes are intra-molecular, but otherwise identical to the reactions in solution. Using the data for acetone and acetic acid in Table 13.7 to calculate the reaction coordinate of the ISM, together with  $\Delta G^0 = 29$  kJ mol<sup>-1</sup> as discussed above, and the classical TST formalism for an intra-molecular reaction gives  $k_{ISM} = 1500$  sec<sup>-1</sup> at 25 °C, in excellent agreement with  $k_{cat} = 1300$  sec<sup>-1</sup> experimentally measured for the TIM-catalysed conversion of DHAP to GAP. This agreement is partially coincidental because there is a small tunnelling correction, calculated to be a factor of 3 at room temperature, which leads to a small overestimate of the experimental values. TIM catalysis is a case where the electrostatic forces and the differential hydrogen bonding are decisive in stabilising the intermediate to the loss of a proton from the  $\alpha$ -position to a carbonyl compound, and, together with the proximity effect, lead to an increase in the rate of the reaction by 15 orders of magnitude.

## 14.9 HYDROPEROXIDATION OF LINOLEIC ACID CATALYSED BY SOYBEAN LIPOXYGENASE-1

Soybean lipoxygenase-1 (SLO) is often used as the prototype for studying the family of lipoxygenases from tissues of different species. They are non-haem iron dioxygenases that catalyse the conversion of unsaturated fatty acids to hydroperoxides. Plant lipoxygenases

aid in germination and participate in the synthesis of fatty acid-derived products involved in wound response and pest deterrent. Mammalian lipoxygenase plays a role in the synthesis of hormones that act in the inflammation of the respiratory and nervous systems [27].

The interest in the hydroperoxidation of linoleic acid catalysed by SLO, which involves formally the abstraction of a hydrogen atom from the C11 position of the substrate by the Fe(III)-OH cofactor, stems from the fact that it exhibits nearly temperature-independent rates and kinetic isotope effects (KIEs) close to 80 [28]. This KIE is much higher than that observed in other H-atom abstractions; for example, that of the  $H+H_2$  versus  $H+D_2$  hydrogen (deuterium) transfer is only  $9.5\pm1.4$  at  $30^\circ\text{C}$  [29]. Such high KIEs were claimed to be inconsistent with the TST view of catalysis [30].

The formal H-atom abstraction of linoleic acid by SLO is a proton-coupled electron transfer, where the electron is transferred from the  $\pi$ -system of the linoleic acid ( $\pi_D$ ) to the iron ( $\text{Fe}_A$ ) and promotes the transfer of the proton from the C11 carbon atom of linoleic acid to the oxygen atom of the Fe-bound OH ligand (Figure 14.12). The  $\pi_D-\text{Fe}_A$  distance is 5.69 Å and the  $\text{Fe}_A-\text{O}$  bond length is 1.86 Å [31], which lead to an electron donor–acceptor distance of 3.83 Å. According to the square-potential barrier expressed by eq. (6.46) and applied in detail to electron tunnelling in the next chapter, it is possible to calculate the electron-tunnelling probability using the barrier height and the donor–acceptor distance. The barrier height is determined by the energy of the relevant electron level in the donor (2.3 V versus NHE [31]), and that in the NHE reference relative to the electron energy at rest in vacuum, 4.44 eV. This gives a barrier height  $V_{\max}-E=6.74$  eV and an electron-tunneling probability of  $4\times10^{-5}$ . This probability multiplied by the frequency of the electron in the donor, typically  $10^{15}\text{ sec}^{-1}$ , gives a reaction frequency 2 orders of magnitude smaller than that of the TST. When the electronic reorganisation cannot accompany the nuclear reorganisation, the reaction becomes non-adiabatic and the reaction frequency is that of the electronic factor. The energy barrier associated with the transfer of the proton is calculated with  $m=1$  and the data for  $\text{H}_2\text{O}$  and benzene (see Table 13.7). These species were chosen because they represent the OH and CH bonds involved in the reaction coordinate and give the reaction energy of  $-23\text{ kJ mol}^{-1}$ , identical to the experimental  $\Delta G^0$  [31]. Finally, the (CH...O) distance was

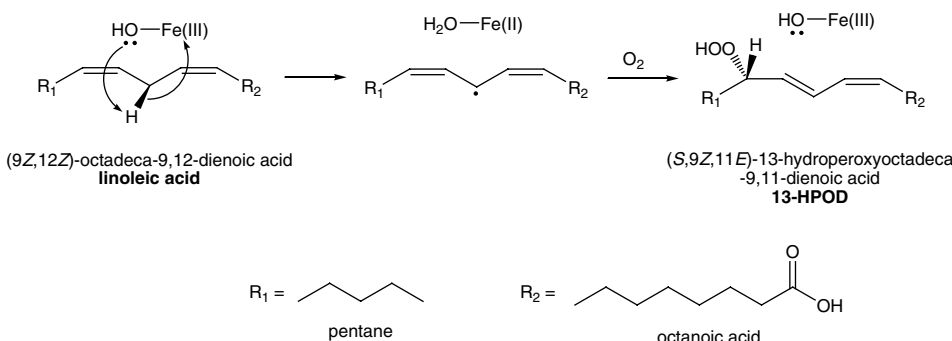


**Figure 14.12** Proton-coupled electron transfer in the hydroperoxidation of linoleic acid catalysed by SLO.

estimated as  $l_{\text{CO}} = 2.88$  [31] or  $2.95 \text{ \AA}$  [32]. With  $D_{0(\text{CHO})} = 10.5 \text{ kJ mol}^{-1}$ , the LS potential gives  $l_{\text{CO}} = 2.9 \text{ \AA}$  and a H-bond stretching frequency of  $217 \text{ cm}^{-1}$ , in good agreement with the available data. Such a significant H-bond energy involving a CH bond has been explained by the strong electron withdrawal effect of the nearby Fe(III) ion [33]. The frequency factor  $5 \times 10^{11} \text{ sec}^{-1}$ , the data for benzene and water in Table 1 and  $l_{\text{CO}} = 2.9 \text{ \AA}$ , give  $k_{\text{ISM}} = 28 \text{ sec}^{-1}$  and  $k_{\text{H}}/k_{\text{D}} = 64$  at  $25^\circ\text{C}$ . This rate and the large KIE include a hydrogen-tunnelling correction of 621 at  $25^\circ\text{C}$ , owing to the thin and high-energy barrier of this reaction. The barrier topography of this atom transfer is determined by the repulsive part of the Morse potential, calculated from the LS potential for the (CH...O) H-bond, which is absent in a typical proton transfer [34]. The calculated rate and KIE are in good agreement with the experimental values,  $k_{\text{cat}} = 327 \pm 14 \text{ sec}^{-1}$  and  $k_{\text{H}}/k_{\text{D}} = 76$  [30], corroborating the good performance of the ISM reaction path and the TST calculation for enzyme-catalysed reactions.

The isomerisation catalysed by TIM and the hydroperoxidation catalysed by SLO follow very different mechanisms and are subject to different stabilisation factors. Nevertheless, they show that Pauling's view of enzyme catalysis remains very influential, in particular his implication of the role of the enzyme in the stabilisation of the transition state of the rate-determining step. In modern words, this has been stated as "the entire and sole source of the catalytic power of enzymes is due to the lowering of the free energy of activation and any increase in the generalised transmission coefficient, as compared to that of the uncatalysed reaction" [35]. Of the factors contributing to the transmission coefficient, tunnelling is decidedly the most important one.

## REFERENCES

- [1] R Wolfenden, MJ Snider, *Acc. Chem. Res.* **34** (2001) 938–945.
- [2] A Brown, *J. Chem. Soc.* **81** (1902) 373.
- [3] L Michaelis, ML Menten, *Biochem. Z.* **49** (1913) 333.
- [4] H Lineweaver, D Burk, *J. Am. Chem. Soc.* **56** (1934) 658.
- [5] D Voet, JG Voet, *Biochemistry*, Wiley, New York, 1995.
- [6] A Kohen, R Cannio, S Bartolucci, JP Klinman, *Nature* **399** (1999) 496–499.
- [7] R Wolfenden, M Snider, C Ridgway, B Miller, *J. Am. Chem. Soc.* **121** (1999) 7419.
- [8] L Pauling, *Chem. Eng. News* **24** (1946) 1375.
- [9] X Zhang, KN Houk, *Acc. Chem. Res.* **38** (2005) 379–385.
- [10] AJ Kirby, *Acc. Chem. Res.* **30** (1997) 290.
- [11] R Breslow, SD Dong, *Chem. Rev.* **98** (1998) 1997–2011.
- [12] J Chen, MA McAllister, JK Lee, KN Houk, *J. Org. Chem.* **63** (1998) 4611–4619.
- [13] JP Guthrie, R Kluger, *J. Am. Chem. Soc.* **115** (1993) 11569.
- [14] RC Davenport, PA Bash, BA Seaton, M Karplus, GA Petsko, D Ringe, *Biochemistry* **30** (1991) 5821.
- [15] JA Gerlt, PG Gassman, *J. Am. Chem. Soc.* **115** (1993) 11552–11568.
- [16] JP Richard, *J. Am. Chem. Soc.* **106** (1984) 4926–4936.
- [17] Y Chiang, AJ Kresge, YS Tang, J Wirz, *J. Am. Chem. Soc.* **106** (1984) 460–462.
- [18] JA Gerlt, PG Gassman, *Biochemistry* **32** (1993) 11943–11952.
- [19] WW Cleland, MM Kreevoy, *Science* **264** (1994) 1887–1890.

- [20] PA Frey, SA Whitt, JB Tobin, *Science* **264** (1994) 1927–1930.
- [21] A Warshel, A Papazyan, PA Kollman, *Science* **1995** (1995) 102–103.
- [22] CN Schutz, A Warshel, *Proteins* **55** (2004) 711–723.
- [23] AR Fersht, J-P Shi, J Knill-Jones, DM Lowe, AJ Wilkinson, DM Blow, P Brick, P Carter, MMY Waye, G Winter, *Nature* **314** (1985) 235–238.
- [24] Q Cui, M Karplus, *J. Phys. Chem. B* **106** (2002) 1768–1798.
- [25] G Jogi, S Rozovsky, AE McDermott, L Tong, *Proc. Natl. Acad. Sci. USA* **100** (2003) 50–55.
- [26] I Kursula, RK Wierenga, *J. Biol. Chem.* **278** (2003) 9544–9551.
- [27] MH Glickman, JP Klinman, *Biochemistry* **35** (1996) 12882.
- [28] A Kohen, JP Klinman, *Acc. Chem. Res.* **31** (1998) 397–404.
- [29] LG Arnaut, AAC Pais, SJ Formosinho, M Barroso, *J. Am. Chem. Soc.* **125** (2003) 5236–5246.
- [30] MJ Knapp, K Rickert, JP Klinman, *J. Am. Chem. Soc.* **124** (2002) 3865–3874.
- [31] E Hatcher, AV Soudackov, S Hammes-Schiffer, *J. Am. Chem. Soc.* **126** (2004) 5763–5775.
- [32] G Tresadern, JP McNamara, M Mohr, H Wang, NA Burton, IH Hillier, *Chem. Phys. Lett.* **358** (2002) 489–494.
- [33] W Siebrand, Z Smedarchina, *J. Phys. Chem. B* **108** (2004) 4185–4195.
- [34] M Barroso, LG Arnaut, SJ Formosinho, *ChemPhysChem.* **6** (2005) 363–371.
- [35] M Garcia-Viloca, J Gao, M Karplus, DG Truhlar, *Science* **303** (2004) 186–195.

# – 15 –

## Transitions between Electronic States

---

### 15.1 MECHANISMS OF ENERGY TRANSFER

The previous chapters dealt with reactions triggered by a strong interaction during the collision between the reactants, manifested in the transfer of thermal energy and in the reorganisation of molecular bonds. The bond-breaking–bond-making process resulting from that interaction leads to the transformation of the reactants into products. The relative nuclear motion in the course of the collision can be associated with the “reaction coordinate” connecting the reactants to the products. Additionally, it is possible to locate a maximum of energy along that reaction coordinate and identify it as the transition state (TS). The TS was characterised by an imaginary frequency, which corresponds to the curvature of the reaction path. The finite value of the imaginary frequency guarantees a smooth transition between the reactants and the products. When these properties are confirmed, the reaction can be described by a single potential energy surface (PES) and is termed adiabatic. Adiabatic reactions can be described in considerable detail by the transition-state theory (TST). However, chemical kinetics is not limited to such systems.

The methods of chemical kinetics can also be applied to the study of transitions between the different electronic states. This study must now be guided by different principles because the initial (reactant) and final (product) states cannot be described by the same PES. Such transitions may occur either with the absorption or emission of light, designated as radiative transitions, or with the conversion of the energy difference between the two states into heat, in which case, they are termed as radiationless transitions. In photochemistry and spectroscopy, the transitions between the electronic states are conveniently illustrated by the so-called Jablonski diagram [1], where the radiative transitions are represented by vertical arrows and the radiationless ones by wavy and/or by dashed lines (Figure 15.1).

The radiative transitions correspond to either the absorption or the emission of light. When the emission of light occurs between states of the same multiplicity, usually in typical organic systems between singlet states, it is called fluorescence. The emission of light associated with the transition between states of different multiplicity, usually between a triplet and a singlet state, is called phosphorescence. When the absorption of radiative energy exceeds the energy of the excited electronic state, the molecule is left in an excited vibrational level of the excited electronic state. If this molecule is in a condensed state, the collision with the neighbouring molecules rapidly relaxes it to the lowest vibrational level of that excited state, the excess vibrational energy is converted into heat and thermal

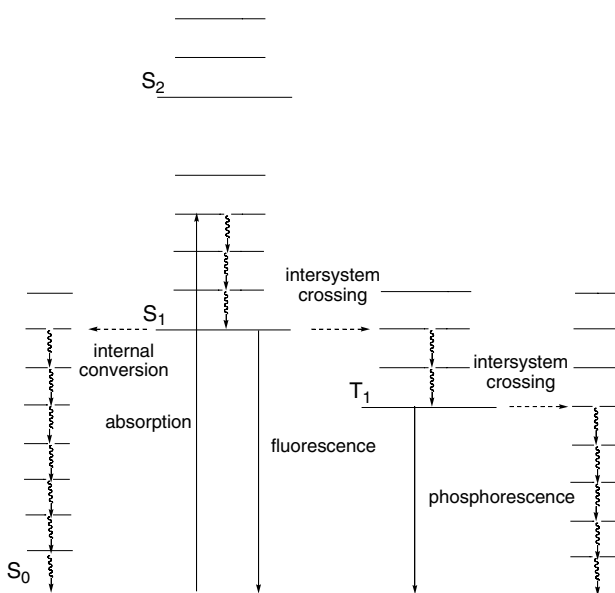


**Figure 15.1** Jablonski diagram illustrating the transitions between the electronic states in a polyatomic molecule, in a condensed phase. The vibrational levels in each electronic state are only schematically represented, because there are likely to be a very large number of vibrational modes that exist in a multi-dimensional surface. The wavy lines represent the vibrational relaxation within the electronic states.

equilibrium is obtained. Under these conditions, the vibrational relaxation is faster than any other process represented in Figure 15.1, and all the subsequent processes occur from the lowest vibrational level of the lowest excited state. According to Kasha [2], following the earlier suggestions of Vavilov: “The emitting level of a given multiplicity is the lowest excited level of that multiplicity”. However, if the molecule is in the gas phase at low pressures, vibrational relaxation is much slower and reversible inter-system crossing may occur. This is more likely for small molecules, with more spaced vibrational states, but has also been observed for anthracene in the gas phase [3]. In summary, in condensed phases, the electronically excited molecule rapidly relaxes to the lowest vibrational state of the electronically excited state. From this state it will undergo an electronic transition to the ground state with conservation of spin that can either be radiative (fluorescence emission) or non-radiative (internal conversion), or may involve a spin flip of one of the electrons in an electronic transition to an isoenergetic, vibrationally excited level of the lowest triplet state (inter-system crossing). In the triplet state, the molecule undergoes rapid vibrational relaxation to its lowest vibrational level, and from here it will return to the ground state either radiatively (phosphorescence emission) or non-radiatively (inter-system crossing to a high vibrational level of the ground state, followed by vibrational relaxation).

Excited electronic states can be formed as a result of high temperatures, highly exothermic chemical reactions (chemiluminescence), radiative recombination of electrons

and holes (electroluminescence) or more commonly, absorption of radiation. In the last case, if monochromatic light of intensity  $I_0$  is incident normal to a sample of homogeneous absorbing solution, the intensity of the transmitted light will be

$$I_t = I_0 10^{-\varepsilon l C} \quad (15.1)$$

where  $C$  is the molar concentration ( $1 \text{ M} = 1 \text{ mol dm}^{-3}$ ) of the molecules that absorb light,  $\varepsilon$  their molar absorptivity coefficient (sometimes called extinction coefficient) in per molar per centimetre at the wavenumber (inverse of the wavelength) of the incident light and  $l$  the length (in centimetre) of the optical path in the solution. The molar absorption coefficient at a given wavenumber,  $\varepsilon(\bar{v})$ , is used to obtain the absorption cross section, which is a parameter frequently used in optics

$$\sigma(\bar{v}) = \frac{2303\varepsilon(\bar{v})}{N_A} = 3.81 \times 10^{-19} \varepsilon(\bar{v}) \text{ (cm}^2\text{)} \quad (15.2)$$

Both the molar absorption coefficient and the absorption cross sections are measures of the electronic transition probability. A further important measure of this is the oscillator strength,  $f$ , given for the transition between a lower state 1 and an upper state 2, which is proportional to the area of the absorption band,

$$f_{12} = \frac{2303m_e c^2}{\pi e^2 N_A n_D} \int \varepsilon(\bar{v}) d\bar{v} \quad (15.3)$$

where  $m_e$  is the mass and  $e$  the charge of an electron and  $n_D$  the refractive index of the solution.

An excited atom may decay spontaneously to the ground state with the emission of a photon of energy

$$E_2 - E_1 = h\nu_{21} = \hbar\omega_{21} \quad (15.4)$$

where the angular oscillation frequency is  $\omega = 2\pi\nu$ . Einstein represented the transition probability for spontaneous emission for our system of two states, 1 and 2, by  $A_{21}$ . However, the excited atom in the presence of a radiation field may also relax to the ground state by interaction with the incident radiation in the process termed stimulated emission. This is the process that forms the basis of the laser. Einstein called the corresponding transition probability  $B_{21}$ . Microscopic reversibility requires that the transition probability for stimulated emission must be equal to the transition probability for absorption

$$B_{21} = B_{12} \quad (15.5)$$

Einstein obtained a relation between spontaneous and stimulated emission, using the relation between the number of atoms in the two states

$$\frac{n_1}{n_2} = e^{-E_1 - E_2 / k_B T} = e^{h\nu_{21} / k_B T} \quad (15.6)$$

and Planck's expression for the radiation density of a black body at temperature  $T$

$$I(v) = \frac{8\pi h v^3}{c^3} \frac{1}{e^{hv/k_B T} - 1} \quad (15.7)$$

When an atomic system is in equilibrium with the radiation field, as many transitions occur in the direction  $1 \rightarrow 2$  as in the opposite direction,  $2 \rightarrow 1$ . In this case, the equilibrium condition will be

$$I(v)(n_1 B_{12} - n_2 B_{21}) - A_{21} n_2 = 0 \quad (15.8)$$

Using eqs. (15.5)–(15.7) in eq. (15.8), gives

$$A_{21} = \frac{8\pi h v^3}{c^3} B_{21} = 8\pi h \bar{v}^3 B_{21} \quad (15.9)$$

Assuming that at time  $t = 0$  the external radiation field is removed and that all atoms are in the excited state, the decay to the ground state follows the (first-order) radiative decay law

$$n_2(t) = n_2(0) e^{-A_{21}t} \quad (15.10)$$

and the radiative (sometimes termed natural) lifetime of fluorescence is  $\tau_F = 1/A_{21}$ .

The distinction between electronic transitions involving states of the same spin multiplicity (fluorescence and internal conversion) and states of different spin multiplicity (phosphorescence and inter-system crossing) is due to the existence of selection rules for electronic transitions. One of the most important rules is the spin selection rule, which is expressed as  $\Delta S = 0$  (i.e. the change of the spin of an electron during a spectroscopic transition is forbidden). The electron is a fermion with spin quantum numbers  $s = +\frac{1}{2}$  or  $-\frac{1}{2}$ , whereas the photon is a boson with  $s = 1$ . A photon absorption or emission does not change the spin state of the electron directly, and phosphorescence is a spin-forbidden process. Inter-system crossing also involves a change in the spin of an electron and, consequently, it is also a spin-forbidden transition. The spin-forbidden nature of these processes is of electronic origin, but can be circumvented by interaction with the medium, especially, when heavy atoms or paramagnetic species are present. Under these conditions, spin is no longer a pure quantum number and significant spin-orbit coupling occurs, owing largely to relativistic effects. Heavy atoms also facilitate the inter-system crossing and phosphorescence when they are present in the molecule. The simplest way to account for the spin-forbidden nature of these processes is to introduce a spin-forbidden factor  $\chi_0 < 1$  in the expression for the rate of electronic transition between states of different spin multiplicity. This accounts for the fact that such transitions are much slower than internal conversion and fluorescence. In view of these spin restrictions and given that the ground state of organic molecules is a singlet state ( $S_0$ ), the lowest excited singlet state of such molecules ( $S_1$ ) has a much shorter lifetime than the corresponding triplet state ( $T_1$ ). Kasha suggested a value of  $\chi_0 = 10^{-6}$  for the inter-system crossing from  $T_1$  to  $S_0$  in aromatic hydrocarbons.

Chemical reactions between two reactants in different electronic states, leading to two products in electronic states that preserve the total spin multiplicity, can also be called radiationless transitions. Two frequently encountered examples are electron and electronic-energy

transfers. Here, electron transfers are understood as processes where only one electron is transferred from one molecule or ion to another molecule or ion, without the breaking or making of any bonds. These processes are also termed outer-sphere electron transfers. They will be discussed in detail in the next chapter. Electronic-energy transfers may occur through three mechanisms: radiatively (the so-called “trivial mechanism”, involving emission of one molecule followed by re-absorption by another), non-radiatively through coulombic (mainly dipole–dipole) interaction (the Förster mechanism [4]) or non-radiatively through electron exchange (the Dexter mechanism [5]).

The radiative or trivial mechanism of inter-molecular energy transfer can be expressed as a sequence of two independent steps



where  $D'$  represents the excited energy donor and  $A$  is the acceptor. The rate of this mechanism is proportional to the fluorescence rate constant of the donor, the concentration of excited molecules and the probability of absorption by  $A$ .

$$v_{\text{rad}} \propto k_f^D [D'] P_{\text{abs}}^A \quad (15.11)$$

From the above discussion on the spin selection rule, it is implicit in this formulation that the states  $D$ ,  $D'$  and  $A$ ,  $A'$  involved in radiative energy transfer will have the same spin multiplicity. However, the pair  $A$ ,  $A'$  may have spin multiplicity different from that of the pair  $D$ ,  $D'$ . The probability of light absorption by  $A$  is proportional to its concentration and to the spectral overlap between the donor emission and the acceptor absorption. The most distinct features of this mechanism are its long range, its dependence of the overlap between the fluorescence of the donor and the absorption of the acceptor, its dependence on the size and shape of the vessel utilised and the fact that it leaves the lifetime of the donor unchanged. Radiative energy transfer is observed mainly in optically thick samples.

The two mechanisms of non-radiative electronic-energy transfer differ in the nature of the interaction between the energies of the donor and that of the acceptor. In the Förster or coulombic mechanism there is an electrostatic interaction between the transition dipole moment corresponding to the electronic de-excitation of the donor and that corresponding to the electronic excitation of the acceptor, and the two transitions occur simultaneously. The energy lost by the donor molecule is acquired by the acceptor molecule in a resonant fashion, and can take place at distances much larger than molecular sizes because the interaction between two point dipoles decreases with their distance ( $R$ ) as  $R^{-3}$  [6]. This process corresponds to the coupling of two oscillators of electromagnetic field by a “virtual” rather than a “real” photon. It is the dominant energy-transfer mechanism except when the dipole strength of the acceptor transition is low or the fluorescence yield of the donor is vanishingly small. Figure 15.2 illustrates the change in donor and acceptor electronic configurations taking place in the course of the Förster energy-transfer mechanism.

Triplet states do not meet the requirements for efficient Förster energy transfer. Yet, triplet–triplet energy transfers, where the donor is initially in a triplet state and the acceptor in the ground (singlet) state and leading to the donor in the ground (singlet) state and

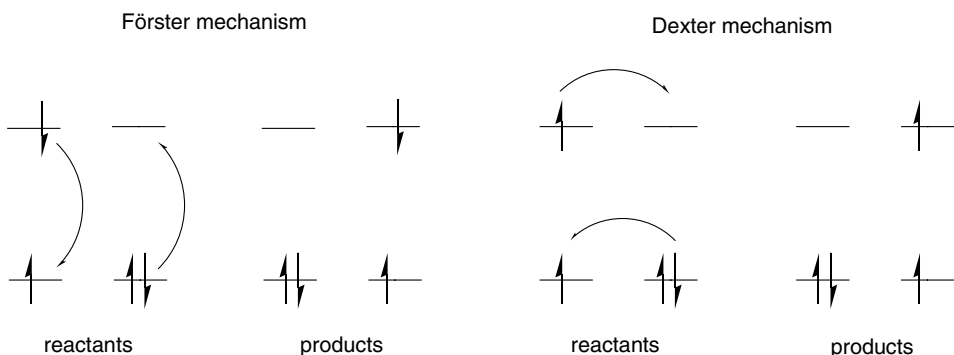


**Figure 15.2** Electronic configurations in: (a) Förster energy transfer; (b) Dexter energy transfer.

the acceptor in a triplet state, are relatively common between organic molecules. These require the acceptor to have a triplet state of lower energy than the donor. A particularly important case of triplet-energy transfer is the transfer of energy from a triplet state to molecular oxygen, whose ground state is a triplet ( ${}^3\Sigma_g^-$ ) and whose first singlet ( ${}^1\Delta_g$ ) state is 94 kJ mol<sup>-1</sup> above the ground state. In this case, the two reactants are triplets and the two products are singlets. This is an example of a process called triplet–triplet annihilation. This process is more commonly associated with the case when two identical organic molecules in their triplet states ( $T_1$ ) meet and yield a singlet ground state ( $S_0$ ) and a highly excited singlet state  $S_n^*$ , which collects the excitation energies of both the partners. This process frequently leads to delayed fluorescence (known as P-type delayed fluorescence from its observation with the aromatic hydrocarbon pyrene). Here the emission has the same spectrum as normal fluorescence, but has the lifetime of the triplet state. The transfer is still allowed because it follows Wigner's spin rule and the process is governed by spin statistics. Initially, it can be characterised by the formation of an intermediate pair state  $T_1 + T_1 \leftrightarrow {}^{1,3,5}(T_1 \dots T_1)$ , that subsequently decays to  $S_0 + S_n^*$ . The reverse process, where a highly excited singlet state dissociates into two triplets is also known and is termed singlet fission.

Such processes can be conceptualised as the tunnelling of an electron from one partner to the other, while another electron tunnels in the opposite direction, leaving the overall spin multiplicity intact (Figure 15.2). This mechanism, first described by Dexter, requires the overlap of the wavefunctions of the two partners in space and is triggered by the electron exchange interaction. Dexter energy transfer is also possible for singlet–singlet energy transfers, but it takes place at shorter distances than the Förster energy transfer.

Electron and triplet energy transfers have certain features in common. For example, such reactions may occur with relatively high rates even when the electron (or energy) donor is physically separated from the electron (or energy) acceptor by distances of 10 Å. However, rather than the concerted transfer of two electrons pictured for triplet-energy transfers in Figure 15.2, electron transfers involve the transfer of one electron only. The understanding of the factors that govern the rates of energy and electron transfers requires the resolution of the time-dependent Schrödinger equation.

## 15.2 THE “GOLDEN RULE” OF QUANTUM MECHANICS

Quantum mechanics establishes a simple expression for the rate constant of a transition between an initial and a final state when these states are only subject to a weak interaction. The formalism of weak interactions was originally developed for spectroscopic transitions, but later found application in energy and electron transfers.

The time-dependent Schrödinger equation, for a time-independent Hamiltonian, has the form

$$\mathbf{H}\Psi(x, y, z, t) = i\hbar \frac{d\Psi(x, y, z, t)}{dt} \quad (15.12)$$

and its more familiar application is to represent the motion of a particle as that of a wave packet. Here, eq. (15.12) is employed to describe the time development of the system from its initial state to the final one. The general solution for this equation of motion is a linear superposition of the stationary states

$$\Psi(x, y, z, t) = \sum_n a_n \Psi_n = \sum_n a_n \Psi_n \exp\left(-\frac{i}{\hbar} E_n t\right) \quad (15.13)$$

where  $\psi_n$  is a function of the space coordinates. When the system is subject to a perturbation, the coefficients  $a_n$  become functions of time during the perturbation and remain constant in the unperturbed system. For example, if the system is initially in a stationary state defined by  $n = 1$  and undergoes a transition to the stationary state defined by  $n = 3$ , then, during the transition,  $a_1$  will decrease from unity to zero, while  $a_3$  will increase from zero to unity, inverting the weight of the contributions  $\Psi_1$  and  $\Psi_3$ . The rate of change from  $a_1$  to  $a_3$  is a measure of the rate of transition from the first to the third stationary state. The calculation of this rate is one of the central problems of the theories of spectroscopic and radiationless transitions.

In the most relevant cases for these transitions, the perturbing interaction is limited in time and space. For example, the system is unperturbed before it interacts with an electromagnetic wave, and it is free again from the perturbation after sufficient time has elapsed. This suggests that the total Hamiltonian can be considered as the sum of two terms:

$$\mathbf{H} = \mathbf{H}_0 + V \quad (15.14)$$

where the time-independent operator  $\mathbf{H}_0$  describes the unperturbed system and  $V$  is the perturbation. This perturbation may be explicitly time-dependent, as in the case of a transient electromagnetic field, or not, as in the case of an applied field.

Replacing eq. (15.14) in eq. (15.12) and omitting the coordinates to simplify the form of the equation,

$$(\mathbf{H}_0 + V)\Psi = i\hbar \frac{d\Psi}{dt} \quad (15.15)$$

and the solutions can be written as

$$\Psi = \sum_j c_j \psi_j \exp\left(-\frac{i}{\hbar} E_j t\right) \quad (15.16)$$

where  $\psi_j$  represents the full set of eigenfunctions with the associated eigenvalues  $E_j$  of the unperturbed system Hamiltonian  $\mathbf{H}_0$ , when the coefficients  $c_j$  are time-dependent. Replacing eq. (15.16) in eq. (15.15) and exchanging the left and right sides

$$\sum_j \left( c_j E_j \psi_j + i\hbar \frac{dc_j}{dt} \psi_j \right) \exp\left(-\frac{i}{\hbar} E_j t\right) = \sum_j c_j (\mathbf{H}_0 \psi_j + V \psi_j) \exp\left(-\frac{i}{\hbar} E_j t\right) \quad (15.17)$$

which can be reduced to

$$\sum_j i\hbar \frac{dc_j}{dt} \psi_j \exp\left(-\frac{i}{\hbar} E_j t\right) = \sum_j c_j V \psi_j \exp\left(-\frac{i}{\hbar} E_j t\right) \quad (15.18)$$

because each term  $\mathbf{H}_0 \psi_j$  on the left-hand side of eq. (15.17) cancels with the corresponding  $E_j \psi_j$  term on the right-hand side of the same equation. An expression for  $dc_j/dt$  can be obtained taking the inner product of  $\mathbf{H}\Psi$  with one of the stationary states. Representing the other stationary state by the index  $k$ , the inner product corresponds to

$$\int \sum_j i\hbar \frac{dc_j}{dt} \psi_k^* \exp\left(\frac{i}{\hbar} E_k t\right) \psi_j \exp\left(-\frac{i}{\hbar} E_j t\right) d\tau = \int \sum_j c_j \psi_k^* \exp\left(\frac{i}{\hbar} E_k t\right) V \psi_j \exp\left(-\frac{i}{\hbar} E_j t\right) d\tau \quad (15.19)$$

where  $\psi_k^*$  is the complex conjugate of  $\psi_k$ , and the integration is over all the space, represented by  $\tau$ . Given that the stationary states of the Hamiltonian are orthogonal

$$\int \psi_k^* \psi_j \, d\tau = \delta_{kj} \quad (15.20)$$

and adopting the shorthand notation for the matrix element of the perturbation between the unperturbed eigenstates

$$V_{kj} = \int \psi_k^* V \psi_j \, d\tau \quad (15.21)$$

and defining the transition frequency

$$\omega_{kj} = \frac{E_k^{(0)} - E_j^{(0)}}{\hbar} \quad (15.22)$$

gives a set of coupled first-order differential equations

$$i\hbar \frac{dc_k}{dt} = \sum_j V_{kj} c_j e^{i\omega_{kj} t}, \quad k = 1, 2, 3, \dots \quad (15.23)$$

In matrix notation, this is equivalent to

$$i\hbar \frac{d}{dt} \begin{pmatrix} c_1 \\ c_2 \end{pmatrix} = \begin{pmatrix} V_{11} & V_{12} e^{-i\omega_{12} t} \\ V_{21} e^{-i\omega_{21} t} & V_{22} \end{pmatrix} \begin{pmatrix} c_1 \\ c_2 \end{pmatrix} \quad (15.24)$$

No approximations have yet been made and eq. (15.24) is exact. The values of  $c_j$  determined by this equation are related to the probability of finding the system in any particular state at any later time. Unfortunately, it is not generally possible to find exact solutions to this equation. The solution of this complicated linear system invokes the perturbation approximation, and the method is called *time-dependent perturbation theory*.

The solution of eq. (15.23) depends critically on the initial conditions. Assuming, for simplicity, that the system at the initial time  $t_0 = -\infty$  is in one of the stationary states of the unperturbed Hamiltonian, and that  $\mathbf{H}_0$  possesses only discrete energy levels, the following initial conditions are introduced:

$$c_s(-\infty) = 1, \quad c_k(-\infty) = 0 \quad \text{if } k \neq s \quad (15.25)$$

The index  $s$  represents the initial stationary state. A successive approximation method can be used to solve eq. (15.23) subject to these initial conditions. The initial values of the coefficients  $c_k$  are introduced in the right-hand side of eq. (15.23). For  $k \neq s$ , the approximate equations

$$i\hbar \frac{dc_k}{dt} = V_{ks} e^{i\omega_{ks}t}, \quad k \neq s \quad (15.26)$$

are thus obtained. These equations are only valid for values of  $t$  such that  $c_k(t) \ll c_s(t) \approx 1$ , if  $k \neq s$ .

Eq. (15.26) can be immediately integrated when the perturbation  $V$  does not itself depend on time, although the time development of the system with the Hamiltonian (15.14) is, nevertheless, conveniently described in terms of transitions between the eigenstates of the unperturbed Hamiltonian  $\mathbf{H}_0$ . Taking the initial time as  $t_0 = 0$

$$i\hbar \int_0^t dc_k = V_{ks} \int_0^t e^{i\omega_{ks}t} dt, \quad k \neq s \quad (15.27)$$

and using eq. (15.22), the coefficients

$$c_k(t) = V_{ks} \frac{1 - e^{i\omega_{ks}t}}{E_k^{(0)} - E_s^{(0)}} \quad (15.28)$$

are obtained for  $k \neq s$ , if  $c_k(0) = 0$  and  $c_s(0) = 1$ .

If the system is known to have been in the initial discrete state  $s$  at  $t = 0$ , the probability that it will be in the unperturbed final eigenstate  $k \neq s$  at time  $t$  is given by

$$|c_k(t)|^2 = 2|V_{ks}|^2 \frac{1 - \cos(\omega_{ks}t)}{(E_k^{(0)} - E_s^{(0)})^2} \quad (15.29)$$

where the relation

$$\cos(x) = \frac{1}{2}(e^{ix} + e^{-ix}) \quad (15.30)$$

was employed. The total probability of transition to all the final states, labelled  $f$ , which form a quasi-continuum of states per unit energy interval, is given by

$$\sum_{k \in f} |c_k(t)|^2 = 2 \int |V_{ks}|^2 \frac{1 - \cos(\omega_{ks}t)}{(E_k^{(0)} - E_s^{(0)})^2} \rho_f(E_k^{(0)}) dE_k^{(0)} \quad (15.31)$$

where  $\rho_f(E)$  represents the density of final unperturbed states. The assumption that the final states form a quasi-continuum justified the use of an integral rather than the sums on the right-hand side of eq. (15.31). Within this approximation, it is of interest to formulate the time rate of change of the total transition probability

$$w = \frac{d}{dt} \sum_{k \in f} |c_k(t)|^2 = \frac{2}{\hbar^2} \int |V_{ks}|^2 \frac{\sin(\omega_{ks}t)}{\omega_{ks}} \rho_f(E_k^{(0)}) dE_k^{(0)} \quad (15.32)$$

It is usual practice to assume that both  $|V_{ks}|^2$  and  $\rho_f(E_k^{(0)})$  are approximately constant over an energy range  $\Delta E$  in the neighbourhood of  $E_s$ . Additionally, the function  $\sin(\omega_{ks}t)/\omega_{ks}$  has a pronounced peak at  $E_k^{(0)} = E_s^{(0)}$  for  $t$  values which satisfy the relation

$$t \gg \hbar/\Delta E \quad (15.33)$$

as illustrated in Figure 15.3. This expresses the fact that the transitions that tend to conserve the unperturbed energy are dominant. If the right-hand side of eq. (15.33) corresponds to a very short time, there is a considerable range of  $t$  values, such that the inequality is fulfilled and yet the initial state  $s$  is not appreciably depleted. For such a range of  $t$  values, eq. (15.32) can be simplified to

$$w = \frac{2}{\hbar} |V_{ks}|^2 \rho_f(E_s^{(0)}) \int_{-\infty}^{+\infty} \frac{\sin(\omega_{ks}t)}{\omega_{ks}} d\omega_{ks} \quad (15.34)$$

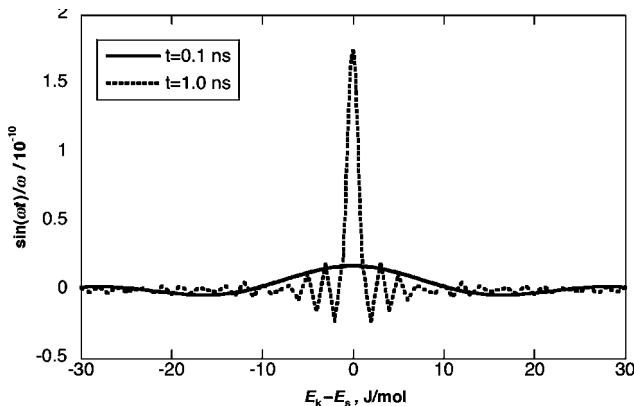


**Figure 15.3** Dependence of the function  $\sin(\omega_{ks}t)/\omega_{ks}$  on the energy difference between the unperturbed initial and final states, calculated for the values of  $t$  indicated in the plot.

where the condition of eq. (15.33) was employed to replace the limits of the integral by  $-\infty$  and  $+\infty$ . Given the standard integral

$$\int_{-\infty}^{+\infty} \frac{\sin(ax)}{x} dx = \pi \quad \text{when } a > 0 \quad (15.35)$$

the transition probability per unit time becomes

$$w = \frac{2\pi}{\hbar} |V_{ks}|^2 \rho_f(E_s^{(0)}) \quad (15.36)$$

Fermi called eq. (15.36) the *Golden Rule of time-dependent perturbation theory* because of its prevalence in radiationless transitions. Sometimes it is referred to as Fermi's Golden Rule.

The matrix element of the perturbation between the eigenstates  $V_{ks}$  is expressed in units of energy, the density of states  $\rho_f E_k^{(0)}$  in reciprocal energy units, and  $w$  in per second. A typical case where the Golden Rule is applicable is the internal conversion of a large molecule, following its electronic excitation. For example, the energy of the first excited singlet state ( $S_1$ ) of anthracene relative to that of its ground state ( $S_0$ ) is 316 kJ mol<sup>-1</sup>. At this energy, the density of vibrational states in  $S_0$  is extremely high. Typically, for such molecules, this is in the range of  $10^{11} - 10^{17}$  states J<sup>-1</sup> mol<sup>-1</sup>, and the  $S_1$  state will relax into an isoenergetic level of the manifold of highly excited vibrational states of  $S_0$ , a process already defined as internal conversion. Subsequent vibrational relaxation in the  $S_0$  state converts the electronic excitation into heat. It must be recalled that this is not the only decay process available to the  $S_1$  state. It may also decay radiatively by fluorescence, or undergo inter-system crossing to the manifold of the triplet states.

### 15.3 RADIATIVE AND RADIATIONLESS RATES

Classically, charged particles radiate when they are accelerated. The strength of radiation is proportional to the square of the electric dipole moment, which is

$$\vec{\mu}_{21} = \int \Psi_2 [e\vec{r}_{21}] \Psi_1 d\tau = e \langle \Psi_2 | \vec{r}_{21} | \Psi_1 \rangle \quad (15.37)$$

where  $\vec{r}_{21}$  stands for the electron position vector. The absorption oscillator strength that describes the strength of the radiative transitions is defined as

$$f_{12} = \frac{8\pi^2 m_e c \bar{v}}{3h} \frac{|\mu_{12}|^2}{e^2} = 1.085 \times 10^{-5} \bar{v}_{\max} \left( \frac{\mu_{12}}{e} \right)^2 \quad (15.38)$$

where the numerical value applies when  $\bar{v}$  is expressed in per centimetre and  $|\mu_{12}|/e$  in angstrom. The oscillator strength is a dimensionless quantity.

The absorption of light is mainly the result of the interaction between the oscillating electric vector of the electromagnetic radiation with the charged particles within the molecules. The transition probability coefficient in the absorption from a lower electronic state 1 to an upper electronic state 2 corresponds to Einstein's coefficient of absorption

$$B_{12} = \frac{8\pi^3}{3h^2} |\mu_{12}|^2 \quad (15.39)$$

Eliminating  $\mu_{12}$  and  $f_{12}$  using eqs. (15.3) and (15.38) in the above expression gives the absorption probability in the gas phase ( $n_D=1$ ) in terms of experimentally accessible quantities

$$B_{12} = \frac{2303c}{hN_A} \int_0^\infty \frac{\varepsilon(\bar{v}) d\bar{v}}{\bar{v}} \quad (15.40)$$

The radiative rate can now be expressed in terms of these quantities using eq. (15.9),

$$k_r = A_{21} = \frac{64\pi^4 v^3}{3hc^3} |\langle \Psi_2 | e\vec{r}_{21} | \Psi_1 \rangle|^2 = \frac{8 \times 2303\pi c}{N_A} \bar{v}^2 \int_0^\infty \varepsilon(\bar{v}) d\bar{v} \quad (15.41)$$

This relation is only strictly applicable to two-level systems, such as atomic systems, where the transitions have sharp lines and in a medium of refractive index  $n_D=1$ . The electric dipole radiation dominates the mechanism of radiative decay in molecular systems. For molecular systems in solution, Strickler and Berg proposed a modified equation that gives good results for the radiative rate [7]

$$k_{SB} = \frac{8 \times 2303\pi c}{N_A} n_D^2 \langle \bar{v}^{-3} \rangle^{-1} \int \frac{\varepsilon(\bar{v}) d\bar{v}}{\bar{v}} = 2.88 \times 10^{-9} n_D^2 \langle \bar{v}^{-3} \rangle^{-1} \int \frac{\varepsilon(\bar{v}) d\bar{v}}{\bar{v}} \quad (15.42)$$

where

$$\langle \bar{v}^{-3} \rangle^{-1} = \frac{\int F(\bar{v}) d\bar{v}}{\int F(\bar{v}) \bar{v}^{-3} d\bar{v}} \quad (15.43)$$

and  $F(\bar{v})$  is the molecular fluorescence intensity distribution (i.e. its spectrum). When the fluorescence is the mirror image of the absorption, the radiative rates calculated with the Strickler–Berg equation compare well with the experimental rates obtained from the fluorescence quantum yield and lifetime of the donor molecules

$$k_f = \frac{\Phi_f}{\tau_D} \quad (15.44)$$

Eq. (15.42) relates the radiative energy transfer rate constant to the molecular properties. The corresponding rate, eq. (15.11), involves the probability of absorption by A, which can be expressed as

$$P_{abs}^A \propto [A] l \int_0^\infty F'_D(\bar{v}) \varepsilon_A(\bar{v}) d\bar{v} \quad (15.45)$$

where  $l$  is the path length of absorption, and the spectral overlap involves the normalised spectral distribution of the donor emission  $F'_D(\bar{v})$  and the molar absorption coefficient of the acceptor  $\varepsilon_A(\bar{v})$ . The normalisation of the donor emission is given by

$$F'_D(\bar{v}) = \frac{F_D(\bar{v})}{\int_0^\infty F_D(\bar{v}) d\bar{v}} \quad (15.46)$$

As mentioned before, radiative energy transfer originates from the interaction between the oscillating electric vector of the electromagnetic radiation and the charged particles within the molecules. Another possible interaction between the excited donor and the ground-state acceptor molecule is the electric dipole–dipole interaction, which is the basis of the Förster mechanism, schematically presented in Figure 15.2. The dipole–dipole interaction energy in the vacuum between two dipoles  $\vec{\mu}_1$  and  $\vec{\mu}_2$  at a distance  $R$  between their centres, has the form

$$V_{12} = \frac{1}{R^3} \left[ \vec{\mu}_1 \otimes \vec{\mu}_2 - \frac{3(\vec{\mu}_1 \otimes \vec{R})(\vec{\mu}_2 \otimes \vec{R})}{R^2} \right] \quad (15.47)$$

A quantitative treatment using the Golden Rule with this interaction energy leads to the following expression for the rate of Förster energy transfer

$$k_F = \frac{9000(\ln 10)\kappa^2\Phi_f}{128\pi^5 n_D^4 N_A R^6 \tau_D} \int_0^\infty \frac{F_D(\bar{v})\varepsilon_A(\bar{v})d\bar{v}}{\bar{v}^4} = \frac{1}{\tau_D} \left( \frac{R_0}{R} \right)^6 \quad (15.48)$$

where  $\kappa$  is an orientation factor (for a random directional distribution the average value is  $\kappa^2 = \frac{2}{3}$ ), the donor fluorescence intensity  $F_D$  is normalised to unit area on a wavenumber scale, and the decadic molar absorption coefficient of the acceptor  $\varepsilon_A$  is in the usual units (per molar per centimetre). The reason why the emission shape needs to be normalised to unity, while the absorption shape does not, is the presence of the term  $\tau_D^{-1}$  that already contains information on the absolute magnitude of the emitting transition moment. The above expression emphasises the fact that the probability of energy transfer is proportional to the square of the interaction energy and decreases, therefore, with the sixth power of the distance. The critical transfer distance  $R_0$  is the distance at which the energy transfer and the spontaneous decay of the excited donor are equally probable. Typically, values between 30 and 100 Å are calculated for aromatic donors.

Electric dipole–dipole coupling is the strongest if the corresponding optical transitions in both molecules are allowed for electric dipole radiation. This is not the case of triplet-energy transfer (Figure 15.2), which must follow an alternative mechanism. Dexter proposed that for such cases it is necessary to include explicitly the spin wavefunctions in the matrix element of the perturbation, eq. (15.21). The molecular wavefunction  $\psi$  is expressed as the product of a spacial  $\varphi(\vec{r})$  and a spin  $\xi(\vec{s})$  electronic wavefunction

$$\begin{aligned} \langle V_{12} \rangle &= \int \varphi_D^{*}(\vec{r}_1) \varphi_A^{*}(\vec{r}_2) V_{12} \varphi_D(\vec{r}_1) \varphi_A^{*}(\vec{r}_2) \times \xi_D^{*}(\vec{s}_1) \xi_A^{*}(\vec{s}_2) \xi_D(\vec{s}_1) \xi_A^{*}(\vec{s}_2) \\ &\quad - \int \varphi_D^{*}(\vec{r}_1) \varphi_A^{*}(\vec{r}_2) V_{12} \varphi_D(\vec{r}_2) \varphi_A^{*}(\vec{r}_1) \times \xi_D^{*}(\vec{s}_1) \xi_A^{*}(\vec{s}_2) \xi_D(\vec{s}_2) \xi_A^{*}(\vec{s}_1) \end{aligned} \quad (15.49)$$

where  $\vec{r}_1$  and  $\vec{r}_2$  denote the spacial coordinates of the electrons involved and the apostrophe denotes an excited state. The first integral is the Coulomb term with  $V_{12}$  given by eq. (15.47), and is different from zero when the spins of the electrons remain unchanged. The second integral is an exchange integral with  $V_{12} = e^2/r_{12}$  in vacuum, where  $r_{12}$  is the distance between the two electrons. This second integral represents the electrostatic interaction between the two charged clouds, and dies off exponentially with the distance

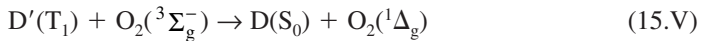
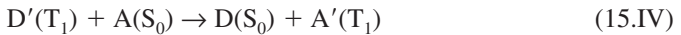
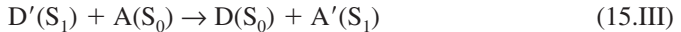
between the donor and the acceptor. Unless  $\xi'_D = \xi'_A$  and  $\xi_D = \xi_A$ , the integral vanishes, but  $\xi'$  is not necessarily equal to  $\xi$ . If  $s'_D$  and  $s_A$  are the initial spin quantum numbers of the two participating molecules, the resultant spin quantum number of the two species taken together must have one of the values

$$s'_D + s_A, s'_D + s_A - 1, s'_D + s_A - 2, \dots |s'_D - s_A| \quad (15.50)$$

It follows that the spin quantum numbers of the resulting species can only have values  $s_D$  and  $s'_A$  if at least one of the values

$$s_D + s'_A, s_D + s'_A - 1, s_D + s'_A - 2, \dots |s_D - s'_A| \quad (15.51)$$

is common to the series above. Thus, processes such as



are spin allowed for an exchange mechanism. The treatment of this perturbation with the Golden Rule, gives an exchange transfer rate of the form

$$k_D = \frac{2\pi}{\hbar} \Gamma \exp(-2R/\ell) \int_0^\infty F_D(\bar{v}) A_A(\bar{v}) d\bar{v} \quad (15.52)$$

where  $\Gamma$  and  $\ell$  reflect the ease of electron tunnelling between the donor and the acceptor and are not simply related to measurable quantities. They will be further discussed in this chapter under Sections 15.6 and 15.8. The donor emission  $F_D$  and the acceptor absorption  $A_A$  spectra are normalised to unity, such that the integrals of  $F_D$  and  $A_A$  are both equal to unity. The most salient features of this equation are the exponential dependence on the inter-molecular distance and the normalisation of both emission and absorption in eq. (15.52), which makes the exchange transfer rates independent of the oscillator strengths of the two transitions.

The overlap integrals appearing in eqs. (15.45), (15.48) and (15.52) reflect the spacial overlap between the wavefunctions of the initial unperturbed state  $s$  and the final unperturbed state  $k$ , and have their origin in the first of the two factors entering the Golden Rule,  $|V_{ks}|^2$  in eq. (15.36). The calculation of the spacial overlap almost invariably employs the Born–Oppenheimer approximation, which, based on the difference of masses between electrons and nuclei, treats the nuclei as stationary points with the electrons moving around them. In practice, this consists of expressing the molecular wavefunction  $\psi$  as the product of an electronic ( $\varphi_e$ ) and a nuclear ( $v_v$ ) wavefunction. The simplest case is that of a diatomic molecule with translational and rotational motions that give rise to a continuum of energies at the temperatures under consideration, and with a vibrational motion described by a harmonic oscillator. Representing the distance between the two nuclei by  $R$ , the Born–Oppenheimer approximation is expressed as

$$\psi(x, R) = \varphi_e(x; R) v_v(R) \quad (15.53)$$

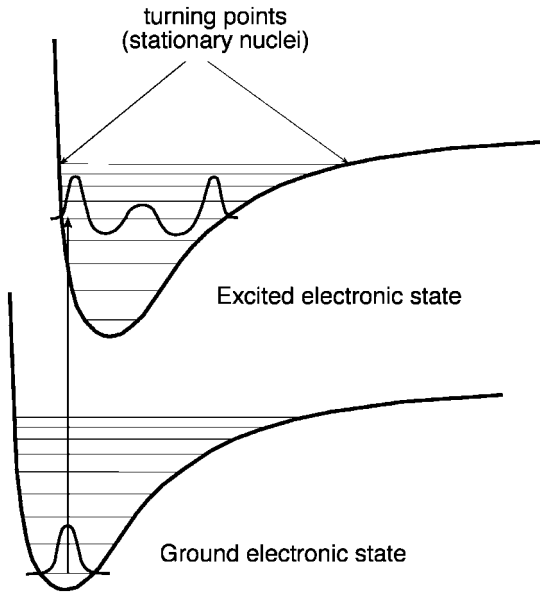


**Figure 15.4** Electronic transition corresponding to the absorption of light by the ground state of a diatomic molecule. The final state, reached immediately after the electronic transition, is the vibrational state of the electronically excited state that has the largest overlap with the lowest vibrational state of the electronic ground state.

The representation  $(x;R)$  denotes the parametric dependence of the electronic wavefunction on the inter-nuclear distance.

Substituting eq. (15.53) into eq. (15.21) and assuming that only the electronic distribution is perturbed, gives

$$\int \psi_k^* V \psi_j d\tau = \int \varphi_k^* v_{v'}^* V \varphi_s v_v d\tau_e d\tau_n = \int \varphi_k^* V \varphi_s d\tau_e \int v_{v'}^* v_v d\tau_n \quad (15.54)$$

The first factor

$$V_{ks}^e = \int \varphi_k^* V \varphi_s d\tau_e \quad (15.55)$$

measures the extension of the electronic redistribution induced by the transition from the initial state  $s$  to the final state  $k$ . The second factor

$$J_{v',v} = \int v_{v'}^* v_v d\tau_n \quad (15.56)$$

is the overlap integral between the vibrational wavefunctions of the initial ( $v$ ) and final ( $v'$ ) states, which is called the *Franck–Condon factor* for the  $k, v' \leftarrow s, v$  transition. According to eq. (15.36), the transition probability, or intensity, is proportional to  $|J_{v',v}|^2$ . Figure 15.4 represents an electronic transition that takes place at a fixed nuclear geometry, following the Franck–Condon principle. The vibrational relaxation takes place entirely in the excited state, after the electronic transition, and takes the system to the lowest vibrational state of the electronically excited state.

### 15.4 FRANCK–CONDON FACTORS

The Franck–Condon factor of an electronic transition from the vibrational level  $v = 0$  of the electronic ground state to the corresponding level  $v' = 0$  of the electronic excited state has a simple analytical solution when the vibrational motion is described by a harmonic oscillator. In this case, the vibrational wavefunctions of the ground vibrational levels is described by a normal (Gaussian) distribution function

$$F(x) = \frac{1}{\sqrt{2\pi}\sigma_x} \exp\left[-\frac{1}{2}\left(\frac{x-x_e}{\sigma_x}\right)^2\right] \quad (15.57)$$

illustrated in Figure 15.5. As shown in the figure, the Gaussian is centred in its average  $x_e$  and the variance  $\sigma^2$  is given by the inflection points of the distribution function. It is also convenient to characterise this distribution by its full-width at half-maximum

$$\Delta\bar{v}_{1/2} = 4\sigma\sqrt{\ln 2} \quad (15.58)$$

More specifically, the wavefunction of the ground vibrational state of a harmonic oscillator with a force constant  $f$  and a reduced mass  $\mu$ , has the form

$$\begin{aligned} v_0 &= \left(\frac{1}{\alpha\sqrt{\pi}}\right)^{1/2} \exp\left[-\frac{(R-R_e)^2}{2\alpha^2}\right] \\ &\qquad\qquad\qquad \alpha^2 = \hbar/\sqrt{f\mu} \\ v'_0 &= \left(\frac{1}{\alpha\sqrt{\pi}}\right)^{1/2} \exp\left[-\frac{(R-R'_e)^2}{2\alpha^2}\right] \end{aligned} \quad (15.59)$$

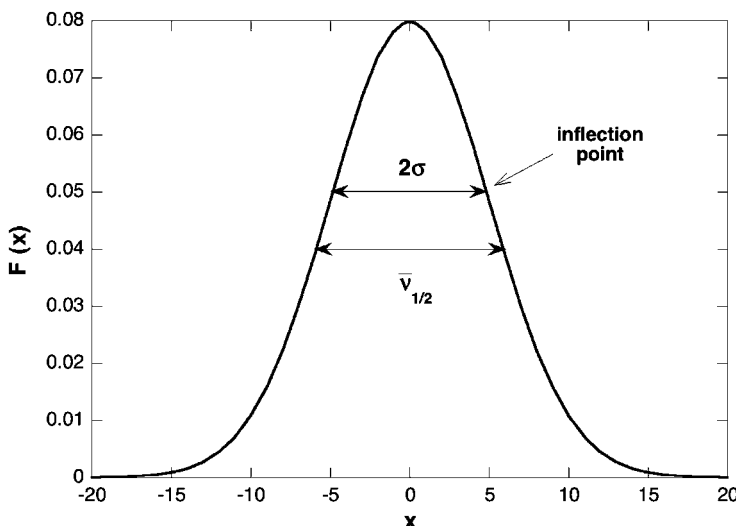


**Figure 15.5** Normal (Gaussian) distribution function, centred in its average,  $x_e = 0$ .

The overlap integral between these identical but displaced oscillators is

$$J_{0',0} = \int_{-\infty}^{+\infty} v_{0'}^* v_0 dR = \frac{1}{\alpha\sqrt{\pi}} \int_{-\infty}^{+\infty} \exp\left[-\frac{(R-R_e)^2 + (R-R'_e)^2}{2\alpha^2}\right] dR \quad (15.60)$$

The integral can be evaluated making the substitution of the variables

$$\alpha z = R - \frac{1}{2}(R_e + R'_e) \quad (15.61)$$

which yields

$$J_{0',0} = \frac{1}{\sqrt{\pi}} \exp\left[-\frac{(R_e - R'_e)^2}{4\alpha^2}\right] \int_{-\infty}^{+\infty} e^{-z^2} dz \quad (15.62)$$

where the integral now has a standard form and gives  $\sqrt{\pi}$ . Thus, the overlap is

$$J_{0',0} = \exp\left[-\frac{(R_e - R'_e)^2}{4\alpha^2}\right] \quad (15.63)$$

Considering that the intensity of the  $0' \leftarrow 0$  transition is proportional to  $|J_{v',v}|^2$ , it attains its maximum when the bond lengths of the ground and excited states are identical, and diminishes as  $(R_e - R'_e)^2$  increases. This effect is illustrated in Figure 15.6, where it is also

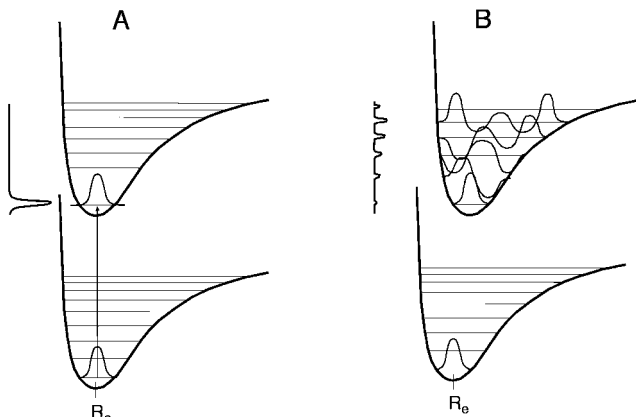


**Figure 15.6** Electronic transitions illustrating the intensity expected for the vibronic band of the absorption spectrum: (a) totally allowed transition following the Franck–Condon principle; (b) partially allowed transition according to the same principle.

shown that the intensities of the transitions to higher vibrational states of the electronically excited state attain their maxima for  $R_e \neq R'_e$  and may dominate the absorption spectrum. The  $0' \leftarrow 0$  transition is a purely electronic transition, while the  $v' \leftarrow 0$  transitions are vibronic (electronic + vibrational) transitions, subject to selection rules.

At room temperatures, the molecules are generally in their lowest vibrational state of the electronic ground state. Upon light absorption, the electron is promoted from the vibrational level  $v = 0$  of the ground state to a vibrational level  $v'$  of the excited state. For parabolas with the same force constant  $f$ , but minima displaced by  $d = |R_e - R'_e|$ , as shown in Figure 15.7, the progression of the vibronic bands follows a Poisson distribution, already presented in eq. (5.20),

$$J_{v',0} = \exp[-S] \frac{S^{v'}}{v'!} \quad (15.64)$$

where  $S$  is a reduced displacement,

$$S \equiv \left( \frac{d}{2\sigma_R} \right)^2 \quad (15.65)$$

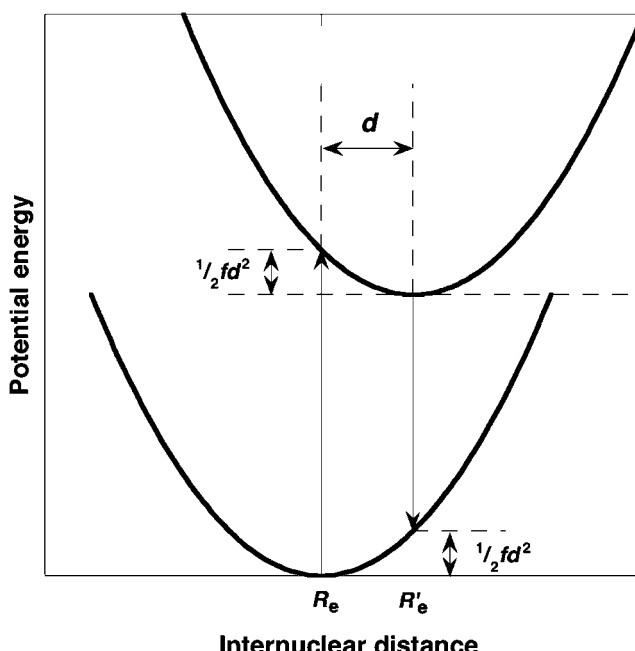


**Figure 15.7** Schematic representation of light absorption and fluorescence emission between electronic states described by identical (same force constant  $f$ ) but displaced ( $R_e \neq R'_e$ ) parabolas. The absorption is, necessarily, at higher energies than the fluorescence.

and  $\sigma_R$ , the root mean square amplitude of the zero-point oscillation in the electronic ground state, is defined as

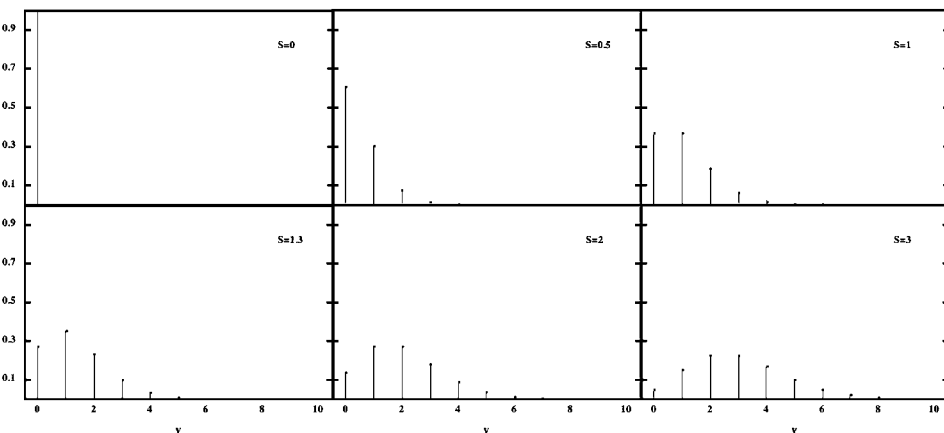
$$\sigma_R^2 \equiv \langle (R - R_e)^2 \rangle_0 = \frac{1}{2} \frac{\hbar}{\sqrt{\mu f}} = \frac{\alpha^2}{2} \quad (15.66)$$

Within the harmonic oscillator approximation, the force constant and the reduced mass are related to the angular frequency of the classical oscillator ( $\omega$ , expressed in per second) and to the wavenumber of the vibration ( $\bar{v}$ , expressed in  $\text{cm}^{-1}$ ) by

$$\omega = 2\pi c \bar{v} = \sqrt{\frac{f}{\mu}} \quad (15.67)$$

Figure 15.8 illustrates the progression of the peaks expected for different values of  $S$ .

The Franck–Condon factors given by eq. (15.64) for the transfer from the lowest vibrational level of the initial electronic state to the  $v'$  vibrational levels of the final electronic state are particularly simple to calculate for diatomic molecules, in view of the straightforward relation between the observed frequencies and the parameters involved in the calculation of  $S$ . Table 15.1 presents the spectroscopic constants of  $\text{O}_2$ ,  $\text{N}_2$  and  $\text{H}_2$ , in different electronic states. They represent the cases of small ( $\text{O}_2$ ), medium ( $\text{N}_2$ ) and large ( $\text{H}_2$ ) changes in bond lengths upon electronic excitation from the ground state to the excited one. The adjustments of the bond lengths minimise the energies of the systems in their electronic states, which have the electronic configurations illustrated in Figure 15.9. Pauling's relation between bond lengths and bond orders can also be employed to evaluate the chemical bond order of these excited states. As usual, for bonds between the same atoms, a longer bond corresponds to a lower bond order and, consequently, to a weaker bond. Although all the examples presented in the table correspond to longer bonds in the excited state, it is possible to

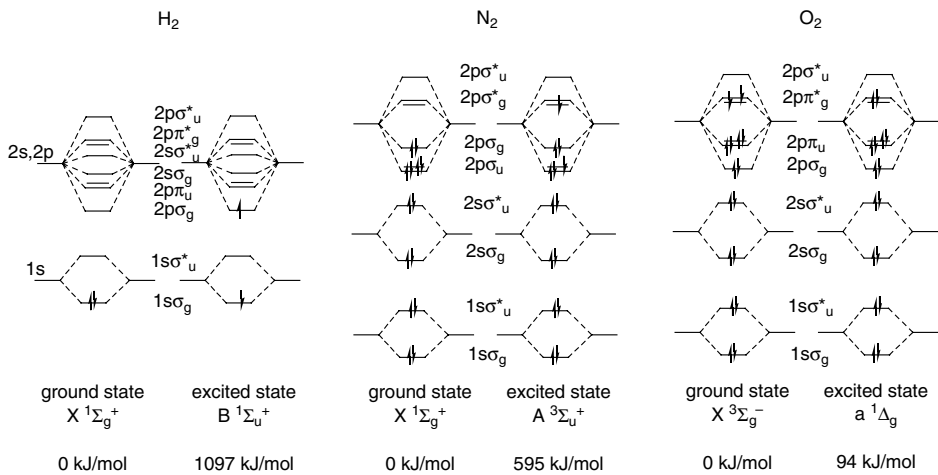


**Figure 15.8** Poisson distribution for different values of the parameter  $S$ . The number of peaks in the spectrum increases when the geometry of the excited state differs more significantly from that of the ground state.

**Table 15.1**

Spectroscopic constants of molecular oxygen ( $\mu = 8.000$ ), nitrogen ( $\mu = 7.004$ ) and hydrogen ( $\mu = 0.5041$ )

Molecule	Electronic state	$\bar{v}$ (cm $^{-1}$ )	$R_e$ (Å)	$f$ (kJ mol $^{-1}$ Å $^{-2}$ )
O <sub>2</sub>	X $^3\Sigma_g^-$	1580	1.2074	$7.086 \times 10^3$
O <sub>2</sub>	a $^1\Delta_g$	1509	1.2155	$6.463 \times 10^3$
N <sub>2</sub>	X $^1\Sigma_g^+$	2358	1.0976	$13.817 \times 10^3$
N <sub>2</sub>	A $^3\Sigma_u^+$	1460	1.293	$5.296 \times 10^3$
H <sub>2</sub>	X $^1\Sigma_g^+$	4395	0.7416	$3.455 \times 10^3$
H <sub>2</sub>	B $^1\Sigma_u^+$	1357	1.2927	$0.329 \times 10^3$

**Figure 15.9** Electronic configurations of the electronic states indicated for O<sub>2</sub>, N<sub>2</sub> and H<sub>2</sub>.

find excited states with shorter bonds, when the electronic transition corresponds to the excitation of an anti-bonding electron. The table also reveals that changes in bond lengths are associated with changes in force constants, and that the approximations used to obtain eq. (15.64) are not very realistic. However, Figure 15.10 shows that, using the average value for  $S$  obtained with the data for the two electronic states and eq. (15.64), the Franck–Condon factors calculated with the harmonic model are in reasonable agreement with the more exact values calculated with Morse oscillators [8,9]. The largest discrepancies are observed for the transition between the electronic states of N<sub>2</sub> considered in this example.

The same principles can be used to simulate the absorption, fluorescence and phosphorescence spectra of polyatomic molecules. In such cases the changes of the bond lengths are not generally known and the progression of the vibronic bands is used to extract the value of  $S$ . It then represents the collective relative change in the bond lengths associated with the electronic excitation. An additional difficulty is that the absorption spectrum in condensed phases, at room temperature, is not a series of narrow peaks. Rather, it is made of absorption bands with an appreciable width. The width of these bands (described as the

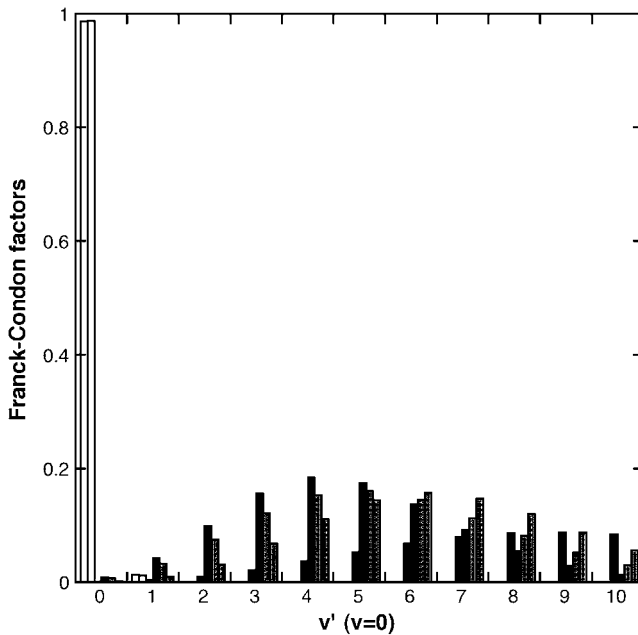


**Figure 15.10** Franck–Condon factors calculated using Morse or harmonic oscillators for the  $X^3\Sigma_g^-$  to a  $^1\Delta_g$  transition in  $O_2$  (white bars),  $X^1\Sigma_g^+$  to  $A^3\Sigma_u^+$  transition in  $N_2$  (black bars) and  $X^1\Sigma_g^+$  to  $B^1\Sigma_u^+$  transition in  $H_2$  (shaded bars). In each set, the first bar refers to the Morse oscillator and the second to the harmonic oscillator.

inhomogeneous broadening) is related to the distribution of molecular energies within each electronic level as well as to interactions with the medium (or solvent). It can be assumed that the translational and rotational motions originate a continuum of energy at the temperatures under consideration. Under this assumption, it is reasonable to describe the energy distribution by a Gaussian function. Thus, the absorption spectrum can be simulated by a sum of the peaks corresponding to the vibronic transitions, each one of them multiplied by a Gaussian that reflects the continuous distribution of energy  $\varepsilon$  within each vibrational level and fitted to the experimental bandwidth,

$$\alpha(\varepsilon) = \sum_{v'=0}^{\infty} \exp[-S_A] \frac{S_A^{v'}}{v'!} \frac{1}{\sqrt{2\pi\sigma_A^2}} \exp\left\{-\frac{[(E'_0 - E_0) + v'\hbar\omega_A - \varepsilon]^2}{2\sigma_A^2}\right\} \quad (15.68)$$

Identically, for the emission from  $v' = 0$  of an electronically excited state to the vibronic levels of the ground electronic state

$$\iota(\varepsilon) = \sum_{v=0}^{\infty} \exp[-S_D] \frac{S_D^v}{v!} \frac{1}{\sqrt{2\pi\sigma_D^2}} \exp\left\{-\frac{[(E'_0 - E_0) - v\hbar\omega_D - \varepsilon]^2}{2\sigma_D^2}\right\} \quad (15.69)$$

where  $E_0$  and  $E'_0$  are the energies of the ground and excited states in their lowest vibrational levels, respectively.

Figure 15.11 illustrates the simulation of normalised anthracene absorption and fluorescence spectra using eqs. (15.68) and (15.69), respectively. This figure also illustrates the singlet–triplet absorption of anthracene measured as the triplet excitation spectrum of a single crystal of the anthracene [10]. The excitation spectrum was obtained by observing the intensity of blue fluorescence as a function of the wavelength of the exciting light, because the direct singlet–triplet absorption is strongly forbidden. For the same reason, the phosphorescence was measured in a hydrocarbon matrix at 77 K, although a room-temperature spectrum of anthracene has also been measured in ultrapure and de-oxygenated cyclohexane [11]. The energies of the excited states ( $E'_0 - E_0$ ), the frequencies of the vibrational progressions  $\omega$ , the widths of the vibronic bands  $2\sigma$ , and the values of  $S$  that reflect the relative intensities of the vibronic bands were adjusted to fit the absorption as well the fluorescence spectra. The best fit to the experimental spectra requires a higher excited-state energy for the absorption ( $E_S = 316 \text{ kJ mol}^{-1}$ ) than for the fluorescence ( $E_S = 313 \text{ kJ mol}^{-1}$ ).

In condensed phases, a difference between the spectral positions of the band maxima (or the band origin) of the absorption and fluorescence arising from the same electronic origin are very frequently observed. In most cases, the fluorescence maximum occurs at a lower wavenumber than the absorption and their difference is called Stokes shift. Anthracene is amenable to the treatment of its vibronic progressions using a single vibrational frequency whose value is much greater than the width of the vibronic bands. Under these conditions, it is possible to identify both the  $0' \leftarrow 0$  transition in absorption and the corresponding  $0 \leftarrow 0'$  band in fluorescence. The Stokes shift measured as the difference between these band maxima,  $200 \text{ cm}^{-1}$ , is probably due to the solvent relaxation. However, in many systems, several vibrational progressions are associated with the electronic excitation and

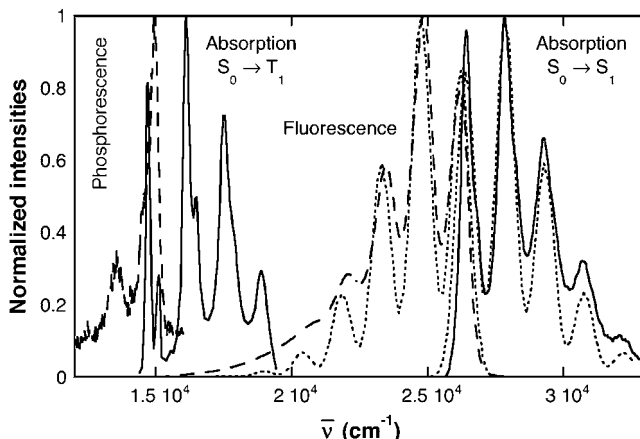


**Figure 15.11** Absorption and emission spectra of anthracene. These are at room temperature, except for the phosphorescence that was measured at 77 K. The singlet–triplet absorption is the triplet excitation spectrum in single-crystal anthracene. The dotted lines are the simulated absorption ( $E_S = 26,400 \text{ cm}^{-1}$ ,  $\sigma_A = 350 \text{ cm}^{-1}$ ,  $S_A = 1.18$ ,  $\bar{v}_A = 1450 \text{ cm}^{-1}$ ) and fluorescence ( $E_S = 26200 \text{ cm}^{-1}$ ,  $\sigma_D = 350 \text{ cm}^{-1}$ ,  $S_D = 1.18$ ,  $\bar{v}_D = 1450 \text{ cm}^{-1}$ ) spectra.

their overlap leads to the observation of only one broad band for the absorption and another one for the fluorescence, in transitions between the same electronic states. In such cases, the Stokes shift has quantum contributions from the vibrational progressions and classical contributions from the solvent relaxation.

Empirically, the singlet-state energy is best determined from the intersection between normalised absorption and fluorescence spectra. The same principle could be applied to the triplet energy, but this is not usually feasible because the singlet-to-triplet absorption is very difficult to observe. Alternatively, the triplet energy is estimated from the origin of the phosphorescence spectrum. Non-spectroscopic techniques, such as photoacoustic calorimetry, often provide a better estimate of the triplet energies.

## 15.5 RADIATIONLESS TRANSITION WITHIN A MOLECULE

The Franck–Condon factors discussed above are relevant for radiative transitions from the lowest vibrational level of the initial state to a series of vibrational levels of the final state. In each radiative transition, the exact energy difference between the two states is either supplied or released by photons. Radiationless transitions must also conserve energy, but cannot use photons for their energy balance. Internal conversion takes place from the lowest vibrational level of the  $S_1$  state to isoenergetic, very high vibrational levels of the  $S_0$  state. It has already been indicated that there is a very large density of vibrational states of  $S_0$  at the energy of  $S_1$ . The same applies to the inter-system crossing from  $T_1$  to  $S_0$ . Jortner and Ulstrup [12] showed that for isothermal transfers and for sufficiently high temperatures, the Franck–Condon factor, which represents the overlap between the ground vibrational wavefunction of the initial state and the vibrational wavefunction of the final electronic state, takes the form

$$J_0 = \frac{1}{\hbar\omega} \frac{1}{\sqrt{2\pi S \coth(\hbar\omega/2k_B T)}} \exp\left[-\frac{\sqrt{2\mu}}{\hbar} \sqrt{\Delta E^\ddagger} d \tanh(\hbar\omega/4k_B T)\right] \quad (15.70)$$

For the unfavourable case of a CH stretching vibration,  $\omega = 5.65 \times 10^{14}$  sec $^{-1}$ ,  $\tanh(\hbar\omega/4k_B T) = 0.9986$  at  $T = 298$  K and the exponential term is identical to that of the tunnelling transmission probability through a barrier formed by intersecting parabolas, eq. (6.37). This demonstrates that the Franck–Condon vibrational overlap factors, which determine the rates of molecular group nuclear-tunnelling processes, can be expressed in terms of a tunnelling rate.

The first calculation of Franck–Condon factors in terms of nuclear tunnelling preceded this formal demonstration [13]. Using the WKB approximation for tunnelling through intersecting parabolas, the tunnelling rate can be expressed as

$$k_{\text{WKB}} = \chi v \exp\left[-\frac{\sqrt{2\mu}}{\hbar} \sqrt{D - E_v} \Delta x\right] \quad (15.71)$$

where  $\chi$  is the electronic forbidden factor ( $\chi \ll 1$  for non-adiabatic transitions),  $v$  is the frequency of the vibrational mode attempting the transition,  $\mu$  its reduced mass,  $D - E_v$  is

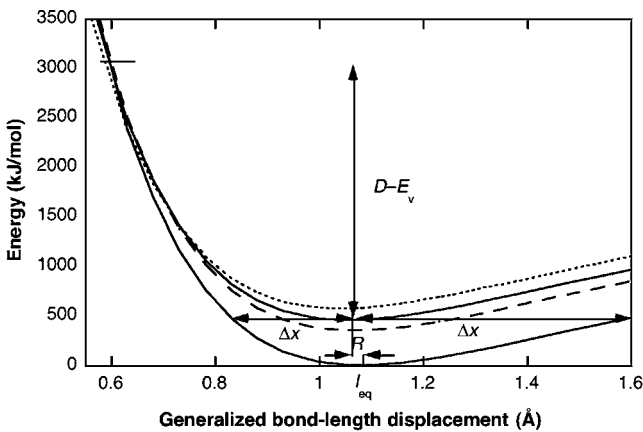


**Figure 15.12** Anharmonic potential energy curves of the generalised CH vibrational modes of benzene in the ground state, first singlet state (solid line), second singlet state (dotted line) and first triplet state (dashed line). The tunnelling barrier width,  $\Delta x$ , is indicated for the repulsive as well as the attractive sides. The height of the tunnelling barrier in the repulsive side,  $D - E_v$ , is measured from the bottom of the  $S_1$  state to its crossing with the  $S_0$  state. The tunnelling barrier in the attractive side is the generalised CH bond dissociation energy.

the barrier height and  $\Delta x$  the barrier width illustrated in Figure 15.12. This figure represents the generalised CH vibrational modes of benzene. In the process of converting a polyatomic molecule into a diatomic molecule,  $C_1H_1$ , it is convenient to define the relative number of atoms involved in the transition as  $\eta = n_H/(n_H + n_C)$  where  $n_H$  and  $n_C$  are the number of hydrogen and carbon atoms, respectively [14]. As a first approximation, the contribution of the CC bonds to the internal conversion or inter-system crossing is neglected, and the effective vibration is  $\eta/0.5$  times smaller than the CH stretching mode. The corresponding barrier width is  $0.5/\eta$  times smaller and, according to the tunnel effect theory (TET) [13,15,16], eq. (15.18) is modified to

$$k_{\text{TET}} = \gamma v \exp \left[ -\frac{\sqrt{2\mu_{\text{CH}}}}{\hbar} \sqrt{D - E_v} \frac{\Delta x}{2\eta} \right] \quad (15.72)$$

Clearly, for benzene eq. (15.72) is identical to eq. (15.71), but for the other aromatic hydrocarbons, the relative number of CH modes is somewhat lower and the rate is reduced.

The minima of the CH bonds represented in this figure in their  $S_0$  and  $S_1$  states are displaced because each CH bond contracts by  $\Delta r \approx 0.01$  Å upon electronic excitation. This contraction directs the crossing of the curves to their repulsive side. McCoy and Ross [17] expressed the electronic transitions in polycyclic aromatic hydrocarbons in terms of a bond-length displacement coordinate  $\Delta R$ ,

$$\Delta R = \left( \sum_j \Delta r_j^2 \right)^{1/2} \quad (15.73)$$

where  $\Delta r_j$  denotes the change in the length of the  $j$ th bond. This gives approximately  $\Delta R = 0.025 \text{ \AA}$  for benzene, which is representative of the other aromatic hydrocarbons because the increase in the number of bonds is probably associated with a smaller CH bond contraction of each bond. The crossing between the generalised CH vibrational modes can now be calculated from the intersection of their Morse curves

$$D_{e,\text{CH}} \left\{ 1 - \exp \left[ -\beta(l - l_{\text{eq,CH}}) \right] \right\}^2 = D_{e,\text{CH}} \left\{ 1 - \exp \left[ -\beta(l - (l_{\text{eq,CH}} - R)) \right] \right\}^2 + E_{S_1} \quad (15.74)$$

knowing the excitation energy and the CH Morse curve parameters of Appendix III. The width of the barrier is given by the displacement of the ground-state curve at the energy of  $S_1$ . The reaction frequency, for a fully allowed process ( $\chi = 1$ ) is just that of the CH frequency,  $\nu = 9.0 \times 10^{13} \text{ sec}^{-1}$ . However, there is one final detail before the internal conversion rates of aromatic hydrocarbons can be calculated: the Morse curve must be adapted to describe the generalised mode.

It has long been recognised that the role played by CH stretching vibrations in radiationless transitions of aromatic molecules is better described in terms of local rather than normal modes of vibration [18]. The concept of a normal mode arises from the analysis of vibrational motions for infinitesimal amplitudes. However, reactivity is most often associated with large vibrational amplitudes. The concept of local modes derives from an analysis of vibrational motion for such large amplitudes. For higher energies, the molecules oscillate according to a pattern that is closer to a local mode than to a normal mode. The vibrational energy of polyatomic molecules is evenly distributed among a number of equivalent chemical bonds and the bond-dissociation energy is much greater than the dissociation energy of one of these bonds. Henry and Siebrand [19] showed that the stretching overtone spectrum of benzene is accurately reproduced assuming that the six local CH bonds of benzene vibrate independently. Additionally, Formosinho [20] showed that in the treatment of local modes as independent oscillators, the generalised CH vibration is expressed by a force constant  $f_{\text{CH}}\sqrt{n_{\text{H}}}$ , as shown in eq. (8.29) and Figure 8.8. Given the relation between the force constant and the Morse parameter,  $f = 2D_e\beta^2$ , the generalised CH bond-dissociation energy can be written as

$$D_{e,\text{CH}} = \sqrt{n_{\text{H}}} D_e \quad (15.75)$$

where  $D_e$  is the bond-dissociation energy of a CH bond, given in Appendix III. With the Morse parameters for the CH bond of benzene, its singlet-state energy and  $\Delta R = 0.025 \text{ \AA}$ , the intersection of the curves in eq. (15.74) occurs at  $D - E_v = 2.63 \times 10^3 \text{ kJ mol}^{-1}$ . The width of the barrier at  $E_{S_1} = 459 \text{ kJ mol}^{-1}$  is  $\Delta x = 0.247 \text{ \AA}$  and the Franck–Condon factor for eq. (15.72) is  $3 \times 10^{-11}$ . Assuming a fully allowed transition,  $\chi\nu = 9.0 \times 10^{13} \text{ sec}^{-1}$ , the calculated internal conversion rate is  $3 \times 10^3 \text{ sec}^{-1}$ . The contribution of tunnelling in the repulsive side is lower than the experimental value,  $4 \times 10^4 \text{ sec}^{-1}$  [21], because the internal conversion in benzene has an equally important contribution from the attractive side. This is not seen for the other aromatic hydrocarbons represented in Figure 15.13, because of their higher  $D_{e,\text{CH}}$  values and lower excited state energy. Figure 15.13 also shows the results obtained with similar calculations for the internal conversions from the  $S_2$  to  $S_1$  states and inter-system crossing from  $T_1$  to  $S_0$  [16]. The displacements between these

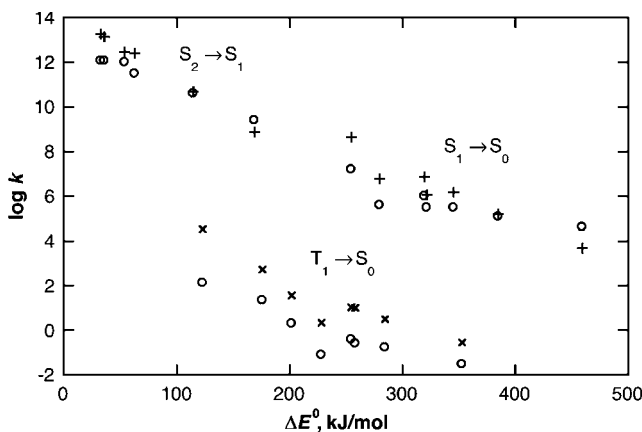


**Figure 15.13** Calculated (crosses and plus signs) and experimental (open symbols) internal conversion rates in benzene, naphthalene, phenanthrene, anthracene, pyrene, coronene, tetracene and azulene. The calculated inter-system crossing rates from  $T_1$  to  $S_0$  were multiplied by  $\chi = 10^{-6}$ .

curves are expected to be smaller than that between  $S_1$  and  $S_0$ . Consequently,  $\Delta R = 0.015 \text{ \AA}$  was employed. The inter-system crossing rate was calculated with the non-adiabatic factor suggested by Kasha ( $\chi = 10^{-6}$ ). However, the calculations show that the non-adiabaticity is even stronger,  $\chi < 10^{-6}$ .

Internal conversion and inter-system crossing rates exhibit a free-energy dependence which is remarkably different from those of the reactions discussed in the previous chapters. As the exothermicity of the internal conversion increases, its rate becomes smaller. This is known as the *energy-gap law* of radiationless transitions [22].

## 15.6 TRIPLET-ENERGY (OR ELECTRON) TRANSFER BETWEEN MOLECULES

Whereas in internal conversions and inter-system crossings only one molecule is involved, in energy (or electron) transfers one species donates energy (or an electron) while another accepts it. Each of these species must be represented by curves such as those of Figure 15.7, describing its initial and final electronic states. For simplicity, the discussion below addresses directly the case of a triplet energy transfer through the Dexter mechanism, but the same reasoning also applies to electron transfers.

The transfer of energy is subject to the restrictions of the Franck–Condon principle (a vertical transition, where the nuclei remain in their initial positions as the electron is transferred) and to the conservation of energy (the energy decrease in one molecule is identical to the simultaneous energy increase in the other one). Figure 15.14a shows that for two identical molecules, which necessarily have the same triplet energy, these conditions are only met for a small fraction of the donor and acceptor molecules. This was also illustrated by the experimental data for anthracene in Figure 15.11. As the triplet energy of the acceptor decreases and the triplet energy transfer becomes more exothermic, there is a

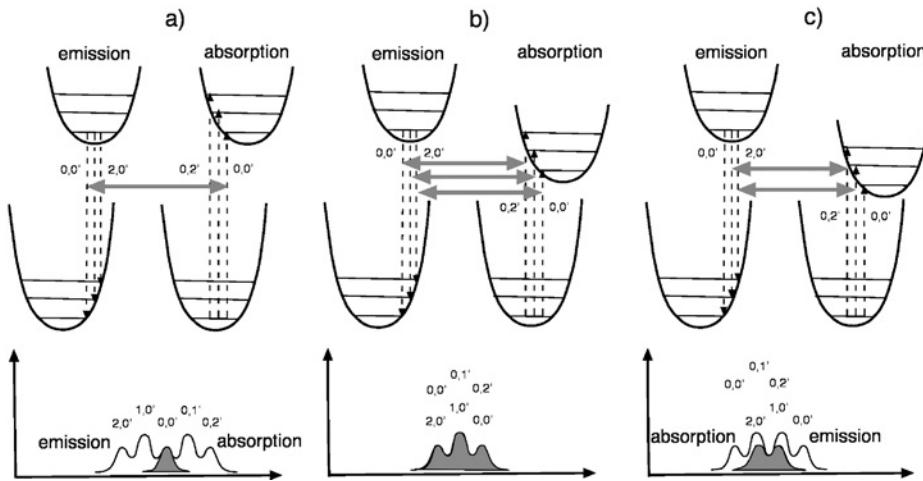


**Figure 15.14** Correspondence between the transfer of energy from an electronically excited donor to an acceptor in its ground state (upper diagrams) and the corresponding emission and absorption spectra. Only the coupled transitions identified in the upper diagrams conserve energy and may occur. (a) Transfer between identical molecules. (b) Exothermic transfer that maximises the spectral overlap. (c) Highly exothermic transfer, beyond the optimal spectral overlap.

better overlap between the donor emission and the acceptor absorption spectra. This overlap goes through a maximum, shown in Figure 15.14b, and then decreases for even more exothermic reactions (Figure 15.14c). This latter situation is similar to that of the energy-gap law.

The simplest way to calculate the transfer rate from the initial state  $s$  to the final state  $k$  is to use the classical expression for the transfer rate at a given energy  $E$  such that  $E > \Delta E^\ddagger$ , where  $\Delta E^\ddagger$  is the energy of the crossing point between the two states. Such an expression is the product between the probability of conversion at the crossing point ( $P_{ks}$ ) and the frequency of passage over the crossing point

$$w(E) = 2vP_{ks} \quad (15.76)$$

There is a factor of 2 in this expression because the energetic condition  $E > \Delta E^\ddagger$  requires that the turning point of the vibration exceeds the distortion to attain the crossing point,  $|x_v| > |x^\ddagger|$ , such that the conversion between the two states is attempted twice during each vibrational motion.

The classical probability of transition probability was first formulated by Landau and Zener [23,24], and was presented in eq. 5.53. Using the notation of this chapter

$$P_{ks} = \frac{2\pi}{\hbar} |V_{ks}^e|^2 \frac{1}{r|s_s - s_k|} \quad (15.77)$$

where  $r = dx/dt$  is the velocity of passage over the crossing point at  $x^\ddagger$ , and  $s_s$  and  $s_k$  the slopes of the potential energy curves describing the initial and final states at that point,  $dV(x^\ddagger)/dx$ ,

respectively. For the specific case of electronic states represented by unidimensional harmonic oscillators with the same force constant  $f$ , the difference between the slopes is

$$|s_s - s_k| = \left| \frac{d}{dx} \left( \frac{1}{2} f x^2 \right) - \frac{d}{dx} \left[ \frac{1}{2} f (d-x)^2 - \Delta E^0 \right] \right| = fd \quad (15.78)$$

The velocity of the vibrational motion of this oscillator is defined as the length travelled per unit time. Given the classical amplitude of the oscillation with an energy  $E$

$$x_v = \sqrt{\frac{2E}{\mu\omega^2}} \quad (15.79)$$

the velocity of passage over  $x^\ddagger$  is

$$r = \omega \sqrt{(x_v)^2 - (x^\ddagger)^2} \quad (15.80)$$

Rearranging the above expressions leads to the expression for the rate of transfer at an energy  $E > \Delta E^\ddagger$

$$w(E) = \frac{2}{\hbar} |V_{ks}|^2 \frac{1}{\sqrt{fd^2} \sqrt{f[(x_v)^2 - (x^\ddagger)^2]}} \quad (15.81)$$

The actual classical transfer rate at a given temperature  $T$  requires averaging over a Boltzmann distribution of energies

$$w = \frac{\int_E^\infty w(E) e^{-E/k_B T} dE}{\int_0^\infty e^{-E/k_B T} dE} \quad (15.82)$$

This procedure yields a compact result because

$$\int_0^\infty e^{-E/k_B T} dE = k_B T \quad (15.83)$$

and eq. (15.79) can be used to express the other integral involved as

$$\int_{\Delta E^\ddagger}^\infty (E - \Delta E^\ddagger)^{-1/2} e^{-E/k_B T} dE = \sqrt{\pi k_B T} e^{-\Delta E^\ddagger/k_B T} \quad (15.84)$$

The resulting expression

$$w = \frac{2\pi}{\hbar} |V_{ks}|^2 \frac{1}{\sqrt{2\pi f d^2 k_B T}} \exp\left(-\frac{\Delta E^\ddagger}{k_B T}\right) \quad (15.85)$$

can be further modified using the quadratic relation between the energy barriers and the reaction energies, discussed in Chapter 7, eq. (7.6),

$$(\Delta E^0 - \lambda)^2 = 4\lambda\Delta E^\ddagger \quad (15.86)$$

and associating the reorganisation energy with the displacement between the curves representing the electronic states (Figure 15.7),

$$\lambda = \frac{1}{2} f d^2 \quad (15.87)$$

The final expression for the *classical rate for triplet-triplet (or electron) transfer*,

$$w = \frac{2\pi}{\hbar} |V_{ks}^e|^2 \frac{1}{\sqrt{4\pi\lambda k_B T}} \exp\left[-\frac{(\Delta E^0 - \lambda)^2}{4\lambda k_B T}\right] \quad (15.88)$$

must be regarded with the caution that follows from the numerous approximations involved in its derivation. First, the problem of energy transfer between molecules is multi-dimensional, whereas in deriving the above expression only one effective frequency was used. Second, the Landau-Zener probability is only valid when  $|V_{ks}^e| \ll 1/\mu r^2$ , that is, for an electronic coupling of 5 kJ mol<sup>-1</sup> the reorganisation energy must exceed 20 kJ mol<sup>-1</sup>, which involves a difficult balance between having enough adiabaticity and at the same time a transfer rate that is competitive with the radiative lifetime. Third, the quadratic relation between the energy barriers and reaction energies must be obeyed. Finally, the classical model assumes that the electronic states cross at a given energy, used to define the activation energy  $\Delta E^\ddagger$ , but in fact there are two molecules (and four electronic states) in the reactants, and as many in the products. The crossing point is not rigorously defined and is replaced by the reorganisation energy defined in eq. (15.87), where it is assumed that all the electronic states have the same frequency  $\omega$ . However, the value of  $\lambda$  is not calculated from the energy of the crossing point, but from the displacement of the electronic states in each species (Figure 15.7).

A more fundamental approach to the problem of energy transfer can be made by writing the classical probability distribution for the donor in the excited state that takes the form at  $R$

$$v(R) = \left( \frac{f}{2\pi k_B T} \right)^{1/2} \exp\left(-\frac{f(R - R_e)^2}{2k_B T}\right) \quad (15.89)$$

This has a clear analogy with the wavefunction of the harmonic oscillator at its ground vibrational state, eq. (15.59). The energy transfer involves a vertical transition between the two energy curves of the donor. Given  $v(R)$ , the distribution of energies associated with the donor,  $\iota(\epsilon')$ , which represents the energies required to transfer the triplet energy from the donor, is

$$\iota(\epsilon') = \frac{1}{\sqrt{2\pi\sigma_D^2}} \exp\left[-\frac{(\epsilon' + E_D - \lambda_D)^2}{2\sigma_D^2}\right] \quad (15.90)$$

where  $E_D$  is the triplet energy of the donor,  $\sigma_D^2 = k_B T/f$  the square of the standard deviation of the respective Gaussian distribution and  $\lambda_D$  the difference between the energy of the

triplet state in its equilibrium geometry and the energy it would have in that state at the equilibrium configuration of the ground state eq. (15.87). The centre of the Gaussian distribution is placed at the ground-state equilibrium configuration of the donor, with an energy  $E_D - \lambda_D$  that is lower than its triplet energy (Figure 15.15) [25]. This displacement is related to the difference between the nuclear configuration of the initial triplet state and the final ground state of the donor. This energy difference,  $\lambda_D$ , is the reorganisation energy of the donor. A similar spectrum can be formulated for the ground-state acceptor,

$$\alpha(\varepsilon) = \frac{1}{\sqrt{2\pi\sigma_A^2}} \exp\left[-\frac{(\varepsilon + E_A + \lambda_A)^2}{2\sigma_A^2}\right] \quad (15.91)$$

where  $E_A$  is the triplet energy of the acceptor and  $\lambda_A$  its reorganisation energy.

Mathematically, the possibility that the energy taken from the donor is between  $\varepsilon'$  and  $\varepsilon' + d\varepsilon'$ , is  $\iota(\varepsilon')d\varepsilon'$  and the possibility that the energy given to the acceptor is between  $\varepsilon$  and  $\varepsilon + d\varepsilon$ , is  $\alpha(\varepsilon)d\varepsilon$ . To conserve energy in the process, the transfer from a particular energy  $\varepsilon'$  in the donor distribution  $\iota(\varepsilon')$  must be paired with the transfer in the acceptor distribution  $\alpha(\varepsilon)$  of the same energy. In Figure 15.15 this corresponds to a horizontal process. Mathematically, the probability of transition with  $\varepsilon'$  between  $\varepsilon'$  and  $\varepsilon' + d\varepsilon'$  and  $\varepsilon$  between  $\varepsilon$  and  $\varepsilon + d\varepsilon$ , is  $\iota(\varepsilon')d\varepsilon'\alpha(\varepsilon)d\varepsilon$ , with  $\varepsilon' = \varepsilon$ . The density of states in eq. (15.36) is this probability per unit of energy. Thus, dividing the probability of transition by one of the energy intervals, and integrating over the other one, gives the total density of states

$$J = \int_{-\infty}^{+\infty} \iota(\varepsilon) \alpha(\varepsilon) d\varepsilon = \frac{1}{2\pi\sqrt{\sigma_D^2 \sigma_A^2}} \int_{-\infty}^{+\infty} \exp\left[-\frac{(\varepsilon + E_D - \lambda_D)^2}{2\sigma_D^2} - \frac{(\varepsilon + E_A + \lambda_A)^2}{2\sigma_A^2}\right] d\varepsilon \quad (15.92)$$

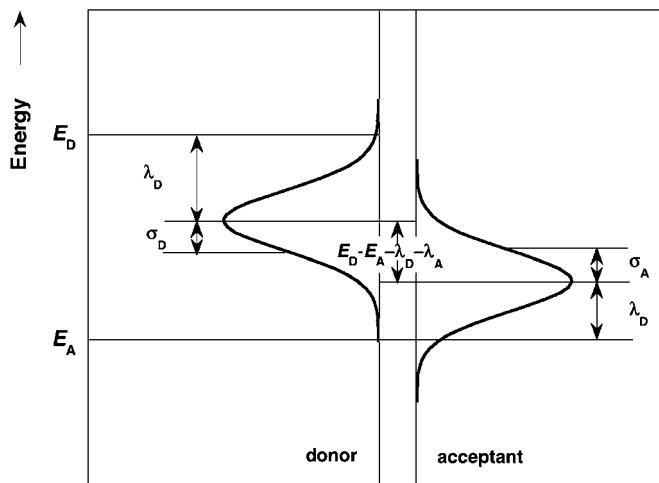


**Figure 15.15** Probability distribution of energies required for triplet energy transfer from a donor to an acceptor. The conservation of energy requires that the transfer is a horizontal process in this diagram, and the nuclear coordinates must pre-organise accordingly.

If we make the substitution

$$\begin{aligned} a &= -\lambda_A - E_A \\ d &= \lambda_D - E_D \end{aligned} \quad (15.93)$$

the exponential term can be rewritten

$$\exp\left\{-\frac{[\varepsilon-a]^2}{2\sigma_A^2}-\frac{[\varepsilon-d]^2}{2\sigma_D^2}\right\}=\exp\left[\frac{\sigma_A^2 a + \sigma_D^2 d}{\sigma_A^2 \sigma_D^2} \varepsilon - \frac{\sigma_A^2 + \sigma_D^2}{2\sigma_A^2 \sigma_D^2} \varepsilon^2\right] \exp\left(-\frac{\sigma_A^2 a^2 + \sigma_D^2 d^2}{2\sigma_A^2 \sigma_D^2}\right) \quad (15.94)$$

to indicate the presence of the standard integral

$$\int_{-\infty}^{+\infty} e^{c_1 x - c_2 x^2} dx = \sqrt{\pi/c_2} \exp\left[\frac{c_1^2}{4c_2}\right] \quad (15.95)$$

and express the overlap integral in a more compact form

$$J = \int_{-\infty}^{+\infty} \iota(\varepsilon) \alpha(\varepsilon) d\varepsilon = \frac{1}{\sqrt{4\sigma^2 \pi}} \exp\left\{-\frac{[\Delta E^0 - \lambda]^2}{4\sigma^2}\right\} \quad (15.96)$$

where  $\sigma^2 = (\sigma_D^2 + \sigma_A^2)/2$ ,  $\lambda = \lambda_D + \lambda_A$ , and the reaction energy is the difference between the triplet energies of the donor and the acceptor,  $\Delta E^0 = E_D - E_A$ .

Introducing this Franck-Condon weighted density of states in the Golden Rule, gives

$$w = \frac{2\pi}{\hbar} |V_{ks}^e|^2 \frac{1}{\sqrt{4\sigma^2 \pi}} \exp\left[-\frac{(\Delta E^0 - \lambda)^2}{4\sigma^2}\right] \quad (15.97)$$

This expression for the Golden Rule is identical to the classical expression, eq. (15.88), when  $\sigma^2 = \lambda k_B T$ . However, it was initially formulated as  $\sigma^2 = k_B T/f$ . This difference can be solved with the transformation

$$\sigma^2 = \frac{\hbar\omega}{2f} \coth\left(\frac{\hbar\omega}{2k_B T}\right) \quad (15.98)$$

which approaches  $\lambda k_B T$  at high temperatures ( $k_B T \gg \hbar\omega/2$ ) and  $k_B T/f$  at low temperatures ( $k_B T \ll \hbar\omega/2$ ). In view of this connection between a classical behaviour at high temperatures and the temperature independence at low temperatures, eq. (15.97) is a *semi-classical rate for triplet-triplet energy (or electron) transfer* [26]. This formulation takes the reorganisation energy of the donor as the difference in its energy when in the triplet state, but having the same geometry as the ground state. This is the Stokes shift between the maxima of the emission and absorption envelopes of the donor, without specific consideration of the vibronic bands. The same applies to the acceptor. Hence, this reorganisation energy includes the vibrational as well as solvent contributions to the Stokes shift.

The semi-classical rate is a significant improvement in the definition of the reaction coordinate for triplet energy transfer. It relates the reorganisation energy of each reactant to the displacement of the corresponding initial and final states along the reaction coordinate, without having to assume the presence of a crossing between the reactive states. It is also less restrictive on the size of the electronic coupling. However, the connection between the high and low temperatures was introduced in an *ad hoc* fashion, and does not recognise that vibronic transitions change the overlap substantially. Further improvement in the treatment of the quantum effects can be achieved with a quantum-mechanical formulation.

The full quantum-mechanical treatment of the vibrations coupled to the changes of the electronic state is rather sophisticated. A convenient simplification is to consider only one vibrational mode for the donor,  $\omega_D$ , and another one for the acceptor,  $\omega_A$ . This is a dramatic simplification, but the result can be generalised to multi-mode processes using a suitable procedure. Another simplification is the classical treatment of the low-frequency modes, attributed to the medium and to low vibrational frequencies of the reactants and products. This is a good approximation if  $\hbar\omega \ll k_B T$ . For example,  $\bar{v} < 100 \text{ cm}^{-1}$  corresponds to a spacing of  $< 1 \text{ kJ mol}^{-1}$  between the vibrational levels, which is less than the thermal energy at room temperature,  $RT = 2.5 \text{ kJ mol}^{-1}$ . A difference of  $200 \text{ cm}^{-1}$  between the simulation of the anthracene absorption and emission was found in Figure 15.11.

For a system with the restrictions mentioned above, the Franck–Condon factor for triplet energy transfer combines the description of the vibrational levels done by eqs. (15.68) and (15.69), with the reorganisation energies included in eqs. (15.90) and (15.91). Integrating as in eq. (15.92), gives

$$J_{v',v} = \frac{1}{\sqrt{4\pi\sigma^2}} \sum_{v=0}^{\infty} \sum_{v'=0}^{\infty} e^{-S_D} e^{-S_A} \frac{S_D^{v'}}{v'!} \frac{S_A^v}{v!} \exp \left[ -\frac{(\Delta E^0 - \lambda + v'\hbar\omega_D + v\hbar\omega_A)^2}{4\sigma^2} \right] \quad (15.99)$$

where

$$\sigma^2 = \frac{\sigma_D^2 + \sigma_A^2}{2} = (\lambda_D + \lambda_A)k_B T = \lambda k_B T \quad (15.100)$$

as a consequence of the approximation made for the low frequency modes. The overlap integral  $J_{v',v}$  is also known as the Franck–Condon weighted density of states. The corresponding triplet energy transfer rate is

$$w = \frac{2\pi}{\hbar} |V_{ks}^e|^2 \frac{1}{\sqrt{4\pi\sigma^2}} \sum_{v=0}^{\infty} \sum_{v'=0}^{\infty} e^{-S_D} e^{-S_A} \frac{S_D^{v'}}{v'!} \frac{S_A^v}{v!} \exp \left[ -\frac{(\Delta E^0 - \lambda + v'\hbar\omega_D + v\hbar\omega_A)^2}{4\sigma^2} \right] \quad (15.101)$$

Setting  $\omega_D = \omega = \omega_A$ ,  $\sigma_D = \sigma = \sigma_A$  and  $S = S_D + S_A$  gives, after some algebraic manipulations, the result

$$w = \frac{2\pi}{\hbar} |V_{ks}^e|^2 \frac{1}{\sqrt{4\pi\lambda k_B T}} \sum_{v=0}^{\infty} e^{-s} \frac{S^v}{v!} \exp \left[ -\frac{(\Delta E^0 - \lambda + v\hbar\omega)^2}{4\lambda k_B T} \right] \quad (15.102)$$

This expression for the *quantum-mechanical rate for triplet energy (or electron) transfer* remains numerically indistinguishable from eq. (15.101) even when  $\omega_D$  and  $\omega_A$  differ by as much as 10% [27].

The overlap between the vibronic bands of the reactants and products is illustrated in Figure 15.16 [25]. This representation is inspired by the model developed by Marcus [28,29] for electron transfer, which will be discussed in detail in Chapter 16. The curve for the reactants represents the potential energy of the system when the donor is in the triplet state and the acceptor in the ground state. The product curve represents the system when the donor is in the ground state and the acceptor in the triplet state. The Franck–Condon principle requires that the nuclear configuration is the same immediately after the transfer, that is, the transfer is vertical. Conservation of energy requires that the transfer is horizontal. The only possible way to meet both requirements is at the crossing point. However, the reaction coordinate should have as many dimensions as there are degrees of freedom for nuclear motion in the system, and the crossing point is, in fact, a large ensemble of

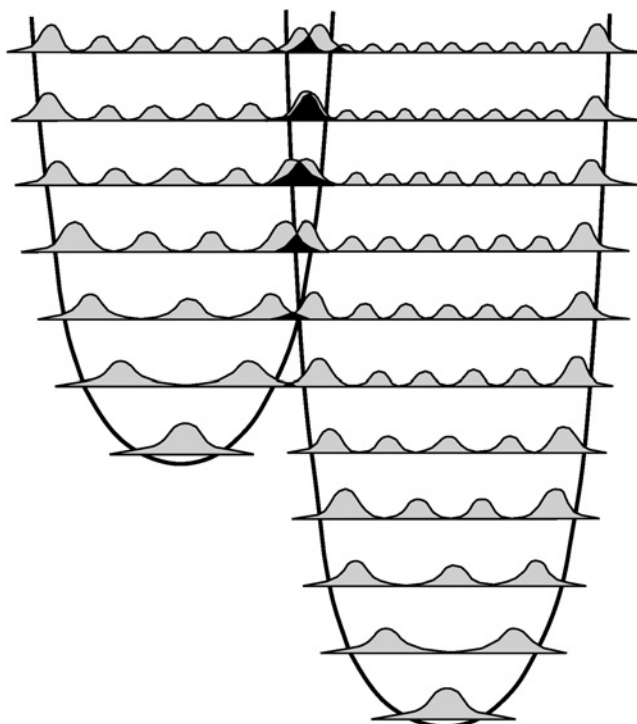


**Figure 15.16** Nuclear motion accompanying triplet energy transfers, emphasising the quantum nature of the vibrational modes. The vibrational energy levels are shown with the squares of the vibrational wavefunctions superimposed on them. The reaction coordinate represents a combination of the positions of all the nuclei disturbed by the electronic transition, as it evolves from the reactants (excited donor and ground-state acceptor) to the products (ground-state donor and excited acceptor).

nuclear configurations. Some of these are represented in Figure 15.14, which gives a more exact microscopic description of the energy transfer process.

The expression obtained for the quantum-mechanical rate is based on the description of the initial and final states of the electronic transition as displaced harmonic oscillators. Additionally, the derivation was based on a single vibrational mode for each reactant. It was assumed that an average vibrational frequency could describe the modes that promote the electronic transition and accept the excess energy released in the course of that transition. However, a more detailed analysis of the absorption and emission bands of the aromatic hydrocarbons that are most amenable to simulations with displaced harmonic oscillators, reveals that even these systems have “shoulders” in the main progression bands, which are probably associated with other vibrational modes. Figure 15.17 shows the overlap between the fluorescence of naphthalene and the absorption of anthracene modelled with the high-frequency progression band discussed above, but it is evident that a subsidiary medium-frequency band, probably associated with CCC bending vibrations, is also present.

For these multi-mode processes it is still possible to employ the average-mode approximation [27,30], and take  $S$  as the sum of the  $S_j$  values for the coupled high- and medium-frequency vibrations

$$S = \sum_j S_j \quad (15.103)$$

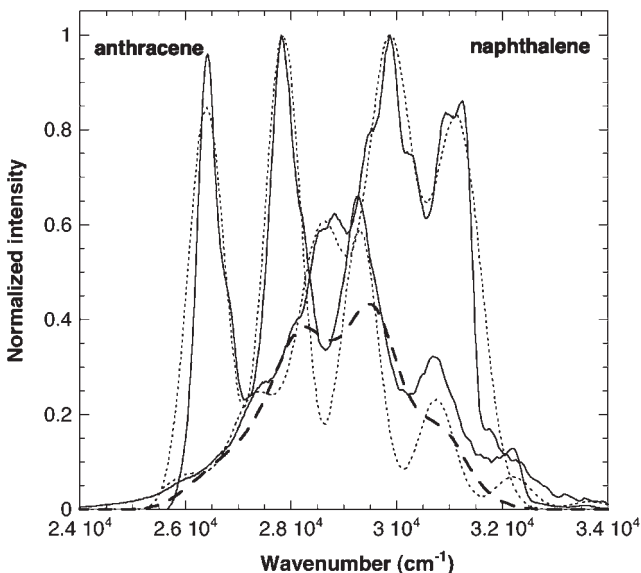


**Figure 15.17** Normalised fluorescence of naphthalene ( $E_S = 31150 \text{ cm}^{-1}$ ) and absorption of anthracene ( $E_S = 26400 \text{ cm}^{-1}$ ), modelled by one vibrational mode each. Naphthalene:  $\bar{v}_D = 1420 \text{ cm}^{-1}$ ,  $\sigma_D = 150 \text{ cm}^{-1}$ ,  $S_D = 0.82$ ; Anthracene:  $\bar{v}_D = 1450 \text{ cm}^{-1}$ ,  $\sigma_D = 150 \text{ cm}^{-1}$ ,  $S_D = 0.70$ . Solid lines: experimental spectra; dotted lines: simulated spectra; dashed line: calculated spectral overlap.

and  $\hbar\omega$  as the weighted average of the quantum spacing

$$\hbar\omega = \frac{\sum_j S_j \hbar\omega_j}{\sum_j S_j} \quad (15.104)$$

The average-mode approximation combines the vibrational progressions needed for a better simulation of absorption and emission spectra. Unfortunately, for triplet-energy (and electron) transfers the relevant singlet–triplet absorption and phosphorescence (or charge-transfer bands) are rarely available for such simulations. It should also be noted that bimolecular transfer rates tend to be controlled by diffusion when the overlap is large, and that for small overlaps minor errors in the simulation of the spectra lead to large errors in  $J_{v',v}$ . Moreover, when the reaction energies exceed 60 kJ mol<sup>-1</sup>, the higher frequency modes such as the CH stretching vibrations become better energy acceptors than the CC modes, and the information carried by the absorption and fluorescence spectra is of little use. Finally, highly exothermic reactions result in the population of highly excited vibrational levels, as illustrated in Figure 15.14, and these are strongly anharmonic. The participation of additional accepting modes in the reaction coordinate and the increased anharmonicity of the accepting modes as the reactions become more exothermic make it very unlikely that the reorganisation energy is independent of the reaction energy.

The observation of large deuterium isotope effects is a good diagnostic for the participation of CH or other bonds to hydrogen in the reaction coordinate for energy or electron transfer. The paradigmatic example is the quenching of O<sub>2</sub>(<sup>1</sup>Δ<sub>g</sub>) in solution. The bimolecular rate constant of radiationless deactivation of singlet oxygen drops from  $4.3 \times 10^3$  M<sup>-1</sup> sec<sup>-1</sup> in H<sub>2</sub>O to  $2.6 \times 10^2$  M<sup>-1</sup> sec<sup>-1</sup> in D<sub>2</sub>O, a KIE of 16.5. The rate is further reduced to 0.75 M<sup>-1</sup> sec<sup>-1</sup> in perfluorodecalin, a solvent without C–H bonds. This spectacular effect is due to the deactivation by coupled vibronic O<sub>2</sub>(<sup>1</sup>Δ<sub>g</sub>, v' = 0 → v' = m) and vibrational X–H(v = 0 → v = n) transitions [31]. Charge recombinations between aromatic hydrocarbons and tetracyanoethylene have much smaller KIE, usually not exceeding a factor of 2, with the particularity that the deuteration of methyl hydrogens in methylated benzene donors gives a larger KIE than that of phenyl hydrogens [32].

Absorption and fluorescence are usually registered using a continuous irradiation of the sample, that is, in steady-state conditions. It is also possible to measure both absorption and fluorescence intensities at different wavelengths as a function of time. Ware and co-workers [33] followed the fluorescence spectra after excitation on the nanosecond timescale, and observed a redshift of the fluorescence maxima as a function of time. Ultra-fast techniques have more recently been employed to measure the time-dependence of absorption and fluorescence spectra, and confirmed the generality of this phenomenon for charge-transfer transitions in condensed phases, known as the “dynamic Stokes shift”.

The time evolution of the fluorescence spectrum of a suitable probe molecule, following excitation by an ultra-short optical pulse, can be used to monitor the dynamic Stokes shift response function

$$S(t) = \frac{\bar{v}(t) - \bar{v}(\infty)}{\bar{v}(0) - \bar{v}(\infty)} \quad (15.105)$$

where  $\bar{v}(x)$  represents the peak of the fluorescence spectrum at times  $t$ , zero and infinity. Expressed in this way, the frequencies need not be referenced to their (usually unknown) gas-phase values. This function carries information on the polar solvation dynamics. The fastest processes develop on a 10 fsec timescale and correspond to the intra-molecular relaxation of high-frequency modes. These processes remain very difficult to follow, such that on the scale of tens of femtoseconds and extending to the picoseconds, there is a continuous shift of the fluorescence spectrum to the red as solvent relaxation proceeds. Solvation is non-exponential in time, and cannot be interpreted with only one time constant. This is in conflict with the description of the dielectric constant of polar solvents by the frequency dependence of the Debye dispersion [34]

$$\varepsilon(\omega) = \varepsilon_{\text{op}} + \frac{\varepsilon - \varepsilon_{\text{op}}}{1 - i\omega\tau_D} \quad (15.106)$$

where  $\varepsilon$  and  $\varepsilon_{\text{op}} (= n_D^{-2})$  are the static and optical (infinite) frequency dielectric constants and  $\tau_D$  is the Debye relaxation time. This simple model of a polar solvent as a dielectric continuum predicts a single exponential shift of the fluorescence spectrum with a time constant approximately equal to the solvent longitudinal relaxation time  $\tau_L = (\varepsilon_{\text{op}}/\varepsilon)\tau_D$ , whereas the dynamic Stokes shifts reveal several time constants, some of which are considerably shorter than  $\tau_L$ . Water is a particularly “fast” solvent, with >50% of the solvation response happening within the first 50 fsec [35], which corresponds roughly to  $660 \text{ cm}^{-1}$  in frequency. This should be compared with  $\tau_D = 8.2 \text{ psec}$ ,  $\varepsilon_{\text{op}} = 4.21$ ,  $\varepsilon = 78.3$  and  $\tau_L = 440 \text{ fsec}$  for water. The ultra-fast relaxation of water was assigned to the vibrational (rotational) motions of the water molecule. It has a particular incidence on preventing the re-crossing of the reaction free-energy barrier, because it shows that water can stabilise the reaction products before they may re-cross to the reactants and reduce the reaction rate. However, the description of the full range of  $S(t)$  requires additional frequencies. In water, some of these frequencies are associated with the hindered translation of the hydrogen-bonded network ( $180 \text{ cm}^{-1}$ ), the hydrogen-bonding bend ( $60 \text{ cm}^{-1}$ ), and the diffusive motions ( $2\text{--}10 \text{ cm}^{-1}$ ). In fact, the entire dielectric dispersion spectrum of  $\varepsilon(\omega)$  must be considered in the simulation of  $S(t)$ , including the low-frequency part, which is well described by the Debye formula, and the high-frequency part, which contains various contributions from inter- and intra-molecular vibrational modes of the solvent. Fleming and co-workers employed seven frequencies in the range indicated above to reproduce the dynamic Stokes shift that they observed in water [36].

The subsequent processes take place from the lowest vibrational level of the first singlet state and have already been discussed. One additional point to take into consideration is that internal conversion leaves the ground state with an excess of heat, which may correspond to temperatures in excess of 1000 K. Its cooling occurs within 1–10 psec, with the shorter times associated with polar molecules in polar environments [37].

Another experimental method to probe the Franck–Condon excited state is resonance Raman spectroscopy. Recall that Raman scattering is an inelastic process entailing a transition to a virtual or real molecular state (or sum of states), and a nominally instantaneous return to the ground state, but in a higher or lower vibrational state. In resonance Raman spectroscopy the incident radiation nearly coincides with the frequency of the electronic transition of the sample. Only a few vibrational modes contribute to the scattering of the

radiation, which simplifies the Raman spectrum and enhances its intensity. The modes that show resonance Raman activity are the same as those that are Franck–Condon active in the electronic transition, and their degree of enhancement is related to their displacement upon formation of the excited state. Consequently, the analysis of vibrational Raman lines obtained in resonance with charge-transfer transitions can, in principle, reveal the complete set of mode-specific reorganisation energies associated with the charge separation or recombination accompanying the electronic transition [38,39]. This technique has been applied to many charge transfers, in particular, in transition-metal complexes and in organic donor–acceptor complexes. A widely used transition-metal complex that has been studied using resonance Raman spectroscopy is the Ru(bpy)<sub>3</sub><sup>2+</sup> complex in water. Fourteen totally symmetric vibrational modes were found to be active in the metal-to-ligand charge transfer, with frequencies ranging from 283 to 1608 cm<sup>-1</sup>. The total reorganisation energy was divided among these modes, including metal–ligand stretching and bending modes, and ligand (bipyridine) localised modes. The hexamethylbenzene–tetracyanoethylene (HMB–TCNE) complex is a typical example of organic donor–acceptor complexes studied by resonance Raman spectroscopy. There are some differences in the reported results among the several groups that have studied this system, but more than 10 vibrational modes are associated with the electronic transition [32,40,41]. The high-frequency modes seem to be the most populated, but the very low frequency donor–acceptor mode at 165 cm<sup>-1</sup> is also strongly populated. The contribution of the solvent and of each vibrational mode to the total reorganisation energy  $\lambda$  remains unsettled. In CCl<sub>4</sub>, where the contribution of the solvent to the reorganisation energy should be very small,  $\lambda$  values between 45 and 56 kJ mol<sup>-1</sup> were proposed [32,40]. These values of  $\lambda$  do not include the contributions from the CH bonds, that are necessary to explain the KIE mentioned above, but could not be assessed from the resonance Raman spectra.

The picture emerging from ultra-fast techniques and resonance Raman spectroscopy is that a large spectrum of solvent frequencies, extending to 1000 cm<sup>-1</sup> in water, and a large number of vibrational frequencies, down to 165 cm<sup>-1</sup> in donor–acceptor complexes, contribute to the energy barrier of electron and triplet-energy transfers in solution. A detailed description of these transfers requires the quantum treatment of a very large number of vibrational modes and a wide dielectric dispersion spectrum for the solvent. Jortner [42] presented a multi-mode formalism and compared its results for the HMB–TCNE complex using nine modes, with the average-mode approximation and with a model using a high single mode with the same reorganisation energy as the multi-mode. The average-mode approximation underestimates the Franck–Condon factor when the reaction exothermicity exceeds 85 kJ mol<sup>-1</sup>. In contrast, a high-frequency single mode combined with the correct reorganisation energy gives a good account of the Franck–Condon factors. The lesson to be learnt is that even an incomplete model that is good enough to reproduce the relevant absorption and emission spectra is also adequate to calculate the Franck–Condon factors. The calculation of the electron or triplet-energy transfer rates additionally requires an estimate of the electronic coupling.

## 15.7 ELECTRONIC COUPLING

The factor  $(4\sigma^2\pi)^{-1/2}$  included in eq. (15.101) is associated with the coupling between the electronic and the nuclear motions. Consequently, it cannot be exclusively assigned to the

nuclear or to the electronic factor. This factor is expressed in per unit of energy and when associated with  $|V_{ks}^e|^2$  and with  $2\pi/\hbar$ , gives the electronic factor in per second, that is, as a frequency.

To relate the electronic coupling to the molecular parameters, it is necessary to return to eq. (15.37) and express the wavefunction of the ground ( $\Psi_1$ ) and excited ( $\Psi_2$ ) states in terms of the wavefunctions of the initial and final unperturbed states,  $\psi_s$  and  $\psi_k$ , respectively. The resolution of this simple two-state problem captures the physics of the electronic coupling. The interaction between the unperturbed wavefunctions is expressed as two linear combinations of  $\psi_s$  and  $\psi_k$ , corresponding to the ground and excited states  $\Psi_1$  and  $\Psi_2$ , of energies  $E_1$  and  $E_2$ , where  $E_1 < E_2$ ,

$$\begin{aligned}\Psi_1 &= c_s \psi_s + c_k \psi_k \\ \Psi_2 &= c_s \psi_s - c_k \psi_k\end{aligned}\quad (15.107)$$

The coefficients of the linear combinations are normalised ( $c_s^2 + c_k^2 = 1$ ). When the overlap integral is zero ( $S_{ks} = \langle \psi_k | \psi_s \rangle = 0$ ), the energies of the adiabatic states are given by the secular determinant

$$\begin{vmatrix} V_{ss} - E & V_{ks} \\ V_{ks} & V_{kk} - E \end{vmatrix} = 0 \quad (15.108)$$

where  $V_{ss}$  and  $V_{kk}$  are the energies of the initial and final unperturbed states, respectively, and  $V_{ks}^e$  is the electronic matrix element coupling the two non-adiabatic states. The roots of this determinant are

$$\begin{aligned}E_1 &= \frac{V_{ss} + V_{kk}}{2} - \frac{\left[ \Delta_{ks}^2 + 4(V_{ks}^e)^2 \right]^{1/2}}{2} \\ E_2 &= \frac{V_{ss} + V_{kk}}{2} + \frac{\left[ \Delta_{ks}^2 + 4(V_{ks}^e)^2 \right]^{1/2}}{2}\end{aligned}\quad (15.109)$$

where  $\Delta_{ks} = (V_{kk} - V_{ss}) \geq 0$ . The difference between the adiabatic and non-adiabatic energies is

$$(E_2 - E_1)^2 = \Delta_{ks}^2 + 4(V_{ks}^e)^2 \quad (15.110)$$

Knowing the adiabatic energies  $E_1$  and  $E_2$ , the coefficients  $c_s$  and  $c_k$  can be calculated from the equations

$$\begin{aligned}\begin{pmatrix} V_{ss} - E_1 & V_{ks}^e \\ V_{ks}^e & V_{kk} - E_1 \end{pmatrix} \begin{pmatrix} c_s \\ c_k \end{pmatrix} &= 0 \\ \begin{pmatrix} V_{ss} - E_2 & V_{ks}^e \\ V_{ks}^e & V_{kk} - E_2 \end{pmatrix} \begin{pmatrix} -c_k \\ c_s \end{pmatrix} &= 0\end{aligned}\quad (15.111)$$

Following the convention that  $E_2 \geq E_1$ , these equations give:

$$\begin{aligned} E_1 &= V_{ss} - \left| \frac{c_k}{c_s} V_{ks}^e \right| = V_{kk} - \left| \frac{c_s}{c_k} V_{ks}^e \right| \\ E_2 &= V_{ss} + \left| \frac{c_s}{c_k} V_{ks}^e \right| = V_{kk} + \left| \frac{c_k}{c_s} V_{ks}^e \right| \end{aligned} \quad (15.112)$$

and the product of the two mixing coefficients is related to the electronic coupling matrix element

$$|c_s c_k| = \frac{|V_{ks}^e|}{E_2 - E_1} \quad (15.113)$$

This is an important relation because it is possible to express the factor  $|c_s c_k|$  as a function of the spectroscopic parameters of charge-transfer reactions. When the degree of charge transfer approaches unity, these are effectively the electronic couplings of electron-transfer reactions. The electronic couplings of electron transfer can later be related to those of the triplet-energy transfers and the kinetic description of such processes in terms of molecular parameters can be completed. The only approximation involved in the derivation of this relation for a two-state system is the orthonormality of the electronic states involved ( $S_{ks} = 0$ ).

There are two important classes of spectroscopic transitions where an electronic transition is associated with a full charge transfer within a molecule or a complex: inter-valence absorption bands and charge-transfer (exciplex with full charge transfer) emission. The most pronounced inter-valence bands are found in mixed-valence complexes and were first described by Taube, who received the Nobel Prize in 1983 for his work on the mechanisms of electron-transfer reactions. Mixed-valence complexes are characterised by the presence of two metal centres in different oxidation states separated by a bridging ligand. One of the earliest examples of a stable mixed-valence complex is the Creutz–Taube ion illustrated in Figure 15.18. Its inter-valence band is observed at 1570 nm. Figure 15.18 also shows a rhenium complex where a similar optical electron transfer occurs. In this case the inter-valence band is associated with the optical transfer of an electron from the py-PTZ ligand to the 4,4'-(CH<sub>3</sub>)<sub>2</sub>bpy ligand separated by  $\approx 6$  Å. Its inter-valence band is characterised by  $\bar{\nu}_{\max} = 1.99 \times 10^4$  cm<sup>-1</sup>,  $\varepsilon_{\max} = 2.4$  M<sup>-1</sup> cm<sup>-1</sup> and  $\Delta \bar{\nu}_{1/2} = 3.50 \times 10^3$  cm<sup>-1</sup> [43].

The other type of charge-transfer band is fluorescence from an exciplex, when it has a high degree of charge transfer. An exciplex is a complex formed between an electron donor and an electron acceptor, normally with one of them in the S<sub>1</sub> state. The fingerprint of exciplex formation is the observation of a broad and structureless emission, redshifted relative to the emission of the molecular components of the exciplex. The stability of the exciplex comes from the mixture of pure locally excited, charge transfer and ground states

$$\Psi_{ex} = c_{le} \Psi_{le} [A D^*] + c_{ct} \Psi_{ct} [A^\bullet - D^{\bullet+}] + c_{gs} \Psi_{gs} [A D] \quad (15.114)$$

where  $c_{le}$ ,  $c_{ct} \gg c_{gs}$ . A high degree of charge separation,  $c_{ct} \gg c_{le}$ , requires that the following conditions are met: the exciplex fluorescence is weak ( $\Phi_F < 0.15$ ), the separation

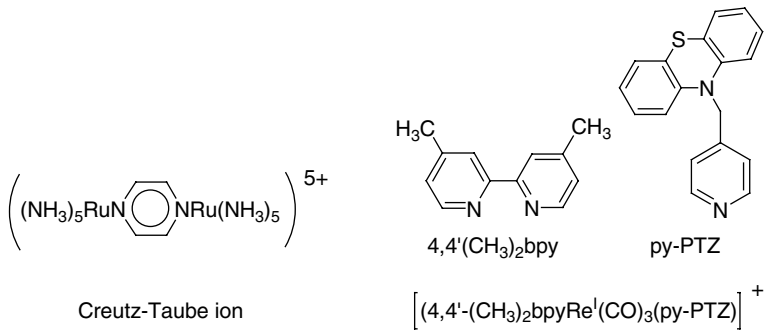


**Figure 15.18** Complexes that show inter-valence bands and ligand-to-ligand charge transfer absorption bands.

between the exciplex and molecular emission ( $>5000 \text{ cm}^{-1}$ ) and the dipole moment of the exciplex ( $\mu_{\text{ex}}$ ) are large. The magnitude of  $\mu_{\text{ex}}$  depends on the charge-separation distance. For example, exciplexes formed between aromatic hydrocarbons and other planar molecules typically have a separation of 3.3 Å between their planes, and for this separation, a full charge separation has  $\mu_{\text{ex}} = 16 \text{ D}$ . These conditions are met in the exciplex formed between excited pyrene and fumaronitrile, which is characterised by  $\Phi_F = 0.10$ ,  $\bar{v}_{\text{ex}} = 2.2 \times 10^4 \text{ cm}^{-1}$ ,  $\mu_{\text{ex}} = 19 \text{ D}$ , and a lifetime of 18 nsec in heptane [44].

The intensity of the absorption bands is given by eq. (15.38), and the electric dipole moment by eq. (15.37). Replacing the wavefunctions of this equation by those of eq. (15.54), yields

$$\begin{aligned} \vec{\mu}_{12} &\equiv c_s c_k (\vec{\mu}_k - \vec{\mu}_s) \\ \vec{\mu}_s &\equiv -e \left\langle \psi_s \sum \vec{r}_i \psi_s \right\rangle \\ \vec{\mu}_k &\equiv -e \left\langle \psi_k \sum \vec{r}_i \psi_k \right\rangle \end{aligned} \quad (15.115)$$

when  $S_{ks} = 0$  and  $\vec{\mu}_{ks} = 0$ . Under this approximation and recognising that the difference between the dipole moments of the unperturbed states is

$$(\vec{\mu}_k - \vec{\mu}_s) = e \Delta r \quad (15.116)$$

where  $\Delta r$  is the distance separating the electron donor and acceptor moieties, eqs. (15.113) and (15.22) lead to

$$\frac{\vec{\mu}_{12}}{e} \equiv \frac{|V_{ks}^e| \Delta r}{h v_{\max}} \quad (15.117)$$

The oscillator strength defined in eq. (15.38) can now be expressed as

$$f_{\text{ks}} = 1.085 \times 10^{-5} \frac{|V_{\text{ks}}^e|^2 (\Delta r)^2}{\bar{v}_{\text{max}}} \quad (15.118)$$

Its relation to the absorption bands was established in eq. (15.3). When the shape of such a band can be described by a Gaussian curve, as is approximately the case of intra-valence bands, the integral can be obtained analytically

$$\int \varepsilon(\bar{v}) d\bar{v} = \sqrt{\frac{\pi}{4 \ln(2)}} \varepsilon_{\text{max}} \Delta \bar{v}_{1/2} \quad (15.119)$$

and the expression for the oscillator strength is reduced to

$$f_{\text{ks}} = 4.61 \times 10^{-9} \varepsilon_{\text{max}} \Delta \bar{v}_{1/2} \quad (15.120)$$

The numerical values of the expressions above apply when  $\varepsilon_{\text{max}}$  is expressed in per molar per centimetre, the bandwidth at half-height is expressed in per centimetre and  $\Delta r$  is in angstrom.

It is now possible to relate the electronic coupling with the properties of the absorption band combining eqs. (15.118) and (15.120),

$$|V_{\text{ks}}^e|^2 = \frac{4.3 \times 10^{-4} \varepsilon_{\text{max}} \Delta \bar{v}_{1/2} \bar{v}_{\text{max}}}{(\Delta r)^2} \quad (15.121)$$

Using the data obtained by Meyer and co-workers for the ligand-to-ligand charge-transfer absorption bands of the complex represented in Figure 15.18 gives  $V_{\text{ks}}^e = 45 \text{ cm}^{-1}$  ( $= 0.53 \text{ kJ mol}^{-1}$ ). This value of the electronic coupling is within the limits required by radiationless transition theories.

Combining eq. (15.117) with eqs. (15.37) and (15.41), leads to a compact expression relating the electronic coupling to the charge-transfer emission band

$$|V_{\text{ks}}^e|^2 = \frac{3h^3 c^3 k_F}{64\pi^4 v_{\text{max}} (\Delta\mu)^2} \quad (15.122)$$

This expression is more useful when it explicitly includes the factors associated with the refractive index of the medium  $n_D$ , and the vacuum permittivity  $(4\pi\varepsilon_0)^{-1}$ ,

$$|V_{\text{ks}}^e|^2 = \frac{3\varepsilon_0 h^3 c^3 k_F}{16\pi^3 n_D^3 \bar{v}_{\text{max}} (\Delta\mu)^2} = 3.0 \times 10^6 \frac{k_F}{n_D^3 \bar{v}_{\text{max}} (\Delta\mu)^2} \quad (15.123)$$

where the numerical value applies when the frequency of the maximum emission is expressed in per centimetre, the fluorescence rate is in per second and the change in dipole moment is in debye. Using the data for the pyrene/fumaronitrile exciplex emission in heptane ( $n_D = 1.385$ ) mentioned earlier and using eq. (15.44) to estimate the fluorescence rate

constant, gives  $V_{\text{ks}}^e = 890 \text{ cm}^{-1}$  ( $= 10.6 \text{ kJ mol}^{-1}$ ). The value of  $V_{\text{ks}}^e$  for the emission of an exciplex ( $\Delta r = 3.3 \text{ \AA}$ ) with a nearly complete charge transfer is 20 times larger than that of  $V_{\text{ks}}^e$  for the ligand-to-ligand ( $\Delta r = 6 \text{ \AA}$ ) charge-transfer absorption. The increase in the donor–acceptor separation by  $2.7 \text{ \AA}$  decreases the electronic coupling by a factor of 400 and the rate should decrease by a factor of  $1.6 \times 10^5$ .

The distance dependence of the electronic factor was explored in detail by Closs and co-workers [45–47]. Using a 4-biphenyl or a 4-benzophenyl group as the donor, connected via a rigid spacer with a 2-naphthyl group, as illustrated in Figure 15.19, it was possible to demonstrate that the rate constants of intra-molecular long-range electron, hole and triplet-energy transfers can be written in the form

$$k = k_0 \exp[-\beta(\Delta r)] \quad (15.124)$$

where  $\Delta r$  is specifically the edge-to-edge separation between the donor and the acceptor, and the rate constant at contact  $k_0$  includes the contribution of the Franck–Condon factors, presumed constant along the reaction series. Additionally, the distance-dependent coefficient for triplet-energy transfers was shown to be equal to the sum of the corresponding coefficients for the electron and hole transfers,  $\beta_{\text{te}} = \beta_{\text{el}} + \beta_{\text{hl}}$ . This is the experimental confirmation that the Dexter mechanism of triplet-energy transfer can be viewed as a simultaneous double-electron exchange.

The problem of electron or triplet-energy transfer through a rigid spacer is similar to that of a particle in a double-well potential (Figure 15.20). This has an exact quantum-mechanical solution. The resolution of the Schrödinger equation for this system gives a splitting of the energy levels in the two potential wells owing to the tunnelling of the electron through the barrier. The splitting is

$$E_2 - E_1 = 8 \frac{E\Phi}{E + \Phi} \frac{1}{1 + \Gamma l} \exp[-\Gamma(\Delta r)] \quad (15.125)$$

where  $l$  is the size of the potential well,  $E$  the energy of the electron,  $\Phi$  the height of the barrier and

$$\Gamma = \frac{1}{\hbar} \sqrt{2m_e \Phi} \quad (15.126)$$

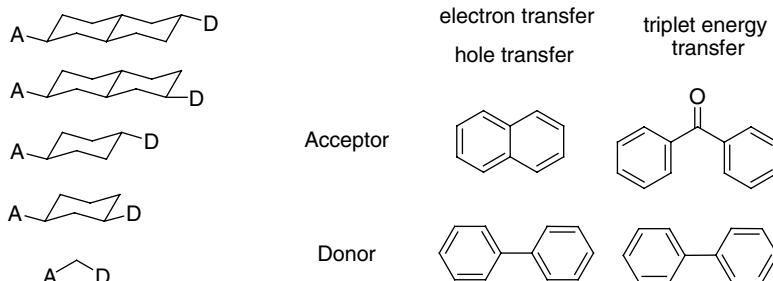


**Figure 15.19** Molecular structures of some covalently linked donor–acceptor systems.

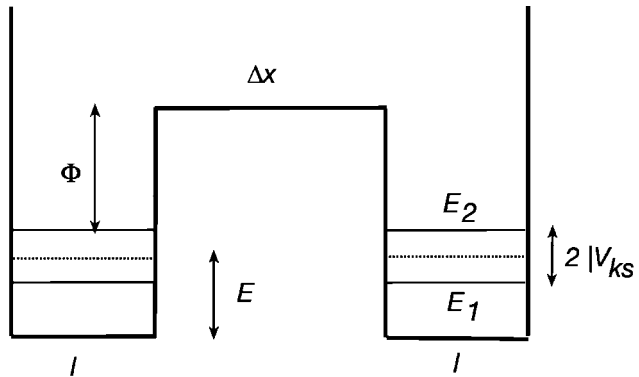


**Figure 15.20** Double square-potential well, with symmetrical wells of length  $l$  separated by a barrier of height  $\Phi$  and edge-to-edge distance  $\Delta x$ .

The size of the potential well and the energy of the electron are related. For cata-condensed aromatic hydrocarbons, Platt [48] proposed a simple relation

$$E = \frac{\hbar^2}{2ml} n^2, \quad n = 0, 1, 2, \dots \quad (15.127)$$

where  $l$  is the perimeter of the aromatic system. For example, the triplet state energy of anthracene,  $228 \text{ kJ mol}^{-1}$ , corresponds to a perimeter  $l = 23.9 \text{ \AA}$ , which is a rather realistic value.

The electronic coupling of the symmetric wells is related to the splitting

$$|V_{\text{ks}}^e| = \frac{E_2 - E_1}{2} \quad (15.128)$$

and gives

$$|V_{\text{ks}}^e|^2 = \left( 4 \frac{E\Phi}{E + \Phi} \frac{1}{1 + \Gamma l} \right)^2 \exp[-2\Gamma(r - r_0)] \quad (15.129)$$

Typically, the electronic barrier is  $\Phi = 3 \pm 1 \text{ eV}$ . This, together with the parameters of naphthalene calculated above and the factor  $2\pi/\hbar$  of the Golden Rule, gives a relatively constant pre-exponential factor, which is typical for aromatic hydrocarbons,

$$\frac{2\pi}{\hbar} \left( 4 \frac{E\Phi}{E + \Phi} \frac{1}{1 + \Gamma l} \right)^2 = (5.4 \pm 0.1) \times 10^{14} \text{ eV sec}^{-1} \quad (15.130)$$

The Franck–Condon factor can be expressed in per electron volt and the resulting transfer rate is in per second. This pre-exponential factor is approximately equal to the frequency of the electronic movement in an aromatic hydrocarbon,  $v_{\text{el}} = 10^{15} \text{ sec}^{-1}$ . Another way of arriving at essentially the same formulation is to describe the distance dependence of

electron transfer as the tunnelling of the electron from the donor to the acceptor, through a square-potential barrier, eq. (6.46).

$$v = v_{\text{el}} \exp[-\beta(\Delta r)] \quad (15.131)$$

where  $\beta = 2\Gamma$ .

In the gas phase, the height of the barrier in eq. (15.126) is the ionisation energy of the donor, or, in the original scanning transmission microscopy experiments [49,50], the average work functions of the metal surface and probe. In an electron transfer between rigidly linked donor-acceptor systems, the height of the barrier is the difference between the energy of the electron in the donor and in the medium separating it from the acceptor, because the electron tunnels through matter and the decay of its wavefunction with the distance from the edge of the classically allowed region depends on the properties of that matter. The energy difference between the electron at rest in vacuum and the electron in the donor ( $\Phi_0$ ) is simple to calculate from the reduction potential of the donor versus NHE or versus SCE, knowing that the absolute potentials of NHE and SCE are  $\Phi_0(\text{NHE})=4.44$  eV and  $\Phi_0(\text{SCE})=4.71$  eV. Some examples of such calculations are shown in Figure 15.21. A simple correction for the stabilisation of the energy of the electron tunnelling through matter is [51]

$$\Phi = \frac{\Phi_0}{\varepsilon_{\text{op}}} \quad (15.132)$$

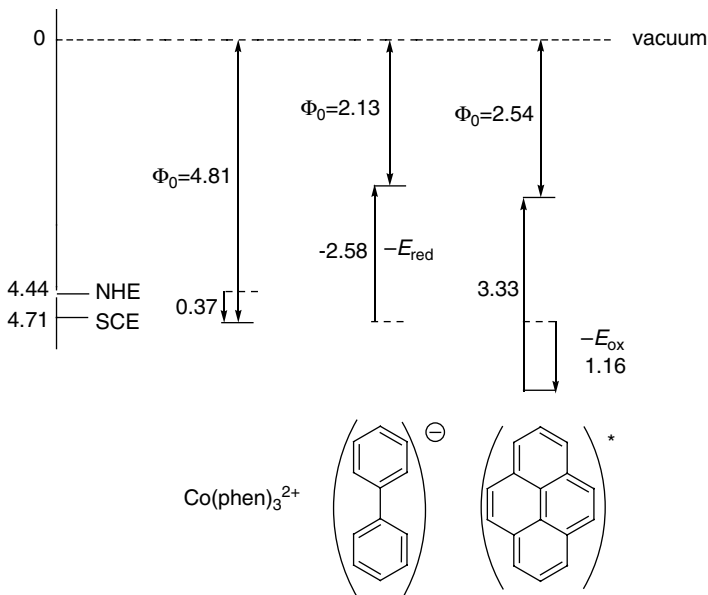


**Figure 15.21** Calculation of the barrier height for electron tunnelling through vacuum, using  $E^0 = 0.37$  V versus NHE for  $\text{Co}(\text{phen})_3^{2+/\beta^+}$ ,  $E^{\text{red}} = -2.58$  V versus SCE for biphenyl, and  $E^{\text{ox}} = 1.16$  V versus SCE for pyrene together with  $E_{\text{S}1} = 3.33$  eV.

since only the optical dielectric constant of the medium separating the electron donor and acceptor,  $\epsilon_{\text{op}} = (n_D)^2$ , is fast enough to follow the electronic transition itself. These equations together lead to

$$v = v_{\text{el}} \exp \left[ -\frac{2}{\hbar} \sqrt{2m_e \frac{\Phi_0}{n_D^2}} \Delta r \right] = v_{\text{el}} \exp \left[ -1.025 \frac{\sqrt{\Phi_0}}{n_D} \Delta r \right] \quad (15.133)$$

where the constant applies when the electron barrier is expressed in electron volts and the distances in angstrom.

The relation of the electron-tunnelling decay coefficient to molecular properties of the reactants and, in particular, to the energy of the electron in the donor, is often obscured by the difficulty of separating the Franck–Condon factors from the electronic factors. Changing the donor with the purpose of changing the energy of the electron and testing the energy dependence of the electronic factor also changes the Franck–Condon factor of the reaction. However, Figure 15.14 shows that there is a reaction energy that maximises the Franck–Condon factor. Krongauz [52] used the free-energy dependence of the Franck–Condon factors to select, from a variety of acceptors, the species that maximise the Franck–Condon factor of each donor. The couples of optimised nuclear factors were then selected for the distance-dependence study in 2-methyltetrahydrofuran (MTHF) glass at 77 K. The results are shown in Figure 15.22, together with the electron-tunnelling decay

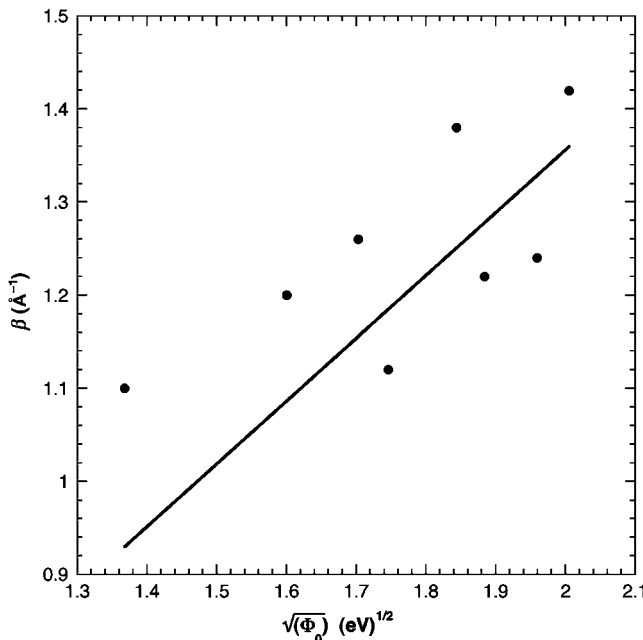


**Figure 15.22** Experimental and calculated distance-dependence of the electronic factor as a function of the energy of the electron in MTHF at 77 K.

coefficient of eq. (15.133) calculated with  $n_D=1.5$ . The square root dependence on the binding energies of the electrons is reasonably well obeyed and the optical dielectric constant is found to be an appropriate scaling factor.

### 15.8 TRIPLET-ENERGY (AND ELECTRON) TRANSFER RATES

The expectation arises that accurate Franck–Condon factors could be calculated by a model incorporating a suitable high frequency and a good estimate of the reorganisation energy. In terms of the relations presented above

$$\lambda = \frac{1}{2} \sum_{i=1}^m f_i d_i^2 = \frac{1}{2} f_{\text{eff}} d_{\text{eff}}^2 \quad (15.134)$$

The effective force constant of the high frequency ( $f_{\text{eff}}$ ) is determined by the dominant vibronic progression. In the spectra of aromatic hydrocarbons this corresponds to  $\hbar\omega \approx 1400 \text{ cm}^{-1}$ , which with  $\mu_{\text{CC}} = 6 \text{ amu}$ , gives  $f = 4.2 \times 10^3 \text{ kJ mol}^{-1} \text{ \AA}^{-2}$ , close to the force constant of the breathing mode of an aromatic ring obtained by normal mode analysis of aromatic hydrocarbons. Resonance Raman spectroscopy shows that in polyatomic systems there are many modes that contribute to  $\lambda$ . However, for diatomic molecules the Stokes shift reports on the effective displacement, and thus these are particularly appropriate to test the validity of the methods employed to calculate  $\lambda$  because there is no ambiguity in the calculation of  $f_{\text{eff}}$  or  $d_{\text{eff}}$ . Table 15.2 presents some homonuclear diatomic molecules and ions, presented in pairs that differ only in one bonding or anti-bonding electron. They are also a good testing ground for the calculation of  $\lambda$  for electron-transfer reactions because the change in the electronic configuration corresponds to a change in the bond order by 0.5 and Pauling's relation is obeyed. In fact, Figure 6.14, illustrating Pauling's relation between bond orders and bond lengths, also includes some of these systems.

The comparison between the bond-length changes of the systems indicated in Table 15.2 requires some reference state. Considering that these systems follow Pauling's relation, the reference state can be found multiplying  $|l_{\text{ox}} - l_{\text{red}}|$  by the respective bond orders, or, better, the average of the bond order  $n_{\text{av}}$ , because the effective displacement is independent of the choice of the initial and final states. This takes into account the fact that smaller bond

**Table 15.2**

Bond lengths and displacements (in angstrom) of diatomic molecules and ions with bond-order differences of 0.5

System electronic configuration	$\text{H}_2^+/\text{H}_2$	$\text{F}_2/\text{F}_2^-$	$\text{O}_2/\text{O}_2^-$	$\text{O}_2^+/\text{O}_2$	$\text{N}_2/\text{N}_2^-$
$\text{X } ^2\Sigma_g^+/\text{X } ^1\Sigma_g^+$					
$l_{\text{ox}}/l_{\text{red}}$	1.052/0.7414	1.4119/1.88	1.2075/1.35	1.1164/1.2075	1.0977/1.19
$l_{\text{ox}} - l_{\text{red}}$	0.311	-0.47	-0.14	-0.0911	-0.09
Bond orders	0.5/1.0	1.0/0.5	2.0/1.5	2.5/2.0	3.0/2.5
$d_{\text{eff}}$	0.259	0.475	0.158	0.112	0.090

orders are more sensitive to bond-order changes than large bond orders. For the same reason, the product  $n_{av}|l_{ox} - l_{red}|$  must be divided by the sum of the equilibrium bond lengths. The success of this procedure of reducing the effective displacement to a common reference state can be assessed from the average and standard deviation of the reduced bond-length changes:  $0.106 \pm 0.016$ . A similar procedure was followed by the ISM to obtain the reduced bond-length changes of bond-breaking–bond-making reactions. It was shown in Chapter 7 that the fundamental equation obtained for isothermal processes was, eq. (7.9),

$$d_{\text{eff}} = \frac{a' \ln(2)}{n^*} (l_D + l_A) = \frac{0.108}{n^*} (l_D + l_A) \quad (15.135)$$

where  $n^*$  is now  $n_{av}$ , because no bonds are broken in the electronic transitions involved in Tables 15.1 and 15.2.

The scaling factor  $a' = 0.156$  of hydrogen-atom and proton transfers seems to be transferable to triplet-energy and electron transfers. This is not totally unexpected because the reference system chosen for bond-breaking–bond-making reaction,  $\text{H} + \text{H}_2$ , does not have significant steric effects and the resonance at the transition state is minimal. These are also properties of triplet-energy and electron transfers. The effective displacements calculated with eq. (15.135) are presented in Table 15.2 and compared with the spectroscopic data in Figure 15.23. For the systems selected for this test, the performance of eq. (15.135) is particularly encouraging. However, it must be emphasised that these systems were selected

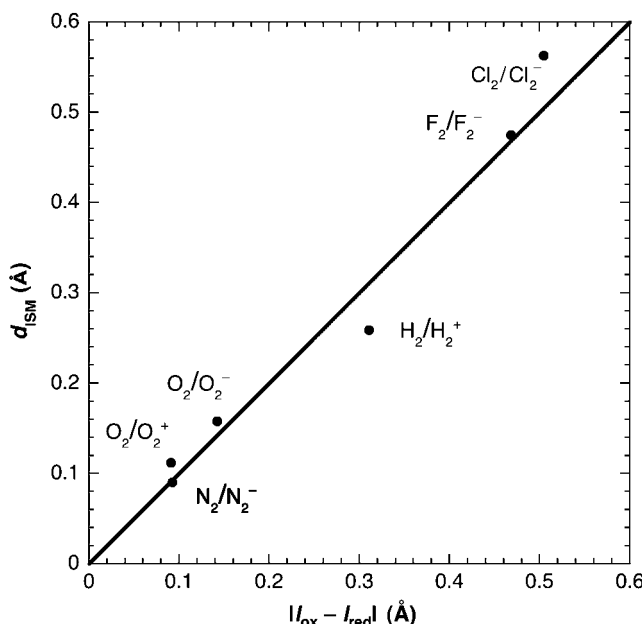


**Figure 15.23** Correlation between the effective displacements calculated by the ISM and the experimental data on the diatomic molecules of Table 15.2.

for their adherence to Pauling's relation in discrete increments of 0.5 in the bond order. For example, the electronic transition from the  $^3\Sigma_g^-$  state to the  $^1\Delta_g$  state of molecular oxygen, shown in Table 15.1, does not involve the same type of change in bond order and its effective displacement cannot be calculated from eq. (15.135).

The generalisation of this method to polyatomic systems is straightforward. For example, benzene formally has three double bonds and three single bonds, that is  $n = 1.5$ . Its cation has one bonding electron less and the total bonding is reduced to  $n = 1.42$ , thus  $n_{av} = 1.44$ . The CC bond length of benzene is 1.397 Å and normal mode analysis gives  $f = 3.87 \times 10^3$  kJ mol $^{-1}$  Å $^{-2}$ . With these values eq. (15.135) gives  $d_{eff} = 0.207$  Å and  $\lambda(\text{benzene}) = 82.7$  kJ mol $^{-1}$ . Another example is TCNE, with its four triple bonds, one double bond and four single bonds, which lead to  $n = 2.0$ . Its anion has  $n = 1.94$  and, consequently,  $n_{av} = 1.97$ . With the average bond length of 1.301 Å for the neutral and 1.291 Å for the anion, and the corresponding average force constants of  $6.42 \times 10^3$  and  $6.19 \times 10^3$  kJ mol $^{-1}$  Å $^{-2}$ , respectively, the reorganisation energy for this redox couple is  $\lambda(\text{TCNE}) = 63.7$  kJ mol $^{-1}$ . The charge transfer in the HMB/TCNE charge-transfer complex should be intermediate between these two values. As mentioned before, resonance Raman spectroscopy suggests that the total reorganisation energy is between 45 and 56 kJ mol $^{-1}$  for this system, which may be increased upon consideration of the role of the CH bonds. Again, this is an encouraging agreement between eq. (15.135) and the experimental data.

The heuristic validation of eq. (15.135) for the calculation of effective displacements for triplet-energy and electron transfers under the specified conditions has interesting consequences. The isomorphism of eqs. (15.135) and (7.9), suggests that the energy dependence of the effective displacement should have the form of eq. (7.8), or, more precisely,

$$d_{eff} = \frac{a'}{2n^{\ddagger}} \ln \left\{ \frac{1 + \exp(\sqrt{2n^{\ddagger}} \Delta E^0 / \Lambda)}{1 - [1 + \exp(\sqrt{2n^{\ddagger}} \Delta E^0 / \Lambda)]^{-1}} \right\} (l_D + l_A) \quad (15.136)$$

where  $\Lambda$  is a parameter that accounts for the coupling of the reaction energy with vibrational modes other than the high-frequency mode selected for the reaction coordinate. An empirical choice of  $\Lambda$ , guided by the best fit to the energy dependence of a series of reactions, gives the correct reorganisation energy and, together with the high-frequency mode and the electronic coupling, leads to good estimates of the reaction rates. A detailed interpretation of eq. (15.136) is postponed to Chapter 16, where it is applied to electron-transfer reactions. For the moment, it is just emphasised that  $d_{eff}$  increases with  $\Delta E^0$ , that is, the *reorganisation energy tends to increase with the driving force* of the reaction.

The most convincing argument for the relation between molecular structure, spectroscopy and kinetics developed in this chapter, is to calculate triplet-energy transfer rates using the Franck–Condon factors and electronic couplings given by the molecular models. An interesting system to test these relations is the triplet-energy transfer from a biacetyl molecule trapped inside a hemicarcerand cage to aromatic hydrocarbons in free solution. This system has two very convenient features: first, biacetyl is one of the few organic molecules phosphorescing at room temperature and second, it is possible to study experimentally an extended range of reaction energies [53,54]. The fluorescence of biacetyl overlaps

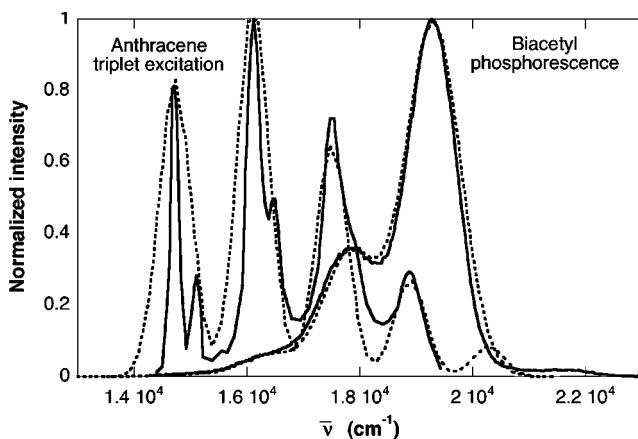


**Figure 15.24** Biacetyl phosphorescence and anthracene triplet excitation spectra. The simulated spectra (dotted lines) used  $E_D = 19,300 \text{ cm}^{-1}$ ,  $\bar{v}_D = 1470 \text{ cm}^{-1}$ ,  $\sigma_D = 480 \text{ cm}^{-1}$  and  $S_D = 0.35$  for biacetyl, and  $E_A = 14,720 \text{ cm}^{-1}$ ,  $\bar{v}_A = 1390 \text{ cm}^{-1}$ ,  $\sigma_A = 280 \text{ cm}^{-1}$  and  $S_A = 1.25$  for anthracene.

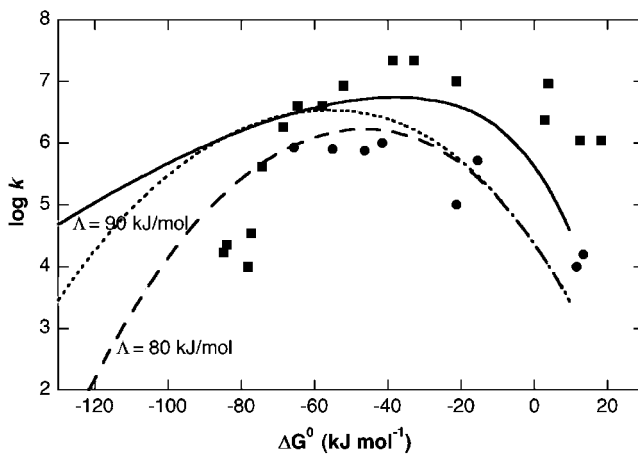


**Figure 15.25** Rate constants for the triplet energy transfer from biacetyl, through a hemicarcerand cage, to aromatic hydrocarbons in solution. The full line represents the Golden Rule calculations and the other lines the ISM calculations differing in the parameters shown in the plot.

with its phosphorescence in steady-state emission spectra, but registering the spectrum with a 10  $\mu\text{sec}$  delay gives enough time for the biacetyl fluorescence to disappear, as illustrated in Figure 15.24 [27]. This figure also shows the triplet-excitation spectrum of anthracene, already previously shown in Figure 15.11. The simulation of this spectrum requires at least two modes, with frequencies  $1390$  and  $380 \text{ cm}^{-1}$ , but only the single, high-frequency approximation for each reactant will be pursued here.

Golden Rule calculations using eq. (15.101) with the reorganisation energy given by eq. (15.100) and the parameters indicated in Figure 15.24 give the rates presented in

Figure 15.25 when the electronic coupling is fitted ( $V_{\text{ks}}^e = 0.1 \text{ cm}^{-1}$ ) to reproduce the fastest experimentally observed triplet-energy transfer rate from biacetyl, through a hemi-carcerand cage, to an aromatic hydrocarbon in solution. The Golden Rule reproduces the general energy dependence of the rates, although this formulation tends to overestimate the rates in the range of reaction energies where the energy-gap law is followed. The same figure also presents calculations with the ISM using  $\Lambda$  as an adjustable parameter. The molecular parameters of the aromatic hydrocarbon are those of benzene discussed above, and for biacetyl the following parameters were employed:  $f = 5.91 \times 10^3 \text{ kJ mol}^{-1} \text{ \AA}^{-2}$ ,  $l = 1.30 \text{ \AA}$ ,  $n = 1.58$  [27]. With  $\Lambda = 90 \text{ kJ mol}^{-1}$  the ISM reproduces the Golden Rule calculations, but a lower value of  $\Lambda$  yields a better agreement with the experimental data. The implications of these results for electron transfers are discussed in the next chapter.

## REFERENCES

- [1] A Jablonski, *Z. Physik*. **94** (1935) 38–46.
- [2] M Kasha, *Discuss. Farad. Soc.* **9** (1950) 14–19.
- [3] SJ Formosinho, AM da Silva, *Mol. Photochem.* **9** (1979) 257–275.
- [4] T Förster, *Ann. Phys.* **2** (1948) 55.
- [5] DL Dexter, *J. Chem. Phys.* **21** (1953) 836–850.
- [6] T Förster, *Discuss. Farad. Soc.* **27** (1959) 7–17.
- [7] SJ Strickler, RA Berg, *J. Chem. Phys.* **37** (1962) 814–822.
- [8] M Halmann, I Laulicht, *J. Chem. Phys.* **43** (1965) 438–448.
- [9] M Halmann, I Laulicht, *J. Chem. Phys.* **44** (1966) 2398–2405.
- [10] P Avakian, E Abramson, RG Kepler, JC Caris, *J. Chem. Phys.* **39** (1963) 1127–1128.
- [11] KH Grellmann, H-G Scholz, *Chem. Phys. Lett.* **62** (1979) 64–71.
- [12] J Jortner, J Ulstrup, *Chem. Phys. Lett.* **63** (1979) 236–239.
- [13] SJ Formosinho, *J. Chem. Soc., Farad. Trans. 2*:70 (1974) 605.
- [14] W Siebrand, in AB Zahn (Ed.), *The Triplet State*. Cambridge Univ. Press, 1967, p. 31.
- [15] SJ Formosinho, LG Arnaut, *Adv. Photochem.* **16** (1991) 67.
- [16] EG Azenha, AC Serra, M Pineiro, MM Pereira, J Seixas de Melo, LG Arnaut, SJ Formosinho, AMdAR Gonsalves, *Chem. Phys.* **280** (2002) 177–190.
- [17] EF McCoy, IG Ross, *Aust. J. Chem.* **15** (1962) 573–590.
- [18] OS Mortensen, W Siebrand, AW Tarr, *Chem. Phys.* **125** (1988) 231–245.
- [19] BR Henry, W Siebrand, *J. Chem. Phys.* **49** (1968) 5369–5376.
- [20] SJ Formosinho, *J. Chem. Soc., Farad. Trans. 2*:72 (1976) 1313–1331.
- [21] JB Birks: *Photophysics of Aromatic Molecules*, Wiley, London, 1970.
- [22] R Englman, J Jortner, *Mol. Phys.* **18** (1970) 145.
- [23] L Landau, *Phys. Z. Sowjetunion* **1** (1932) 88.
- [24] C Zener, *Proc. Roy. Soc. (London) A* **137** (1932) 696.
- [25] D DeVault, *Q. Rev. Biophys.* **13** (1980) 387–564.
- [26] JJ Hopfield, *Proc. Natl. Acad. Sci. USA* **71** (1974) 3640–3644.
- [27] C Serpa, LG Arnaut, SJ Formosinho, KR Naqvi, *Photochem. Photobiol. Sci.* **2** (2003) 616.
- [28] RA Marcus, *J. Chem. Phys.* **24** (1956) 966–978.
- [29] RA Marcus, *Farad. Discuss. Chem. Soc.* **29** (1960) 21.
- [30] JP Claude, KM Omberg, DS Williams, TJ Meyer, *J. Phys. Chem. A* **106** (2002) 7795–7806.
- [31] R Schmidt, *J. Photochem. Photobiol. A Chem.* **80** (1994) 1–5.

- [32] K Kulinowski, IR Gould, NS Ferris, AB Myers, *J. Phys. Chem.* **99** (1995) 17715–17723.
- [33] WR Ware, P Chow, SK Lee, *Chem. Phys. Lett.* **2** (1968) 356–358.
- [34] PY Chen, TJ Meyer, *Chem. Rev.* **98** (1998) 1439–1477.
- [35] R Jimenez, GR Fleming, PV Kumar, M Maroncelli, *Nature* **369** (1994) 471–473.
- [36] MJ Lang, XJ Jordanides, X Song, GR Fleming, *J. Chem. Phys.* **110** (1999) 5884–5892.
- [37] SA Kovalenko, R Schanz, VM Farztdinov, H Hennig, NP Ernsting, *Chem. Phys. Lett.* **323** (2000) 312–322.
- [38] AB Myers, *Chem. Rev.* **96** (1996) 911–926.
- [39] JT Hupp, RD Williams, *Acc. Chem. Res.* **34** (2001) 808–817.
- [40] K Wynne, C Galli, RM Hochstrasser, *J. Chem. Phys.* **100** (1994) 4797–4810.
- [41] BM Britt, JL McHale, DM Friedrich, *J. Phys. Chem.* **99** (1995) 6347–6355.
- [42] M Bixon, J Jortner, J Cortes, H Heitele, ME Michel-Bayerle, *J. Phys. Chem.* **98** (1994) 7289–7299.
- [43] NE Katz, SL Mecklenburg, DK Graff, P Chen, TJ Meyer, *J. Phys. Chem.* **98** (1994) 8959–8961.
- [44] C Serpa, PJS Gomes, LG Arnaut, SJ Formosinho, J Pina, J Seixas de Melo, *Chem. Eur. J.* **12** (2006).
- [45] GL Closs, LT Calcaterra, NJ Green, KW Penfield, JR Miller, *J. Phys. Chem.* **90** (1986) 3673.
- [46] GL Closs, M.D. Johnson, JR Miller, P. Piotrowiak, *J. Am. Chem. Soc.* **111** (1989) 3751.
- [47] GL Closs, P Piotrowiak, JM MacInnis, GR Fleming, *J. Am. Chem. Soc.* **110** (1988) 2652.
- [48] JR Platt, *J. Chem. Phys.* **17** (1949) 481.
- [49] G Binnig, H Rohrer, *Angew. Chem. Int. Ed. Engl.* **26** (1987) 606.
- [50] G Binnig, H Rohrer, C Gerber, E Weibel, *Physica* **109 & 110B** (1982) 2075.
- [51] LG Arnaut, LG Formosinho, *J. Photochem. Photobiol. A: Chem.* **100** (1996) 15.
- [52] VV Krongauz, *J. Phys. Chem.* **96** (1992) 2609.
- [53] F Pina, AJ Parola, E Ferreira, M Naestri, N Armaroli, R Ballardini, V Balzani, *J. Phys. Chem.* **99** (1995) 12701–12703.
- [54] ZS Romanova, K Deshayes, P Piotrowiak, *J. Am. Chem. Soc.* **123** (2001) 11029–11036.

This page intentionally left blank

# – 16 –

## Electron Transfer Reactions

---

### 16.1 RATE LAWS FOR OUTER-SPHERE ELECTRON EXCHANGES

Electron transfers are another prototype of chemical reactions as paradigmatic as H-atom or proton-transfer reactions. Furthermore, these are chemical processes ubiquitous in chemistry and biology. They are important from a historical point of view in the development of chemical kinetics, and are scientifically relevant in many physical, chemical, biological and technological processes.

The field of electron-transfer reactions in solution has only developed since World War II and initially was centred on inorganic processes. Two kinds of mechanisms are invoked for ET reactions in transition-metal complexes. One, the *inner-sphere mechanism*, where the two reactants share one or more ligands in their first coordination shell in the activated complex and the electron transfer is considered to occur via the bridging ligand. This requires bond breaking followed by bond forming. The other is the *outer-sphere mechanism*, where the first coordination shells of the two reactants remain intact with respect to the number and kind of ligands present. The latter mechanism is the focus of this chapter, because bond-breaking–bond-forming reactions have already been extensively discussed in this book.

Let us consider the isothermal process for the transfer of one electron between hydrated iron (II) and (III) species

$$\frac{d\left[^*\text{Fe}^{3+}\right]}{dt} = k_2 \left[\text{Fe}^{3+}\right] \left[^*\text{Fe}^{2+}\right] - k_{-2} \left[\text{Fe}^{2+}\right] \left[^*\text{Fe}^{3+}\right] \quad (16.1)$$

This is a *self-exchange* reaction, where the products are identical to the reactants. For it to be followed experimentally, the iron species normally are marked radioactively (represented by  $*$ ). If the reaction is followed, for example, in terms of  ${}^*\text{Fe}_{(\text{aq})}^{3+}$ , the rate law can be written as:

$$\frac{d\left[^*\text{Fe}^{3+}\right]}{dt} = k_2 \left[\text{Fe}^{3+}\right] \left[^*\text{Fe}^{2+}\right] - k_{-2} \left[\text{Fe}^{2+}\right] \left[^*\text{Fe}^{3+}\right] \quad (16.1)$$

by simplifying the representation of the ionic species in terms of the chemical symbol of the metallic element and of the electric charge. Since second-order rate constants in the

forward and reverse directions are equal,  $k = k_2 = k_{-2}$ . If we represent the initial concentration of reactants by  $a$  and the concentration of products by  $x$ , we can write

$$\frac{dx}{dt} = k(a-x)^2 - kx^2 \quad (16.2)$$

which can be rearranged to

$$\frac{dx}{dt} = ka^2 - 2kax \quad (16.3)$$

or

$$\frac{dx}{dt} = ka(a-2x) \quad (16.4)$$

As a consequence, we have

$$\frac{dx}{a-2x} = ka dt \quad (16.5)$$

This equation can be integrated

$$\int_0^x \frac{dx}{a-2x} = \int_0^t ka dt \quad (16.6)$$

The result requires knowledge of the value of the standard integral

$$\int_0^x \frac{dx}{a-bx} = \frac{1}{b} \ln(a+bx) \quad (16.7)$$

and thus

$$-\frac{1}{2} \ln(a-2x) = kat + \text{constant} \quad (16.8)$$

The value of the constant of integration is obtained by solving eq. (16.8) for  $t = 0$ , where  $x = 0$ ,

$$\ln \frac{a-2x}{a} = -2kat \quad (16.9)$$

or

$$\frac{a-2x}{a} = \exp(-2kat) \quad (16.10)$$

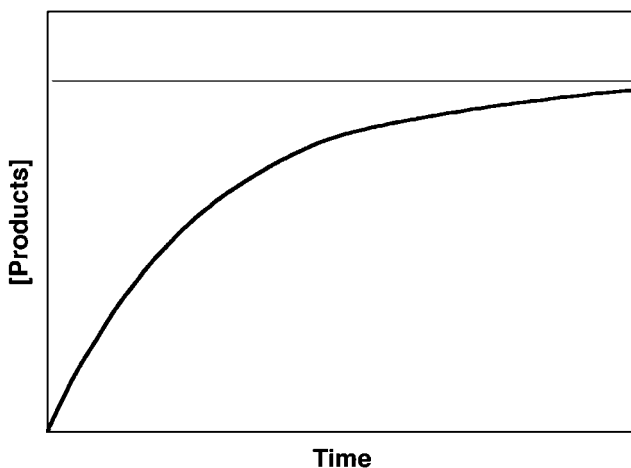


**Figure 16.1** Change in the concentration of the products with time in a reaction following mechanism 16.I. If the concentrations of the two reactants are identical, the concentration of the products tends to half of the initial concentration of the reactants.

**Table 16.1**

Rate constants of electron self-exchange reactions in transition-metal complexes, measured in water at room temperature<sup>a</sup>

Metal complexes	$k$ ( $\text{mol}^{-1} \text{ dm}^3 \text{ sec}^{-1}$ )
$\text{Fe(OH}_2\text{)}_6^{3+/2+}$	1.1
$\text{Fe(CN)}_6^{3-/4-}$	19
$\text{Cr(OH}_2\text{)}_6^{3+/2+}$	$\leq 2 \times 10^{-5}$
$\text{Co(en)}_3^{3+/2+}$	$7.7 \times 10^{-5}$
$\text{Fe(phen)}_6^{3+/2+}$	$3.3 \times 10^8$
$\text{Co(bpy)}_3^{2+/1+}$	$2 \times 10^9$

<sup>a</sup>Data from ref. [1]. Ligands: en = ethylenediamine; phen = 1,10-phenanthroline; bpy = 2,2'-bipyridine.

Figure 16.1 displays the profile of the concentration of the products as a function of time in a self-exchange reaction, according to eq. (16.9).

Table 16.1 lists typical values of rate constants for self-exchange reactions of transition-metal complexes with different kinds of ligands in aqueous solutions; the rates cover 14 orders of magnitude. The collection of the vast majority of such data became experimentally feasible only through the availability of several metal radioactive isotopes due to the Manhattan project. The surprising result for the chemists at the end of the 1940s and beginning of the 1950s of the twentieth century was the slowness of many such processes.

In contrast, in the beginning of the 1980s, Gray [2] and collaborators showed that electrons can be transferred in proteins over distances of 15–20 Å on a biologically relevant timescale of milliseconds to microseconds. This appears to be consistent with

a significant effect producing slow rates for electron transfers due to bulk solvent. Anticipating an alternative view, one should be aware that the electronic nature of the reactive bonds in hydrated transition-metal ions and in donor and acceptor complexes in proteins are entirely different. As it will be shown in due course, such a direct comparison is therefore not meaningful from a theoretical point of view.

## 16.2 THEORIES OF ELECTRON-TRANSFER REACTIONS

### 16.2.1 The classical theory of Marcus

ET reactions between molecular species in cases where no bond-breaking–bond-forming processes occur are usually considered to be very different in nature from atom-transfer reactions. For the latter case, we can use a Born–Oppenheimer adiabatic potential-energy surface and there is a strong interaction with the attacking atom, which effectively determines the barrier for the reaction. In contrast, for the former processes the interaction between the electron donor and its acceptor is very weak, the nuclear configuration of the products resembles that of the reactants and, in retrospect with a certain naivety, chemists expected that ET would in general be fast processes, and would mainly be diffusion controlled.

The current view is that the electron-transfer event itself is a fast activationless process; the barrier for the reaction stems from the necessity to adjust the orientation of the solvent dipoles around ions and the lengths of some bond in the inner-coordination shells prior to the transfer step. According to this view, which was due largely to Rudolph Marcus [3], for the solvent, and to Noel Hush [4], for the metal-ligand bond lengths, there are no proper transition states in electron-transfer reactions, because the solvent molecules are not in equilibrium distribution with the charges of the oxidised and reduced species.

The theoretical formalism proposed to estimate the rates of ET reactions is known as the theory of Marcus (TM) [3,5,6]. However it is relevant to make a distinction between two components of the theory. One component is concerned with the estimation of the intrinsic barrier,  $\Delta G(0)^{\ddagger}$ , for homonuclear reactions in terms of molecular parameters of the reactants, which we will call TM-1. The other component of the theory addresses the effect of the reaction energy,  $\Delta G^0$ , on the reaction rates, presented in Chapter 7 in terms of the quadratic expression of Marcus (eq. (7.6)); this will be called TM-2. It is currently employed to estimate the rates of cross-reactions, when the reaction energies of the heteronuclear reactions are known together with the rates of the corresponding homonuclear reactions.

In general terms, the theory of Marcus involves a model for ET reactions based on the approximation that the inner-coordination sphere energy is independent of the outer-sphere reorganisation. In its classical formulation, TM provides the rate for a self-exchange reaction such as reaction (16.I)

$$k_{\text{MT}} = \kappa_{\text{el}} Z \exp \left[ - \left( w_r + \Delta G_v^* + \Delta G_s^* \right) / RT \right] \quad (16.11)$$

which involves collision frequency factor,  $Z$  (taken as  $Z = 10^{11} \text{ M}^{-1} \text{ sec}^{-1}$ );  $\kappa_{\text{el}}$  is an electronic transmission factor ( $\kappa_{\text{el}} = 1$  for adiabatic reactions and  $\kappa_{\text{el}} < 1$  for non-adiabatic

reactions). The reaction energy barrier is made up of three contributions: (i) a small electrostatic term,  $w_r$ , the electrostatic work required to bring the two reactants together; (ii) an external reorganisation of the solvent dipoles,  $\Delta G_s^*$ ; and (iii) an internal reorganisation of the metal-ligand bonds in the inner-coordination shell,  $\Delta G_v^*$ . Within the framework of TM-1, the explicit formulae of these terms, taking energies in kJ mol<sup>-1</sup> and radii in Å, are:

$$w_r = \frac{e^2 z_{\text{ox}} z_{\text{red}}}{\epsilon r \left[ 1 + r \sqrt{\frac{8\pi N_A^2 e^2 I}{10^{33} \epsilon RT}} \right]} = \frac{1389 z_{\text{ox}} z_{\text{red}}}{\epsilon r \left[ 1 + 50.3r \sqrt{\frac{I}{\epsilon T}} \right]} \quad (16.12)$$

$$\Delta G_s^* = \frac{e^2}{4} \left( \frac{1}{2r_{\text{ox}}} + \frac{1}{2r_{\text{red}}} - \frac{1}{r} \right) \left( \frac{1}{n_D^2} - \frac{1}{\epsilon} \right) = 347.3 \left( \frac{1}{r_{\text{av}}} - \frac{1}{r} \right) \left( \frac{1}{n_D^2} - \frac{1}{\epsilon} \right) \quad (16.13)$$

$$\Delta G_v^* = \frac{1}{2} c_n \frac{f_{\text{ox}} f_{\text{red}}}{f_{\text{ox}} + f_{\text{red}}} (l_{\text{ox}} - l_{\text{red}})^2 \quad (16.14)$$

$$e^2 = \frac{e_0^2 N_A}{4\pi\epsilon_0} \quad (16.15)$$

In the above expressions  $e_0$  is the elementary charge,  $N_A$  the Avogadro constant,  $\epsilon_0$  the permittivity of vacuum,  $n_D$  and  $\epsilon$  are the refractive index and the static dielectric constants of the solvent, respectively,  $I$  the ionic strength of the solution and  $r$  the distance between the centres of the reactants in the collisional complex, assumed to be equal to  $2r_{\text{av}} = (r_{\text{ox}} + r_{\text{red}})/2$ ;  $f_{\text{ox}}$  and  $f_{\text{red}}$  are the stretching vibrations for the two reactants in the oxidised and reduced forms, and  $l_{\text{ox}}$  and  $l_{\text{red}}$  are the equilibrium lengths of the metal-ligand bonds in the same species. The parameter  $r$  corresponds to the diameter of the spherical symmetric transition-metal complexes which can be estimated from the relation  $r = (r_x r_y r_z)^{1/3}$ . Finally,  $c_n$  is the coordination number, i.e. the number of metal-ligand bonds involved in the reaction coordinate.

By end of the 1950s, the experimental data on ET in transition-metal complexes was insufficient for a reliable comparison with the theoretical ideas of Marcus and Hush. However, by the beginning of the 1960s, Norman Sutin [7] had obtained a considerable amount of kinetic data on such systems and was able to test the theoretical ideas available. The idea of accounting for an internal reorganisation is due to N. Hush, but eq. (16.14) is not, in fact, the expression originally proposed. Instead, Sutin employed another expression available from spectroscopy to account for the minimal energy rearrangement for bond length changes and this expression was empirically found to be more convenient to express  $\Delta G_v^*$ .

The rates were calculated according to TM-1 assuming the following approximations: (i) near adiabaticity ( $\kappa_{\text{el}} \approx 1$ ); (ii) dielectric continuum model for the solvent; (iii) intermediate distortions between oxidised and reduced species for the internal modes; and (iv) separation between internal modes and medium modes (either high-frequency vibrational modes or low frequency). This last approximation is implicit in eqs. (16.12)–(16.15). The separation between the inner-sphere,  $\Delta G_v^*$ , and the outer-sphere,  $\Delta G_s^*$ , reorganisation

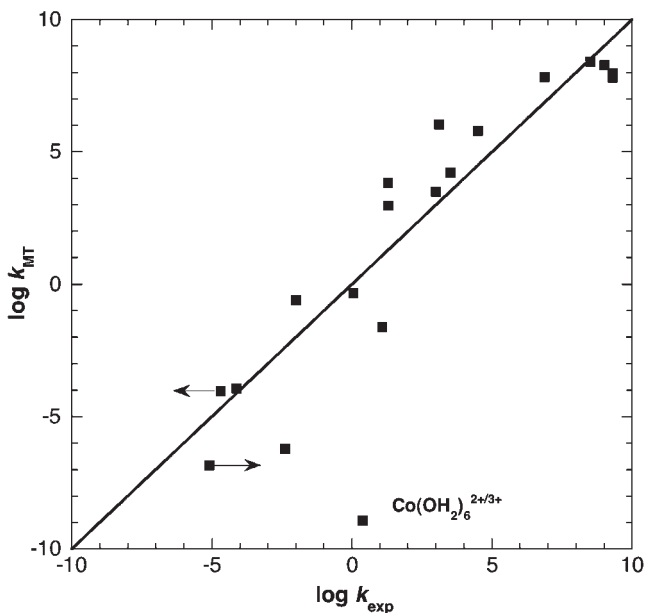


**Figure 16.2** Comparison between electron self-exchange rates of transition-metal complexes calculated by TM-1 and experimental data, in aqueous solutions at room temperature (from ref. [1]).

energies distinguishes between high-frequency vibrational modes associated to the reactants and products, and low-frequency solvent modes. Additionally, the low-frequency modes must have much larger vibrational amplitudes to give a comparable contribution for the energy barrier.

The success of such ideas can be judged from the excellent agreement of the theoretical calculations with the experimental self-exchanges rates in transition-metal complexes (Figure 16.2). In spite of this initial success, an anomaly has persisted for the reaction  $\text{Co}_{(\text{aq})}^{3+}/\text{Co}_{(\text{aq})}^{2+}$ ; TM-1 underestimates the rate by *ca.* eight orders of magnitude. Rudolph Marcus called this “the soldier marching the wrong way”!

The theory of Marcus was not only able to account for the kinetics of self-exchange reactions (TM-1), but could also estimate rates for moderately exothermic processes where  $\Delta G^0 < 0$ . Marcus further develop the theory, TM-2, to relate the rates for which  $\Delta G^0 = 0$ , to cross reactions



In TM-2 Marcus assumes that the reactants ( $\text{Red}_1 + \text{Ox}_2$ ) can be represented by one single parabola and that the same is valid for the products. The parabolas are vertically separated by  $\Delta G^0$ , and horizontally displaced by a distance that yields the activation energy as the crossing point between reactants and products curves, as illustrated in Figure 15.16. When

the work terms are neglected, the parabolas illustrated in this figure lead to the following relation between self-exchange and cross-reaction rate constants:

$$k_{12} = (k_{11} k_{22} K_{12} f_{12})^{1/2} \quad (16.16)$$

$$\ln f_{12} = \frac{(\ln K_{12})^2}{4} \left[ \ln \left( \frac{k_{11} k_{22}}{(k_B T / h)^2} \right) \right]^{-1} \quad (16.17)$$

These predictions of the theory have also met with a remarkable success.

TM-1 and TM-2 are collectively known as the theory of Marcus. However, the approximations involved in the derivation of the two formalisms are different. The approximations involved in TM-2 have already been discussed with respect to Figure 15.16.

Another great success of TM was the prediction of new pattern of reactivity for very exothermic electron transfers (the existence of an *inverted region*, to be discussed later in Section 16.5). The prediction of such pattern of reactivity against the scientific consensus at the time reveals how those simple ideas of Marcus, based on his quadratic equation, grasped one of the essential features of physical reality in this field, one which has important implications for fundamental biological processes such as photosynthesis.

### 16.2.2 Solute-driven and solvent-driven processes

In order to assess the solvent contribution to the electron-transfer processes in solution, it is useful to represent the potential energy surface for an electron self-exchange reaction in solution by a bi-dimensional diagram. One-dimension is for the internal coordinate of reactants and products and the other for the solvent, an ill-described average for the distance approach and orientation with respect to reactants and products. Two extreme limits can be considered for such PES. In the first case, the overall force-constant for motions of solvent molecules,  $f_s$ , is much lower than that for reactants and products,  $f_v$  ( $f_v/f_s \geq 5$ ). Figure 16.3 illustrates such a surface and the reaction path for the corresponding electron transfers. Solvent motion is relatively slow, after a fast initial reorientation of the solvent molecules which requires very little energy. There is also some solvent relaxation after the electron-transfer event, close to the configuration of the products. Nevertheless, the main part of the reaction-path is due to rearrangements of the internal coordinate, and this type of diagram represents a *solute-driven* reaction. The “transition state” configuration of these processes is very close to that of the “diabatic path” indicated by Evans and Polanyi, as shown in the same figure.

When the energy barriers provided by internal motions are extremely low, the force constant for solvent interactions becomes significant and a large percentage of the interactions along the reaction coordinate is due to solvent motions. Molecules spend a long time in the transition-state region and dynamic motions of solvent molecules can determine the kinetics. These are the *solvent-driven* reactions. The role of the dynamic effect of solvents can be excluded for the vast majority of ET reactions, which we will consider. Exceptions are the virtually “activationless processes”, i.e., cases where  $\Delta G^* < 5 \text{ kJ mol}^{-1}$ . In the limits

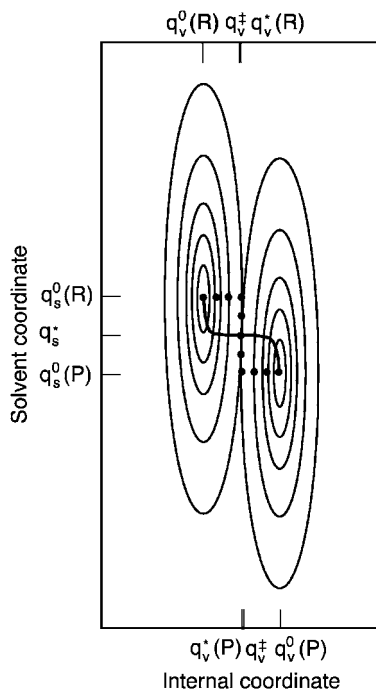


**Figure 16.3** Equipotential curves representing reactant and product in an electron exchange reaction as a function of a solvent reorganisation coordinate and an internal coordinate, both treated as harmonic. The heavy line represents the classical reaction path (path of steepest descent from the top of the barrier). The dotted line represents the Evans–Polanyi “diabatic path”, whose energy dependence is determined by the generalised internal coordinate  $q_v$ . In this plot,  $f_v/f_s = 5$  and the energy change from  $q_v^0(R)$  to  $q_v^‡$  is very close to the energy change from  $[q_v^0(R), q_s^0(R)]$  to  $[q_v^*, q_s^*]$ .

of solute- and solvent-driven reactions, a one-dimensional representation of the reaction is reasonable. However, the ET reaction is better represented by a two-dimensional diagram when the force constants of solvent and of reactants/products are within a factor of 2 of each other.

The second type of effect, which solvent molecules can induce, is of a static nature. Solvent molecules may modify the rearrangements in the internal coordinate of a solute-driven reaction through non-specific (dipole moment, polarisability, etc.) or specific (hydrogen bonding) effects. We are not concerned at this stage with changes produced by the solvent on the reaction energy,  $\Delta G^0$ , because we are dealing with self-exchange processes. Non-specific interactions with solvent molecules can cause small changes in force constants and bond lengths, but in general these effects tend to compensate and are of small magnitude. In general, such contributions to the energy barrier, together with some external reorganisation of the solvent molecules, are of the order  $\Delta G^* < 5 \text{ kJ mol}^{-1}$  and can be neglected.

### 16.2.3 Critique of the theory of Marcus

The approximations in which the classical theory of Marcus is based have been mentioned above. They require a discussion between the effects of having enough interaction between the reactants in the collisional complexes to achieve adiabaticity, but not enough to decrease the barrier. The near-adiabaticity assumed for ET reactions, may not be applicable to all molecular systems, in particular when spin changes are involved or when the redox-active orbitals of the two reactants cannot approach each other very closely. On the other hand, if the redox partners interact very strongly, the electron coupling will increase to a point where its value reduces the energy barrier appreciably.

For the total reorganisation energy barrier,  $\Delta G_{\text{total}}^*$ , TM-1 appears to have a sound physical basis. Nevertheless, upon critical examination there are worrying features with respect to the two pillars,  $\Delta G_s^*$  and  $\Delta G_v^*$ . The separation between internal and medium modes corresponds in hydrated transition-metal ions to the treatment of the first hydration sphere as a static medium with an optical dielectric constant  $\epsilon_{\text{op}} = n_D^2$  and the second hydration shell as a dielectric continuum characterised by the bulk dielectric constant of water. Electron transfer of hydrated transition-metal ions is, in general, a very slow process and this is thought to be due mainly to the water-molecule dipole reorientation around the ions. However, the ratio of the force constants for hydrated metal ions in the first (internal contribution) and second coordination (external contribution) shells, is  $ca. f_v/f_s \approx 8$ . From the previous arguments, one would expect for such a regime the electron transfer to be predominantly solute-driven. In addition, in the presence of hydrated metal ions there is almost no free volume for expansion in the second hydration shell and the large difference in force constants cannot be compensated by differences in configurational changes [8].

The success of TM in the estimation of self-exchange reactions in Figure 16.2 now starts to create some problems. We have to explore the possibility that TM-1 works because an overestimate of the solvent contribution  $\Delta G_s^*$  in polar media is compensated by an underestimate in the internal reorganisation  $\Delta G_v^*$ .

The most effective way to assess empirically the role of solvent reorganisation in electron-transfer reactions is to study self-exchange reactions involving one uncharged partner, in various solvents. Under such conditions the work term is zero ( $w_r = 0$ ), and the decrease in the solvent dielectric constant should lead to a decrease of  $\Delta G_s^*$  in eq. (16.13), and to a logarithmic dependence of the rates on  $\gamma = n_D^{-2} - \epsilon^{-1}$ . The results presented in Figure 16.4 argue against the effect of the solvent reorganisation on electron-transfer reactions proposed by the TM. A compensation of effects due to solvent dynamics has been excluded, at least for the ferrocene self-exchange [9]. According to Li *et al.*, TM currently overestimates  $\Delta G_s^*$  by a factor of 2 in polar media and the source of error is due to the fact that during the Born charging of an ion, the dielectric constant of the solvent is considered to be constant [10,11].

The limiting case to assess the role of solvent reorganisation for an electron-transfer reaction is the absence of bulk solvent, that is, the gas phase. The study of gas-phase electron transfers has the same simplifying and complicating features as the study of  $S_N2$  reactions in the gas phase, discussed in detail in Chapter 11. The reaction coordinate can be defined more precisely, but, on the other hand, the formation of precursor and successor complexes makes the interpretation of the kinetics more elaborate. For very negative

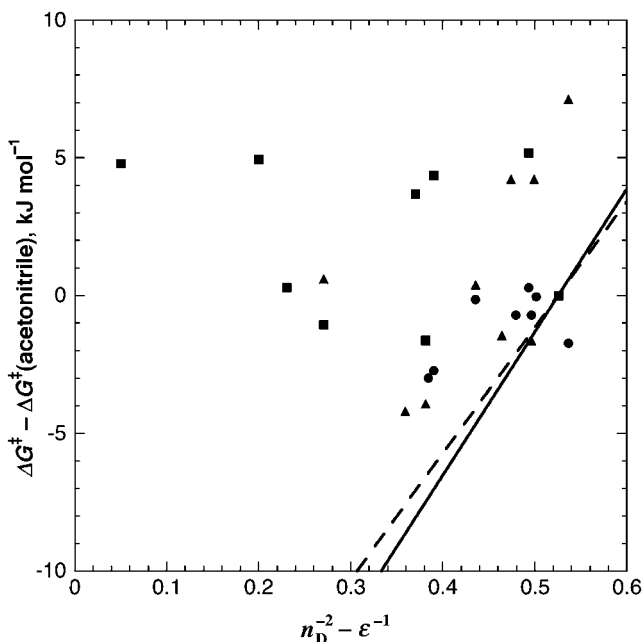


**Figure 16.4** Solvent dependence of the free energy of activation of self-exchanges as a function of the solvent optical and static dielectric constants. The free energies were obtained from the experimental rates using the frequency factor from transition-state theory, and are relative to those in acetonitrile. Tetracyanoethylene<sup>0/-</sup>: squares [12] and solid line, calculated with eq. (16.13) using  $r = 6.7 \text{ \AA}$ ; ferrocene<sup>0/+</sup>: circles [13] and dashed line, calculated with eq. (16.13) using  $r = 7.6 \text{ \AA}$ ; sesquibicyclic hydrazine 22/u22: triangles [14].

enthalpies of formation of such complexes the rates may be very fast even when the central barrier is high (Figure 11.14). The maximum rate of a bimolecular ion–molecule reaction for a small molecule exchanging an electron with the corresponding ion, is very well described by the Langevin collision rate

$$k_L = 2\pi e \sqrt{\frac{\alpha}{\mu}} = 2.34 \times 10^{-9} \sqrt{\frac{\alpha'}{\mu}} \quad (16.18)$$

where  $\alpha$  is the polarisability of the neutral species and  $\alpha'$  its polarisability volume. When the polarisability volume is expressed in  $\text{\AA}^3$  and the reduced mass in amu, the numerical constant gives the collision rate in  $\text{cm}^3 \text{ molecule}^{-1} \text{ sec}^{-1}$ . For example, the Langevin collision rate of the electron exchange  $\text{O}_2/\text{O}_2^-$  ( $\alpha' = 1.56 \text{ \AA}^3$ ,  $\mu = 8.00 \text{ amu}$ ) is  $k_L = 1.03 \times 10^{-9} \text{ cm}^3 \text{ sec}^{-1}$ , or  $6.2 \times 10^{11} \text{ M}^{-1} \text{ sec}^{-1}$ . The self-exchange rate constant obtained experimentally for the gas-phase reaction of  $^{18}\text{O}_2^+$  with  $^{16}\text{O}_2$  is  $2.5 \pm 0.2 \times 10^{11} \text{ M}^{-1} \text{ sec}^{-1}$  [15]. This is almost half of  $k_L$ , which is the maximum expected for a symmetric charge-transfer

reaction at thermal energy, since on each collision the system has effectively an equal probability of forming the products or of going back to the reactant state. Similar results have been obtained for other gas-phase self-exchanges such as  $\text{DBr}^+/\text{HBr}$  ( $\alpha' = 3.61 \text{ \AA}^3$ ,  $\mu = 40.5 \text{ amu}$ ,  $k_L = 4.2 \times 10^{11} \text{ M}^{-1} \text{ sec}^{-1}$ ), which has a very similar thermal rate constant,  $2.4 \times 10^{11} \text{ M}^{-1} \text{ sec}^{-1}$  [16]. These examples confirm that the gas-phase self-exchange rates of small molecules and their ions are very fast, and show the relation with their polarisability and reduced mass, but indicate that they are unrelated to the corresponding Franck–Condon factors.

The apparent contradiction between the principles of the Golden Rule developed in Chapter 15 and the fast gas-phase electron self-exchanges can be resolved by taking a closer look at the electronic couplings involved with these reactions. The formation of stable ion–molecule complexes and the small size of the reactants, favours electronic coupling between the two reactants. Detailed calculations for the  $\text{H}_2^+/\text{H}_2$  system reveal that the electronic interaction leads to a very large energy splitting, and that it can be considered as an  $\text{H}_4^+$  system with an energy splitting of  $533 \text{ kJ mol}^{-1}$  between ground and excited states at the equilibrium geometry of the ground state ( $1.59 \text{ \AA}$  between the parallel axis defined by the two sets of nuclei, with a bond dissociation energy of  $76 \text{ kJ mol}^{-1}$ ) [17]. The electronic coupling in the  $\text{O}_2/\text{O}_2^-$  system is smaller, but it is still  $56 \text{ kJ mol}^{-1}$ , in agreement with the larger distance between the two moieties ( $3.18 \text{ \AA}$  for the same geometry as described above, and a complexation energy of  $12 \text{ kJ mol}^{-1}$ ) [18]. For such large electronic couplings, Morokuma expressed doubts about the idea that the non-adiabatic approach to electron transfers should be preferred over the adiabatic approach with a proper transition state [18]. The electronic couplings of self-exchanges involving small molecules in the gas phase are very high and such systems are not good models for self-exchanges in solution.

This difficulty can be overcome by studying larger systems in the gas phase. For example, the exchange of one electron between ferrocene,  $\text{Fe}(\text{Cp})_2$ , and ferricinium ion,  $\text{Fe}(\text{Cp})_2^+$ , has been studied in many different solvents and in the gas phase. The symmetry of equilibrium conformation of  $\text{Fe}(\text{Cp})_2$  in the gas phase is  $D_{5h}$  (Figure 16.5). The most stable complex formed between  $\text{Fe}(\text{Cp})_2$  and  $\text{Fe}(\text{Cp})_2^+$  in the gas phase maintains this symmetry, with the centres of the four cyclopentadienyl rings and the two metals considered to be along the same straight line. The complexation energy in this configuration is  $24.3 \text{ kJ mol}^{-1}$  and the distance between the two iron atoms is  $6.75 \text{ \AA}$  [19]. At such a distance the calculated electronic coupling is only  $135 \text{ cm}^{-1}$  ( $1.6 \text{ kJ mol}^{-1}$ ) and the self-exchange can be regarded as slightly non-adiabatic, both in solution and in the gas phase. In fact, this electronic coupling is such as to place the reaction at the limit between adiabatic and non-adiabatic processes ( $\kappa_{\text{el}} \approx 1$ ). The Langevin collision rate of the electron exchange  $\text{Fe}(\text{Cp})_2/\text{Fe}(\text{Cp})_2^+$  ( $\alpha' = 19 \text{ \AA}^3$ ,  $\mu = 93 \text{ g mol}^{-1}$ ) is  $k_L = 6.4 \times 10^{11} \text{ M}^{-1} \text{ sec}^{-1}$ , but the experimental self-exchange rate is only  $1.5 \times 10^{11} \text{ M}^{-1} \text{ sec}^{-1}$  at  $350 \text{ K}$  [20]. The experimental rate is significantly less than half the Langevin rate, which is the maximum anticipated for an efficient electron exchange during the lifetime of each ion–molecule encounter pair. The actual observed efficiency is  $0.2 \pm 0.1$ . The branching fraction for a precursor with energy  $E$  is defined as

$$BF(E) = \frac{k_{\text{et}}(E)}{k_{\text{et}}(E) + k_d(E)} \quad (16.19)$$

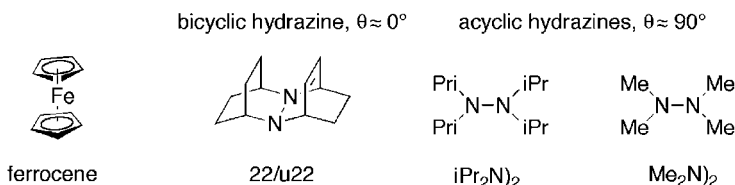


**Figure 16.5** Molecular structures of species studied for their self-exchanges in different solvents and in the gas phase. The angle  $\theta$  is lone pair/lone pair dihedral angle.

where  $k_{et}$  is the self-exchange between precursor and successor complex and  $k_d$  the dissociation of the precursor complex in the isolated ion + molecule reactants. The microscopic efficiency at a given temperature can be expressed as a function of the canonical branching fraction

$$\Phi(T) = \frac{k_{obs}(T)}{k_L(T)} = \frac{BF(T)}{1+BF(T)} \quad (16.20)$$

In the simplest approximation, where the first-order  $k_{et}$  and  $k_d$  rate constants have the same frequency factors, the difference between the rates can be assigned to the difference in activation energies. The activation energy of  $k_d$  is the complexation energy,  $24.3\text{ kJ mol}^{-1}$ . The efficiency of  $0.2 \pm 0.1$  can be obtained when, under these approximations, the activation energy of the self-exchange is  $28.0 \pm 2.5\text{ kJ mol}^{-1}$ . It is of interest that the temperature dependence of the  $\text{Fe}(\text{Cp})_2/\text{Fe}(\text{Cp})_2^+$  self-exchange in acetonitrile gives an enthalpy of activation of  $24\text{ kJ mol}^{-1}$  [21]. This is very similar to the gas-phase value and consistent with the solvent independence illustrated in Figure 16.4.

The solvent independence and the large gas-phase barrier required to explain the inefficiency of the  $\text{Fe}(\text{Cp})_2/\text{Fe}(\text{Cp})_2^+$  self-exchange is not compatible with the  $\Delta G_s^*$  and  $\Delta G_v^*$  values of eqs. (16.13) and (16.14), respectively. Using the refractive index ( $n_D = 1.341$ ) and static dielectric constant ( $\epsilon = 37$ ) of acetonitrile, together with a metal–metal distance of  $7.6\text{ \AA}$ , eq. (16.13) gives  $\Delta G_s^* = 24\text{ kJ mol}^{-1}$ . Using the metal–ring centre distances and associated force constants for  $\text{Fe}(\text{Cp})_2$  and  $\text{Fe}(\text{Cp})_2^+$  given in Appendix III, eq. (16.14) leads to  $\Delta G_s^* = 1\text{ kJ mol}^{-1}$ , when  $c_n = 4$  because of the presence of two vibrating bonds in each reactant. The success of TM in estimating the self-exchange barrier of  $\text{Fe}(\text{Cp})_2/\text{Fe}(\text{Cp})_2^+$  in acetonitrile but not in the gas phase substantiates the suspicion that it overestimates the solvent contribution  $\Delta G_s^*$  in polar media and that is compensated by an underestimate of the internal reorganisation  $\Delta G_v^*$ . In the gas phase, this compensation cannot take place and the model fails to reproduce the experimental barrier of the  $\text{Fe}(\text{Cp})_2/\text{Fe}(\text{Cp})_2^+$  exchange.

An interesting case study involving organic molecules is the self-exchange of alkylhydrazines $^{0+/}$ , some of which are illustrated in Figure 16.5. These self-exchanges are particularly interesting because the molecules are approximately spherical, the active orbitals in the electron-transfer process are centred on the nitrogen atoms, and they are isolated from the other partner by a “hydrocarbon layer”. The sphere centred on the NN bond has

a radius of 3.93 Å for 22/u22 and 4.34 Å for iPr<sub>2</sub>N)<sub>2</sub>. In addition, the self-exchanges of alkylhydrazines are much slower than those of the more common aromatic hydrocarbons, and, in solution, they can be studied far from the limit of diffusion-controlled rates.

The solvent independence of the 22/u22 self-exchanges was presented in Figure 16.4. The gas-phase electron exchange reaction in the Me<sub>2</sub>N<sub>2</sub>)<sub>2</sub>/Me<sub>2</sub>N<sub>2</sub>)<sub>2</sub><sup>+</sup> complex was studied by Nelsen and co-workers. The heat of association of the complex is −54 kJ mol<sup>−1</sup> and the activation energy is 23 kJ mol<sup>−1</sup>, which means that the central barrier for the self-exchange in the complex is 77 kJ mol<sup>−1</sup> [22]. This barrier is very close to that obtained in acetonitrile, 72 kJ mol<sup>−1</sup>, and similar results were obtained for eight other compounds, which led Nelson [23] to conclude that “There is apparently a closer correspondence of ET barriers in the presence and absence of solvent than most people expected”. In fact, eq. (16.13) with  $r = 8$  Å and the data of acetonitrile gives  $\Delta G_s^* = 23$  kJ mol<sup>−1</sup>, but the barrier in the gas phase is not less than in the acetonitrile. These data indicate that electron transfers in organic systems also involve a completely solute driven processes.

#### 16.2.4 ISM as a criterion for solute-driven electron transfers

The energy barrier of the Fe(Cp)<sub>2</sub>/Fe(Cp)<sub>2</sub><sup>+</sup> self-exchange can also be explored with the ISM, under the approximations discussed in Chapter 15 for the use of this model in the calculation of Franck–Condon factors. According to ISM, the sum of bond distortions from the equilibrium to the transition-state configuration is, for a self-exchange reaction

$$d_0 = |l_r^\ddagger - l_r| + |l_p^\ddagger - l_p| = \frac{0.108}{n^\ddagger} (l_{\text{ox}} + l_{\text{red}}) \quad (16.21)$$

where the term “transition state” is used to describe the activated nuclear configuration that the reactants must reach to transfer an electron. The bond orders are preserved along the reaction coordinate for an electron transfer, and  $n^\ddagger$  represents the average bond order of the two reactants. For Fe(Cp)<sub>2</sub> this requires an analysis of its electronic configuration, as shown in Figure 16.6.

The principal bonding interaction occurs between the d<sub>xz</sub> and d<sub>yz</sub> orbitals (transforming together as e<sub>1''</sub>) and the e<sub>1''</sub> symmetry-adapted linear combinations of ligand orbitals. Their excellent overlap gives delocalised  $\pi$ -type metal-ring bonds. The d<sub>x<sup>2</sup>-y<sup>2</sup></sub> and d<sub>xy</sub> (e<sub>2'</sub>) orbitals interact with e<sub>2'</sub> symmetry-adapted linear combinations of ligand orbitals. The d<sub>z<sup>2</sup></sub> (a<sub>1'</sub>) orbital, although of the same symmetry as the Cp  $\pi$  orbitals and strongly directed towards the ligands, has a nodal surface which coincides with that of the Cp  $\pi$  orbitals and their interaction is weak. The bonding character of the e<sub>2'</sub> and a<sub>1'</sub> orbitals (LUMO; lowest unoccupied molecular orbital) can be assessed by removing one of their electrons to yield Fe(Cp)<sub>2</sub><sup>+</sup>. This process is accompanied by an increase in the bond length and a decrease in the force constant, which is consistent with a decrease in M–Cp bonding. Thus, the bond order of Fe(Cp)<sub>2</sub> must be greater than 1.0, but is probably less than 1.5. In contrast, the bond order of Fe(Cp)<sub>2</sub><sup>+</sup> is reduced with respect to Fe(Cp)<sub>2</sub>, and should be close to 1.0. A reasonable estimate for the Fe(Cp)<sub>2</sub>/Fe(Cp)<sub>2</sub><sup>+</sup> self-exchange is  $n^\ddagger = 1.25$ , which gives  $d = 0.287$  Å.

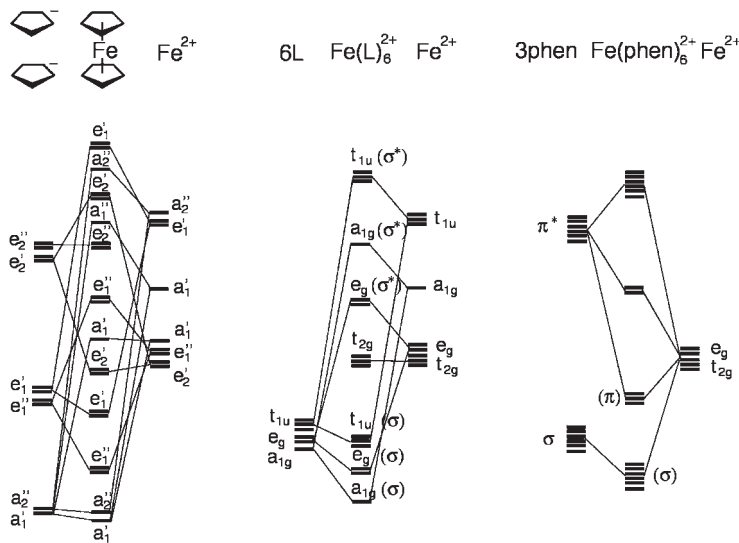


**Figure 16.6** Molecular orbitals of transition-metal complexes, employed to estimate metal-ligand bond orders. Left: ferrocene assuming a  $D_{5h}$  symmetry; in ferrocene and the other 18-electrons bis(cyclopentadienyl) complexes the  $a_1'$  orbital and all the other lower-energy orbitals are full but the  $e_1''$  and higher-energy orbitals are empty. Centre:  $Fe(OH_2)_6^{2+}$  with a  $O_h$  symmetry. Right:  $Fe(phen)_6^{2+}$  with  $O_h$  symmetry, emphasising the role of the ligand  $\pi^*$  orbitals in  $\pi$ -back bonding.

The transition-state energy for a self-exchange is given by

$$\Delta G_0^\ddagger = \frac{1}{2} f_{\text{eff}} \left( \frac{d_0}{2} \right)^2 \quad (16.22)$$

where the value of effective force constant depends on the use of a normal or local mode treatment of the reactive modes, as discussed in Chapter 15. The Cp–M stretch force constants of  $Fe(Cp)_2$  and  $Fe(Cp)_2^+$  are obtained from

$$f_{\text{sym}} = 4\pi^2 \bar{v}_{\text{sym}}^2 c^2 \mu = 3.548 \times 10^{-4} \bar{v}_{\text{sym}}^2 \mu \quad (16.23)$$

where the constant involves the symmetric stretching frequency expressed in  $\text{cm}^{-1}$ , the reduced mass in amu and the force constant in  $\text{kJ mol}^{-1} \text{\AA}^{-2}$ . These values for the force constants rely on a simple three-body model where the central atom does not move within the symmetrical stretching regime, and each Cp ring is considered in the first approximation as a point mass equal to 65 amu, that is,  $\mu = 65$  amu. The Cp–M–Cp symmetric stretching occur at  $\bar{v}_{\text{sym}} = 303 \text{ cm}^{-1}$  for  $Fe(Cp)_2$  and at a slightly lower frequency for  $Fe(Cp)_2^+$ , consistent with its longer Cp–M bond. The anti-symmetric mode is observed at a higher frequency,  $\bar{v}_{\text{asym}} = 478 \text{ cm}^{-1}$ . In Chapter 15, we discussed the difference between

local and normal mode behaviour, and concluded that CH bonds in aromatic hydrocarbons are best described as a local modes. Local mode behaviour is expected from small inter-bond coupling constants between anharmonic vibrational modes. The inter-bond coupling constant is related to the vibrational splitting between symmetric and anti-symmetric stretching vibrations. For example, the CH symmetric stretching of benzene ( $a_{1g}$  symmetry,  $\bar{v}_1$  in the Herzberg notation) occurs at  $3062\text{ cm}^{-1}$ , whereas the CH anti-symmetric stretching ( $b_{1u}$  symmetry,  $\bar{v}_5$ ) occurs at  $3068\text{ cm}^{-1}$ , an inter-bond coupling of  $\xi = |\bar{v}_{\text{sym}} - \bar{v}_{\text{asym}}|/2 = 3\text{ cm}^{-1}$ . This is in contrast with the  $a_{1g}$  symmetry ring-breathing mode ( $\bar{v}_2 = 992\text{ cm}^{-1}$ ) and  $b_{2u}$  symmetry alternating elongation–contraction CC mode ( $\bar{v}_9 = 1310\text{ cm}^{-1}$ ), which have a coupling  $\xi = 159\text{ cm}^{-1}$  and are best described as normal modes. The splitting between symmetric ( $\bar{v}_1$ ) and anti-symmetric ( $\bar{v}_3$ ) metal-ligand stretching vibrations in octahedral hexaammine or hexaaqua complexes is also small ( $\xi = 10–20\text{ cm}^{-1}$ ) and these have to be treated as local modes. However, the values observed for metallocenes ( $\xi = 90 – 60\text{ cm}^{-1}$ ) are intermediate between those of typical local and normal mode behaviour. Using a local mode behaviour, the calculated barrier is  $\Delta G^\ddagger = 26.5\text{ kJ mol}^{-1}$ , intermediate between the value inferred from the gas-phase efficiency and the enthalpy of activation in acetonitrile.

The Franck–Condon factor of the  $\text{Me}_2\text{N}_2)_2/\text{Me}_2\text{N}_2)_2^+$  exchange is principally associated with changes in the NN bond. The X-ray geometries of the similar  $i\text{Pr}_2\text{N}_2)_2$  and  $i\text{Pr}_2\text{N}_2)_2^+$  compounds are known, and reveal a decrease in the NN bond length from  $1.394$  to  $1.333\text{ \AA}$  when the neutral [24] is oxidised to the cation [25], concomitant with the change in the lone pair/lone pair dihedral angle  $\theta$  from *ca.*  $90^\circ$  to  $0^\circ$ . Clearly, the removal of a non-bonding electron from a nitrogen atom leads to an increase in bonding, and the N–N bond acquires some three-electron bond character. For simplicity, this bond can still be characterised with  $n^\ddagger = 1$ , which is probably an underestimate but compensates for the neglect of changes in the other bonds. With  $n^\ddagger = 1$ , the N–N bond lengths discussed above and the corresponding force constants given in Appendix III, eq. (16.21) give  $d_0 = 0.2945\text{ \AA}$ , which, using eq. (16.22), leads to  $\Delta G^\ddagger = 78\text{ kJ mol}^{-1}$ . In this case there is no ambiguity as to the nature of the local or normal mode behaviour of the N–N mode, because only one bond is involved in the reaction coordinate, and the force constant is the average of the neutral and cation N–N force constants. The barrier calculated by this model is in excellent agreement with the barriers observed in the gas phase and in solution.

We could suggest that within the ISM formalism we can explain all the ET data. However, reducing the role of the solvent to a thermodynamic effect, which is reflected in  $\Delta G^0$ , and, occasionally, to specific interactions (hydrogen bonding, heat sink) with the redox centres, is a major change in the paradigm shared by most practitioners of this field. We need to reconsider the view that TM offers to get a more coherent picture of solvent effects on such reactions and, in general, within the field of chemical kinetics. In contrast with TM, ISM, employs a common theoretical formalism for many important types of chemical transformations, which stresses the role of the electronic properties of reactive bonds and also of reaction energy in chemical reactivity. This formalism was discussed in detail in the previous chapters, and will be pursued further in this chapter in the interpretation of the rates of electron-transfer reactions.

### 16.3 ISM AND ELECTRON-TRANSFER REACTIONS

#### 16.3.1 Representing ET reactions by the crossing of two potential-energy curves

Electron-transfer reactions, such as the  $\text{Fe}(\text{OH}_2)_6^{3+/2+}$  self-exchange, mechanism 16.I, do not involve any bond breaking. In this specific case the Fe–O bonds linked to the 6 water molecules of the first coordination shells of Fe(III) remain intact. However, this does not mean that there is not a substantial distortion of the Fe–O bonds in the electron-transfer process. In fact, such a bond rearrangement is fundamental for the electron-transfer step and allows it to occur.

The molecular orbitals for the  $\sigma$  metal-ligand bonds in  $\text{Fe}(\text{OH}_2)_6^{2+}$  arise from the interaction of 6 metal 4s,  $4p_x$ ,  $4p_y$ ,  $4p_z$ ,  $3d_{x^2-y^2}$ ,  $3d_{z^2}$  orbitals with the corresponding ligand  $\sigma$  orbitals sharing the same symmetry (Figure 16.6). When we consider the distribution of electron spins in the d-orbitals for the ligand fields of  $\text{Fe}(\text{OH}_2)_6^{3+}$  and  $\text{Fe}(\text{OH}_2)_6^{2+}$ , it becomes evident that electron transfer goes from a  $t_{2g}(\pi)$  orbital of one species to an orbital of the same symmetry in the other ion. This means that the bond order of each bond is preserved,  $n = 1$ , and that no electronic restriction exists for such a transfer. For this electron transfer, the spin changes by  $1/2$ ,  $S(\text{Fe}^{3+}) = 5/2$  and  $S'(\text{Fe}^{2+}) = 4/2$ , where S and S' are the spin quantum numbers of oxidised and reduced species.

Let us assume, for simplicity, that the hydrated iron ions are each bonded to a single water molecule and, therefore, have a single Fe–O bond.

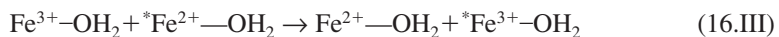
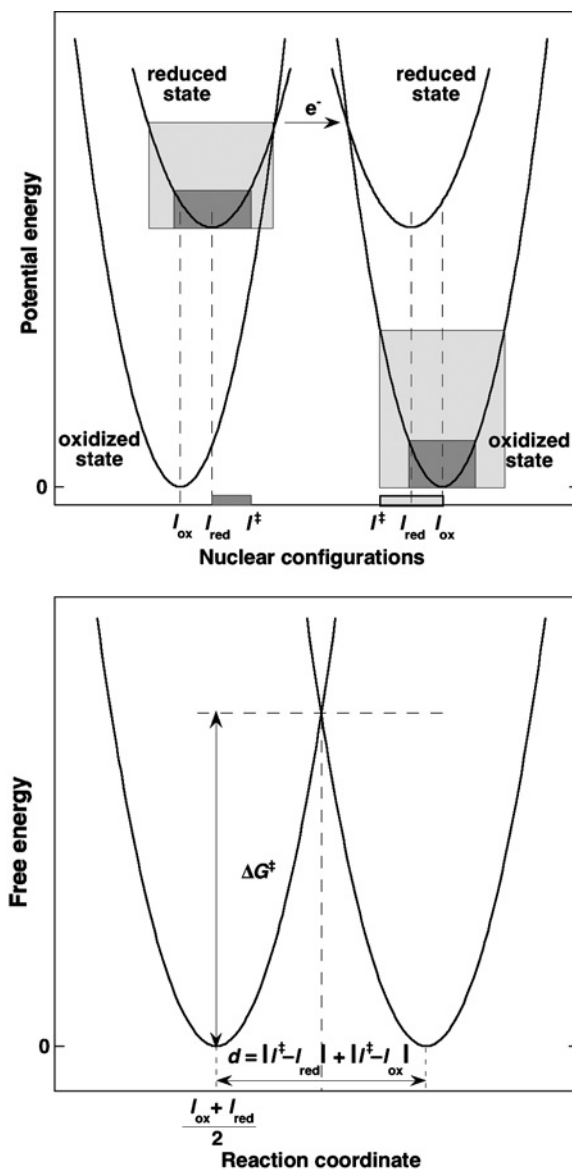


Figure 16.7 represents in qualitative terms the potential-energy curves for the two metal–water bonds of the oxidised and reduced species. According to the Franck–Condon principle, the  $\text{Fe}^{3+}\text{—O}$  and  $\text{Fe}^{2+}\text{—O}$  bonds have to reach to a common configuration, which we will loosely call a “transition state”, before the electron is transferred. The products then relax from their configuration at the “transition state” to their equilibrium bond lengths. A more useful representation of the reaction coordinate combines both reactants and products with in the same curve. At the “transition state”, the identical nuclear configurations of the Fe–O bonds can be regarded as having the same value of  $n^\ddagger$ , because the same bond length between the same two atoms must correspond to the same electronic configuration, and hence to the same bond order. This principle is also the basis of ISM, and we can anticipate that the nuclear distortion from equilibrium to the transition state of a self-exchange reaction should have the form of eq. (16.21). The usefulness of this equation rests on the transformation of the two Fe–O bond coordinates into a single coordinate that accounts for the concerted changes taking place in the two bonds in different regions of the space. The nature of this transformation is the same as that discussed in the connection between Figures 15.14 and 15.16 in Chapter 15. Its appropriateness ultimately depends on the ability to reproduce the correct energy of the “transition state”.

We must provide a note of caution on interpretation of the crossing between the reactants and products curves in Figure 16.7. The crossing is represented as weakly avoided, assuming a weak electronic coupling between reactants and products curves. This is



**Figure 16.7** Transformation of the reaction coordinate according to ISM. The shaded areas in the upper panel reflect the probabilities of finding the reactants in the reduced and oxidised states in the nuclear configurations. The ISM reaction coordinate is the sum of the two reactants bond distortions from equilibrium to transition-state configurations.

consistent with non-adiabatic electron transfers, where the energy of the crossing point corresponds to the activation energy. The limit between adiabatic and non-adiabatic reactions can be defined, rather arbitrarily, as an electronic coupling of  $4 \text{ kJ mol}^{-1}$  ( $330 \text{ cm}^{-1}$ ), which is enough to let the electronic factor approach unity, but not sufficient to reduce the barrier appreciably. A stronger non-adiabaticity ( $|V_{\text{ks}}| \ll 4 \text{ kJ mol}^{-1}$ ) does not significantly change the energy of the crossing point, but reduces the reaction frequency.

According to eq. (16.22), the energy of the crossing point depends on the value of the effective force constant. In TM-1, eq. (16.14), the force constant is obtained from a symmetrisation procedure and then multiplied by the number of bonds in the reaction coordinate. In ISM, the transformation in Figure 16.7 corresponds to placing the two reactants in an average energy position, to obtain a thermoneutral process for a self-exchange, and their effective force constant is also the average of the force constants for the oxidised and reduced species.

$$f_r = \frac{f_{\text{ox}} + f_{\text{red}}}{2} \quad (16.24)$$

The same treatment is used to obtain the effective force constant of products,  $f_p$ . Eq. (16.24) is an effective way to consider the equation of Scheme (16.III) as divided by two, since the energy barrier for the reaction is defined for 1 mol of reactants. For consistency, the same averaging procedure is also applied to equilibrium bond lengths.

$$l_{r,\text{eq}} = \frac{l_{\text{ox,eq}} + l_{\text{red,eq}}}{2} \quad (16.25)$$

We will subsequently represent such lengths in a more simplified manner by  $l_{\text{ox}}$  and  $l_{\text{red}}$ . It must be emphasised that eq. (16.21) already accounts for the existence of two reactants (and two products) in the reaction coordinate, because it gives the sum of the bond extensions in the two species.

### 16.3.2 Adiabatic self-exchanges of transition-metal complexes

Following ISM, the sum of bond length extensions to the transition state in a self-exchange is given by eq. (16.21). Since the bond order of  $\text{Fe}^{3+}-\text{OH}_2$  and  $\text{Fe}^{2+}-\text{OH}_2$  is approximately that of a single bond (bond order  $n = 1$ ), we take the transition-state–bond order to be unity,  $(n_{\text{ox}} + n_{\text{red}})/2 = n^{\ddagger} = 1$ . The real molecular system contains 6 single bonds in each reactant, mechanism (16.I), because each Fe ion has 6 water molecules in the first coordination shell. In view of the small inter-bond coupling of the  $\text{Fe}^{3+}-\text{OH}_2$  bonds in these complexes, the 6 iron–oxygen bonds behave as local modes, and their effective force constant is

$$f = f_r = f_p = \sqrt{6} \frac{f_{\text{ox}} + f_{\text{red}}}{2} \quad (16.26)$$

The energy barrier,  $\Delta G^\ddagger$ , will be given by

$$\Delta G^\ddagger = \frac{1}{2} \sqrt{6} \frac{f_{\text{ox}} + f_{\text{red}}}{2} \left( \frac{d}{2} \right)^2 \quad (16.27)$$

or taking into consideration eq. (16.21),

$$\Delta G^\ddagger = \frac{\sqrt{6}}{16} (f_{\text{ox}} + f_{\text{red}}) \left[ \frac{0.108}{n^\ddagger} (l_{\text{ox}} + l_{\text{red}}) \right]^2 \quad (16.28)$$

With the relevant structural data listed in Appendix III, one estimates

$$\Delta G^\ddagger = \frac{\sqrt{6}}{16} (1.53 + 0.96) \times 10^3 \text{ kJ mol}^{-1} \text{ \AA}^{-2} \left[ \frac{0.108}{1} (1.98 + 2.10) \text{\AA} \right]^2 \quad (16.29)$$

and  $\Delta G^\ddagger = 74 \text{ kJ mol}^{-1}$ .

The frequency for conversion of the reactants species to the common activated configuration is that of the stretching frequency modes of the Fe–O bonds within the hydrated metal ions:  $\bar{v}_{\text{ox}} = 490 \text{ cm}^{-1}$  and  $\bar{v}_{\text{red}} = 389 \text{ cm}^{-1}$ . With an average frequency  $\bar{v}_N = 440 \text{ cm}^{-1}$ , the frequency factor for the process,  $\bar{v}$ , is that of the nuclear motions,  $\bar{v}_N$ ,

$$v = v_N = \omega c = 1.3 \times 10^{13} \text{ sec}^{-1} \quad (16.30)$$

when the effective electronic frequency is greater than this value. This is true when  $|V_{ks}^\text{el}| > 300 \text{ cm}^{-1}$  ( $3.6 \text{ kJ mol}^{-1}$ ) for  $\lambda = 4\Delta G^\ddagger = 296 \text{ kJ mol}^{-1}$ , as discussed in Section 15.7. Under these conditions, which are in the borderline region between non-adiabatic and adiabatic processes, the rate constant is given by:

$$k_{\text{ISM}} = K_c v_N \exp\left(-\frac{\Delta G^\ddagger}{RT}\right) \quad (16.31)$$

where  $K_c$  is the equilibrium constant for the formation of reactant pairs separated by a distance  $r$ . According to the Eigen–Fuoss model, the stability constant of the precursor complex is

$$K_c = \frac{4\pi N_A r^3}{3000} \exp\left(-\frac{w_r}{RT}\right) \quad (16.32)$$

and its numerical value ranges from  $0.1 \text{ M}^{-1}$  for the  $\text{Fe(OH}_2)_6^{3+/2+}$  exchange when the ionic strength is  $0.55 \text{ M}$ , to  $0.8 \text{ M}^{-1}$  for the  $\text{Fe(Cp)}_2^{+/-}$  exchange. Lower values of  $r$  decrease  $K_c$  but increase  $|V_{ks}^\text{el}|$ . For the small range of  $|V_{ks}^\text{el}|$  that corresponds to nearly adiabatic reactions where  $\bar{v} \approx \bar{v}_N$ , these effects tend to self compensate and the neglect of  $|V_{ks}^\text{el}|$  in the reduction of  $\Delta G^\ddagger$ , can be offset by the assumption that  $K_c \approx 1 \text{ M}^{-1}$ . Thus, for bimolecular electronic transfers in solutions with a high ionic strength or those involving one uncharged

partner, we can use the assumption that  $K_c \approx 1 \text{ M}^{-1}$ . Under these approximations, the rate constant estimated by ISM for the reaction  $\text{Fe(OH}_2\text{)}_6^{3+/2+}$  at 298 K, is  $k_{\text{ISM}} = 1.2 \text{ M}^{-1} \text{ sec}^{-1}$ , in very good agreement with the experimental rate constant,  $k_{\text{exp}} = 1.1 \text{ M}^{-1} \text{ sec}^{-1}$ .

Given the approximate nature of these calculations, the frequency factor for bimolecular electron transfers in transition-metal complexes can be taken as  $K_c \bar{v}_N = 10^{13} \text{ M}^{-1} \text{ sec}^{-1}$ . With this pre-exponential factor and the barrier calculated above for the  $\text{Fe(Cp)}_2/\text{Fe(Cp)}_2^+$  exchange,  $\Delta G^\ddagger = 26.5 \text{ kJ mol}^{-1}$  with  $n^\ddagger = 1.25$ , we obtain  $k_{\text{ISM}} = 2.1 \times 10^8 \text{ M}^{-1} \text{ sec}^{-1}$ . The experimental rate in acetonitrile, extrapolated to zero ionic strength, is  $9.3 \times 10^6 \text{ M}^{-1} \text{ sec}^{-1}$  [21]. It could be anticipated that the calculated rate would be an upper limit for the experimental values in solution because the bonding character of the  $e_2'$  and  $a_1'$  orbitals was overemphasised. With  $n^\ddagger = 1$ , a lower limit for this parameter, the calculated rate is  $k_{\text{ISM}} = 5.0 \times 10^5 \text{ M}^{-1} \text{ sec}^{-1}$ .

### 16.3.3 Outer-sphere electron transfers with characteristics of an inner-sphere mechanism

Another representative class of outer-sphere electron transfers is the exchange between iron(II/III)—phenanthroline complexes



The metallic centres in the collisional complex are well separated, by at least  $r_{\text{Fe,Fe}} = 13.6 \text{ \AA}$ , due to the size of the ligands. In contrast, for the  $\text{Fe(OH}_2\text{)}_6^{3+/2+}$  complexes the corresponding distance is much smaller, and an electron can easily jump between the two iron atoms leading to a nearly adiabatic reaction, as illustrated in Figure 16.8. In  $\text{Fe(phen)}_3^{3+/2+}$  complexes the distance is too large for a nearly adiabatic electron jump from one metal centre

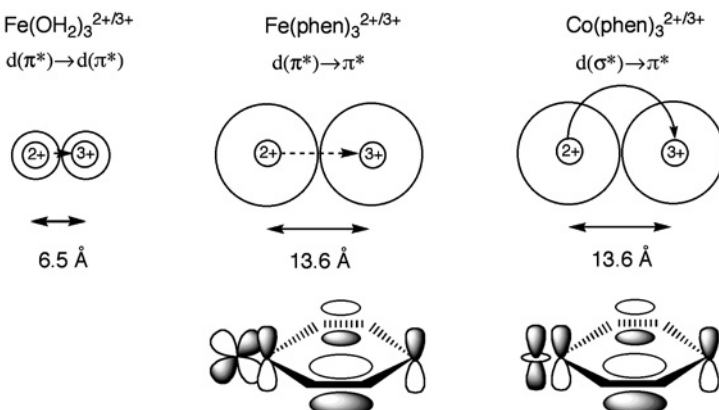


**Figure 16.8** Schematic illustration of the distances involved in electron transfers between metal centres, with the emphases on the favourable orbital overlap between the active redox orbitals of iron and the phenanthroline  $\pi^*$  (LUMO) orbital, and the zero overlap between the redox active orbitals of cobalt and the same ligand orbital.

to the other. However, although the electron is exchanged between  $d(\pi)$  orbitals centred in metal ions separated by 13.6 Å, the ligand  $\pi^*$  (LUMO) has a good overlap with the  $d(\pi)$  iron orbital and provides a conductive *bridge* for the transfer of the electron from metal to the other. This orbital connection, also illustrated in Figure 16.8, favours a nearly adiabatic electron transfer between iron–phenanthroline complexes.

In addition to providing a conducting bridge for the transfer of an electron, the good overlap between the  $\pi^*$  (LUMO) orbitals of the ligands and the  $t_{2g}$  ( $d_{xy}$ ,  $d_{xz}$ ,  $d_{yz}$ ) orbitals of the metal also allows for the possibility of  $\pi$  bonding. Pi bonding in coordination complexes is most relevant in terms of chemical reactivity when the ligand has empty  $\pi^*$  orbitals, or  $\pi$  acceptor ligands. In this case, the ligand  $\pi^*$  orbitals have energies greater than, but near those of the metal  $t_{2g}$  orbitals, with which they overlap. As a result, they form molecular orbitals, with the bonding orbitals being lower in energy than the initial metal  $t_{2g}$  orbitals. The corresponding anti-bonding orbitals are higher in energy than the  $e_g$   $\sigma$  anti-bonding orbitals. Metal ion d electrons occupy the bonding orbitals, resulting in increased bonding strength and bond orders. This metal-to-ligand  $\pi$  bonding is also called  $\pi$  back bonding, with electrons from d orbitals of the metal donated to the ligands [26]. In the first approximation, the number of bonding orbitals increases to 9, and the average bond order of the  $\text{Fe}(\text{phen})_3^{2+}$  complex is  $n = 1.5$ . Using the local-mode approximation for the six modes involved in the reaction coordinate and  $n^\ddagger = 1.5$ , the barrier calculated with the data on the Fe–N bonds listed in Appendix III, is  $\Delta G^\ddagger = 35 \text{ kJ mol}^{-1}$ . This barrier together with  $K_c \bar{v}_N = 10^{13} \text{ M}^{-1} \text{ sec}^{-1}$  gives  $k_{\text{ISM}} = 7.3 \times 10^6 \text{ M}^{-1} \text{ sec}^{-1}$ , which is lower than the experimental value,  $k_{\text{exp}} = 3.3 \times 10^8 \text{ M}^{-1} \text{ sec}^{-1}$ . This difference indicates the need for modification of the assumptions used to derive the parameters employed in the calculation. Figure 16.9 shows that a resonance effect in the transition state of an electron transfer involving metal–ligand  $\pi$  back bonding may shift electronic density around the metal–ligand bonds in the activated common configuration, such that  $n^\ddagger = 2$ . This effect is equivalent to the maximum electron inflow inside the transition state provided by the electrophilicity index of Parr. The importance of resonance in electron transfers was emphasised earlier for gas-phase reactions, and Eberson and Shaik [27] have argued that it also plays an important role in solution when there is a good overlap between the two LUMO of the two reactants. With  $n^\ddagger = 2$  and the data in Appendix III, eq. (16.28) gives  $\Delta G^\ddagger = 20 \text{ kJ mol}^{-1}$  and eq. (16.31) gives  $k_{\text{ISM}} = 3 \times 10^9 \text{ M}^{-1} \text{ sec}^{-1}$ . Since this value is very close to the rate of diffusion in water,  $k_{\text{diff}} = 7 \times 10^9 \text{ M}^{-1} \text{ sec}^{-1}$ , the observed rate constant,  $k_{\text{obs}}$ , should be corrected for the effect of diffusion as given by the expression

$$\frac{1}{k_{\text{obs}}} = \frac{1}{k_{\text{diff}}} + \frac{1}{k_{\text{ISM}}} \quad (16.33)$$

which leads to a rate in much agreement with experiment,  $k_{\text{obs}} = 2 \times 10^9 \text{ M}^{-1} \text{ sec}^{-1}$ .

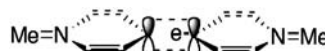
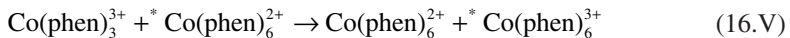


**Figure 16.9** Electronic interaction between metal–ligand complexes when the ligands have empty  $\pi^*$  orbitals, leading to transition-state bond orders  $n^\ddagger = 2$ .

## 16.4 NON-ADIABATIC SELF-EXCHANGES OF TRANSITION-METAL COMPLEXES

### 16.4.1 A source of non-adiabaticity: orbital symmetry

An important example of non-adiabatic electron transfer is the self-exchange process of the phenanthroline complex of cobalt (II and III),



Although this appears to be identical to reaction (16.IV), the rate of electron transfer is considerably slower, *ca.* seven orders of magnitude,  $k = 12 \text{ M}^{-1} \text{ sec}^{-1}$ . This dramatic difference is related to the nature of the orbitals involved. In contrast to the reactions of  $\text{Fe}(\text{phen})_3^{3+/2+}$ , where the transfer of the electron occurs from a  $d(t_{2g})$  orbital, of  $\pi$  symmetry, the active redox orbitals of  $\text{Co}(\text{phen})_3^{2+}$  are  $d(e_g)$  orbitals, of  $\sigma^*$  symmetry. The overlap of this orbital with the LUMO orbital of the ligand is zero for symmetry reasons, as illustrated in Figure 16.8. Therefore, the  $\pi^*$  LUMO orbital of the ligand cannot operate as a conducting wire between the two Co-metal centres which are  $13.6 \text{ \AA}$  apart. The only way that the electron can be transferred from one ion to the other is through quantum mechanical tunnelling.

### 16.4.2 Electron tunnelling at a distance

The expressions for quantum mechanical tunnelling were presented in Chapter 6 and the application, to electron transfers is discussed in Chapter 15. Briefly, the electron-tunnelling probability through a square-potential barrier can be calculated when the height and width of the barrier are known. In electron transfer between the cobalt centres indicated above, the width of the tunnelling barrier is the metal-to-metal distance,  $r = 13.6 \text{ \AA}$ . In aromatic hydrocarbons, where the LUMO is delocalised over all the conjugated bonds, it is more appropriate to define the tunnelling barrier as the distance between the edges of the aromatic systems. The distance-dependence of tunnelling probability is

$$\chi_r = \exp(-\beta r) \quad (16.34)$$

where  $\beta$  is an electronic decay coefficient, also called a *distance-dependence factor*, which is given by the expression:

$$\beta = \frac{4\pi}{h} \sqrt{2m_e \Phi} = 1.025 \sqrt{\Phi} \quad (16.35)$$

where the numerical value corresponds to the barrier height  $\Phi$  expressed in eV and  $\beta$  given in  $\text{\AA}^{-1}$ . We explained in Chapter 15 that the barrier height is related to the energy difference between the electron at rest in the vacuum, in the highest occupied molecular orbital

(HOMO) of the donor,  $\Phi_0$ , and to the refractive index of the material separating the donor and acceptor

$$\Phi = \frac{\Phi_0}{n_D^2} \quad (16.36)$$

$\Phi_0$  is also the absolute potential of the electron in the donor, and can be estimated from the electrode potential of the metal complex,  $E^0$ , measured with respect to the normal hydrogen electrode (NHE). Taking  $\Phi_0(\text{NHE}) = 4.44 \text{ eV}$ , the absolute potential of the electron in the donor is

$$\Phi_0 = 4.44 + E^0 \quad (16.37)$$

In this example, the reduction potential of  $\text{Co}(\text{phen})_3^{3+}$  is  $E^0 = 0.37 \text{ eV}$ , and for the phenanthroline spacer,  $n_D(\text{phen}) = 1.62$ . With the relevant set of data, we obtain  $\Phi_0 = 4.81, 1.833$  and  $\beta = 1.388 \text{ \AA}^{-1}$ . From eq. (16.34) with a separation distance of the metal centres of  $r = 13.6 \text{ \AA}$ , the probability for the tunnelling of electron is quite low,  $\chi_r = 6.3 \times 10^{-9}$ .

The calculations of non-adiabaticity of electron transfers require the assessment of the frequency of the electron transfer under the effect of the separation distance. The reaction frequency is the product of an electronic frequency,  $v_{\text{el}} = 10^{15} \text{ sec}^{-1}$ , and the probability of transfer at a distance  $r$ , i.e.,  $v_{\text{el}}\chi_r$ . The electron transfer is a nearly adiabatic process when it is controlled by the nuclear motion,  $v_N < v_{\text{el}}\chi_r$ , but becomes strongly non-adiabatic when it is controlled by the effective electronic frequency motion,  $v_N > v_{\text{el}}\chi_r$ .

#### 16.4.3 Non-adiabaticity due to spin forbidden processes

Some electron exchanges of cobalt complexes involve changes in spin configuration, from low-spin to high-spin such that  $S' \neq S \pm 1/2$ , and this can lead to another source of non-adiabaticity. The spin forbidden factor,  $\chi_s$ , is entirely empirical within the present formalism, as well as within the TM formalism. For the complexes  $\text{Co}(\text{phen})_3^{3+/2+}$  experimental evidence, also supplemented by quantum mechanical calculations, suggest that  $\chi_s \approx 10^{-3}$ , and as a rule of thumb we will employ this value for spin-forbidden electron transfers in transition-metal complexes. Where no heavy metals or paramagnetic species are involved, we expect to have  $\chi_s \ll 10^{-3}$ , as shown in Chapter 15 for aromatic hydrocarbons.

Finally, when the reaction barrier is estimated, the rate constant will be given by

$$k = K_c v_{\text{el}} \chi_r \chi_s \exp\left(-\frac{\Delta G^\ddagger}{RT}\right) \quad (16.38)$$

For the self-exchange reaction of  $\text{Co}(\text{phen})_3^{3+/2+}$  the frequency factor will be  $v = (10^{15})(6.3 \times 10^{-9})(10^{-3}) = 6.3 \times 10^3 \text{ sec}^{-1}$ , and  $K_c \approx 1 \text{ M}^{-1}$ , as usual. With the structural data in Appendix III, we can estimate  $\Delta G^\ddagger = 15 \text{ kJ mol}^{-1}$  and obtain a rate constant  $k_{\text{ISM}} = 14 \text{ M}^{-1} \text{ sec}^{-1}$ , which compares very well with the experimental data at room temperature,  $k_{\text{exp}} = 12 \text{ M}^{-1} \text{ sec}^{-1}$ .

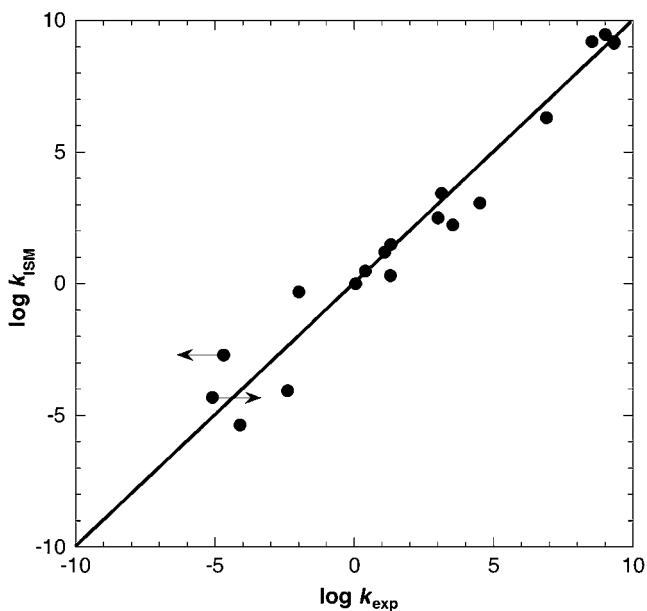


**Figure 16.10** Comparison between electron self-exchange rates of transition-metal complexes calculated by ISM and experimental data, in water at room temperature, from ref. [1].

Figure 16.10 illustrates the results from application of ISM for the self-exchange rates in transition-metal complexes. These are at least as good as those provided by TM-1, but can also treat the “anomalous” case of the  $\text{Co}(\text{OH}_2)_6^{3+/2+}$  system. This reveals that ISM provides an alternative view for electron-transfer self-exchange reactions in transition-metal complexes. It is a view not in terms of solvent- and solute-driven reactions, as in the formalism of Marcus, but entirely in terms of solute-driven reactions. The relevant factors are force constants, the sum of the equilibrium bond lengths of oxidised and reduced species and the electronic properties of the same bonds (*bond orders*).

## 16.5 ELECTRON SELF-EXCHANGES OF ORGANIC MOLECULES

Electron-transfer reactions occur frequently between organic molecules and their radical cations or anions. A good example is the reaction between naphthalene and its radical anion



One electron is transferred from a  $\pi$  orbital. The bond extensions occur on the carbon skeleton and do not significantly involve the CH bonds. The reactive bonds are therefore considered to be the CC bonds of the aromatic ring. Assuming that the carbon–carbon

stretching modes behave as normal modes, the effective force constant for naphthalene is given by

$$f_{\text{ox}} = \frac{\sum_{i=1}^n f_i}{n} \quad (16.39)$$

Vibrational data are available from normal mode analysis of vibrational spectra, in particular from the symmetric stretching modes that employ valence force fields. For naphthalene, we obtain  $f_{\text{ox}} = 3.81 \times 10^3 \text{ kJ mol}^{-1} \text{ \AA}^{-2}$ . Using the same averaging manner, we can estimate the average bond length

$$l_{\text{ox}} = \frac{\sum_{i=1}^n l_i}{n} \quad (16.40)$$

From the structural data the result is  $l_{\text{ox}} = 1.398 \text{ \AA}$ . The same procedure can be employed for the radical anion data, but for the majority of the cases such experimental data are not available. Therefore, we will employ, without any significant error, the data for the neutral species, since quantum mechanical calculations show that the changes in CC bond lengths are very small between neutral and mono-charged aromatic species. Additionally, the changes in the bond lengths tend to be compensated by opposing changes in the force constants. In contrast, changes in  $n^\ddagger$  quite significantly affect the energy barriers, and require a more detailed consideration of the bond orders in the neutral and anion species.

For the neutral naphthalene molecule, the average bond order of the carbon–carbon bonds is

$$n_{\text{ox}} = \frac{5 \times 2 + 6}{11} = 1.455 \quad (16.41)$$

resulting from the 5 C = C and 6 C–C bonds of the naphthalene aromatic ring. For the radical anion the extra electron has an anti-bonding character,  $\pi$ , and the bond order can be written as

$$n_{\text{red}} = n_{\text{ox}} - \frac{0.5}{11} = 1.409 \quad (16.42)$$

Using eq. (11.12) one obtains  $n^\ddagger = 1.43$ .

The energy barrier for local mode behaviour is given by eq. (16.27). For normal modes, the equivalent expression is

$$\Delta G^\ddagger = \frac{1}{2} \frac{f_{\text{ox}} + f_{\text{red}}}{2} \left( \frac{d}{2} \right)^2 \quad (16.43)$$

With the structural data mentioned above and the value  $n^\ddagger = 1.43$ , eqs. (16.13) and (16.29) lead to  $\Delta G^\ddagger = 21.2 \text{ kJ mol}^{-1}$ .

The nuclear frequency factor for ET in these organic systems is the frequency of the CC stretching vibration of  $1600 \text{ cm}^{-1}$ , or  $\nu_N = 4.8 \times 10^{13} \text{ sec}^{-1}$ . The separation distance between the planes defined by the aromatic rings is typically the van der Waals contact distance

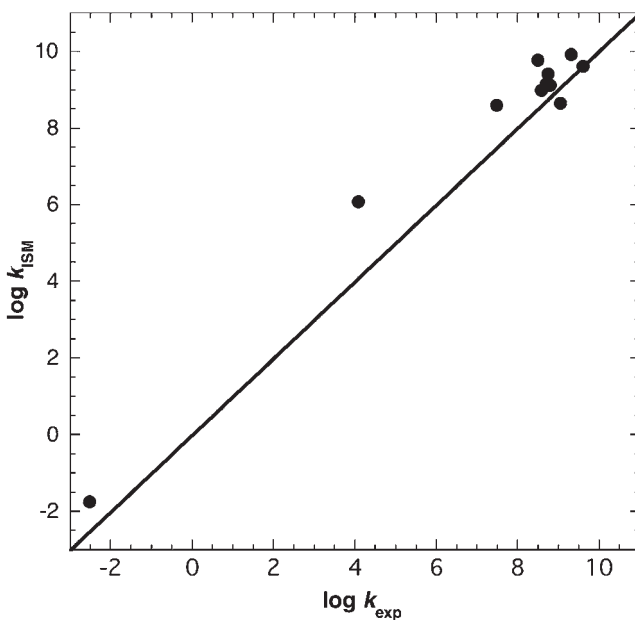


**Figure 16.11** Comparison between electron self-exchange rates of organic species calculated by ISM and experimental data, in acetonitrile at room temperature, from ref. [1].

of  $3.5 \text{ \AA}$ . For a typical distance parameter of  $\beta = 1.2 \text{ \AA}^{-1}$ , this leads to a probability of electron transfer  $\chi_r \approx 1.5 \times 10^{-2}$ . Thus the electronic frequency factor, for a spin allowed process, is  $\nu = \nu_{\text{el}} \chi_r = (10^{15} \text{ sec}^{-1})(1.5 \times 10^{-2}) = 1.5 \times 10^{13} \text{ sec}^{-1}$  and since  $\nu_{\text{el}} \chi_r$  and  $\nu_N$  are of comparable magnitude, the electron transfer has a slightly non-adiabatic character. As usual, we take  $\nu = 10^{13} \text{ sec}^{-1}$  and  $K_c = 1 \text{ M}^{-1}$ .

The rate constant for the exchange of an electron between naphthalene and its radical anion is  $k_{\text{ISM}} = 1.8 \times 10^9 \text{ M}^{-1} \text{ sec}^{-1}$  at  $T = 298 \text{ K}$ . Using the diffusion-controlled rate in acetonitrile,  $k_{\text{dif}} = 1.9 \times 10^{10} \text{ M}^{-1} \text{ sec}^{-1}$ , eq. (16.33) allows the estimation of  $k_{\text{obs}} = 1.6 \times 10^9 \text{ M}^{-1} \text{ sec}^{-1}$ , which is within an order of magnitude of the experimental value in the absence of effects due to ion pairing,  $k_{\text{exp}} = 6.2 \times 10^8 \text{ M}^{-1} \text{ sec}^{-1}$ . Somewhat dramatically, the electron exchange between  $i\text{Pr}_2\text{N}_2)_2$  and  $i\text{Pr}_2\text{N}_2)_2^+$  is much slower,  $k_{\text{exp}} = 3.0 \times 10^{-3} \text{ M}^{-1} \text{ sec}^{-1}$  at  $298 \text{ K}$  in acetonitrile. Using the barrier calculated above,  $\Delta G^\ddagger = 78 \text{ kJ mol}^{-1}$ , and the experimental contact distance of  $8.68 \text{ \AA}$ , we calculate, for  $\beta = 1.2 \text{ \AA}^{-1}$ ,  $\nu_{\text{el}} \chi_r = 3.0 \times 10^{10} \text{ M}^{-1} \text{ sec}^{-1}$  and  $k_{\text{ISM}} = 6.4 \times 10^{-4} \text{ M}^{-1} \text{ sec}^{-1}$  at  $T = 298 \text{ K}$ , in good agreement with the experimental value. Figure 16.11 compares the rates estimated for several organic self-exchange reactions by ISM and the experimental rates.

## 16.6 INVERTED REGIONS

In a family of reactions with a constant intrinsic barrier,  $\Delta G^\ddagger(0)$ , the quadratic equation of Marcus led this scientist to predict the existence of an inversion on the effect of reaction

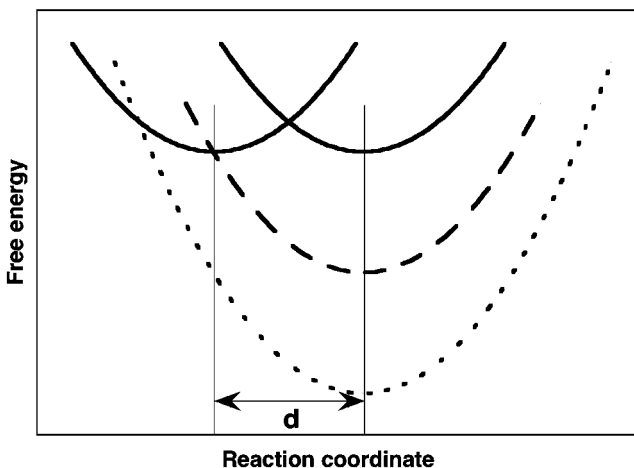


**Figure 16.12** Crossing of potential energy curves representing the reactants and products of increasingly exothermic electron transfers. For a sufficiently exothermic reaction, the barrier vanishes (dashed curve), and the rate attains its maximum value. In even more exothermic reactions the crossing of the curves moves up from the minimum of the reactants curve, a reaction barrier reappears (dotted curve), and the rate decreases. This decrease in the rate in very exothermic electron transfers is the “inverted region”.

energy,  $\Delta G^0$ , on energy barriers,  $\Delta G^\ddagger$ , for very exothermic reactions [28]. From eq. (7.11) we can formulate the quadratic equation as

$$\Delta G^a = \Delta G^a(0) + \frac{\Delta G^0}{2} + \frac{(\Delta G^0)^2}{16\Delta G^a(0)} \quad (16.44)$$

This equation can be differentiated to give

$$\frac{d\Delta G^a}{d\Delta G^0} = \frac{1}{2} + \frac{1}{8} \frac{\Delta G^0}{\Delta G^a(0)} \quad (16.45)$$

Usually the derivative  $(d\Delta G^\ddagger/d\Delta G^0)$  has a positive sign, which means that a decrease in  $\Delta G^0$  also leads to a decrease in  $\Delta G^\ddagger$  and, consequently, promotes an increase in the rate constants. However, when  $\Delta G^0 < -4\Delta G^\ddagger(0)$ , eq. (16.45) shows that  $(d\Delta G^\ddagger/d\Delta G^0)$  becomes negative. This means that a decrease in  $\Delta G^0$  now leads to an increase in  $\Delta G^\ddagger$  and, consequently, leads to a decrease in the rate constants. Figure 16.12 illustrates the appearance of an *inverted region* in terms of a curve-crossing model. A considerable advantage for the use of uni-dimensional representations for ET processes is the representation of the inverted regions. Such regions are not amenable to any physical representation for multi-dimensional potential energy surfaces.

In spite of the fact that such a prediction of Marcus appeared to be in contradiction with the scientific consensus at the time, several researchers persistently searched for this

effect. A convenient way to produce very exothermic reactions is by preparation of electronically excited states,  $A^*$ , as reacting species using ultraviolet or visible light excitation. Excited states are better oxidants and reductants than the same species in their ground states, and as a consequence photochemical reactions often lead to electron-transfer processes. Let us consider an acceptor of electron,  $A$ , that is subsequently excited by light



where  $I_{\text{abs}}$  represents the intensity of the light absorbed. In the presence of a donor molecule,  $D$ , an electron-transfer reaction can occur



Such a photo-induced reaction can be followed experimentally through the competition with the fluorescence emission of  $A^*$



and with non-radiative decay processes



with rate constants  $k_F$  and  $k_{\text{nr}}$ , respectively.

Under steady state conditions for  $A^*$

$$\frac{d[A^*]}{dt} = I_{\text{abs}} - (k_F + k_{\text{nr}})[A^*] - k_{\text{et}}[D][A^*] \quad (16.46)$$

from which

$$[A^*] = \frac{I_{\text{abs}}}{k_F + k_{\text{nr}} + k_{\text{et}}[D]} \quad (16.47)$$

The intensity of the fluorescence emission,  $I_{\text{abs}}$ , in the presence of donor molecules

$$I_F = k_F [A^*] = \frac{k_F I_{\text{abs}}}{k_F + k_{\text{nr}} + k_{\text{et}}[D]} \quad (16.48)$$

while that in the absence of the donor is

$$I_F^0 = \frac{k_F I_{\text{abs}}}{k_F + k_{\text{nr}}} \quad (16.49)$$

From these two equations, we can see that a study of the ratio of intensities,  $I_F^0/I_F$ ,

$$\frac{I_F^0}{I_F} = \frac{k_F + k_{\text{nr}} + k_{\text{et}}[D]}{k_F + k_{\text{nr}}} \quad (16.50)$$

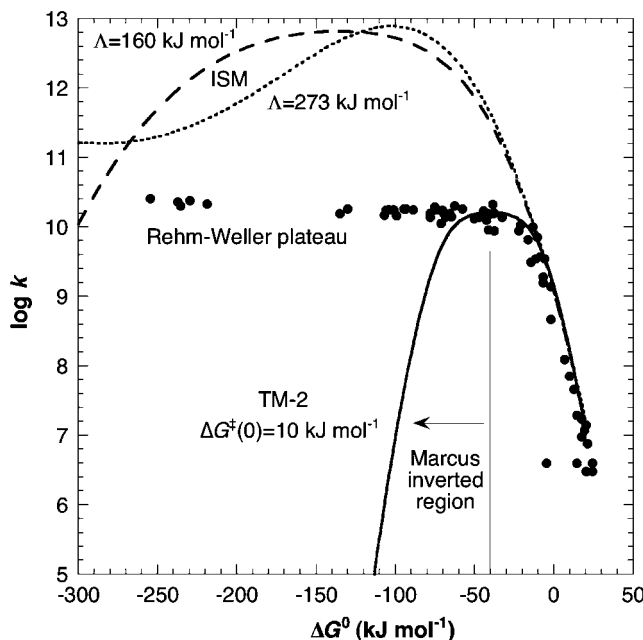


**Figure 16.13** Rehm–Weller behaviour in the bimolecular photoinduced electron transfer in acetonitrile. The experimental points are from ref. [29]. The rate constants of the reactions with  $\Delta G^0 < -50 \text{ kJ mol}^{-1}$  are diffusion controlled. ISM calculations employed  $f_r = f_p = 3.8 \times 10^3 \text{ kJ mol}^{-1} \text{ Å}^{-2}$ ,  $l_r + l_p = 2.8 \text{ Å}$ ,  $n^\ddagger = 1.41$  and  $\Lambda = 160$  or  $273 \text{ kJ mol}^{-1}$ . The intrinsic barrier of TM-2 was fitted to reproduce the rates in the normal region with  $Z = 10^{11} \text{ M}^{-1} \text{ sec}^{-1}$ .

as a function of the  $[D]$  leads to the familiar Stern–Volmer form (see also eq. (3.21) and Figure 9.4).

$$\frac{I_F^0}{I_F} = 1 + \frac{k_{et}}{k_F + k_{nr}} [D] \quad (16.51)$$

The quenching of fluorescence of  $A^*$  expressed by the ratio  $I_F^0/I_F$  is a linear function of the concentration of the quencher, i.e., the donor in the present case. The intercept of the plot is one, and the slope is  $k_{et}\tau$ , where  $k_{et}$  is the rate of electron transfer and  $\tau$  the lifetime of  $A^*$  in the absence of quencher,

$$\tau^{-1} = (k_F + k_{nr})^{-1} \quad (16.52)$$

The lifetime of  $A^*$  is obtained through independent measurements under non-steady-state conditions as described in Chapter 3.

Figure 16.13 presents the studies of Rehm and Weller [29] of the quenching of fluorescence of naphthalene and derivatives by amines in acetonitrile solution for the range of

reaction energies  $\Delta G^0$  between +25 and  $-250 \text{ kJ mol}^{-1}$ . In contrast with the predictions of Marcus, no inverted region is observed, and for very exothermic reactions ( $\Delta G^0 < -50 \text{ kJ mol}^{-1}$ ) the rate is constant and diffusion controlled.

According to eqs. (7.1) and (7.2), using the general expression for the calculation of the sum of bond extensions

$$d = \frac{a'}{2n^\ddagger} \ln \left\{ \frac{1 + \exp(\sqrt{2n^\ddagger} \Delta G^0 / \Lambda)}{1 - \left[ 1 + \exp(\sqrt{2n^\ddagger} \Delta G^0 / \Lambda) \right]^{-1}} \right\} (l_{\text{ox}} + l_{\text{red}}) \quad (16.53)$$

This relation between  $d$  and  $\Delta G^0$  offers a method to estimate energy barriers for very exothermic reactions. This method differs from the Marcus cross-relation, TM-2, expressed by eqs. (16.16) and (16.17), and illustrated in Figure 16.12. TM-2 is based on a constant  $d$ , independent of the value of  $\Delta G^0$ , whereas ISM contemplates an increase of  $d$  with an increase in the absolute value of the reaction energy,  $|\Delta G^0|$ . TM-2 corresponds to the limiting situation of  $\Lambda \gg |\Delta G^0|$  in ISM. This is important because the Rehm–Weller pattern of reactivity can now be reproduced with the structural data of naphthalene and amines and a dynamic parameter  $150 < \Lambda < 280$ , in  $\text{kJ mol}^{-1}$ . This is in fact the only parameter adjusted to the experimental data. With the same set of spectroscopic and thermodynamic parameters TM-2 predicts the onset of an inverted region for  $\Delta G^0 < -50 \text{ kJ mol}^{-1}$ . Alternative explanations for the observance of the Rehm–Weller plateau rather than the Marcus inverted region in photo-induced charge separations have relied on long-distance electron transfers for the most exothermic reactions and on the formation of electronically excited radical ions as the primary photochemical product. The presently available experimental data does not support the first hypothesis, but the second cannot be excluded for some of the most exothermic reactions [30]. However, this latter explanation can only reduce the extent of the discrepancy between the prediction of the inverted region and the observation of the diffusion-limited plateau, and not the discrepancy itself.

Instead of dealing with systems where the donor and acceptor molecules have to diffuse and collide for the electron-transfer process to occur, in 1986 Closs, Miller and collaborators have studied long-distance intra-molecular electron transfers in molecular systems where the donor and the acceptor species are covalently linked by a rigid hydrocarbon spacer. The system designed by Closs and Miller is the electron transfer from the 4-biphenyl anion to a series of aromatic molecules, with the anion being prepared by electron addition using pulse radiolysis. As Figure 16.14 shows, ISM can reproduce the new pattern of reactivity well with an adjusted  $\Lambda$  parameter,  $\Lambda = 280 \text{ kJ mol}^{-1}$ . This inverted region shows some asymmetry towards the low-energy side owing to the increase of  $d$  with  $|\Delta G^0|$ .

Inverted regions have been observed in very exothermic inter-molecular electron transfers and in other systems where the relative motions of donor and acceptor are somewhat restricted. In such conditions, diffusion is not the rate-determining step and a wider kinetic window is open for the observation of the inverted region. Another example of such systems is the charge recombination of contact radical-ion pairs formed after charge

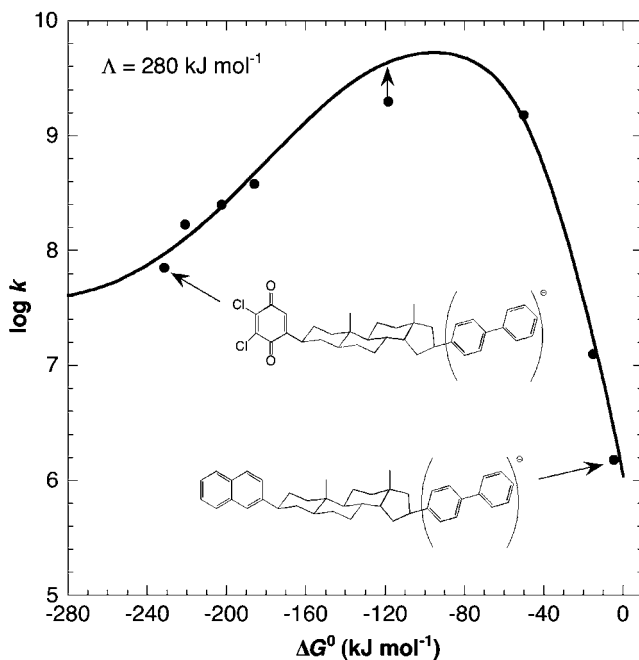


**Figure 16.14** Intra-molecular electron transfer in methyltetrahydrofuran (points) [31]. ISM calculations (line) employed  $f_r = f_p = 4.1 \times 10^3 \text{ kJ mol}^{-1} \text{ Å}^{-2}$ ,  $l_r + l_p = 2.78 \text{ Å}$ ,  $n^\ddagger = 1.45$  and  $\Lambda = 280 \text{ kJ mol}^{-1}$ .

separation in a weakly polar solvent. The reaction mechanism resembles that of portrayed by (16.VII)–(16.X), but with weakly polar solvents the separation of the ions is thermodynamically unfavourable, and in this case the dominant decay pathway of the ions is their charge recombination



The system shown in Figure 16.15 consists of ion pairs formed between aromatic hydrocarbon radical cations and the fumaronitrile radical anion, in supercritical fluids and saturated hydrocarbon solvents.

The systems indicated in Figure 16.15 involve ultra-exothermic electron transfers and show that the “inverted region” does not extend indefinitely to higher exothermicities. When the reaction exothermicity exceeds  $-300 \text{ kJ mol}^{-1}$ , charge recombination rates increase again. It has been shown that this is not due to a change in the decay mechanism [32]. Rather, it is a consequence of eq. (16.53). The existence of a “double-inverted region” had been predicted prediction for ultra-exothermic electron transfers [33], and can be rationalised with Figure 16.16. The increase in the reorganisation energy with  $|\Delta G^0|$  reflects the increased participation of other reactant modes in the reaction coordinate as more energy

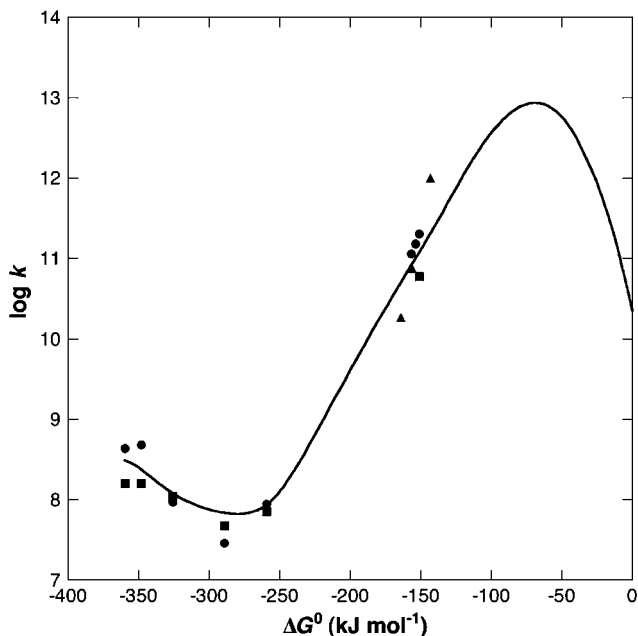


**Figure 16.15** Charge recombination rates in ion pairs formed between aromatic hydrocarbon radical cations and the fumaronitrile radical anion, in heptane and cyclohexane (squares), supercritical  $\text{CO}_2$  (circles) and other supercritical fluids (triangles). ISM calculations (line) used  $f_r = f_p = 4.8 \times 10^3 \text{ kJ mol}^{-1} \text{ Å}^{-2}$ ,  $l_r + l_p = 2.7 \text{ Å}$ ,  $n^\ddagger = 1.8$ ,  $\Lambda = 290 \text{ kJ mol}^{-1}$ , and a frequency factor that accounts for the energy of the electron in the donor.

has to be dissipated by the reactants. The empirical value of  $\Lambda$  is restricted to a very limited range in the case of the double-inverted regions ( $\Lambda \approx 290 \text{ kJ mol}^{-1}$  for organic systems), but for the inverted region a good fit can be obtained either with  $\Lambda = 280 \text{ kJ mol}^{-1}$  or  $\Lambda = 145 \text{ kJ mol}^{-1}$ . The Rehm–Weller plateau is expected when  $\Lambda$  is between 150 and  $280 \text{ kJ mol}^{-1}$ . Lower  $\Lambda$  values imply much larger increases in the sum of bond extensions with  $|\Delta G^0|$ . The dynamic parameter has a small dependence on the nature of the solvent, and varies more with the nature of the electron-transfer reactions. The parameter  $\Lambda$  is expected to be lower for the activated configurations with a limited number of degrees of freedom. This appears to be the case when one compares charge recombinations processes in contact ion-pairs ( $\Lambda = 300 \text{ kJ mol}^{-1}$ ) and in solvent separated ion-pairs ( $\Lambda = 350 \text{ kJ mol}^{-1}$ ). Figure 16.17 illustrates the diversity of free-energy relationships that result from the values of  $\Lambda$  discussed above.

Finally, inverted regions have also been observed in electron transfers between redox centres embedded in proteins. This is both the case of modified intra-protein electron transfers briefly mentioned before [2,34], and of the reaction centres in photosynthetic bacteria [35].

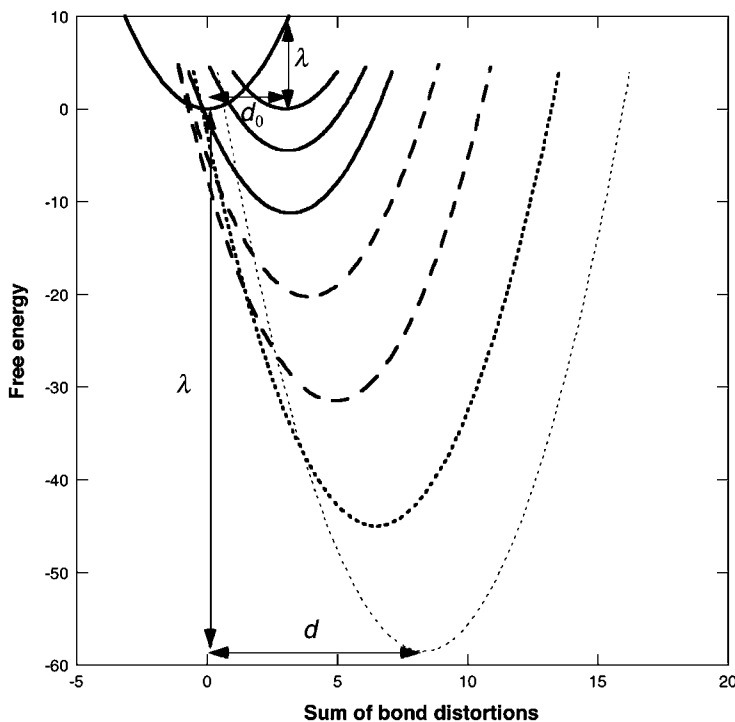


**Figure 16.16** The sum of reactant and product bond distortions from equilibrium to transition-state configurations ( $d$ ) increases with the free energy of the reactions ( $\Delta G^0$ ). This increase in  $d$  leads to an increase in the total reorganisation energy ( $\lambda$ ). The activation energy, given by the crossing between reactant and product curves, first decreases with  $\Delta G^0$  (full lines), goes through a minimum, increases in the inverted region (dashed lines), goes through a maximum, and decreases again in double-inverted region (dotted lines).

## 16.7 ELECTRON TRANSFER AT ELECTRODES

### 16.7.1 The Tafel equation

Electrochemistry deals principally with chemical and physical phenomena at interfaces between an electronic conductor (typically a metal or a semiconductor) and an ionic conductor such as electrolyte solution, as affected by the electric potential of the solid conductor. An electrochemical reaction involves a current going through the interface, hence the passing of either electrons or ions. But even if the current is carried through by ions, an electron-transfer step often occurs within the ions, which must be either generated or discharged by an exchange of electrons.

Figure 16.18 illustrates pictorially some of the relevant features of a solid/liquid interface [36]. For simplicity we will consider mainly metal electrodes. Electron transfer occurs between the solid surface layer and the dissolved species. Beneath this surface layer, for metals there is a constant potential in which no electron localisation is possible.

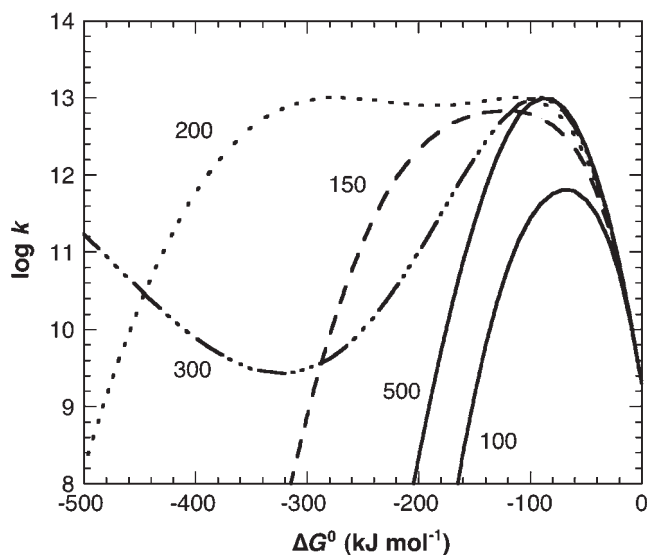


**Figure 16.17** Free-energy dependences of adiabatic electron transfers according to ISM. The calculations used  $v = 10^{15} \text{ sec}^{-1}$ ,  $f_r = f_p = 3.77 \times 10^3 \text{ kJ mol}^{-1} \text{ Å}^{-2}$ ,  $l_r + l_p = 2.80 \text{ Å}$ ,  $n^\ddagger = 1.435$  and the values of  $\Lambda$  indicated in the plot.

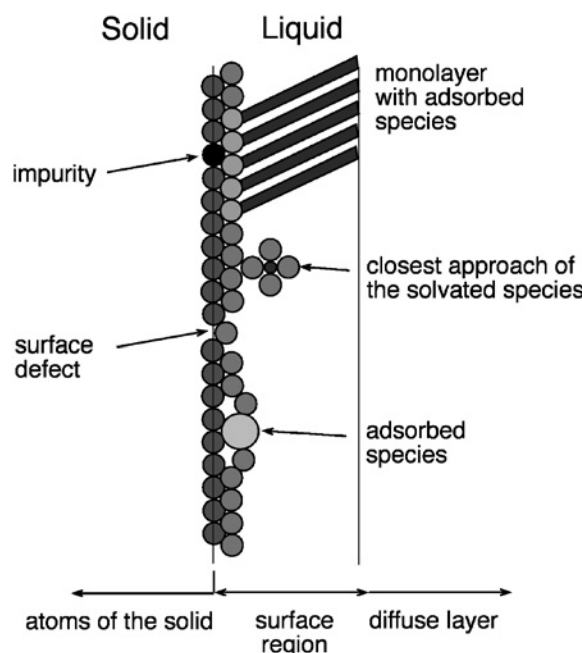


**Figure 16.18** Representation of the interface electrode/solution, illustrating some of the species that can be found in this region.

In an electrochemical cell there are usually two electrodes: one, the *reference electrode*, at a constant potential and the other, the *working electrode*, where more positive or negative potentials are applied to produce electrochemical reactions through the transfer of electrons. If more negative potentials are applied to the working electrode, the energy of the electrons in the metal is increased, such that the energy can be higher than that of the LUMO of any oxidant species present in solution and, consequently, at the metal/liquid interface. Under these circumstances, a flow of electrons can occur from the metal electrode to the solution, the so-called reduction current. Alternatively, more positive potentials,  $E$ , can be applied to the working electrode. The energy level of the electrons in the metal is lowered, and an electron can be transferred from the HOMO of a species in solution to the metal. Hence an oxidation electric current is generated. The creation of these reduction and oxidation currents is illustrated in Figure 16.19. The critical potential for such processes depends on the standard potential,  $E^0$ , of the reactant.

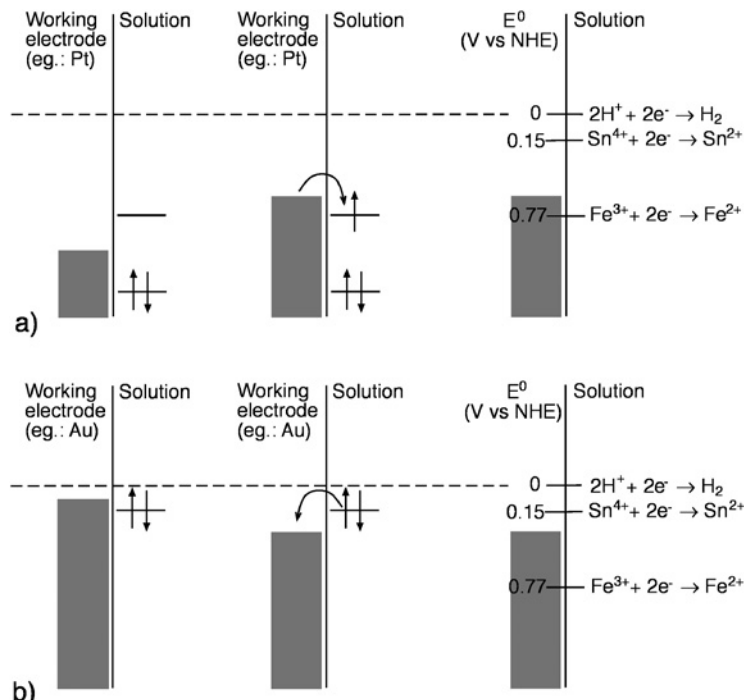


**Figure 16.19** (a) Reduction: initially (left) the energy of the electrons in the working electrode is too low to reduce the species in solution, but on increasing the energy of these electrons (centre) an electron transfer to the LUMO of that species will occur; the right panel shows the reduction potentials of  $\text{Fe}^{3+}$  and  $\text{Sn}^{4+}$ , and an energy level of the electrons in the electrode that allows for the reduction of  $\text{Fe}^{3+}$  but not of  $\text{Sn}^{4+}$ . (b) Oxidation: initially (left) the energy of the electrons in the working electrode is too high to oxidise the species in solution, but decreasing the energy of these electrons (centre) an electron transfer from the HOMO of that species will occur; the right panel shows the oxidation potentials of  $\text{Fe}^{2+}$  and  $\text{Sn}^{2+}$ , and an energy level of the electrons in the electrode that allows for the oxidation of  $\text{Sn}^{2+}$  but not of  $\text{Fe}^{2+}$ . The initial potential of the electrodes corresponds to their equilibrium in solution (no current).

The driving force for these heterogeneous reactions can be achieved by varying the electrode potential according to

$$\Delta G_{\text{het}}^0 = F(E - E^0) \quad (16.54)$$

where  $F$  is the Faraday constant ( $F = 96\,485\, \text{C mol}^{-1}$ ). This equation reveals that kinetic processes at electrodes can be drastic and continuously modified by changing the electrode potential. This is a unique feature of electrochemical processes. For metals, which contain a large concentration of mobile electrons in thermal equilibrium, any change in the potential of the metal is communicated to the energy levels in the metal that, in turn, communicate with the electrolyte to follow the electrode potential. This situation is unlike that at semi-conductor-electrolyte interfaces, where the change in the electrode potential may not result in a change in the energy level of charge carriers available to the electrolyte. For metals, at interfaces, the induced charge resides on the surface. For semiconductors, owing to their low free-carrier density, the induced charge can be distributed over relatively large distances from surfaces. The potential, which the reactant species experience in solution is less than the real potential energy difference between the electrode and the solution, because of the presence of solvent molecules and other molecular species (including counter ions) adsorbed at the surface of the metal electrode.

The rate of the electronic transfer is associated with the intensity,  $i$ , of the electric current that goes through the electrode, where  $i$  represents the number of electrons which react with the active species per unit of time

$$i \text{ (amperes)} = \frac{dQ}{dt} \text{ (coulombs second}^{-1}\text{)} \quad (16.55)$$

Since electrode reactions are heterogeneous process, the rates are defined by  $\text{mol sec}^{-1}$  per unit area,

$$v = \frac{i}{nFA} \text{ mol sec}^{-1} \text{ cm}^{-2} \quad (16.56)$$

Here  $n$  is the number of electrons transferred in each elementary process and  $A$  the active surface of the electrode.

The kinetics of electron transfers at electrodes are usually studied in terms of the current intensity as a function of the potential. When  $i = 0$ , the potential of the electrode is that of equilibrium,  $E_{\text{eq}}$ . The application of a potential different from  $E_{\text{eq}}$  corresponds a polarisation of the electrode, whose magnitude is called the *overpotential*,  $\eta$ ,

$$\eta = E - E_{\text{eq}} \quad (16.57)$$

The measurement of a certain  $i$  is always associated with the presence of overpotential. However, the dependence of  $i$  upon  $\eta$  is complicated by the existence of several elementary steps displayed in Figure 16.20 and associated with the effect of the electrical double-layer [37]. This *double-layer effect* is due to the electrostatic work necessary to bring the electroactive ion to a charged interface.

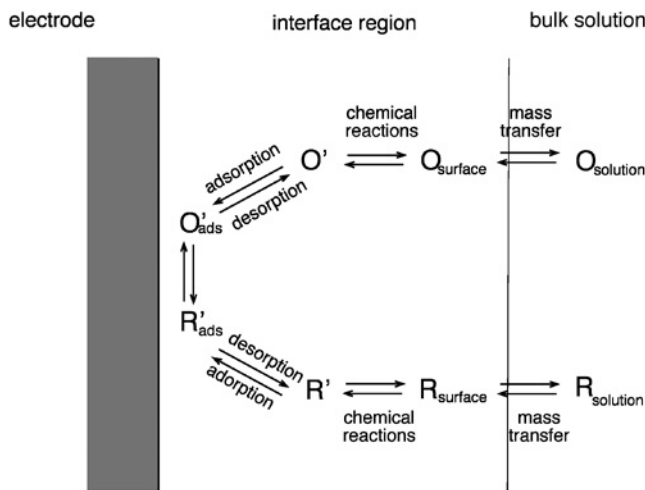
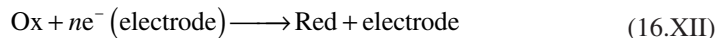


**Figure 16.20** Pathway of a general electrode reaction.

For the low-intensity regime, Tafel in 1905 showed that the overpotential is linearly related to the intensity,

$$\eta = a + b \log i \quad (16.58)$$

where  $a$  and  $b$  are constants. To understand this empirical relation of Tafel, let us consider the reaction



The rate of reduction is proportional to the concentration of the oxidant species at the surface of the electrode,  $[\text{Ox}]_s$ , at a certain instant of time

$$v_{\text{red}} = k_{\text{red}} [\text{Ox}]_{0,t} = \frac{i_c}{nFA} \quad (16.59)$$

Here  $i_c$  is the intensity of the cathodic current. In an analogous manner for the oxidation reaction we can write

$$v_{\text{ox}} = k_{\text{ox}} [\text{R}]_{0,t} = \frac{i_a}{nFA} \quad (16.60)$$

where  $i_a$  is the anodic current. The net rate of reaction is the difference between the rates of reduction (cathodic reaction) and oxidation (anodic reaction)

$$v = v_{\text{red}} - v_{\text{ox}} = k_{\text{red}} [\text{O}]_{0,t} - k_{\text{ox}} [\text{R}]_{0,t} = \frac{i}{nFA} \quad (16.61)$$

where

$$i = i_c - i_a = nFA \left( k_{\text{red}} [\text{O}]_{0,t} - k_{\text{ox}} [\text{R}]_{0,t} \right) \quad (16.62)$$

Assuming that the rates follow Arrhenius behaviour, we can write

$$\begin{aligned} k_{\text{red}} &= k^0 e^{-znf(E-E^{0'})} \\ k_{\text{ox}} &= k^0 e^{(1-\alpha)nf(E-E^{0'})} \end{aligned} \quad (16.63)$$

where  $f = F/RT$ . To obtain the Tafel equation, one needs to relate the activation energies of the reduction and oxidation reactions with the reaction energy as shown in Figure 16.21 [37]. The model displayed in the figure is the Butler–Volmer model for the kinetics at electrodes. A change on the electrode potential,  $E$ , leads to a change in the energy of the electron relative to the electrode, and the curve relative to the process  $\text{Ox} + ne^- \rightarrow$  moves up or down on the vertical scale of that figure. For an increase variation in  $E$ , that curve moves up, the barrier for the oxidation decreases, and this decrease is proportional to the energy of the reaction. The proportionality factor is  $(1 - \alpha)$ , where  $\alpha$  is called the cathodic *transfer coefficient*. Thus one can write for the anodic barrier

$$\Delta G_a^\ddagger = \Delta G_{0a}^\ddagger - (1 - \alpha)nFE \quad (16.64)$$

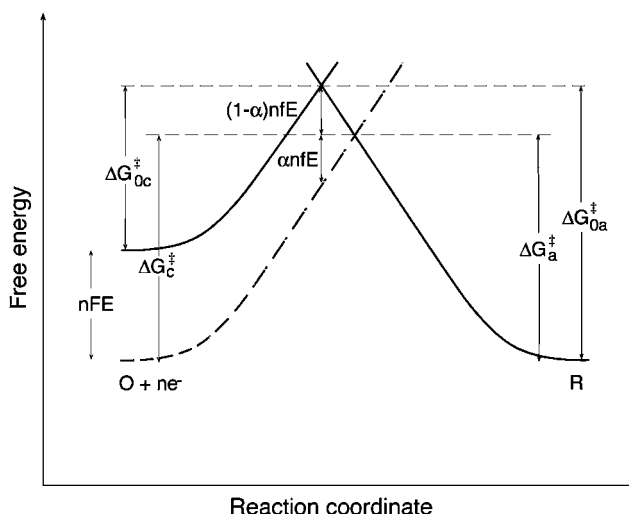


**Figure 16.21** Effects of a change in potential on the free energy of activation for oxidation and reduction.

and the corresponding expression

$$\Delta G_c^{\ddagger} = \Delta G_{0c}^{\ddagger} + \alpha nFE \quad (16.65)$$

for the cathodic barrier.

The coefficient  $\alpha$  is usually taken as the fraction of the electron residing on the activated complex and  $(1-\alpha)$  that fraction still in the metal at the transition-state configuration. The parameter  $\alpha$  is also called the *Tafel coefficient*.

Substituting eqs. (16.64) and (16.65) into eq. (16.63) leads to

$$\begin{aligned} k_{\text{red}} &= A_{\text{red}} e^{-\Delta G_{0c}^{\ddagger}/RT} e^{-\alpha nFE} \\ k_{\text{ox}} &= A_{\text{ox}} e^{-\Delta G_{0a}^{\ddagger}/RT} e^{(1-\alpha)nFE} \end{aligned} \quad (16.66)$$

When there is equilibrium at the interface with a solution containing equal amounts of Ox and Red, the rates in the forward and reverse directions are equal, and an intrinsic rate constant,  $k^0$ , can be defined

$$k^0 = A_{\text{red}} e^{-\Delta G_{0c}^{\ddagger}/RT} = A_{\text{ox}} e^{-\Delta G_{0a}^{\ddagger}/RT} \quad (16.67)$$

and,

$$\begin{aligned} k_{\text{red}} &= k^0 e^{-\alpha nF(E-E^0)} \\ k_{\text{ox}} &= k^0 e^{(1-\alpha)nF(E-E^0)} \end{aligned} \quad (16.68)$$

where  $E^0$  is the formal potential of the electroactive species. Further, substituting these expressions into eq. (16.62) one gets

$$i = nFAk^0 \left( [O]_{0,t} e^{-\alpha nF(E-E^0)} - [R]_{0,t} e^{(1-\alpha)nF(E-E^0)} \right) \quad (16.69)$$

The equation of Tafel is a particular case of eq. (16.69).

### 16.7.2 Calculations of rate constants

The transfer of electrons between a metal or a semi-conductor electrode and a dissolved or surface-bound reactant is no different in kind from the homogenous processes, previously described. In the model proposed by Marcus the electrochemical rate constant,  $k_{\text{het}}$ , is given by

$$k_{\text{het}} = Z\chi \exp\left(-\frac{\Delta G_{\text{het}}^*}{RT}\right) \quad (16.70)$$

where  $Z$  is the frequency factor for the electrode reaction and  $\chi$  an electronic transmission factor.

Several expressions have been proposed for the pre-exponential factor. In terms of a translational partition function,  $Z$  is

$$Z = \sqrt{\frac{RT}{2\pi\mu}} \quad (16.71)$$

where  $\mu$  is the reduced mass of the reactant. For a hydrated metal ion this leads to typical values of  $Z = 5 \times 10^3 \text{ cm sec}^{-1}$ . Another expression for  $Z$  is

$$Z = (\delta r_e) v_n \quad (16.72)$$

where  $\delta r_e$  is the reaction zone thickness within which electron transfer with the electrode surface occurs, and  $v_n$  the effective nuclear activation frequency. It is common to take  $\delta r_e = 1 \text{ \AA}$ , but differences in opinion exist on the appropriate value for  $v_n$ , with some people taking it as the typical nuclear frequency  $v_n = 10^{13} \text{ sec}^{-1}$ , and others as the reciprocal of the solvent longitudinal relaxation time  $v_n = (\tau_L)^{-1}$  [38,39]. For reactions in aqueous solutions these two approaches give  $Z = 1 \times 10^5 \text{ cm sec}^{-1}$  and  $Z = 2 \times 10^4 \text{ cm sec}^{-1}$ , respectively. When eqs. (16.71) and (16.72) are employed, it is usually assumed that the electrochemical reaction is adiabatic,  $\chi \approx 1$ . An alternative expression, where adiabaticity is not implicit, is

$$Z\chi = \Gamma v_{el} e^{-\beta(r-r_0)} \quad (16.73)$$

where  $\Gamma$ , a factor that converts bulk into surface concentration of the reactant, is of the order of  $10^{-7} \text{ cm}$  [40];  $\Gamma$  represents the precursor complex equilibrium constant  $K_c$  and is also called the “reactive thickness”. The other parameters have their usual meaning;  $r$  represents the distance of a metal-ion to the electrode and  $r_0$  the width of the internal Helmholtz plane (IHP), because at this distance electron transfer can be considered a tunnelling process from the electrode to the ion, with unit probability. The interaction of the adsorbed solvent molecules with the electrode allows a conductive pathway for the electron through an empty anti-bonding orbital of the solvent molecules. The distance dependence of the electronic transmission factor in eq. (16.73) is similar to that expressed by eq. (16.34). The value of the pre-exponential factor given by eq. (16.73) for the reduction of  $\text{Fe(OH}_2)_6^{3+}$  in aqueous solution can be estimated from its reduction potential with respect to NHE,  $E_{red} = 0.38 \text{ V}$ , which, following eq. (16.37), gives  $\Phi_0 = 4.82 \text{ eV}$ . If one considers that in the diffuse double-layer the refractive index of water is that of the bulk,  $n_D = 1.33$ , then  $\beta = 1.692 \text{ \AA}^{-1}$ . With  $\Gamma = 10^{-7} \text{ cm}$ ,  $r - r_0 = 3 \text{ \AA}$ , which is the van der Waals diameter of a water molecule [41], and  $v_{el} = 10^{15} \text{ sec}^{-1}$ , eq. (16.73) gives  $Z\chi \approx 6 \times 10^5 \text{ cm sec}^{-1}$ . Thus, depending on the approximations assumed, the value of the pre-exponential factor in electrochemical reactions ranges from  $5 \times 10^3$  to  $6 \times 10^5 \text{ cm sec}^{-1}$ .

A positive charge placed at the interface near a metallic electrode induces an opposing negative charge in the metal. This effect, equivalent to an *image force*, leads to a decrease in the width and a sharpening of the barrier for the electron to tunnel from the metal to the transition-metal ion. Instead of the usual rectangular barrier, the image-force effect barrier can be approximated by a kind of parabolic potential [42]. However, for solutions in

the 0.1–1 M concentration range typically employed in kinetic experiments, the image force interaction will be reduced and can be neglected. Thus, the probability of tunnelling given by eq. (16.34) also applies to electrochemical processes.

Marcus has pointed out that the energy barrier for a heterogeneous process should be half of that for the homogeneous process in solution,  $\Delta G_{\text{hom}}^*$ , described above,

$$\Delta G_{\text{het}}^* = \frac{1}{2} \Delta G_{\text{hom}}^* \quad (16.74)$$

because the response of the metal electrode to the transfer of the electron with the redox species does not involve energy changes [43], and the reactions can be effectively described as if only one reactant is present.

Curtiss *et al.* [44] have carried out measurements for reaction rates of the electrochemical oxidation of  $\text{Fe}(\text{OH}_2)_6^{2+}$  to  $\text{Fe}(\text{OH}_2)_6^{3+}$  at a gold electrode in a 0.5 M  $\text{HClO}_4$  aqueous solution. The experimental design of a pressurised flow-system allowed electrochemical studies over a vast range of temperatures, from 25 to 250 °C. A good Arrhenius behaviour was found with  $E_a = 56.8 \pm 1.5 \text{ kJ mol}^{-1}$ , a frequency factor of  $Z = 6 \times 10^5 \text{ cm sec}^{-1}$  and a Tafel coefficient  $\eta = 0.425 \pm 0.01$ , independent of the temperature. The measured standard rate constant at 25 °C is  $k_{\text{het}} = 6 \times 10^{-5} \text{ cm sec}^{-1}$ .

The activation energy of the electrochemical oxidation of  $\text{Fe}(\text{OH}_2)_6^{2+}$  can be calculated with the structural and electronic data in Appendix III for  $\text{Fe}(\text{OH}_2)_6^{3+/2}$ ,  $f_r = f_{\text{ox}} = 3.75 \times 10^3 \text{ kJ mol}^{-1} \text{ Å}^{-2}$ ,  $f_p = f_{\text{red}} = 2.35 \times 10^3 \text{ kJ mol}^{-1} \text{ Å}^{-2}$ ,  $l_{\text{ox}} + l_{\text{red}} = 4.08 \text{ Å}$ , together with  $n^\ddagger = 1$ , valid for a normal outer-sphere process. The barrier for the heterogeneous reaction is, using eq. (16.74),  $\Delta G_{\text{het}}^\ddagger = 36 \text{ kJ mol}^{-1}$ , which is 20 kJ mol<sup>-1</sup> lower than the experimental activation energy. Using an intermediate value for the pre-exponential factor,  $Z\chi \approx 5 \times 10^4 \text{ cm sec}^{-1}$ , the calculated rate 25 °C,  $k_{\text{het}} = 2 \times 10^{-2} \text{ cm sec}^{-1}$ , is much higher than the experimental value. However, the estimated Tafel coefficient ( $\eta_{\text{ox}} = 0.44$ ) at  $\Delta G^0 = 0$  is in close agreement with experiment, provided one considers the asymmetry of the potential energy curves (see eq. (7.1)).

Part of the discrepancy between the calculated and experimental electrochemical oxidation rates of  $\text{Fe}(\text{OH}_2)_6^{2+}$  is due to electrostatic double-layer effects upon the apparent rate constants for electrochemical exchange. The “standard” rate constants measured at the formal potential for the redox couple concerned must be corrected for double-layer effects to obtain the “corrected” rate [45]. Such corrections depend on the electrode, electrolyte, Tafel coefficient, potential and charge of the redox couple. For the electrochemical exchange of the  $\text{Fe}(\text{OH}_2)_6^{2+/3+}$  couple at the mercury/aqueous surface at 25 °C, the correction for the double-layer effects increase the rate from  $2 \times 10^{-5}$  to  $1 \times 10^{-4} \text{ cm sec}^{-1}$  [38]. Thus, the discrepancy noted above is reduced to a factor of 200.

The double-layer effects are significantly reduced when one of the partners in the redox couple is uncharged. This is the case of ferrocene, which was treated in detail for gas phase and homogenous solution self-exchanges. The standard rate constants for the electro-oxidation of ferrocene at a platinum electrode in acetonitrile range from 0.02 to 220 cm sec<sup>-1</sup> [46]. Some of the observed scatter is related to differences in electrolyte nature and concentration, or in temperature, but also reflects the experimental errors of some of the techniques employed. Fawcett and Opallo reviewed these data and recommended a

rate between 1 and 4 cm sec<sup>-1</sup> [46]. Using the data for Fe(Cp)<sub>2</sub><sup>0/+</sup> in Appendix III and assuming local mode behaviour, ISM calculations with  $n^\ddagger = 1$  give  $\Delta G_{\text{het}}^\ddagger = 21 \text{ kJ mol}^{-1}$ . Taking  $Z\chi \approx 5 \times 10^4 \text{ cm sec}^{-1}$ , this gives  $k_{\text{het}} = 10 \text{ cm sec}^{-1}$  at 25 °C, in good agreement with the experimental rate.

### 16.7.3 Asymmetry in Tafel plots

Hupp and Weaver [47] have extended the usual Tafel plots to regimes of strong overpotential in the anodic and cathodic regions for the system Cr(OH<sub>2</sub>)<sub>6</sub><sup>2+</sup>/Cr(OH<sub>2</sub>)<sub>6</sub><sup>3+</sup> and have found a significant asymmetry in the plots. Under exothermic conditions the plot is virtually linear in the cathodic region over a 500 mV range according to the Butler–Volmer model, but has a strong downward curvature in the anodic region. For example, at an overpotential of 700 mV the cathodic reduction of Cr(OH<sub>2</sub>)<sub>6</sub><sup>3+</sup> at Hg-electrode is 200 times faster than the anodic oxidation of Cr(OH<sub>2</sub>)<sub>6</sub><sup>2+</sup> at the same overpotential.

The asymmetry of the plots is related first to the asymmetry of reactants and products. In the anodic oxidation the reactant is Cr(OH<sub>2</sub>)<sub>6</sub><sup>2+</sup> and the product is Cr(OH<sub>2</sub>)<sub>6</sub><sup>3+</sup>, hence  $f_r = f_{\text{red}}$  and  $f_p = f_{\text{ox}}$ . On the other hand, in the cathodic reduction the reactant is Cr(OH<sub>2</sub>)<sub>6</sub><sup>3+</sup> and the product is Cr(OH<sub>2</sub>)<sub>6</sub><sup>2+</sup>, hence  $f_r = f_{\text{ox}}$  and  $f_p = f_{\text{red}}$ . The potential-energy curves of reactant and product are asymmetric for each reaction, and this asymmetry is reversed between electrochemical oxidation and reduction. With the data available in Appendix III, this contribution to the asymmetry of the cathodic reduction of the Cr(OH<sub>2</sub>)<sub>6</sub><sup>2+</sup>/Cr(OH<sub>2</sub>)<sub>6</sub><sup>3+</sup> couple system can be shown to be given by  $f_r = f_{\text{ox}} = 3.75 \times 10^3 \text{ kJ mol}^{-1} \text{ Å}^{-2}$  and  $f_p = f_{\text{red}} = 2.35 \times 10^3 \text{ kJ mol}^{-1} \text{ Å}^{-2}$ .

The pre-exponential factor provides another source of asymmetry. The barrier for tunnelling is raised by the application of an anodic overpotential and lowered by applying a cathodic one. Where there is overpotential the barrier for tunnelling varies according to the expression:

$$\Phi = \frac{\Phi_0 - \Delta G_{\text{het}}^0}{n_D^2} \quad (16.75)$$

However, these two contributions are not enough to account for the full asymmetry in the Tafel plots, although they can account for a factor of *ca.* 40 times faster rates for the anodic process when compared with the cathodic ones. Further corrections are needed to account for the experimental data. An additional contribution may be due to a difference in entropy change for the cathodic and anodic processes.

Using the force constants mentioned above, and taking  $l_r + l_p = 4.13 \text{ Å}$  and  $n^\ddagger = 1$ , ISM calculations give  $\Delta G_{\text{het}}^\ddagger = 36.4 \text{ kJ mol}^{-1}$ . The frequency factor for the electrochemical exchange must be less than that employed for the Fe(OH<sub>2</sub>)<sub>6</sub><sup>2+/3+</sup> and Fe(Cp)<sub>2</sub><sup>0/+</sup> exchanges, because the Cr(OH<sub>2</sub>)<sub>6</sub><sup>2+/3+</sup> couple exchanges a  $\sigma^*$  electron and we have seen that this is a non-adiabatic process. In homogeneous self-exchanges, the frequency of the Cr(OH<sub>2</sub>)<sub>6</sub><sup>2+/3+</sup> exchange is a factor of 240 lower than that of the Fe(OH<sub>2</sub>)<sub>6</sub><sup>2+/3+</sup> exchange [1]. Assuming that the same factor applies to electrochemical exchanges, we take  $Z\chi \approx 2 \times 10^2 \text{ cm sec}^{-1}$  and estimate  $k_{\text{het}} = 8 \times 10^{-5} \text{ cm sec}^{-1}$  at 25 °C. At this temperature, the standard rate constant is

$2 \times 10^{-5}$  cm sec $^{-1}$  and the double-layer corrected rate constant is  $2 \times 10^{-6}$  cm sec $^{-1}$  [45]. In this case the double-layer correction decreases the rate because the potential drop across the diffuse layer is negative. In view of all the approximations and corrections involved, the calculations provide a reasonable estimate of the experimental rate.

#### 16.7.4 Electron transfer at surfaces through a blocking layer

An outer-sphere electron-transfer process should be independent of the nature of the electrode and of the electrolyte medium. Nevertheless, experimental electron-transfer rates are strongly dependent on the electrodes and of their surface history.

Long-distance electron-transfer processes at metal/electrolyte interfaces have been studied with ferrocene groups positioned at a fixed distance from a gold electrode using self-assembled monolayers of a mixed ferrocene-substituted alkyl thiol,  $\text{Fe}(\text{Cp})_2\text{CO}_2(\text{CH}_2)_{16}\text{SH}$  diluted with unsubstituted alkane thiols,  $\text{CH}_3(\text{CH}_2)_{15}\text{SH}$ . Monolayers at Au appear to be reasonably homogeneous and the kinetic electrochemical data obtained by Chidsey [48] under those conditions appear to be free from heterogeneities and double-layer effects that lead to kinetic dispersions found by other authors. Figure 16.22 shows this system. The inferred structure for the C-16 alkyl layer employed in these experiments corresponds to an estimated distance from the surface of 19 Å. In these systems, electron

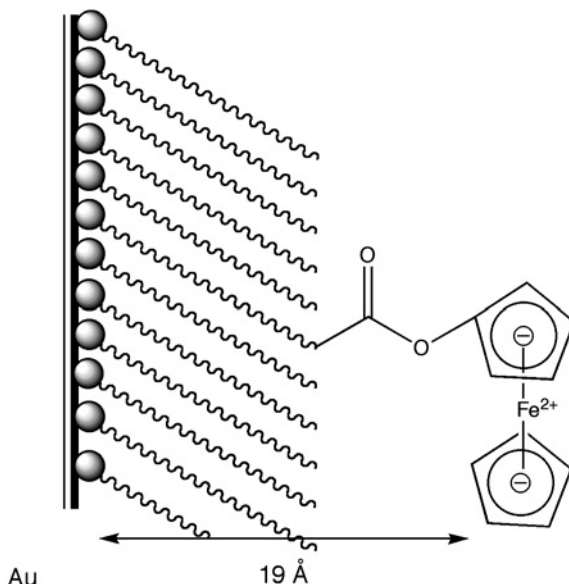


**Figure 16.22** Ferrocene covalently linked to an alkanethiol adsorbed to the surface of a gold electrode. The ferrocene-substituted alkylthiol is diluted in other alkanethiols to minimise the interactions between ferrocenes and favour a homogenous coverage of the electrode. The stability of the monolayer is due to the strong adsorption of the sulphur atom at the surface of the gold electrode.

transfer has the characteristics of an intra-molecular processes and, therefore the rate constants are in units of  $\text{sec}^{-1}$ ; at the standard potential the rate is  $k_{\text{het}} = 1.25 \text{ sec}^{-1}$  at 298 K.

The pre-exponential factor for this electrochemical exchange can be calculated with eq. (16.73) making  $\Gamma = 1$ . Assuming the monolayer has a refractive index  $n_D = 1.6$ , making  $r - r_0 = 19 \text{ \AA}$  and taking the absolute potential of ferrocene  $\Phi_0 = 5.17 \text{ eV}$ , the frequency factor becomes  $10^3 \text{ sec}^{-1}$ . This with the activation free energy already calculated for the  $\text{Fe}(\text{Cp})_2^{0/+}$  couple,  $\Delta G_{\text{het}}^\ddagger = 21 \text{ kJ mol}^{-1}$ , gives  $k_{\text{het}} = 0.2 \text{ sec}^{-1}$  at 298 K. It is rewarding to see that in this system, free from double-layer effects and uncertainties in the pre-exponential factor, the calculate rate is in good agreement with the experiment.

A more rigorous treatment must consider that in a metal electrode there is a continuum of energy levels and, therefore, a manifold of activated complexes for electron transfers (Figure 16.23). In the previous approach, the sum over activated complexes was replaced by a *single activated complex* with properties corresponding to the Fermi level. For the present kinetic data it is worth avoiding such a simplification.

The density of electronic states in the electrode,  $\rho$ , close to the Fermi level of the metal, is dependent on the Fermi energy ( $\varepsilon_F$ ), on the number of conducting electrons provided by each atom ( $N$ ), and can be estimated within the model of a free electronic gas

$$\rho(\varepsilon_F) = \frac{3N}{2\varepsilon_F} \quad (16.76)$$

For gold, each atom contributes  $N = 1$  to the electronic gas and  $\varepsilon_F = 5.51 \text{ eV}$ . Hence the density of states for gold at the Fermi level is  $\rho(\varepsilon_F) = 0.27 \text{ states eV}^{-1} \text{ atom}^{-1}$ .

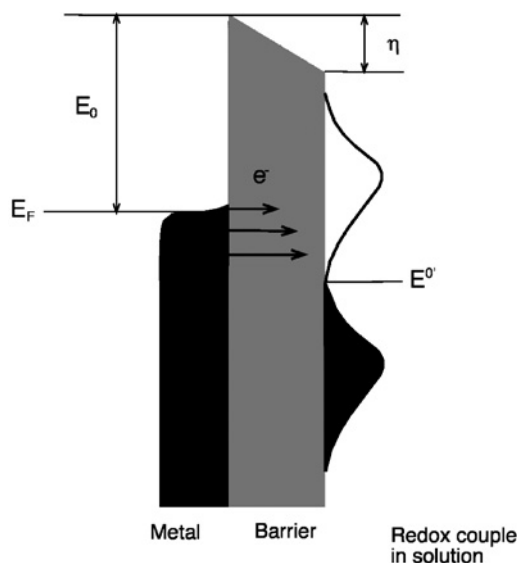


**Figure 16.23** Representation of the electron transfers for the several electronic levels of the metal.

The distribution of the electrons in a metal follows Fermi–Dirac statistics

$$\begin{aligned} f_{\text{red}}(\varepsilon) &= \frac{1}{1 + \exp(\varepsilon/k_B T)} \\ f_{\text{ox}}(\varepsilon) &= \frac{\exp(\varepsilon/k_B T)}{1 + \exp(\varepsilon/k_B T)} \end{aligned} \quad (16.77)$$

For reduction, such a statistical distribution favours the energy levels of lower energy, since the high-energy levels are less populated. Nevertheless, the barrier for the electron transfer decreases with an increase in the energy levels of the electrons to be transferred. Consequently, the rate for the reduction process is proportional to

$$\rho(\varepsilon_F) f_{\text{red}}(\varepsilon) \exp\left(-\frac{\varepsilon^\ddagger}{k_B T}\right) \quad (16.78)$$

where  $\varepsilon^\ddagger$  is the energy barrier for the level of energy  $\varepsilon$ . The probability of electron transfer attains a maximum for the electrochemical potential of the electrons in the metal.

The probability of electron transfer from an ion or molecule to an electrode follows the same formalism, and also attains a maximum for the electrochemical potential of the electrons in the metal

$$\rho(\varepsilon_F) f_{\text{ox}}(\varepsilon) \exp\left(-\frac{\varepsilon^\ddagger}{k_B T}\right) \quad (16.79)$$

The experimental electron-transfer rate is given by the integral for all the elementary rates from each energy level. The factor of non-adiabaticity needs also to be taken into account and the overall rate is given by

$$k_{\text{ele}} = v_{\text{el}} \rho(\varepsilon_F) RT \int \chi_r f(\varepsilon) \exp\left(-\frac{\varepsilon^\ddagger}{k_B T}\right) d\left(\frac{\varepsilon}{k_B T}\right) \quad (16.80)$$

Here the integral is carried out for all the levels thermally populated.

Figure 16.24 presents the ISM calculations for the system of Chidsey together with the results for the Butler–Volmer model; the monolayer is described as before with a refractive index  $n_D = 1.6$  and the absolute potential of ferrocene is  $\Phi_0 = 5.17$  eV. The calculations incorporated the correction of the images forces for tunnelling of the electrons. All the models interpret the rates well at the standard potential.

The Butler–Volmer model overestimates the effect of overpotential on the rates and has a symmetric behaviour. The more complete calculations with ISM rates with  $\Lambda = 350$  kJ mol<sup>-1</sup>, are in fair agreement with experiment for the cathodic reduction and, with respect to the Butler–Volmer approach, present some asymmetry due to a more favourable non-adiabatic factor for tunnelling of the electrons in reduction. There is no close agreement for data in the anodic region. Incorporating a correction with a lower  $\Lambda$  into the Butler–Volmer model

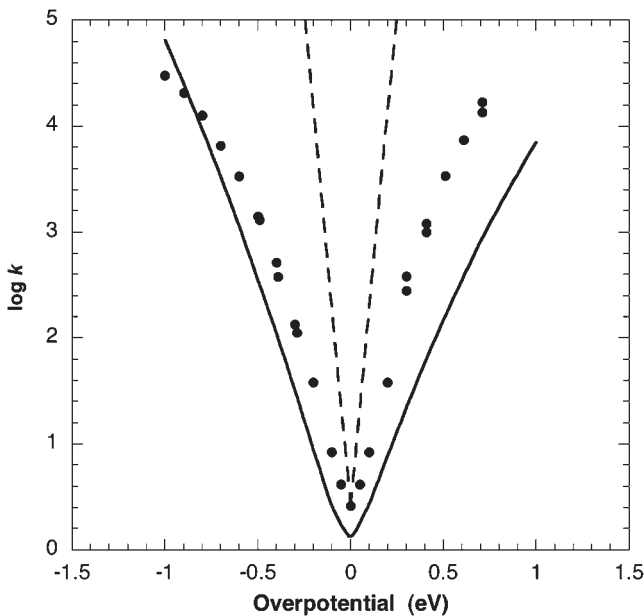


**Figure 16.24** Tafel plots for a first-order electron-transfer rate, at 298 K, on a gold electrode covered with a monolayer of *n*-alkylthiols, some of them covalently linked to ferrocenes. The points are the experimental data of Chidsey [48], the dashed line represents the Butler–Volmer model calculated with  $k_0 = 1.25 \text{ sec}^{-1}$  and  $\alpha = 0.5$ , and the full line was calculated with ISM [49].

does not appear to be valid, because it would decrease the rate constants even more, which would increase the disagreement still further. A possible solution would be the incorporation of the transfer of holes from the electrode to the molecular species in the oxidation region of the process.

## REFERENCES

- [1] SJ Formosinho, LG Arnaut, R Fausto, *Prog. React. Kinet.* **23** (1998) 1.
- [2] JR Winkler, HB Gray, *Chem. Rev.* **92** (1992) 369.
- [3] RA Marcus, *J. Chem. Phys.* **24** (1956) 966.
- [4] NS Hush, *J. Chem. Phys.* **28** (1958) 962.
- [5] RA Marcus, N Sutin, *Biochim. Biophys. Acta* **811** (1985) 265.
- [6] RA Marcus, *Angew. Chem. Int. Ed. Engl.* **32** (1993) 1111.
- [7] N Sutin, *Annu. Rev. Nucl. Sci.* **12** (1962) 285.
- [8] SJ Formosinho, LG Arnaut, *J. Mol. Struct. (Theochem)* **130** (1994) 105.
- [9] A Zahl, R van Eldik, M Matsumoto, TW Swaddle, *Inorg. Chem.* **42** (2003) 3718.
- [10] X-X Li, K-X Fu, Q Zhu, M-H Shan, *J. Mol. Struct. (Theochem)* **671** (2004) 239.
- [11] K-X Fu, X-X Li, Q Zhu, Z Gong, S-Z Lu, Z-M Bao, *J. Mol. Struct. (Theochem)* **715** (2005) 157.
- [12] G Grampp, A Kapturkiewicz, W Jaenicke, *Ber. Bunsenges. Phys. Chem.* **94** (1990) 439.

- [13] GE McManis, RM Nielson, A Gochev, MJ Weaver, *J. Am. Chem. Soc.* **111** (1989) 5533.
- [14] SF Nelsen, Y Kim, SC Blackstock, *J. Am. Chem. Soc.* **111** (1989) 2045.
- [15] R Derai, PR Kemper, MT Bowers, *J. Chem. Phys.* **82** (1985) 4517.
- [16] J Xie, RN Zare, *J. Chem. Phys.* **96** (1992) 4293.
- [17] C-Y Lee, AE DePristo, *J. Am. Chem. Soc.* **105** (1983) 6775.
- [18] K Ohta, K Morokuma, *J. Phys. Chem.* **91** (1987) 401.
- [19] MD Newton, K Ohta, E Zhong, *J. Phys. Chem.* **95** (1991) 2317.
- [20] DE Richardson, JR Eyler, *Chem. Phys.* **176** (1993) 457.
- [21] K Kirchner, S-Q Dang, M Stebler, HW Dodgen, S Wherland, JP Hunt, *Inorg. Chem.* **28** (1989) 3604.
- [22] SF Nelsen, DT Rumack, M Meot-Ner (Mautner), *J. Am. Chem. Soc.* **109** (1987) 1373.
- [23] SF Nelsen, A Konradsson, TL Jentzsch, JJ O'Konek, JR Pladziewicz, *J. Chem. Soc. Perkin Trans. 2* (2001) 1552. SF Nelsen, MN Weaver, JR Pladziewicz, LK Ausman, TL Jentzsch, JJ O'Konek, *J. Phys. Chem. A*, **110** (2006) 11665.
- [24] SF Nelsen, MT Ramm, RF Ismagilov, MA Nagy, DA Trieber, DR Powell, X Chen, JJ Gengler, Q Qu, JL Brandt, JR Pladziewicz, *J. Am. Chem. Soc.* **119** (1997) 5900.
- [25] SF Nelsen, L-J Chen, DR Powell, FA Neugebauer, *J. Am. Chem. Soc.* **117** (1995) 11434.
- [26] GL Miessler, DA Tarr, *Inorganic Chemistry*, Prentice Hall, New Jersey, 1998.
- [27] L Eberson, SS Shaik, *J. Am. Chem. Soc.* **112** (1990) 4484.
- [28] RA Marcus, *Faraday Discuss. Chem. Soc.* **29** (1960) 21.
- [29] D Rehm, A Weller, *Isr. J. Chem.* **8** (1970) 259.
- [30] E Vauthay, *J. Photochem. Photobiol. A: Chem.* **179** (2006) 1.
- [31] GL Closs, LT Calcaterra, NJ Green, KW Penfield, JR Miller, *J. Phys. Chem.* **90** (1986) 3673.
- [32] C Serpa, PJS Gomes, LG Arnaut, SJ Formosinho, J Pina, J Seixas de Melo, *Chem. Eur. J.* **12** (2006) 5014.
- [33] LG Arnaut, SJ Formosinho, *J. Mol. Struct. (Theochem)* **233** (1991) 209.
- [34] LG Arnaut, SJ Formosinho, *J. Photochem. Photobiol. A: Chem.* **118** (1998) 173.
- [35] LG Arnaut, SJ Formosinho, *J. Photochem. Photobiol. A: Chem.* **111** (1997) 111.
- [36] AJ Bard, HD Abrufa, CE Chidsey, LR Faulkner, SW Feldberg, K Itaya, M Majda, O Melray, RW Murray, MD Porter, MP Soriaga, HS White, *J. Phys. Chem.* **97** (1993) 7147.
- [37] AJ Bard, LR Faulkner, *Electrochemical Methods*, Wiley, Nova Iorque, 1980.
- [38] JT Hupp, MJ Weaver, *Inorg. Chem.* **22** (1983) 2557.
- [39] DK Phelps, AA Kornyshev, MJ Weaver, *J. Phys. Chem.* **94** (1990) 1454.
- [40] RJD Miller, G McLendon, A Nozik, W Schmickler, F Willig, *Surface Electron Transfer Processes*, Wiley, New York, 1995.
- [41] RA Pierotti, *J. Phys. Chem.* **69** (1965) 281.
- [42] JG Simmons, *J. Appl. Phys.* **34** (1963) 1793.
- [43] RA Marcus, *Ann. Rev. Phys. Chem.* **15** (1964) 155.
- [44] LA Curtiss, JW Halley, J Hautman, NC Hung, Z Nagy, Y-J Rhee, RM Yonco, *J. Electrochem. Soc.* **138** (1991) 2023.
- [45] MJ Weaver, *J. Electroanal. Chem. Interfacial Electrochem.* **93** (1978) 231.
- [46] WR Fawcett, M Opallo, *Angew. Chem. Int. Ed. Engl.* **33** (1994) 2131.
- [47] JT Hupp, MJ Weaver, *J. Phys. Chem.* **88** (1984) 6128.
- [48] CED Chidsey, *Science* **251** (1991) 919.
- [49] LG Arnaut, AAC Pais, SJ Formosinho, *J. Mol. Struct.* **563/564** (2001) 1.

This page intentionally left blank

# Appendix I

## General Data

---

**Table I.1**

Fundamental physical constants

Name	Symbol	Value	Units (SI)
Speed of light <i>in vacuo</i>	$c$	$2.998 \times 10^8$	$\text{m sec}^{-1}$
Elementary charge	$e$	$1.602 \times 10^{-19}$	C
Vacuum permittivity	$\epsilon_0$	$8.854 \times 10^{-12}$	$\text{C}^2 \text{N}^{-1} \text{m}^2$
Avogadro's number	$N_A$	$6.022 \times 10^{23}$	$\text{mol}^{-1}$
Faraday constant	$F$	$9.648 \times 10^4$	$\text{C mol}^{-1}$
Gas constant	$R$	8.314	$\text{J K}^{-1} \text{mol}^{-1}$
Planck constant	$h$	$6.626 \times 10^{-34}$	J sec
Boltzmann constant	$k_B$	$1.381 \times 10^{-23}$	$\text{J K}^{-1}$
Atomic mass unit <sup>a</sup>	amu	$1.661 \times 10^{-27}$	kg
Electron rest mass	$m_e$	$9.109 \times 10^{-31}$	kg
Proton rest mass	$m_p$	$1.673 \times 10^{-27}$	kg

<sup>a</sup>IUPAC recommends the name “unified atomic mass unit” and its representation by the symbol u.

**Table I.2**

Conversion factors

<i>Length</i>					
m	$\mu\text{m}$	nm	$\text{\AA}$	pm	bohr
1	$10^{-6}$	$10^{-9}$	$10^{-10}$	$10^{-12}$	$1.8897 \times 10^{-10}$
<i>Energy</i>					
$\text{J mol}^{-1}$	$\text{cal mol}^{-1}$	erg	eV	$\text{cm}^{-1}$	hartree
1	0.2390	$10^7$	$1.0365 \times 10^{-5}$	$8.361 \times 10^{-2}$	$3.809 \times 10^{-7}$
<i>Pressure</i>					
$\text{N m}^{-2}$	Pa	bar	atm	$\text{lbf pol}^{-2}$	mmHg
1	1	$10^{-5}$	$9.899 \times 10^{-6}$	$1.450 \times 10^3$	$7.501 \times 10^{-3}$

Note:  $1 \text{ N m}^{-1} = 1 \text{ kg sec}^{-2} = 0.6022 \text{ J mol}^{-1} \text{ pm}^{-2} = 6.022 \text{ kJ mol}^{-1} \text{ \AA}^{-2} = 10^{-3} \text{ dyn cm}^{-1}$ . 1 Debye =  $3.336 \times 10^{-30} \text{ C m}$ .

This page intentionally left blank

# Appendix II

## Statistical Thermodynamics

---

In this appendix, we will use statistical thermodynamics to relate the equilibrium constant of a chemical reaction to the microscopic properties of the molecules involved. Our strategy will be to define functions for the microscopic properties of molecules and then to connect these to the change in the free energy of a reaction. The relationship between this property and the equilibrium constant is well known.

We will consider a system of molecules with ideal gas behaviour characterised by fixed values of temperature ( $T$ ), composition (total number of molecules  $N$ ), and volume ( $V$ ). This system is called the canonical ensemble. In this system, there will be, on average,  $n_0$  molecules in the state of given energy  $\varepsilon_0$ ,  $n_1$  molecules in the state  $\varepsilon_1$ , or in general,  $n_j$  molecules in the state  $\varepsilon_j$ . The molecules will be in equilibrium with a thermal bath, but the energy of each molecule can fluctuate. The value of  $T$  is a measure of the average energy of the molecules of the canonical ensemble. Thus, the population of the energetic states is kept practically constant, but the identity of the molecules in each state can change due to molecular collisions.

As the total number of molecules has to remain constant

$$\sum_j n_j = N \quad (\text{II.1})$$

If we also fix the energy of the system

$$\sum_j n_j \varepsilon_j = E \quad (\text{II.2})$$

this is described as a microcanonical ensemble. The number  $n_i$  of molecules having energy  $\varepsilon_i$  is given by Boltzmann's distribution law

$$\frac{n_i}{N} = \frac{e^{-\varepsilon_i/k_B T}}{\sum_j e^{-\varepsilon_j/k_B T}} \quad (\text{II.3})$$

which can also be expressed as a sum over the number of energy levels (or group of states with the same energy)

$$\frac{n_i}{N} = \frac{g_i e^{-\varepsilon_i/k_B T}}{\sum_j g_j e^{-\varepsilon_j/k_B T}} \quad (\text{II.4})$$

where  $g_j$  is a statistical factor which takes account of the number of states with the same energy level  $\varepsilon_j$ . The denominator of this expression

$$Q = \sum g_j e^{-\varepsilon_j/k_B T} \quad (\text{II.5})$$

is called the molecular partition function, and is an indication of the average number of states which are thermally accessible to a molecule at the temperature of the system. As  $T \rightarrow 0$  only the ground state will be thermally accessible, such that  $Q \rightarrow g_0$ , which is the degeneracy for  $\varepsilon_0 = 0$ . Also, as  $T \rightarrow \infty$ , all the levels will become accessible and  $Q \rightarrow \infty$ .

Until this point, we have specified the energy levels relative to an arbitrarily chosen zero energy level. In practice, the energies are normally represented as the difference between the level  $j$  and the level of lowest energy of the molecule,  $\varepsilon_0 = 0$ . Thus, the energy  $E$  must be taken as the value of the internal energy relative to its value at  $T = 0$

$$U = U(0) + E \quad (\text{II.6})$$

where  $U(0)$  is the internal energy at  $T = 0$ .

In addition to the relation between the energy of the system and the molecular partition functions, we must also consider the relationship between the entropy,  $S$ , and the number of configurations, which the molecules can take in this system. If we consider  $N$  molecules, the first of these can be arranged in  $N$  different ways, the second in  $(N-1)$  ways and we can continue in the same fashion until the  $N$ th molecule, which can only be arranged in one way. Thus, the total number of arrangements is

$$N(N-1)(N-2)\cdots 1 = N! \quad (\text{II.7})$$

However, the arrangements in which the molecules have the same energy are equivalent. We only obtain a new distribution when the particles change to different energy levels. When changes are made within the  $n_0$  molecules which exist in the state of energy  $\varepsilon_0$ , we do not produce any new distribution. In the same fashion it can be shown that the possible distributions of the  $n_1$  molecules of the state of energy  $\varepsilon_1$  are indistinguishable, and we can carry on with the other levels in exactly the same way. Consequently, the total number of different distributions of  $N$  molecules having the configuration  $\{n_0, n_1, \dots\}$  is given by the ratio between the total number of permutations and the number of permutations within each energy level

$$W_n = \frac{N!}{n_0! n_1! n_2! \dots} \quad (\text{II.8})$$

where the symbol  $n$  indicates that this distribution refers exclusively to the given configuration, and that the other configurations can be considered within the conditions imposed by (II.1) e (II.2). The above equation allows us to obtain the weight of any given configuration. Taking logarithms, this weight can also be written as

$$\begin{aligned} \ln W_n &= \ln N! - \ln(n_0! n_1! n_2! \dots) \\ &= \ln N! - \sum_j \ln n_j! \end{aligned} \quad (\text{II.9})$$

Using Stirling's approximation, that  $\ln x! \approx x \ln x - x$ , we obtain

$$\begin{aligned}
 \ln W_n &= N \ln N - N - \sum_j (n_j \ln n_j - n_j) \\
 &= N \ln N - \sum_j (n_j \ln n_j) \\
 &= \sum_j (n_j \ln N) - \sum_j (n_j \ln n_j) \\
 &= \sum_j \left( n_j \ln \frac{N}{n_j} \right)
 \end{aligned} \tag{II.10}$$

The quantitative relationship between the statistical entropy and the molecular disorder is given by the Boltzmann relationship

$$S = k_B \ln W \tag{II.11}$$

where  $W$  is the weight of the most probable configuration of the system. It should be noted that as  $T \rightarrow 0$  all the molecules are in the lowest energy level, and  $e^{N!} = n_0!$ , from which  $\ln W = 0$ . Substituting eq. (II.10) into (II.11), we obtain

$$\begin{aligned}
 S &= -k_B \sum_j \left( n_j \ln \frac{n_j}{N} \right) \\
 &= -k_B \sum_j n_j \left( -\frac{\varepsilon_j}{k_B T} - \ln Q \right) \\
 &= \frac{1}{T} \sum_j n_j \varepsilon_j + k_B N \ln Q \\
 &= \frac{1}{T} E + k_B N \ln Q
 \end{aligned} \tag{II.12}$$

Now, by using eq. (II.6) we obtain

$$S = \frac{U - U(0)}{T} + k_B N \ln Q \tag{II.13}$$

The energy and entropy, which are related in this equation to the molecular partition function, are statistical entities, defined by particles which do not interact except to maintain the equilibrium conditions. To obtain similar relationships for real systems, it is necessary to apply statistical mechanics to the calculation of the thermodynamic entities, which correspond to the molar quantities of particles, or that is  $N$  approaches  $N_A$ . In this treatment it is convenient to use the canonical ensemble already discussed and presented in Figure II.1. This ensemble consists of a very large number of systems,  $N$ , each containing 1 mol of molecules and separated from the others by diathermic walls, which allow heat conduction but do not allow particles to pass. The set of all the systems is isolated from the outside and has a fixed energy  $E$ , which is the energy of the canonical ensemble.

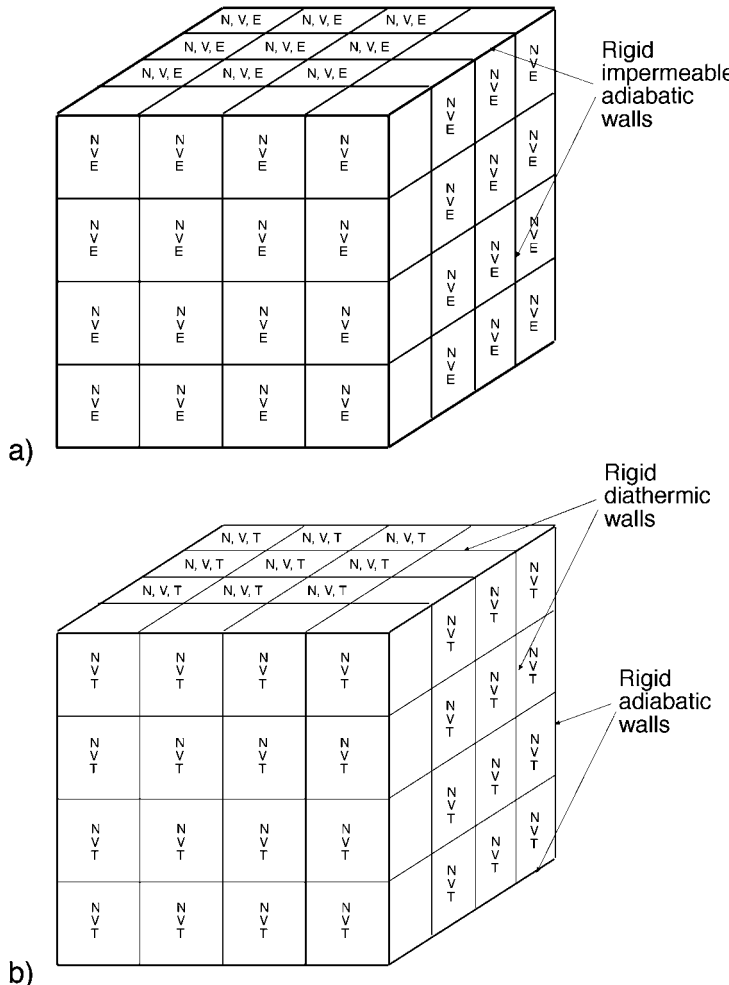


**Figure II.1** Schematic representations of ensembles of systems. (a) Microcanonical ensemble of  $N=64$  systems each with the same  $N$ ,  $V$  e  $E$ . (b) Canonical ensemble of  $N=64$  systems with the same  $N$ ,  $V$  e  $T$ ; the systems are in thermal contact and the total energy  $E$  of the 64 replicas is a constant, although it fluctuates from one system to the other.

Each particular system within the ensemble can occupy the energy states  $E_0, E_1, E_2, \dots, E_j$ , and the total energy of the state  $j$  of the system is given by

$$E_j = \varepsilon_j(1) + \varepsilon_j(2) + \dots + \varepsilon_j(N) \quad (\text{II.14})$$

where  $\varepsilon_j(s)$  is the energy of molecule  $s$  in the state  $j$ , etc. We should note that the canonical ensemble, with fixed values of  $N$ ,  $V$  and  $E$ , is a member of a micro-canonical ensemble.

If, at any one time, we have  $\mathbf{n}_0$  systems in the state of energy  $E_0$ ,  $\mathbf{n}_1$  in the state of energy  $E_1$ , and, in general,  $\mathbf{n}_j$  systems in the state  $E_j$ , the weight of the distribution  $\{\mathbf{n}_0, \mathbf{n}_1, \mathbf{n}_2, \dots\}$  is now given by

$$W_n = \frac{N!}{n_0! n_1! n_2! \dots} \quad (\text{II.15})$$

and the canonical distribution is

$$\frac{\mathbf{n}_i}{N} = \frac{e^{-E_i/k_B T}}{Q} \quad (\text{II.16})$$

where  $Q$  is the canonical partition function which can be related to the molecular partition function given the relationship between the sum over the states of the system and the sum over molecular states

$$\begin{aligned} Q &= \sum_j e^{-E_j/k_B T} \\ &= \sum_j e^{-\epsilon_j(1)/k_B T - \epsilon_j(2)/k_B T - \dots - \epsilon_j(N)/k_B T} \\ &= \left( \sum_j e^{-\epsilon_j(1)/k_B T} \right) \left( \sum_j e^{-\epsilon_j(2)/k_B T} \right) \dots \left( \sum_j e^{-\epsilon_j(N)/k_B T} \right) \\ &= \left( \sum_j e^{-\epsilon_j/k_B T} \right)^N = Q^N \end{aligned} \quad (\text{II.17})$$

Eq. (II.16) represents the probability that a member of the canonical ensemble has a given energy,  $E_j$ . This is given by the product of two functions, one which decreases exponentially with the energy and another, which gives the number of permitted states with a particular energy, and which increases very strongly with energy. The result of these two opposing effects is a distribution strongly centred on the average energy of the members of the ensemble.

$$E = \frac{\mathbf{E}}{N} \quad (\text{II.18})$$

In the thermodynamic limit of  $N \rightarrow \infty$  there is always one configuration of the canonical ensemble which becomes clearly dominant, from which it is possible to calculate the thermodynamic properties of the ensemble. In fact, we can ignore configurations in which the energy  $\mathbf{E}$  is only present in one or a few systems. In this limit, the internal energy of one system of the ensemble can be written in the form

$$U = U(0) + E = U(0) + \frac{\mathbf{E}}{N} \quad (\text{II.19})$$

On the other hand, it is only of interest to consider the weight of the most probable distribution of the ensemble, which is given by the product of the average weights of the most

probable distributions of each system of the ensemble.

$$W = W^N \quad (\text{II.20})$$

Using this equation in conjunction with the Boltzmann formula for the entropy, eq. (II.11), we obtain

$$S = k_B \ln W^{1/N} = \frac{k_B}{N} \ln W \quad (\text{II.21})$$

Following the arguments which led to expression (II.13), for the canonical ensemble we can obtain

$$S = \frac{U - U(0)}{T} + k_B \ln Q \quad (\text{II.22})$$

If it is possible to identify all the molecules, such as in case of a solid, where the positions in the crystal lattice can be defined in terms of the coordinate positions, eq. (II.17) can be used. However, for the case where the molecules cannot be differentiated, e.g. with an ideal gas, it is necessary to count over all the sums of the molecular states of indistinguishable molecules, and weigh the result by the number of possible permutations,  $N!$ . For this case

$$Q = \frac{Q^N}{N!} \quad (\text{II.23})$$

As we already know the relationship between the canonical partition functions, the internal energy and entropy of a system, it is possible to connect the thermodynamic functions with the partition functions, which in turn are related to the spectroscopic data for the individual molecules.

The Helmholtz free energy

$$A = U - TS \quad (\text{II.24})$$

for  $T=0$  leads to  $A(0) = U(0)$ . Substituting into eq. (II.22), we obtain

$$A - A(0) = -k_B T \ln Q \quad (\text{II.25})$$

As the Gibbs free energy is given by

$$G = A + pV \quad (\text{II.26})$$

and for perfect gases  $pV=nRT$ , eq. (II.25) can be used to write

$$\begin{aligned} G - G(0) &= A - A(0) + nRT \\ &= -k_B T \ln Q + nRT \end{aligned} \quad (\text{II.27})$$

As ideal gases consist of indistinguishable molecules, we obtain

$$\begin{aligned} G - G(0) &= -Nk_B T \ln Q + k_B T \ln N! + nRT \\ &= -nN_A k_B T \ln Q + k_B T (N \ln N - N) + nRT \\ &= -nRT \ln \left( \frac{Q}{N} \right) \end{aligned} \quad (\text{II.28})$$

since  $N = nN_A$  and  $R = k_B N_A$ . Also, as the standard Gibbs free energy of a reaction  $A + B \rightleftharpoons \ddot{\gamma}$  is related to its equilibrium constant

$$\Delta G^0 = -RT \ln K_{\text{eq}} \quad (\text{II.29})$$

it is also possible to express the equilibrium constant of a reaction in terms of partition functions of reactants and products. Since, for an ideal gas at  $T=0$  we obtain  $G(0)=A(0)=U(0)$ , it can be shown that, for any reaction at equilibrium, the difference of molar free energy between products and reactants is equal to their difference in molar internal energy, and this is given by the difference in zero point energy between the products and reactants. This energy difference is normally given as

$$\Delta E^0 = U_{\ddot{\gamma}}^0(0) - U_A^0(0) - U_B^0(0) \quad (\text{II.30})$$

The remaining free-energy difference between reactants and products can be related to their standard molar partition functions

$$Q_A^0 = \frac{Q_A}{n}, \quad Q_B^0 = \frac{Q_B}{n}, \quad Q_{\ddot{\gamma}}^0 = \frac{Q_{\ddot{\gamma}}}{n} \quad (\text{II.31})$$

where these refer to 1 mol of ideal gas in the standard state of  $p^0 = 1$  atm, such that the standard molar volume  $V_m^0 = RT/p^0$ . Thus,

$$\Delta G^0 = \Delta E^0 - RT \ln \left( \frac{Q_{\ddot{\gamma}}^0/N_A}{(Q_A^0/N_A)(Q_B^0/N_A)} \right) \quad (\text{II.32})$$

from which

$$\ln K_{\ddot{\gamma}} = \ln \left( \frac{Q_{\ddot{\gamma}}^0/N_A}{(Q_A^0/N_A)(Q_B^0/N_A)} \right) - \frac{\Delta E^0}{RT} \quad (\text{II.33})$$

and

$$K_{\ddot{\gamma}} = \frac{Q_{\ddot{\gamma}}^0 N_A}{Q_A^0 Q_B^0} e^{-\Delta E_0/RT} \quad (\text{II.34})$$

This page intentionally left blank

# Appendix III

## Parameters Employed in ISM Calculations

---

**Table III.1**

Morse curve parameters, ionisation potentials and electron affinities for the calculation of atom and proton transfer rates<sup>a</sup>

	$l_{\text{eq}}^a(\text{\AA})$	$D^0_{298}(\text{kJ mol}^{-1})$	$\omega_e(\text{cm}^{-1})$	$I_p(\text{eV})$	$E_A(\text{eV})$
H <sub>2</sub>	0.74144	435.99	4161	13.598	0.75419
CH <sub>4</sub>	1.0870	438.9	2917	9.843	0.08
CH <sub>3</sub> CH <sub>3</sub>	1.0940	423.0	2954	8.117	-0.26
CH <sub>3</sub> CH <sub>2</sub> CH <sub>3</sub>	1.107	409.1	2887	7.37	-0.321
(CH <sub>3</sub> ) <sub>3</sub> CH	1.122	404.3	2890	6.70	-0.156
CH <sub>3</sub> COCH <sub>3</sub>	1.103	411.3	2939		
CH <sub>3</sub> OCH <sub>3</sub>	1.121	402.2	2817	6.90	-0.017
CH <sub>3</sub> OH	1.0936	401.8	2844	7.562	
CH <sub>3</sub> CHO	1.128	373.8	2822	7.00	0.423
CH <sub>2</sub> O	1.116	368.5	2783	8.14	0.313
CH <sub>3</sub> C <sub>6</sub> H <sub>5</sub>	1.111	375.7	2934	7.2488	0.912
CH <sub>2</sub> =CH <sub>2</sub>	1.087	465.3	3026	8.25	0.667
C <sub>6</sub> H <sub>6</sub>	1.101	473.1	3062	8.32	1.096
HCN	1.0655	527.6	3311	14.170	3.862
CH≡CH	1.060	556.1	3374	11.610	2.969
CH <sub>3</sub> NH <sub>2</sub>	1.099	390.4	2820	6.29	
(CH <sub>3</sub> ) <sub>3</sub> SiH	1.485	377.8	2107	7.03	0.971
SiH <sub>4</sub>	1.4798	384.1	2187	8.135	1.405
(CH <sub>3</sub> ) <sub>3</sub> SnH	1.700	322	1815	7.10	1.70
GeH <sub>4</sub>	1.5251	349.0	2106	7.948	1.61
NH <sub>3</sub>	1.012	452.7	3337	10.780	0.771
PH <sub>3</sub>	1.4200	351.0	2323	9.824	1.25
AsH <sub>3</sub>	1.511	319.2	2116	9.85	1.27
H <sub>2</sub> O	0.9575	498	3657	13.017	1.8277
OH	0.96966	427.6	3737.76	13.618	1.4611
CH <sub>3</sub> OH	0.9451	436.0	3681	10.720	1.57
H <sub>2</sub> S	1.3356	381.6	2615	10.422	2.317
H <sub>2</sub> Se	1.47	334.9	2345	9.845	2.2125
CH <sub>3</sub> SH	1.340	365.3	2610	9.262	1.867
C <sub>6</sub> H <sub>5</sub> SH	1.36	348.5	2597	8.6	2.26
HF	0.9169	569.87	3962	17.423	3.448

(continued)

**Table III.1** (continued)

	$l_{\text{eq}}^{\text{a}}$ (Å)	$D^0_{298}$ (kJ mol $^{-1}$ )	$\omega_{\text{e}}$ (cm $^{-1}$ )	$I_{\text{p}}$ (eV)	$E_{\text{A}}$ (eV)
HCl	1.27455	431.62	2886	12.968	3.6144
HBr	1.41444	366.35	2559	11.814	3.3636
HI	1.60916	298.41	2230	10.451	3.059
CF <sub>3</sub> H	1.098	449.5	3036	8.76	1.869
F <sub>2</sub>	1.41193	158.78	892	17.423	3.448
Cl <sub>2</sub>	1.988	242.58	557	12.968	3.6144
Br <sub>2</sub>	2.281	192.81	317	11.814	3.3636
I <sub>2</sub>	2.666	151.09	213	10.451	3.0590

<sup>a</sup>Data from LG Arnaut, AACC Pais, SJ Formosinho, M Barroso, *J. Am. Chem. Soc.* **125** (2003) 5236.

**Table III.2**

Harmonic oscillator parameters for the simplified calculation of atom and proton transfer rates

Bond	$f_{\text{XH}}$ (kJ mol $^{-1}$ Å $^{-2}$ )	$l_{\text{XH}}$ (Å)
CH	$2.90 \times 10^3$	1.07
NH	$3.82 \times 10^3$	1.01
ROH	$4.21 \times 10^3$	0.97
HOH	$4.21 \times 10^3$	0.958
HF	$5.80 \times 10^3$	0.917

**Table III.3**

Morse curve parameters employed in ISM calculations of S<sub>N</sub>2 reaction rates<sup>a</sup>

Molecule	$D_{\text{e}}$	$\omega$	$l_{\text{eq}}$
	(kJ mol $^{-1}$ )	(cm $^{-1}$ )	(Å)
CH <sub>3</sub> —CH <sub>3</sub> CH <sub>3</sub>	368 <sup>b</sup>	1054 <sup>b</sup>	1.512
CH <sub>3</sub> —SiH <sub>2</sub> CH <sub>3</sub>	368 <sup>c</sup>	770 <sup>d</sup>	1.873
CH <sub>3</sub> —GeH <sub>2</sub> CH <sub>3</sub>	314	651	1.957
CH <sub>3</sub> —SnH <sub>2</sub> CH <sub>3</sub>	205	541	2.177
CH <sub>3</sub> —NHCH <sub>3</sub>	259	1143	1.474
CH <sub>3</sub> —PHCH <sub>3</sub>	264	664	1.868
CH <sub>3</sub> —AsHCH <sub>3</sub>	234	607	1.973
CH <sub>3</sub> —SbHCH <sub>3</sub>	201	597	2.162
CH <sub>3</sub> —OCH <sub>3</sub>	276	1014 <sup>b</sup>	1.405
CH <sub>3</sub> —SCH <sub>3</sub>	280	723	1.801
CH <sub>3</sub> —SeCH <sub>3</sub>	280	648	1.948

(continued)

**Table III.3 (continued)**

Molecule	$D_e$	$\omega$	$l_{eq}$
	(kJ mol <sup>-1</sup> )	(cm <sup>-1</sup> )	(Å)
CH <sub>3</sub> –TeCH <sub>3</sub>	146	470	2.200
F–CH <sub>3</sub>	452 <sup>b</sup>	1049 <sup>b</sup>	1.351
Cl–CH <sub>3</sub>	347 <sup>b</sup>	732 <sup>b</sup>	1.764
Br–CH <sub>3</sub>	293 <sup>b</sup>	611 <sup>b</sup>	1.951
I–CH <sub>3</sub>	234 <sup>b</sup>	533 <sup>b</sup>	2.027

<sup>a</sup>All data were calculated by the PM3 method in ref. LG Arnaut, AACC Pais, SJ Formosinho, *J. Mol. Struct.*, **563/564** (2001) I, except where indicated. <sup>b</sup> From *NIST Standard Reference Database # 69 (Feb, 2000)*. <sup>c</sup> From DF McMillen, Dm Golden, *Ann. Rev Phys. Chem.*, **33** (1982) 493. <sup>d</sup> From similar compounds in AA Zavitsas, C Chatgilialoglu, *J. Am. Chem. Soc.*, **117** (1995) 10645.

**Table III.4**

Harmonic oscillator parameters for the calculation of electron transfer rates<sup>a</sup>

Complex or Molecule <sup>b</sup>	Electronic configuration	$f_{red}$ (kJ mol <sup>-1</sup> Å <sup>-2</sup> )	$f_{ox}$ (kJ mol <sup>-1</sup> Å <sup>-2</sup> )	$l_{red}$ (Å)	$l_{ox}$ (Å)
Fe(CN) <sub>6</sub> <sup>4-/3-</sup>	(π) <sup>6</sup> /(π) <sup>5</sup>	1.38 × 10 <sup>3</sup>	1.44 × 10 <sup>3</sup>	1.88	1.88
Cr(OH <sub>2</sub> ) <sub>6</sub> <sup>2+/3+</sup>	(π) <sup>3</sup> (σ*) <sup>1</sup> /(π) <sup>3</sup>	0.96 × 10 <sup>3</sup>	1.53 × 10 <sup>3</sup>	2.15	1.98
Mn(OH <sub>2</sub> ) <sub>6</sub> <sup>2+/3+</sup>	(π) <sup>3</sup> (σ*) <sup>2</sup> /(π) <sup>3</sup> (σ*) <sup>1</sup>	0.96 × 10 <sup>3</sup>	1.53 × 10 <sup>3</sup>	2.177	1.991
V(OH <sub>2</sub> ) <sub>6</sub> <sup>2+/3+</sup>	(π) <sup>6</sup> /(π) <sup>5</sup>	0.96 × 10 <sup>3</sup>	1.53 × 10 <sup>3</sup>	2.131	1.992
Fe(OH <sub>2</sub> ) <sub>6</sub> <sup>2+/3+</sup>	(π) <sup>4</sup> (σ*) <sup>2</sup> /(π) <sup>3</sup> (σ*) <sup>2</sup>	0.96 × 10 <sup>3</sup>	1.53 × 10 <sup>3</sup>	2.10	1.98
Co(OH <sub>2</sub> ) <sub>6</sub> <sup>2+/3+</sup>	(π) <sup>5</sup> (σ*) <sup>2</sup> /(π) <sup>6</sup>	0.96 × 10 <sup>3</sup>	1.53 × 10 <sup>3</sup>	2.081	1.873
Ru(OH <sub>2</sub> ) <sub>6</sub> <sup>2+/3+</sup>	(π) <sup>6</sup> /(π) <sup>5</sup>	1.16 × 10 <sup>3</sup>	1.82 × 10 <sup>3</sup>	2.11	2.03
Co(NH <sub>3</sub> ) <sub>6</sub> <sup>2+/3+</sup>	(π) <sup>5</sup> (σ*) <sup>2</sup> /(π) <sup>6</sup>	0.78 × 10 <sup>3</sup>	1.48 × 10 <sup>3</sup>	2.19	1.97
Ru(NH <sub>3</sub> ) <sub>6</sub> <sup>2+/3+</sup>	(π) <sup>6</sup> /(π) <sup>5</sup>	1.23 × 10 <sup>3</sup>	1.52 × 10 <sup>3</sup>	2.14	2.12
Co(phen) <sub>3</sub> <sup>2+/3+</sup>	(π) <sup>5</sup> (σ*) <sup>2</sup> /(π) <sup>6</sup>	0.68 × 10 <sup>3</sup>	1.38 × 10 <sup>3</sup>	2.11	1.91
Fe(phen) <sub>3</sub> <sup>2+/3+</sup>	(π) <sup>6</sup> /(π) <sup>5</sup>	1.44 × 10 <sup>3</sup>	1.42 × 10 <sup>3</sup>	1.97	1.97
Ru(bpy) <sub>3</sub> <sup>2+/3+</sup>	(π) <sup>6</sup> /(π) <sup>5</sup>	1.32 × 10 <sup>3</sup>	1.32 × 10 <sup>3</sup>	2.056	2.034
Fe(Cp) <sub>2</sub> <sup>0/+</sup>	(a <sub>1g</sub> ) <sup>2</sup> (e <sub>2g</sub> ) <sup>4</sup> /(a <sub>1g</sub> ) <sup>2</sup> (e <sub>2g</sub> ) <sup>3</sup>	1.90 × 10 <sup>3</sup>	1.75 × 10 <sup>3</sup>	1.649	1.677
Anthracene <sup>0/-</sup>			3.77 × 10 <sup>3</sup>		1.406
22/u22 <sup>+0</sup>		1.92 × 10 <sup>3</sup>	1.40 × 10 <sup>3</sup>	1.497	1.349
iPr <sub>2</sub> N) <sub>2</sub> <sup>+0</sup>		4.50 × 10 <sup>3</sup>	9.95 × 10 <sup>3</sup>	1.394	1.333

<sup>a</sup>Data from SJ Formosinho, LG Arnaut, R Fausto, *Prog. React. Kinet.* **23** (1998) 1, except Fe(cp)<sub>2</sub><sup>0/+</sup> which are from E Diana, R Rossetti, PL Stanghellini, SFA Kettle, *Inorg. Chem.* **36** (1997) 382 and TN Doman, CR Landis, B Bosnich, *J. Am. Chem. Soc.* **114** (1992) 7264.

<sup>b</sup> phen: 1,10-phenanthroline; bpy: 2,2'-bipyridyl; Cp: cyclopentadienyl; anthracene data are representative of most aromatic molecules, and the differences between  $f_{ox}$  and  $f_{red}$  are compensated using the differences between  $l_{ox}$  and  $l_{red}$ . For the structures of the hydrazines 22/u22 and iPr<sub>2</sub>N)<sub>2</sub>, see Figure 16.5.

This page intentionally left blank

# Appendix IV

## Semi-classical Interacting State Model

---

### IV.1 VIBRATIONALLY ADIABATIC PATH

The classical reaction path of an atom transfer reaction



given by the intersecting/interacting state model (ISM) in Chapter 6, eq. (6.81)

$$\begin{aligned} V_{\text{cl}}(n) &= (1-n)V_{\text{BC}}(n) + nV_{\text{AB}}(n) + n\Delta V^0 \\ &= (1-n)D_{\text{e,BC}} \left\{ 1 - \exp \left[ \gamma_{\text{BC}} \ln(1-n) \right] \right\}^2 + nD_{\text{e,AB}} \left\{ 1 - \exp \left[ \gamma_{\text{AB}} \ln(n) \right] \right\}^2 + n\Delta V^0 \\ \gamma_{\text{BC}} &= \frac{a'_{\text{sc}} (l_{\text{BC,eq}} + l_{\text{AB,eq}}) \beta_{\text{BC}}}{m} \\ \gamma_{\text{AB}} &= \frac{a'_{\text{sc}} (l_{\text{BC,eq}} + l_{\text{AB,eq}}) \beta_{\text{AB}}}{m} \end{aligned} \quad (\text{IV.1})$$

must be augmented by zero-point energy corrections along the reaction coordinate  $n$ ,  $Z(n)$ , to yield the vibrationally adiabatic path

$$V_{\text{ad}}(n) = V_{\text{cl}}(n) + Z(n) \quad (\text{IV.2})$$

This, together with a procedure to calculate tunnelling corrections, transforms classical ISM into semi-classical ISM. This appendix presents the background material necessary for such a treatment.

The zero-point energy of the reactants is directly calculated from the Morse curve of the BC bond

$$\bar{v}_{\text{BC}} = \frac{1}{2\pi c} \sqrt{\frac{f_{\text{BC}}}{\mu_{\text{BC}}}} = \frac{1}{2\pi c} \sqrt{\frac{2\beta_{\text{BC}}^2 D_{\text{BC}}}{\mu_{\text{BC}}}} = 2.3738 \times \beta_{\text{BC}} \sqrt{\frac{D_{\text{BC}}}{\mu_{\text{BC}}}} \quad (\text{IV.3})$$

where  $c$  is the speed of light,  $f_{\text{BC}}$  the force constant of the BC bond, and the numerical conversion factor is included to give the result in  $\text{cm}^{-1}$  when the spectroscopic constant  $\beta$  is expressed in  $\text{\AA}^{-1}$ , the reduced mass  $\mu_{\text{BC}}$  in amu and the electronic dissociation energy  $D_{\text{BC}}$

in J. The zero-point energy of the reactants is then

$$Z_{BC} = \frac{1}{2} hc \bar{v}_{BC} \quad (IV.4)$$

while similar expressions give the zero-point energy of the products,  $Z_{AB}$ . These expressions ignore the very small anharmonic correction of the Morse curves associated with the fundamental vibrational level.

The normal modes of vibration of the linear tri-atomic transition state  $\{A\cdots B\cdots C\}^\ddagger$  are the symmetric stretching, the anti-symmetric stretching and two degenerate bending modes. For a stable tri-atomic molecule, the symmetric and anti-symmetric stretchings are calculated from Wilson's equation

$$w_\pm = \frac{f_{ab}(\mu_A + \mu_B) + f_{bc}(\mu_C + \mu_B) \pm \sqrt{(f_{ab}\mu_A - f_{bc}\mu_C)^2 + (f_{ab} + f_{bc})^2 \mu_B^2 + 2(f_{ab} - f_{bc})(f_{ab}\mu_A - f_{bc}\mu_C)\mu_B}}{2} \quad (IV.5)$$

where, using the nomenclature of Wilson,  $\mu_i = m_i^{-1}$ ,  $f_{ij}$  are the force constants of the fragments  $ij$ , and the cross terms and bendings were neglected. The solution obtained with the subtraction of the square root term,  $w_-$  is associated with the symmetric stretch, and that obtained with the addition,  $w_+$ , with the asymmetric stretch. The latter has an imaginary frequency and corresponds to the curvature of the classical reaction coordinate. If we make  $f_{ab} = f_{bc}$ , we obtain

$$\mu = \frac{2}{\mu_A + 2\mu_B + \mu_C + \sqrt{(\mu_A - \mu_C)^2 + 4\mu_B^2}} \quad (IV.6)$$

We note that this equation has the correct limits: if all the masses are identical, then  $\mu = m/3$ ; if A and C are much heavier than B, then  $\mu = m_B/2$ . The reduced mass  $\mu$  is that of the anti-symmetric stretch of a tri-atomic molecule with  $D_{\infty h}$  symmetry, as expected for a linear transition state. As will be seen below, the tunnelling correction employs eq. (IV.6) for calculating the reduced mass.

The symmetric and anti-symmetric stretching frequencies along the reaction path are obtained from

$$\begin{aligned} \bar{v}_{\text{sym}}(n) &= \frac{1}{2\pi} \sqrt{w_-} [1 - y(n)] \\ \bar{v}_{\text{asym}}(n) &= \frac{1}{2\pi} \sqrt{w_+} y(n) \end{aligned} \quad (IV.7)$$

using eq. (IV.5) and the fractional force constants  $f_{ab}(n)$  given by the equation of Bürgi and Dunitz [1]

$$\begin{aligned} f_{bc}(n) &= 2D_{BC} (\beta_{BC})^2 (1-n)^{2\beta_{BC}} \\ f_{ab}(n) &= 2D_{AB} (\beta_{AB})^2 n^{2\beta_{AB}} \end{aligned} \quad (IV.8)$$

where  $a = 0.26$  is Pauling's constant, and  $y(n)$  is the switching function

$$\begin{aligned}
 y(n) &= \cosh \left[ \frac{l_{BC}}{l_{BC} + l_{AB}} \frac{\ln(n^{\ddagger})}{\ln(n/0.5)} \right]^{-1} && \text{for } n < 0.5 \\
 y(n) &= 0 && \text{for } n = 0.5 \\
 y(n) &= \cosh \left[ \frac{l_{AB}}{l_{BC} + l_{AB}} \frac{\ln(1-n^{\ddagger})}{\ln((1-n)/0.5)} \right]^{-1} && \text{for } n > 0.5
 \end{aligned} \tag{IV.9}$$

The switching function attenuates the frequencies to provide the correct asymptotic limits: when  $n \rightarrow 0$  then  $\bar{v}_{\text{asym}}(n) \rightarrow \bar{v}_{\text{BC}}$  and  $\bar{v}_{\text{sym}}(n) \rightarrow 0$ , when  $n \rightarrow 0.5$  then  $\bar{v}_{\text{asym}}(n) \rightarrow 0$  and  $\bar{v}_{\text{sym}}(n) \rightarrow 1/(2\pi\sqrt{w_-})$ , when  $n \rightarrow 1$  then  $\bar{v}_{\text{asym}}(n) \rightarrow \bar{v}_{\text{AB}}$  and  $\bar{v}_{\text{sym}}(n) \rightarrow 0$ .

ISM is a unidimensional reactivity model and cannot offer a method to calculate the two degenerate bending frequencies. However, there is a good linear correlation between the symmetric stretching and bending frequencies of many tri-atomic systems (Figure IV.1). From the slope of the empirical relation (slope = 0.43), we obtain the bending frequency

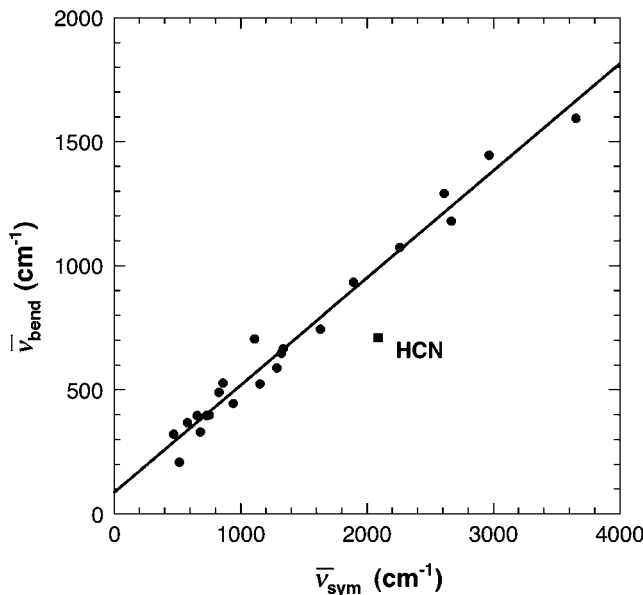


**Figure IV.1** Correlation between bending and symmetric stretching frequencies of tri-atomic molecules. Systems included in the correlation are H<sub>2</sub>O, D<sub>2</sub>O, H<sub>2</sub>S, D<sub>2</sub>S, H<sub>2</sub>Se, D<sub>2</sub>Se, CH<sub>2</sub>CO, SO<sub>2</sub>, NO<sub>2</sub>, CO<sub>2</sub>, CS<sub>2</sub>, F<sub>2</sub>O, Cl<sub>2</sub>O, ClCN, BrCN, ICN, SCN<sup>-</sup>, SC<sup>-</sup>O, NNO, O<sub>3</sub>, ClO<sub>2</sub> and SCl<sub>2</sub> from references [2,3]. The correlation coefficient is 0.989 and the slope is 0.43. The HCN system does not fit the correlation, presumably because the force constants of the two bonds and the masses of the end atoms are very different.

from the symmetric stretching frequency and get, for the transition state

$$Z_{\ddagger} = \frac{1}{2} hc \left[ \bar{v}_{\text{sym}}^{\ddagger} + 2(0.43 \bar{v}_{\text{sym}}^{\ddagger}) \right] \quad (\text{IV.10})$$

The above equation emphasises the fact that we are calculating the bending contribution from the symmetric stretching, and that we assume a linear transition state, i.e., there are two degenerate bending vibrations.

Now we have all the elements to calculate the zero-point energy corrections along the reaction coordinate

$$Z(n) = \frac{1}{2} hc \left\{ \bar{v}_{\text{sym}}(n) + 2[0.43 \bar{v}_{\text{sym}}(n)] + \bar{v}_{\text{asym}}(n) \right\} \quad (\text{IV.11})$$

and include them in eq. (IV.2) to obtain the vibrationally adiabatic path.

The asymptotic limits of the stretching frequencies are closely related to those of the electrophilicity index  $m$ . In the reactants we have  $m_{\text{BC}} = 1$  and the Morse curve of BC is from the spectroscopy of the isolated molecule. Also for the products  $m_{\text{AB}} = 1$ , for the same reasons. At the transition state,  $m(n)$  attains its maximum value, given by eq. (6.67)

$$m^{\ddagger} = \frac{I_p + E_A}{I_p - E_A} \quad (\text{IV.12})$$

Thus, we may consider that  $m(n)$  varies along the reaction coordinate much in the same manner as the stretching frequencies, and it is possible to calculate this from.

$$m(n) = \frac{I_p + E_A}{I_p - E_A} [1 - y(n)] \quad (\text{IV.13})$$

The energy of the maximum point along the vibrationally adiabatic path, eq. (IV.2), minus the zero-point energy of the reactants is the vibrationally adiabatic barrier.

$$\Delta V_{ad}^{\ddagger} = V_{ad}^{\ddagger}(n) - Z_{\text{BC}} \quad (\text{IV.14})$$

In practise, this maximum is found numerically, using steps of  $\Delta n = 0.01$  or smaller. Note that the maximum of the vibrationally adiabatic barrier may not coincide with that of the classical reaction path,  $n^{\ddagger}$ .

## IV.2 TUNNELLING CORRECTIONS

A very accurate method to calculate tunnelling correction along a unidimensional reaction path involves the semi-classical approximation [4]. The transmission coefficient and the transmission probabilities are

$$\kappa(T) = 1 + \frac{2}{k_B T} \int_{\varepsilon_0}^{\Delta V_{ad}^{\ddagger}} \sinh \left( -\frac{\Delta V_{ad}^{\ddagger} - \varepsilon}{k_B T} \right) G(\varepsilon) d\varepsilon \quad (\text{IV.15})$$

$$\begin{aligned}
 G(\varepsilon) &= \left\{ 1 + \exp[2\gamma(\varepsilon)] \right\}^{-1} & \varepsilon_0 \leq \varepsilon \leq \Delta V_{ad}^{\ddagger} \\
 &= 1 - G(2\Delta V_{ad}^{\ddagger} - \varepsilon), & \Delta V_{ad}^{\ddagger} \leq \varepsilon \leq 2\Delta V_{ad}^{\ddagger} - \varepsilon_0 \\
 &= 1 & 2\Delta V_{ad}^{\ddagger} - \varepsilon_0 < \varepsilon
 \end{aligned} \tag{IV.16}$$

respectively, while the barrier penetration integral is

$$\gamma(\varepsilon) = \frac{2\pi}{h} \int_{s_-}^{s_+} \sqrt{2\mu[V_a(s) - \varepsilon]} \, ds \quad \varepsilon < \Delta V_{ad}^{\ddagger} \tag{IV.17}$$

the threshold energy  $\varepsilon_0$  is the limiting value of the vibrationally adiabatic potential energy for exothermic or endothermic reactions

$$\varepsilon_0 = \max[V_a(s = -\infty), V_a(s = +\infty)] \tag{IV.18}$$

the reduced mass is given by eq. (IV.6), and  $s_+$  and  $s_-$  are the classical turning points, i.e., the locations at which  $V_a(s) = \varepsilon$ .

Hydrogen-atom or proton-transfer transfers between heavy atoms often lead to vibrationally adiabatic paths with two maxima. Formally, the resolution of this problem should be made in the framework of the canonically unified theory [5]. In practice, given the approximate nature of our treatment, it suffices to use TST with  $\Delta V_{ad}^{\ddagger}$  equal to the value for the maximum point. For these cases, the tunnelling correction of the particles with energies between that of the highest of the two maxima and the minimum between these is calculated for the highest barrier only.

### IV.3 SEMI-CLASSICAL RATE CONSTANTS

The semi-classical expression for the reaction rate constant given by transition-state theory

$$k_{\text{scTST}} = \kappa(T) \sigma \frac{k_B T}{h} \frac{Q^{\ddagger}}{Q_A Q_{BC}} e^{-\Delta V_{ad}^{\ddagger}/RT} \tag{IV.19}$$

can be calculated with the tunnelling correction and vibrationally adiabatic barrier described above, and the partition functions given by eqs. (6.20), (6.21) and (6.25). Here,  $\sigma$  is the statistical factor that accounts for the degeneracy of the reaction path. For a linear tri-atomic transition state, this expression can be simplified to

$$\begin{aligned}
 k_{\text{sc}} &= A \exp\left(-\frac{\Delta V_{ad}^{\ddagger}}{RT}\right) \\
 A &= \sigma \kappa(T) \frac{6.82 \times 10^{10}}{\sqrt{T}} \left( \frac{m_A + m_B + m_C}{m_A (m_B + m_C)} \right)^{3/2} \\
 &\times \frac{I_{ABC}}{I_{BC}} \frac{1 - \exp(-\bar{v}_{BC} hc/k_B T)}{\left[1 - \exp(-\bar{v}_{\text{sym}} hc/k_B T)\right] \left[1 - \exp(-0.43 \bar{v}_{\text{sym}} hc/k_B T)\right]^2} \text{ dm}^3 \text{ mol}^{-1} \text{ sec}^{-1}
 \end{aligned} \tag{IV.20}$$

where  $I_{ABC}$  and  $I_{AB}$  are the moments of inertia of the transition state and of the reactants, respectively.

In summary, the partition functions are calculated assuming that the system involves a linear tri-atomic transition-state, a diatomic reactant molecule and an atom. The classical transition-state geometry is obtained at the maximum of eq. (IV.1). The zero-point energy corrections are calculated with eq. (IV.11). The tunnelling correction is calculated using the semi-classical approximation, which requires numerical quadratures of eqs. (IV.15) and (IV.17). The total computational effort of calculating one rate constant at one given temperature is less than one second in any modern personal computer. This efficiency of the calculations makes it possible to perform semi-classical ISM calculations on-line, through the Internet. Such calculations can be made, free of charge, at the site: <http://www.ism.qui.uc.pt:8180/ism/>

## REFERENCES

- [1] H-B Bürgi, JD Dunitz, *J. Am. Chem. Soc.* **109** (1987) 2924.
- [2] G Herzberg, *Molecular Spectra and Molecular Structure. II. Infrared and Raman Spectra of Polyatomic Molecules*, Van Nostrand, New York, 1945.
- [3] K Nakamoto, *Infrared Spectra of Inorganic and Coordination Compounds*, Wiley, New York, 1963.
- [4] BC Garrett, DG Truhlar, *J. Phys. Chem.* **83** (1979) 2921.
- [5] BC Garrett, DG Truhlar, RS Grev, GS Schatz, RB Walker, *J. Phys. Chem.* **85** (1981) 3806.

# Appendix V

## The Lippincott–Schroeder Potential

---

### V.1 LIPPINCOTT—SCHROEDER (LS) POTENTIAL

The presence of a hydrogen bond along the reaction coordinate is included in the ISM reaction path using the Lippincott–Schroeder (LS) potential [1]. This empirical potential relates the H-bond binding energies ( $D_{AB}$ ) to the AB equilibrium distances ( $l_{AB, eq}$ ) and to the AB stretching frequency ( $\bar{v}_{AB}$ ) in the B ··· H–A hydrogen-bonded complex (charges omitted).

$$V_{LS} = V_{HA} + V_{HB} + V_{rep} + V_{el} \quad (V.I)$$

The LS potential is expressed as a sum of four terms

$$V_{LS} = V_{HA} + V_{HB} + V_{rep} + V_{el} \quad (V.1)$$

where the first two terms represent covalent interactions and have the form

$$\begin{aligned} V_{HA} &= D_{HA} \left[ 1 - \exp(-\alpha_{LS}) \right] \\ V_{HB} &= D_{H\cdots B} \left[ 1 - \exp(-\beta_{LS}) \right] - D_{H\cdots B} \end{aligned} \quad (V.2)$$

$D_{HA}$  and  $D_{H\cdots B}$  are the bond-dissociation energies of the unperturbed HA and H···B bonds, and

$$\begin{aligned} \alpha_{LS} &= \frac{\kappa_{HA} (l_{HA} - l_{HA,eq})^2}{2l_{HA}} \\ \beta_{LS} &= \frac{\kappa_{H\cdots B} (l_{H\cdots B} - l_{H\cdots B,eq})^2}{2l_{H\cdots B}} \\ \kappa_{HA} &= f_{HA} l_{HA,eq} / D_{HA} \\ \kappa_{H\cdots B} &= f_{H\cdots B} l_{H\cdots B,eq} / D_{H\cdots B} \end{aligned} \quad (V.3)$$

In these expressions,  $l$  (or  $f$ ) are the bond lengths (or the harmonic force constants) of the unperturbed HA and H···B bonds. The data for the unperturbed H···B bond are not usually known. However, Lippincott and Schroeder introduced the approximation

$$\kappa_{\text{H}\cdots\text{B}} = g\kappa_{\text{HA}} \quad (\text{V.4})$$

where  $g = 1.45$ , and showed that  $g$  is transferable to all B···H–A systems [2]. Additionally they assumed that

$$\begin{aligned} D_{\text{H}\cdots\text{B}} &= D_{\text{HA}}/g \\ l_{\text{H}\cdots\text{B},\text{eq}} &= l_{\text{HB}} \end{aligned} \quad (\text{V.5})$$

which provide all the approximations necessary to calculate the covalent contributions. The covalent contributions for a hydrogen bond between two oxygen atoms are indicated in Figure V.1.

Lippincott and Schroeder expressed the repulsive term as a negative exponential and the electrostatic one as a negative power of the AB distance. Both these terms involve empirical constants. They were modified to reduce the number of constants and the following expression was obtained:

$$V_{\text{rep}} + V_{\text{el}} = A \left[ \exp(-bl_{\text{AB}}) + \frac{l_{\text{AB},\text{eq}}}{2l_{\text{AB}}} \exp(-bl_{\text{AB},\text{eq}}) \right] \quad (\text{V.6})$$

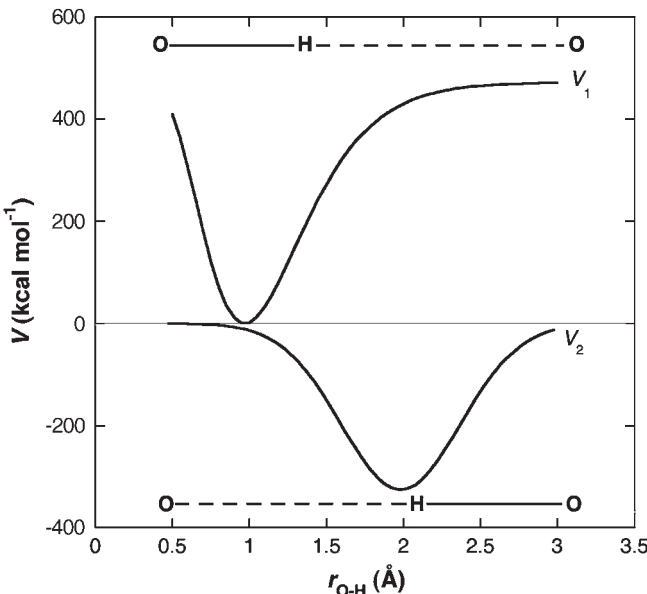


**Figure V.1** Covalent contributions to the LS potential for a hydrogen bond between two oxygen atoms.

The first derivative of the potential expresses the parameter  $A$  as a function of the repulsion constant  $b$ , and the set of parameters defined above

$$A = \frac{D_{\text{H}\cdots\text{B}}\kappa_{\text{H}\cdots\text{B}}}{2} \left[ 1 - \left( \frac{l_{\text{H}\cdots\text{B}}}{l_{\text{AB,eq}} - l_{\text{HA}}} \right)^2 \right] \exp(-\beta) / \exp(-bl_{\text{AB,eq}})(b - 1/2l_{\text{AB,eq}}) \quad (\text{V.7})$$

The only parameter left to be fitted to the experimental data is the repulsion constant  $b$ . Lippincott and Schroeder chose the value  $b = 4.8 \text{ \AA}$ . Figure V.2 illustrates the covalent, electrostatic and repulsive contributions to hydrogen bonds between two oxygen atoms, as a function of the distance between the oxygen atoms. With the data presently available on the H-bond lengths and strengths, a better description of the relation between these two quantities can be achieved with  $b = 9 \text{ \AA}$ . This was the value employed in the simulations presented in Figure 13.12, but the original value was implemented in the LS–ISM reaction path because the differences in the calculated rates are negligible.

Another important quantity in the LS potential is the force constant of the AB hydrogen bond. This can be obtained from the second derivative of the potential.

$$\begin{aligned} f_{\text{AB}} &= B + A \exp(-bl_{\text{AB,eq}}) \frac{(bl_{\text{AB,eq}})^2 - 1}{(l_{\text{AB,eq}})^2} \\ B &= \frac{D_{\text{H}\cdots\text{B}}\kappa_{\text{H}\cdots\text{B}}}{(l_{\text{H}\cdots\text{B}})^3} \exp(-\beta) \left[ (l_{\text{H}\cdots\text{B,eq}})^2 - \frac{\beta}{2} (l_{\text{H}\cdots\text{B}} + l_{\text{H}\cdots\text{B,eq}})^2 \right] \end{aligned} \quad (\text{V.8})$$

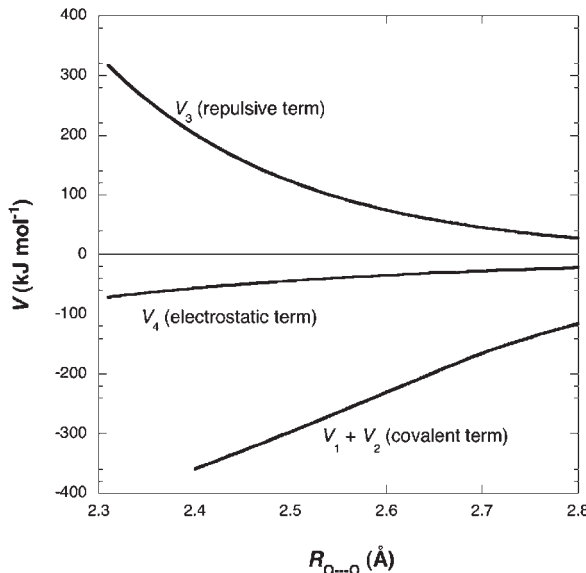


**Figure V.2** Covalent, electrostatic and repulsive contributions to LS potentials representing hydrogen bonds between two oxygen atoms, as a function of the distance between the oxygen atoms.

The importance of this force constant results from its relation to the AB vibrational frequency

$$\bar{v}_{AB} = \frac{1}{2\pi c} \sqrt{\frac{f_{AB}}{\mu_{AB}}} \quad (V.9)$$

The LS potential does not include a correction for the change of translational and rotational degrees of freedom on dissociation of the hydrogen bond. Such corrections are small and have been neglected. However, the experimental H-binding energies,  $D_{AB}$ , are corrected for the zero-point energy of the AB vibration,  $Z_{AB}$ , to obtain the electronic binding energy of the H-bond,  $D_{e,AB}$ . This is done calculating  $\bar{v}_{AB}$  from  $D_{AB}$ , to obtain a first approximation for  $Z_{AB}$ , and then recalculating the LS potential and its properties with  $D_{AB} + Z_{AB}$ .

## V.2 THE LS-ISM REACTION PATH

The vibrationally adiabatic path of ISM and the LS potential are combined to reflect the fact that a hydrogen-bonded complex brings the structure of the reactants closer to that of the transition state, as shown in Mechanism (V.I). A hydrogen bond can be regarded as an incipient proton transfer, and the bond order at the precursor complex is no longer  $n=0$ , but the bond order of the  $B \cdots H$  bond in that complex,  $n_{H \cdots B}$ . Similarly, for the products, the bond order is not  $n=1$  but the bond order of the  $H \cdots A$  bond in the successor complex,  $(1-n_{H \cdots A})$ . Thus, for a proton transfer in condensed media, the reaction coordinate  $n$  is only defined in the interval  $[n_{H \cdots B}, (1-n_{H \cdots A})]$ . The precursor and successor complexes are included in the classical reaction path of ISM with a simple transformation of the reaction coordinate [3]

$$V_{cl}(n) = (1-j)V_{HA}(1-j) + jV_{HB}(j) + k\Delta V_{cl}^0 - D_{e,AB} \quad (V.10)$$

where

$$\begin{aligned} j &= n - n_{H \cdots B} && \text{for } n_{H \cdots B} \leq n \leq n^\ddagger \\ j &= n - (1 - n_{H \cdots A}) && \text{for } n^\ddagger < n \leq (1 - n_{H \cdots A}) \\ k &= (n - n_{H \cdots B}) / (1 - n_{H \cdots B} - n_{H \cdots A}) && \text{for } n_{H \cdots B} \leq n \leq (1 - n_{H \cdots A}) \end{aligned} \quad (V.11)$$

and  $\Delta V_{cl}^0$  will be given by eq. (13.84), after correction for the difference in zero-point energies between reactants and products ( $Z_{BC}$  and  $Z_{AB}$ ).

The LS-ISM vibrationally adiabatic path is then calculated adding the zero-point energies along the reaction path, as indicated in eq. (IV.2), but including also  $Z_{AB}$ .

## V.3 RATE CONSTANTS FOR PROTON TRANSFER ALONG AN H-BOND

The rate of the reaction illustrated by mechanism (V.I) is the product between the concentration of the transition states at the top of the barrier  $[\ddagger] = [B \cdots H \cdots A]$ , and the frequency

at which they pass over the barrier. Since the transition states are in thermal equilibrium with the hydrogen-bonded reactants, so

$$\left[ \ddot{\cdot} \right] = \left[ B^+ \cdots H - A \right] e^{-\Delta^{\ddagger} V_{ad}/RT} \quad (V.12)$$

and these can be related to the concentration of the separated reactants

$$K_c = \frac{\left[ B^- \cdots H - A \right]}{\left[ B^- \right] [H - A]} \quad (V.13)$$

this rate can be expressed as:

$$k_{H\text{ bond}} = \kappa(T) \bar{v}_{\text{TST}} K_c e^{-\Delta^{\ddagger} V_{ad}/RT} \quad (V.14)$$

where the tunnelling correction is included as usual. In the spirit of the transition-state theory, we assume that the reaction frequency is the “universal” transition-state frequency

$$\bar{v}_{\text{TST}} = \frac{k_B T}{h} \quad (V.15)$$

but we note that other choices are also possible. For example, the AB hydrogen bond frequency  $\bar{v}_{AB}$  has been described as a restricted translation of the  $H_2O$  molecules along the O–H···O direction [4], and is also a sensible choice for the reaction frequency. From weakly H-bonded systems such as  $H_2O \cdots HCN$  ( $D_{0AB} = 4 \text{ kJ mol}^{-1}$ ) to strongly H-bonded systems such as  $H_2O \cdots HOH_2^+$  ( $D_{0AB} = 29 \text{ kJ mol}^{-1}$ ),  $\bar{v}_{AB}$  ranges from 80 to  $500 \text{ cm}^{-1}$ , and correspond to reaction frequencies between  $2 \times 10^{12}$  and  $1.5 \times 10^{13} \text{ sec}^{-1}$ . Eq. (V.15) gives  $6 \times 10^{12} \text{ sec}^{-1}$  at room temperature. The numerical results are very similar, but the use of the frequency factor in H-bonded systems has a stronger physical motivation. This is the frequency employed in LS-ISM/scTST calculations. Proton transfers in enzymes have the properties of intra-molecular reactions and are also calculated with this frequency factor.

The LS-ISM reaction path can also be implemented in the calculations offered at the site: <http://www.ism.qui.uc.pt:8180/ism/>.

## REFERENCES

- [1] ER Lippincott, R Schroeder, *J. Chem. Phys.* **23** (1955) 1099–1106.
- [2] R Schroeder, ER Lippincott, *J. Phys. Chem.* **61** (1957) 921.
- [3] M Barroso, LG Arnaut, SJ Formosinho, *Chem. Phys. Chem.* **6** (2005) 363–371.
- [4] GE Walrafen, MR Fisher, MS Hokmabadi, W-H. Yang, *J. Chem. Phys.* **85** (1986) 6970–6982.

This page intentionally left blank

# Appendix VI

## Problems

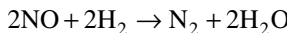
---

1. What are the orders of the following reactions, given the corresponding reaction half-lives:

- (a) The decomposition of ammonia on a tungsten filament, with the following half-lives,  $t_{1/2}$ , at different initial pressures,  $p_0$ :

$p_0$ (mmHg)	12	48	72	120
$t_{1/2}$ (sec)	52.5	210	315	525

- (b) The reaction



at the stoichiometric composition, for which the following  $t_{1/2}$  values have been measured at 826 °C for the initial pressure of the reactants  $p_0$ :

$p_0$ (mmHg)	251	288	340
$t_{1/2}$ (sec)	180	140	100

- (c) The pyrolysis of acetaldehyde at 518 °C and at the initial pressure of 360 mmHg, which has the fractional lifetimes  $t_{1/2}$  and  $t_{3/4}$  of 420 and 1220 sec, respectively.

2. The initial rates,  $v_0$ , for the reaction  $2\text{A} + \text{B} = \text{C} + \text{D}$  are shown in the following table:

$[\text{A}]_0$ (mol dm <sup>-3</sup> )	$[\text{B}]_0$ (mol dm <sup>-3</sup> )	$v_0$ (mol dm <sup>-3</sup> sec <sup>-1</sup> )
0.025	0.100	0.01
0.050	0.100	0.02
0.100	0.100	0.04
0.100	0.050	0.01
0.100	0.025	0.0025

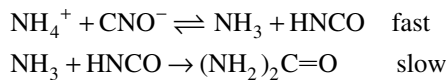
What is the rate law and what is the value of the rate constant?

3. A live plant has some radioactivity owing to the presence of  $^{14}\text{C}$  that shows 15.3 counts per minute per gram of carbon. In the cave of Lascaux in France some samples of coal

have a radioactivity of 2.25 counts per minute per gram of carbon. What is the age of the samples of coal, knowing that the  $^{14}\text{C}$  half-life is 5669 years?

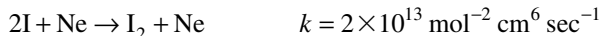
4. The rate constant for the reaction:  $\text{H}^+ + \text{OH}^- \rightarrow \text{H}_2\text{O}$  is  $1.3 \times 10^{11} \text{ dm}^3 \text{ mol}^{-1} \text{ sec}^{-1}$ . Non-equilibrium concentrations of protons and hydroxide ions can be induced in temperature jump experiments. (a) Calculate the half-life for the neutralisation process if (i)  $[\text{H}^+] = [\text{OH}^-] = 10^{-3} \text{ M}$  and (ii)  $[\text{H}^+] = [\text{OH}^-] = 5 \times 10^{-5} \text{ M}$ . (b) Under the same conditions, calculate the half-life of the hydroxide ion if  $\text{pH} = 6$ .

5. The initial rate of formation of urea increases by a factor of 2 when one doubles the concentration of ammonium cyanate. The suggested mechanism of urea formation is



- (a) What is the rate law for this mechanism?
- (b) Is the mechanism in agreement with the effect of  $[\text{NH}_4\text{CNO}]$ ?

6. What fast reaction technique could you choose to follow the recombination



at 333 K?

7. The rate of the reaction

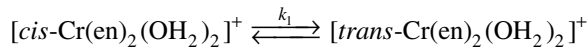


was measured in terms of the total pressure  $P_t$  at 500 °C as follows:

$P_t$ (mmHg)	55	60	79	89	102	105
Time (sec)	0	60	360	600	1200	1500

- (a) Verify that the decomposition follows a first-order process.
- (b) Calculate the rate constant and the half-life of the reaction.

8. The reaction



is first order in both directions with  $k_1 = 3.3 \times 10^{-4} \text{ sec}^{-1}$  and  $K_e = 0.16$  at 25 °C.

- (a) Show that

$$k_1 t = \frac{x_e}{a_0} \ln \left( \frac{x_e}{x_e - x} \right)$$

where  $a_0$  is the initial amount of the *cis*-form and  $x$  the amount converted into the *trans*-form; the amount of the *trans*-form at equilibrium is  $x_e$ .

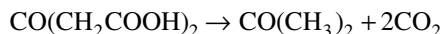
- (b) Starting with pure *cis*-form, how long would it take for 75% of the equilibrium amount of the *trans*-form to be formed?

9. *N*-Methylnicotinamide ( $\text{NcMe}^+$ ) is a model of the biologically important electron transport agent nicotinamide adenine dinucleotide ( $\text{NAD}^+$ ). One electron reduction of  $\text{NcMe}^+$  produces the corresponding pyridinyl radical,  $\text{NcMe}\cdot$ , whose decay can be monitored spectrophotometrically at 400 nm. Data from a study of absorbance against time are given below for the reaction of this pyridinyl radical in buffered aqueous solution (pH 7.2).

Time (μsec)	20	100	200	400	600	800	1200	1600	∞
Absorbance at 400 nm	0.0273	0.0186	0.0128	0.0081	0.0060	0.0047	0.0026	0.0022	0.0

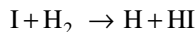
- (a) Determine the order of this reaction.  
 (b) Derive an expression that you can use to determine the rate constant. Given the value  $\epsilon_{400\text{nm}} = 8900 \text{ dm}^3 \text{ mol}^{-1} \text{ cm}^{-1}$  for the molar absorption coefficient of the pyridinyl radical, and that the measurements were made in 1 cm cuvettes, calculate the rate constant for the decay of this species.

10. In aqueous solutions, the following decarboxylation reaction:



is a first-order process with an activation energy of  $192.9 \text{ kJ mol}^{-1}$ . At  $10^\circ\text{C}$  the half-life of the reaction is 107 min. What is the rate constant at  $50^\circ\text{C}$ ?

11. The rate constant for the elementary reaction

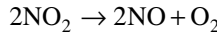


is

$$k = 1014.1 \text{ e}^{-140/RT} \text{ mol}^{-1} \text{ dm}^3 \text{ sec}^{-1}$$

(Note:  $E_a$  is in  $\text{kJ mol}^{-1}$ ). What is the activation energy for the reaction in the reverse direction if  $\Delta H = 137.3 \text{ kJ mol}^{-1}$  for the above reaction?

12. The decomposition of nitrogen oxide

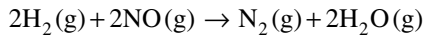


occurs at high temperatures, via the activated complex  $\{\text{NO}_2\cdot\text{Ar}\}^\ddagger$  in a sequence of two elementary steps. The net change in the first of these is



- (a) What is the second reaction, which when combined with reaction (i), gives the complete reaction?
- (b) At temperatures around 600 K the rate law is second order and proceeds via a different activated complex  $\{\text{NO}_2\cdot\text{NO}_2\}^\ddagger$ . Which one of the activated complexes is expected to lead to a lower activation energy?

#### 13. The rate law for the reaction



is

$$v = k[\text{NO}]^2 [\text{H}_2]$$

Which of the following mechanisms is in agreement with the rate law?

Mechanism I:	$2\text{H}_2 + 2\text{NO} \rightarrow \text{N}_2 + 2\text{H}_2\text{O}$	slow
Mechanism II:	$\text{H}_2 + \text{NO} \rightarrow \text{N} + \text{H}_2\text{O}$	fast
	$\text{N} + \text{NO} \rightarrow \text{N}_2 + \text{O}$	fast
Mechanism III:	$2\text{NO} \rightleftharpoons \text{N}_2\text{O}_2$	fast equilibrium
	$\text{N}_2\text{O}_2 + \text{H}_2 \rightarrow \text{N}_2\text{O} + \text{H}_2\text{O}$	slow
	$\text{N}_2\text{O} + \text{H}_2 \rightarrow \text{N}_2 + \text{H}_2\text{O}$	fast

#### 14. The initial rate of reaction between iodate and iodide ions



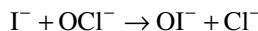
has been measured at 298 K at constant ionic strength and pH:

Experiment number	1	2	3	4	5
$10^2 [\text{IO}_3^-] (\text{mol dm}^{-3})$	3.8	4.5	5.0	3.8	4.5
$10^2 [\text{I}^-] (\text{mol dm}^{-3})$	3.0	3.0	3.6	5.0	7.0
$10^8 v_0 (\text{mol dm}^{-3} \text{ sec}^{-1})$	0.84	1.17	3.00	6.46	34.8

(Data: Barton *et al.*, *J. Chem. Soc. Faraday Trans. I* (1976) **72** 568).

- (a) Estimate the partial orders of the reaction and the pseudo-rate constant.
- (b) From the rate law, what can be deduced about the composition of the activated complex for the rate-determining step?

15. The reaction between hypochlorite ion and iodide ion in alkaline solutions

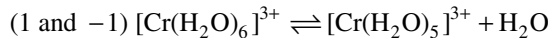


has a rate law

$$\frac{d[\text{OI}^-]}{dt} = k[\text{I}^-][\text{OCl}^-][\text{OH}^-]^{-1}$$

- (a) What can be said about the composition of the activated complex in the rate-determining step?
- (b) Propose a mechanism for the reaction.

16. (a) Propose a rate law which is consistent with the following mechanism:



- (b) Under what conditions can the reaction be considered to be a first-order process?

17. Chlorine water is used in water treatment and in the destruction of dissolved organic matter. In this system, a fast equilibrium is established between dissolved chlorine  $\text{Cl}_2 (+\text{H}_2\text{O})$  and hypochlorous acid ( $\text{HOCl}$ ),



In the oxidation of propan-2-ol by chlorine water, two possible rate-determining steps can be considered:

- (1)  $\text{Cl}_2 (\text{aq}) + \text{propan-2-ol} \rightarrow \text{products}$
- (2)  $\text{HOCl} (\text{aq}) + \text{propan-2-ol} \rightarrow \text{products}$

At pH 1 and room temperature, with the initial concentration of  $[\text{Cl}_2 (\text{aq})]_0 = 1.5 \times 10^{-3} \text{ mol dm}^{-3}$ , and  $[\text{propan-2-ol}]_0 = 2.01 \times 10^{-2} \text{ mol dm}^{-3}$ , the alcohol was oxidised with the initial rate law

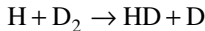
$$-\frac{d[\text{oxidant}]}{dt} = k_{\text{obs}} [\text{oxidant}]$$

where oxidant refers to a combination of  $\text{Cl}_2$  and  $\text{HOCl}$ . Addition of chloride ions ( $> 10^{-2} \text{ mol dm}^{-3}$ ) accelerated the oxidation rate and a plot of  $(k_{\text{obs}})^{-1}$  versus  $[\text{Cl}^-]^{-1}$  was linear. On the basis of the above, suggest kinetic methods for distinguishing between the two possible mechanisms.

(Data: Venkatasubramanian and Srinivasan, *Indian J. Chem.* (1972) **10** 1085).

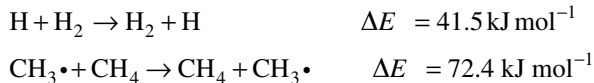
18. In 1867 the Austrian chemist Leopold Pfaundler proposed that for reactions in the vapour phase at high temperatures only molecules that possess energy close to the dissociation

limit could react. Using his ideas, it would appear that the internal energy of complexes, such as HDD in the reaction

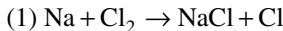


would be sufficient to keep the atoms bonded together for a certain period, even though it is close to the dissociation energy of  $\text{D}_2$ , *ca.*  $422 \text{ kJ mol}^{-1}$ . However, 70 years later, chemists found that the activation energy of the above reaction is much lower than this (close to  $50 \text{ kJ mol}^{-1}$ ).

- (a) Explain why the reaction barriers of elementary chemical steps are actually considerably lower than the dissociation energies of the reactant molecules.
- (b) Interpret, in structural terms, the relative energy barriers for the two reactions:

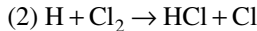


19. In the 1930s, Michael Polanyi studied the sodium–chlorine reaction in highly dilute flames:



The gases were mixed by diffusion and the product NaCl (which is a solid) was deposited on the walls of the vessel. An emission of sodium-*D* radiation was observed; such an emission requires an energy of  $202 \text{ kJ mol}^{-1}$ .

- (a) What can be the source of energy for the formation of electronically excited  $\text{Na}^*(^2\text{P})$  which leads to chemiluminescence?
- (b) In the 1950s, his son, John Polanyi, studied another highly exothermic reaction



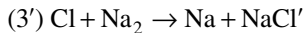
However, in this case, the emission was in the infrared region. How can one interpret such contrasting behaviours?

Relevant bond dissociation energies in  $\text{kJ mol}^{-1}$ : Na–Na = 77; Cl–Cl = 242.7; H–Cl = 431.4; Na–Cl = 407.9.

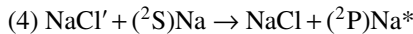
Polanyi concluded that another reaction must occur:



Although this energy release would be sufficient to produce  $\text{Na}^*(^2\text{P})$ , quenching experiments show that the energy released in reaction (3) does not pass into the sodium atom, but produces vibrationally excited  $\text{NaCl}'$ ,



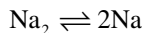
The vibrationally excited NaCl' molecule then transfers its energy to a sodium atom, which becomes electronically excited



- (c) The energy release in  $\text{H} + \text{Cl}_2 \rightarrow \text{HCl}' + \text{Cl}$  ( $\Delta H^0 = -188.7 \text{ kJ mol}^{-1}$ ) passes into the vibrational energy of the products, a large part going into translational and rotational energy since the PES is repulsive).
20. (a) According to the hard-sphere collision theory, what is the frequency factor for the elementary reaction  $\text{D} + \text{H}_2 \rightarrow \text{H}_2 + \text{D}$  at 300 K, with a collision molecular diameter of  $2.5 \text{ \AA}$ ?
- (b) Relate the collision diameter of  $1.0 \text{ \AA}$  with the reaction cross section,  $\sigma$ , of an elementary reaction.
- (c) The collision theory was developed by Trautz and Lewis. In 1918 Lewis calculated a pre-exponential factor of  $3.5 \times 10^{-7} \text{ dm}^3 \text{ mol}^{-1} \text{ sec}^{-1}$  for the reaction  $2\text{HI} \rightarrow \text{H}_2 + \text{I}_2$  at 556 K in excellent agreement with the experimental value. However, this agreement was somewhat unfortunate, since it led to undue confidence in the theory and delayed the development of the subject for some years. Would that be the case if the calculation had been carried out for the reaction
- $$\text{K} + \text{Br}_2 \rightarrow \text{KBr} + \text{Br}$$
21. For a Maxwell–Boltzmann distribution show that the activation energy,  $E_a$ , of an elementary reaction can be related with the collision cross section,  $\sigma(E)$ , by the expression
- $$E_a = \frac{\int_{E_0}^{\infty} \sigma(E) E^2 \exp\left[-\frac{E}{RT}\right] dE}{\int_{E_0}^{\infty} \sigma(E) E \exp\left[-\frac{E}{RT}\right] dE} - \frac{3}{2} RT$$
- where  $E$  is the total energy of the molecular system and  $E_0$ , the onset energy for a reactive collision ( $\sigma(E) = 0$  for  $E < E_0$ )
- (a) What is the meaning of the two terms in the previous equation?
- (b) Show that for a collision cross section of the kind  $\sigma = \sigma_0 \frac{\sqrt{(E - E_0)}}{E}$  the activation energy is almost independent of the energy.
- (c) Show that for a hard sphere model one has  $\frac{E_a}{E_0} = 1 + \frac{RT}{2E_0}$ . For values of  $E_0 = 50 \text{ kJ mol}^{-1}$  discuss the experimental possibilities to investigate the change of  $E_a$  with temperature in the range 200–1000 K.
22. The elementary reaction
- $$\text{H} + \text{Cl}_2 \rightarrow \text{HCl} + \text{Cl}$$

has the following distribution of energies in the products:  $f_{\text{vib}} = 39\%$ ,  $f_{\text{rot}} = 7\%$  and  $f_{\text{trans}} = 54\%$ . Represent the most relevant features of the potential energy surface (PES) along the reaction valley.

23. Estimate the equilibrium constant for the dissociation reaction in the vapour phase



at 1000 K. The relevant data to estimate the partition functions are:  $B = 0.1546 \text{ cm}^{-1}$ ;  $\bar{v} = 159.2 \text{ cm}^{-1}$ ;  $D_0 = 70.4 \text{ kJ mol}^{-1}$ . The ground state is a duplet electronic state.

24. The reaction  $2\text{HI} \rightarrow \text{H}_2 + \text{I}_2$  has a second-order rate constant that depends on temperature as follows:

$T (\text{K})$	556	629	647	700	716	781
$k_2 (\text{dm}^3 \text{ mol}^{-1} \text{ sec}^{-1})$	$3.5 \times 10^{-7}$	$3.02 \times 10^{-6}$	$8.59 \times 10^{-5}$	$1.16 \times 10^{-3}$	$1.16 \times 10^{-3}$	$3.95 \times 10^{-2}$

Calculate the enthalpy and the entropy of activation for the standard state  $1 \text{ mol dm}^{-3}$ .

25. The thermal decomposition of  $\text{F}_2\text{O}$  in the vapour phase has an experimental rate law

$$-\frac{d[\text{F}_2\text{O}]}{dt} = k_1[\text{F}_2\text{O}]^2 + k_{11}[\text{F}_2\text{O}]^{3/2}$$

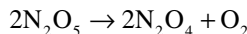
(a) Show that this law is consistent with the mechanism

- (1)  $\text{F}_2\text{O} + \text{F}_2\text{O} \rightarrow \text{F} + \text{OF} + \text{F}_2\text{O}$
- (2)  $\text{F} + \text{F}_2\text{O} \rightarrow \text{F}_2 + \text{OF}$
- (3)  $\text{OF} + \text{OF} \rightarrow 2\text{F} + \text{O}_2$
- (4)  $2\text{F} + \text{F}_2\text{O} \rightarrow \text{F}_2 + \text{F}_2\text{O}$

(b) Derive the rate law for the disappearance of  $\text{F}_2\text{O}$ .

- (c) Under what reaction conditions is the decomposition of  $\text{F}_2\text{O}$  a reaction of order 3/2 in relation to this reagent?
- (d) Under the above conditions, how is the overall activation energy of the reaction related to those of the corresponding elementary processes?

26. The decomposition of nitrogen pentoxide



is suggested to follow the mechanism:

- (1)  $\text{N}_2\text{O}_5 \rightarrow \text{NO}_2 + \text{NO}_3$
- (2)  $\text{NO}_2 + \text{NO}_3 \rightarrow \text{N}_2\text{O}_5$
- (3)  $\text{NO}_2 + \text{NO}_3 \rightarrow \text{NO}_2 + \text{O}_2 + \text{NO}$
- (4)  $\text{NO} + \text{N}_2\text{O}_5 \rightarrow 3\text{NO}_2$

Step (2) has activation energy close to zero, while step (3) is a reasonably endothermic process. Step (4) is also a fast process.

- (a) What is the rate-determining step?
- (b) What is the rate law?

27. For the isomerisation of bicyclooct-7-ene, the following kinetic data were obtained:

$T$ (K)	508.7	517.1	521.5	529.1	535.5	551.8	558.1
$k (\times 10^{-4} \text{ sec}^{-1})$	0.376	0.763	1.08	1.93	3.32	10.5	16.6

- (a) Calculate the activation energy for the reaction.
- (b) Calculate the pre-exponential factor ( $A$ ) and comment on its value.
- (c) What is the rate constant for the reaction at 239° C?

28. The table below presents relevant data for the sigmatropic-shift reaction of hexa-1,5-diene, which is illustrative of pericyclic reactions. Substituents can cause changes in the reaction energy and/or in the bond order at the transition state,  $n^\ddagger$ . Select reaction series where linear free-energy relationships (LFER) can be established.

No.	Substituent	$\Delta G^\ddagger$	$\Delta G^0$	$n^\ddagger$
1	H	174.1	0	0.49
2	Allylvinyl ether	137.9	-71.1	0.40
3	2-phenyl	148.4	0	0.524
4	2,5-diphenyl	129.6	0	0.560
5	3,4-dimethyl	163.0	-18	0.490
6	3,3-dicyano	133.8	-18.8	0.534
7	3,4-diphenyl	129.6	-18.8	0.542
8	3-phenyl	150.0	-9.5	0.514

Energies in kJ mol<sup>-1</sup>.

(Data: Formosinho, *Tetrahedron* (1986) **42** 4557–4562).

29. (a) In the quadratic equation of Marcus

$$\Delta G^\ddagger = \Delta G(0)^\ddagger \left( 1 + \frac{\Delta G^0}{4 \Delta G(0)^\ddagger} \right)^2$$

what is the meaning of the symbols  $\Delta G^\ddagger$ ,  $\Delta G(0)^\ddagger$  and  $\Delta G^0$ ?

- (b) In a family of reactions under what conditions can this Marcus equation lead to a LFER?
- (c) Relate  $\Delta G(0)^\ddagger$  to structural factors of force constants,  $f$ , bond lengths,  $l$  and bond-order at the transition state,  $n^\ddagger$ .

30. Use the quadratic equation of Marcus to verify the Reactivity–Selectivity Principle (RSP) for a reaction with an intrinsic barrier of 10 kJ mol<sup>-1</sup>.

Hint: estimate the corresponding values indicated in the following table for the energies  $\Delta G^0$  and selectivities  $S$ .

Reactant	Reactant	$\Delta G^0$ (kJ mol <sup>-1</sup> )	$\Delta G^\ddagger$ (kJ mol <sup>-1</sup> )	S
A	X	-10		
	Y	-12		
B	X	10		
	Y	12		

31. The following first-order rate constants  $k_1$  were obtained for the isomerisation of cyclopropane:

$P$ (mmHg)	84.1	11.0	2.89	0.569	0.120	0.067
$10^4 k_1$ (sec <sup>-1</sup> )	2.98	2.23	1.54	0.857	0.392	0.303

(Data: Pritchard *et al.*, Proc. Roy. Soc. London A (1953) **217** 563).

Use the data to verify the simple Lindemann equation.

32. The photodissociation of pure diazo-*n*-propane vapour ( $\text{CH}_3\text{CH}_2\text{CHN}_2$ ) with a mercury lamp ( $\lambda > 300$  nm) yields propylene (represented by S), resulting from collisional stabilisation



and products such as ethane and ethylene (represented by D) from the direct dissociation of the vibrationally hot nascent propylene  $\text{Pr}^*$



The ratio of the decomposition products varies with pressure as follows:

What would be predicted if the Lindemann approach was verified?

[D]/[S]	0.344	0.182	0.123	0.0854	0.072	0.0452	0.033
$P$ (kPa)	0.123	0.330	0.664	1.07	1.33	2.26	3.06

(Data: Figuera *et al.*, J. Phys. Chem. (1974) **78** 1348).

33. A substance  $A_2$  decomposes in the vapour phase



and presents the following values of concentration as function of time, at atmospheric pressure:

At constant pressure:

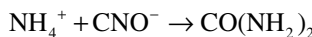
[A <sub>2</sub> ] (mol dm <sup>-3</sup> )	1.00	0.67	0.47	0.37	0.24	0.16	0.10
t (min)	0	5	10	15	20	30	40

As can be seen,  $\log [A_2]$  does not vary in a linear fashion with time. However, when the kinetics of the reaction are studied at a constant volume, the following data is obtained:  
At constant volume:

$[A_2]$ (mol dm $^{-3}$ )	1.0	0.79	0.62	0.50	0.42	0.26	0.15
$t$ (min)	0	5	10	15	20	30	40

In these experimental conditions,  $\log [A_2]$  is a linear function of time, revealing that the reaction is a first-order process with  $k = 0.046 \text{ min}^{-1}$ . How can one interpret such findings?

### 34. The synthesis of urea



was studied at 30 °C in mixtures of water/glycol. The rate constant of the reaction depends on the dielectric constant of the medium as follows:

$10^3 k$ (dm $^3$ mol $^{-1}$ min $^{-1}$ )	6.25	11.3	14.1	19.1	26.5	38.4
$\epsilon$	76.7	63.5	60	55	50	45

- (a) Interpret the influence of the dielectric constant of the medium on the rates?
- (b) What would be the effect of  $\epsilon$  if the reaction involved  $\text{CO}_2$  rather than  $\text{CNO}^-$ ?

### 35. Predict the effects of

- (a) increasing ionic strength
- (b) increasing dielectric constant of the medium

on the rates of the following reactions in aqueous solutions:

- (i)  $[\text{Fe}(\text{H}_2\text{O})_6]^{3+} + [\text{Fe}(\text{CN})_6]^{4-} \rightarrow [\text{Fe}(\text{H}_2\text{O})_6]^{2+} + [\text{Fe}(\text{CN})_6]^{3-}$
- (ii)  $\text{CH}_3\text{CH}(\text{OCH}_3)_2 + \text{H}_3\text{O}^+ \rightarrow \text{CH}_3\text{CHO} + 2\text{CH}_3\text{OH} + \text{H}^+$
- (iii)  $[\text{Co}(\text{NH}_3)_5\text{Br}]^{2+} + \text{H}_2\text{O} \rightarrow [\text{Co}(\text{NH}_3)_5(\text{H}_2\text{O})]^{3+} + \text{Br}^-$
- (iv)  $\text{SO}_3^{2-} + \text{ClO}^- \rightarrow \text{SO}_4^{2-} + \text{Cl}^-$

36. The diffusion coefficient for iodine atoms in carbon tetrachloride solution at 25 °C is  $D = 2 \times 10^{-9} \text{ m}^2 \text{ sec}^{-1}$ . Given that the atomic radius of iodine is 0.2 nm, calculate the maximum rate constant predicted for the recombination of iodine atoms under these conditions.

37. Radiolysis of water produces a reducing species, z, in addition to hydrogen atoms, hydroxyl radicals and various other species



The second-order rate constants for the reaction of z with  $\text{Ag}^+$  ions in water show the following variation with ionic strength:

Ionic strength ( $\text{mmol dm}^{-3}$ )	0	0.625	3.60	10.4	16.3	29.8	38.5	44.6	56.2
$k (10^{10} \text{ dm}^3 \text{ mol}^{-1} \text{ sec}^{-1})$	3.20	3.05	2.85	2.67	2.37	2.16	1.91	1.82	1.62

What is the charge of z? Also suggest a structure for this species.

38. The rate constant of the reaction between persulphate ion and iodide ion varies with ionic strength  $I$  as follows:

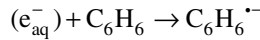
$I \times 10^3 (\text{mol dm}^{-3})$	2.45	3.65	4.45	6.45	8.45	12.45
$k (\text{mol}^{-1} \text{ dm}^3 \text{ sec}^{-1})$	1.05	1.12	1.16	1.18	1.26	1.39

- (a) Estimate the product of the charge of the two ions,  $Z_A Z_B$ .
- (b) Given the kinetic data below for reaction of the muonium,  $Mu$ , with ions at  $25^\circ\text{C}$ , what is the electric charge of  $Mu$ ?

Reaction	$k (10^8 \text{ mol}^{-1} \text{ dm}^3 \text{ sec}^{-1})$	
	$I < 0.02 \text{ mol dm}^{-3}$	$I = 0.9 \text{ mol dm}^{-3}$
$Mu + \text{Cu}^{2+}$	65	63.5
$Mu + \text{SCN}^-$	0.62	0.74

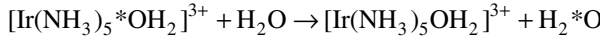
(Data: Yean *et al.*, *Hyperfine Interaction* (1979) **6** 409).

39. In a study of the reactions of the hydrated electron ( $e_{\text{aq}}^-$ ) at  $298 \text{ K}$ , a half-life ( $t_{1/2}$ ) in pure water of  $1.2 \text{ msec}$  was observed, while in the presence of benzene ( $5 \text{ mmol dm}^{-3}$ ), this was reduced to  $9.9 \mu\text{sec}$ . Assuming that the concentration of benzene is much greater than that of the hydrated electron, and that the decay in the presence of benzene is due to the bimolecular reaction



calculate the second-order rate constant for this reaction, and show if this is diffusion controlled (viscosity of water is  $0.890 \text{ mPa sec}$ ).

40. (a) Calculate the volume of activation  $\Delta V^\ddagger$  of the reaction



studied at  $60.5^\circ\text{C}$ , using data on the variation of the rate constant  $k$  as a function of the hydrostatic pressure  $P$  given below:

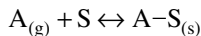
$P (\text{kPa})$	1	59	1027	2020	3310
$10^5 k (\text{dm}^3 \text{ mol}^{-1} \text{ sec}^{-1})$	2.82	4.01	4.56	4.59	5.80

\*: Indicates labelling with  $^{18}\text{O}$ .

(Data: Tong and Swaddle, *Inorg. Chem.* (1974) **13** 1538).

- (b) Interpret in terms of structural changes and solvent effects the observed effect of  $P$  on the rates.

41. A reaction catalysed on a metal surface



shows the following data for the volume of the gas adsorbed as a function of pressure at 298 K:

$P$ (Pa)	25.3	129.3	253.3	540
$V$ (cm <sup>3</sup> )	0.042	0.163	0.221	0.321

- (a) Is the data consistent with a Langmuir adsorption isotherm?  
 (b) What is the volume adsorbed,  $V_\infty$  when all the active sites are occupied?

42. The adsorption of CO on platinum

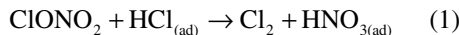


has a rate,  $v_d$ , given by the expression

$$v_d = \frac{d\Gamma_{CO_{ads}}}{dt} = \frac{k_B T}{h} \frac{q_\ddagger}{q_0(CO_{ads})} \Gamma_{CO_{ads}} \exp(-\frac{E_a}{RT})$$

- (a) At 600 K,  $v_d = 0.0012$  mol m<sup>-2</sup> sec<sup>-1</sup>,  $\sigma = 0.5$ ,  $E_d = 134$  kJ mol<sup>-1</sup> and  $N_s = 10^{19}$  m<sup>-2</sup>. What can be said about the ratio of the partition functions  $q_\ddagger$  and  $q_0(CO_{ads})$  for the activated complexes for CO desorption and adsorbed CO, respectively?  
 (b) Explain the meaning of the symbols employed above.

43. In the atmosphere, the halogen reservoir compound, ClONO<sub>2</sub> is converted to Cl<sub>2</sub> on polar stratospheric cloud surfaces by heterogeneous reactions. This leads to destruction of polar ozone through reactions on ice surfaces such as



Reaction (1) is the most important heterogeneous reaction to convert photochemically inert ClONO<sub>2</sub> and HCl into photochemical active chlorine.

As with reaction (1), reaction with HONO on the ice surface is a nucleophilic reaction. A possible mechanism for the reaction is the following:



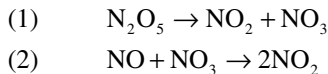
- (a) write the rate of reaction  $\xi = -d[HONO]/dt$  in terms of the pressure of HONO,  $P_{\text{HONO}}$ .
- (b) If one defines the reaction probability,  $\gamma = \xi/\phi$ , where  $\phi_{\text{HONO}}$  is the flux of HONO impinging on the HX-treated ice surface, show that  $\gamma = \xi \sqrt{(2\pi m k_B T)/P_{\text{HONO}}}$ ;  $m_w$  is the molecular weight of HONO.

44. Nitrogen is adsorbed on activated charcoal. The adsorbed volumes per gram of charcoal as function of the gas pressure at 196 K are as shown:

$P(\text{N}_2)$ (atm)	3.5	10.0	16.7	25.7	33.5	39.2
$V(\text{N}_2)$ (ml g <sup>-1</sup> )	101	136	153	162	165	166

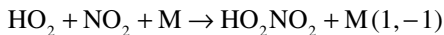
Verify that the data follow a Langmuir isotherm.

45. The reaction  $\text{NO} + \text{N}_2\text{O}_5 \rightarrow 3\text{NO}_2$  is suggested to follow the mechanism:



- (a) What is  $[\text{NO}_3]$  under steady-state conditions?
- (b) What are the rate laws for the disappearance of nitrogen pentoxide and for the formation of nitrogen dioxide?

46. Peroxynitric acid ( $\text{HO}_2\text{NO}_2$ , PNA) plays an important role in atmospheric chemistry as a gas-phase reservoir for  $\text{NO}_x$  ( $\text{NO}$  and  $\text{NO}_2$ ) and  $\text{HO}_x$  in the stratosphere as well as the troposphere. The lifetime of PNA at the middle latitudes in the upper troposphere and lower stratosphere is in the range of 10–12 h. However, at the higher temperatures found in the lower troposphere and even in the middle of the upper stratosphere,  $\text{HO}_2\text{NO}_2$  degradation can be dominated by thermal decomposition (reaction –1)

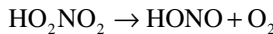


The standard enthalpy of reaction is  $\Delta_f H_{298\text{ K}}^0 = -100.4 \pm 2.1 \text{ kJ mol}^{-1}$ . The rate coefficients vary with temperature as indicated in the following table.

$T$ (K)	$k_{-1}$ (sec <sup>-1</sup> )
331.3	0.21
334.4	0.37
341.6	1.06
342.4	1.87
343.2	1.1
347.3	1.47
349.9	3.18

(Data: T Gierczak *et al.*, *J. Phys. Chem. A* (2005) **109** 586–596).

- (a) Is the Arrhenius equation verified?  
 (b) PNA can also thermally dissociate to give



This reaction which is exothermic,  $\Delta_r H_{298\text{ K}}^0 = -26.8 \text{ kJ mol}^{-1}$ , is believed not to compete with the thermal decomposition of PNA to yield only  $\text{NO}_2$  and  $\text{HO}_2$  (reaction (-1)). Why?

47. The decomposition of ethane into ethene and hydrogen in the presence of nitrous oxide is suggested to follow the mechanism:

- (1)  $\text{C}_2\text{H}_6 + \text{NO} \rightarrow \text{C}_2\text{H}_5\cdot + \text{HNO}$
- (2)  $\text{C}_2\text{H}_5\cdot \rightarrow \text{H}\cdot + \text{C}_2\text{H}_4$
- (3)  $\text{H}\cdot + \text{C}_2\text{H}_5 \rightarrow \text{C}_2\text{H}_4 + \text{H}_2$
- (4)  $\text{H}\cdot + \text{NO} \rightarrow \text{HNO}$
- (5)  $\text{HNO} \rightarrow \text{H}\cdot + \text{NO}$
- (6)  $\text{C}_2\text{H}_5\cdot + \text{HNO} \rightarrow \text{C}_2\text{H}_6 + \text{NO}$

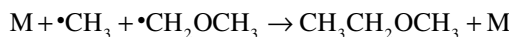
- (a) What is the role of  $\text{NO}$ ?  
 (b) Assuming that a fast equilibrium is established between the pairs of reaction steps 1 and 6 ( $K_1$ ) and 4 and 5 ( $K_2$ ), write the rate law for the decomposition.

48. The decomposition of dimethylether follows the mechanism

- (1)  $\text{CH}_3\text{OCH}_3 \rightarrow \cdot\text{CH}_3 + \cdot\text{OCH}_3$
- (2)  $\cdot\text{CH}_3 + \text{CH}_3\text{OCH}_3 \rightarrow \text{CH}_4 + \cdot\text{CH}_2\text{OCH}_3$
- (3)  $\cdot\text{CH}_2\text{OCH}_3 \rightarrow \cdot\text{CH}_3 + \text{HCHO}$
- (4)  $\cdot\text{CH}_3 + \cdot\text{CH}_2\text{OCH}_3 \rightarrow \text{CH}_3\text{CH}_2\text{OCH}_3$

Radicals are indicated by the symbol ( $\bullet$ ).

- (a) Establish the rate law of this decomposition.  
 (b) What is the order of the reaction if the termination step is



49. The oxidation of a hydrocarbon  $\text{RH}$  can occur via the following chain reaction mechanism:

- (1)  $\text{RH} + \text{O}_2 \rightarrow \text{HO}_2\cdot + \text{R}\cdot$
- (2)  $\text{R}\cdot + \text{O}_2 \rightarrow \text{RO}_2\cdot$
- (3)  $\text{RO}_2\cdot + \text{RH} \rightarrow \text{ROOH} + \text{R}\cdot$
- (4)  $2\text{R}\cdot \rightarrow \text{R}_2$

- (a) Predict the order of the reaction.  
 (b) Relate the activation energy,  $E_a$ , of the oxidation with that of the individual steps.
50. The termolecular reactions for removal of oxygen atoms in the presence of an inert gas



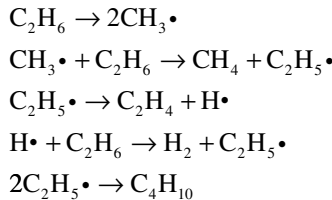
have the following rates  $k_3$  for the cases  $\text{M} = \text{Ar}$  and  $\text{M} = \text{CO}_2$ ,

	$T$ (K)	213	298	335	386
Ar	$10^{-8} k_3 (\text{dm}^6 \text{ mol}^{-2} \text{ sec}^{-1})$	5.39	1.86	1.38	1.01
$\text{CO}_2$	$10^{-8} k_3 (\text{dm}^6 \text{ mol}^{-2} \text{ sec}^{-1})$	34.9	12.0	8.96	6.55

(Data: Mulcahy and Williams, *Trans. Faraday Soc.* (1968) **64** 59).

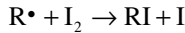
Show that the  $k_3$  values conform to the Arrhenius equation, with negative activation energy values.

51. By applying the steady-state hypothesis to the species  $\text{CH}_3$  and  $\text{C}_2\text{H}_5$  show that a mechanism:



would lead to an overall rate law of one-half order.

52. In free radical polymerisation reactions, iodine,  $\text{I}_2$ , can destroy the active centres because it reacts with radicals as follows:



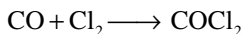
and the iodine atoms produced in these reactions do not initiate further polymerisations. Thus iodine inhibits polymerisation by acting as a radical scavenger. Propose an explanation for such behaviour.

53. The polymerisation of styrene in toluene, with benzoyl peroxide acting as a catalyst, shows the following initial rates of reaction as a function of the concentration of the monomer at 25 °C:

[Styrene] (mol dm <sup>-3</sup> )	0.86	2.59	4.33	6.04	7.78
$v_0$ (mol dm <sup>-3</sup> h <sup>-1</sup> )	3.5	15.5	31.0	47.0	64.0

What is the order of the reaction?

54. Propose a mechanism for the reaction



with an experimental rate law

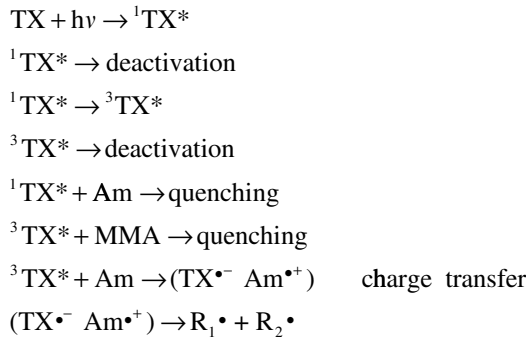
$$v = k [\text{Cl}_2]^{3/2} [\text{CO}]$$

Hint: consider that one is leading with a stoichiometric rate law.

55. Photopolymerisation of methyl methacrylate (MMA) can be photoinitiated by thioxanthone (TX). The polymerisation rate,  $R_p$ , can be expressed by the equation

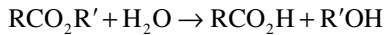
$$R_p = \frac{k_p}{\sqrt{k_t}} \sqrt{\phi_i} \sqrt{I_a} [M]$$

- (a) Propose a simple mechanism that accounts for such a rate expression.
- (b) Photopolymerisation can be initiated by TX in the presence of an amine (Am), but does not occur in the absence of amine. Interpret these findings.
- (c) A possible mechanism for photoinitiation is the following:



Radicals  $\text{R}_1^{\bullet}$  and  $\text{R}_2^{\bullet}$  can initiate polymerisation. The absence of photopolymerisation in the absence of amine indicates that the interaction of TX triplets with the monomer does not lead to polymerisation).

56. The hydrolysis of an ester,  $\text{RCO}_2\text{R}'$  ( $5 \times 10^{-5}$  mol dm $^{-3}$ ), in 9.5% ethanol–water at pH 12.50 and at 30° C was followed spectrophotometrically by observing the formation of the product  $\text{R}'\text{OH}$ . Absorbance values for the product at its maximum are given below at various times after the start of the reaction.



Time $t$ (h)	0	2	5	9	26	48	81	144	$t = \infty$
Absorbance	0.022	0.038	0.064	0.098	0.233	0.348	0.424	0.462	0.472

- (a) Assuming pseudo-first-order kinetics, calculate the rate constant for this reaction.  
 (b) The pseudo-first-order rate constants for this reaction at the same temperature at various pH values are

pH	$k (10^{-5} \text{ sec}^{-1})$	12.67	12.80	12.90	13.71
		1.42	4.35	5.53	40.8

What is the overall rate law for the hydrolysis and the specific rate constant?

57. The mutarotation of glucose in water follows first-order kinetics, but the reaction is catalysed by acids. (a) Calculate the rate constants for the catalysed and the non-catalysed reaction for the experimental data in aqueous solutions of  $\text{HClO}_4$ .

[Acid] ( $\text{mol dm}^{-3}$ )	$k_{\text{obs}} (10^{-3} \text{ min}^{-1})$
$10^{-4}$	5.4
0.0048	6.0
0.0247	8.92
0.0325	10.02

- (b) Predict the effect of using a carbon acid on the catalysed rate constant  $k_{\text{cat}}$ .

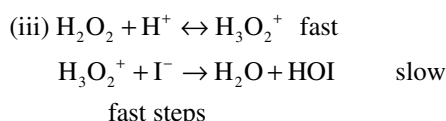
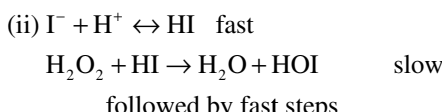
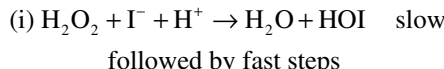
58. Under certain experimental conditions the rate law of the reaction



is

$$d[\text{I}_3^-]/dt = k[\text{H}_2\text{O}_2][\text{I}^-][\text{H}^+]$$

- (a) Verify whether any of the following mechanisms interprets the experimental rate law:



- (b) Propose possible steps that follow the rate-determining step in mechanism (i).  
 (c) Propose structures for the activated complexes in the rate-determining steps of the proposed mechanisms.

59. The reaction of formation of monoiodoacetone in aqueous solution



has a rate law

$$-\frac{d[\text{I}_2]}{dt} = k[\text{CH}_3\text{COCH}_3][\text{H}^+]$$

that is zero order in iodine. Propose a mechanism for the reaction.

60. The iodation of acetone is catalysed by acids. The catalytic rate constant,  $k_{\text{cat}}$ , has the following values according to the nature of the acid HA ( $K_a$ , acid dissociation constant):

Acid catalyst	$K_a$	$k_{\text{cat}} (10^6 \text{ mol}^{-1} \text{ dm}^3 \text{ sec}^{-1})$
Dichloroacetic	$5.7 \times 10^{-2}$	220
Monochloroacetic	$1.4 \times 10^{-3}$	34
Glycollic	$1.54 \times 10^{-4}$	8.4
Acetic	$1.8 \times 10^{-5}$	2.4
Trimethylacetic	$9.1 \times 10^{-6}$	1.9

- (a) Are we dealing with a general or a specific acid–base catalysis?  
 (b) Calculate the Brønsted coefficient.

61. The initial rate of hydrolysis of adenosine triphosphate catalysed by myosin at constant enzyme concentration, varies as shown:

$r_0 (\text{mmol dm}^{-3} \text{ sec}^{-1})$	0.080	0.114	0.154	0.174	0.189
$[S_0] (\text{mmol dm}^{-3})$	0.01	0.02	0.05	0.1	0.25

Calculate the Michaelis constant and  $r_{0,\text{max}}$ .

62. The hydrolysis of urea is catalysed by the enzyme urease



The dependence of the rate on the substrate concentration is given in the following table:

$v (\text{mol dm}^{-3} \text{ sec}^{-1})$	0.120	0.226	0.362	0.600	0.846
$[\text{urea}] (\times 10^3 \text{ mol dm}^{-3})$	0.32	0.65	1.29	3.27	8.30

- (a) Derive the Michaelis-Menten equation.  
 (b) Show whether the above reaction obeys this equation, and if so determine the appropriate kinetic parameters.

63. Benzene absorbs ultraviolet light at  $\lambda = 258$  nm. With normal irradiation sources a molecule is excited by a single photon. Under such conditions can one carry out the reaction  $\text{C}_6\text{H}_6 \xrightarrow{h\nu} \text{C}_6\text{H}_5 + \text{H}$ ,  $\Delta H_f = 468 \text{ kJ mol}^{-1}$ ?

On photoirradiation with high-intensity lasers, each molecule can absorb two or more photons at the same time. For biphotonic absorptions what is the absorption wavelength required to produce the dissociation of benzene?

64. Planck radiation formula eq. (15.7) gives the distribution of energy per unit volume per unit frequency. The same formula for the distribution of energy per unit volume per wavelength is

$$I(\lambda) = \frac{8\pi hc}{\lambda^5} \frac{1}{e^{hc/\lambda k_B T} - 1}$$

- (a) From this expression obtain Wien's displacement law for the change in the wavelength of maximum black-body irradiance with temperature, making  $\partial I(\lambda)/\partial \lambda = 0$  and  $\exp(hc/\lambda k_B T) - 1 \approx \exp(hc/\lambda k_B T)$ .
- (b) Obtain the Stefan–Boltzmann law for the total power per unit area from a black-body radiator, using the radiated power per unit area as a function of wavelength

$$\frac{dP}{d\lambda} \frac{1}{A} = \frac{2\pi hc^2}{\lambda^5} \frac{1}{e^{hc/\lambda k_B T} - 1}$$

that differs from the expression above by the factor  $c/4$  which involves an integration over all angles. The integration from  $\lambda = 0$  to  $\lambda = \infty$  is conveniently made with the substitutions  $x = hc/\lambda k_B T$  and  $dx = -hc/\lambda^2 k_B T d\lambda$ , and using the standard form integral

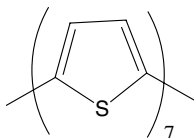
$$\int_0^\infty \frac{x^3}{(e^x - 1)} dx = \frac{\pi^4}{15}$$

- (c) The amount of incoming solar radiation on the outer surface of Earth's atmosphere, the solar constant, can be calculating from Stefan–Boltzmann law, knowing that the surface temperature of the Sun is 6000 K and that the irradiance from a sphere of radius  $R$  is proportional to  $R^{-2}$ . Calculate the solar constant using the radius of the Sun =  $6.5 \times 10^5$  km and the average Earth–Sun distance =  $1.5 \times 10^8$  km.
- (d) The Earth intercepts radiation passing through a disc of area  $\pi R_E^2$ . Calculate the absorbed solar radiation taking as the fraction of incident radiation that is reflected back into space, called the albedo,  $\alpha = 0.31$  and  $R_E = 6370$  km.
- (e) Consider the equilibrium between the absorbed solar radiation, calculated above, and the emitted terrestrial radiation, given by  $4\pi R_E^2 \sigma T_E^4$ , and calculate the radiative equilibrium temperature of the Earth,  $T_E$ .
- (f) The Earth's surface temperature is 300 K. Calculate the wavelength of its maximum irradiance, and the wavelength of the maximum absorbance of the Sun.

- (g) Provide an explanation for the difference between the radiative equilibrium temperature of the Earth and its surface temperature.

65. Oligothiophenes are conjugated polymers that have been investigated as materials for molecular electronics, including organic light-emitting diode (OLED) displays (Seixas de Melo *et al.*, *J. Chem. Phys.* 2001 **115** 5625).

- (a) Use the Strickler–Berg equation to calculate the radiative rate of decay of the excited singlet state of



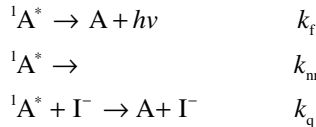
in dioxane ( $n_D = 1.422$ ), knowing that  $\langle \bar{v}^{-3} \rangle^{-1} = 5.59 \times 10^{12} \text{ cm}^{-3}$  and  $\int \epsilon(\bar{v}) \bar{v}^{-1} d\bar{v} = 1.19 \times 10^4 \text{ M}^{-1} \text{ cm}^{-1}$ .

- (b) Compare the calculated value with the experimental radiative rate knowing that the observed lifetime and fluorescence quantum yield are 0.85 nsec and 0.336, respectively.
- (c) How does the radiative rate of the singlet state change when the molar absorption coefficient increases?

66. Ruthenium (II) polypyridyl complexes have been extensively employed in solar cells. Their decadic molar extinction coefficients  $\epsilon$  are *ca.*  $10^4 \text{ M}^{-1} \text{ cm}^{-1}$  in the visible range.

- (a) Calculate the corresponding light capture cross sections in square nanometre.
- (b) The radius of  $\text{Ru(bpy)}_3^{2+}$  is 0.68 nm. Using the area occupied by this dye on the surface of an electrode, calculate the percentage of the incident light with a wavelength matching the maximum absorption of  $\text{Ru(bpy)}_3^{2+}$  that is absorbed.
- (c) Although it is tempting to overlay multi-layers of the dye on the electrode to increase its light absorption, this is generally a mistaken tactic because the energy transfer between sensitiser molecules is rarely efficient and the outer dye layers act only as a light filter. Alternatively, using nanocrystalline particles with diameters of 10–20 nm, it is possible to reach dye surface concentrations of  $\Gamma = 3 \times 10^{16} \text{ cm}^{-2}$ . Calculate the percentage of the incident light absorbed by a film with this concentration of  $\text{Ru(bpy)}_3^{2+}$ , knowing that the absorbance is given by  $A = \Gamma\sigma$  (Grätzel and Moser, *Electron Transfer in Chemistry*, Ed. I. Gould, vol. 5 (2001), Wiley-VCH, p. 587).

67. Iodide ions quench the fluorescence of anthracene (A) in aqueous solutions in the scheme



- (a) Derive an equation relating the fluorescence intensities in the presence ( $I$ ) and absence ( $I^0$ ) of iodide to  $[I^-]$ .
- (b) Given the following experimental results for the quenching of anthracene fluorescence by iodide ion:

$[I^-]$ (mol dm $^{-3}$ )	0	0.001	0.003	0.005	0.010
Relative fluorescence intensity	100	94.8	86.1	78.8	64.8

and the experimental fluorescence lifetime of anthracene in water ( $\tau = 1/(k_f + k_{nr}) = 4.9$  nsec), calculate  $k_q$ .

- (c) Is the quenching diffusion controlled?
68. The resin matrix of dental materials has important influence on the chemical and physical properties of light cure resins. The organic formulations also include photoinitiating systems that absorb light. From there free radicals start the conversion of the oligomer blend to a polymeric cross-linked network. Camphorquinone (CQ) is widely used in dental resin mixed with an amine. However, CQ is a solid, yellow compound with an unbleachable chromophore.

- (a) How can one reduce the amount of CQ to be used in the resin formulations?
- (b) Assuming that the potential of photoactivation to initiate the polymerisation reaction is proportional to the number of photons available at each wavelength, what are the two main factors that will influence photopolymerisation efficiency?
- (c) For dentistry it seems very desirable to have some parameter that takes into account the spectral properties of the photoinitiators as well as the spectral output of the dental light curing units (LCU). Such a parameter has been defined by Miguel Neumann and co-workers in terms of photon absorption efficiency (PAE). Other authors have defined such a parameter in terms of energy. What kind of parameter should one employ?
- (d) Table A below presents the normalised PAE for four dental photoinitiators irradiated with different light sources and Table B the properties of the photoinitiators and the concentrations employed.

Why is phenylpropanedione (PPD) the most efficient initiator? Why is it that for all initiators the light emission device UBIS is always better than UBI? The initiator lucirin is very inefficient with LED, why?

**Table A**

PAEs of dental photoinitiators and LCUs

Photoinitiators	Quartz–tungsten lamp Optilux ( $\lambda_{\max} = 493$ nm)	LED ultrablue I (UBI) ( $\lambda_{\max} = 467$ nm)	LED ultrablue IS (UBIS) ( $\lambda_{\max} = 454$ nm)
CQ	2.7	4.4	4.5
PPD	10.9	7.8	11.3
Irgacure 819	2.6	0.8	0.9
Lucirin TPO	2.7	0.2	0.3

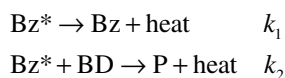
**Table B**

Properties and experimental conditions of the photoinitiators

Photoinitiators	$\lambda_{\max}$ (nm)	$\epsilon_{\max}$ ( $L \text{ mol}^{-1} \text{ cm}$ )	Concentration (wt%)
CQ	470	28	0.15
PPD	398	150	0.039
Irgacure 819	370	300	0.046
Lucirin TPO	381	520	0.037

(Data: Neumann *et al.*, *J. Dentistry* **33** (2005) 525–532).

69. Benzophenone in an electronically excited state,  $\text{Bz}^*$ , in a solution of benzhydrol, BD, is quenched at room temperature according to the following kinetic scheme:



P is a product of the reaction.

- (a) For the set of conditions  $[\text{BD}] > [\text{Bz}]$  show how  $[\text{Bz}^*]$  and  $[\text{P}]$  vary with time.
- (b) Determine the quantum yield of product formation,  $\phi_p$ , with  $k_1 = 2.6 \times 10^5 \text{ sec}^{-1}$  and  $k_2 = 5.0 \times 10^6 \text{ M}^{-1} \text{ sec}^{-1}$  when  $[\text{BD}] = 10^{-2} \text{ M}$ .

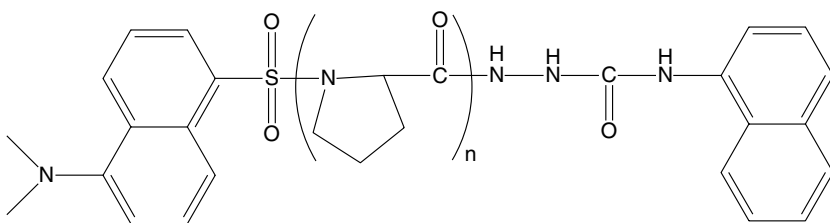
70. Aminoaromatic carbonyl compounds such as Michler's ketone (MK) (4,4'-bis(*N,N*-dimethylamino)benzophenone) are ideally suited as photoinitiators since they have large extinction coefficients, charge-transfer states and relatively long triplet lifetimes in solution. MK derivatives are also unique in that they can photoproduce two different types of free-radical intermediates  $\text{R}_1^\bullet$  and  $\text{R}_2^\bullet$ .

The experimentally determined order of reaction with respect to photoinitiator concentration dependence, monomer and light intensity for the photopolymerisation of MMA deviate from normal photopolymerisation kinetics. McGinniss *et al.* (McGinniss *et al.*, *Macromolecules* 1978 **11** 393) reported a rate for photopolymerisation of MMA photoinitiated by 4,4'-bis(diethylamino)benzophenone (DEABP), measured by the rate of conversion of MMA to polymer (PMMA),

$$R_p = k I_a^{0.3-0.5} [\text{DEABP}]^{0.2-0.4} [\text{MMA}]^{1.2-1.3}$$

Propose mechanistic interpretations for the above observations of low order for the initiator, higher order for the monomer and lower order for light intensity.

71. Electronic excitation energy transfer following the Förster mechanism can be used as a spectroscopic ruler. Verify the prediction of the  $R^6$  donor–acceptor distance dependence using the oligomers of poly-L-proline substituted with an  $\alpha$ -naphthyl group as the energy donor and a dansyl group as the energy acceptor knowing the transfer efficiencies  $E$



$R$ (Å)	21	25	27	30	33	36	40	42	46
$E$	0.97	0.83	0.72	0.62	0.50	0.40	0.28	0.26	0.13

(Data: Stryer and Haugland, *PNAS* (1967) **58** 719).

72. Using the harmonic approximation calculate the Franck–Condon factor  $J_{0,v''}$ , with  $v'' = 0\text{--}19$ , for the  $\text{A}^3\Sigma_u^+ \rightarrow \text{X}^1\Sigma_g^+$  transition in  $\text{Br}_2$ , knowing that for the excited state  $R_e = 2.695$  Å and  $\bar{v} = 153$  cm $^{-1}$ , whereas for the ground state  $R_e = 2.281$  Å and  $\bar{v} = 325.32$  cm $^{-1}$ .

(Data: Coxon, *J. Mol. Spectrosc.* (1971) **41** 566).

73. The electron self-exchange reaction for  $[\text{Co}(\text{OH}_2)_6]^{3+/2+}$  in water has an experimental rate constant for electron transfer  $k_{\text{exp}} = 2.4$  M $^{-1}$  sec $^{-1}$ . There is a low-lying electronic state that bypasses the spin-forbidden character of the reaction from the ground state, and the electron transfer can be considered adiabatic. The relevant structural data for the reaction is as follows:

Complex	Electronic configuration	Force constant (kJ mol $^{-1}$ Å $^{-2}$ )		Bond lengths (Å)	
		$f_{\text{red}}$	$f_{\text{ox}}$	$l_{\text{red}}$	$l_{\text{ox}}$
$[\text{Co}(\text{OH}_2)_6]^{3+/2+}$	$(\pi)^5(\sigma^*)^2/(\pi)^6$	$9.6 \times 10^2$	$1.53 \times 10^3$	2.081	1.873

Estimate the rate constant for the reaction at 298 K:

- (a) Using Marcus Theory with the radius of each reactant  $r_{\text{av}} = 6.5$  Å and the collision frequency factor  $Z = 10^{11}$  M $^{-1}$  sec $^{-1}$ .
- (b) Using ISM with a reaction frequency of  $K_c v_N = 10^{13}$  sec $^{-1}$ .
74. The experimental rate of electron transfer for the reaction of the iron-cyclopentadienyl complex has been measured through NMR line broadening as described in Section 3.2.2. The rate constant at 298 K in acetone is  $k_{\text{exp}} = 8 \times 10^6$  M $^{-1}$  sec $^{-1}$  at an ionic strength 0.15 M.
- (a) From the structural data listed in Table 16.2 estimate the energy barrier,  $\Delta G^\ddagger$ , assuming a coordination number for iron of 2; the bond lengths listed are the distance from the Fe atom to the centre of the cyclopentadienyl ring.
- (b) Calculate the theoretical rate constant for a typical value of  $v_N = 10^{13}$  sec $^{-1}$ .

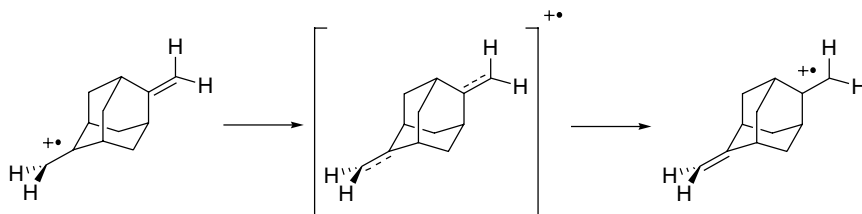
75. The paramagnetic encounter complex between tetracyanoethylene acceptor (TCNE) and its radical-anion (TCNE $^{\cdot-}$ ) has a donor–acceptor separation of 2.9 Å. The complex

$(TCNE)_2^{*-}$  has an inter-valence absorption band with an absorption maximum at 1515 nm in dichloromethane. Calculate its electronic coupling matrix element knowing that, in this solvent, the extinction coefficient is  $1.2 \times 10^3 \text{ M}^{-1} \text{ cm}^{-1}$  and that the full-width at half-maximum is  $3 \times 10^3 \text{ cm}^{-1}$ , assuming a Gaussian band shape.

(Data: Rosoka *et al.*, *Chem. Phys.* (2006) **324** 117).

76. In the first scanning transmission microscopy experiment, a logarithmic dependence of the tunnel current on tip-sample separation was found. Calculate the tunnelling decay coefficient of this distance dependence, knowing that the sample was in platinum and the tip was made of tungsten, and that their work functions are 5.03 and 4.55 eV, respectively.

77. High-level *ab initio* calculations were employed to calculate the PES for electron transfer in bis(methylene) adamantyl radical cation



where the electron transfer is symmetrical, with the change in bond orders from 1.5 to 2 in one bond associated with the change from 2 to 1.5 in the other bond. Depending on the level of theory, the reorganisation energy was estimated to be 76 or 55 kJ mol<sup>-1</sup>.

(Data: Blancafort *et al.*, *J. Am. Chem. Soc.* (2005) **127** 3391).

Estimate the reorganisation energy for this electron transfer using the effective displacement of ISM and representing the double bond by the parameters of ethylene ( $l_D = 1.342 \text{ \AA}$ ,  $f_D = 5.77 \times 10^3 \text{ kJ mol}^{-1} \text{ \AA}^{-2}$ ) and the radical cation moiety by the parameters of benzene ( $l_A = 1.397 \text{ \AA}$ ,  $f_A = 3.87 \times 10^3 \text{ kJ mol}^{-1} \text{ \AA}^{-2}$ ).

## Answers

1. (a) zero order; (b) second order; (c) second order—the ratio between  $t_{3/4}$  and  $t_{1/2}$  is 3 times for a second-order reaction; 2 times for a first-order reaction and 1.7 for a one-half order reaction.

2.  $v = k [A] [B]^2$ ;  $k = 40 \text{ mol}^{-2} \text{ dm}^6 \text{ sec}^{-1}$ .

3. 15,700 years.

4. (a)  $t_{1/2} = 0.78 \text{ nsec}$ ; (b)  $t_{1/2} = 154 \text{ nsec}$ .

5. (a)  $v = k K [\text{NH}_4^+] [\text{CNO}^-]$ ;  $K$  is the equilibrium constant of the first step and  $k$  the rate constant of the slow process; (b) The addition of salt to water leads to complete dissociation into  $\text{NH}_4^+$  and  $\text{CNO}^-$ .

6. flash photolysis.

7.  $= 1.56 \times 10^{-3} \text{ sec}^{-1}$ ;  $t_{1/2} = 442 \text{ sec}$ .

8. 580 sec.

9. (a) second-order  $2\text{NcMe}\bullet \rightarrow \text{products}$  (a plot of 1/absorbance against time is linear); (b) the slope of the plot of 1/absorbance against time is  $2k/\epsilon_{400\text{nm}}l$ . Using the above molar absorption coefficient and  $l = 1 \text{ cm}$  gives  $k = 1.2 \times 10^9 \text{ dm}^3 \text{ mol}^{-1} \text{ sec}^{-1}$ .

10.  $k = 166.8 \text{ min}^{-1}$ .

11. 2.7 kJ mol $^{-1}$ .

12. (a)  $\text{O} + \text{NO}_2 \rightarrow \text{NO} + \text{O}_2$ ; (b)  $\{\text{NO}_2\cdot\text{NO}_2\}^\ddagger$ .

13. Mechanism III.

14. (a)  $v = k [\text{IO}_3^-]^2 [\text{I}^-]^4$ ;  $k = 7.2 \text{ dm}^{15} \text{ mol}^{-5} \text{ sec}^{-1}$ ; (b) The experimental rate law demonstrates that the activated complex for the rate-determining step contains one iodate ion *plus* one iodide ion, *plus* an undefined number of protons because the reaction is carried out at constant pH, *plus* an undefined number of water molecules because the reaction takes place in aqueous solutions. Kinetic data seldom reveal what happens after the rate-determining step.

15. (a)  $\{\text{IClOH}(\text{OH}_2)_n\}^\ddagger$ ; (b) One possible mechanism is

- (i)  $\text{OCl}^- + \text{H}_2\text{O} \rightleftharpoons \text{HOCl} + \text{OH}^-$  fast
- (ii)  $\text{HOCl} \rightarrow \text{ICl} + \text{OH}^-$  slow
- (iii)  $\text{ICl} + 2\text{OH}^- \rightarrow \text{OI}^- + \text{Cl}^- + \text{H}_2\text{O}$  fast

while another possibility is:

- (i)  $\text{OCl}^- + \text{H}_2\text{O} \rightleftharpoons \text{HOCl} + \text{OH}^-$  fast
- (ii)  $\text{I}^- + \text{HOCl} \rightarrow \text{HOI} + \text{Cl}^-$  slow
- (iii)  $\text{OH}^- + \text{HOI} \leftrightarrow \text{H}_2\text{O} + \text{OI}^-$  fast.

16. (a)  $(d[[\text{Cr}(\text{H}_2\text{O})_5\text{NCS}]^{2+}]/dt) = k_1 - k_2 [[\text{Cr}(\text{H}_2\text{O})_6]^{3+}]/(k_{-1} + k_2 [\text{NCS}^-])$ ; (b)  $[\text{NCS}^-] \ll (k_{-1}/k_2)$ .

17. For the first mechanism where  $\text{Cl}_2$  (aq) is the coreactant with the alcohol:  $(k_{\text{obs}})^{-1} = \{k_1[\text{Cl}_2(\text{aq})]_0 + K/(k_1[\text{Cl}_2(\text{aq})]_0 [\text{H}^+]) (1/[\text{Cl}^-])\}$ ; when HOCl (aq) is the coreactant with the alcohol a plot of  $(k_{\text{obs}})^{-1}$  should be linear with  $[\text{Cl}^-]$ .

18. (b) the length of the CH bond is greater than that of the HH bond.

19. (a) The reaction  $\text{Na} + \text{Cl}_2 \rightarrow \text{NaCl} + \text{Cl}$  ( $\Delta H^0 = -165.2 \text{ kJ mol}^{-1}$ ) does not release enough energy to form the electronically excited  $\text{Na}^*$ .

20. (a)  $7.8 \times 10^{-5} \text{ m}^3 \text{ mol}^{-1} \text{ sec}^{-1}$ ; (b)  $\sigma = 3.1 \text{ \AA}^2$ ; (c) the calculation would underestimate considerably the experimental value, since this a harpoon reaction.

21. The first term represents the average energy of molecules undergoing reaction and the second term the average energy of colliding molecules.

22. This corresponds to a repulsive or late downhill surface.
23.  $V = 8.2 \times 10^{-2} \text{ m}^3 \text{ mol}^{-1}$ ; some of the partition functions are:  $q_{\text{Na}}^{\text{el}} = 2$ ;  $q_{\text{Na}_2}^{\text{rot}} = 2246$ ;  $q_{\text{Na}_2}^{\text{vib}} = 4.88$ ;  $K = 2.42$ .
24.  $\Delta H^\ddagger = 181 \text{ kJ mol}^{-1}$ ;  $\Delta S^\ddagger = -48 \text{ J K}^{-1} \text{ mol}^{-1}$ .
25. (a)  $-d[\text{F}_2\text{O}]/dt = 2k_1 [\text{F}_2\text{O}]^2 + k_2 [\text{F}] [\text{F}_2\text{O}]$ ; the steady state for F leads to the following relations for the rates of the elementary step:  $0 = R_1 - R_2 + 2R_3 - 2R_4$  and for OF is  $0 = R_2 - 2R_3$ . Then we obtain  $[\text{F}] = (k_1[\text{F}_2\text{O}]/k_4)^{1/2}$  and  $k_1 = 2k_1$  and  $k_{\text{II}} = k_2(k_1/k_4)^{3/2}$ .
26. (a) step 3; (b)  $v = k_3(k_1/(k_2 + k_3)) [\text{N}_2\text{O}_5] \approx (k_3k_1/k_2) [\text{N}_2\text{O}_5]$ .
27. (a)  $E_a = 180 \text{ kJ mol}^{-1}$ ; (b)  $A = 14.1$ ; (c)  $5.5 \times 10^{-5} \text{ sec}^{-1}$ .
28. Substituents 1, 3 and 4 have a zero reaction energy and the series of substituents 5, 6 and 7 have  $\Delta G^0 \approx -18.5 \text{ kJ mol}^{-1}$ . In each of these series one verifies an LFER between  $\Delta G^\ddagger$  and  $\Delta G^0$ .
29.  $\Delta G(0)^\ddagger$  is constant throughout the family; (b) for harmonic oscillators  $\Delta G(0)^\ddagger = (1/8)f[(0.108)/n^\ddagger](2l)^2$ .
- 30.
31.  $1/k^1$  versus  $1/P$  is not linear.
32. For the Lindemann approach the rates  $k_S$  and  $k_D$  would be independent of energy. In terms of ideal gas law one would have  $[\text{D}]/[\text{S}] = k_D/k_S[\text{M}] = RT k_D/k_S P$  and one should expect a linear relation of  $[\text{D}]/[\text{S}]$  versus  $P^{-1}$ . This is not verified; the plot has a pronounced downward curvature. The rate of decomposition should increase with an increase in the vibrational energy.
33. In terms of the general definition of the rate,  $v$ , as a function of the amount of the reactant,  $dn_{\text{A}_2} = V d[\text{A}_2] + [\text{A}_2] dV$ , where  $V$  is the volume, one has  $v = d[\text{A}_2]/dt + [\text{A}_2]/V dV/dt$ . This becomes the usual rate expression when the volume remains constant. At constant pressure the volume increases with time, since the total number of molecules is  $(1-x)n_{\text{A}_2} + 2xn_{\text{A}_2}$ , where  $x$  is the fraction of decomposition.
34. (a)  $\log k$  varies linearly with the reciprocal of  $\epsilon$ . The slope is positive because the ions in the rate-determining step have electric charges of opposite signs; (b) the rates would be independent of  $\epsilon$ .
35. With increases in both ionic strength and dielectric constant the rate of reaction (i) decreases while that of reaction (iv) increases, while reactions (ii) and (iii), in principle, are unaffected.
36.  $3.0 \times 10^6 \text{ m}^3 \text{ mol}^{-1} \text{ sec}^{-1} = 3.0 \times 10^9 \text{ dm}^3 \text{ mol}^{-1} \text{ sec}^{-1}$ .
37.  $-1$ ; the species is the hydrated electron.
38. (a)  $Z_A Z_B \approx 2$ ; (b) muonium is electrically neutral.
39.  $1.4 \times 10^7 \text{ dm}^3 \text{ mol}^{-1} \text{ sec}^{-1}$ ; from the viscosity of water, assuming that benzene and the hydrated electron have comparable sizes the diffusion-controlled rate constant is  $7.4 \times 10^9 \text{ dm}^3 \text{ mol}^{-1} \text{ sec}^{-1}$ , so the rate is considerably lower than diffusion control.
40.  $\Delta V^\ddagger = -4.8 \text{ cm}^3 \text{ mol}^{-1}$ ; (b) With the approach of the ions of the same charge sign, there is an intensification of the electric field, leading to an increase in electrostriction and a resulting decrease in volume. These effects tend, in general, to be more important than the

volume changes owing to the change in the volume of the reactant molecules themselves as they pass into the activated complex. In the present case the structural effects dominate since one of the species is neutral.

41. The adsorption follows a Langmuir isotherm because  $1/V$  is a linear function of  $1/P$ ; (b)  $V_\infty = 0.475 \text{ cm}^3$ .

42. (a) The ratio  $q_\ddagger/q_0(\text{CO}_{\text{ads}}) = 53.6$ . Usually  $q_\ddagger/q_0 > 1$  is interpreted in terms of a mobile activated complex. (b)  $\sigma$  is the fraction of occupied sites;  $N_s$  the number of sites per square metre on the platinum surface;  $E_a$  is the energy barrier for desorption;  $\Gamma_{\text{Coads}}$  is the concentration of the adsorbed CO per unit area,  $\Gamma_{\text{Coads}} = \sigma N_s / L = 0.5 \times 10^{19} / L = 8.3 \times 10^{-6} \text{ mol m}^{-2}$ , where  $L$  is the Avogadro constant. The partition function  $q_\ddagger$  differs from  $q^\ddagger$  by  $k_B T/h$ .

43. (a) rate  $\xi = k P_{\text{HONO}} [\text{HX}_{\text{(ad)}}]$  with  $k = k_{11} k_2 / (k_{-11} + k_2)$ ; (b) This is an application of the Hertz–Knudsen equation.

44.

45. (a)  $[\text{NO}_3]_{\text{st}} = (k_1/k_2) ([\text{N}_2\text{O}_5]/[\text{NO}])$ ; (b)  $(-\text{d}([\text{N}_2\text{O}_5]/\text{dt}) = k_1[\text{N}_2\text{O}_5]; (\text{d}[\text{NO}_2]/\text{dt}) = 3k_1[\text{N}_2\text{O}_5]$ .

46. reaction (–1) is a more exothermic process by *ca.* 73.6 kJ mol<sup>–1</sup>.

47. a catalyst;  $\text{d}[\text{H}_2]/\text{dt} = (k_3 K_1/K_2)[\text{C}_2\text{H}_6]$ .

48. (a)  $r = k [\text{CH}_3\text{OCH}_3]$ ; initiation first-order,  $\bullet\text{CH}_3$   $\beta$ -radical,  $\bullet\text{CH}_2\text{OCH}_3$   $\mu$ -radical, termination  $\beta\mu$ ; (b)  $r = k' [\text{CH}_3\text{OCH}_3]^{1/2}$ .

49. (a) the fate of the less reactive radical  $\text{HO}_2\bullet$  is not indicated and can be ignored in the kinetic treatment, which only uses steady-state conditions for  $\text{R}\bullet$ ;  $[\text{R}\bullet] = (k_1 [\text{RH}] [\text{O}_2]/2k_4)^{1/2}$ ;  $\text{d}[\text{ROOH}]/\text{dt} = k_2 (k_1/2k_4)^{1/2} [\text{RH}]^{1/2} [\text{O}_2]^{3/2}$ ; (b)  $E_a = E_2 + \frac{1}{2}E_1 - \frac{1}{2}E_4$ .

50. For both examples  $E_a = -6.6 \text{ kJ mol}^{-1}$ .

51.

52. A prototype reaction such as  $\text{CH}_3 + \text{I}_2 \rightarrow \text{CH}_3\text{I} + \text{I}$  is a fast process,  $k = 8.4 \times 10^9 \text{ mol}^{-1} \text{ dm}^3 \text{ sec}^{-1}$  at 300 K. However, a possible subsequent step for the propagation of the chain such as  $\text{CH}_4 + \text{I} \rightarrow \text{CH}_3\text{I} + \text{H}$  is so endothermic that the rate constant is *ca.*  $k = 8.4 \times 10^{-29} \text{ mol}^{-1} \text{ dm}^3 \text{ sec}^{-1}$  and the chain is quenched. Rates estimation on Java program at <http://www.ism.qui.uc.pt:8180/ism/>. Termination reactions  $\text{R}\bullet + \text{I} \rightarrow \text{RI}$  are fast processes.

53. 1.32.

54.  $\text{Cl}_2 \rightleftharpoons 2\text{Cl}$  fast equilibrium

$\text{Cl} + \text{CO} \rightleftharpoons \text{ClCO}$  fast equilibrium

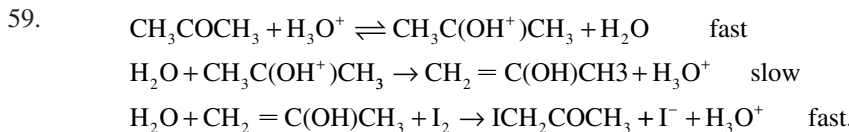
$\text{ClCO} + \text{Cl}_2 \longrightarrow \text{COCl}_2 + \text{Cl}$  slow

55.(a) The mechanism is identical to that proposed in the text. In the rate of polymerisation expression  $k_p$  is the rate constant of the propagation step,  $k_t$  the rate constant of the termination step,  $\phi_i$  the photoinitiation quantum yield,  $I_a$  intensity of the light absorbed and  $[\text{M}]$  the concentration of the monomer.

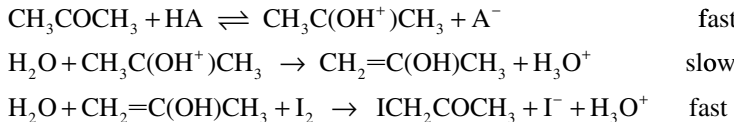
56. (a)  $k = 2.78 \times 10^{-2} \text{ h}^{-1} = 7.76 \times 10^{-6} \text{ sec}^{-1}$ ; from the increase in rate with pH, rate =  $k [\text{RCO}_2\text{R'}][\text{OH}^-]$ , and  $k = 8.2 \times 10^{-4} \text{ dm}^3 \text{ mol}^{-1} \text{ sec}^{-1}$ .

57.  $k_{\text{cat}} = 0.145 \text{ mol}^{-1} \text{ dm}^3 \text{ min}^{-1}$ ;  $k_{\text{non-cat}} = 5.3 \times 10^{-3} \text{ min}^{-1}$ ; (b) since a carbon acid would have a transition state bond order closer to  $n^\ddagger \approx 0.5$ ,  $k_{\text{cat}} < 0.145 \text{ mol}^{-1} \text{ dm}^3 \text{ min}^{-1}$  and eventually there is no acid catalysis.

58. The composition of the activated complex is  $\{\text{H}_2\text{O}_2\text{HI}\}^\ddagger$ . Mechanism (i) is a termolecular process, which is more likely if some collision complex is formed, either between  $\text{H}_2\text{O}_2$  and  $\text{H}^+$  or between  $\text{I}^-$  and  $\text{H}^+$ , and during the lifetime of such a complex a collision with the other reactant occurs. However, the presence of such complexes corresponds effectively to the other proposed mechanisms. Mechanism (iii) is the one that leads to products from the activated complex of the rate-determining step with the minimum rearrangement.



60. (a) General acid–base catalysis; the mechanism presented in the previous question can be rewritten in general terms:



(b)  $\alpha = 0.6$ . If the reaction were a specific acid –catalysis, the rate law would be  $v = kK_a [\text{acetone}] ([\text{HA}]/[\text{A}^-])$ .

61.  $K_M = 0.0145$ ;  $r_0 = 0.196 \text{ mmol dm}^{-3} \text{ sec}^{-1}$ .

62.  $K_M = 2.6 \times 10^{-3} \text{ mol dm}^{-3}$ .

63. no;  $\lambda = 510 \text{ nm}$ .

64. (a)  $T\lambda_{\text{max}} = hc/5k_B = 2.88 \times 10^6$  when  $T$  is in Kelvin and  $\lambda$  in nanometre.

(b) 
$$\frac{P}{A} = \frac{2\pi^5 k^4}{15h^3 c^2} T^4 = \sigma T^4 = [5.670 \times 10^{-8} \text{ W m}^{-2} \text{ K}^{-4}] T^4.$$

(c)  $S = 5.67 \times 10^{-8} (6000)^4 (6.5 \times 10^5 / 1.5 \times 10^8)^2 = 1380 \text{ W m}^{-2}$ .

(d)  $(1 - 0.31) 1380 \pi (6,370,000)^2 = 1.214 \times 10^{17} \text{ W}$ .

(e)  $T_E = 255 \text{ K}$ .

(f)  $\lambda_{\text{max}}(\text{Earth}) = 9600 \text{ nm}$  and  $\lambda_{\text{max}}(\text{Sun}) = 480 \text{ nm}$ .

(g) The infrared radiation emitted by the Earth is absorbed by  $\text{H}_2\text{O}$ ,  $\text{CO}_2$  and  $\text{O}_3$  present in the atmosphere, which are transparent to the visible radiation of the Sun, contributing to the “greenhouse effect”.

65. (a)  $3.9 \times 10^8 \text{ sec}^{-1}$ .

(b) the value from the quantum yield and lifetime is  $4.0 \times 10^8 \text{ sec}^{-1}$  and the agreement is excellent.

(c) the radiative rate increases.

66. (a)  $\sigma = 0.0038 \text{ nm}^2$ .

(b)  $A = \pi r^2 \sigma$ ; incident photons absorbed =  $1-10^{-A}$ ; incident light absorbed = 1.3%.

(c) incident light absorbed = 93%.

67. (b)  $k_q = 1.1 \times 10^{10} \text{ dm}^3 \text{ mol}^{-1} \text{ sec}^{-1}$ ; this is very close to the calculated value for the diffusion-controlled rate constant in water ( $7.4 \times 10^9 \text{ dm}^3 \text{ mol}^{-1} \text{ sec}^{-1}$ ), and the quenching is diffusion controlled.

68. (a) Since CQ has an unbleachable chromophore, large amounts will lead to undesirable yellowing, affecting the final aesthetic appearance of cured material. A possible strategy is to include other photoinitiators that act synergistically with CQ. An addition of an amine might also reduce the amount of CQ; (b) (i) the spectral properties of the photolysing reaction, which should ideally overlap with the absorption spectrum of the photoinitiator and (ii) the mechanism by which the polymerisation process is triggered by the excited photoinitiating species. For example, for CQ the mechanism for photoinitiation is an electron/proton transfer process whereas for PPD it is photocleavage. (c) The number of photons is more relevant for photoinitiation; PAE can thus be used to identify the best mechanism for photochemical process with specific photoinitiators. (d) PPD is the most efficient initiator, mainly owing to its low molecular weight, the good overlap with the LCUs' emission spectra and an extinction coefficient *ca.* 5 times higher than CQ. The LCU UBIS is always somewhat more efficient owing to the shift of the output to shorter wavelengths where the photoinitiators have their absorption maxima. The narrow spectral irradiance of the LEDs employed is not appropriate for curing Lucirin that has maximum absorption well within the ultraviolet region.

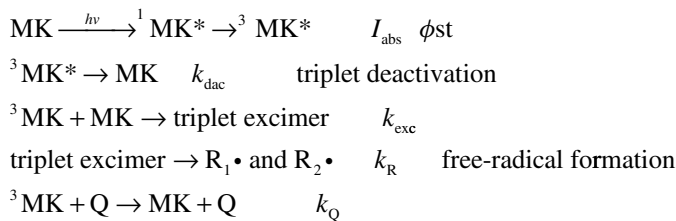
69. Bz\* decays in a first-order process with a rate constant  $k = k_1 + k_2 [\text{BD}]$ ;  $\phi_p = 0.16$ .

70. Deviations from normal kinetic orders might be attributable to primary radical or photoproduct termination interactions with growing polymer radicals or formation of relatively inactive transfer radicals. The low-order kinetic for the initiator is consistent with primary initiator radical competition for the monomer and other deactivation pathways. A following simplified mechanism can be proposed:

- (1)  $\text{R}\cdot + \text{M} \rightarrow \text{M}\cdot$
- (2)  $\text{M}\cdot + \text{M} \rightarrow \text{P}\cdot$
- (3)  $\text{R}\cdot + \text{R}\cdot \rightarrow \text{absorbing photoproducts}$
- (4)  $\text{R}\cdot + \text{photoproducts} \rightarrow \text{termination}$
- (5)  $\text{R}\cdot + \text{P}\cdot \rightarrow \text{termination}$
- (6)  $\text{P}\cdot + \text{photoproducts} \rightarrow \text{termination}$

Variations in light intensity are also consistent with screen effects owing to photoproduct formation.

The following mechanism has been proposed:



Show that the rate of the ketone disappearance is given by

$$-\frac{d[\text{MK}]}{dt} = I_{\text{abs}} \phi_{\text{st}} - k_{\text{dac}} [{}^3\text{MK}] + k_{\text{exc}} [{}^3\text{MK}] [\text{MK}] / [\text{Q}] - [{}^3\text{MK}] [\text{Q}]$$

71. The straight line of a plot of  $\ln(E^{-1}-1)$  versus  $\ln(R)$  has a slope of 6.1, very close to the theoretical slope.

72.

$v''$	0	1	2	3	4	5	6	7	8	9
$J_{0,v''}/1000$	0.0	0.0	0.0	0.1	0.4	1.4	3.6	7.9	15.3	26.4
$v''$	10	11	12	13	14	15	16	17	18	19
$J_{0,v''}/1000$	40.9	57.7	74.5	88.8	98.3	101.6	98.4	89.7	77.3	63.0

73. (a)  $k_{\text{Marcus}} = 1.2 \times 10^{-9} \text{ M}^{-1} \text{ sec}^{-1}$ .

(b)  $k_{\text{ISM}} = 6 \text{ M}^{-1} \text{ sec}^{-1}$ .

74. (a)  $\Delta G^\ddagger = 38 \text{ kJ mol}^{-1}$ .

(b)  $k_{\text{ISM}} = 2 \times 10^6 \text{ M}^{-1} \text{ sec}^{-1}$ .

75.  $V^e = 1100 \text{ cm}^{-1}$ .

76.  $\beta = 2.24 \text{ \AA}^{-1}$ .

77.  $\lambda = 69 \text{ kJ mol}^{-1}$ .

This page intentionally left blank

# Subject Index

- Ab initio, theories 115, 116  
Absolute-rate theory *see* Transition-state theory  
Abstraction reactions 28  
Acetaldehyde decomposition 308  
Acetone iodination 39, 41, 42  
Acid-base catalysis 321–358  
    and Acid-base strength 338  
    General 321, 326–330, 377  
    Mechanisms of 40, 321, 338  
    Salt effects 342–343  
    Specific 326–329  
Acidity functions 343–345  
    Hammett 343  
Activated complex 202, 217, 235, 236,  
    239–241, 243, 244, 248, 263, 264, 267,  
    344, 376, 437, 475, 480  
Activation energy 3, 11, 18, 41–43, 157, 158,  
    161, 168, 175, 176, 215, 223, 232, 267,  
    270, 284, 288, 293, 306, 309, 324, 326,  
    442, 454  
    and ISM 178  
    Calculation of 4, 43  
Empirical 3, 25, 41, 178, 180, 199  
of Catalyzed reactions 29–30, 324, 375  
Temperature dependence 175, 177, 260  
Activation  
    Enthalpy of 174, 375, 451, 377  
    Entropy of 121, 144, 237, 241, 244  
    Gibbs free energy of *see also* free energy  
        193, 199, 241  
    Volume of 247, 249  
Active centres 255  
Activity coefficients 236, 238, 239, 245, 342,  
    344  
Adiabatic energy 177, 422  
Adiabaticity 155, 156, 165, 413, 441, 445, 476  
Adsorption 251–255  
    Activated 253  
    Active centres 252–255  
    Associative chemisorption 254–255, 269  
    Competitive 258–259  
    Dissociative 257, 269  
Ideal 256  
Isotherms 256–259  
Nonideal 253–255  
Rates 258  
Statistical mechanics treatment 263–265, 271  
Thermodynamics 260  
Van der Waals 251  
    with Dissociation 257–258  
Alkali metal reactions 137  
Ammonia decomposition on surfaces 259  
Analysis of kinetic results 78–83  
Anthracene 395, 406, 410, 416, 418, 427, 433  
Anthraquinone 64, 65  
Arrhenius equation 4, 25, 260, 326, 375  
Arrhenius intermediate 322, 325, 328  
Ascorbic acid, oxidation 47, 49  
Associative mechanism 248, 249, 277–279  
Atom combinations, on surfaces 255, 270  
Atom formation, on surfaces 269  
Adatom 252, 253, 268, 271  
Aspirin 335–338, 377  
Azocoll papain 46, 48, 112  
Atom-molecule complex mechanism 295–298  
Autocatalysis 29  
Bell-Evans-Polanyi relationship 175  
Benzophenone 70  
Benzhydrol 70  
Biacetyl 61–63, 432–434  
Bimolecular reactions 99, 104  
    in Gas phase 121, 177  
    on Surfaces 265  
Bodenstein, M. 84, 300  
Bond dissociation energy 159, 172, 276, 408,  
    409, 447  
Bond-energy-bond-order (BEBO) method 167  
Born-Oppenheimer approximation 398, 440  
Bovine serum albumin 54  
Branching chains 310, 312, 313, 317  
    Degenerate 316  
Branching factor 313, 317  
Bromine atoms, reaction with H<sub>2</sub> 295, 301, 304

- Bromine-hydrogen reaction 295–298  
 Brönsted-Bjerrum equation 245  
 Brönsted equation 194–196, 339, 349, 359  
 Brönsted relationships 194, 339, 351
- Cage effect 229  
 Catalysis  
   Acid-base 194, 321–358, 377  
   Activation energies 324, 326  
   by Ions 327, 328  
   Enzyme 46–47, 104, 109, 277, 323, 325,  
     351, 361–383  
   Intramolecular 337, 338  
   of Chain reactions 319  
   of Hydrogenations, heterogeneous  
     homogeneous 29  
   of Polymerization 318–319  
   Surface 364  
 Catalytic constant 194, 339, 365, 373  
 Catalytic hydrogenation 29  
 Chain-ending step 299  
 Chain length 305, 307, 309  
 Chain-propagating step 295, 305  
 Chain reactions, catalysis of 319  
 Chemiluminescence 137, 386  
 Chemisorption 251, 253, 254, 269  
 Christiansen's theory of unimolecular  
   reactions 209–212  
 Chlorine, reaction with alkali metals 137  
   with Hydrogen 298–300, 304  
   with Nitric oxide 349  
 Chymotrypsin 368, 369  
 Collision cross section 117, 517  
 Collision frequency factor 4, 117, 147, 214,  
   440  
 Collision theory 4, 116, 117, 119–122,  
   132, 133, 135, 143, 144, 147, 167,  
   212, 215  
 Collisions, strong 385  
 Collisions in solution 226  
 Combustion 310, 311, 314, 316, 317  
 Compensation effects 200  
 Competition 51, 56–61, 155, 259, 269, 297,  
   372, 464  
 Complex reactions 18, 39–41  
   Mechanisms classification 84  
   Rate equations 84–89  
 Consecutive reactions 84  
 Continuous flow 51, 52
- Conventional transition-state theory *see*  
   Transition-state theory  
 Cool flames 317  
 Coulombic energy 389  
 Cross-reactions 288, 291, 440, 442  
 Cross section, reaction 117, 133, 271  
 Crossing, PES 135–137, 155, 411  
 Cyclopentadienyl iron, complexes 450  
 Cyclopropane isomerisation 152, 153, 216,  
   218, 220, 222
- Degenerate branching 316  
 Degrees of freedom 133, 146, 156, 214–216,  
   219, 265, 417, 468, 508  
 Density of states 217–219, 255, 395,  
   414–416, 480  
 Desorption rates 256, 258  
 Detonation 310  
 Deuterium-hydrogen exchange 158, 382  
 Deuterium-methane exchange 419  
 Dexter mechanism 75, 389, 397, 410, 426  
 Dielectric constant, effect on rates 234,  
   240–242, 379, 420  
 Differential method 77  
 Diffusion-controlled reactions 225–228,  
   233, 457  
   Ionic reactions 235  
 Dimethoxybenzene 72  
 Diphenylcyclopentadienone 36, 37, 80  
 Dipole-dipole reactions 125, 389, 397  
 Direct reaction 271  
 Dispersion angle 127  
 Displacement 145, 162, 165, 408, 409, 413,  
   416, 421, 430–432  
   ISM ( $d_{ISM}$ ) 431  
   Reduced ( $s$ ) 402  
 Disproportionation 21  
 Dissociative mechanism 277, 278  
 Distance dependence factor 458  
 Distribution of collisions in solution 225  
 Distribution of energy 4, 142, 154, 216, 405  
 Dividing surface 219  
 Double inverted region 467–469  
 Double-sphere model 240  
 Dynamic parameter 183, 186, 192, 466, 468
- Einstein, A. 387, 395  
 Eigen, M. 52, 345–347, 357  
 Elastic scattering 126

- Electric field jumps 54–55  
Electron, hydrated 234, 235  
Electron-jump mechanism 456  
Electronic coupling 413, 416, 421–430,  
    432, 434  
Electrostriction 243, 244, 248  
Electron transfer reactions 58, 382, 423,  
    437–482  
    Adiabatic 440, 454–456  
    Electrodes, at 469–482  
    Marcus theory, 440–443, 445, 475  
    Non-adiabatic 440, 454, 458  
    Self-exchanges 437, 454, 458, 460–462  
    Spin forbidden 410, 459  
Electron tunnelling 382, 398, 428, 429, 458  
Electrophilicity index 172–174, 176, 178, 190,  
    285, 287, 302, 352, 355, 357, 457  
Elementary reactions 4, 13, 21, 23, 77, 190, 196,  
    223–249, 271, 288, 292, 298, 301, 375  
Encounters 226  
Energisation 209, 210, 218  
Energy of activation *see* Activation energy  
Energy distribution 10, 132, 133, 140, 405  
Energy flow 215, 218–220  
Energy gap law 410, 434  
Energy transfer 54, 57, 61, 63, 67, 75, 385,  
    390, 396, 397, 410, 413, 414, 416, 417,  
    421, 423, 426, 432, 434  
    Intermolecular 218, 389  
    Intramolecular mechanisms 218, 220  
    Triplet-triplet 66, 389, 390, 410, 413, 430  
Enthalpy of activation 174, 375, 451  
Entropy of activation 121, 144, 241, 244, 376  
Enzyme catalysis 46–47, 104, 109, 277, 323,  
    361–383  
    Influence of pH 373  
    Influence of temperature 375–376  
    Transient-phase kinetics 367  
Equilibrium, statistical mechanics 144, 146  
Ester hydrolysis 108, 361  
Ethane decomposition 298, 309  
Exchange reactions 18, 248, 249, 290,  
    292, 439  
Excitation 10, 28, 60, 64, 66, 67, 69, 71, 73,  
    141, 219, 355, 389, 395, 403, 404, 406,  
    408, 433, 464  
Explosion limits 311, 314  
Extent of reaction 15–17, 24, 40  
Eyring, H. 143  
Family of reactions 183, 184, 186, 189, 190,  
    193, 356, 357, 462  
Fast reactions 18, 50, 235  
Femtochemistry 72–75  
Ferrocene 59, 445, 447, 450, 456, 477,  
    479–482  
Fick, law 230  
Flames 137, 317  
Flash photolysis 61–65, 67  
Flow systems 51, 52  
Fluorescence 60, 61, 386, 406  
Force constant 8, 190–193, 195, 203, 205, 221,  
    454, 461  
Foreign-gas effect 210, 211, 215  
Förster mechanism 389, 397  
Franck-Condon factors 27, 400–407, 421, 426,  
    429, 430, 432, 447, 449  
Franck-Condon principle 27, 399, 401, 410,  
    417, 452  
Franck-Rabinowitch effect 229  
Free radical combinations 172, 295, 309  
Frequency factor *see* Pre-exponential factor  
  
Gas-phase reactions 30, 84, 289, 290, 310,  
    446, 457  
General acid-base catalysis 327, 329, 330,  
    350, 377  
Gibbs energy of activation 199  
Golden rule 220, 391, 395, 397, 398, 415, 427,  
    433, 434, 447  
Goldfinger-Letort-Niclause rules 309–310  
Grotthuss mechanism 346  
  
Half-life 79–82, 107, 361  
Halides, reaction with alkali metals 137  
Halogenation of acetone 39, 42  
Halogens reactions, 203  
    with Alkali metals 137  
    with Nitric oxide 349  
Hamiltonian 129, 130, 391–393  
Hammond, postulate of 202, 203  
Hammett relationship 197  
Heterogeneity of surfaces 479  
Heterogeneous reactions, comparison with  
    homogeneous reactions 477  
    *See also* Surface reactions  
Hinselwood, treatment of unimolecular  
    reactions 212–215  
Hydrated electron 234, 235

- Hydration shell 347, 445  
 Hydrazines 446, 449  
 Hydrocarbon decompositions 305  
 Hydrocarbon oxidation 196  
 Hydrogen atoms, 28, 204, 281, 304, 306  
   Reaction with H<sub>2</sub> 304  
   Reaction with HBr 304  
 Hydrogen bonds 55, 345–347, 355,  
   379–381, 507  
 Hydrogen-bromine reaction 295–298  
 Hydrogen-chlorine reaction 298–300  
 Hydrogen-deuterium exchange 158, 382  
 Hydrogen-iodine reaction 300–301  
 Hydrogen ion catalysis *see* proton transfer  
 Hydrogen ions, combination with OH<sup>−</sup> ions  
   330  
 Hydrogen-oxygen reaction 310–314
- Image force 476, 477  
 Impact parameter 122–124, 126, 131  
 Induction period 317, 367  
 Inelastic scattering 420  
 Inert-gas effect 84, 302  
 Initiation of oxidation 316  
   of Polymerization 318  
 Inner-sphere reactions 437, 456  
 Integration, method of 89  
   Laplace transforms 89–93  
   Markov chains 99–103  
   Matrix method 94–97  
   Monte Carlo method 103–106  
   Runge-Kutta method 97–99  
 Internal conversion of energy 386, 388, 395,  
   407–410  
 Intermolecular energy transfer 218, 389  
 Internal pressure *see* Pressure  
 Interchange mechanism 277, 278  
 Interacting-state model *see* ISM  
 Intersecting-state model *see* ISM  
 Intramolecular energy transfer 218, 220  
 Intrinsic barrier 176, 184, 192, 193, 196, 206,  
   284, 357, 440, 462  
 Inverted region 443, 462–469  
 Iodine-acetone reaction 39, 41  
 Iodine-atom combination 228  
 Iodine-hydrogen reaction 300–301  
 Ion-dipole reactions 280  
 Ion-molecule reaction 280, 289, 446  
 Ion-pair (ionic) yield 276, 277, 342, 379, 468
- Ionic reactions  
   Diffusion control 232, 235, 457  
   Ionic recombinations 467, 468  
   Ionic strength, effects 31, 49, 83, 244–246  
   ISM 167–186, 192, 220, 285, 301, 352, 357,  
    431, 449, 452, 482  
   Isokinetic temperature 200  
   Isolation method 83, 106–107  
   Isomerization of cyclopropane 152, 153, 216,  
    218, 220, 222  
   Isotope effects 156, 338, 357, 382  
   Primary 157, 351  
   Secondary 158, 160  
   Isotope exchange reactions 157, 158, 357
- Jablonski diagram 385, 386  
 Jortner, J. 220, 407, 421
- Kasha, rule of 386  
 Kinetic-isotope effects 156–160  
 Kinetic results, analysis of 33, 78, 277  
 Kinetic theory of collisions 115
- Laidler, K. 298, 321, 324  
 Landau and Zener, transition probability 411  
 Langevin collision rate 446, 447  
 Langford-Gray classification of mechanisms  
   276  
 Langmuir-Hinshelwood mechanisms 262, 263,  
   268–270  
 Langmuir isotherm 256–259  
 Langmuir-Rideal mechanisms 262, 263  
 Laser-induced reactions 67–68  
 Lennard-Jones potential 125–127  
 Lifetime 9, 10, 28, 56–58, 60–62, 68, 69, 72,  
   95, 96, 388–390, 396  
 Light intensity 27, 43, 64  
   Actinometry 44, 46  
   Ferrioxalate 44, 45  
 Lindemann-Christiansen hypothesis  
   209–212  
 Linear Gibbs-energy relationships (LFER)  
   193–201, 356  
 Lineweaver-Burk plot 366, 371  
 Lippincott-Schroeder (LS) potential 345, 346,  
   505–509  
 Local random matrix theory (LRMT) 218–220  
 Lotka, reaction 102, 103  
 Luminescence quenching 60–61

- Marcus and Coltrin path 165, 166  
Marcus (RRKM) theory of unimolecular reactions 215–218  
Marcus theory *see* electron transfer  
Marcus equation 191, 192, 292, 463  
Maxwell-Boltzmann distribution 12, 118, 119, 145, 213  
Menschutkin reactions 30, 224, 225, 239  
Methane, reaction with H atoms 152, 181  
Methylcoumarin 95, 97  
Methylpropane 34–37, 77–79  
Methyl radical reactions 19, 152, 181  
Methyl transfer reactions 280–282, 285, 288–290  
Michaelis-Menten equation 111, 323, 363–368, 374  
Microscopic reversibility 21, 89, 387  
Minimum-energy path (MEP) 6, 7, 11, 133, 155, 165  
Molecular beams 126, 127, 132, 268  
Molecular dynamics 4, 115–142  
Molecularity 3, 210  
of Reactions 13, 273, 277  
Morse potential 158–160, 171, 404  
  
Nitric oxide 119, 209, 267  
Nitrobenzoic acid 197  
Naphthalene 61–63, 233, 410, 418, 427, 460, 461, 465, 466  
Normal modes 216–219, 409, 451, 461, 500  
Norrish, R. 61, 62  
Nuclear magnetic resonance (NMR) 56–60  
  
Opposing reactions 2, 88, 89  
Order of reaction 3, 23, 34–39, 77, 80, 82  
Outer-sphere reactions 437, 440, 456, 477  
Oxidation, gas-phase  
of Hydrocarbons 316  
of Hydrogen 270, 311  
  
Parallel reactions 84–86  
Parr, electrophilicity index 172, 190, 285, 352, 457  
Partition functions 143, 146–151, 154, 156, 177, 178, 216, 235, 264, 265–267, 351, 352, 488, 492, 493, 503, 504  
Pauling relationship 168, 169, 403, 430, 432  
Persulfate ions, reactions 41  
pH dependence of rates 329, 330  
  
pH effects in enzyme kinetics 373–375  
pH jump 55  
Phosphorescence 60, 385, 386, 388, 404, 406, 407, 419, 433  
Photoacoustic calorimetry (PAC) 67, 69, 407  
Photochemical reactions 61, 167, 228, 298, 300, 464  
Photodissociation 74  
Photolysis 46  
Flash 61–65  
Poisoning of surfaces 259  
Poisson distribution 122, 402, 403  
Polanyi, J. 140, 142  
Polanyi, M. 4. 137, 140, 143  
Polymerization 317–319  
Porter, G. 61, 62  
Potential-energy surfaces (PES) 4, 116, 135, 149, 215, 218, 385, 440, 443, 463  
Attractive 138  
Calculation of 4, 11  
DMBE 150, 164, 180, 181, 183  
Early barrier 140  
Empirical 134, 136  
Late barrier 140  
Profile 31, 325  
Repulsive 138  
Pre-equilibrium approximation 107, 108  
Pre-exponential factor 3, 4, 118, 158, 178, 179, 237, 244, 289, 293, 351, 355, 377, 476, 478, 480  
for Solution reactions 223  
Temperature dependence 25  
Pressure, influence on rates  
External 238, 246–249  
Internal 68, 237–240  
Pressure jump 54  
Probability of reaction 130, 133  
Pross and Shaik diagrams 282–285  
Protolytic mechanisms 327  
Proton mobility 345–350  
Proton transfer reactions 321–359, 382  
Prototropic mechanisms 327  
Pulse radiolysis 65–67  
Pulsed lasers 55, 62, 65, 68, 69, 74  
Pyrolysis 305–310  
  
Quantum effects 156, 416  
Quantum mechanical tunnelling 132, 160–167, 355, 407–410, 458

- Quantum yield 45, 46, 60, 61, 69, 166, 167, 396  
 Quasiequilibrium 144, 146, 154, 344  
 Quenching 39, 60, 62, 419, 465
- Radiation hypothesis 3, 209  
 Radioactive decay 80  
 Radiationless transitions 385, 388, 391, 395, 407–410, 425  
 Radiative rates 395  
 Rate-determining step 13, 22, 23, 34, 40, 77, 106, 111–113, 277, 325, 330, 334, 335, 344, 347, 368, 376, 466  
 Reaction cross section 133, 271  
 Reaction dynamics 104, 115, 139  
 Reaction path 6, 28, 163, 165, 190, 289, 381, 385, 499, 502, 503, 505, 508  
 Reaction probability 100, 119  
 Reactivity-selectivity principle (RSP) 203–205  
 Recombination of radicals 228, 314, 466, 468  
 Re-crossing 155, 420  
 Reduced mass 8, 118, 119, 159, 165, 182, 286, 400, 403, 407, 446, 447, 450, 476, 499, 500, 503  
 Refractive index 387, 396, 425, 441, 448, 459, 476, 478, 480, 481  
 Rehm-Weller plateau 465, 466, 468  
 Relationships *see* structure-reactivity  
 Relaxation methods 52–56  
 Relaxation time 53, 56, 57, 420, 476  
 Relaxation, vibrational 67, 386, 395, 399  
 Reorganisation energy 284, 413–416, 419, 421, 430, 432, 433, 441, 445, 467  
 Reynolds number 51  
 Reversible reactions 20, 21, 52, 84, 88, 89, 91, 94, 112, 143  
 Rice-Herzfeld mechanisms 306, 308  
 Rice-Ramsperger-Kassel Marcus (RRKM) treatment 215–218  
 Ritchie equation 205
- Saddle point 6, 7, 134, 154, 155, 167  
 Salt effects 31, 245, 342–343  
 Scattering 71, 122, 126, 128, 132, 134, 135  
 Rainbow 127  
 Secondary recombination 228  
 Semiempirical calculations 167  
 Separability of motions 5–6, 115  
 Serine proteases 368, 369, 377, 379  
 Single Photon counting (SPC) 69–72
- Slater's treatment of unimolecular reactions 219  
 Sodium reactions 137  
 Solvent effects 30, 223–225, 274, 280, 289–294  
 Soybean lipoxygenase 381  
 Specific acid-base catalysis 326–329  
 State-to-state kinetics 132  
 Statistical factors 151–154  
 Steady-state hypothesis 108, 210, 227, 228, 266, 295, 296, 308, 318, 324, 333, 348  
 Steric factor 135, 144  
 Stern-Volmer equation 61, 465  
 Stimulated emission 387  
 Stopped-flow method 52, 367  
 Strong collisions  
 Structure-reactivity relationships  
 Bell-Evans-Polanyi 175, 176, 196, 206  
 Electronic effect (Ritchie) 205  
 Linear (LFER) 193–201  
 Quadratic (QFER) 189–193
- Substitution reactions  
 $S_N1$  mechanism 274–276  
 $S_N2$  mechanism 274–276
- Substituent effects 338  
 Successive (consecutive) reactions 84, 86–88  
 Surface heterogeneity 479  
 Surface reactions  
 Activation energies 260–261  
 Bimolecular 265–267  
 Inhibition 258, 260, 261  
 Mechanisms 268–271  
 on Nonuniform surfaces 253  
 Poisoning 259  
 Transition-state theory 263–267  
 Surface structure 253–255  
 Sutin, N. 441  
 Symmetry number 154
- Tafel equation 469–475  
 Taft relationship 196–201  
 Temperature, and reaction rates 25–26  
 Temperature-jump method 53–54  
 Thermodynamic formulation of rates 235  
 Trajectory 21, 104, 117, 118, 122, 123, 126, 129, 130, 132–137, 154, 155, 166, 167  
 Transfer coefficient 474

- Transfer of energy 390, 410, 411  
Transition-state theory  
    Adiabatic 156  
    Assumptions 144  
    Conventional 144–147, 216  
    Thermodynamic 147  
    Variational 155  
Transition state bond order 169, 170, 178, 186, 190, 192, 205, 207, 225, 454, 457, 461  
Transitions, between states 385–435  
Transmission coefficient 156, 383, 502  
Triose-phosphate isomerase 379  
Tunnel effect theory 160–167, 407–410  
Tunnelling *see* Quantum mechanical tunnelling  
Ultrasonic absorption 55–56  
Unimolecular reactions 209–222, 263–265  
van't Hoff equation 25, 53, 260  
van't Hoff intermediate 324–326, 333  
Vibrational relaxation *see* Relaxation, vibrational  
Vibrationally adiabatic path 182, 499–502  
Volume of activation 247, 249, 288  
Zero-order kinetics 82–83, 259, 323  
Zero-point energy 132, 174, 264, 302, 356, 357  
    and Isotope effects 156–160, 419  
Zewail, A. 74  
Zundel ion 346, 347

This page intentionally left blank